EARTHQUAKE ENGINEERING RESEARCH CENTER

AN EXPERIMENTAL STUDY OF THE BEHAVIOR OF DUAL STEEL SYSTEMS

by

ANDREW S. WHITTAKER
CHIA-MING UANG
VITELMO V. BERTERO

COLLEGE OF ENGINEERING

UNIVERSITY OF CALIFORNIA AT BERKELEY

. Title and Subtitle	5. Report Date
ın Experimental Study of the Behavior of Dual Steel Systems	July 1990
	6.

. Author(s)	8. Performing Organization Rept. No.
ı.S. Whittaker, C-M Uang, and V.V. Bertero	UCB/EERC-88/14

. Performing Organization Name and Address	10. Project/Task/Work Unit No.
Earthquake Engineering Research Center University of California, Berkeley .301 S 46th St. Richmond, CA 94804	
	11. Contract(C) or Grant(G) No.
	(C)
	(G) ECE82-08141 ECE84-19739

2. Sponsoring Organization Name and Address	13. Type of Report & Period Covered
National Science Foundation :800 G. St. NW Washington, DC 20550	
	14.

5. Supplementary Notes

6. Abstract (Limit: 200 words)

This report compares the behavior of 0.3-scale models of a concentrically braced (CBDS) and an eccentrically braced (EBDS) dual system. These two dual systems, six stories in height, were tested on the earthquake simulator at the University of California at Berkeley, as part of the U.S.-Japan Cooperative Earthquake Research Program. The models were similitude scaled replicas of full-scale test structures (prototypes) that were pseudo-dynamically tested in the Building Research Institute in Tsukuba, Japan, and which satisfied the seismic requirements of the 1985 UCB, 1984 ATC 3-06 and 1986 SEAOC. The performances of the two models are compared for minor, moderate and severe earthquake shaking. The performance of the EBDS was clearly superior to that of the CBDS. The roles of the DMRFs in both models are studied and recommendations are made regarding their minimum stiffness and strength requirements in CBDSs and EBDSs.

The values of response modification factors used to derive design response spectra from an assumed linear elastic design response spectra for CBDSs and EBDSs are reviewed in this report; in both instances, the ATC and SEAOC response modification factors are significantly higher than the values obtained form the earthquake simulator testing of the models. A rational procedure for the design of steel structures sited in regions of high seismic risk is presented.

17. Document Analysis   a. Descriptors

b. Identifiers/Open-Ended Terms

c. COSATI Field/Group

18. Availability Statement	19. Security Class (This Report)	21. No. of Pages
Release Unlimited	unclassified	352
	20. Security Class (This Page) unclassified	22. Price

i.a

U.S.-JAPAN COOPERATIVE EARTHQUAKE RESEARCH PROGRAM

AN EXPERIMENTAL STUDY OF THE BEHAVIOR OF DUAL STEEL SYSTEMS

by

Andrew S. Whittaker

(Forell/Elsesser Engineers, San Francisco, CA)

Chia-Ming Uang

(Northeastern University, Boston, MA)

Vitelmo V. Bertero

(University of California at Berkeley, Berkeley, CA)

ABSTRACT

This report presents, summarizes and compares the behavior of 0.3-scale *models* of a concentrically braced dual system (CBDS) and an eccentrically braced dual system (EBDS). These two dual systems, six stories in height, were tested on the earthquake simulator at the University of California at Berkeley, as part of the U.S.-Japan Cooperative Earthquake Research Program.

The *models* were similitude scaled replicas of full-scale test structures (*prototypes*) that were pseudo-dynamically tested in the Building Research Institute in Tsukuba, Japan. The *prototypes* satisfied the seismic requirements of the 1985 UBC, 1984 ATC 3-06 and 1986 SEAOC.

The performances of the two *models* are compared for minor, moderate and severe earthquake shaking. The performance of the EBDS was clearly superior to that of the CBDS. The roles of the DMRSFs in both *models* are studied in this report and recommendations are made regarding their minimum stiffness and strength requirements, in CBDSs and EBDSs, respectively.

Response modification factors are currently used by the ATC and SEAOC to derive design response spectra from an assumed linear elastic design response spectra. The values of the factors used for CBDSs and EBDSs are reviewed in this report; in both instances, the ATC and SEAOC response modification factors are significantly higher than the values obtained from the earthquake simulator testing of the *models*. Analysis of the test results suggest that realistic response modification factors for CBDSs and EBDSs, for the period range of $0.5 \leq T_1 \leq 1.00$ second, are $R_{CBDS} = 2.5$ and $R_{EBDS} = 5.0$.

A rational procedure for the design of steel structures sited in regions of high seismic risk is presented in the final chapters of this report. This procedure satisfies the serviceability requirements for minor earthquake shaking and prevents collapse, or life-threatening damage, during severe earthquake shaking.

ACKNOWLEDGMENTS

Table of Contents

List of Tables

List of Figures

CHAPTER 1

INTRODUCTION

1.1 Earthquake Resistant Steel Framing Systems

The comprehensive design of a structure required to withstand severe earthquake shaking should satisfy the requirements of a number of limit states that can be categorized as follows: *Serviceability Limit State*; *Damageability Limit State*; and *Collapse Limit State*. These design limits states, as they apply to earthquake engineering, can be described as follows.

A design for the serviceability limit state requires that, for minor frequent earthquake ground motions, the bare structure and the associated non-structural components should suffer little or no damage and that discomfort to the occupants should be minimal. Structural damage is typically avoided by providing the structure with sufficient strength to remain elastic. Non-structural damage and occupant discomfort is precluded by ensuring that the structure has sufficient stiffness to prevent excessive deformations [1].

A damageability limit state design would require that a structure remain undamaged but would accept minor non-structural damage in the event of moderate earthquake shaking. This limit state is compatible with minor inelastic behavior in certain critical structural locations; the deformations produced as a result of the inelastic behavior, although small, may result in limited non-structural damage.

A design for the collapse limit state guards against the collapse of both the structure and the non-structural elements during very infrequent, severe earthquakes. Furthermore, design for the collapse limit state guards against that non-structural damage that might jeopardize the safety of the occupants and the occupants of adjacent structures. To prevent structural collapse, the structure must be able to absorb and dissipate large amounts of energy.

In general, those structural systems which possess a significant degree of redundancy with large ductility and stable hysteretic behavior will perform satisfactorily in major seismic events.

- 2 -

A dual system, that is, one comprised of at least two different, yet compatible structural systems, should satisfy these requirements.

Allowing the structure to reach the latter two limit states is justified on purely an economic basis; the costs associated with providing a non-essential building with sufficient strength and stiffness to preclude any damage in either moderate or severe earthquakes is usually prohibitive and may be significantly larger than that required to rectify the resulting damage.

To date, three basic structural framing systems have been used for the design and construction of low, medium and high-rise steel buildings.

The first type of framing system, the *ductile moment-resisting space frame* (DMRSF), is depicted in Figure 1.1a. This structural system is used more extensively than the concentrically braced frame (described below) for two principal reasons. The DMRSF is advantageous from the architectural standpoint as it provides unobstructed space between columns, and, it has enhanced energy absorption and dissipation characteristics. The DMRSF does however have a number of shortcomings for buildings of five or more stories; these shortcomings include: (1) to comply with serviceability displacement limits, member sizes significantly larger than those required for a comparable braced system are necessary; (2) the possibility of significant non-structural damage at the damageability level; and (3) life threatening damage at the collapse level.

The second of these systems, the *concentrically braced frame* is shown in Figure 1.1b. In this system, diagonal bracing elements with coincidental centerlines form a vertically cantilevered truss; as a result the lateral story forces are resisted primarily via axial forces in the bracing members. As such, its high elastic stiffness makes it an efficient framing system for minor earthquake shaking; the performance of the CBF in the inelastic range however is not as impressive [2]. The inelastic cyclic performance of such a system has shown that repeated yielding of the bracing elements causes a marked reduction in brace capacity and pinched hysteresis loops. This results in a significant decrease in the ability of the concentrically braced

structure to absorb and dissipate energy; brace failure leads to unacceptably large inter-story drifts and thus non-structural damage. For the construction of essential facilities, that is, structures that must remain fully operational following severe earthquakes, the CBF is an attractive structural system when the seismic response of the facility will be limited to linear elastic behavior in order to preclude damage. However, as demonstrated in Chapter 7, in order for a CBF to remain elastic during severe earthquake shaking, it must be designed for lateral forces appreciably higher than those specified by current earthquake-resistant design regulations in the United States.

The third of these systems, the *eccentrically braced frame* (EBF), is shown in Figure 1.1c. In the eccentrically braced frame, axial forces in the bracing elements are transferred to either the columns or other braces via beam flexure and shear in an element known as an active link [3,4]. Four types of eccentrically braced frames, the D-braced, the split K-braced, the V-braced and the inverted V-braced frames are shown in Figure 1.2. If an EBF is correctly analyzed, proportioned and constructed, it possesses greater ductility and energy absorption and dissipation capacity than the more traditional CBF. Moreover, for a similar level of energy absorption and dissipation capacity to the DMRSF, it offers significant advantages in terms of drift control and overall material cost.

In recent years, there has been a trend towards combining either of the two bracing systems with a DMRSF to form a so-called *dual system*. The role of the DMRSF in the concentrically braced dual system (CBDS) is to provide additional energy dissipation capacity to the dual system and to supply a line of defense against structural collapse in the event of the failure of the concentric braces. The importance of the latter contribution, that is, the improvement in the redundancy of the structural system, is discussed in Chapter 7. The role of the DMRSF in the eccentrically braced dual system (EBDS) is similar to that for the CBDS. However, as the stable energy dissipation capacity of an EBF is superior to that of a CBF [5], the increase in energy dissipation capacity of an EBDS due to the presence of the DMRSF is less marked than for the CBDS.

1.2 U.S.-Japan Cooperative Earthquake Research Program

The overall objective of the U.S.-Japan Cooperative Research Program [6] is to improve seismic safety practices through studies to determine the relationship between full-scale tests, small-scale tests, component tests and analytical studies for reinforced concrete (Phase 1) and steel (Phase 2) structures. The research program has been tailored to:

- analyzing and testing building systems as realistically as possible,

- reviewing the effectiveness of current earthquake resistant design procedures and structural systems in light of the experimental results,

- research that is of practical interest and value to the engineering profession.

In order to meet the Phase 2 objectives of the research program, the Joint Technical Coordinating Committee (JTCC) decided to sequentially test two full-scale, six story, dual steel buildings designed to the then current United States and Japanese codes of practice.

The concentrically braced *prototype* was constructed and pseudo-dynamically tested in the Large-Size Structures Laboratory of the Building Research Institute (B.R.I.) in Tsukuba, Japan. Following the completion of the testing of the concentrically braced *prototype*, the concentric braces were removed and eccentric braces installed for the testing of the eccentrically braced *prototype*. The objective of the pseudo-dynamic testing program was to generate displacements in the *prototypes* that were sufficiently large enough ($\approx 2\%$ inter-story drift index) to ascertain their strengths, ductility and failure mechanisms [7,8].

In addition, a series of tests on reduced-scale models of the *prototypes*, connections, structure sub-assemblages and composite floor systems was undertaken. Two medium-scale models (hereafter referred to as the *models*) of the *prototypes* were designed, constructed and tested on the earthquake simulator of the University of California at Berkeley in Richmond, California. That testing program and its results form the basis of this report.

1.3 Objectives and Scope of the Studies at the University of California

1.3.1 General

The principal objective of the studies at Berkeley was to investigate the behavior of the *model* dual systems, experimentally and analytically, under the application of realistic earthquake ground motions. In order to satisfy the objectives of the U.S.-Japan Co-operative Research Program, the integrated analytical and experimental studies undertaken at the University of California at Berkeley were conducted in three phases.

1.3.2 First Phase: Preliminary Analytical Studies

Review of the Designs of the CBDS and EBDS Prototypes:

In light of the results obtained in the full-scale tests in Japan, a thorough review of the analysis and design of both the CBDS and EBDS was conducted. Its purpose was to check whether the design of *prototype* dual systems represented the best possible design and construction practice in the USA; any detected weakness could then be rectified in the construction of the *models*.

The initial analysis and design of the concentrically braced *prototype* was undertaken in accordance with the 1979 edition of the Uniform Building Code and the 1981 Japanese Aseismic Code [9]. After testing the *models*, the *prototypes* were re-analyzed and their designs re-evaluated in accordance with:

- The 1985 edition of the Uniform Building Code (UBC) [10].

- The 1984 edition of Applied Technology Council Recommendations (ATC 3-06) [11].

- The 1986 edition of the SEAOC "Recommended Lateral Force Requirements" [12]

The results of the three analyses are presented in part in Chapter 2 and References 1 and 2.

The results of some of these analytical studies and the physical limitations of the Berkeley earthquake simulator were used to select the length scale of the *models* tested at Berkeley [2].

Seismic Performance of the Prototypes:

The seismic performance of the two *prototypes* was reviewed prior to the construction of the *models* and some of the *models'* connection details were modified as a result [1,2].

1.3.3 Second Phase: Earthquake Simulator Studies

Selection of Materials, Fabrication and Instrumentation:

The results of the first phase were assessed to ascertain whether modifications to the structural shapes used in the *prototypes* were necessary. The material and geometric characteristics of the W steel sections were closely measured in order to facilitate accurate similitude scaling in the *models*. The concentrically braced *model* was constructed first, subject to the guidelines outlined above and elaborated upon in Reference 2. After testing, the concentric bracing was removed and the resulting DMRSF was then tested to evaluate its dynamic characteristics; the results of these tests are presented and discussed in Reference 2. The eccentrically braced *model* was then constructed by installing the eccentric bracing in all six stories of the DMRSF in the bay adjacent to the location of the concentric braces.

Earthquake Simulator Testing of the Models:

The objective of the experimental programs was to subject the *models* to earthquake simulator motions that would elicit structural response that could be broadly categorized into the following:

- Serviceability Limit State Response.

- Damageability Limit State Response.

- Collapse Limit State Response.

Details of the testing program for the CBDS and the EBDS are presented in References 1 and 2, respectively.

1.3.4 Third Phase: Data Evaluation and Correlation Studies

In References 1 and 2, selected earthquake simulator test results were presented for the eccentrically and concentrically braced *models*, respectively. These reports discussed in detail

the behavior of the *prototypes* and the fabrication, construction, instrumentation and earthquake simulator testing of the *models*. In addition, these two reports analyzed a portion of the earthquake simulator test results and then correlated these experimental results with (1) the analytical studies of the *models'* responses and (2) the responses of the *prototypes*.

As noted in Section 1.2, one objective of the U.S.-Japan Cooperative Earthquake Research Program was to review the effectiveness of current earthquake resistant design procedures and structural systems in light of the experimental results - this is the primary objective of this dissertation.

1.4 Report Objectives and Scope

This is the third and final report dealing with the experimental response of the *model* dual systems studied on the earthquake simulator. Some results of the earthquake simulator testing, previously reported in References 1 and 2, are reproduced in this report for completeness. The concentrically braced *model* (CBDS *model*) was principally tested with the 1978 Miyagi-Ken-Oki (MO) N00E earthquake ground motion whereas the eccentrically braced *model* (EBDS *model*) was subjected to both the Miyagi-Ken-Oki earthquake ground motion and the 1952 Kern County Taft N21E earthquake ground motion. In Reference 2, Uang and Bertero described three tests of the CBDS in detail; these tests were denoted as MO-06, MO-33 and MO-65, where the numerical suffix indicates the peak ground acceleration. In Reference 1, Whittaker et al. described five tests of the EBDS in detail; these tests were denoted as Taft-08, Taft-27, Taft-57, Taft-66 and Sine-70. In order to compare the performance of the these two framing systems, results from two other tests of the EBDS are presented and these will be referred to as the MO-07 and MO-28.

The primary objectives of this report are to compare the behavior and performance of the CBDS and EBDS *models* that were tested on the earthquake simulator and to assess the implications of the test results for the design and construction of dual steel systems in regions of high seismic risk. In order to provide the information necessary to compare the behavior of

the CBDS and EBDS, the design (Chapter 2), construction (Chapters 3 and 4) and earthquake simulator testing (Chapters 5 and 6) of the *models* are presented in this report. In Chapter 7, the responses of both of the *model* dual systems are evaluated and compared in terms of:

- Strength versus Deformation relationships

- Energy Distributions and Energy Dissipation Capacities

- Response Modification Factors

- Lateral Force Distributions

- Low-Cycle Fatigue and Incremental Collapse

- DMRSF Responses

In Chapter 8: the responses of the CBDS and EBDS *models* to severe earthquake shaking are summarized; conclusions are drawn with respect to the suitability of CBDSs and EBDSs for regions of high seismic risk; recommendations for the design of dual systems in regions of high seismic risk are presented, and a rational design procedure for steel structures is proposed in Section 8.3.

1.5 Literature Review

A review of the currently available literature on eccentrically and concentrically braced frames is presented in References 1 and 2, respectively. In addition to these two EERC Reports, a number of papers and reports have been published recently that discuss these two framing systems.

Concentrically Braced Frame:

Khatib, Mahin and Pister [13] studied the seismic response of chevron braced dual steel systems in order to: investigate the parameters that affect inelastic force redistribution in dual systems; determine the sensitivity of the dual system's response to these parameters; develop optimal proportioning guidelines to improve the response of dual systems; and formulate design recommendations for possible inclusion in the seismic regulations. Khatib showed that

the response of chevron braced frames and the tendency of chevron braced frames to form soft stories are extremely sensitive to the characteristics of the ground excitation. Statically adding the individual strengths of concentrically braced frames and moment resisting space frames was shown to be incorrect. The interaction forces that are developed when concentrically braced frames and moment resisting space frames are forced by compatibility to undergo the same displacements in the dual system, reduce the total strength available in the dual system to resist external loads.

Tang and Goel [14] conducted a series of dynamic analyses of concentrically braced steel structures in order to study their earthquake resistance. Their objectives were to assess the safety level of this type of building if it was designed and constructed in accordance with current seismic regulations. Tang and Goel concluded that: concentrically braced structures can perform very well during severe earthquake ground motions if the bracing members are ductile; braced structures can be designed for smaller lateral forces than those specified by current codes if the bracing members are ductile, and "..if properly designed, braced non-moment frames can be more economical and can perform as well as dual systems during severe earthquakes ...". The first and second conclusions are based in part on the assumption that tubular braces can, through the appropriate choice of b/t ratios, respond in a ductile manner - this issue is discussed in Chapters 7 and 8. The third conclusion is, in the author's opinion, extremely questionable because it completely ignores the beneficial effects of redundancy in a structural system, such as the back-up DMRSF in a dual system.

Eccentrically Braced Frame:

Ricles and Popov [15] investigated, both experimentally and analytically, the behavior of composite shear links and concluded that: composite links have greater initial elastic strength and stiffness than bare steel links; the energy dissipation capacity of a composite link is greater than that of a bare steel link for identical deformation histories, and the concrete floor slab is not as effective as transverse beams at either end of the link for preventing lateral-torsional buckling. Ricles and Popov [16], prior to undertaking a series of dynamic nonlinear analyses

of three different eccentrically braced frames, developed a multilinear element to describe the behavior of composite shear links. The conclusions drawn by Ricles from these analyses include the following: careful consideration must be given to the selection of the section sizes for the links so that the relationship of *(required strength/supplied strength)* for the links should be uniform over the height of the structure in order to enhance the energy dissipation capacity of the EBF; the design axial forces in the braces should be increased to the point whereby they are based on link shear forces of $1.7V_p$ in lieu of the current $1.5V_p$, and the extent of the link end moment transferred into the eccentric braces should be thoroughly reviewed in order to prevent the yielding or buckling of the eccentric braces.

Engelhardt [17] showed that depending upon the geometry and member sizes of the eccentrically braced frame, plastic hinges may develop in the beam and brace outside the link and that a significant loss of frame strength and inelastic deformation capacity may result. Engelhardt is currently testing links that yield predominantly in flexure (moment links); the effects of web stiffener spacing, connection detailing, link rotation capacity and yielding of the beam and brace outside of the link are under investigation.

On the subject of dual systems, the emphasis in the past has centered on the elastic interaction between reinforced concrete shear walls and moment frames. Khan et al. [18] discussed this form of interaction and presented a series of influence curves that related the distribution of the story shear force between the shear walls and the frame members to a wide range of structural parameters. The elastic interaction between the shear walls, which have a similar deformation pattern to braced frames under lateral loading, and moment frames, is now well understood; however, their interaction in the inelastic range is poorly understood. As noted in Reference 1, the stiffness and strength compatibility of these two framing systems and the torsional redundancy of the entire dual system may dictate whether the dual system can withstand severe earthquake shaking. The strength and stiffness compatibility of the braced frames and the DMRSF in the dual system is discussed in Chapters 7 and 8 of this report.

CHAPTER 2

PROTOTYPE DUAL SYSTEMS

2.1 Selection of the Prototype Dual Systems

A full-scale, six story, two bay by two bay office building utilizing composite construction was chosen as the subject for intensive investigation. The design and construction of this building was intended to be representative of a medium-rise office building constructed in both the United States and Japan.

The plan view and frame elevations of the six story test building are shown in Figures 2.1 and 2.2, for the CBDS and EBDS *prototypes*, respectively. The structure, 49.21×52.49 ft in plan and 73.43 ft high, consists of three frames parallel to the loading direction; two ductile moment-resisting space frames on Grid Lines A and C and a chevron braced frame on Grid Line B. Transverse to the loading direction there are three frames; two cross-braced frames on Grid Lines 1 and 3 and an unbraced frame on Grid Line 2. All column-to-girder connections in the transverse frames were bolted, shear type connections. The cross-bracing provided lateral stiffness in the transverse direction and greatly increased the torsional stiffness of the structure.

The composite floor system, shown in Figure 2.3, was constructed using lightweight reinforced concrete cast on 1.6 mm thick, standard steel floor decking supported by steel W girders. To develop full composite action, shear studs were provided to transfer the shear forces developed on the slab-to-girder interface. The lightweight concrete had a specified strength of 3.0 ksi and the slab's wire mesh reinforcement consisted of 0.24 inch (6mm) diameter deformed bars on a 4 inch square grid.

2.2 Design of the Prototype Dual Systems

The design criteria, loads and procedure were reported in detail by Foutch et al. [19] for the CBDS *prototype*. The design criteria adopted for the CBDS *prototype* were as follows:

(i) The design gravity and earthquake loads should be representative of those specified in both the United States and Japan.

(ii) Allowable stresses under earthquake loading could be increased by one-third above those values specified for gravity or permanent loading.

(iii) Girders and columns should be W sections of ASTM-A36 steel.

(iv) Bracing members should be ASTM A500 Grade B steel tubing and should be designed to resist both tension and compression.

(v) Girders in the braced bay should be designed for gravity loads without consideration of the supporting effect provided by the braces.

(vi) Girder-to-column connections should be designed as moment connections in the loading direction and shear connections in the transverse direction. The strength of the connections should satisfy the requirements of the Japanese Aseismic Design Code [9].

The design of the concentrically braced *prototype* was complicated by the significant differences between the design practices in the United States and Japan. Although significant efforts were made by the design group to design a structure that was consistent with the 1979 Uniform Building Code, the 1981 Japanese Aseismic Code and professional practice in both countries, compromises were necessary in the selection of the design gravity loads (Table 2.1) and the seismic loads.

Total gravity dead loads of 90 psf, 75 psf and 30 psf were used for the typical floors, roof and exterior wall areas, respectively (Table 2.1). The design live loads were 60 psf and 20 psf for the typical floors and roof, respectively; live load reduction was used for the sizing of the primary girders.

The seismic design loads were based on a total base shear of **0.197** W_{drw} at the working stress level [7,8,19,20] and were estimated using the 1981 Japanese Aseismic Design Code. The total base shear of $0.197W_{drw}$ was equivalent to a UBC design base shear of $0.113W_{drw}$, where the braced bay was designed for 125% of the design base shear and the DMRSF was designed for 50% of the design base shear. The latter is 100% larger than required by the UBC for a DMRSF in a dual system and was used to reconcile the significant differences in the minimum strength requirements of the 1979 Uniform Building Code and the 1981 Japanese Aseismic Code. The minimum strength requirements of the 1981 Japanese Aseismic Code are generally significantly higher than the minimum strength requirements of the seismic regulations in the United States. Accordingly, the seismic design loads can be considered to be consistent for the *prototype* being sited on firm ground in the United States or on soft soil in Japan [7].

The distribution of the seismic forces between the braced frame and the DMRSF is also different in the United States and Japan. The 1981 Japanese Aseismic Code distributes 66% of the total base shear to the braced frame (=$0.13W_{drw}$) and 34% to the DMRSF (=$0.067W_{drw}$), that is, the nominal strength of the DMRSF is approximately 50% of the braced frame. In the United States, the concentrically braced frame is designed to resist 125% of the total base shear and the DMRSF is designed to resist 25% of the total base shear, that is, the nominal strength of the DMRSF is only 20% of the braced frame. Clearly, the strength of the *prototype's* DMRSF is significantly higher than that required by the seismic regulations in the United States.

The design reactive weight, W_{drw}, of 1356 kips excluded the live loads and the weight of the external walls and internal partitions. The live load was excluded because it is not commonly considered as part of the reactive weight for seismic design in the United States. The weight of the external walls and internal partitions were excluded from the reactive weight because they were not included in the pseudo-dynamic testing of the *prototypes*. In addition, the inclusion of these loads in the design reactive weight would have resulted in a stronger

structure that could not have been suitably damaged by the actuators at the B.R.I. testing facility [7,8,19].

The design procedure, connection details and construction details for the CBDS *prototype* are presented by Uang and Bertero [2], Foutch et al. [7,8,19] and Yamanouchi et al. [20] and are not reproduced in this report.

Table 2.2 lists the W section sizes used for the column, girder and brace members in both the CBDS and EBDS *prototypes*; the mark numbers are shown in Figures 2.1 and 2.2. The floor weights of the *prototype* are presented in Table 2.3; the second column contains those dead loads noted in Table 2.1 multiplied by the corresponding contributing areas; the third column contains the loads in the second column excluding the weight of the external wall and the fourth column notes the as-tested weights of the individual floors. The measured material properties of the *prototypes'* structural steel and lightweight concrete are presented in References 1, 2, 7 and 8.

The beam and column sizes were not changed for the testing of the eccentrically braced *prototype* because it was not feasible for this multi-phase testing program. The design of the shear links and of the eccentric braces were based on the test results for isolated shear links [3,4,21,22,23]. The design of the shear links and of the eccentric braces was constrained by: (1) the geometry of the existing concentrically braced *prototype*; and (2) the existing steel W sections in the concentrically braced frame (Frame B). A shear link length of 28 inches (711 mm) was chosen for all six levels of the *prototype*; web stiffener thickness and spacing were based upon the research findings of Manheim [23]. The eccentric braces were designed to remain elastic at a load level consistent with the ultimate shear strength of the corresponding links.

2.3 Pseudo-Dynamic Testing of the Prototypes

The pseudo-dynamic earthquake simulation testing of the *prototypes* was conducted in three stages:

Stage 1 Testing - Concentrically Braced Dual System:

The 1978 Miyagi-Ken-Oki (MO) N00E earthquake record was used as the input signal for the testing of the CBDS *prototype*. The three tests of the CBDS had different levels of peak acceleration and were classed as follows:

(i)   **Minor Test** - Serviceability Limit State

        MO - Peak acceleration of 65 gals or 6.6%g

(ii)   **Moderate Test** - Damageability Limit State

        MO - Peak acceleration of 250 gals or 25.5%g

(iii)   **Final Test** - Collapse Limit State

        MO - Peak acceleration of 500 gals or 51.0%g

The Japanese researchers conducted free and forced vibration tests to evaluate the natural frequencies, mode shapes and modal damping ratios of the CBDS *prototype*.

Stage 2 Testing - Eccentrically Braced Dual System:

Five earthquake simulation tests on the EBDS *prototype* were conducted in Stage 2; two tests utilized the 1952 Kern County Taft N21E earthquake record [24] and the remaining three utilized a sinusoidal signal whose period approximately equaled the fundamental period of the EBDS *prototype*. The three tests using sinusoidal input were all part of the one test conducted after the Taft 500 gals test. The five tests can be classed as follows:

(i)   **Minor Tests** - Serviceability Limit State

        Taft - Peak acceleration of 65 gals or 6.6%g

        Sine - Peak acceleration of 97 gals or 9.9%g

(ii)   **Moderate Test** - Damageability Limit State

        Sine - Peak acceleration of 270 gals or 27.5%g

(iii) **Final Tests** - Collapse Limit State

        Taft - Peak acceleration of 500 gals or 51.0%g

        Sine - Peak acceleration of 320 gals or 32.6%g

The procedure used to install the eccentric bracing and repair the structural slab prior to the commencement of the Stage 2 testing is described in detail in Reference 25. The results of these five tests and the associated vibration tests are presented by Kawakami et al. [25], Yamanouchi et al. [26] and the B.R.I. Steel Group [27].

Stage 3 Testing - Unbraced Frame:

The testing of the unbraced *prototype* used the NS component of the 1940 El Centro earthquake record with a peak acceleration of 350 gals (35.6%g) as the input signal. The results of this test and the associated free vibration tests are presented in Reference 28.

2.4 Prototype Design Review - UBC 1985

2.4.1 General

The concentrically and eccentrically braced *prototypes* would be classified by the UBC as dual systems consisting of ductile moment-resisting space frames and braced frames. The UBC stipulates the following design criteria for dual systems:

- The moment-resisting space frames and braced frames shall resist the design lateral force in accordance with their relative rigidities.

- The ductile moment-resisting space frames shall resist not less than 25% of the design lateral force.

- The braced frame acting independently of the ductile moment-resisting space frame shall resist the design lateral forces.

If these three criteria are satisfied, the UBC assigns a horizontal force factor (K) of 0.8 to the structure; structures designed using such a factor must incorporate ductile moment-resisting space frames. Furthermore, in regions of high seismic risk (Seismic Zones 3, 4 and part of

Zone 2), all members in the braced frames must be designed for 125% of the design lateral force (Section 2312 (j) 1G). The factor of 1.25 is intended to compensate for the limited ductility in axially loaded compression members and relates primarily to concentrically braced frames.

2.4.2 Design Loading

The analysis of the *prototype* was based on gravity (dead and live) loads and earthquake loads. Wind loads are negligible with respect to earthquake loads in Seismic Zone 4 and were ignored in the analyses.

Gravity Loading: The dead and live loads listed in Table 2.1 were used as the gravity loads for the analysis and design of the *prototype*. The weight of the external wall was included as a design dead load but not as a reactive weight for the reasons cited in Section 2.2. Live load reductions as and when permitted by the UBC were considered in formulating the gravity loads.

Earthquake Loading: In accordance with UBC Clause 2312, the equivalent lateral force procedure was used to calculate the design lateral loads. The UBC design base shear (V_b) at the working stress level is determined as follows:

$$V_b = C_s W = Z \, I \, K \, C \, S \, W \qquad (2.1)$$

where Z, I, K, C, S and W, respectively, are the coefficients that depend on the seismic zone, building importance, type of building frame, period of the building, soil properties and the reactive weight of the building (=1356 kips). The following values, consistent with the original design [20], were used to calculate the design lateral loads:

$Z = 1.0$ for a building in Seismic Zone 4

$I = 1.0$ for nonessential buildings

$K = 0.8$ for a dual braced system

$S = 1.5$ for site conditions not evaluated

$$T = \frac{0.05h_n}{\sqrt{D}} = 0.05\frac{70.5'}{\sqrt{49.2'}} = 0.50 \text{ second}$$

$$C = \frac{1.0}{15\sqrt{T}} = 0.094.$$

The design base shear given by Equation 2.1 is

$$V_b = 0.113 \; W = 0.113 \times 1356 = 153.4 \text{ kips.} \tag{2.2}$$

The lateral force distribution corresponding to Equation 2.2 and Clause 2312 of the UBC is given by the following equation:

$$F_x = V_b \frac{W_x h_x}{\sum\limits_{i=1}^{n} W_i h_i} \tag{2.3}$$

where F_x, W_x, W_i, h_x and h_i are the lateral force at level 'x', the reactive weights at levels 'x' and 'i', respectively, and the heights above the base to levels 'x' and 'i', respectively. The resulting lateral force distribution is presented in Table 2.4. Torsional moments, equivalent to the story shear acting at an eccentricity of 5% of the maximum building dimension, were included in the analyses.

2.4.3 Discussion of the UBC Analyses

The following loading combinations were considered:

(i)   1.0 DL + 1.0 LL   (Dual System)

(ii) 1.0 DL + 1.0 LL ± 1.0 EQ   (Dual System)

(iii) 1.0 DL + 1.0 LL ± 1.25 EQ   (Braced Frame Alone)

(iv) 1.0 DL + 1.0 LL ± 0.25 EQ   (DMRSF Alone)

The three dimensional analyses of the *prototypes* were performed using the substructuring option in the SAP-80 [29] computer program.

Concentrically Braced Dual System:

The critical load case for the concentrically braced frame was (1.0 DL + 1.0 LL ± 1.25EQ) and for the ductile moment-resisting space frame, the critical load case was (1.0 DL + 1.0 LL ± 0.25 EQ).

The stress ratios in the columns, beams and bracing elements in the braced frame were satisfactory provided that the beams outside the braces were assumed to be restrained over their entire lengths and that an effective length factor equal to 0.7 was chosen for the concentric braces. The horizontal components of the brace forces were included as axial forces in the beams framing into the concentric brace-to-beam connection. The stress ratios in the column and beam elements of the ductile moment-resisting space frame were also less than unity. The peak lateral displacements and inter-story drift ratios are shown in Table 2.5. The inter-story drift indices were calculated by multiplying the inter-story drifts, resulting from the application of the design lateral forces, by a factor equal to 1.0/K, in accordance with UBC Clause 2312. All of the inter-story drift indices were significantly less than the specified limit of 0.5%.

Eccentrically Braced Dual System:

The critical load case for the eccentrically braced frame was (1.0 DL + 1.0 LL ± 1.25EQ) and for the ductile moment-resisting space frame, the critical load case was (1.0 DL + 1.0 LL ± 0.25 EQ).

The stress ratios in the columns, beams, bracing elements and shear links in the braced frame were satisfactory provided that the beams framing into either side of the links were assumed to be fully restrained against lateral-torsional buckling. The horizontal components of the eccentric brace forces were included as axial forces in the beams framing into the shear links.

The stress ratios in the column and beam elements of the ductile moment-resisting space frame were less than unity. The peak lateral displacements and inter-story drift ratios are shown in Table 2.5; the inter-story drift indices were calculated by multiplying the inter-story drifts, resulting from the application of the design lateral forces, by a factor equal to 1.0/K, in

accordance with UBC Clause 2312. All of the inter-story drift indices were significantly less than the specified limit of 0.5%.

2.5 Prototype Design Review - ATC 3-06 1984

2.5.1 General

The *prototype* would be classified by ATC 3-06 as a dual system and to be consistent with Section 2.4, it was assigned to Seismic Performance Category C. ATC 3-06 lists the following design criteria for a dual system:

- The special moment frames and the braced frames shall resist the total seismic force in proportion to their relative rigidities.

- The special moment frames shall be capable of resisting at least 25% of the prescribed seismic force.

The ATC regulations, in a manner similar to the UBC, does not differentiate between concentrically and eccentrically braced frames; the dual braced system is assigned a response modification factor (R) equal to six. This factor is used to reduce the ATC 3-06 linear elastic design response spectra (LEDRS) to an inelastic derived response spectra (IDRS).

2.5.2 Design Loading

The ATC analysis was based upon the gravity loads noted in Section 2.4.2 and the earthquake loads presented below.

Earthquake Loading: The ATC lateral force procedure was used to calculate the design lateral loads; the *prototype* would be classified as a *regular* building in both plan and elevation. The ATC seismic base shear (V_b) at the level of first significant yielding is determined as follows:

$$V_b = C_s W \tag{2.4}$$

where C_s and W are the seismic design coefficient and the reactive weight (=1356 kips), respectively. The seismic design coefficient is calculated as follows:

$$C_s = \frac{1.2A_v S}{RT^{2/3}}$$ (2.5)

where A_v, S, R and T, respectively, are coefficients depending upon the seismic zone, soil properties, the type of structure and the period of the building. To be consistent with the UBC analysis, the following values of the ATC parameters were chosen:

$$A_a = A_v = 0.4$$

$$S = 1.5 \text{ for site conditions not evaluated}$$

$$R = 6.0 \text{ is the response modification factor for dual systems}$$

$$T = \frac{0.05h_n}{\sqrt{L}} = 0.05\frac{70.5'}{\sqrt{49.2'}} = 0.50 \text{ second.}$$

On the basis of Equations 2.4 and 2.5, the seismic design coefficient is equal to 0.190. However, ATC 3-06 states that for Soil Type 3 (S=1.5) and $A_a \geq 0.3$ the value of C_s can be calculated as follows:

$$C_s = \frac{2.0A_a}{R} = 0.133$$ (2.6)

and the resulting design seismic base shear at the level of first significant yielding is

$$V_b = 0.133 \times W = 0.133 \times 1356 = 180.7 \text{ kips.}$$ (2.7)

The lateral seismic shear force distribution corresponding to Equation 2.7 and Section 4.3 of ATC 3-06 is determined as follows:

$$F_x = C_{vx}V_b$$ (2.8)

$$C_{vx} = \frac{W_x(h_x)^k}{\sum\limits_{i=1}^{n} W_i h_i}$$ (2.9)

where k (=1 in this instance) is a factor relating to the period of the building and the remaining terms are defined in Section 2.4.2. The resulting lateral force profile is presented in Table 2.6. Torsional moments, equivalent to the story shear acting at an eccentricity of 5% of the building dimension, perpendicular to the loading direction, were included in the analyses.

2.5.3 Discussion of the ATC Analyses

The following loading combinations were considered:

(i) $1.2Q_D + 1.0Q_L \pm 1.0Q_E$ (Dual System)

(ii) $0.8Q_D \pm 1.0Q_E$ (Dual System)

(iii) $1.2Q_D + 1.0Q_L \pm 0.25Q_E$ (SMRSF Alone)

(iv) $0.8Q_D \pm 0.25Q_E$ (SMRSF Alone)

The influence of non-orthogonal loading was included in the analyses using the simplified approach noted in ATC Section 3.7.2, that is, 100% of the seismic forces in one direction and 30% of the seismic forces in the perpendicular direction were assumed to act concurrently.

Concentrically Braced Dual System:

The critical load case for the CBDS was $(1.2\ Q_D + 1.0\ Q_L \pm 1.0\ Q_E)$ and the critical load case for the special moment resisting space frame (SMRSF) was $(1.2\ Q_D + 1.0\ Q_L \pm 0.25\ Q_E)$. The stress ratios in all the structural elements in both the braced and unbraced frames were less than unity. The inclusion of the bi-directional ground motion had only a minor influence on the computed stress levels. The peak lateral displacements and inter-story drift ratios are shown in Table 2.7. The design story drifts were calculated using the calculated elastic drifts multiplied by the deflection amplification factor ($C_d = 5.0$ for a dual system) given in Table 3-B of ATC 3-06. As an office building, the *prototype* would be classified into Seismic Hazard Exposure Group 2; the calculated inter-story drift indices were significantly less than the limiting value of 1.5%.

Eccentrically Braced Dual System:

The critical load case for the EBDS was $(1.2\ Q_D + 1.0\ Q_L \pm 1.0\ Q_E)$ and the critical load case for the special moment frames was $(1.2\ Q_D + 1.0\ Q_L \pm 0.25\ Q_E)$. The stress ratios in all the structural elements in both the braced and unbraced frames were less than unity. The inclusion of the bi-directional ground motion had only a minor influence on the computed stress levels. The peak lateral displacements and inter-story drift ratios are shown in Table 2.7. The design story drifts were calculated using the calculated elastic drifts multiplied by the deflection amplification factor ($C_d = 5.0$ for a dual system) given in Table 3-B of ATC 3-06. As an office building, the *prototype* would be included in Seismic Hazard Exposure Group 2; the calculated inter-story drift indices were significantly less than the limiting value of 1.5%.

2.6 Prototype Design Review - SEAOC 1986

2.6.1 General

In accordance with the SEAOC recommendations, the design of a dual braced system must satisfy the following requirements:

- The moment-resisting space frames and the braced frame shall resist the lateral loads in proportion to their relative rigidities.

- The specially detailed moment-resisting space frames shall be capable of resisting at least 25% of the base shear.

The SEAOC recommendations differentiates between concentrically and eccentrically braced dual systems by assigning different coefficients and design regulations to the two framing systems. To obtain an inelastic derived response spectrum, SEAOC reduces its smoothed linear elastic design response spectrum by a factor denoted as R_w. This factor serves a similar function to the response modification factor (R) used in ATC 3-06. The factor R_w equals 10 and 12, respectively, for concentrically braced and eccentrically braced dual systems incorporating special moment resisting space frames (SMRSFs).

2.6.2 Design Loading

The SEAOC analysis was based upon the gravity loads noted in Section 2.4.2 and the earthquake loads presented below.

Earthquake Loading: A static force procedure was used to calculate the design lateral loads. The SEAOC design base shear at the working stress level is determined using the following formula:

$$V_b = \frac{ZIC}{R_w} W = C_s W \tag{2.10}$$

where Z, I, C and R_w, respectively, are coefficients depending on the seismic zone, the building occupancy, the soil type, the building period and the type of building frame.

Concentrically Braced Dual System:

To be consistent with the UBC analysis, the following values of these parameters were chosen:

$$Z = 0.4 \quad \text{for Seismic Zone 4}$$

$$I = 1.0 \quad \text{for a nonessential structure}$$

$$R_w = 10 \quad \text{for a concentrically braced dual system}$$

$$S = 1.5 \quad \text{for site conditions not evaluated}$$

$$T = C_t(h_n)^{3/4} = 0.020(70.5')^{3/4} = 0.5 \text{ second}$$

$$C = \frac{1.25S}{T^{2/3}} = 3.03.$$

For a structure in Seismic Zone 4 founded on Soil Type S_3, C_{max} can be taken as 2.25. On the basis of Equation 2.10, the design base shear (V_b) is

$$V_b = 0.090 \ W = 0.090 \times 1356 = 122.0 \text{ kips.} \tag{2.11}$$

The lateral force distribution corresponding to Equation 2.11 and Section 1E4 is determined through the use of an equation similar to that used by the UBC (Equation 2.3). The SEAOC

lateral force distribution on the CBDS is shown in Table 2.8.

Eccentrically Braced Dual System:

To be consistent with the UBC analysis, the following values of these parameters were chosen:

$$Z = 0.4 \quad \text{for Seismic Zone 4}$$

$$I = 1.0 \quad \text{for a nonessential structure}$$

$$R_w = 12 \quad \text{for an eccentrically braced dual system}$$

$$S = 1.5 \quad \text{for site conditions not evaluated}$$

$$T = C_t(h_n)^{3/4} = 0.030(70.5')^{3/4} = 0.7 \text{ second}$$

$$C = \frac{1.25S}{T^{2/3}} = 2.38.$$

For a structure in Seismic Zone 4 founded on Soil Type S_3, C_{max} can be taken as 2.25. On the basis of Equation 2.10, the design base shear (V_b) is

$$V_b = 0.075 \ W = 0.075 \times 1356 = 101.8 \text{ kips.} \tag{2.12}$$

The lateral force distribution corresponding to Equation 2.12 and Section 1E4 is determined through the use of an equation similar to that used by the UBC (Equation 2.3). The SEAOC lateral force distribution on the EBDS is shown in Table 2.8.

Torsional moments, equivalent to the story shear acting at an eccentricity of 5% of the building dimension, perpendicular to the loading direction, were included in the analyses.

2.6.3 Discussion of the SEAOC Analyses

The following loading combinations were considered:

(i) $\quad 1.0P_{DL} + 1.0P_{LL} \pm 1.0P_{EQ} \qquad$ (Dual System)

(ii) $\quad 1.0P_{DL} + 1.0P_{LL} \pm 0.25P_{EQ} \qquad$ (DMRSF Alone)

The influence of non-orthogonal loading was included in the analyses using the simplified approach noted in SEAOC Section 1H(c)2 and outlined in Section 2.5.3.

Concentrically Braced Dual System:

The critical load case for the concentrically braced dual system was $(1.0 \ P_{DL} + 1.0 \ P_{LL} \pm 1.0 \ P_{EQ})$ and the critical load case for the special moment resisting space frames was $(1.0 \ P_{DL} + 1.0 \ P_{LL} \pm 0.25 \ P_{EQ})$. The stress ratios in all of the structural elements in both the braced and unbraced frames were significantly smaller than unity.

In an attempt to guard against collapse in the event of severe earthquake shaking, SEAOC requires that the columns be capable of resisting earthquake forces that are assumed to be $3 \ R_w/8$ times higher than the design earthquake forces. The column compressive stresses did not exceed $1.7 \ F_a$ under the application of $(1.0 \ P_{DL} + 1.0 \ P_{LL} \pm 3.75 P_{EQ})$, or F_y under the application of $(1.0 \ P_{DL} \pm 3.75 \ P_{EQ})$, where $3.75 = 3 \ R_w/8$.

The lateral displacements and inter-story drift ratios are shown in Table 2.9; all of the inter-story drift ratios were substantially less than the code specified limit of $0.03/R_w$ (=0.0030) or 0.30%. The SEAOC requirements in Section 4G1 for bracing members and Section 4G3 for chevron bracing (that is, that the chevron braces be designed for 1.5 times the prescribed seismic forces) were satisfied by the *prototype's* concentric bracing.

Eccentrically Braced Dual Steel System:

The critical load case for the eccentrically braced dual system was $(1.0 \ P_{DL} + 1.0 \ P_{LL} \pm 1.0 \ P_{EQ})$ and the critical load case for the special moment resisting space frames was $(1.0 \ P_{DL} + 1.0 \ P_{LL} \pm 0.25 \ P_{EQ})$. The stress ratios in all structural elements in both the braced and unbraced frames were significantly smaller than unity. Similarly, the column compressive stresses did not exceed $1.7 \ F_a$ under the application of $(1.0 \ P_{DL} + 1.0 \ P_{LL} \pm 4.5 \ P_{EQ})$, or F_y under the application of $(1.0 \ P_{DL} \pm 4.5 \ P_{EQ})$, where $4.5 = 3 \ R_w/8$. The lateral displacements and inter-story drift ratios are shown in Table 2.9; all of the inter-story drift ratios were substantially less than the code specified limit of $0.03/R_w$ (=0.0025) or 0.25%. Section 4H of the

SEAOC guidelines deals with the design and proportioning of eccentrically braced frames; these clauses and the manner in which they relate to the *prototype* are discussed in Reference 1. The eccentrically braced frame in the *prototype* dual system satisfied all the requirements of SEAOC Section 4H [1].

2.7 Review of the 1985 UBC, 1984 ATC and 1986 SEAOC

The *prototype* design base shear coefficients for the 1985 UBC, 1984 ATC 3-06 and 1986 SEAOC recommendations are listed in Table 2.10 for both the CBDS and EBDS.

The UBC requires that the braced frames resist 125% of the design base shear (Section 2.4.1) and that the DMRSF resist 25% of the design base shear. The design base shear is evaluated at the working stress level and the design and proportioning of the members is based on the working stress, or allowable stress, method.

ATC 3-06 requires that the braced frames resist that percentage of the design base shear that is distributed to them in accordance with their relative rigidities and that the DMRSF resist 25% of the design base shear. Elastic analysis of the dual systems distributed approximately 80% of the lateral forces to the braced frames; accordingly, 80% of the design base shear was assigned to the braced frame in Table 2.10. The ATC design base shear is evaluated at a level of first significant yielding and and the design and proportioning of the members are based on a strength method.

The 1986 SEAOC requires that: (1) the braced frames in a CBDS resist 150% of the prescribed seismic forces ($\approx 0.8\times150\% = 120\%$ of the design base shear force); and (2) the braced frames in an EBDS resist that percentage of the design base shear that is distributed to them in accordance with their relative rigidities ($\approx 80\%$ in this instance - see above). The design base shear is evaluated at the working stress level and the design and proportioning of the members are based on the working stress, or allowable stress, method.

The UBC and SEAOC coefficients are extrapolated to yielding levels in Table 2.10 by including a one-third increase in the allowable stresses for earthquake loading, that is, by

assuming an average working stress of $0.8 \times F_y$, that is, $0.6F_y \times 1.33$. For comparison purposes, the base shear coefficients listed in Table 2.10 were derived assuming deformation compatibility between the braced and unbraced frames, that is, by directly summing the strengths of the braced and unbraced frames. This assumption is non-conservative because: the stiffnesses of the braced frames (CBF and EBF) were significantly greater than that of the DMRSF, and the interaction forces that are developed between the braced and unbraced frames in a dual system will reduce the total strength available in the dual system to resist the earthquake loading [13].

For the CBDS, the UBC coefficient exceeds that of the ATC by 52% and that of SEAOC by 29%. For the eccentrically braced frame, the UBC coefficient exceeds that of the ATC by 52% and that of SEAOC by 111%.

Since the *prototype* dual systems were designed for a base shear coefficient of 0.197, the *prototype* dual systems cannot be considered as representative of CBDSs and EBDSs designed in accordance with either the UBC, ATC or SEAOC.

2.7.2 Elastic and Inelastic Drift Levels

The limiting elastic inter-story drift indices for the UBC, ATC and SEAOC are listed below. The UBC and SEAOC inter-story drift indices have been extrapolated to a level of first significant yield by assuming a maximum working stress equal $0.8F_y$ (see above), that is, by multiplying the UBC and SEAOC working stress inter-story drift index limits by 1.25 (=1/0.8).

UBC : $= 0.0050 \times K \times 1.25 = 0.0050$ for CBDSs and EBDSs

ATC : $= 0.0030$ for CBDSs and EBDSs

SEAOC : $= \dfrac{0.03}{R_w} \times 1.25 = 0.0038$ for CBDSs

$= 0.0031$ for EBDSs

On the basis of the base shear coefficients and inter-story drift indices presented above, the story stiffnesses required by the UBC and SEAOC for the CBDS and EBDS are significantly less than that required by the ATC.

The maximum inelastic inter-story drift indices implicitly or explicitly specified by the UBC, ATC and SEAOC, are as follows:

$$\text{UBC}: \ = \frac{3}{K} \times 0.005 \times K = 0.0150 \ \text{ for CBDSs and EBDSs}$$

$$\text{ATC}: \ = 0.0150 \ \text{ for CBDSs and EBDSs}$$

$$\text{SEAOC}: \ = \frac{0.03}{R_w} \times \frac{3R_w}{8} = 0.0112 \ \text{ for CBDSs and EBDSs}.$$

Note that SEAOC specifies different inter-story drift index limits for the CBDS and EBDS at the serviceability level. This is a questionable approach because in this limit state, damage is precluded and the restrictions on the maximum inter-story drift index should relate to occupant discomfort and the preclusion of damage to the non-structural elements. SEAOC specifies identical limits on the inelastic inter-story drift index for both the CBDS and the EBDS. This is also highly questionable unless non-structural damage controls the maximum acceptable inter-story drifts. If this is not the case, the larger ductility supplied by the EBDS with respect to the CBDS should be accounted for by less stringent drift requirements for the EBDS.

2.7.3 Comparison of Code Design Base Shear Spectra

Concentrically Braced Dual System:

The 1985 UBC, 1984 ATC and 1986 SEAOC design base shear spectra (C_s in Equations 2.1, 2.4 and 2.10) are presented in Figure 2.4 for CBDSs sited on rock or firm ground (Figure 2.4a) and soft soil (Figure 2.4b). The soft soil site was categorized as Type 3 in accordance with all three seismic regulations. In Figure 2.4, the UBC and SEAOC design base shear forces have been extrapolated to a level of first significant yielding in the manner described above. On the rock site for periods less than 0.3 second, the ATC design base shear forces are significantly greater than either the UBC or SEAOC (47% and 21%, respectively) whereas on the soft soil site, both the UBC and ATC design base shear forces are significantly greater than those of SEAOC (24% and 15%, respectively) for periods less than 0.75 second.

Eccentrically Braced Dual System:

The 1985 UBC, 1984 ATC and 1986 SEAOC design base shear spectra (C_s in Equations 2.1, 2.4 and 2.10) are presented in Figure 2.4 for EBDSs sited on rock or firm ground (Figure 2.4a) and soft soil (Figure 2.4b). The soft soil site was categorized as Type 3 in accordance with all three seismic regulations. On the rock site for periods less than 0.3 second, the ATC design base shear forces are significantly greater than either the UBC or SEAOC (5% and 47%, respectively), whereas on the soft soil site, both the UBC and ATC design base shear forces are significantly greater than those of SEAOC (38% and 48%, respectively) for periods less than 0.75 second.

Although the ATC and SEAOC linear elastic design response spectra are similar for both rock and soft soil sites, there is a significant difference between their respective response modification factors for CBDSs and EBDSs. The ATC response modification factors for CBDSs and EBDSs are both equal to six. SEAOC's response modification factors for CBDSs and EBDSs, are 8.0 (=10/1.25) and 9.6 (=12/1.25), respectively, if the SEAOC design base shear spectra are scaled to a level of first significant yielding.

2.7.4 Discussion of Code Guidelines

The ATC's use of a *strength* method to design and proportion structural systems assumed to undergo significant inelastic deformation is conceptually far superior to the working stress design methods used by the UBC and SEAOC. The use of strength methods in conjunction with realistic elastic and inelastic design response spectra is a cornerstone of a rational approach to the earthquake resistant design of buildings.

The requirement in the 1985 UBC that the braced frame resist 125% of the design base shear significantly increases the *effective* UBC base shear coefficient - this increase is clearly evident in Table 2.10. A dual system designed strictly in accordance with 1984 ATC 3-06 or the 1986 SEAOC minimum strength requirements will have a significantly lower strength than if it was designed to just satisfy the minimum strength requirements of the 1985 UBC. Clearly, the reduction in the minimum strength requirements of the seismic regulations in the

United States will increase the vulnerability of dual systems sited in regions of high seismic risk. On the basis of results presented by Whittaker et al. [1] and Uang and Bertero [2], these reductions cannot be justified for dual steel systems.

SEAOC acknowledges the superior performance of the eccentrically braced frame over the concentrically brace frame by increasing the value of R_w from 10 (CBDS) to 12 (EBDS) and by requiring that the concentric bracing resist 150% of the prescribed seismic forces. The EBF design guidelines (Section 4H) reflect the results of the recent research in this field and offer a simple, yet effective means by which to design eccentrically braced frames.

CHAPTER 3

MODEL DUAL SYSTEMS

3.1 General

In this chapter, the selection, design, construction and instrumentation of the CBDS and EBDS *models* are discussed. In Section 3.2, the Earthquake Simulator test facilities at the University of California at Berkeley are briefly discussed. The rationale for selecting the *models'* scaling factors and a summary of the *models'* fabrication and construction are presented in Section 3.3. The instrumentation of the *models* dual systems is discussed in Section 3.4 and a brief introduction to the data acquisition process is given in Section 3.5.

3.2 Earthquake Simulator Test Facilities

The CBDS and EBDS *models* were tested on the earthquake simulator in the Earthquake Simulator Laboratory (ESL) of the University of California at Berkeley.

The main feature of the ESL is a 20 ft by 20 ft earthquake simulator table. The table is 12 inches thick, heavily reinforced and post-tensioned; it weighs approximately 45 tons (100 kips). During testing, a pit beneath the table is pressurized to counterbalance the weight of the table and the model. A 12 inch gap between the table and the foundation wall is sealed by a 24 inch wide strip of reinforced nylon fabric. The maximum allowable air pressure on the nylon fabric is 4 psi and as a result, the maximum weight on the earthquake simulator table is limited to 130 kips. The table and model are supported by screw-jacks beneath the table when the pit is not pressurized.

The earthquake simulator is driven by seven actuators, four 25 kip vertical actuators and three 50 kip horizontal actuators. The vertical actuators do not support gravity loads during testing. A passive stabilizing system is present (with further assistance from the vertical actuators which act as active stabilizers) to control the pitching motion of the earthquake simulator

table generated by the model's overturning moments. The nominal overturning capacity of the earthquake simulator is approximately 1700 ft-kips. A detailed discussion of the earthquake simulator characteristics is given by Rea and Penzien [31]. Figure 3.1 depicts the earthquake simulator in plan and elevation and details the limitations on its dynamic performance [31]. The types of signals that can be input to the earthquake simulator include:

- Periodic Motion - the input waveform is selected from those available in the function generator and passed to an *MTS* controller which generates the table displacement command signal.

- Random Motion - white noise, filtered white noise, shot noise and other stochastic records, in the form of digitized displacement time histories, are passed through a *Preston* D/A converter, which converts the digitized signal to an analog signal. The analog signal is then passed to an *MTS* controller which generates the table displacement command signal.

- Earthquake Ground Motion - an earthquake acceleration record is selected from a library of records and then integrated in either the time domain or the frequency domain to produce a digitized displacement time history. The digitized displacement time history is then passed through a *Preston* D/A converter, which converts the digitized signal to an analog signal. The analog signal is then passed to an *MTS* controller which generates the table displacement command signal.

3.3 Design of the CBDS and EBDS Models

3.3.1 General

A primary objective of the Berkeley studies was to design, construct and test the largest possible steel models of the CBDS and EBDS *prototypes* that could be accommodated on the earthquake simulator [1,2].

The *models* were designed to comply with the similitude requirements for a reduced scale model of the *prototype* shown in Figure 2.1. The most suitable model was determined to be an

artificial mass simulation model [2] which satisfied similitude requirements for geometry and loading parameters. Furthermore, this model complied with all material requirements except mass density. To satisfy the latter requirement, lead ballast was attached to the roof and floor slabs in such a manner that it did not affect the stiffness of the *models* [2].

As noted in the previous section, the maximum payload of the earthquake simulator is approximately 130 kips. Assuming that the *models'* foundation and reference frame weighed approximately 15 kips, the maximum possible weight of the *models* was of the order of 115 kips. As the weight of the *prototype* was 1154 kips, the maximum length factor that could be used was $\sqrt{115/1154}=0.316$. A length scale factor of 0.3048 (hereafter denoted as 0.3) was adopted for the *models*. The scale factor of 0.3 satisfied the weight, height and plan limitations of the earthquake simulator. The weights of the *prototypes'* floor and roof slabs, the similitude scaled weights and the weights of the *models'* floor and roof slabs are presented in Table 3.1.

Details regarding the fabrication of the *models* are presented in References 1 and 2, and are not restated herein.

3.3.2 Mechanical Characteristics of the CBDS and EBDS Models

Girders, Columns and Transverse X-Bracing:

Grade 50 X10 steel provided the best match (to a uniaxial strain level of 12%) for the mechanical characteristics of the steel used in the *prototypes*. Thus, this steel was used to fabricate the *models'* W sections. Grade 50 X10 steel was unavailable in #14 gage (0.0747 inches) and Grade 50 Cor10 steel was used for this plate thickness. The stress-strain curves for these two steels are presented in Figure 3.2. The X-bracing in Frames 1 and 3 were double angle sections rolled from ASTM A500 Grade B steel (Figure 3.2).

CBDS Bracing Elements:

The bracing elements in Frame B were fabricated from Grade 50 Cor10 steel with a yield stress of 55 ksi and an ultimate stress of 74 ksi [2]. The concentric braces were fabricated from two strips of Cor10 plate, each bent to form angle sections and consequently welded to

form the required square hollow sections.

EBDS Bracing Elements:

The bracing elements in Frame B were standard cold formed rectangular hollow sections produced from ASTM A500 Grade B Steel (Figure 3.2).

Composite Floor System:

The composite floor system was constructed from steel metal decking, shear studs and lightweight concrete. A detailed description of the composite floor system is given in References 1 and 2. The *models'* steel decking was 0.018 inch thick metal sheeting, fabricated from ASTM A446 Grade A steel; the steel decking was sandblasted to remove its galvanized coating. The profile of the metal decking is shown in Figure 3.3. The spacing of the shear studs satisfied the AISC requirements for full composite action between the steel W sections and the lightweight concrete slab. A graded lightweight coarse aggregate (maximum size of 0.25 inch) and normal weight sands were used for the concrete mix [1,2]. The nominal 28 day strength was 4.0 ksi, close to the target strength of 4.17 ksi. At the time of testing the EBDS *model*, the compressive strength and modulus of elasticity of its concrete, measured using 3 inch by 6 inch cylinders, were 5.2 and 2,775 ksi, respectively. The strength and stiffness of the *models'* concrete were approximately 20% greater than that of the *prototype*. The wire mesh reinforcement was 0.0625 inch in diameter on a 1 inch pitch. Its yield stress and ultimate tensile stress were 79 and 85 ksi, respectively.

3.4 Instrumentation of the CBDS and EBDS Models

The instrumentation was designed to record global structural response and local element response, especially at certain critical regions. One hundred and seventy-six channels of data were collected for each test; the instrumentation incorporated accelerometers, linear potentiometers (LPs), direct current linear voltage displacement transducers (DCDTs), strain gages, strain rosettes and clip gages.

Linear potentiometers and DCDTs were used to monitor the global displacement response of the *models*. These instruments were attached to either a lightweight trussed steel portal frame that straddled the *models* in the transverse direction or, an instrumentation frame located off the earthquake simulator table parallel to Grid Line 3. Both instrumentation frames were very stiff and had very small periods of vibration.

Earthquake Simulator Table Response:

Ten channels of data recorded the motion of the earthquake simulator table during each test. These channels recorded the following information (refer to Figures 2.1 and 2.2 for the reference system):

(i)   Channels 1-2 : Linear variable displacement transducers (LVDTs) mounted in the earthquake simulators horizontal actuators measured the displacement time history at two locations (x-direction).

(ii) Channel 3   : The average of two accelerometers mounted beneath the table was used to measure its horizontal acceleration time history (x-direction).

(iii) Channel 4   : The average of four accelerometers mounted beneath the table was used to measure its vertical acceleration time history (z-direction).

(iv) Channels 5-7 : The pitch (x-z plane), roll (y-z plane) and twist (x-y plane) acceleration time histories (rad/sec^2) of the table were measured using the response of the four vertical and two horizontal accelerometers mounted beneath the table.

(v)   Channels 8-10 : The vertical displacement time history of the table was measured using LVDTs mounted in the table's vertical actuators (z-direction).

Global Response of the Models:

The parameters used to quantify the global structural response include lateral displacements, inter-story drifts, accelerations, story shear forces and the overturning moments at each floor level. The following instrumentation was used to evaluate these time history responses:

(i)   At each floor level on Frames A and B, total horizontal displacements and accelerations were measured using DCDTs, LPs and accelerometers.

(ii)   The relative vertical displacements of the *models* were measured at their roof levels using a trussed reference frame mounted on the *models'* foundation. A total of six transducers (DCDTs) was used to measure the vertical displacement of the *models*.

(iii)   The relative transverse (parallel to Grid Line 1) displacements of the *models* were measured at the roof level by two transducers (DCDTs) attached to the transverse reference frame.

Local Response of the Models:

The instrumentation used to capture the local element response quantities in both the CBDS and EBDS *models* is described below. Additional details and a list of the transducers used to acquire data for the testing of both the CBDS and EBDS are presented in References 1 and 2. The structural steel in both the CBDS and EBDS was coated with a whitewash paint that distorted and peeled upon yielding of the steel, thereby identifying yielded sections of the *models*.

Braces: Concentrically Braced Dual System [2]:

Brace Force: In the lower four stories, four strain gages were installed at the upper quarter point of each of the braces. This permitted the axial force and biaxial bending moments to be calculated from the known brace material properties. In the upper two stories, only two strain gages were installed per brace due to the limited number of data acquisition channels.

Brace Axial Deformation: Transducers (DCDTs) were installed in the lower four stories to measure the total axial deformation of the braces.

Braces: Eccentrically Braced Dual System [1]:

Brace Force: In the lower three stories, four strain gages were installed at the quarter point of each brace adjacent to its upper end and combined into two data channels per brace. Because of the limited number of data acquisition channels, two strain gages were installed at the

quarter points of each brace in the remaining three stories. For all twelve braces, the strain gages were calibrated to measure axial force prior to their installation in the EBDS *model*.

Brace Axial Deformation: Transducers (DCDTs) were installed in the lower two stories of the EBDS *model* to measure the axial deformation of the braces.

Columns:

Column Shear: The columns were instrumented to determine the story shear distribution in the *models*. One strain rosette was applied to each side of the column web (for the web parallel to Frame B) or to the column flange (for the flange parallel to Frame B) at the column mid-height; the output from these two rosettes was combined into a single channel to increase the resolution of the channel data [1,2]. All nine columns in the first story were instrumented; in the upper five stories, the columns in Frames A and B were instrumented and the shear forces in the columns in Frame C were assumed to be identical to those in the corresponding columns in Frame A.

Column Axial Force and Bending Moment: Two strain gages (combined into one channel) per column flange were installed $17\frac{1}{8}$ inches below the underside of the L2 floor beams in all nine columns to calculate the axial force and bending moments in the first story columns. The columns' axial forces and bending moments were estimated in the manner described in Section 5.4.

Column Axial Deformation: Transducers (DCDTs) were installed adjacent to the Frame B columns in the lower two stories to record column axial deformations permitting evaluation of its influence on inter-story drift.

Column Base Rotation [2]: The base of the first story columns in Frame B were instrumented with DCDTs to measure the column end rotations.

Shear Links: Eccentrically Braced Dual System [1]:

Shear Strain: In the lower three shear links, four transducers (DCDTs) at each level were used to measure the shear strains (Figure 3.4); the shear strains in the two half-panels were averaged

in order to obtain the average shear strain in the link. In the upper three stories, two transducers (DCDTs) at each level were used to measure the shear strains. These transducers captured both flexural and shear deformation. However, for shear links, the flexural deformations are generally insignificant. For example, for the shear link at Level L2 with equal end moments of opposite sign (double curvature) and applied shear forces up to 170% of the link's nominal plastic shear capacity, the flexural contribution to the total deformation of the link was less than 2% [1]. The diagonal DCDT displacements were therefore assumed to be kinematically related to shearing strains alone. The measured displacements were transformed into shear strains in a manner similar to that described by Roeder [21].

Axial Strain and Deformation: In order to estimate the axial forces and bending moments in the shear links, the lower three links were instrumented with strain gages that were installed on the links' flanges (Figure 3.4a). DCDTs were installed at the underside of the links' flanges and at the centroid of the links' webs to measure the axial deformations of the links.

3.5 Data Acquisition

The earthquake simulator's data acquisition system functions in the following manner. The transducers (load cells, strain gages, DCDTs, accelerometers etc) are powered by *Pacific* signal conditioners which provide the excitation voltage for the transducers, amplify the transducer output and then lowpass filter the output with a cut-off frequency of 100 Hz. The *Preston* multiplexer scans the signal conditioners and sequentially reads each channel at a burst rate of 500kHz, that is, for two adjacent channels (#100 and #101 for example), the true read time difference is two microseconds. The scanning rate, that is, the number of times per second each channel is sampled, is limited by the maximum throughput rate of the operating system ($\approx$ 50 kHz) and was set at 100 and 200 samples per second, for the Taft and Miyagi-Ken-Oki earthquake simulator tests, respectively. The analog signal from the multiplexer is then passed through a *Preston* A/D converter to convert the signal to a digital form. The digital record is then stored on hard disk on the in-house VAX 11-750.

An interactive data analysis and graphics package [32], S, was used to process the acquired data; the package was expanded to include bandpass filters, numerical intergration and differentiation, response spectra evaluation and so on.

A block diagram of the earthquake simulator control and data acquisition system is presented in Figure 3.5.

CHAPTER 4

DYNAMIC CHARACTERISTICS
OF THE MODELS

4.1 General

Uang et al. [2] discussed the characteristics of the CBDS *model* during its construction phase and the testing period. The static and dynamic characteristics of the EBDS *model* were monitored in a similar manner at various stages in its testing program [1]. The objectives of these tests were threefold; first, to assess the variation in the *models'* dynamic characteristics as a function of the level of accumulated damage; second, to correlate the performances of the *models* with each other and with the *prototypes* tested in Tsukuba, Japan, and finally, to evaluate the reliability of currently available analytical techniques to predict the dynamic characteristics and response of braced steel structures.

The correlation of the *prototypes'* responses with their respective *models'* responses is presented in References 1 and 2 and is not reproduced in this report.

The reliability of computer programs such as DRAIN-2D [33], DRAIN-2DX [34] and ANSR-1 [35] for predicting both the elastic and inelastic response of planar braced steel structures was demonstrated in References 1 and 2; interested readers should consult these references for a detailed discussion of the applicability of these computer programs.

In this chapter, the mechanical and dynamic characteristics of both the CBDS and EBDS *models* will be presented; these characteristics will be reviewed and discussed in later chapters whereupon the behavior of these two dual systems is discussed.

4.2 CBDS and EBDS System Identification

Various techniques were used to evaluate the dynamic characteristics of the *model* dual systems; these were the static flexibility method, free vibration testing, forced vibration testing

and ambient vibration testing. The first three testing methods were used for both the CBDS and EBDS; ambient vibration testing was used for the CBDS only and interested readers should consult Reference 2 for details of this testing method. The first three testing methods are briefly discussed below.

Static Flexibility Method (Unit Loading Test):

The static flexibility test was used to determine the dynamic characteristics of the *models* assuming a lumped mass system. The static flexibility test set-up is illustrated schematically in Figure 4.1. As shown in Figure 4.1, the *model* was laterally loaded at each floor level by a very stiff beam; the lateral force was applied to the loading beam by two cables that extended to the laboratory floor. The load was applied by tightening turnbuckles in both cables simultaneously while monitoring the load levels with load cells. The vertical component of the cable force and the weight of the loading beam was carried by tubular steel columns anchored to the laboratory floor. Lateral loads were sequentially applied at each level of the *model*. The measured displacements of each story at each stage of the loading process yielded the flexibility coefficients (f_{ij}) of the *model* corresponding to six lateral degrees of freedom and enabled the *model's* flexibility matrix (F) to be constructed. The *model's* flexibility matrix was inverted to obtain its stiffness matrix ($\underline{K}$).

The natural periods and mode shapes were evaluated by solving the following six degree-of-freedom eigenvalue problem:

$$\underline{K}\Phi = \underline{\Omega}\,\underline{M}\,\underline{\Phi} \tag{4.1}$$

where $\underline{K} = \underline{F}^{-1}$ = Stiffness Matrix

$\underline{M}$ = Mass Matrix

$\underline{\Phi}$ = Eigenvector or mode shape matrix

$= [\phi_1 \ \phi_2 \ \text{.......} \ \phi_6]$

$\underline{\Omega}$ = Eigenvalue matrix

$$\underline{\Omega} = \begin{bmatrix} w_1{}^2 & & & \\ & w_2{}^2 & & \\ & & \ddots & \\ & & & w_6{}^2 \end{bmatrix}$$

Equation 4.1 was transformed into a standard eigenvalue problem through the use of a diagonal, non-zero mass matrix. By premultiplying the left- and right-hand sides of (4.1) by the square root of the inverse of the mass matrix, (4.1) can be rewritten as:

$$\underline{M}^{-\frac{1}{2}} \, \underline{K} \, \underline{M}^{-\frac{1}{2}} \underline{M}^{\frac{1}{2}} \, \underline{\Phi} = \underline{M}^{-\frac{1}{2}} \, \underline{M}^{\frac{1}{2}} \underline{M}^{\frac{1}{2}} \, \underline{\Phi} \, \underline{\Omega} \tag{4.2}$$

or,

$$\overline{\underline{K}} \, \overline{\underline{\Phi}} = \overline{\underline{\Phi}} \, \underline{\Omega} \tag{4.3}$$

where,

$$\overline{\underline{K}} = \underline{M}^{-\frac{1}{2}} \, \underline{K} \, \underline{M}^{-\frac{1}{2}} \tag{4.4}$$

$$\overline{\underline{\Phi}} = \underline{M}^{\frac{1}{2}} \, \underline{\Phi} \tag{4.5}$$

Solving Equation 4.3, a symmetric eigenvalue problem, directly yields the frequencies (ω_i) of the original eigenproblem. The mode shapes of the original system (ϕ_i) are obtained by solving Equation 4.5 for $\underline{\Phi}$.

Free Vibration Tests:

Two methods were used to measure the free vibration response of the *models*:

Method 1: The *model* was given a small lateral displacement by loading it at the roof level via two cables attached to Frames A and C; turnbuckles were inserted in both cables to adjust the frame displacements. The two cables were attached to a single cable (a Y configuration) and anchored to the laboratory floor. A 3/8 inch diameter threaded rod was inserted into the cable close to the floor and loaded until the appropriate displacement was achieved at the roof level. The threaded rod was then cut and the *model's* free vibration decay was then recorded by the earthquake simulator's data acquisition system.

Method 2: A small acceleration pulse was input to the earthquake simulator; the *model's* free vibration decay was then recorded by the earthquake simulator's data acquisition system.

The dynamic characteristics of both the CBDS and EBDS *models* were evaluated from their free vibration responses obtained using both Method 1 and Method 2. The following procedure, depicted in Figure 4.2, was used to estimate the natural periods of vibration and modal damping ratios:

(i) The displacement and acceleration time histories were transformed into the frequency domain using a Fast Fourier Transform (FFT) algorithm. The dominant peaks in the Fourier amplitude spectra of the response are associated with the natural frequencies of the *model.*

(ii) Appropriate roll-on and roll-off frequencies were selected above and below the peaks in the Fourier amplitude spectra and the band-passed frequency domain response was then transformed back into the time domain using an Inverse Fast Fourier Transform (IFFT) algorithm.

(iii) The band-passed time domain response of step (ii) was then treated as the free vibration decay response of a single degree-of-freedom system (SDOFS). The natural frequency of vibration was then calculated by either the zero response crossing method or by determining the frequency associated with the peak of the FFT noted in step (i). The modal damping ratios were evaluated using the conventional logarithmic decrement approach [36].

(iv) Steps (ii) and (iii) were repeated with different roll-on and roll-off frequencies to ascertain the sensitivity of the damping ratios to the roll-on and roll-off frequencies.

The mode shapes of the EBDS *model* [1] were evaluated using the amplitude and phase angle of the peaks of the Fourier amplitude spectra noted in step (i) for the recorded response at all six floor levels.

Forced Vibration Tests:

The forced vibration response of the *model* was evaluated using a force generator mounted on its roof. The force generator was a small shaking table; it provided a constant acceleration of up to 0.6g in the frequency range of 2 to 20 Hz and it could generate a maximum force amplitude of 30 lbf with 50 lb of weight atop it [2]. The frequency of the input was varied from test to test, at and around the expected periods of vibration of the *model*. The normalized response to the input was evaluated as a function of the exciting frequency; the frequency associated with the peak normalized response and the half-power bandwidth method [36] were used to evaluate the natural frequencies and modal damping ratios, respectively.

4.3 Dynamic Characteristics of the CBDS and EBDS Models

The dynamic characteristics of the *models* were evaluated prior to the earthquake simulator testing and are presented below.

Static Flexibility Tests:

The static flexibility method described in Section 4.2 was used to evaluate the flexibility and stiffness matrices of the CBDS and EBDS *models*; these matrices are presented in Tables 4.1 and 4.2, respectively. The stiffness matrices were evaluated by inverting a symmetric flexibility matrix calculated as $f_{ij}^* = (f_{ij} + f_{ji})/2$. The mass matrix used in the eigen analysis was derived from the last column of Table 3.1. The natural periods and mode shapes of the *models* are also listed in Tables 4.1 and 4.2 and the mode shapes are shown in Figure 4.3.

Free Vibration Tests:

The natural periods and damping ratios of the *models,* evaluated from the Method 1 free vibration tests, are listed in Table 4.3. The differences between the periods and damping ratios determined from the Method 1 and Method 2 test results, are discussed in Section 6.2.

Forced Vibration Tests:

The natural periods and damping ratios of the *models* are listed in Table 4.3.

4.4 Summary

Static Flexibility Test:

The static flexibility test, the most time consuming of the three techniques used, is a semi-analytical technique that requires prior knowledge of the mass matrix to determine the mode shapes and modal frequencies of the structure being tested.

The inaccuracies inherent with the static flexibility method stem from the assumption of a diagonal mass matrix, the resolution of the LPs measuring the floor displacements and the accuracy of the load cells in the cables loading the *model*. The mode shapes and modal frequencies determined from static flexibility test results relate to the *model* in a fixed-base configuration and not in the air-supported condition in which it was tested. In addition, the flexibility test provides no information regarding the modal damping ratios. The principal advantage of the static flexibility test is that a significant number of mode shapes and modal frequencies can be obtained for no more effort than required to evaluate the first few mode shapes and modal frequencies.

Clearly, the static flexibility test method is not suitable for the system identification, that is the determination of f_{ij}, T_i and ϕ, of real buildings. However, for the system identification of the two *models*, the static flexibility test method proved to be a useful tool in confirming the modal frequencies obtained by other techniques as well as providing a means by which to verify the analytical stiffness matrices [1,2].

Free Vibration Test:

The free vibration tests, both Methods 1 and 2, were used throughout the testing program to monitor the change in the dynamic characteristics of both the CBDS and the EBDS. Method 1 was used to evaluate the dynamic characteristics (T_i, ξ_i, ϕ_i) of both *models* in a

fixed-base condition. Method 2 was used frequently during the earthquake simulator testing program (Tables 5.1 and 5.2) to monitor the change in the dynamic characteristics of the *models* in the air-supported configuration. In this testing program, both methods were only capable of measuring the dynamic characteristics of the CBDS and the EBDS in the first three modes. This resulted from the lack of resolution in the linear potentiometers recording the free vibration displacement response of the *model* and the dominance of the first mode in that response.

Forced Vibration Test:

Forced vibration testing was used prior to earthquake simulator testing to evaluate the dynamic characteristics (T_i, ξ_i) of the *models* in a fixed-base condition. This technique can be used for the identification of a building's flexibility matrix by sequentially applying cyclic loading of a constant amplitude at each assumed degree-of-freedom and measuring the building's response at the remaining degrees-of-freedom. Forced vibration testing was used to evaluate only the modal frequencies and damping ratios in this testing program.

Summary:

A series of system identification experiments was undertaken to evaluate the dynamic characteristics of the *models*. Three techniques for evaluating the dynamic characteristics of models were implemented for both the CBDS and EBDS *models*.

The variation in T_1 and T_2, determined using all three techniques, was less than 5% for both the CBDS and the EBDS. All three techniques proved to be successful in determining the major dynamic characteristic of both *models*, that is, their respective fundamental frequencies.

It is generally difficult to compare the dynamic response of two different buildings if there are significant differences in their dynamic characteristics. The elastic response of a building to earthquake shaking is generally controlled by the first few natural periods and modal damping ratios, that is, T_1, T_2, ξ_1 and ξ_2. If there is a significant difference in these parameters for the buildings being studied, it is difficult to compare their elastic and inelastic

behavior, even if identical earthquake ground motions are used. The small differences between the two lowest natural periods (T_1 and T_2) and between the mode shapes (ϕ_1 and ϕ_2) of the CBDS and the EBDS, eliminated this potential problem. The behavior of the CBDS *model* and the behavior of the EBDS *model* are directly compared wherever possible, in the following chapters of this report.

CHAPTER 5

EARTHQUAKE SIMULATOR TESTING
OF THE MODELS

5.1 General

The earthquake simulator input motions and testing programs for both the CBDS and EBDS *models* are described in Section 5.2 and 5.3, respectively. Aspects of the data reduction process are discussed in Section 5.4. The methods used to analyze the test data from the energy standpoint are discussed in Section 5.5.

5.2 Earthquake Simulator Input Motions

The *models* were subjected to four different earthquake acceleration records: 1978 Miyagi-Ken-Oki N00E component; 1971 Pacoima Dam S14W component; 1952 Kern County Taft N21E component and an artificial harmonic signal (Sine).

MIYAGI-KEN-OKI N00E, June 12, 1978.

The real-time Miyagi-Ken-Oki (MO) earthquake acceleration record (recorded at Tohoku University) resulted from an earthquake with a Richter Magnitude of 7.4. The MO earthquake acceleration record has a long duration of strong motion shaking, a peak acceleration of 26%g, and a reasonably broad frequency content. A truncated, time-scaled version of this acceleration record was used for testing the CBDS and EBDS *models*. The frequency content of the time-scaled Miyagi-Ken-Oki record is strongest at and around the fundamental frequency of the model. The energy content of the MO record is concentrated in three distinct bursts around the 4, 6 and 8.5 second marks of the time-scaled record.

PACOIMA DAM S14W, February 9, 1971.

The real-time Pacoima Dam earthquake acceleration record resulted from an earthquake with a Richter Magnitude of 6.4. It has a moderate duration of strong motion shaking and a peak

acceleration of 117%g. A truncated, time-scaled version of this acceleration record was used for EBDS Tests No. 29 and 30. For EBDS Tests No 27 and 28, a truncated version of the real-time acceleration record was used to develop the command signal.

TAFT N21E, July 21, 1952.

The real-time Taft earthquake acceleration record resulted from an earthquake with a Richter magnitude of 7.2. It has a long duration of strong motion shaking, a peak acceleration of 15.6%g, and a broad frequency content. The time-scaled acceleration record was derived from the earthquake acceleration records processed by the California Institute of Technology [24]. A truncated, time-scaled version of this acceleration record was used to test the CBDS and EBDS *models*. The frequency content of the time-scaled Taft record, although broad, is strongest in and around the fundamental frequency of the *models*. The energy content of the time-scaled Taft record is concentrated in two major bursts around the 3 and 7 second marks of the time-scaled signal.

SINE INPUT

The artificial sinusoidal earthquake ground motion was used to test the EBDS only. The sinusoidal input consisted of over 4 seconds of sinusoidal acceleration followed by two rectangular acceleration pulses. The motion was designed to excite the EBDS initially in its fundamental mode and then to subject it to two severe acceleration pulses.

All four acceleration time histories noted above were numerically integrated and baseline corrected to obtain the digitized displacement command signals for the earthquake simulator's actuators. The digitized record was then passed through a *Preston* D/A converter and then processed by an *MTS* controller to generate the analog displacement command signal for the earthquake simulator.

Of the three recorded earthquake ground motions noted above, only the Miyagi-Ken-Oki and Taft earthquake records are discussed in this report. The damage potential of these earthquakes can be compared by means of input energy spectra, $E_I(\xi, T, \eta)$. Although the elastic input energy is not necessarily representative of the actual input energy to a building during an

earthquake, it is convenient to compare the elastic input energy per unit mass (E_I/m) for both of these earthquake records. The SDOF energy spectra were evaluated using the computer program NONSPEC [37]. NONSPEC analyzes the inelastic response of viscously damped single-degree-of-freedom systems subjected to either base acceleration input or external load excitation. These SDOF input energy spectra, evaluated for a damping ratio of 2% and anchored to peak accelerations of 0.5g, are presented in Figure 5.1 together with the fundamental periods of the CBDS and EBDS *models*. The elastic input energy per unit mass is maximized for the Miyagi-Ken-Oki record at a period of approximately 0.6 second. For the Taft earthquake record, the input energy is maximized at a period of approximately 0.4 second. Assuming elastic response in the SDOFS, the input energy for the Taft record is greater than that of the Miyagi-Ken-Oki record for both the CBDS and EBDS *models*. Thus, the energy demand on the EBDS subjected to the Taft record with a peak acceleration of 0.5g is significantly greater than the energy demand on the CBDS subjected to the Miyagi-Ken-Oki record with a peak acceleration of 0.5g, that is, the Taft earthquake ground motion has greater damage potential than the Miyagi-Ken-Oki ground motion for similar levels of peak acceleration.

5.3 Earthquake Simulator Test Programs

The programs for testing the *models* were chosen in order to subject them to a variety of earthquake records whose peak intensities were varied to elicit response in both the elastic and inelastic range. Tables 5.1 and 5.2 list the test schedules for the CBDS [2] and the EBDS [1], respectively, noting where appropriate, the maximum table acceleration, the peak base shear, the maximum roof displacement and the associated roof drift index. As indicated in these tables, the earthquake simulator tests were categorized into four groups.

The first group of tests were of a diagnostic nature; as such, they were low amplitude tests undertaken to verify the performance of the earthquake simulator, the instrumentation and the data acquisition system in addition to obtaining *serviceability limit state* response in the

models. In these tests, the peak table accelerations varied between 0 and 15%g.

The second group of tests generated *damageability limit state* response. This series of tests was designed to produce minor structural damage in the *models* in the form of brace buckling (CBDS) and shear link yielding (EBDS) as well as yielding in the critical regions of the ductile moment-resisting space frames. In these tests, the peak table accelerations varied between 15%g and 35%g.

The third group of tests brought about *collapse limit state* response. This series of tests was designed to produce major structural damage in the *models*. In these tests, the peak table accelerations exceeded 40%g.

The fourth group of tests simulated the effects of *after-shocks* on the *models*. This series of tests was conducted after brace buckling in the CBDS and after major yielding in the shear links in the EBDS.

The variation of the dynamic characteristics of the CBDS and EBDS *models* with the degree of structural damage, was investigated by undertaking free vibration tests prior to, and after, a number of the earthquake simulator tests. The results of these tests are discussed in Section 6.2.

5.4 Data Reduction

5.4.1 Data Noise

Electronically recorded data inevitably contains both high and low frequency noise. One hundred and seventy-six channels of data were collected during each test of both the CBDS and EBDS *models*. The transducer output from the first 128 channels was lowpass filtered by the signal conditioners. The output from the remaining 48 channels contained a significant amount of high frequency noise and in a number of cases, low frequency noise.

A time domain numerical filter developed by Ormsby [38,39] was used to remove high and low frequency noise from the response time histories. The Ormsby filter involves the

convolution of the digitized response time history and a filter weighting function. The truncation caused by including a finite number of terms generally leads to leakage of the frequency response; the leakage of the high and low frequency components was minimized through the use of transition zones [39] that were selected on a trial-and-error basis. A discussion of numerical filtering is presented by Blondet [39]; interested readers should consult this reference for further details.

The problems associated with identifying and removing high and low frequency noise from the CBDS and EBDS response time histories, are discussed below.

High Frequency Noise:

All one hundred and seventy-six channels of data were lowpass filtered to remove high frequency noise above 20Hz. This cut-off frequency (f_c) was chosen for the following two reasons. First, the filtered response time histories still contained frequencies beyond the *models'* first three modal frequencies (Table 4.3). As the simulated earthquake responses of the *models* were primarily in their lowest two modes (ϕ_1 and ϕ_2), the filtered data captured the true response of the *models*. Secondly, the amplitudes of the Fourier spectra of the time-scaled earthquake records were negligible above 20 Hz, that is, there were no high frequency components in the input to excite higher modes in the *models*. A roll-off frequency (f_r) [39] of 21 Hz was used in conjunction with the cut-off frequency of 20 Hz.

High frequency noise is easily identified; an example of a transducer signal, with and without high frequency noise is presented in Figure 5.2 [1]. In order to illustrate the differences between the uncorrected and filtered signals, a brace deformation time history has been lowpass filtered using a cut-off frequency of 12 Hz and a roll-off frequency of 13 Hz. It should be noted that the filtered deformation response of the brace still contains that component of the random noise within the passband of the filter.

Low Frequency Noise:

Low frequency noise appears in the form of either: (1) a permanent offset in the channel data; or (2) as an harmonically varying baseline in the channel data. An example of the latter form of low frequency noise is shown in Figure 5.3a; the time history shown in Figure 5.3a is the lowpass filtered (f_c=20 Hz) fifth inter-story drift response of the EBDS during the Taft-08 Test [1]. The corrected response was obtained by removing the frequency content below 0.5 Hz from the time history. The cut-off frequency was chosen on the basis of the Fourier amplitude spectrum of the Taft-08 time-scaled acceleration time history; this time history has negligible frequency content below 0.5 Hz. Accordingly, the removal of the frequency content below 0.5 Hz will not alter the true inter-story drift response. The error function, that is, the low frequency noise, is also shown in Figure 5.3a; the highpass filtered response is shown in Figure 5.3b.

Permanent offsets were observed in lateral displacement and axial strain gage time histories for the damageability and collapse limit state tests; these offsets reflect permanent deformation and in these instances, the channel data was not filtered. In those transducers whose readings at the end of a test must decay to zero, for example, accelerometers and column web shear rosettes, the permanent offsets were unacceptable. It was assumed that the drift in the channel reading increased uniformly over the duration of the test. The signal was corrected by rotating the abscissa to remove the permanent offset. In these tests, the acceleration data rarely required correction; the column shear rosettes were corrected as necessary.

5.4.2 Sign Convention

The following sign convention, shown in Figure 5.4, was used in this report: (1) *Lateral displacement, inter-story drift and acceleration:* positive to the right (south) and positive upwards; (2) *Brace axial strain, axial deformation and axial force:* positive for elongation and tension; (3) *Story and column shear force:* positive shear force induced by positive inter-story drift; (4) *EBDS Link shear force and shear strain:* positive shear strain upwards and to the right (south), positive shear force generates positive shear strain.

5.4.3 Relative Lateral Displacement and Inter-story Drift Calculations

The relative displacement of the *ith* floor (v_i) was calculated by subtracting the rigid body displacement of the earthquake simulator table from the total displacement of the *ith* floor.

The *ith* inter-story drift (δ_i) was calculated as the difference between the relative displacements of the adjacent floors, that is:

$$\delta_i = v_{i+1} - v_i \tag{5.1}$$

The inter-story drift index (Θ^i) in the *ith* story was calculated as:

$$\Theta^i = \frac{\delta_i}{h_i} \tag{5.2}$$

where h_i is the height of the *ith* story.

5.4.4 Story Force Calculations

Story Shear:

Two methods were used to calculate the story shear force, that is, the shear forces in the columns and the horizontal components of the axial forces in the braces:

Inertia Force:

The story shear force was calculated by summing the inertia forces of each floor above the story under consideration. These inertia forces were calculated by multiplying the measured floor absolute accelerations by the corresponding floor weights (from Table 3.1). The advantage of this technique is that the calculation is straightforward if the accelerometers are accurately calibrated and if the floor weights are known accurately. The disadvantage of this technique is that the damping force is not included in the story shear force. The equilibrium equation of motion in vector form is:

$$\underline{f}_I = -(\underline{f}_S + \underline{f}_D) \tag{5.3}$$

where $\underline{f}_I$, $\underline{f}_S$ and $\underline{f}_D$ are the inertia force, the restoring force and the damping force vectors, respectively. The story shear force is generally related to the restoring force vector alone and

therefore, this method is reliable when the damping forces are small.

Shear Force Summation:

The story shear force was calculated by adding the column shear forces that were estimated from the strain rosette measurements to the horizontal components of the brace forces; this is a more rigorous method of calculating the story shear forces.

Summary:

These two methods were compared for a low intensity test of the EBDS with a peak acceleration of 7.8%g (Test No 7 in Table 5.2) [1]. The results of the two methods are presented in Figure 5.5; the difference between them is negligible and their correlation coefficient is approximately equal to one. For the testing of the CBDS, the inertia force method was used to evaluate the story shear forces after brace buckling [2]. For the testing of the EBDS, the second method was used to evaluate the story shear forces because the pre-calibrated braces remained elastic throughout the EBDS's testing program.

The total story shear force at level i (V_i^{TOTAL}) can be divided into two components as follows:

$$V_i^{TOTAL} = V_i^{BRACE} + V_i^{DMRSF} \tag{5.4}$$

where V_i^{TOTAL} = total shear force in the *ith* story

$\qquad V_i^{DMRSF}$ = shear force resisted by the DMRSF in the *ith* story

$\qquad\qquad$ = sum of the column shear forces in the *ith* story

$\qquad V_i^{BRACE}$ = shear forces resisted by the braces in the *ith* story

$\qquad\qquad$ = sum of the horizontal components of the brace forces in the *ith* story.

The column shear forces in Frame B are included in the latter term in Equation 5.4.

Overturning Moment:

The overturning moment at level i (OTM_i) was calculated using the floor inertia forces as follows:

$$OTM_i = \sum_{j=i}^{6}(m_j\ddot{v}_j^t)(h_j-h_i) \tag{5.5}$$

where m_j, $\ddot{v}_j^t$, h_j and h_i are the mass of the jth floor, the total acceleration of the jth floor and the heights of the jth and ith floors above the earthquake simulator table, respectively.

5.4.5 Element Force Calculations

Column Axial Force and Bending Moment:

All nine first story columns were instrumented with shear strain rosettes and uniaxial strain gages [1,2]. The computer program UNCOLA [40] was used to calculate the resultant axial force and the resultant bending moment from the axial strain measurements. The bending moments at both ends of the first story columns were determined by equilibrium using the estimated bending moments (UNCOLA output) and column shear forces (Figure 5.6).

Brace Force:

CBDS Brace Force:

To calculate the axial force in the unbuckled concentric braces, the average brace axial strains were multiplied by the measured Young's modulus (E_s=29,000 ksi). After either in-plane or out-of-plane brace buckling, the axial force and the biaxial bending moments at the instrumented cross-section were calculated from the strain readings on its four sides. Although the strain gages were installed at the upper quarter point of the braces and close to an analytical inflection point, the strain gages measured significant flexural yielding excursions upon brace buckling. The measured strain time histories were used to trace the corresponding stress states using the measured mechanical characteristics of the brace material.

A modified version [2] of the computer program UNCOLA [40] was used to calculate the axial force and biaxial bending moment resultants from the strain time histories. The stress-

strain relationship of the brace material was modeled using a Ramberg-Osgood constitutive relationship. Assuming Bernoulli's hypothesis that plane sections remain plane, strain values at three different locations at a section are sufficient to define the complete strain distribution. The axial force and biaxial moments were calculated after a least-squares fit was used on the four strain readings to determine the strain distribution. As only two strain gages were installed on the concentric braces in the upper two stories; in-plane bending was assumed and only the axial force and the in-plane bending moments were estimated [2].

EBDS Brace Force:

Each eccentric brace was calibrated prior to its installation in the *model* so that the strain gage readings produced axial force directly. The eccentric braces were calibrated in this manner because their responses were expected to remain elastic.

EBDS Link Shear Force:

Since the shear force in the composite link could not be directly measured, the vertical component of the eccentric brace force minus that portion of shear force in the adjacent beam was assumed to be equal to the link shear force. On the basis of strain rosette readings taken after EBDS Test 23 (Table 5.2), the shear force in the adjacent beam was estimated to be 7% of the vertical component of the eccentric brace force [1].

5.4.6 Member Designation

The member designations of the columns, beams and braces in the CBDS and EBDS *models* are shown in Figures 5.7 and 5.8, respectively.

5.5 Energy Input, Distribution and Dissipation

Although earthquake resistant design based upon energy methods is not envisaged at this stage, the use of energy methods to design, detail and categorize connections and critical regions is attractive. Useful energy equations have been developed by a number of researchers for SDOFS and MDOFS [1,2,41].

The input energy (E_I) is the integral with respect to time of the input power (P_I). The kinetic energy (E_K) is proportional to the absolute velocity ($\dot{v}^t$) squared. The elastic strain energy (E_S) is recoverable and is stored in the structure by elastic deformation. The cumulative viscous damped energy (E_μ) is the integral with respect to time of the energy dissipated by a number of mechanisms that include viscous damping and aerodynamic damping; the damping force is assumed to be proportional to relative velocity ($\dot{v}$). The cumulative hysteretic energy (E_H) is that energy dissipated by inelastic activity in the structure, integrated with respect to time.

The cumulative energy balance in a structure, as a function of time, can be expressed as follows:

$$E_K + E_A + E_\mu - E_I \qquad (5.6)$$

where E_A (= E_S + E_H) is the cumulative absorbed energy and the remaining terms are described above. For the *models*, a six degree-of-freedom lumped mass system was assumed and these terms can be quantified as follows:

Input Energy (E_I) :

$$E_I - \int(\sum_{i-1}^{6} m_i \ddot{v}_i^t)\, dv_g - \int(\sum_{i-1}^{6} m_i \ddot{v}_i^t)\, \dot{v}_g dt - \int P_I\, dt \qquad (5.7)$$

where m_i = floor mass at level i

$\ddot{v}_i^t$ = absolute lateral acceleration at level i - $\ddot{v}_i$ + $\ddot{v}_g$

$\ddot{v}_i$ = relative lateral acceleration at level i

v_g = base motion displacement

$\dot{v}_g$ = base motion velocity

$\ddot{v}_g$ = base motion acceleration

P_I = input power (kip–inch/sec)

The input power is equal to the base shear force (V_b) multiplied by the ground velocity ($\dot{v}_g$) if the base shear is evaluated using the inertia force method ($=\sum m_i \ddot{v}_i^t$). If the base shear force is evaluated by summing the column shear forces and the horizontal components of the axial forces in the braces, the assumption that the input energy can be estimated as $\int(V_b\dot{v}_g dt)$ is theoretically incorrect because the damping forces in the first story are neglected. However, as shown in Figure 5.5, the differences between evaluating the base shear force by either the inertia force or story shear force summation methods are, for all practical purposes, negligible.

Kinetic Energy (E_K) :

$$E_K = \frac{1}{2}\dot{v}^{tT}\underline{m}\dot{v}^t = \frac{1}{2}\sum_{i-1}^{6}m_i(\dot{v}_i^t)^2 \tag{5.8}$$

where $\underline{m}$ = diagonal mass matrix

$\underline{\dot{v}}^t$ = absolute lateral velocity vector

$\dot{v}_i^t$ = absolute lateral velocity at level i

The absolute velocity ($\dot{v}_i^t$) at a given level was calculated by numerically differentiating the absolute horizontal displacements.

Absorbed Energy (E_A) :

$$E_A = \int \underline{f}_S^T d\underline{v} = \sum_{i-1}^{6}\int f_{Si}dv_i \tag{5.9}$$

$$= E_S + E_H$$

where $\underline{f}_S$ = restoring force vector

f_{Si} = restoring force acting at level i

= difference in the story shear forces above and below level i

v_i = relative lateral displacement at level i.

A transformation [1,2] can be used to express E_A in terms of the story shear and the inter-story drift:

$$E_A = \int \underline{V}^T d\underline{\delta} = \sum_{i=1}^{6} \int V_i d\delta_i \qquad (5.10)$$

where V_i = story shear force at level i

δ_i = the inter-story drift in the ith story.

The absorbed energy is calculated by integrating the story shear with respect to the corresponding inter-story drift. The absorbed energy can be divided into recoverable elastic strain energy (E_S) and the non-recoverable inelastic hysteretic energy (E_H). The elastic strain energy is calculated as follows:

$$E_S = \sum_{i=1}^{6} \frac{V_i^2}{2K_i} \qquad (5.11)$$

where K_i is the unloading stiffness of the V_i versus δ_i curve; for these studies, it was assumed to be equal to the initial tangent stiffness. The inelastic hysteretic energy is therefore calculated as follows:

$$E_H = E_A - E_S = \sum_{i=1}^{6} \int V_i d\delta_i - \sum_{i=1}^{6} \frac{V_i^2}{2K_i} \qquad (5.12)$$

Viscous Damped Energy (E_μ) :

The viscous damped energy is calculated as follows:

$$E_\mu = \int \underline{f}_D^T d\underline{v} = \sum_{i=1}^{6} \int f_{Di} dv_i \qquad (5.13)$$

$$= \int q^T d\underline{\delta} = \sum_{i=1}^{6} \int q_i d\delta_i$$

where q_i is the damping force in the ith story. The viscous damped energy is difficult to evaluate explicitly and in this report was evaluated by reformulating Equation 5.6 as follows:

$$E_\mu = E_I - E_A - E_K. \qquad (5.14)$$

CHAPTER 6

EARTHQUAKE SIMULATOR TEST RESULTS

6.1 General

As noted in Tables 5.1 and 5.2, the CBDS and EBDS *models* were subjected to twenty and twenty-four simulated earthquake ground motions, respectively.

The results of all of these tests are not presented in this report and further details regarding the response of the CBDS and EBDS models can be found in References 2 and 1, respectively. In order to satisfy one of the primary objectives of this report, that is, to compare the behavior of the individual systems at various intensities of earthquake loading, the results of the following tests are presented in Sections 6.3 through 6.6:

Serviceability Limit State:

CBDS: Test No. 7 (Table 5.1) - Miyagi-Ken-Oki record; peak acceleration = 6.3%g.

EBDS: Test No. 11 (Table 5.2) - Miyagi-Ken-Oki record; peak acceleration = 7.0%g.

Damageability Limit State:

CBDS: Test No. 27 (Table 5.1) - Miyagi-Ken-Oki record; peak acceleration = 33.5%g.

EBDS: Test No. 17 (Table 5.2) - Miyagi-Ken-Oki record; peak acceleration = 27.5%g.

Collapse Limit State:

CBDS: Test No. 29 (Table 5.1) - Miyagi-Ken-Oki record; peak acceleration = 64.9%g.

EBDS: Test No. 23 (Table 5.2) - Taft record; peak acceleration = 57.3%g.

These six tests will be designated as MO-06, MO-07, MO-33, MO-28, MO-65 and Taft-57 in this report.

The variations in the natural periods and damping ratios of the CBDS and EBDS *models* over the course of the test program are summarized in Section 6.2. Descriptions of the structural damage incurred by the CBDS and EBDS *models* are presented in References 2 and 1,

respectively.

As peak ground acceleration (PGA) does not suitably describe the intensity of an earthquake ground motion, the ATC [11] introduced the concept of effective peak acceleration (EPA). The EPA suggested by the ATC for seismic design in regions of high seismic risk is 0.4g. In this report, EPA is used as a damage potential index for the direct comparison of the input motions for the Miyagi-Ken-Oki Tests noted above. The EPA was evaluated from the 5% damped, linear elastic response spectrum for the measured earthquake simulator table motion as follows:

(i)   The line of constant acceleration of best fit to the spectral shape in the period range of 0.055 to 0.275 second was selected. In order to comply with the similitude laws, the period range of 0.1 to 0.5 second (used by the ATC to evaluate the EPA) was time scaled by the same factor $(=1/\sqrt{1.811})$ used for scaling the acceleration time histories.

(ii)   The acceleration ordinate of the line was divided by a factor of 2.5 to obtain the EPA.

The technique for evaluating EPA is depicted in Figure 6.1 for the time-scaled Miyagi-Ken-Oki earthquake record with a peak acceleration of 65%g.

6.2 Variation of Natural Periods and Damping Ratios

The natural period and damping ratio variations for the first three modes of the CBDS and EBDS *models* are presented in Tables 6.1 and 6.2. The natural periods and damping ratios in the last row of Table 6.1 and the first row of Table 6.2 represent the dynamic characteristics of the models without any bracing, that is, a DMRSF. Figures 6.2 and 6.3 depict the variation of natural periods and damping ratios with the sequence of testing for both the CBDS and EBDS, respectively.

As a consequence of the CBDS, EBDS and DMRSF having identical total masses and mass distributions the fundamental periods noted in Tables 6.1 and 6.2 can be used to evaluate the ratio of the effective stiffnesses of the CBDS and EBDS to that of the DMRSF alone:

$$\frac{K_{CBDS}}{K_{DMRSF}} = \left[\frac{1/0.342}{1/0.672}\right]^2 = 3.9 \tag{6.1}$$

and

$$\frac{K_{EBDS}}{K_{DMRSF}} = \left[\frac{1/0.316}{1/0.672}\right]^2 = 4.5, \tag{6.2}$$

respectively. Clearly, the concentric and eccentric braces increased the stiffnesses of the *models* significantly in the elastic range.

The ratio of the stiffness of the EBDS to that of the CBDS is

$$\frac{K_{EBDS}}{K_{CBDS}} = \left[\frac{1/0.316}{1/0.342}\right]^2 = 1.17. \tag{6.3}$$

The ratio of the stiffnesses of the EBDS and CBDS is contrary to what would be generally expected because a CBDS is typically stiffer than an EBDS. The relationship between elastic lateral stiffness and link length as a function of bay length (e/L) [4] is presented in Figure 6.4; a value of e/L equal to zero corresponds to a concentrically braced frame. For constant brace sizes, Figure 6.4 suggests that for an e/L ratio of 0.1 and an h/L ratio of 1.0, the stiffness of the eccentrically braced frame is between 60% and 70% of that of the concentrically braced frame (for the EBDS *model*, e/L=0.095 and h/L=1.2). As noted in Equation 6.3, the stiffness of the EBDS is 17% higher than that of the CBDS; the large discrepancy between this result and that suggested by Figure 6.4 is a result of the larger brace sizes used in the EBDS. The cross-sectional areas of the EBDS's braces were 18%, 91%, 91%, 132%, 158% and 177% greater than those of the CBDS's braces in the first to sixth stories, respectively.

The variations in the natural periods and viscous damping ratios over the duration of the testing program were relatively small for both the CBDS and EBDS. The fundamental period of the CBDS increased by approximately 10% (from 0.361 second to 0.392 second) over the duration of the CBDS's testing program and the fundamental period of the EBDS increased by approximately 5% (from 0.316 second to 0.333 second) over the duration of its testing

program. The free and forced vibration tests employed low levels of excitation and hence, the natural periods and damping ratios presented in Tables 6.1 and 6.2 and Figure 6.2 are lower bounds to the values that existed during the earthquake simulations. Unless noted otherwise, the natural frequencies and damping ratios listed in Tables 6.1 and 6.2 relate to the air-supported earthquake simulator table and model system. The damping ratio in this system was appreciably higher than that in the fixed base model (2.2% versus 0.7% for the EBDS) because of the damping in the earthquake simulator's vertical and horizontal actuators and passive stabilizers. The increase in the fundamental period of the complete system with respect to the fixed base model (0.316 second to 0.326 second for the EBDS) resulted from the axial flexibility of the earthquake simulator's vertical actuators and passive stabilizers which introduced a rotational degree of freedom into the air-supported earthquake simulator table and model system.

6.3 Serviceability Limit State

6.3.1 Concentrically Braced Dual System - MO-06 Test

Response Time Histories:

The measured table horizontal acceleration and displacement and the corresponding linear elastic response spectrum for 0%, 2%, 5%, 10% and 20% damping are shown in Figure 6.5; the EPA of this test was 0.046g. The relative lateral displacement, inter-story drift, lateral inertia force and story shear force time histories at each level are shown in Figures 6.6 to 6.9, respectively. The lateral displacement time histories indicate that the response was primarily in the first mode and that there was little contribution from higher modes. The time histories of the total story shear force and the story shear force resisted by the concentric braces are shown in Figure 6.9. The base overturning moment time history is shown in Figure 6.10. The overturning moment resisted by the concentric braces is also shown in Figure 6.10 and is approximately one-quarter of the total overturning moment.

Story Shear and Inter-Story Drift Relationships:

The total story shear and inter-story drift relationships for each story of the CBDS are presented in Figure 6.11. The response in all six stories of the CBDS was linear with only small deviations from expected elastic behavior.

The deviations from the expected elastic response can be attributed to the limited resolution of the linear potentiometers measuring the total displacement of each floor ($\pm$ 0.02 inch). The total displacement of each floor included the rigid body displacement of the earthquake simulator platform; the relative displacement of each floor was obtained by subtracting the rigid body displacement from the total displacement. The inter-story drifts were calculated by subtracting the relative displacements of the adjacent floors. Therefore, the errors inherent in estimating the inter-story drifts, due to the limited resolution of the LPs can be of the order of $\pm$ 0.04 inch, or, approximately 75% of the maximum inter-story drift measured during the MO-06 Test.

Maximum Response Envelopes:

The envelopes of maximum response of relative displacements, inter-story drifts, story shear forces, inertia forces and overturning moments over the height of the *model* are shown in Figure 6.12 and summarized in Table 6.3. It is clear from Figure 6.12 that in the elastic range, the concentric braces in each story resisted most of the story shear and that the maximum inter-story drifts were approximately uniform over the height of the *model*. The concentric braces resisted approximately 80%, 60%, 60%, 65%, 55% and 60% of the story shear in the first to sixth stories, respectively.

The distribution and magnitude of the overturning moments over the height of the *model* are important as they are a reflection of both the lateral force distribution (see below) and the likelihood of developing tension in the perimeter columns. The nearly cubic distribution of overturning moments over the height of the *model* was a reflection of an inertia force profile that was bounded by an inverted-triangular profile (henceforth termed a triangular profile) and a parabolic profile.

The lateral displacement, inertia force, story shear, inter-story drift and overturning moment profiles over the height of the *model* at the times of maximum base shear and maximum roof displacement are shown in Figure 6.13. The inertia force profiles are bounded by a triangular profile and a parabolic profile; the former is consistent with the design lateral force profile assumed by the UBC and ATC for masses evenly distributed over the height of a structure and in the period range under consideration ($T < 0.7/\sqrt{1.811}$). The relationship between the inertia force profile, the first few natural periods of the structure and the frequency content of the earthquake ground motion is extremely important. Figure 6.5c indicates that the SDOFS pseudo-acceleration responses to the MO-06 record for the first two natural periods of the CBDS are of the same order. This result is reflected in the inertia force time histories (Figure 6.8) where the contribution of the second mode is evident in the response of the upper levels of the *model*. The reduction in the inertia forces at the roof level from those at the sixth floor (Figures 6.12 and 6.13) is a result of the reactive weight of the roof slab being approximately 15% less than that of the other five floors, and this masks the effect of the second mode on the inertia force profiles.

The maximum inter-story drift index of 0.15% occurred in the fourth story. The maximum base shear coefficient (V_b/W_{al}) of 0.14 exceeded the UBC design base shear coefficient ($=0.113$) for this low amplitude, serviceability limit state earthquake. As the *model* was not designed in accordance with the UBC, this result is not a reflection of the overstrength inherent in concentrically braced dual systems designed in accordance with the UBC but rather a comparison between the *design* base shear in a region of high seismic risk ($=0.113W_{drw}$) and the base shear that was developed during *minor* earthquake shaking.

Lateral Force Distribution:

The inherent differences in the displacement profiles of a braced frame and a DMRSF under lateral loading cause interaction forces to be developed between them when they are combined into a dual system. These interaction forces lead to a lateral shear force distribution within a story which is not proportional to the stiffnesses of the individual systems in the story.

In extreme cases, this "braced frame - moment frame" interaction can cause the story shear force carried by the DMRSF in the upper levels of a structure to exceed the total story shear while the braced frame carries a story shear force of the opposite sense.

Furthermore, the distribution of lateral force between the braced frame and the DMRSF can have a profound effect on the relationship between their respective story shears and over-turning moments and thus the applicability of certain capacity design procedures.

The distributions of lateral force between the concentrically braced bay and the DMRSF at the times of maximum base shear and maximum lateral displacement, shown in Figure 6.14, show no evidence of this form of interaction; the same conclusion can be drawn from Figure 6.12. This result can be attributed primarily to the moderate height of the *model* and the small axial deformations in the braced bay columns.

Energy Distribution:

The method described in Section 5.5 was used to calculate the input energy, the kinetic energy and the strain energy time histories. The viscous damped energy (E_μ) was calculated as:

$$E_\mu = E_I - E_K - E_S.$$ (6.4)

Figure 6.15 shows the input energy, the kinetic energy, the viscous damped energy and the elastic strain energy time histories for the MO-06 Test. The energy input to the CBDS during this test was extremely small; the maximum input energy was approximately 2.5 kip-in and this was measured at 8.25 seconds in the test. All of the cumulative input energy was dissipated by equivalent viscous damping in the CBDS.

6.3.2 Eccentrically Braced Dual System - MO-07 Test

Response Time Histories:

The measured table horizontal acceleration and displacement and the corresponding linear elastic response spectrum for 0%, 2%, 5%, 10% and 20% damping are shown in Figure 6.16; the EPA of this test was 0.054g. The relative lateral displacement, inter-story drift, lateral

inertia force and story shear force time histories at each level are shown in Figures 6.17 to 6.20, respectively. The lateral displacement time histories indicate that the response was primarily in the first mode and that there was little contribution from higher modes. The time histories of the total story shear force and the story shear force resisted by the eccentric braces are shown in Figure 6.20. The base overturning moment time history is shown in Figure 6.21; the overturning moment resisted by the eccentric braces is also shown in this figure. The eccentric braces resisted approximately one-quarter of the total overturning moment.

Story Shear and Inter-story Drift Relationships:

The total story shear and inter-story drift relationships for each story of the EBDS are presented in Figure 6.22. The response was linear in all six stories of the EBDS with only minor deviations from the expected elastic response.

Maximum Response Envelopes:

The envelopes of maximum response of relative displacements, inter-story drifts, story shear forces, inertia forces and overturning moments over the height of the *model* are shown in Figure 6.23 and summarized in Table 6.4. The eccentric braces in the lower five stories resisted approximately 80% of the story shear. In the sixth story, the eccentric braces resisted approximately 70% of the story shear. This 10% decrease is a result of the smaller size of the sixth story eccentric braces compared with those in the fifth story; the columns and beams in these two stories were identical. The maximum drift in the first story was greater than that in the remaining stories because the floor-to-floor height in the first story was approximately 30% greater than in the remaining five stories (Figure 2.1). The nearly cubic distribution of overturning moments over the height of the *model* was a reflection of the inertia force profile that varied between triangular and parabolic.

The lateral displacement, inertia force, story shear, inter-story drift and overturning moment profiles over the height of the *model* at the times of maximum base shear and maximum roof displacement are shown in Figure 6.24. The inertia force profiles are bounded by a triangular profile and a parabolic profile in a manner similar to that seen for the CBDS in

Figures 6.12 and 6.13. Figure 6.16c indicates that the SDOFS pseudo-acceleration responses to the MO-07 record at the first two natural periods of the EBDS are approximately the same. This result is reflected in the inertia force time histories in Figure 6.19 where the contribution of the second mode is evident in the response of the upper levels of the *model*. The reduction in the inertia forces at the roof level from those at the sixth floor (Figures 6.23 and 6.24) is a result of the reactive weight of the roof slab being approximately 15% less than that of the other five floors, and this masks the effect of the second mode on the inertia force profiles.

The maximum inter-story drift index of 0.10% occurred in the third story while the maximum first inter-story drift index was 0.09%. The maximum base shear coefficient (V_b/W_{at}) of 0.107 was approximately equal to the UBC design base shear coefficient (=0.113) for this low amplitude, serviceability limit state earthquake. As the *model* was not designed in accordance with the UBC, this result is not a reflection of the overstrength inherent in dual steel systems designed in accordance with the UBC but rather a comparison between the *design* base shear in a region of high seismic risk (=$0.113W_{drw}$) and the base shear that was developed during *minor* earthquake shaking.

Lateral Force Distribution:

The distributions of lateral force between the eccentrically braced bay and the DMRSF at the times of maximum base shear and maximum lateral displacement, shown in Figure 6.25, show no evidence of interaction which might cause the story shear force carried by the upper levels of the DMRSF to exceed the total applied story shear. As noted in Section 6.3.1, this can be attributed primarily to the moderate height of the *model* and the small axial deformations in the braced bay columns.

Energy Distribution:

The method described in Section 5.5 was used to calculate the input energy, the kinetic energy and the strain energy time histories. Figure 6.26 shows the input energy, the kinetic energy, the viscous damped energy and the elastic strain energy time histories for the MO-07 Test. The energy input to the EBDS during this test was extremely small; the maximum input

energy was approximately 1.6 kip-in and this was measured at 6.75 seconds in the test. All of the cumulative input energy was dissipated by equivalent viscous damping in the EBDS.

6.4 Damageability Limit State

6.4.1 Concentrically Braced Dual System - MO-33 Test

Response Time Histories:

The measured table horizontal acceleration and displacement and the corresponding linear elastic response spectrum for 0%, 2%, 5%, 10% and 20% damping are shown in Figure 6.27; the EPA of this test was 0.21g. The relative lateral displacement, inter-story drift, lateral iner-tia force and story shear force time histories at each level are shown in Figures 6.28 to 6.31, respectively. The lateral displacement time histories indicate that the response was primarily in the first mode and that there was little contribution from higher modes.

The time histories of the total story shear force and the story shear force resisted by the concentric braces are shown in Figure 6.31. The story shear force resisted by the concentric braces was calculated by subtracting the sum of the column shear forces from the total story shear force. In Figure 6.31, the brace story shear forces required to initiate brace buckling (V_y^{bb}), calculated as $2\ P_{cr}\cos\theta$ (where P_{cr} = brace buckling load) [2] are also shown. The axial forces in the concentric braces reached 88%, 93%, 86%, 92%, 92% and 67% of their respec-tive buckling loads in the first to sixth stories, respectively. The base overturning moment time history is shown in Figure 6.32 in conjunction with the overturning moment resisted by the concentric braces. Since the concentric braces in the first story did not buckle during the MO-33 Test, the percentage of the total overturning moment resisted by the concentric braces remained relatively constant over the duration of the test.

Story Shear and Inter-story Drift Relationships:

The total story shear and inter-story drift relationships for each story of the CBDS are presented in Figure 6.33. The brace story shear (the horizontal component of the concentric

brace force) and inter-story drift and the DMRSF story shear and inter-story drift relationships for each story are presented in Figures 6.34 and 6.35, respectively.

Minor yielding is evident in the first and second stories although the axial forces in the concentric braces in these stories did not exceed their nominal buckling loads. This inelastic behavior can be attributed to the yielding in the braced bay columns in the lower two stories for a small number of cycles, yielding in the composite girders in addition to cracking in the composite slabs above the concentric brace-to-beam junction. The third, fourth and sixth stories responded elastically while the fifth story exhibited inelastic behavior stemming primarily from the minor buckling of Braces Br9 and Br10 [2].

The columns in all six stories of the DMRSF, except those in the braced bay columns of the bottom two stories, responded in a linear elastic manner and therefore did not contribute to the hysteretic energy dissipation in this test.

The six story shear ratios (SSR), defined as V_{brace}/V_{total}, or the portion of the total story shear resisted by the concentric braces, are shown in Figure 6.36. The results in Figure 6.36 confirm that the concentric braces in the first to fourth stories and in the sixth story remained elastic (SSR $\approx$ constant) but that those in the fifth story underwent minor buckling [2] (SSR reduced from the elastic level).

Maximum Response Envelopes:

The envelopes of maximum response of relative displacements, inter-story drifts, story shear forces, inertia forces and overturning moments over the height of the *model* are shown in Figure 6.37 and summarized in Table 6.5. It is clear from Figure 6.37 that the concentric braces in each story resisted most of the story shear; that the maximum inter-story drifts were approximately uniform over the height of the *model* and thus the lateral displacement profiles were approximately triangular. The nearly cubic distribution of overturning moments over the height of the *model* was a reflection of the inertia force profile that was bounded by a triangular profile and a parabolic profile.

The lateral displacement, inertia force, story shear, inter-story drift and overturning moment profiles over the height of the *model* at the times of maximum base shear and maximum roof displacement are shown in Figure 6.38. Figure 6.27 indicates that the SDOF pseudo-acceleration response to the MO-33 record at the first two natural periods of the CBDS are of the same order. This result is reflected in the inertia force time histories in Figure 6.30 where the contribution of the second mode is evident in the response of the upper levels of the *model*. The reduction in the inertia forces at the roof level from those at the sixth floor (Figures 6.37 and 6.38) is a result of the smaller mass of the roof slab in comparison with that of the other five floors, rather than the effect of the second and higher modes.

The maximum inter-story drift index of 0.69% occurred in the fifth story and the maximum first inter-story drift was 0.51%. The maximum base shear coefficient (V_b/W_{at}) of 0.56 exceeded significantly the UBC design base shear coefficient (=0.113) and exceeded the nominal yielding strength of the *model* (=$0.3W_{at}$) for this damageability limit state earthquake. Since the *model* was not designed in accordance with the UBC, this result is not a reflection of the overstrength inherent in concentrically braced dual systems designed in accordance with the UBC but rather a comparison between the *design* base shear in a region of high seismic risk (=$0.113W_{drw}$) and the base shear that was developed during *moderate* earthquake shaking.

Lateral Force Distribution:

The distributions of lateral force between the concentrically braced bay and the DMRSF at the times of maximum base shear and maximum lateral displacement, shown in Figure 6.39, show no evidence of "braced frame - moment frame" interaction; the same conclusion can be drawn from Figure 6.37. This can be attributed to the moderate height of the *model* and the small axial deformations in the braced bay columns.

Column Axial Force and Bending Moment Interaction:

Axial strains due to gravity load effects and residual strains were not included in the column axial strain time histories since all of the data channels were initialized prior to each test. The axial forces in the columns due to gravity loads were calculated assuming a uniform

distribution of gravity load over the plan area of each floor and using a tributary area approach. The end moment (M) and axial force (N) interaction curves for the first story columns in Frames A and B are shown in Figures 6.40 and 6.41, respectively. The AISC [42] M-N yield surface, based upon linear elastic-perfectly plastic material properties, is also shown in these two figures. The columns in the braced bay (Columns $1C_{B1}$ and $1C_{B2}$) were subjected to a significantly higher axial force demand than those in the DMRSF. Figure 6.41 suggests that Columns $1C_{B1}$ and $1C_{B2}$ yielded in axial compression and tension at their bases during this test; this yielding contributed to the dissipation of the input energy during this test. The negligible change in the axial force in Column $1C_{A2}$ is a result of this column being located approximately on the neutral axis of the CBDS in the plane of earthquake shaking.

Concentric Brace Response:

The axial force versus axial deformation responses for Braces Br1 and Br2 (Story 1), Braces Br3 and Br4 (Story 2), Brace 6 (Story 3) and Brace 8 (Story 4) are presented in Figures 6.42 and 6.43. The response for all of the concentric braces in the lower four stories was linear and therefore consistent with the earlier observations. The axial deformations in the concentric braces in the fifth and sixth stories were not measured and thus the hysteretic behavior of these braces is unavailable.

Energy Distribution:

The method described in Section 5.5 was used to calculate the input energy, the kinetic energy and the strain energy time histories. For the level of excitation used in this test, the input energy is dissipated as both hysteretic energy and viscous damped energy. Figure 6.44 shows the input energy, the kinetic energy, the elastic strain energy, the hysteretic energy and the viscous damped energy time histories for the MO-33 Test. Three distinct bursts of input energy can be identified for this test at 4, 6 and 8 seconds; brace buckling in the fifth story was initiated by the first burst of input energy.

6.4.2 Eccentrically Braced Dual System - MO-28 Test

Response Time Histories:

The measured table horizontal acceleration and displacement and the corresponding linear elastic response spectrum for 0%, 2%, 5%, 10% and 20% damping are shown in Figure 6.45; the EPA of this test was 0.19g. The relative lateral displacement, inter-story drift, lateral inertia force and story shear force time histories at each level are shown in Figures 6.46 to 6.49, respectively. The lateral displacement time histories indicate that the displacement response was primarily in the first mode and that there was little contribution from higher modes. The time histories of total story shear force and the story shear force resisted by the eccentric braces are shown in Figure 6.49. The base overturning moment time history is shown in Figure 6.50; the overturning moment resisted by the eccentric braces is also shown in this figure.

Story Shear and Inter-story Drift Relationships:

The total story shear and inter-story drift relationships for each story of the EBDS are presented in Figure 6.51. The brace story shear (the horizontal component of the concentric brace force) and inter-story drift and the DMRSF story shear and inter-story drift relationships for each story are presented in Figures 6.52 and 6.53, respectively.

Nonlinear behavior was confined to the lower two stories and the upper four stories responded elastically. The nonlinear behavior can be attributed to yielding in the lower two shear links, yielding in the composite girders as well as cracking in the composite slabs above the lower two shear links.

In all six stories, the DMRSF responded in a linear elastic manner and therefore did not contribute to the hysteretic energy dissipation in this test.

The six story shear ratios (SSR), shown in Figure 6.54, indicate that despite yielding in the shear links at Levels L2 and L3, the percentage of the story shear resisted by the eccentric braces remained relatively constant.

Maximum Response Envelopes:

The envelopes of maximum response of relative displacements, inter-story drifts, story shear forces, inertia forces and overturning moments over the height of the *model* are shown in Figure 6.55 and summarized in Table 6.6. The maximum drift in the first story was greater than that in the remaining stories because the floor-to-floor height in the first story was approximately 30% greater than in the remaining stories (Figure 2.1). The nearly cubic distribution of overturning moments over the height of the *model* was a reflection of the inertia force profile that was bounded by a triangular profile and a parabolic profile.

The lateral displacement, inertia force, story shear, inter-story drift and overturning moment profiles over the height of the *model* at the times of maximum base shear and maximum roof displacement are shown in Figure 6.56. The inertia force profiles are bounded by a triangular profile and a parabolic profile and are similar to the CBDS's inertia force profiles shown in Figures 6.37 and 6.38. Figure 6.45c indicates that the SDOFS pseudo-acceleration response to the MO-28 record at the first two natural periods of the EBDS are approximately the same. This observation is reflected in the inertia force time histories in Figure 6.49 where the contribution of the second mode is evident in the response of the upper levels of the *model*. The reduced inertia forces at the roof level from those at the sixth floor (Figures 6.55 and 6.56) are a result of the reactive weight of the roof slab being approximately 15% less than that of the other five floors, and this masks the effect of the second mode on the inertia force profiles.

The maximum inter-story drift index of 0.62% occurred in the first story. The maximum base shear coefficient (V_b/W_{at}) of 0.50 exceeded both the UBC design base shear coefficient (=0.113) and the nominal yielding strength of the *model* (=$0.3W_{at}$) by a factor of 1.66 for this damageability limit state earthquake. As the *model* was not designed in accordance with the UBC, this result is not a reflection of the overstrength inherent in dual systems designed in accordance with the UBC but rather a comparison between the *design* base shear in a region of high seismic risk (=$0.113W_{drw}$) and the base shear that was developed during *moderate* earthquake shaking.

Lateral Force Distribution:

The distributions of lateral force between the eccentrically braced bay and the DMRSF at the times of maximum base shear and maximum lateral displacement, shown in Figure 6.57, show no evidence of "braced frame - moment frame" interaction.

Column Axial Force and Bending Moment Interaction:

The end moment (M) and axial force (N) interaction curves for the first story columns in Frames A and B are shown in Figures 6.58 and 6.59, respectively. The AISC [42] M-N yield surface, based upon linear elastic-perfectly plastic material properties, is also shown in these two figures. Although the columns in the braced bay (Columns $1C_{B2}$ and $1C_{B3}$) were subjected to a significantly higher axial force demand than those in the DMRSF, no yielding in these columns was observed. The negligible change in the axial force in Column $1C_{A2}$ is a result of this column being located approximately on the neutral axis of the EBDS in the plane of earthquake shaking.

Eccentric Brace Response:

The current philosophy for the design of bracing members in eccentrically braced frames is to keep the brace's capacity above what is required to reach the ultimate strength of the associated shear link, and thus to ensure that the bracing member remains elastic. The brace axial force versus axial deformation relationships for the eccentric braces in the first two stories (Braces Br1, Br2, Br3 and Br4) are presented in Figure 6.60, along with their nominal buckling loads (P_{cr}) and tensile strengths (T_y). The brace response was linear in all four of these braces. The axial deformations in the concentric braces in the third, fourth, fifth and sixth stories were not measured and thus the hysteretic behavior of these braces is unavailable.

Shear Link Response:

The relationships between link shear force and shear strain for the Level 2 to Level 6 shear links are presented in Figure 6.61. The maximum shear strains ranged from 1.2% (0.012 radian) in Link L2 to 0.20% (0.0020 radian) in Link L6. The Link L2 shear force versus shear

strain relationship is presented in Figure 6.62; the shear yielding strength (V_p) and the corresponding shear strain (γ_y) of the bare steel link are also shown in this figure. The peak shear force in this composite shear link was 26.9 kips, that is, 170% of the nominal shear yielding strength of the bare steel link.

Energy Distribution:

The method described in Section 5.5 was used to calculate the input energy, the kinetic energy and the strain energy time histories. For the level of excitation used in this test, the input energy is dissipated as both hysteretic energy and viscous damped energy. Figure 6.63 shows the input energy, the kinetic energy, the elastic strain energy, the hysteretic energy and the viscous damped energy time histories for the MO-28 Test. The shear links dissipated in excess of 35% of the input energy; 80% of the energy dissipated by the links was dissipated in Link L2.

6.5 Collapse Limit State

6.5.1 Concentrically Braced Dual System - MO-65 Test

Response Time Histories:

The measured table horizontal acceleration and displacement and the corresponding linear elastic response spectrum for 0%, 2%, 5%, 10% and 20% damping are shown in Figure 6.64; the EPA of the MO-65 Test was 0.41g which is approximately equal to the value assumed by the ATC 3-06 [11] for seismic design in a region of high seismic risk. The relative lateral displacement, inter-story drift, lateral inertia force and story shear force time histories at each level are shown in Figures 6.65 to 6.68, respectively. The lateral displacement time histories indicate that the *model* responded primarily in its first mode. As a result of buckling of the concentric braces in the lower five stories [2], the natural period of the *model* elongated to approximately 0.45 second during the MO-65 Test; a 25% increase over its natural period of 0.361 second prior to the MO-06 Test, but substantially less than the natural period of the DMRSF (= 0.672 second).

The time histories of total story shear and the story shear forces resisted by the concentric braces are shown in Figure 6.68. In Figure 6.68, the brace story shear forces required to initiate brace buckling (V_y^{bb}), calculated as $2\,P_{cr}\cos\theta$ (where P_{cr} = brace buckling load) [2] are also shown. The axial forces in the concentric braces reached 99%, 91%, 115%, 109%, 112% and 110% of their nominal buckling loads in the first to sixth stories, respectively. Although all the braces in the lower five stories buckled, only the braces in the fifth story ruptured and lost their axial strengths. This result is contradictory to that suggested above by the nominal buckling loads of the braces and strongly suggests that other factors, such as residual stresses, imperfections and lack of initial straightness can have a significant effect on the shear resistance of a concentrically braced frame.

It is important to differentiate between brace buckling and brace rupture. Brace buckling does not necessarily imply any loss of strength; brace rupture is associated with the complete loss of the brace's axial strength. The rupture of the fifth story braces was preceded by: (1) their overall buckling, followed by (2) local buckling at their respective midheights in the plastic hinge regions; leading to (3) very high curvatures and strains in the buckled sections of the tubular braces; and consequently (4) tearing or fracture of the brace material in the buckled regions. The problems associated with preventing (2), (3) and (4) after overall buckling has occurred is discussed briefly in Chapter 7 and by Uang and Bertero [2].

The base overturning moment time history is shown in Figure 6.69; the overturning moment resisted by the concentric braces is also shown in this figure. Despite the buckling of the first story braces, the percentage of the total overturning moment resisted by the braces remained relatively constant over the duration of the test.

Story Shear and Inter-story Drift Relationships:

The total story shear and inter-story drift relationships for each story are presented in Figure 6.70. The brace story shear (the horizontal component of the concentric brace force) and inter-story drift and the DMRSF story shear and inter-story drift relationships for each story are presented in Figures 6.71 and 6.72, respectively. The strength and deformation response is

nonlinear in all but the sixth story. The greatest strength degradation occurs in the fifth story. In the lower four stories, the inelastic behavior is confined to the concentrically braced bay with the response of the DMRSF being elastic to inter-story drift index levels approaching 1.20%. As a consequence of the rupture of the concentric braces in the fifth story, the shear resistance of the concentrically braced bay at this level was lost completely and the DMRSF resisted the total story shear force. The fifth story response of the CBDS clearly demonstrates the undesirable effects of poor post-buckling behavior in a concentrically braced frame; that is, strength and stiffness degradation and loss of energy dissipation capacity.

The six story shear ratios (SSR), defined as V_{brace}/V_{total}, or the portion of the total story shear resisted by the concentric braces, are shown in Figure 6.73. The results in Figure 6.72 confirm those presented in Figures 6.70 and 6.71. The story shear ratios in the lower three stories remained relatively constant despite buckling of the concentric braces in these stories. In the fourth story, severe brace buckling was associated with the bursts of input energy at the 6 and 8-9 second marks in this test. As a result of the rupture of the concentric braces in the fifth story, the shear resistance of the fifth story of the concentrically braced bay was completely lost just prior to the 9 second mark in the test.

Maximum Response Envelopes:

The envelopes of maximum response of relative displacements, inter-story drifts, story shear forces, inertia forces and overturning moments over the height of the *model* are shown in Figure 6.74 and summarized in Table 6.7. The inertia force profiles varied between a parabolic profile and a rectangular profile. The maximum inter-story drift indices exceeded the UBC, ATC and SEAOC yielding level inter-story drift index limits (0.5%, 0.3%, and 0.38% respectively) and exceeded the UBC, ATC and SEAOC ultimate inter-story drift index limits in the fifth story and the SEAOC ultimate inter-story drift index limit in the fourth story. The distribution of overturning moments over the height of the *model* was bounded by a cubic function and a parabolic function and was a reflection of the inertia force profile.

The lateral displacement, inertia force, story shear, inter-story drift and overturning moment profiles over the height of the *model* at the times of maximum base shear and maximum roof displacement are shown in Figure 6.75. The responses at the time of maximum base shear are similar to those maximum responses shown in Figure 6.74; the exception being the inertia force profile that was parabolic at the time of maximum base shear as opposed to the more rectangular envelope of maximum inertia forces. At the times of maximum lateral roof displacement (at 8.86 seconds for maximum positive displacement and 8.61 seconds for maximum negative displacement), the concentric braces in the fifth story had started to rupture, leading to the formation of a soft fifth story; this is evident in the lateral displacement and inertia force profiles.

The maximum inter-story drift index of 1.89% occurred in the fifth story while the maximum first inter-story drift was 0.87%. The maximum base shear coefficient (V_b/W_{at}) of 0.73 exceeded significantly the UBC design base shear coefficient (=0.113) and exceeded the nominal yielding strength of the *model* (=$0.3W_{at}$) by a factor of 2.43 for this collapse limit state earthquake. As the *model* was not designed in accordance with the UBC, this result is not a reflection of the overstrength inherent in concentrically braced dual systems designed in accordance with the UBC but rather a comparison between the *design* base shear in a region of high seismic risk (=$0.113W_{drw}$) and the base shear that was developed during *severe* earthquake shaking.

Lateral Force Distribution:

The distributions of lateral force between the concentrically braced bay and the DMRSF at the times of maximum base shear and maximum lateral displacement are shown in Figure 6.76. The total lateral force distribution in both cases reflects the formation of a soft fifth story. The maximum base shear forces (at 6.25 seconds for maximum positive base shear and at 4.34 seconds for maximum negative base shear) were measured prior to brace rupture and therefore the lateral force distributions at these times are significantly different from those that were measured at the times of maximum lateral roof displacement (see above). At the times of

maximum base shear, the lateral forces on the fifth story of the concentrically braced frame were, as a result of the degradation of the strength of the fifth story braces, smaller than those measured during the MO-33 Test (Figure 6.39) and approximately one-third of the corresponding total lateral force. At the time of maximum negative roof displacement, the shear resistance of the concentrically braced bay was completely lost and the inertia forces at this level were carried by the DMRSF alone.

Column Axial Force and Bending Moment Interaction:

The end moment (M) and axial force (N) interaction curves for the first story columns in Frames A and B are shown in Figures 6.77 and 6.78, respectively. The AISC [42] M-N yield surface, based upon linear elastic-perfectly plastic material properties, is also shown in these two figures. The columns in the braced bay (Columns $1C_{B1}$ and $1C_{B2}$) were subjected to a significantly higher axial force demand than those in the DMRSF. Figure 6.78 suggests that Columns $1C_{B1}$ and $1C_{B2}$ yielded primarily in axial compression and tension at their bases during this test; this yielding contributed to the dissipation of the input energy during this test. The M-N points outside the yield surface at the bases of Columns $1C_{B1}$ and $1C_{B2}$ were a result of material strain-hardening at these locations. The negligible change in the axial force in Column $1C_{A2}$ is a result of this column being located approximately on the neutral axis of the CBDS in the plane of earthquake shaking.

The yielding of the columns in the braced bay had a beneficial effect on the energy dissipation capacity of the CBDS. However, it is of paramount importance to maintain the integrity of the vertical load carrying system and therefore, dissipating energy in the columns of a DMRSF is undesirable. Capacity design procedures that base the column design axial forces on both the gravity loads and the maximum strength of the concentric braces would, if used in conjunction with the strong column - weak girder design philosophy, improve the performance of these columns.

Concentric Brace Response:

The axial force versus axial deformation response for Braces Br1 and Br2 (Story 1), Braces Br3 and Br4 (Story 2), Brace 6 (Story 3) and Brace 8 (Story 4) are presented in Figures 6.79 and 6.80. The axial deformations of the concentric braces in the fifth and sixth stories were not measured and thus the hysteretic behavior of these four braces is unavailable. All of the six braces represented in these two figures buckled to some degree with Brace Br8 showing the largest degradation in strength (both compression and tension) and stiffness.

The unstable hysteresis of a tubular brace in the post-buckling range can be clearly seen in the response of Brace Br8. The loss of strength and stiffness in this brace appears in the brace shear and inter-story drift relationship (Figure 6.71) and in the brace story shear response profiles (Figure 6.75).

A detailed analysis of the response of the concentric braces in the CBDS is given by Uang and Bertero [2].

Energy Distribution:

The method described in Section 5.5 was used to calculate the input energy, the kinetic energy and the strain energy time histories. For the level of excitation used in this test, the input energy is dissipated primarily by inelastic behavior. Figure 6.81 shows the input energy, the kinetic energy, the elastic strain energy, the hysteretic energy and the viscous damped energy time histories for the MO-65 Test. The viscous damped energy time history was calculated as:

$$E_\mu = E_I - E_K - E_S - E_H \qquad (6.5)$$

where E_H was calculated using Equation 5.12. Three distinct bursts of input energy can be identified for this test at 4, 6 and 8-9 seconds; brace failures in the fifth story were initiated by the burst of input energy between the 8 and 9 second mark.

The distribution of the hysteretic energy (E_H) over the height of the *model* is shown in Figure 6.82; the distribution is relatively uniform over the height of the *model* in the lower five

stories but the contribution of the sixth story to the energy dissipation capacity of the *model* was negligible. The first story dissipated the greatest amount of input energy. This should be the case because for similar inter-story drifts with relatively stable behavior, the maximum first story shear forces were of the order of twice those in the fifth story. The fifth story dissipated the second largest amount of input energy because of the large drifts that developed as a result of brace rupture and the subsequent formation of a soft fifth story. After brace rupture, the fifth story hysteretic energy was dissipated solely by the DMRSF and although DMRSFs have proven to be stable energy dissipators, their energy dissipation is generally associated with inter-story drifts that are unacceptably large.

6.5.2 Eccentrically Braced Dual System - Taft-57 Test

Response Time Histories:

The measured table horizontal acceleration and displacement and the corresponding linear elastic response spectra for 0%, 2%, 5%, 10% and 20% damping are shown in Figure 6.83; the EPA of the Taft-57 Test was 0.44g which is 110% of the value used by the ATC 3-06 [11] for seismic design in a region of high seismic risk. The relative lateral displacement, inter-story drift, lateral inertia force and story shear force time histories at each level are shown in Figures 6.84 to 6.87, respectively. The lateral displacement time histories indicate that the *model* responded primarily in its first mode. Because of yielding in the shear links, especially at Levels L2 and L3 [1], the natural period of the *model* elongated to approximately 0.40 second during the Taft-57 Test; a 22% increase over its natural period of 0.326 second prior to testing but substantially less than the natural period of the DMRSF (= 0.672 second).

The time histories of total story shear and the story shear forces resisted by the eccentric braces are shown in Figure 6.87. The base overturning moment time history is shown in Figure 6.88; the overturning moment resisted by the eccentric braces is also shown in this figure.

Story Shear and Inter-story Drift Relationships:

The total story shear and inter-story drift relationships for each story are presented in Figure 6.89. The brace story shear (the horizontal component of the eccentric brace force) and

inter-story drift and the DMRSF story shear and inter-story drift relationships for each story are presented in Figures 6.90 and 6.91, respectively.

Nonlinear behavior was confined to the lower two stories of the *model* and the upper four stories of the *model* responded elastically. The nonlinear behavior can be attributed to yielding in the lower two shear links, yielding in the composite girders and cracking of the composite slabs above the lower two shear links.

Except for the bases of the braced bay columns, the DMRSF responded in a linear elastic manner in all six stories and did not contribute significantly to the energy dissipation in this test.

The six story shear ratios (SSR), shown in Figure 6.92, indicate that despite yielding in the shear links at Levels L2 and L3, the percentage of the story shear resisted by the eccentric braces remained relatively constant. The intermittent drop in the percentage of the first story shear force resisted by the eccentric braces corresponded to the times of significant yielding in Link L2 and the consequent decrease in the tangent stiffness of the the braced bay in the first story.

Maximum Response Envelopes:

The envelopes of maximum response of relative displacements, inter-story drifts, story shear forces, inertia forces and overturning moments over the height of the *model* are shown in Figure 6.93 and summarized in Table 6.8. Figure 6.93a indicates that the shear resistance of the braced bay was smaller in the first story than in the second story. Although the shear capacity of Links L2 and L3 were nominally identical, the floor-to-floor height in the first story was 30% greater than that in the second story. Accordingly, the horizontal component of the eccentric brace force, which is limited by the link's shear strength, was smaller in the first story than in the second story.

The ultimate lateral strength of the first story braced bay (defined as the maximum possible lateral load imparted to the first story eccentric braces) was reached during this test. In the *model*, Link L2 acted as a structural *fuse* and limited the axial forces that could be imparted to

the eccentric braces in the first story and therefore prevented their buckling. The DMRSF resisted all of the first story shear force beyond the ultimate lateral strength of the braced bay.

The lateral displacement, inertia force, story shear, inter-story drift and overturning moment profiles over the height of the *model* at the times of maximum base shear and maximum roof displacement are shown in Figure 6.94. The inertia force profiles are approximately rectangular in shape and are similar to those for the CBDS shown in Figure 6.74. Figure 6.83c indicates that the SDOFS responses to the Taft-57 record at the first two natural periods of the EBDS are approximately the same (Figure 6.83). This result is reflected in the inertia force time histories in Figure 6.87 where the contribution of the second mode is evident in the responses of the upper levels of the *model*.

The maximum inter-story drift index of 1.28% occurred in the first story. The maximum base shear coefficient (V_b/W_{at}) of 0.845 exceeded the UBC design base shear coefficient (=0.113) by a factor exceeding seven and exceeded the nominal yielding strength of the *model* (=$0.3W_{at}$) by a factor of 2.82 for this collapse limit state earthquake. As the *model* was not designed in accordance with the UBC, this result is not a reflection of the overstrength inherent in dual steel systems designed in accordance with the UBC but rather a comparison between the *design* base shear in a region of high seismic risk (=$0.113W_{drw}$) and the base shear that was developed during *severe* earthquake shaking.

Lateral Force Distribution:

The distributions of lateral force between the eccentrically braced bay and the DMRSF at the times of maximum base shear and maximum lateral displacement are shown in Figure 6.95. The total lateral force distribution in both cases reflects the formation of a soft first story.

Column Axial Force and Bending Moment Interaction:

The end moment (M) and axial force (N) interaction curves for the first story columns in Frames A and B are shown in Figures 6.96 and 6.97, respectively. The AISC [42] M-N yield surface, based upon linear elastic-perfectly plastic material properties, is also shown in these two figures. The columns in the braced bay (Columns $1C_{B2}$ and $1C_{B3}$) were subjected to a

significantly higher axial force demand than those in the DMRSF. Lüders bands were noted at the bases of both braced bay columns ($1C_{B2}$ and $1C_{B3}$) on the completion of the test and this observation is consistent with the information presented in the interaction curves. Yielding lines were not observed at the bases of the columns in Frames A and C. The negligible change in the axial force in Column $1C_{A2}$ is a result of this column being located approximately on the neutral axis of the EBDS in the plane of earthquake shaking.

Eccentric Brace Response:

The brace axial force versus axial deformation relationships for the eccentric braces in the first two stories (Braces Br1, Br2, Br3 and Br4) are presented in Figure 6.98 along with their nominal buckling loads (P_{cr}) and tensile strengths (T_y). The brace response was linear in all four of these braces. The axial deformations in the eccentric braces in the third, fourth, fifth and sixth stories were not measured and thus the hysteretic behavior of these eight braces is unavailable.

Shear Link Response:

The relationships between link shear force and shear strain for the Level 2 to Level 6 shear links are presented in Figure 6.99. The maximum shear strains ranged from 8.0% (0.08 radian) in Link L2 to 0.3% (0.003 radian) in Link L6. The Link L2 shear force versus shear strain relationship is presented in Figure 6.100; the shear yielding strength (V_p) and the corresponding shear strain (γ_y) of the bare steel link are also shown in this figure. The peak shear force in this composite shear link was 33.6 kips, that is, 210% of the nominal shear yielding strength of the bare steel link.

Energy Distribution:

The method described in Section 5.5 was used to calculate the input energy, the kinetic energy and the strain energy time histories. For the level of excitation used in this test, the input energy is dissipated primarily by inelastic behavior. Figure 6.101 shows the input energy, the kinetic energy, the elastic strain energy, the hysteretic energy and the viscous damped energy time histories for the Taft-57 Test. The viscous damped energy time history

was calculated using Equation 6.5. The distribution of the hysteretic energy (E_H) over the height of the *model* is shown in Figure 6.102, the distribution is highly non-uniform with the energy dissipation being concentrated in the lower two stories. The contribution of the sixth story to the energy dissipation capacity of the *model* was negligible. The distribution of the hysteretic energy dissipated by the shear links (E_L) over the height of the *model* is shown in Figure 6.103. The shear links accounted for nearly the entire hysteretic energy dissipation, dissipating in excess of 90% of the input energy. More than 70% and 15% of the energy dissipated by the shear links was dissipated in Links L2 and L3, respectively.

CHAPTER 7
EVALUATION OF THE EARTHQUAKE
SIMULATOR TEST RESULTS

7.1 General

In Chapter 6, three tests of the CBDS *model* and three tests of the EBDS *model* were described in detail. In this chapter, the pertinent results for these six tests are summarized and the responses of the *models* are compared. The behavior of the *models* at both the global and local levels is discussed in Section 7.2 and their response modification factors are derived and compared in Section 7.3. The lateral force distributions on both the CBDS and EBDS are discussed in Section 7.4. In Section 7.5, the ramifications of low-cycle fatigue and incremental collapse on the design and response of both CBDSs and EBDSs are discussed. The role of the DMRSF in both the CBDS and the EBDS is discussed in Section 7.6.

In Section 7.7, the data acquired during the testing of the CBDS and EBDS is used to compare the measured responses of the multi-degree-of-freedom (MDOF) *models* with the responses predicted using an equivalent single-degree-of-freedom (SDOF) system. This was done in an attempt to validate the use of SDOF response spectra for predicting the response of MDOF dual systems.

The seven limitations noted below must be carefully considered prior to extrapolating the results presented in Chapter 7 to other dual steel systems:

(1) Test Structures:

The *models* were bare steel structures and the interacting effects of non-structural components were not considered. Non-structural components such as internal masonry partitions and external cladding may play an important role in the response of buildings to earthquake shaking. Partitions can have a profound effect on the stiffness and strength of a building; their influence on the strength and deformation characteristics of a building depends on the degree to which they are isolated from the structural frame. A discussion of the effects of partitions on

seismic response of structures is given by Brokken and Bertero [43].

(2) Reactive Weight:

The *prototypes'* as-tested weight (W_{at}) of 1154 kips was significantly less than both the design gravity dead weight of 1742 kips and the design reactive weight (W_{drw}) of 1356 kips. For the design of the *prototypes*, the critical load cases involved a combination of the gravity dead loads (=1742 kips), gravity live loads and earthquake loads that were based upon W_{drw}. The earthquake loads dominated the design forces in the braced frames and because the conclusions presented below are generally related to the nominal yielding strength of the *models* (=$0.3W_{at}$), the lack of consistency between the design gravity dead load and the design reactive weight was not a major drawback to this testing program.

(3) Seismic Regulations:

The CBDS and EBDS *prototypes* were designed for a working stress base shear of approximately $0.2W_{at}$. This design base shear force is significantly higher than that required by current seismic regulations in the United States (Table 2.10). As such, the elastic stiffnesses, elastic strengths and maximum strengths of the CBDS and EBDS *prototypes* and *models* cannot be considered as representative of CBDSs and EBDSs designed according to the seismic regulations in the United States.

The variation of column, beam and brace cross-sectional sizes over the height of the *prototypes* (Figures 2.1 and 2.2 and Table 2.2) must be considered in any evaluation of the response quantities discussed in this chapter. In Chapter 2, it was noted that the *prototypes* were intended to represent a portion of a typical office building. Thus, the structural sections listed in Table 2.2 were not selected using optimization procedures, that is, the minimum required section sizes were generally not used. If optimization procedures had been used to design the *prototypes*, the overstrengths discussed in this chapter would have been significantly reduced.

(4) Torsional Excitation and Stiffness:

The *models* were symmetrically located with respect to the earthquake simulator excitation for all of the tests. Their centers of mass coincided with their centers of stiffness in the loading direction (parallel to Frame B) in each story; therefore, torsional loading was not introduced during testing. X-bracing was installed in Frames 1 and 3 to provide the *models* with a significant strength and stiffness in the transverse direction and significant torsional strength and stiffness.

(5) Foundations:

The foundations for both *models* were restrained against sliding, rocking and uplift; this foundation condition is rarely achieved in real buildings. The axial flexibility of the earthquake simulators vertical actuators and passive stabilizers introduced a rigid body rotational degree of freedom to the *models*. In principle, this effect is similar to that foundation condition associated with skin-friction piles, whereby the axial flexibility of the piles are such that a rigid-body rotational degree of freedom is introduced to the structure.

(6) Earthquake Ground Motions:

Recent earthquakes in Chile (1985) and Mexico (1985) resulted in strong motion records with significantly larger peak accelerations, strong motion durations and input energies, than either the 1978 Miyagi-Ken-Oki S00E or the 1952 Kern County Taft N21E earthquake records. Therefore, although the acceleration-scaled (peak acceleration $\geq$ 0.5g) Miyagi-Ken-Oki and Taft earthquake records were severe ground motions for both the CBDS and EBDS *models*, they should not be considered to be maximum credible ground motions for either the *models* or steel dual systems in general, if ground motions like those recorded at the Llolleo station during the 1985 Chile earthquake can occur in the United States.

(7) Concentric Braces:

In Chapter 3 it was noted that the CBDS *model's* concentric braces were fabricated from bent Grade 50 Cor10 steel plate, and seam welded to form square hollow sections. This

fabrication procedure resulted in a residual stress distribution over the cross-section of the tube that was far more favorable than that which would be typically found in cold-formed tubular sections, that is, the buckling strength of the CBDS *model's* braces would be higher than a cold-formed brace of similar length and geometry [44].

Studies on the cyclic response of concentric braces [2,45,46,47,48,49,50] have concluded that: filling tubular braces with expansive concrete extends the fracture life of tubular sections and improves their hysteretic behavior; the fracture life of square and rectangular tubular sections increases with an increase in slenderness ratio (l/r) and decreases with an increase in breadth-to-thickness (b/t) ratio; the fracture life of cold-formed structural tubes is significantly shorter than for wide-flange shapes; stocky bracing members ($l/r \leq 60$) dissipate more energy than slender bracing members ($l/r \geq 180$), and the fracture strain in cold-formed tubular sections ($\varepsilon_u^{max} \approx 10\%$) is much less than in hot-rolled or annealed tubular sections ($\varepsilon_u^{max} \approx 25\%$). The slenderness and compactness (b/t = breadth-to-thickness) ratios of the CBDS *model's* concentric braces varied between 48 and 78 (assuming an effective length factor, k, of 0.7), and 12 and 21, respectively.

The discussion of the response of the CBF and CBDS presented in the remainder of this chapter and in Chapter 8 implicitly assume braces of the type tested in the CBDS *model* on the earthquake simulator. Extrapolation of these results and conclusions to CBFs/CBDSs incorporating other types of bracing must account for the issues raised above.

7.2 CBDS and EBDS Response Characteristics

7.2.1 Maximum Strength and Global Deformation Responses

The lateral strengths of the CBDS and EBDS are presented in Figure 7.1, as a function of roof drift index, which is defined as the relative lateral roof displacement divided by the height of the *model*. These two curves were constructed from the data acquired from the earthquake simulator testing of the two *models*.

As noted in Chapter 2, the CBDS *prototype* was designed according to the 1979 Uniform Building Code and the 1981 Japanese Aseismic Code [9]. The nominal yielding strength requirements of the 1981 Japanese Aseismic Code for the *models* are also presented in Figure 7.1, in order to provide a basis for the discussion of the overstrengths observed in the *models*.

In deriving the design yielding strengths of the *models*, the braced frame was assumed to be ductile enough to allow development of the yielding strength of the DMRSF. The summation of their individual yielding strengths overestimates the strengths at first significant yielding of both the CBDS and EBDS *models*, because the braced frames yield at inter-story drift indices that are approximately 1% less than the DMRSF's inter-story drift indices at first significant yielding.

For the design of the CBDS *prototype*, the working stress base shear force was $0.197W_{drw}$, of which 66% was apportioned to the bracing (=0.130) and 34% to the DMRSF (=0.067). By factoring the working stress coefficient of 0.197 to the level of first significant yielding ($C_s/0.80$ - see Section 2.7) and accounting for the difference between the as-tested reactive weight (W_{at}) and the design reactive weight (W_{drw}) by multiplying the resulting yielding coefficient by a factor of 1.18 (=1356/1154), the design yielding strength of the CBDS *prototype* is $0.3W_{at}$. That is, the CBDS *prototype* is designed to have a nominal yielding strength of $0.3W_{at}$. Since the CBDS *model* was a similitude scaled version of the CBDS *prototype*, $0.3W_{at}$ is assumed to be the design yielding strength of the CBDS *model*.

The beam and column sizes in the EBDS *prototype* were identical to those in the CBDS *prototype*, because it was impractical to change them for the multi-phase testing program. Foutch [51] analyzed the EBDS *prototype* and found that the total allowable base shear at the working stress level on the first story braced bay was 162 kips, or, $0.12W_{drw}$. By including the strength contribution of the DMRSF (=$0.067W_{drw}$), the EBDS *prototype's* working stress base shear coefficient is equal to $0.187W_{drw}$, or, 95% of the CBDS's coefficient of 0.197. Factoring the working stress coefficient of $0.187W_{drw}$ to the level of first significant yielding ($C_s/0.80$) and accounting for the difference between W_{at} and W_{drw} by multiplying the resulting

yielding coefficient by a factor of 1.18 (=1356/1154), the design yielding strength of the EBDS *prototype* is $0.28W_{at}$. For the purposes of these studies, the design yielding strength of the EBDS *prototype* is assumed to be equal to that of the CBDS *prototype*, namely $0.3W_{at}$. The plastic shear capacities of the shear links at Level L2 of the EBDS *model* (similitude scaled) and the EBDS *prototype* were within 1% of one another. As the remainder of the EBDS *model* was a similitude scaled version of the EBDS *prototype*, $0.3W_{at}$ is also assumed to be the design yielding strength of the EBDS *model*.

In addition to the design yielding strengths of the *models*, the minimum strength and maximum deformation requirements of the 1985 UBC, 1984 ATC and 1986 SEAOC are presented in Figure 7.1. The design yielding strength requirements of these regulations (Table 2.10) have been multiplied by 1.18 to account for the differences between W_{at} and W_{drw}. The minimum strength requirements of these three seismic regulations have been presented to illustrate the significant differences between the seismic regulations currently used in the United States and Japan.

Concentrically Braced Dual System:

The peak shear resistance of the CBDS was $0.73W_{at}$, or 243% of its design yielding strength of $0.3W_{at}$. This occurred at a roof drift index of 0.88%. The peak shear resistance of the CBDS was achieved during the MO-65 Test whose effective peak acceleration (EPA) was 0.40g. The point of peak roof drift index (=0.92%) in Figure 7.1 corresponded to the formation of a soft fifth story.

Eccentrically Braced Dual System:

The peak shear resistance of the EBDS was $0.86W_{at}$, or 285% of its design yielding strength of $0.3W_{at}$. This occurred at a roof drift index of 0.70%. The peak shear resistance of the EBDS was achieved during the Taft-66 Test whose effective peak acceleration (EPA) was 0.53g. The point of peak roof drift index corresponded to the formation of a soft first story.

Comparison and Discussion:

The elastic stiffness of the EBDS was slightly greater than that of the CBDS and this was due primarily to the use of larger bracing members in the EBDS. The maximum shear resistance of the EBDS was 17% greater than that of the CBDS although their design yielding strengths were identical. The greater strength of the EBDS was achieved because the structural elements controlling the response of the EBDS, namely the shear links, were stressed to a level approaching the ultimate tensile stress, while the elements controlling the response of the CBDS, namely the concentric braces, could not strain-harden before buckling. Furthermore, the lightweight concrete slab acted compositely with the steel shear links to increase their shear strengths and therefore the strength of the EBDS, further.

From the standpoint of maximum strength and global displacement, a number of conclusions can be drawn from the results presented above:

• The CBDS and EBDS exhibited strengths significantly greater than both their design yielding strengths and the minimum strengths required by current seismic regulations in the United States. The EBDS was appreciably stronger than the CBDS as a result of strain-hardening in its critical structural elements and the contribution of the concrete slab to the strength of those critical elements.

• The CBDS and EBDS maximum roof drift indices of 0.92% and 0.70%, respectively, were significantly less than the maximum inter-story drift indices deemed acceptable by current seismic regulations in the United States. The CBDS maximum roof drift index of 0.92% was 31% greater than the EBDS's maximum roof drift index, although the EBDS was subjected to an earthquake ground motion with an EPA that was 32% higher than the EPA of the severest earthquake ground motion used to test the CBDS.

Finally, it should be noted that the *models* were designed for base shear coefficients that were significantly greater than the minimum strength requirements of the 1986 SEAOC, namely 0.164 for the CBDS and the 0.100 for the EBDS (Table 2.10). These significantly lower minimum strength requirements for both CBDSs and EBDSs will lead to CBDSs and

EBDSs with maximum strengths that are significantly smaller than those described above for the *models*.

Using the parameters of maximum shear resistance and roof displacement as performance indices, the EBDS was superior to the CBDS. However, these two parameters alone cannot be used to quantify the seismic behavior of structural systems. The strength and deformation response of the individual stories and the energy dissipation capacity of the building at both the global and local levels, will also control the seismic response of a building. The performances of the CBDS and EBDS, as a function of these latter parameters, are discussed in the following three sub-sections.

7.2.2 CBDS and EBDS Story Shear and Deformation Responses

The envelopes of total story shear (V^{TOTAL}), the story shear resisted by the braces (V^{BRACE}) and the story shear resisted by the DMRSF (V^{DMRSF}), as a function of inter-story drift index for the CBDS and EBDS, are shown in Figures 7.2 and 7.3, respectively. The DMRSF story shear includes that shear force resisted by the three columns in Frame B.

The envelopes presented in these three figures were constructed from the results of four tests of the CBDS: the MO-06, MO-16, MO-33 and MO-65 Tests; and four tests of the EBDS: the MO-07, MO-28, Taft-57 and Taft-66 [1] Tests.

Concentrically Braced Dual System:

In the first, second and third stories, the strength versus deformation envelopes were all stable despite the fact that the concentric braces buckled in these stories during the MO-33 and MO-65 Tests. In all three cases however, the braces did not rupture and showed no loss of strength up to inter-story drift indices of 0.87%. The lateral stiffness and strength stiffness of this DMRSF was such that it resisted between 35% and 45% of the inertia forces in these three stories but remained essentially elastic over the course of the testing program.

The concentric braces in the fourth and fifth stories showed signs of strength degradation at inter-story drift indices exceeding 0.5%; the strength degradation resulted from the severe

buckling of Braces Br7, Br8, Br9 and Br10. The rupture of the concentric braces in the fifth story is clearly evident in Figure 7.2 where the V^{BRACE} component becomes negligible for the MO-65 Test at the point of maximum inter-story drift index (=1.89%). In this story, the DMRSF resisted the total story shear following the rupture of the concentric braces, with only a minor degree of inelastic behavior.

Eccentrically Braced Dual System:

Nonlinear behavior was confined to the lower three stories of the EBDS; the response of the upper three stories of the EBDS remained elastic. In the first and second stories, the strength versus deformation envelopes were stable up to inter-story drift indices of approximately 1.3%.

The DMRSF was significantly more flexible than the eccentrically braced frame. It remained essentially elastic throughout the testing program and did not contribute significantly to energy dissipation in the EBDS, even at its maximum inter-story drift index of 1.3%.

7.2.3 Response in the Critical Stories of the CBDS and EBDS

The fifth story of the CBDS and the first story of the EBDS were chosen for comparison purposes because the failures of these *models* were initiated in these two stories. The envelope of fifth story shear force versus fifth inter-story drift index for the CBDS is presented in Figure 7.4 and the envelope of first story shear force versus first inter-story drift index for the EBDS is presented in Figure 7.5. The UBC, ATC and SEAOC minimum strength and maximum deformation requirements, factored to the level of first significant yielding are presented in Table 2.10. In the CBDS envelope presented in Figure 7.4, the strength requirements of the UBC, ATC, SEAOC and the 1981 Japanese Aseismic Code have been factored by the ratio of the design fifth story shear force over the design base shear force. In all four cases, the strength requirements were multiplied by a factor equal to 0.484, because the lateral force distributions suggested by the UBC, ATC, SEAOC and the Japanese Aseismic Code were identical for the CBDS *model*.

Concentrically Braced Dual System:

The peak shear resistance of the fifth story of the CBDS was 42.4 kips, or 270% of its design yielding strength of 15.5 kips. This peak shear corresponded to a fifth inter-story drift index of approximately 1.5%. The peak shear resistance of the concentric braces in the fifth story (that is, the braced bay) was 15 kips (Figure 7.4). This is approximately equal to the design yielding strength of the fifth story of the CBDS and is 50% greater than the design yielding strength of the braced bay in the fifth story (=0.66×15.5).

The shear resistance of the fifth story of the CBDS at the level of first significant yielding was approximately 28 kips, or 180% of the design yielding strength of the fifth story of the CBDS. This occurred at a fifth inter-story drift index of approximately 0.6%. The stiffness of the fifth story of the CBDS was in excess of 100% greater than the minimum stiffnesses required by the UBC, ATC and SEAOC.

Following buckling of the fifth story concentric braces at an inter-story drift index of approximately 0.5%, the shear resistance of the fifth story braced bay degraded rapidly, such that, at a fifth inter-story drift index of 1.5%, the shear resistance of the fifth story braced bay was only 45% of its maximum value. At a fifth inter-story drift index of 1.9%, the shear resistance of the fifth story braced bay was completely lost.

The design yielding strength of the fifth story of the DMRSF is:

$$V_{DMRSF}^5 = 0.484 \times 0.34 \times 0.3 \times 107.1 = 0.484 \times 10.9 = 5.1 \text{ kips}$$

where, the factor 0.484 is as discussed above and 10.9 kips is the design yielding strength of the first story of the DMRSF. The maximum stress ratio (f_a/F_a in AISC [42] nomenclature) in the DMRSF's fifth story beams and columns, based on the most severe of the 1985 UBC's load cases (DL+LL+0.25EQ) for the DMRSF, was 0.5. Limit analyses [1,2] showed that the maximum strength of the fifth story of the DMRSF, assuming a soft fifth story mechanism, was 36.6 kips, or 710% of its design yielding strength. These results clearly indicate that the design of the CBDS's DMRSF is extremely conservative; that is, the lateral stiffness and

strength of the CBDS's DMRSF should be considered to be significantly greater than required for dual systems in the United States. The peak shear resistance of the fifth story of the DMRSF was approximately 40 kips, that is, 108% of its predicted ultimate strength of 36.6 kips. This 8% overstrength can be attributed to strain-hardening in the fifth story columns.

It is evident from Figure 7.4 that the DMRSF played a crucial role in the response of the CBDS. At a fifth inter-story drift index of approximately 0.6%, the DMRSF became the primary lateral load resisting system. The elastic stiffness of the DMRSF in the fifth story was approximately 65% of the elastic stiffness of the concentrically braced frame. The elastic stiffness and strength of the DMRSF permitted the CBDS to develop a strength equal to 273% of the fifth story design yielding strength (=15.5 kips) and the DMRSF stabilized the response of the fifth story of the CBDS up to an inter-story drift index of 1.5%.

Eccentrically Braced Dual System:

The peak shear resistance of the first story of the EBDS was 91.6 kips, or 285% of its design yielding strength of 32.1 kips. This occurred at a first inter-story drift index of approximately 1.28%. The peak shear resistance of the eccentric braces in the first story was 55.2 kips. This is 170% of the design yielding strength of the first story of the EBDS and 260% of the design yielding strength of the braced bay in the first story. The enhanced strength and stiffness of the first story of the EBDS resulted from: the increased strength of Link L2 that resulted from its composite action with the lightweight concrete slab; and the ductility of the eccentrically braced frame ($\mu_{ebf}^1 \approx 3.2$) that enabled the DMRSF to contribute to the strength of the EBDS.

The shear resistance of the first story of the EBDS, at the level of first significant yielding, was approximately 52 kips, or 162% of the design yielding strength of 32.1 kips. This occurred at a first inter-story drift index of 0.40%. The stiffness of the first story of the EBDS was in excess of 115% greater than the minimum stiffness required by the UBC, ATC or SEAOC.

The design yielding strength of the first story of the DMRSF is:

$$V^1_{DMRSF} = 0.34 \times 0.3 \times 107.1 = 10.9 \text{ kips.}$$

Limit analyses [1] showed that the maximum strength of the DMRSF, assuming a soft first story mechanism, was 60.2 kips, that is, 550% of its design yielding strength. The peak shear resistance of the first story of the DMRSF was approximately 36 kips, that is, 60% of its maximum predicted strength.

The shear link at Level L2 of the EBDS failed at a first inter-story drift index of approximately 1.3%; this drift index exceeds that permitted by SEAOC (=1.12%) for EBDSs, but is less than that permitted by the UBC and ATC for steel dual systems. Generally, unless the inter-story drift limits are dictated by the lack of flexibility in the non-structural elements, inter-story drift indices of the order of 1.5% to 2.0% are acceptable. Furthermore, typical DMRSFs are so flexible that they will not yield at levels of inter-story drift index less than 1.25%. Two of the intended roles of the DMRSF in a dual system are: (1) to supply additional strength and stiffness to the primary lateral load resisting system during severe earthquake shaking; and (2) to dissipate a portion of the input energy during severe earthquake shaking. Thus, there is no reason to limit the maximum inter-story drift index in an EBDS to 1.12%, *if* the eccentrically braced frame can be safely deformed to greater levels of inter-story drift index.

It is possible to select the desired strength and elastic stiffness of an eccentrically braced frame through the judicious choice of link lengths and cross-sections [1]. Although Link L2 (Figure 5.8) failed at an inter-story drift index of 1.3%, a first inter-story drift index of between 1.6% and 1.8% could have been achieved without failure by using a longer shear link at Level L2. By using longer shear links, the eccentrically braced frame could have been designed to yield at a first inter-story drift index of approximately 0.6% rather than at 0.4%. Assuming a displacement ductility of three, a maximum first inter-story drift index in excess of 1.5% could have been achieved. At this inter-story drift index, the strength and energy dissipation capacity of the DMRSF could have been mobilized.

Comparison and Discussion:

The failure of the CBDS resulted from the rupture of its concentric braces in the fifth story during the MO-65 Test. The EBDS failed as a result of flange fracture in the shear link at Level L2 (Link L2) during the Sine-70 Test (Table 5.2).

There is a marked difference between the post-elastic responses of the critical stories in the CBDS (fifth story) and the EBDS (first story). Upon buckling and rupture of the fifth story concentric braces, the lateral load carrying capacity of the concentrically braced bay in the fifth story was lost. The rupture of these braces resulted from severe local buckling in the plastic hinge regions at the braces' midspans and ends. These braces exhibited a serious loss of strength and stiffness upon severe buckling, failing in a non-ductile manner. Their failure led to a significant increase in the inter-story drift index in the fifth story (Θ_{max}^5 = 1.89%), exceeding the maximum inter-story drift index limits of the UBC (=1.5%), ATC (=1.5%) and SEAOC (=1.12%). The DMRSF played a critical role in the response of the fifth story of the CBDS because it provided sufficient strength and stiffness for the strength versus deformation response to remain stable after buckling of the concentric braces. As the DMRSF was designed for lateral loads that were more than twice that required by the UBC, its stiffness can also be considered to be significantly greater than the stiffness which would have been obtained by satisfying the minimum UBC requirements. Thus, if a DMRSF designed according to the minimum UBC requirements, had been incorporated into the CBDS instead of the as-tested DMRSF, the strength of the fifth story of the CBDS would have quickly degraded following brace buckling, and significantly larger inter-story drifts would have resulted.

The tangent stiffness of the eccentrically braced bay in the first story of the EBDS was reduced by a factor of five upon yielding of the shear link at Level L2. This reduced the tangent stiffness of the first story of the EBDS by a factor of three. Despite this reduction in the tangent stiffness, the shear resistance of the first story of the EBDS continued to increase with increasing deformation up to the maximum first inter-story drift index of 1.3%.

In a dual system, the advantages of a ductile bracing system during severe earthquake shaking include: a significant capability to dissipate energy in the braced frame; and the ability to mobilize the strength of the DMRSF to complement the strength of the braced frame. The displacement ductility of the *ith* story of either the concentrically or eccentrically braced frame (μ_{bf}^i) can be defined as

$$\mu_{cbf}^i, \mu_{ebf}^i = \frac{\Theta_{max}^i}{\Theta_y^i} \qquad (7.1)$$

where Θ_{max}^i is the *ith* inter-story drift index corresponding to the maximum shear strength of the braced frame in the *ith* story and Θ_y^i is the *ith* inter-story drift index corresponding to the point of first significant yielding in the braced frame in the *ith* story. Note that the drift index at point of maximum shear strength will not necessarily correspond to the maximum drift index. As noted above, the critical stories in the CBDS and EBDS were the fifth and first stories, respectively. For the eccentrically braced frame (EBF) in the EBDS, μ_{ebf}^1 was approximately three, while for the concentrically braced frame (CBF) in the CBDS, μ_{cbf}^5 was of the order of only one; in both instances, Θ_y was between 0.4% and 0.6%. The significant difference in the ductilities of the CBF and EBF is a major difference between CBDSs and EBDSs and influences the roles of the DMRSF in these dual systems.

The strength and stiffness of the concentrically braced frame degraded quickly following brace buckling. At the point of strength degradation in the concentric braces in the fifth story, that is, at $\Theta^5 = 0.6\%$, the DMRSF was forced to assume the role of the primary lateral load resisting system. If the stiffness of the DMRSF in the CBDS *model* had been reduced by approximately 40%, the response of the fifth story of the CBDS would have degraded quickly following brace buckling.

The shear resistance of the first story of the eccentrically braced frame did not degrade following shear yielding of the link at Level L2. The strength of the eccentrically braced bay continued to increase following the yielding of Link L2 up to the point of its failure at a first inter-story drift index of 1.3%. The DMRSF in the EBDS performed its intended role in the

dual system, that is, it provided additional strength and stiffness following yielding of the primary lateral load resisting system. At no stage did the DMRSF replace the eccentrically braced frame as the primary lateral load resisting system. Irrespective of the stiffness of the DMRSF in the EBDS *model*, the response of the first story of the EBDS would have remained stable up to drift levels in excess of those permitted by SEAOC (=1.12%) because the eccentrically braced frame provided stable ductility. The following conclusions can be drawn from the results of the story strength versus deformation envelopes:

- The eccentrically braced frame possessed significant ductility whereas the ductility of the concentrically braced frame was limited by the lack of ductility in its tubular concentric braces.

- The ductility of the eccentrically braced frame permitted the DMRSF to perform its intended role in the dual system, that is, to provide stiffness and strength to the EBDS after the eccentrically braced frame had yielded. The lack of ductility in the concentrically braced frame required the DMRSF to assume the role of the primary lateral load resisting system in order to prevent the premature failure of the CBDS.

7.2.4 Energy Dissipation and Distribution

The use of energy methods as design tools for earthquake resistant design has become a subject for intensive research over the last few years [1,2,41]. The two issues that must be addressed in this field of research are: the need for reliable input energy spectra, and the need for analytical techniques to estimate the energy dissipation capacity of a given building.

Three objectives of a comprehensive earthquake-resistant design are: the use of structural systems with energy absorption and dissipation mechanisms that offer stable hysteretic behavior; the maximization of the energy absorption and dissipation capacities of the structural elements and sub-assemblages in the chosen structural system, and the mitigation of structural damage in the chosen structural system. The latter objective is related to distributing the energy dissipation over the height of a building such that a uniform inelastic deformation profile can be achieved.

Concentrically Braced Dual System:

The CBDS dissipated approximately 400 kip-inches of energy by inelastic behavior during the MO-65 Test (Figure 6.82); of this 400 kip-inches, 29%, 18%, 10%, 20% and 23% were dissipated in the first to fifth stories, respectively; the sixth story remained essentially elastic and did not contribute to energy dissipation in the CBDS.

The energy absorbed by a story of the *model* was defined in Section 5.5 as the integral of the story shear force with respect to the inter-story drift; the energy dissipated by a story was defined as the absorbed energy less the elastic strain energy stored in that story. For a uniform inter-story drift over the height of a building, the first story will dissipate the greatest amount of energy and the top story will dissipate the least amount of energy, because the shear forces are maximized in the first story and minimized in the top story. Due to severe brace buckling in the fourth (Figure 6.80) and fifth stories, the inter-story drifts in these two stories were greater than those in the second and third stories. Therefore, although the story shear forces in the fourth and fifth stories were smaller than those in the lower stories, the larger inter-story drifts in these stories resulted in more energy being dissipated in these two stories than in the second and third stories.

The fifth story strength versus deformation envelope remained stable following severe buckling and rupture of its concentric braces because of the contribution of the DMRSF to the stiffness and strength of the CBDS's fifth story. The DMRSF remained elastic for fifth inter-story drift indices smaller than 1.5%. Therefore, the DMRSF only dissipated energy in the fifth story at inter-story drift indices greater than 1.5%. As such, the DMRSF dissipated only 34% of the total energy dissipated in the fifth story with the concentric braces dissipating the remaining 66% through brace buckling.

Three conclusions can be drawn from the results presented above; namely,

- Energy can be dissipated by the buckling of the concentric braces in a concentrically braced frame provided that brace rupture, due to local buckling, is prevented.

- The inelastic response of the concentric braces was characterized by strength and stiffness degradation (Figures 6.71 and 6.80). Strength and stiffness degradation in the concentric braces led to the loss of their ability to dissipate energy in a stable manner.

- The elastic flexibility of the DMRSF in the CBDS precluded it from contributing to energy dissipation in the CBDS at levels of inter-story drift index below the maximum values permitted by the current earthquake-resistant design regulations in the United States, that is, 1.5% for the UBC and ATC and 1.12% for SEAOC.

Eccentrically Braced Dual System:

The EBDS dissipated approximately 400 kip-inches of energy by inelastic behavior during the Taft-57 Test (Figure 6.102); of this 400 kip-inches, 70%, 19%, 5%, 4% and 2% were dissipated in the first to fifth stories, respectively. The sixth story of the EBDS remained elastic during the Taft-57 Test and did not contribute to its energy dissipation (Figure 6.102).

As a result of the method used to estimate the shear force in the six shear links [1], the link energy time histories shown in Figure 6.103 overestimate, by between 10% and 15%, the energy dissipated by the six shear links. This is the reason for the discrepancy between Figures 6.102 and 6.103, where the energy dissipated by Link L2 exceeds the energy dissipated in the first story. However, it is evident that the shear links in this EBDS dissipated between 85% and 95% of the cumulative input energy.

The DMRSF contributed significantly to the strength and stiffness of the first story of the EBDS following the yielding of the shear link at Level L2 (Figure 7.5). The DMRSF's first story shear versus first inter-story drift index envelope remained essentially linear throughout the testing program, even at the maximum first inter-story drift index of 1.3%. As such, the DMRSF did not contribute to energy dissipation in the first story, except for a small number of cycles during which plastic hinges formed at the bases of Columns $1C_{B2}$ and $1C_{B3}$ (Figure 6.97).

A number of conclusions can be drawn from these test results; namely,

- The shear links at Levels L2 and L3 of the EBDS dominated the energy dissipation capacity of the EBDS.

- Shear links are extremely good energy dissipators and they dissipate energy in a stable, ductile manner for a large number of severe yielding cycles.

- The flexibility of the EBDS's DMRSF precluded it from contributing to energy dissipation in the EBDS at levels of inter-story drift index corresponding to the failure of the EBF (=1.3%).

Comparison and Discussion:

There are two issues regarding energy dissipation that must be considered in comparing the relative merits of the CBDS and EBDS. First, the structural system under consideration must be capable of dissipating a large amount of energy per cycle of loading. Secondly, the structural system must maintain its ability to dissipate energy for a large number of cycles, that is, it must possess stable hysteretic behavior. The second issue is of paramount importance because the earthquake records used to test both the CBDS and EBDS, were characterized by moderate durations of strong motion shaking. Recent earthquakes in Chile (1985) and Mexico (1985) had durations of strong motion shaking that were several times longer than either the Miyagi-Ken-Oki or Taft earthquake records. The cumulative energy demands from the Chile and Mexico earthquakes would be significantly greater than those of the Miyagi-Ken-Oki and Taft earthquake records for structures within a wide range of fundamental periods [52]. Thus, buildings must possess *stable* hysteretic behavior in order to provide good energy dissipation capacity for a *large* number of yielding cycles.

Although the CBDS and the EBDS each dissipated approximately 400 kip-inches of energy during the MO-65 Test (Figure 6.82) and the Taft-57 Test (Figure 6.102), respectively, the hysteretic behavior of those elements dissipating the input energy were significantly different. These differences are discussed below, in terms of the two issues noted above.

The CBDS was subjected to three earthquake simulations with peak accelerations between 15%g and 35%g and one earthquake simulation with a peak acceleration of 65%g (MO-65 Test), prior to the rupture of its concentric braces in the fifth story. The CBDS exhibited a relatively uniform energy dissipation profile over its height during the MO-65 Test, with maximum inter-story drift indices of 0.87%, 0.83%, 0.81%, 1.20%, 1.89% and 0.66%, in the first to sixth stories, respectively. The uniform energy dissipation profile in the lower five stories was a consequence of large inter-story drifts being developed in the fourth and fifth stories. The hysteretic behavior in the fourth and fifth stories was poor (Figures 6.70 and 6.71). The strength and stiffness degradation in the braced bays of these two stories was accompanied by large inter-story drifts, especially in the fifth story where the maximum inter-story drift index reached 1.89%. The ability of the fifth story of the CBDS to dissipate energy was dramatically reduced by the rupture of its concentric braces. Although the concentric braces dissipated a significant amount of energy upon buckling, it was not possible to prevent local buckling at their midspans and ends, and their subsequent rupture in these locations.

It is worth noting that the cumulative duration of strong-motion shaking of the four Miyagi-Ken-Oki earthquake simulation tests was shorter than the strong motion duration of the 1985 Chile earthquake. Thus, one could infer that CBFs and CBDSs are susceptible to failure if they are subjected to earthquakes with long durations of strong-motion shaking because of the potential for strength and stiffness degradation of their concentric braces.

The optimization of energy dissipation in a concentrically braced frame has been considered by Khatib et al. [13]. The *zipper* scheme proposed by Khatib involves lacing several stories of concentric braces together at the brace-to-girder connections (Figure 7.6); this scheme attempts to promote simultaneous buckling in the concentric braces over the height of the concentrically braced frame, thereby maximizing the frame's ability to dissipate energy.

The EBDS was subjected to six earthquake ground motions with peak accelerations between 15%g and 35%g and five earthquake ground motions with peak accelerations exceeding 40%g (Table 5.2). Energy dissipation in the EBDS was dominated by energy dissipation

in its shear links (Figure 6.103). In the Taft-57 Test, the shear links dissipated in excess of 90% of the input energy and of the energy dissipated in the shear links, more than 70% was dissipated in Link L2. Link L2 provided stable hysteretic behavior for a large number of yielding cycles without any evidence of strength degradation, even with shear strains approaching the level associated with severe web buckling (Figure 6.100). Furthermore, Whittaker et al. [1] previously observed that the EBDS's Link L2 survived more than 350 yielding reversals, of which more than 100 exceeded a shear strain ductility of 10. The results presented in this section and in Chapter 6 confirm the results obtained by other researchers [3,4,21] working in the field of eccentrically braced frames, namely: shear links exhibit stable hysteretic behavior for a large number of yielding cycles provided that they are properly designed and fabricated; and as a result shear links are extremely good energy dissipators.

The EBDS exhibited a highly nonuniform energy dissipation distribution. In excess of 70% and 15% of the hysteretic energy dissipation in the EBDS occurred in its first and second stories, respectively, during the Taft-57 Test (Figure 6.102). This nonuniform distribution of energy dissipation resulted in part from the fact that the EBDS was a modified version of the previously tested CBDS. In particular, the shear links in the eccentrically braced frame were not designed specifically for the internal force distribution resulting from the application of the design lateral forces (Section 2.6). The concentration of damage in the first and second stories of the EBDS was undesirable, because the EBDS's potential for energy dissipation in its upper stories was not mobilized. The nonuniform energy dissipation (damage) distribution was reflected in the distribution of shear strains in the shear links over the height of the EBDS. The maximum strains in the shear links varied by a factor of twenty. Ideally, the maximum shear strains in all of the shear links should be identical.

To improve the distribution of energy dissipation and damage in this EBDS and particularly in the eccentrically braced frame (EBF), it would be desirable to force rigid body displacement fields on both sides of the shear links, over the height of the EBF, by lacing the ends of the shear links together (Figure 7.6). This rigid body displacement field would:

maximize the strength of the eccentrically braced frame; maximize the ability of the eccentrically braced frame to dissipate energy; ensure an even distribution of damage, that is, a uniform inter-story drift index, over the height of the EBDS, and reduce the likelihood of failure by low-cycle fatigue and incremental collapse. A comparison of the energy dissipated by a six-story EBF forming a complete mechanism involving all six stories, and forming a soft first story, is presented in Appendix A.

The conclusions that can be drawn from the comparison of the energy dissipation capabilities of the CBDS and EBDS are as follows:

• The brace buckling mechanism can dissipate a significant amount of energy per cycle of loading provided that local buckling is avoided.

• The overriding concern regarding the use of concentrically braced frames incorporating cold-formed tubular braces is the susceptibility of their braces to local buckling and rupture during a severe earthquake with a long duration of strong-motion shaking, such as those recorded in Chile and Mexico in 1985.

• Although suggestions have been made to improve the fracture life of tubular braces, no technique has been developed that will permit the tubular braces to buckle repeatedly without rupture.

• Concentrically braced frames with cold-formed, stocky tubular steel braces exhibit little ductility prior to the degradation of their stiffness and strength. If concentrically braced frames are to be used in regions of high seismic risk, their strengths should be based on a design response spectrum that is not reduced by a ductility factor (see Section 7.3).

• Shear links exhibit stable hysteretic behavior for a large number of severe yielding cycles and are ideally suited for buildings sited in regions of high seismic risk.

• Eccentrically braced frames can provide significant ductility if their shear links are properly designed and fabricated.

7.3 CBDS and EBDS Response Modification Factors

General:

The ATC [11] introduced a Response Modification Factor (R) to derive an inelastic design response spectrum (IDRS) from its linear elastic design response spectrum (LEDRS). The minimum design base shear is then based on this IDRS. The ATC Commentary states that "...the response modification factor, R, and ... have been established considering that structures generally have additional *overstrength* capacity above that whereby the design loads cause significant yield...", and that R "... is an empirical response reduction factor intended to account for both *damping* and the *ductility* inherent in the structural system at displacements great enough to surpass initial yield and approach the ultimate load displacements of the structural system....". The ATC specifies a value of R equal to 6 for steel dual systems incorporating braced steel frames and does not differentiate between CBDSs and EBDSs.

SEAOC [12] also adopts a Response Modification Factor (R_w) to reduce its LEDRS to an IDRS. The factor R_w is larger than R because the SEAOC reduces its LEDRS to a working stress level rather than to the ATC's level of first significant yielding. Assuming a maximum steel stress equal to $0.8\sigma_y$, that is, accounting for the 33% increase in the allowable stresses under earthquake loading ($=0.6\sigma_y \times 4/3$), the SEAOC values of R_w should be 25% greater than the ATC's corresponding R values. SEAOC specifies values of R_w equal to 10 and 12 for CBDSs and EBDSs, respectively. Scaling these values of R_w to yielding levels (R_w^*), the values of R_w^* are equal to 8 and 9.6, respectively. These values are 33% and 60% greater than the ATC recommended values of R for dual steel systems.

In the ensuing discussion, the ATC's definition of the response modification factor is used to estimate the values of R for the CBDS and EBDS *models* from the experimental results.

The response modification factor can be defined as the product of three reduction factors [1]; namely,

$$R = R_\mu \times R_S \times R_\xi \qquad (7.2)$$

These reduction factors are defined as follows:

(i) The ductility factor, R_μ, accounts for the reduction in the required elastic strength, LERS(ξ,T) due to ductility. Newmark and Hall [53] suggest that R_μ be set equal to 1.0, $\sqrt{2\mu - 1.0}$ or μ, depending on the fundamental period of the structure.

(ii) The strength factor, R_S, is defined as

$$R_S = \frac{\text{Maximum Strength Ratio}}{C_y} = \frac{C_s}{C_y} = (\text{OSR}+1) \qquad (7.3)$$

where C_s is equal to the peak shear resistance divided by the reactive weight, C_y is the design yielding strength divided by the reactive weight and OSR is the overstrength. The overstrength can be defined as the peak shear resistance minus the design yielding strength, divided by the reactive weight. Overstrength in a structure results from the use of non-optimal structural sections, material overstrength, inelastic redistribution of internal forces, material strain-hardening and certain code-based minimum requirements. The strength factor associated with a structure designed using optimization techniques will be a function of the latter four parameters.

(iii) The damping factor, R_ξ, accounts for the reduction in the required elastic strength due to an increase in damping resulting from inelastic behavior. The ATC and SEAOC use a 5% damped LEDRS as the basis for developing their design response spectra. The use of 5% damping will overestimate the true level of damping present in the majority of steel buildings in the United States. Accordingly, the damping factor can generally be assumed to be equal to, or less than, one.

The response modification factor for the CBDS can be calculated from the MO-65 Test by comparing the linear elastic response spectrum (LERS) of the MO-65 Test and the design yielding strength of the CBDS *model*. In Figure 7.7, the MO-65 LERS for 2% damping, similitude scaled to full-scale units, is presented in addition to the design yielding strength of the

CBDS ($=0.3W_{at}$) and the maximum shear resistance of the CBDS ($=0.73W_{at}$). For an average value of the CBDS *model's* period, similitude scaled to full-scale units (0.66 to 0.79 second), the total reduction from the MO-65 LERS to the CBDS's design yielding strength of $0.3W_{at}$, is by a factor of 4.5 with a strength factor (R_S) equal to 2.43 and a ductility factor (R_μ) equal to 1.85. As the LERS was constructed for a damping ratio of 2%, which is roughly equal to the first modal damping ratio of the CBDS, the damping factor, R_ξ, is set equal to one. The experimental response modification factor for the CBDS *model* is therefore equal to

$$R_{CBDS} = R_\mu \times R_S \times R_\xi = 1.85 \times 2.43 \times 1.0 = 4.5.$$

In Figure 7.8, the Taft-57 LERS for 2% damping, similitude scaled to full-scale units, is presented in addition to the design yielding strength of the EBDS *model* ($=0.3W_{at}$) and the maximum shear resistance of the EBDS *model* during the Taft-57 Test. For an average value of the EBDS *model's* period, similitude scaled to full-scale units (0.59 to 0.72 second) [1], the total reduction from the Taft-57 LERS to the EBDS's design yielding strength of $0.3W_{at}$, is by a factor of 5.2, with R_S equal to 2.82 and R_μ equal to 1.84. As the LERS was constructed for a damping ratio of 2%, which is roughly equal to the first modal damping ratio of the EBDS, R_ξ, is set equal to one. For the most severe test of the EBDS, that is, the Taft-66 Test [1], the total reduction from the Taft-66 LERS to the EBDS's design yielding strength, is by a factor of 6.0 with R_S equal to 2.85, R_μ equal to 2.12 and R_ξ equal to one [1]. The experimental response modification factor for the EBDS *model* is therefore equal to

$$R_{EBDS} = R_\mu \times R_S \times R_\xi = 2.12 \times 2.85 \times 1.0 = 6.0.$$

Concentrically Braced Dual System:

The measured response modification factor for the CBDS of 4.5 is 75% and 56% of values specified by the ATC (R) and SEAOC (R_w^*), respectively. The measured reduction factor of 4.5 was comprised of a ductility reduction factor of 1.85 and a strength factor of 2.43.

As noted above, the maximum inter-story drift index in the CBDS was 1.89% in its fifth story and this drift level was associated with degradation of the lateral strength of the CBDS's

fifth story. If the permissible level of ductility was based on criteria that precluded drift associated with strength degradation, the maximum inter-story drift index would have been limited to approximately 1.5% for the CBDS *model*. A reduction in the maximum inter-story drift index would have: reduced the displacement ductility (μ) in the fifth story; and therefore reduced the CBDS's ductility factor from the value of 1.85 noted above.

The maximum strength of the first story of the DMRSF was 560% of its design yielding strength, that is, R_S^{DMRSF} is equal to 5.6. This overstrength resulted from internal force redistribution in the DMRSF as well as the initial conservative design of the DMRSF. The overstrength of the DMRSF was the primary reason why the CBDS was able to develop a strength factor of 2.43. For a typical CBDS, designed according to any of the current seismic regulations in the United States, the strength and stiffness of the DMRSF will generally be significantly less than that of the *models'* DMRSF. Therefore, the CBDS's response modification factor of 4.5 should be considered to be an upper bound on the value of R that could be expected in CBDSs designed according to current seismic regulations in the United States.

The maximum strength of a concentrically braced frame (CBF) beyond its strength at the level of first significant yielding is limited by the lack of ductility in its concentric braces because the CBF is unable to redistribute internal forces before reaching the brace's ductility limits. The strength factor for a concentrically braced frame, R_S^{CBF}, designed according to current practice in the United States, is probably limited to approximately 2.0.

The greater the stiffness and strength of the DMRSF in the CBDS, the greater the value of R_S for the CBDS. For a CBDS ($0.5 \le T_1 \le 1.0$ second) incorporating a very flexible DMRSF, a strength factor of between 1.5 and 2.0 would appear to be appropriate because the contribution of the strength of the DMRSF to the CBDS will be limited by the maximum acceptable inter-story drift. That is, the maximum strength of the DMRSF will not be mobilized before the maximum acceptable inter-story drifts are exceeded. For a CBDS ($0.5 \le T_1 \le 1.0$ second) incorporating a stiff DMRSF, such as the one in the *model*, a strength factor of between 2.5

and 3.0 would reflect the contribution of the strength of the DMRSF to the strength of the CBDS.

Eccentrically Braced Dual System:

The EBDS's measured response modification factor of 6.0 was 100% and 62% of values specified by the ATC (R) and SEAOC (R_w^*), respectively. The measured reduction factor of 6.0 was comprised of a ductility reduction factor of 2.12 and a strength factor of 2.85. The maximum shear resistance of the eccentrically braced frame (EBF) was 260% of its design yielding strength; the first story of the EBF had a significant elastic overstrength and strain hardened at a rate of approximately one-fifth of its elastic stiffness. The combined overstrengths of the DMRSF (see above) and the EBF provided the EBDS with a strength factor of 2.85.

The strength factor for an EBF ($0.5 \leq T_1 \leq 1.0$ second) designed according to the 1986 SEAOC, is probably between 1.75 and 2.25. The value of the strength factor, R_S^{EBF}, will depend on the choice of steel for the shear link and the extent of the contribution of composite action to the strength of the shear links. The strength factor for a DMRSF may be as high as five (see above), and in general, the greater the role of the DMRSF in the EBDS, the greater the EBDS's strength factor. For an EBDS ($0.5 \leq T_1 \leq 1.0$ second) incorporating a very flexible DMRSF, a strength factor of between 2.0 and 2.5 would appear to be appropriate. For an EBDS ($0.5 \leq T_1 \leq 1.0$ second) incorporating a stiff DMRSF, such as the one in the *model*, a strength factor of between 2.75 and 3.25 would reflect the contribution of the DMRSF to the strength of the EBDS.

Conclusions:

The *models* were constructed under conditions that were more stringent than those practiced in the construction industry. Furthermore, the *models* were only subjected to earthquake loading in the plane parallel to their braced frames and response of the *models* in the transverse direction was constrained by X-bracing. Finally, the DMRSF in the *models* was significantly stiffer and stronger than required by current seismic regulations in the United States. The response modification factors obtained from the testing of the *models* are therefore considered

to be upper bounds on the factors that could be obtained from the testing of similar full-scale buildings designed according to current seismic regulations in the United States.

Ductility plays the following two roles in the evaluation of a response modification factor. Firstly, if ductility is available in a structure, the required elastic strength can be reduced; for example, the Newmark and Hall procedure [53] can be used to estimate the extent of the ductility reduction factor, R_μ. Secondly, if the primary lateral load resisting elements exhibit stable, ductile behavior, significant internal force redistribution is possible and the potential strength of a given structure can be developed; that is, R_S can be maximized.

These studies have shown that the values of R and R_w currently adopted by the ATC and SEAOC exceed the measured response modification factors for the *models*. On the basis of the results presented above, more appropriate values of R for buildings incorporating cold-formed tubular steel braced framing and composite floor systems, and designed according to current seismic regulations, are as follows:

$$R_{CBF} = 2.0 \qquad (0.5 \text{ second} \leq T_1 \leq 1.0 \text{ second})$$

$$R_{CBDS} = 2.5 \qquad (0.5 \text{ second} \leq T_1 \leq 1.0 \text{ second})$$

$$R_{EBF} = 4.0 \qquad (0.5 \text{ second} \leq T_1 \leq 1.0 \text{ second})$$

$$R_{EBDS} = 5.0 \qquad (0.5 \text{ second} \leq T_1 \leq 1.0 \text{ second})$$

In estimating the values of R for the CBF and CBDS, the effects of strong motion duration were implicitly included by assuming a minimal reduction due to ductility ($R_\mu \approx 1.0$), because rupture of the concentric braces must be avoided in order to maintain the integrity of the primary lateral load resisting system. Furthermore, the R values noted above for the CBDS and EBDS assume that the DMRSF is designed for a percentage of the design base shear which is similar to that prescribed by current seismic regulations in the United States.

Bounds on the applicability of these response modification factors have been set because of the role that ductility plays in their evaluation. For fundamental periods (T_1) of less than

0.5 second, the effect of ductility diminishes such that as $T_1 \rightarrow 0$ second, $R_\mu \rightarrow 1.0$. For fundamental periods greater than 1.0 second, dependence on large ductilities will lead to excessively flexible structures that are unable to develop their potential strengths without exceeding the acceptable levels of inter-story drift.

Clearly the studies presented in this report are extremely limited in their scope. Parametric studies on a wide variety of building structural systems would permit a more accurate assessment of the values of R that could be expected from full-scale buildings. If the current practice of deriving a design response spectrum by reducing the LEDRS by a factor of R, is to be used for the next few decades, then there is an urgent need to establish a rational basis for the values of R specified in seismic regulations in the United States.

7.4 CBDS and EBDS Lateral Force Distribution

The design lateral force distributions for the UBC, ATC and SEAOC were presented in Chapter 2. In all three instances, the design lateral force distributions for the dual systems and the DMRSF were approximately triangular. The lateral force distributions on the CBDS, the concentric braces and the DMRSF are presented in Figures 6.14, 6.39 and 6.76 at the times of maximum base shear force and maximum lateral roof displacement, for the MO-06, MO-33 and MO-65 Tests, respectively. The lateral force distributions on the EBDS, the eccentric braces and the DMRSF are presented in Figures 6.25, 6.57 and 6.95 at the times of maximum base shear force and maximum lateral roof displacement, for the MO-07, MO-28 and Taft-57 Tests, respectively.

Concentrically Braced Dual System:

For the MO-06 Test, the inertia force profiles at the times of maximum lateral roof displacement were similar to the CBDS's fundamental mode shape. The "braced frame-moment frame" interaction in a dual system, which may result in the DMRSF's story shears exceeding the total story shears in the upper stories of the dual system, was not observed. The design lateral force distribution is similar to the inertia force distributions for the MO-06 Test at the

times of maximum roof displacement and maximum positive base shear.

For the MO-65 Test, the inertia force profiles at the times of maximum base shear were triangular in the lower four stories and uniform in the upper two stories. At the time of maximum positive base shear in the CBDS, the inter-story drift indices in the first to sixth stories were 0.71%, 0.66%, 0.68%, 0.66%, 0.84% and 0.48%, respectively. This result suggests that the use of the triangular design lateral force distribution [9] led to a CBDS response in which the damage, measured in terms of maximum inter-story drift index, was distributed relatively uniformly over its height.

Eccentrically Braced Dual System:

For the MO-07 Test, the inertia force profiles at the times of maximum base shear and maximum lateral roof displacement were similar to the EBDS's fundamental mode shape. The "braced frame-moment frame" interaction described above was not observed in the EBDS during the MO-07 Test; this can be attributed to the moderate height of the *model* and the absence of large axial deformations in the braced bay columns. The design lateral force distribution agrees reasonably well with the inertia force profiles for the MO-07 Test at the times of maximum roof displacement.

For the Taft-57 Test, the inertia force profiles at the times of maximum base shear were approximately rectangular, with smaller inertia forces being developed at the roof than at Level 6 because the reactive weight of the roof was only 85% of the reactive weight of the lower floors. At the time of maximum positive base shear in the EBDS, the inter-story drift indices in the first to sixth stories were 1.21%, 0.75%, 0.60%, 0.46%, 0.49% and 0.39%, respectively. The concentration of damage in the first story of the EBDS resulted from the formation of a soft first story. The inertia force profiles at the times of maximum base shear reflect this soft story formation.

Comparison and Discussion:

For a dual system that is expected to undergo significant inelastic response to severe earthquake shaking, the design lateral force distribution and its distribution between the braced

frame and the DMRSF should result in a dual system in which: the maximum inter-story drift index profile is relatively uniform over the height of the dual system, and the energy dissipation capacity of the dual system is maximized. Optimizing the energy dissipation capacity of a dual system generally requires designing it to fail as a complete mechanism involving all of its stories, rather than as a soft story, wherein only a limited number of plastic hinges are formed and the damage is concentrated in only one story.

The energy dissipation capacity of a concentrically braced frame will be maximized if it fails as a mechanism involving brace buckling in all levels of the frame as shown in Figure 7.9a, rather than as a soft story as shown in Figure 7.9b. At the time of maximum base shear, the inter-story drift indices were relatively uniform over the height of the CBDS. For this CBDS, the design lateral force distribution [9] on the CBDS and the internal force distribution between the braced frame and the DMRSF resulted in a desirable energy dissipation distribution. Therefore, the design lateral force distribution can be considered to be correct for a CBDS with a configuration that is similar to the CBDS *model*. It must be noted however that the internal force distribution [9] between the braced frame and the DMRSF was significantly different from that assumed by the UBC, ATC and SEAOC, because the DMRSF was designed for a significantly higher percentage of the total base shear force than required by current seismic regulations in the United States.

The energy dissipation capacity of an eccentrically braced frame will be maximized if it fails as a mechanism involving simultaneous shear yielding in all of its shear links as shown in Figure 7.9c, rather than as a soft story as shown in Figure 7.9d. The EBDS's energy dissipation was concentrated in its first and second stories (Figure 6.102), rather than distributed uniformly over its height, as was the case for the CBDS (Figure 6.82). Specific conclusions regarding the suitability of the design lateral force distribution [9] for EBDSs should not be drawn from the results presented in this report, because the DMRSF's beams and columns were designed as part of a CBDS and not an EBDS. Furthermore, the sizing of the shear links and eccentric braces would have differed significantly from the as-tested sizes, if the design of

the EBDS had not been constrained by the existing beam sizes in the CBDS. A design of the EBDS that was free of these constraints would have resulted in significantly smaller shear links and eccentric braces in the upper five stories of the EBDS. This would have resulted in a more uniform inter-story drift profile in the EBDS, that is, a more uniform damage distribution.

Although the design process is iterative in nature, the initial choice of a lateral force profile will have a major impact on the distribution of member sizes over the height of a building, especially in its upper stories. Because of its importance in earthquake resistant design, further research is needed to develop optimum lateral force distributions for steel dual systems.

7.5 Low-Cycle Fatigue and Incremental Collapse

7.5.1 General

Variable, repeated loading can give rise to structural collapse by either low-cycle fatigue (alternating plasticity) or incremental collapse (crawling collapse). Low-cycle fatigue is associated with a large number of alternating yield cycles. Incremental collapse results from the accumulation, in a given cycle of loading, of plastic deformation in a sufficient number of plastic hinges to permit the structure to move as a rigid body.

As a result of the 1985 Mexico and 1985 Chile earthquakes, attention has been focused on low-cycle fatigue and incremental collapse. The 1985 Chile earthquake record (N10E at Llolleo) has an extremely long duration of strong motion shaking, a large effective peak acceleration and a strong frequency content for natural periods less than 0.7 second. For structures with fundamental periods less than 0.7 second, this earthquake record is, with regard to low-cycle fatigue and incremental collapse, the most damaging earthquake ground motion recorded to date. Consequently, this earthquake record was used to estimate the likelihood of failure of the CBDS and EBDS *models* by either low-cycle fatigue or incremental collapse.

All of the *models'* test results have been similitude scaled to full-scale units in the studies presented in the following sub-sections and, accordingly,

$$T_{CBDS} = 0.367 \times 1.811 = 0.66 \text{ second}$$

$$T_{EBDS} = 0.326 \times 1.811 = 0.59 \text{ second}$$

where, T_{CBDS} and T_{EBDS} were estimated from the free vibration tests conducted prior to the MO-65 and Taft-57 Tests, respectively (Tables 6.1 and 6.2).

7.5.2 Test Results

The CBDS *model* was subjected to a total of three moderate earthquake ground motions and one severe earthquake ground motion prior to the rupture of its fifth story concentric braces. In considering the response of the CBDS to these four ground motions, two factors must be noted, namely: the most severe earthquake ground motion that the CBDS was subjected to, had an effective peak acceleration (EPA) of only 0.4g, and the total duration of strong motion shaking for these four tests was less than that of the 1985 Chile earthquake ground motion.

The EBDS *model* was subjected to a total of seven moderate and six severe earthquakes prior to the failure of its shear link at Level L2: the EBDS *model* was subjected to earthquake ground motions with EPAs in excess of 0.5g, and the EBDS's total duration of strong motion shaking was approximately three times longer than the CBDS's duration of strong motion shaking.

7.5.3 Low-Cycle Fatigue

Cumulative deformation ductility is a better failure index than maximum deformation ductility for structures susceptible to low-cycle fatigue because it is a measure of total inelastic deformation. The cumulative ductility ratio is calculated by summing the absolute value of all of the inelastic deformations and then normalizing the result to Δ_y.

The computer program NONSPEC [37] was used to estimate the cumulative ductility ratio demand on a SDOFS subjected to the 1985 Chile (N10E-Llolleo), the MO-65 Test (CBDS) and the Taft-66 Test (EBDS) earthquake records. The Taft-66 earthquake record was chosen for this study of the EBDS's response, because in terms of EPA and energy input, this

was the most severe test of the EBDS [1].

The strengths of the *models*, expressed as a function of their design reactive weights (W_{drw}) were both $0.60W_{drw}$ ($=0.72 \times 1154/1400$), where their strengths of $0.72W_{at}$ were evaluated using an equal energy method (Figures 7.10 and 7.11). The computed cumulative ductility ratios for the Chile, MO-65 Test and Taft-66 Test earthquake records were 6.67, 3.87 and 8.16, respectively.

Concentrically Braced Dual System:

The stiffness and strength degradation associated with severe brace buckling is a form of low-cycle fatigue. The cumulative ductility ratio of the MO-65 Test ($=3.87$) of the CBDS was only 58% of that demanded by the Chile earthquake ground motion. Since the CBDS's concentric braces buckled and ruptured during the MO-65 Test, the CBDS would have failed undoubtedly by low-cycle fatigue, if it had been subjected to the long duration Chile earthquake record.

Eccentrically Braced Dual System:

Up to the point of its fracture during the Sine-70 Test [1], Link L2 in the EBDS exhibited stable hysteretic behavior and survived a large number of yielding cycles of a shear strain ductility in excess of 10. Note that: (1) the total cumulative deformation ductility demand on Link L2 for all of the moderate and severe tests was of the order of four times that for the Taft-66 Test [1]; and (2) the cumulative ductility ratio for the Taft-66 ($=8.16$) earthquake record was 22% greater than demanded by the Chile earthquake record ($=6.67$). The EBDS did not fail by, nor show signs of failing by, low-cycle fatigue during the Taft-66 Test. Thus, the EBDS would not have failed by low-cycle fatigue, if it had been subjected to the long duration Chile earthquake record.

7.5.4 Incremental Collapse

Incremental or crawling collapse can be initiated by earthquake ground motions that contain either numerous uni-directional acceleration pulses of moderate intensity or a smaller

number of very severe acceleration pulses. The 1978 Miyagi-Ken-Oki and 1952 Taft earth-quake records contain several acceleration pulses, but in general, these pulses are offsetting and the permanent displacements in both the CBDS and EBDS *models* were small. In order to estimate the likelihood of incremental collapse of the CBDS and EBDS, NONSPEC was used to evaluate the maximum displacement ductility and the maximum cyclic displacement ductility for the 1985 Chile, the MO-65 Test (CBDS) and the Taft-66 Test (EBDS) earthquake records. Using the same parameters given in the previous section, the maximum displacement ductility and maximum cyclic displacement ductility were 2.95 and 3.16, respectively, for the Chile earthquake record; 1.89 and 2.01, respectively, for the MO-65 Test earthquake record and 2.73 and 2.84, respectively, for the Taft-66 Test earthquake record.

Concentrically Braced Dual System:

The maximum displacement ductility and the maximum cyclic displacement ductility for the Chile earthquake record were 50% greater than those for the MO-65 Test earthquake record. However, because the CBDS did not fail by incremental collapse during the MO-65 Test, firm conclusions regarding the possibility of its incremental collapse during the Chile earthquake record, cannot be drawn.

Eccentrically Braced Dual System:

The maximum displacement ductility and the maximum cyclic displacement ductility for the Chile earthquake record were similar to those of the Taft-66 Test earthquake record. The EBDS did not fail by incremental collapse during the Taft-66 Test, and only small residual shear strains were observed in Links L2 and L3 upon the completion of all of the severe earth-quake simulator tests. The EBDS would be unlikely to fail by incremental collapse, were it subjected to the Chile earthquake record.

7.5.5 Summary

Categorical conclusions regarding the importance of low-cycle fatigue and incremental collapse in the earthquake-resistant design of dual systems cannot be drawn on the basis of testing two *models* with a limited number of earthquake ground motions, especially *models* that

were considerably stronger than required by current seismic regulations in the United States. Further studies regarding the influence of the type and duration of earthquake ground motions on the likelihood of incremental collapse and low-cycle fatigue are required.

Low Cycle Fatigue:

The failure of CBDSs by low-cycle fatigue appears probable in regions of high seismic risk, unless the applied earthquake record is of extremely short duration and/or the CBDSs have a high nominal yielding strength ($C_y \gtrsim 0.40$ to 0.50). This testing program has shown that concentrically braced frames (CBFs) and CBDSs incorporating cold-formed tubular braces can suffer severe stiffness and strength degradation after only a limited number of minor yielding cycles.

The failure of EBDSs by low-cycle fatigue is unlikely unless the applied earthquake record has an extremely long duration of strong motion shaking, or the EBDS has a very short fundamental period, and/or a very low yielding strength ($C_y \leq 0.20$). This testing program has shown that properly stiffened and fabricated shear links can sustain a very large number of yielding cycles with a high shear strain ductility demand [1].

Incremental Collapse:

It is difficult to draw firm conclusions regarding the incremental collapse of dual systems because the earthquake records used in this testing program did not contain a significant number of uni-directional acceleration pulses.

Concentrically braced frames and CBDSs with extremely flexible DMRSFs, as currently designed and detailed in the United States, are susceptible to failure by incremental collapse because they possess relatively little ductility before the onset of strength and stiffness degradation.

For an EBDS with a fundamental period between 0.7 second and 3.0 seconds and possessing a significant overstrength with respect to the minimum strength requirements of current seismic regulations, failure by incremental collapse is improbable unless the earthquake has an

extremely long duration of strong motion shaking containing a large number of uni-directional acceleration pulses. For an EBDS with a fundamental period less than 0.5 second, the possibility of incremental collapse depends on the expected earthquake ground motions at the site under consideration. An EBDS with a short fundamental period however is undesirable because the DMRSF, if designed for a percentage of the design base shear similar to that prescribed by current seismic regulations, is prevented from contributing to energy dissipation in the EBDS, because of its lack of stiffness compatibility with the stiffer eccentrically braced frame.

7.6 Ductile Moment-Resisting Space Frames in Dual Systems

The DMRSF played significantly different roles in the response of the CBDS and EBDS *models*. Conceptually, the DMRSF is intended to be a secondary supply of strength and energy dissipation to the dual system, or, to act as a secondary line of defense against the collapse of the dual system, in the event of severe earthquake shaking. In the CBDS *model*, the DMRSF assumed the role of the primary lateral load resisting system following the *failure* of the concentrically braced frame. In the EBDS *model*, the DMRSF enhanced the strength of the dual system following the *yielding* of the primary lateral load resisting system, that is, the DMRSF performed its intended role as a secondary supply of strength during severe earthquake shaking.

Despite the important role that the DMRSF plays in the dual system, the UBC, ATC and SEAOC only require that the DMRSF be designed to resist 25% of the minimum design base shear. These seismic regulations place no limits on either the flexibility of the DMRSF, or the relationship between its flexibility and that of the braced frame.

Concentrically Braced Dual System:

The high strength demand on the fifth story of the DMRSF during the MO-65 Test is clearly shown in Figure 6.72; it resulted from the formation of a soft fifth story that was a consequence of brace buckling and rupture. The envelope of the story shears resisted by the

DMRSF during the MO-65 Test is shown in Figure 7.12a in conjunction with the design story shears for the DMRSF (scaled to yielding levels) from the 1981 Japanese Aseismic Code (J.A.C.) [9], and the strength of each story of the DMRSF calculated using limit analysis of individual soft story mechanisms. The significant differences between the story strengths of the DMRSF and the design story shear forces clearly indicate that this DMRSF was conservatively designed. The maximum story shear force demands during the MO-65 Test were 40%, 44%, 40%, 64%, 109% and 27% of the estimated first to sixth story strengths, respectively. The potential strengths of the DMRSF were not developed in the first to fourth stories, nor in the sixth story of the CBDS. In the fifth story of the CBDS, the maximum strength demand on the DMRSF exceeded the strength predicted by limit analysis; the overstrength of the DMRSF can be attributed to strain hardening in the fifth story columns.

The design story shear forces from the Japanese Aseismic Code [9] were exceeded in all six stories of the CBDS by more than a factor of two. The maximum fifth story shear force resisted by the DMRSF was 40.1 kips or 260% of the design yielding strength of the CBDS's fifth story.

The maximum inter-story drift index of 1.89%, measured during the MO-65 Test, exceeded the UBC and ATC limits of 1.5% and the SEAOC limit of 1.12% for CBDSs. However, this DMRSF, one that was significantly stronger than required by the UBC, ATC and SEAOC, was so flexible that it did not yield in the fifth story until the fifth inter-story drift index exceeded 1.5%. Although the DMRSF developed its potential strength in the fifth story, its energy dissipation capacity was not developed because the extent of its plastic deformation was minimal ($\approx$ 0.3% to 0.4% of the story height).

The *models'* DMRSF was designed for 34% of the 1981 Japanese Aseismic Codes's design base shear force of 0.197 W_{drw}, that is, the DMRSF was designed for a base shear force of

$$V_{DMRSF} = \frac{0.34 \times 0.197}{0.8} \times W_{drw} = 0.083 \times W_{drw}$$

at a level of first significant yielding. The minimum strength requirements of the UBC, ATC and SEAOC would require that the DMRSF be required to resist a base shear force, at a level of first significant yielding, equal to

$$V_{UBC} = \frac{0.25 \times 0.113}{0.8} \times W_{drw} = 0.035 \times W_{drw}$$

$$V_{ATC} = 0.25 \times 0.133 \times W_{drw} = 0.033 \times W_{drw}$$

$$V_{SEAOC} = \frac{0.25 \times 0.075}{0.8} \times W_{drw} = 0.023 \times W_{drw}$$

The *models'* DMRSF was therefore significantly stronger than required by any of the seismic regulations in the United States. If the design lateral forces on the DMRSF were reduced to a level that was compatible with the requirements of the UBC, ATC and SEAOC, and the stress ratios in the critical members in the DMRSF [2] were increased to unity by reducing the section sizes, the resulting DMRSF would have been 40% weaker than the *models'* DMRSF. A 40% strength reduction in the DMRSF would have catastrophic consequences for the response of the fifth story of the CBDS during the MO-65 Test. In order to avoid the collapse of the CBDS's fifth story, a twofold increase in the ductility factor (R_μ) would have been required to offset the 40% strength reduction. The yield level drifts in the DMRSF exceeded the code-based limits for severe earthquake shaking. An increase in the fifth inter-story drift index to between 3% and 4%, resulting from a twofold increase in R_μ, would have been totally unacceptable in terms of both non-structural damage and potential structural collapse.

Eccentrically Braced Dual System:

The high strength demand on the first story of the DMRSF during the Taft-57 Test, shown in Figures 6.91 and 6.97, resulted from the formation of a soft first story. The envelope of the story shears resisted by the DMRSF is shown in Figure 7.12b in conjunction with the DMRSF's design story shear forces [9] and the strengths of each story of the DMRSF obtained from limit analysis. The maximum story shear force demands on the DMRSF were 60%, 20%, 23%, 27%, 24% and 26% of its estimated first to sixth story strengths, respectively. The

potential strengths of the DMRSF were not developed in the EBDS and the DMRSF did not contribute significantly to energy dissipation in the EBDS.

The design story shear forces were exceeded in all six stories of the EBDS. The maximum story shear force resisted by the DMRSF was 36.1 kips, or 112% of the design yielding strength of the EBDS ($=0.3W_{at}$) and approximately 40% of the maximum first story shear force.

In the Taft-57 Test, the maximum inter-story drift of 1.28% exceeded the SEAOC limit of 1.12% for EBDSs. However, the flexibility of the DMRSF was such that at a first inter-story drift index of 1.12%, it remained essentially elastic and did not develop its potential strength, nor did it dissipate energy. The SEAOC inter-story drift limits for EBDSs and strength requirements for DMRSFs in dual systems are clearly incompatible. SEAOC should be revised so that the DMRSF can contribute more effectively to the dual system during severe earthquake shaking by: increasing the inter-story drift index limits to at least 1.5%, and implementing minimum stiffness requirements for DMRSFs in EBDSs.

Discussion:

The stiffness and strength of a DMRSF are implicitly related. For a single story, single bay DMRSF using a constant section size throughout, its stiffness is proportional to the section depth cubed and its strength is proportional to the section depth squared. Therefore, the DMRSF's lateral stiffness can be conservatively assumed to be linearly related to its lateral strength.

A number of conclusions can be drawn regarding the role of the DMRSF in the response of both the CBDS and the EBDS *models* and the design requirements for DMRSFs in steel dual systems:

- The design strength of the DMRSF in both the CBDS and EBDS *models* was more than 100% higher than the minimum required by current seismic regulations in the United States.

- The stiffness of the *models'* DMRSF was significantly higher than the stiffness which would have resulted from its design according to current seismic regulations in the United States.

- The strength and stiffness of the DMRSF prevented the collapse of the CBDS following the buckling and rupture of the concentric braces in the fifth story of the concentrically braced frame.

- The DMRSF enhanced the strength and stiffness of the EBDS following the yielding of the primary lateral load resisting system and therefore performed one of its intended roles in the dual system. As a result of the DMRSF being significantly more flexible than the eccentrically braced frame (EBF), it was unable to dissipate a significant amount of energy prior to the failure of the EBF because it could not reach its yielding strength within the drift levels reached by the EBDS.

- The problems associated with lack of strength and stiffness compatibility of the braced frames and the DMRSF in the *models*, will be significantly worse in a dual system that is designed for only the minimum requirements of either the UBC, ATC or SEAOC.

- The SEAOC maximum inter-story drift indices of 1.12% for both CBDSs and EBDSs are too conservative with respect to those permitted by the UBC and ATC (=1.5%). There is no reason to limit inter-story drift indices to 1.12% if (1) the braced frame is sufficiently ductile to develop inter-story drift indices approaching 1.5% to 2.0% safely; and (2) the non-structural components are detailed to accept inter-story drift indices of the order of 1.5% to 2.0%.

- There is an urgent need to rationalize the relative elastic stiffnesses, yielding strengths, deformabilities and ductilities of the braced frames and DMRSFs in dual systems and to implement these findings in seismic regulations in the United States. The implementation of minimum stiffness requirements for DMRSFs in steel dual systems is of paramount importance.

7.7 Inelastic Response and Energy Spectra

7.7.1 General

The inelastic response of multi-degree-of-freedom systems (MDOFS) is often described through the use of single-degree-of-freedom (SDOF) response spectra. The experimental results acquired during this testing program make it possible to evaluate the use of SDOF spectra to predict the MDOF response of dual systems. The computer program NONSPEC [37] was used to construct the inelastic response and energy spectra presented and discussed in Sections 7.7.2 and 7.7.3.

To reduce the response of a MDOFS to a SDOFS, the yielding strength (R_y) and displacement ductility of the equivalent elastic-perfectly plastic (EPP) system must be defined. These two variables were based on the base shear versus roof drift index relationships for both the CBDS and the EBDS. These relationships are presented in Figures 7.10 and 7.11, respectively, and are based upon the equal energy approach. The yielding strengths of both the CBDS and EBDS *models*, expressed as a function of their as-tested reactive weights (107.1 kips), were estimated to be $0.72W_{at}$ (Section 7.5.3).

The MO-65 earthquake record was chosen for this study of the CBDS's response because the effective peak acceleration (EPA) and the input energy were both maximized for the CBDS during this test [2]. The Taft-66 earthquake record was chosen for this study of the EBDS's response because the EPA and the input energy were both maximized for the EBDS during this test [1].

In Sections 7.7.2 and 7.7.3, the test results for the CBDS and EBDS *models* have been scaled to full-scale units, in order to allow a more realistic interpretation of the results.

7.7.2 Inelastic Response Spectra

SDOF inelastic response spectra for the similitude scaled MO-65 Test and Taft-66 Test acceleration records are shown in Figures 7.13a and 7.13b, respectively. These spectra present the relationship between the non-dimensional strength parameter (η), defined as

$$\eta = \frac{C_y}{\ddot{V}_{g\,max}/g} = \frac{R_y}{m\,\ddot{V}_{g\,max}} \qquad (7.4)$$

the ductility (μ), and the fundamental period (T) for 2% damping and values of C_y equal to 0.2, 0.4, 0.6, 0.8, 1.0 and 3.0. The parameters C_y, R_y, m and $\ddot{V}_{g\,max}$ in Equation 7.4 are the seismic yielding coefficient, the yielding strength, the mass and the peak ground acceleration, respectively. For the MO-65 and Taft-66 Tests, $\ddot{V}_{g\,max}$ equaled 0.649g and 0.663g, respectively.

Assuming SDOF spectra are valid for estimating MDOF response, the MO-65 Test and Taft-66 Test inelastic spectra can be used to quantify the overstrength required of CBDSs and EBDSs, designed for the minimum strength requirements of current seismic regulations, in order for them to survive severe earthquake shaking. As the 1986 SEAOC [12] is the only seismic regulation in the United States that distinguishes between CBDSs and EBDSs, its minimum strength requirements will be used as benchmarks for this study.

Concentrically Braced Dual System:

For the CBDS (Figure 7.13a), η equaled 1.1 (=0.72/0.649) and the required displacement ductility (μ), based upon a period of 0.66 second ($\approx$ 0.36×1.811) and a damping ratio of 2%, was 1.5. The CBDS's roof displacement ductility, calculated as shown in Figure 7.10, was approximately 1.45; the SDOF assumption provided an accurate assessment of the required displacement ductility in this instance. The yielding strength and stiffness of the CBDS *model* decreased linearly over its height [2]. At the time of maximum positive base shear, the interstory drift indices in the lower five stories of the CBDS ranged between 0.66% and 0.84% and the displacement ductilities in the lower five stories were relatively uniform. The SDOFS assumption for modeling the MDOFS inelastic response of the CBDS was valid in this instance.

If the CBDS *model* was designed strictly for the minimum strength requirements of the 1986 SEAOC, its nominal strength coefficient at a level of first significant yielding (C_{ty}) would have been 0.16 (Table 2.10). For the MO-65 Test, η would therefore have equaled 0.25

(=0.16/0.649) and the required displacement ductility, based upon the SEAOC derived period of 0.5 second (Section 2.6) and 2% damping, would have exceeded 15. A displacement ductility of 15 is *five* times the ductility implicitly assumed by SEAOC (=3.0) for CBDSs and approximately *ten* times the *model's* maximum roof displacement ductility ($\mu_{ROOF} = 1.45$). This displacement ductility demand for the MO-65 Test earthquake record is far greater than that which could be supplied by any CBDS, irrespective of any techniques used to improve the ductility of the concentric braces. Conversely, the required η for a displacement ductility of 1.45 would have been 1.1 (Figure 7.13a), that is, the CBDS's required strength factor would have been

$$R_S = \frac{C_{max}}{C_{ty}} = \frac{\eta}{C_{ty}} \times \frac{\ddot{V}_{gmax}}{g} = \frac{1.1 \times 0.649}{0.16} = 4.5$$

that is, 83% greater than that measured during the CBDS's testing program (=2.43). Clearly, if the CBDS *model* had been designed for a yielding strength of $0.16W_{at}$ rather than $0.30W_{at}$, it would have collapsed during the MO-65 Test.

Eccentrically Braced Dual System:

For the EBDS (Figure 7.13b), η equaled 1.1 (=0.72/0.663) and the required displacement ductility (μ), based upon a period of 0.6 second ($\approx 0.32 \times 1.811$) and 2% damping, was 2.0. The EBDS's roof displacement ductility, calculated as shown in Figure 7.11, was approximately 1.40 and the SDOF assumption did not accurately predict the required displacement ductility. For the EBDS *model*, whose yielding strength and stiffness varied in an irregular manner over its height [1], the inter-story drift indices at the time of maximum positive base shear ranged from 1.21% in the first story to 0.39% in the sixth story. At the time of maximum positive base shear, the displacement ductilities varied from less than one in the sixth story to approximately two in the first story. As a result of the concentration of inelastic deformation in the first story of the EBDS, the SDOF assumption for modeling the MDOF inelastic response of the EBDS *model* was poorer than for the CBDS, in which the inelastic deformation was uniformly distributed throughout the lower five stories.

If the EBDS *model* could have been designed strictly in accordance with the minimum strength requirements of the 1986 SEAOC, its nominal strength coefficient at a level of first significant yielding (C_{ty}) would have been 0.10 (Table 2.10). For the Taft-66 Test, η would therefore have equaled 0.15 (=0.10/0.663). The required displacement ductility, based upon the SEAOC derived period of 0.7 second (Section 2.6) and 2% damping, would have exceeded 10. A displacement ductility of 10 is approximately *three* times the ductility implicitly assumed by the 1986 SEAOC (=3.6) for EBDSs and in excess of *seven* times the *model's* maximum roof displacement ductility (μ_{ROOF} = 1.4). This displacement ductility demand for the Taft-66 Test earthquake record is far greater than that which could be supplied by any EBDS. Conversely, the required η, for a displacement ductility of 1.4 would have been 1.4 (Figure 7.13b), that is, the EBDS's required strength factor would have been

$$R_S = \frac{C_{max}}{C_{ty}} = \frac{\eta}{C_{ty}} \times \frac{\ddot{v}_{gmax}}{g} = \frac{1.4 \times 0.663}{0.10} = 9.3$$

and more than three times the strength factor measured during the EBDS's testing program. Clearly, if the EBDS *model* had been designed for a yielding strength of $0.10W_{at}$ rather than $0.30W_{at}$, it would have collapsed during the Taft-66 Test.

Discussion:

If a structure fails as a SDOF mechanism involving all of its stories rather than a single story, the SDOF assumption for estimating MDOF inelastic response is reasonable. Achieving this mode of failure is one major objective in earthquake-resistant design. In a CBDS, this mode of failure would involve simultaneous brace buckling in all stories (Figure 7.9a); in an EBDS, it would involve simultaneous yielding in the shear links in all stories (Figure 7.9c). Techniques by which this mode of failure could be achieved have been discussed by Khatib et al. [13] for the CBDS and by Whittaker et al. [1] for the EBDS. The importance of achieving a complete SDOF mechanism is demonstrated in Appendix A for an EBF.

The results of this brief study have shown that smoothed SDOF inelastic design response spectra (IDRS) are a reasonable basis for the preliminary design of MDOF dual systems. To

avoid underestimating the required yielding strength of the MDOF system at the preliminary design stage, the global displacement ductility should be assumed to be significantly smaller than those values assumed by the UBC, ATC and SEAOC. On the basis of the experimental results presented in Chapters 6 and 7, realistic estimates of μ_δ will vary between 1.25 (CBDSs) and 2.00 (EBDSs). It should be noted that the use of realistic IDRS alone will not automatically ensure a safe design because the the issues of low-cycle fatigue and incremental collapse are not included in the IDRS approach. However, if a structural system exhibits stable ductile behavior, such as the EBDS, the problems posed by low-cycle fatigue and incremental collapse can be avoided to a large degree.

The results presented in this section clearly indicate that the overstrength and ductility demands on both the CBDS and EBDS *models*, designed to *just develop* the minimum strengths required by the 1986 SEAOC, during severe earthquake shaking (MO-65 and Taft-66 Tests) are extremely high. These overstrength and ductility demands are far higher than those which could be supplied by either of the *models*. The minimum strength requirements of the 1986 SEAOC (and the 1985 UBC and 1984 ATC 3-06) are clearly too low. These seismic regulations place too great a reliance, albeit implicitly, on a building's overstrength and ductility for acceptable performance during severe earthquake shaking.

7.7.3 Energy Spectra

The SDOFS input energy spectra for the similitude scaled MO-65 and Taft-66 earthquake records are presented in Figures 7.14a and 7.14b, respectively, for values of C_y equal to 3.0, 0.8, and 0.6. A value of C_y equal to 3 corresponds to linear elastic response for both the MO-65 and Taft-66 Test earthquake records.

Concentrically Braced Dual System:

The similitude scaled input energy for the MO-65 Test was 15,255 kip-in (= $432/0.3048^3$). This input energy is indicated in Figure 7.14a. For a value of C_y equal to 0.72, the energy input to a SDOFS with a mass of 2.986 kip/sec^2 (=1154/386.4) and a period of 0.66 second is 11,680 kip-in, that is, 76% of the scaled test result. During the MO-65 Test, the

natural period of the CBDS varied between 0.36 second and 0.45 second; this variation was estimated from the CBDS's relative displacement response time histories using a zero-crossing technique. For a natural period of 0.82 second (=0.45×1.811), the energy input is 26,370 kip-in, or 172% of the scaled test result. Thus, within the bounded range of the fundamental period of the CBDS, the cumulative input energy varied by a factor of 2.25.

Eccentrically Braced Dual System:

The similitude scaled input energy for the Taft-66 Test was 20,447 kip-in (= 579/ 0.3048^3). This input energy is indicated in Figure 7.14b. For a value of C_y equal to 0.72, the energy input to a SDOFS with a mass of 2.986 kip/sec^2 (=1154/386.4) and a period of 0.59 second is 16,962 kip-in, that is, 83% of the scaled test result. During the Taft-66 Test, the natural period of the EBDS varied between 0.33 second and 0.42 second; this variation was estimated from the EBDS's relative displacement response time histories using a zero-crossing technique [1]. For a natural period of 0.76 second (=0.42×1.811), the energy input is 29,065 kip-in, or 142% of the scaled test result. Thus, within the bounded range of the fundamental period of the EBDS, the cumulative input energy varied by a factor of 1.7.

Discussion:

From the results presented above for both the CBDS and EBDS, it appears possible to estimate a reasonable bound on the input energy to a MDOFS using SDOFS energy spectra if the ranges of the yielding strength and fundamental period of the MDOFS can be established. However, it is clear that the energy that can be imparted to a building for a given earthquake ground motion is sensitive to a number of parameters including: the yielding strength, R_y, of the building; the effective fundamental period of the building during the earthquake; the duration of strong motion shaking; the frequency content of the earthquake ground motion, and the stability of the building's hysteretic response. In order to use energy methods in the design process, energy design response spectra (EDRS) must be developed; the influence of these five parameters must be included in the development of these spectra.

The development of energy spectra has been the subject of research by Uang and Bertero [52], Housner [54] and Akiyama [55]. For natural periods greater than one second, the input energy is relatively independent of yielding strength [1,2], and consequently, the degree of inelastic deformation or damage. In this instance, the input energy can be estimated using the zero damped pseudo-velocity spectral ordinate, following the approach suggested by Housner. For natural periods less than one second, there can be a significant increase in the input energy with a reduction in yielding strength [1,2,52]; this is clearly evident in Figures 7.14a and 7.14b, for the MO-65 Test and Taft-66 Test earthquake records, respectively. The dependence of total input energy spectra on yielding strength for fundamental periods less than one second, is a drawback to their development and use in the design process.

Of similar importance to the total input energy is the maximum rate at which the input energy is imparted to the building, that is, the maximum input power. For example, using the MO-65 Test energy time history (Figure 6.81), the total energy input was 434 kip-in. Of this 434 kip-in, more than 400 kip-in was input to the CBDS between the 4 and 10 second marks, at an average rate of 70 kip-in/sec, or, 13 kip-in per half-cycle of loading. However, during each of the half-cycles of loading ($\approx T_1/2$) following the 6 and 8.4 second marks in the MO-65 Test, approximately 70 kip-in of energy was input to the CBDS, that is, five times the average input power. The use of energy spectra in the design process will therefore also require the development of damage laws that can relate the life of a structure, at both the global and local levels, to the number of yielding reversals and the distribution of ductility demand during these reversals.

CHAPTER 8

SUMMARY, CONCLUSIONS AND RECOMMENDATIONS

8.1 Summary

8.1.1 General

In this testing program, two structural systems have been thoroughly investigated. These systems, the concentrically braced dual system (CBDS) and the eccentrically braced dual system (EBDS), are currently being constructed in regions of high seismic risk in the United States. The performance of both the CBDS and the EBDS have been described and summarized in detail in Chapters 6 and 7, in terms of their strength, deformability, ductility, energy dissipation capacity and vulnerability to failure by low-cycle fatigue and incremental collapse. The results of the testing of these two systems are summarized in this section.

8.1.2 Serviceability Limit State

For minor earthquake shaking, the response of the CBDS (MO-06: EPA=0.047g) and the EBDS (MO-07: EPA=0.054g) were similar. The displacement responses of both the CBDS and the EBDS were primarily first mode responses. The story shear time histories in the upper levels of both the CBDS and the EBDS displayed a small amount of second mode response.

The inertia force profiles for the CBDS and the EBDS during the minor earthquake shaking tests were approximately triangular and thus similar to the lateral force distribution that is assumed by the UBC, ATC and SEAOC for the design of CBDSs and EBDSs. The distribution of the inertia forces between the braced frame and the DMRSF in both the CBDS and the EBDS showed no evidence of the "braced frame-moment frame" interaction whereby the story shear force resisted by the DMRSF in its upper stories exceeds the total story shear.

In the MO-06 and MO-07 Tests, the maximum base shear coefficients (V_b/W_{at}) equaled or exceeded the working stress base shear coefficients assumed by current seismic regulations

in the United States for severe earthquake shaking.

The energy dissipation mechanism for both the CBDS and the EBDS during the minor earthquake shaking tests was equivalent viscous damping that involved viscous, structural, and aerodynamic damping.

8.1.3 Damageability Limit State

For moderate earthquake shaking, the global responses of the CBDS (MO-33: EPA=0.21g) and the EBDS (MO-28: EPA=0.19g) were similar. The maximum inter-story drift indices varied between 0.5% and 0.69% in the CBDS and between 0.29% and 0.46% in the EBDS. The maximum base shear coefficients were 0.56 and 0.50, for the CBDS and EBDS, respectively.

The peak shear resistances of both *models* were significantly greater than their design yielding strengths of $0.3W_{at}$, that is, both the CBDS and EBDS exhibited substantial over-strengths. The CBDS and EBDS were both able to supply the significant overstrengths required to withstand moderate earthquake shaking successfully.

The critical elements in the CBDS (5th story concentric braces) and the EBDS (shear link at Level L2) behaved very differently during moderate earthquake shaking. In the MO-33 Test of the CBDS, the concentric braces in the fifth story buckled and the strength of the fifth story braced bay degraded marginally after initial buckling. The maximum displacement ductility in the fifth story of the CBF was approximately 1.3 (Figure 6.34) but this was associated with minor strength degradation. In the MO-28 Test of the EBDS, the shear link at Level L2 yielded and then strain-hardened; the maximum displacement ductility in the first floor of the EBF was approximately 1.4.

The energy dissipation mechanisms for both the CBDS ($E_I \approx 80$ kip–in) and the EBDS ($E_I \approx 50$ kip–in) involved both damping and inelastic behavior in similar proportions. In the CBDS, the hysteretic energy was dissipated primarily by the buckling of the concentric braces. In the EBDS, the hysteretic energy was dissipated by the shear yielding of the shear links at Levels L2 and L3.

8.1.4 Collapse Limit State

For severe earthquake shaking, both the global and critical member responses of the CBDS (MO-65: EPA = 0.40g) and EBDS (Taft-57: EPA = 0.44g) were significantly different. The maximum inter-story drift index in the CBDS was 1.89% (5th story) compared with 1.28% (first story) in the EBDS. The significant difference between the two maximum inter-story drift indices was a result of a major difference in the post-elastic responses of the *models*.

The peak shear resistances of both the CBDS ($0.73W_{at}$) and the EBDS ($0.85W_{at}$) were significantly greater than their design yielding strengths of $0.3W_{at}$; that is, both the CBDS and the EBDS exhibited substantial overstrengths during severe earthquake shaking.

The inertia force profiles measured at the times of maximum base shear for the CBDS and EBDS, were different from the design lateral force distribution used by the seismic regulations in the United States. The failure mechanisms of the *models* are the primary reason for this because the CBDS responded as a soft fifth story and the EBDS responded as a soft first story.

The critical elements in the CBDS (concentric braces) and the EBDS (shear links) behaved very differently during the severe earthquake shaking tests. In the MO-65 Test of the CBDS, the concentric braces in the lower five stories buckled. The strength and stiffness of the concentric braces in the fourth and fifth stories (Figure 6.71) degraded during the MO-65 Test and the fifth story braces ruptured towards the end of the test. The maximum displacement ductility in those braced bays whose strength and stiffness did not degrade (first, second, third and sixth stories) during the MO-65 Test was approximately 1.2. In the Taft-57 Test of the EBDS, the shear links at Levels L2 and L3 yielded and then strain-hardened. The maximum displacement ductility in the first story of the eccentrically braced frame was approximately 3.2 and there was no evidence of either strength or stiffness degradation.

The energy dissipation mechanisms for both the CBDS ($E_I \approx 420$ kip–in) and the EBDS ($E_I \approx 410$ kip–in) involved both damping and inelastic behavior. For severe earthquake shaking, the dissipation of energy by inelastic behavior was dominant for both the CBDS and

EBDS. In the CBDS, the inelastic behavior was concentrated in the concentric braces in the lower five stories and in the fifth story of the DMRSF. In the EBDS, the inelastic behavior was concentrated in the shear links at Levels L2 and L3; the DMRSF made a negligible contribution to energy dissipation in the EBDS during the Taft-57 Test.

8.1.5 CBDS and EBDS Hysteretic Behavior

The hysteretic behavior of the concentrically braced frame (CBF) in the CBDS and in the eccentrically braced frame (EBF) in the EBDS were significantly different. The inelastic cyclic response of the CBF was characterized by strength and stiffness degradation (Figure 6.71), whereas in the EBF, the inelastic cyclic response was ductile and stable (Figure 6.90) for a large number of yielding reversals.

The CBDS was subjected to three moderate earthquake shaking tests (MO-20, MO-27 and MO-33) and one severe test (MO-65). Including the MO-20, MO-27 and MO-33 Tests, the CBDS was subjected to approximately 30 seconds of strong motion shaking (55 seconds in full-scale units) but only 6 seconds (11 seconds in full-scale units) of *severe* earthquake shaking. The strength and stiffness of the fifth story of the CBF degraded towards the end of the MO-65 Test after only eight yielding cycles in its concentric braces.

The EBDS was subjected to five moderate earthquake shaking tests (MO-18, Taft-22, Taft-27, MO-28 and Taft-34) and three severe tests (Taft-40, Taft-57 and Taft-66). Including the moderate tests, the EBDS was subjected to approximately 100 seconds of strong motion shaking (150 seconds in full-scale units). The strength and stiffness of the EBF in the EBDS did not degrade during any of these moderate or severe earthquake simulations. There was strength and stiffness degradation of the first story of the EBF, caused by a fracture of Link L2 during the Sine-70 Test after an additional 25 seconds of severe shaking (approximately 40 seconds in full-scale units) following the Taft-66 Test. The hysteretic response of the EBF remained stable throughout the testing program with the most highly strained shear link, that is, Link L2, responding with more than 350 stable yielding cycles, of which more than 100 exceeded a shear strain ductility of 10.

8.1.6 Response Modification Factors

The ATC [11] and SEAOC [12] reduce their linear elastic design response spectra (LEDRS) to design response spectra by applying response modification factors (R and R_w, respectively). The ATC's response modification factors for CBDSs and EBDSs are 6 and 6, respectively. SEAOC's response modification factors for CBDSs and EBDSs, scaled to a level of first significant yielding, are 8 and 9.6, respectively.

The response modification factors (R) were estimated by considering them to be the product of three fundamental factors:

$$R = R_\mu \times R_S \times R_\xi$$

where R_μ, R_S and R_ξ are the ductility factor, strength factor and damping factor, respectively.

The test results for the CBDS and EBDS *models* enabled their respective response modification factors to be established. For the CBDS, the response modification factor was estimated to be

$$R = R_\mu \times R_S \times R_\xi = 1.85 \times 2.43 \times 1.0 = 4.5.$$

For the EBDS, the response modification factor was estimated to be

$$R = R_\mu \times R_S \times R_\xi = 2.12 \times 2.85 \times 1.0 = 6.0.$$

The *models* were constructed under conditions that were more stringent than those practiced in the construction industry. Furthermore, the *models* were only subjected to earthquake loading in the plane of the braced frame and the transverse responses of the *models* were constrained by transverse X-bracing. Finally, the DMRSF in the *models* was significantly stiffer and stronger than required by current seismic regulations in the United States. These response modification factors are therefore considered to be upper bounds on those factors that could be obtained from testing similar full-scale buildings designed according to the current seismic regulations in the United States.

8.1.7 DMRSF Response in the CBDS and EBDS

The DMRSF in both *models* was significantly stronger and stiffer than required by any of the seismic regulations in the United States.

The DMRSF played an important role in the response of both the CBDS and the EBDS. In the fifth story of the CBDS, the DMRSF had sufficient strength and stiffness to assume the role of the primary lateral load resisting system following the buckling and rupture of the fifth story concentric braces. This prevented the catastrophic failure of the CBDS's fifth story. In the EBDS, the DMRSF enhanced the strength and stiffness of the EBDS after the eccentrically braced frame yielded, but at no stage did it become the primary lateral load resisting system.

Despite the importance of the DMRSF in a dual system, the seismic regulations in the United States pay scant attention to its design as an integral part of the dual system. The UBC, ATC and SEAOC only require that the DMRSF resist 25% of the minimum design base shear force. They place no limits on its flexibility nor any limits on the ratio of its flexibility to that of the braced frame.

The response of the CBDS *model* to severe earthquake shaking (EPA=0.40g) would be deemed unacceptable by the seismic regulations in the United States; the maximum inter-story drift indices exceeded the UBC and ATC limit of 1.5% and the SEAOC limit of 1.12%. However, at the SEAOC inter-story drift index limit of 1.12%, the strength of the DMRSF was not fully mobilized, and the DMRSF could not contribute to energy dissipation in the CBDS. The DMRSF in the CBDS *model* was designed to resist 52% of the design base shear of the concentrically braced frame ($0.34V_b$ compared with $0.66V_b$). The 1986 SEAOC stipulates that the concentrically braced frame resist $1.50V_b$ and that the DMRSF resist $0.25V_b$, or 17% of the design base shear of the concentrically braced frame (CBF). The contribution of the DMRSF to the strength, stiffness and energy dissipation capacity of the CBDS would have been significantly smaller if the DMRSF had been designed to resist 17% rather than 52% of the CBF's design base shear. By limiting the maximum inter-story drift index to 1.12% and by requiring the DMRSF to resist only 17% of the CBF's design base shear, the 1986 SEAOC is

limiting the ability of the DMRSF to prevent the catastrophic failure of the CBDS after buckling and rupture of the concentric braces.

The EBDS *model* responded extremely well to long duration, severe earthquake shaking without strength and stiffness degradation. The DMRSF in the EBDS did not develop its potential strength prior to exceeding the SEAOC maximum inter-story drift index limit of 1.12% and thus, the DMRSF could not contribute to energy dissipation in the EBDS. The DMRSF in the EBDS *model* was designed to resist in excess of 50% of the design base shear of the eccentrically braced frame (EBF). The 1986 SEAOC stipulates that the EBF and the DMRSF resist the lateral loads in proportion to their relative rigidities (Section 2.6), but that the DMRSF be capable of resisting at least 25% of the design base shear. Assuming that the EBF was four times stiffer than the DMRSF (Section 2.7) would require the EBF to resist $0.8V_b$ and the DMRSF to resist $0.25V_b$, or 32% of the design base shear of the EBF. The contribution of the DMRSF to the strength, stiffness and energy dissipation capacity of the EBDS would have been significantly smaller if the DMRSF had been designed to resist only 32% of the EBF's design base shear. By limiting the maximum inter-story drift index to 1.12% and requiring the DMRSF to resist only 32% of the EBF's design base shear, the 1986 SEAOC is limiting the ability of the DMRSF to contribute to the strength and stiffness of the EBDS after yielding of the EBF.

8.2 Conclusions

8.2.1 Introduction

In order to avoid collapse during severe earthquake events, a dual system must: have sufficient strength to remain elastic during such an event, or possess stable, ductile hysteretic behavior for a large number of cycles in order to dissipate the input energy by plastic deformation. The UBC, ATC and SEAOC implicitly assume that general, nonessential buildings will undergo significant inelastic deformation during severe earthquake shaking. These seismic regulations assume that a building is capable of repeatedly achieving its design strength for the

large number of cycles associated with long duration, severe earthquake shaking.

The conclusions presented below relate to the response of the CBDS and EBDS *models* and also to CBDSs and EBDSs in general. These conclusions must be considered within the seven limitations discussed in Section 7.1 and categorized under: (1) Test Structures; (2) Reactive Weight; (3) Seismic Regulations; (4) Torsional Excitation and Stiffness; (5) Foundations; (6) Earthquake Ground Motions, and (7) Concentric Braces. Furthermore, the issues raised in Section 7.2 regarding the extreme susceptibility of stocky cold-formed tubular braces to rupture after only a small number of buckling cycles and the better cyclic performance of other types of bracing members must be considered in reviewing the response of the CBDS *model* to moderate and severe earthquake shaking. In Section 8.2.7, the results of this testing program are used to formulate new guidelines for the design of CBDSs and EBDSs in the United States.

8.2.2 Global Behavior of the CBDS and EBDS Models

From the standpoint of maximum strength and global displacement, a number of conclusions can be drawn from the results presented in Chapter 6 and summarized in Chapter 7 and Section 8.1:

- The elastic stiffness of the EBDS *model* was 17% higher than the elastic stiffness of the CBDS *model* because the cross-sectional areas of the EBDS's braces were 18%, 91%, 91%, 132%, 158% and 177% greater than that of the CBDS's braces in the first to sixth stories, respectively.

- The CBDS and EBDS *models* developed strengths ($0.73W_{at}$ and $0.86W_{at}$, respectively) significantly greater than their design yielding strengths ($=0.3W_{at}$) and the minimum strengths required by current seismic regulations in the United States. The overstrengths in the *models* resulted from the use of non-optimal structural sections, material overstrength, inelastic redistribution of internal forces, material strain-hardening and the need to satisfy certain code-based minimum requirements such as minimum slenderness ratios and compactness ratios.

- The EBDS *model* was 17% stronger than the CBDS *model* as a result of strain-hardening in its critical structural elements and the contribution of the concrete slab to the strength of those critical elements.

- The CBDS *model's* maximum roof drift index of 0.92% was 31% greater than the EBDS *model's* maximum roof drift index, although the EBDS *model* was subjected to an earthquake ground motion with an EPA that was 32% higher than the EPA of the most severe earthquake ground motion used to test the CBDS *model*.

8.2.3 Response of the Critical Stories in the CBDS and EBDS Models

The responses of the critical stories, that is, the stories in which failure was initiated, in the CBDS *model* (fifth) and EBDS *model* (first), were summarized and discussed in Section 7.2. The following conclusions can be drawn from these studies :

- The strength and stiffness of the CBF degraded quickly following severe buckling of its concentric braces after a small number of yielding cycles. At the onset of strength degradation in the fifth story concentric braces ($\Theta^5 = 0.6\%$), the DMRSF was forced to assume the role of the primary lateral load resisting system.

- The strength of the EBF increased following the yielding of Link L2, up to the point of the link's fracture at a first inter-story drift index of 1.3%. The shear link at Level L2 survived more than 350 yielding cycles, of which more than 100 exceeded a shear strain ductility of 10. The DMRSF in the *model* performed its intended role in the EBDS and provided additional strength and stiffness following yielding of the EBF. However, at no stage was it forced to become the primary lateral load resisting system.

- The stable hysteretic behavior of the first story of the EBF ($\mu_{max} = 3.2$) contrasted markedly with the strength-degrading response of the fifth story of the CBF ($\mu_{max} \approx 1.0 \to 1.2$).

- Without considering the extremely important issue of repeated yielding cycles, the stable ductile response of the first story of the EBF was far superior to the strength-degrading

response of the fifth story of the CBF.

8.2.4 Energy Dissipation in the CBDS and EBDS

The general conclusions that can be drawn from the comparison of the energy dissipation capabilities of the CBDS and EBDS are as follows:

- The brace buckling mechanism can dissipate a significant amount of energy per cycle of loading, provided that local buckling of the concentric braces is prevented.

- The primary concern regarding the use of tubular braces in concentrically braced frames is the susceptibility of these braces to rupture after only a small number of yielding cycles. Although suggestions have been made to improve the fracture life of tubular braces, no technique has yet been developed that will permit the tubular braces to repeatedly buckle inelastically without rupture.

- Concentrically braced frames incorporating stocky cold-formed tubular bracing members have minimal ductility prior to the degradation of their stiffness and strength. If concentrically braced frames are to be used in regions of high seismic risk, their strengths should be based on a design response spectrum that is not reduced by a ductility factor (Section 7.3) unless brace rupture can be precluded.

- Adequately stiffened shear links exhibit stable hysteretic behavior for a large number of yielding cycles. As such, eccentrically braced frames are ideally suited for buildings sited in regions of high seismic risk.

- Eccentrically braced frames can develop a significant degree of ductility. Their design strengths can therefore be based on response modification factors that include a ductility reduction factor.

8.2.5 Response Modification Factors

- From the results of the earthquake simulator testing of the CBDS and EBDS *models*, it is concluded that the response modification factors assumed by the ATC and SEAOC for these dual systems are non-conservative.

• For buildings incorporating cold-formed tubular steel braced framing and composite floor systems and designed according to the current seismic regulations, appropriate values of the response modification factor (R) are as follows:

$$R_{CBF} = 2.0 \qquad (0.5 \text{ second} \leq T_1 \leq 1.0 \text{ second})$$

$$R_{CBDS} = 2.5 \qquad (0.5 \text{ second} \leq T_1 \leq 1.0 \text{ second})$$

$$R_{EBF} = 4.0 \qquad (0.5 \text{ second} \leq T_1 \leq 1.0 \text{ second})$$

$$R_{EBDS} = 5.0 \qquad (0.5 \text{ second} \leq T_1 \leq 1.0 \text{ second})$$

In estimating values of R for a CBF and CBDS, the effects of strong motion duration were implicitly included by assuming a minimal reduction for ductility ($R_\mu \approx 1.0$), because rupture of the concentric braces must be avoided in order to maintain the integrity of the primary lateral load resisting system. Furthermore, the R values noted above for the CBDS and EBDS assume that the DMRSF is designed for a percentage of the design base shear which is similar to that prescribed by current seismic regulations in the United States. If brace types other than cold-formed tubular steel sections are used in the concentrically braced frames, the CBF may be able to dissipate more energy and respond in a more stable manner than indicated by this testing program. Improved concentric brace performance would manifest itself in larger R values.

• If optimization procedures are used to design dual systems, the response modification factors noted above should be based on strength factors that are reduced towards a value equal to one, until a study of the overstrength of optimal buildings can be conducted.

• The design of dual systems with fundamental periods less than 0.3 second should be reflected in the use of R factors significantly smaller than those noted above, for two reasons: (1) As $T_1 \to 0$ second, the ductility factor $R_\mu \to 1$ because the required elastic strength cannot be reduced by ductility, and (2) as $T_1 \to 0$ second, the more flexible DMRSF cannot contribute significantly to the strength factor, R_s; that is, the strength factor must be reduced.

8.2.6 SDOF Response Spectra and the Design of MDOF Dual Systems

The results presented in Section 7.7 have shown that smoothed SDOFS inelastic design response spectra (IDRS) are a reasonable basis for the preliminary design of MDOF dual systems. To avoid underestimating the required strength of the MDOF system at the preliminary design stage, the global displacement ductility should be assumed to be significantly smaller than those values assumed by the UBC, ATC and SEAOC. On the basis of the experimental results presented in Chapters 6 and 7, realistic estimates of μ_δ will vary between 1.25 for CBDSs and 2.00 for EBDSs.

Furthermore, the results presented in Section 7.7 indicate that it is possible to estimate a reasonable bound on the input energy to a MDOF system using SDOF energy spectra, if the ranges of the MDOFS's yielding strength and fundamental period can be established. However, it was shown that the input energy is sensitive to a number of parameters that include: the yielding strength, R_y, of the building; the effective fundamental period of the building during the earthquake; the duration of strong motion shaking; the frequency content of the earthquake ground motion, and the stability of the building's hysteretic response. In order to use energy methods in the design process, energy design response spectra (EDRS) must be developed and the influence of these five parameters must be included in their development.

The results presented in Section 7.7 clearly indicate that the minimum strength requirements of the 1986 SEAOC (and the 1985 UBC and 1984 ATC 3-06) are too low. These seismic regulations place too great a reliance, albeit implicitly, on a building's overstrength and ductility, for acceptable performance during severe earthquake shaking.

8.2.7 Recommendations for the Design of Dual Systems

On the basis of earthquake simulator testing of two steel dual systems at the University of California at Berkeley, a number of recommendations for the design of steel dual systems are formulated.

Ductile Moment Resisting Space Frames:

- The seismic regulations in the United States should: increase the minimum required strengths for DMRSFs in dual systems relative to the minimum strengths of braced frames so that the relative strengths of DMRSFs are similar to those used in the *models*, and limit the flexibility of the DMRSF so that it yields before exceeding the code-specified inter-story drift limits or the maximum deformation capacity of the braced frame or both, in order to allow the DMRSF to contribute to energy dissipation in the dual system.

- Since the role of the DMRSF in the CBDS was significantly different from its role in the EBDS, the relationship between the strength of the DMRSF and the concentrically braced frame in the CBDS and the relationship between the strength of the DMRSF and the eccentrically braced frame in the EBDS, should differ (see below).

Concentrically Braced Frames and Dual Systems:

Essential facilities such as hospitals, communication centers and so on, must remain operational after a major earthquake. Therefore, these facilities should be designed to remain elastic during a major earthquake. The concentrically braced dual system can be effective in this application because its stiffness will tend to minimize internal damage in the facility, provided that it remains elastic.

- The minimum strength requirements for concentrically braced frames (CBFs) should be high enough to ensure elastic response during severe earthquake shaking because CBFs possess minimal ductility, and may fail catastrophically by brace rupture during moderate and long duration shaking. The design strength of a CBF should therefore be based on *reliable* linear elastic design response spectra and *realistic* response modification factors ($\approx$ 2.0 : see Section 8.2.5).

- The design strength of a CBDS should be based on *reliable* linear elastic design response spectra and *realistic* response modification factors ($\approx$ 2.5 : Section 8.2.5).

- The DMRSF in a CBDS should be designed for a significantly larger stiffness and a higher percentage of the design base shear than currently required by seismic regulations in the United States. The following guidelines, based on the testing of the CBDS *model*, could be used to design the DMRSF:

$$V_{DMRSF} \approx 40\% - 50\% \text{ of } V_{CBF}$$

$$K_{DMRSF} \approx 30\% - 50\% \text{ of } K_{CBF}.$$

Eccentrically Braced Frames and Dual Systems:

- The design strengths of EBFs and EBDSs should be based on *reliable* linear elastic design response spectra and *realistic* response modification factors (see Section 8.2.5).

- The DMRSF in an EBDS should be designed for a significantly larger stiffness and a higher percentage of the design base shear, than required by current seismic regulations in the United States. The following guidelines, based on the testing of the EBDS *model*, could be used to design the DMRSF :

$$V_{DMRSF} \approx 30\% - 40\% \text{ of } V_{EBF}$$

$$K_{DMRSF} \approx 30\% - 50\% \text{ of } K_{EBF}.$$

8.3 Rational Design Procedures for Steel Structures

8.3.1 General

A rational design method for the earthquake-resistant design of steel structures is currently unavailable. Bertero [30] has suggested an interim method that uses the ATC LEDRS and a realistic value of the response modification factor (R) to estimate the story shear demand. In this section, an outline of one rational design procedure for the design of steel dual systems in regions of high seismic risk is presented. This design method is by no means complete and for its implementation, a large number of parametric studies, both experimental and analytical, must be undertaken. The method described below recognizes the stochastic

nature of the excitation and the inelastic nature of the response of typical buildings to severe earthquake shaking.

8.3.2 A Brief Review of Current Practice

The 1985 UBC [10], 1984 ATC 3-06 [11] and the 1986 SEAOC [12] are three seismic design regulations currently in use in the United States. Although there are significant differences between the UBC, ATC and SEAOC, all three regulations adopt an inelastic response spectrum as the basis for an elastic analysis and design.

The use of elastic design methods for structures assumed to undergo significant inelastic activity is questionable and can be justified only for standard structures whose elastic and inelastic response is well understood, or on the basis that no other design method is available. The rational design method detailed in Section 8.3.3 is philosophically different from the UBC, ATC or SEAOC since it explicitly recognizes the differences between the requirements of the serviceability and collapse limit states and uses design methods that are appropriate to both limit states.

8.3.3 An Outline of a Rational Design Method

General:

The philosophy behind this design procedure is to satisfy serviceability requirements for minor, frequent earthquakes and to avoid collapse or life-threatening damage during major, rare earthquakes (*collapse limit state*).

Design for Serviceability Requirements:

The basic premise in the design for the serviceability limit state is that any form of structural or non-structural damage is avoided during frequent minor earthquakes. The ATC LEDRS [11] is currently anchored to an effective peak acceleration of 0.4g for seismic design in regions of high seismic risk; these spectra are inappropriate for design for serviceability requirements. As any form of damage is precluded in the serviceability limit state, the use of a smoothed linear elastic design response spectrum (LEDRS) is both the simplest and the most

appropriate means by which to design buildings. In this instance, the LEDRS should be anchored to effective peak accelerations of the order of 0.05g to 0.10g depending upon the seismicity of the region. The effective peak accelerations should reflect the characteristics of low-level ground motions previously recorded at the particular site, or other sites of similar seismicity and local and global geology.

The seismic design forces should be based on the LEDRS noted above with no reduction for ductility or overstrength, that is, R equal to one. A procedure similar to that prescribed by the ATC [11] which accounts for the effects of orthogonal loading, torsional loading and so on, could be used to analyze and design the building. If the building being designed is a dual system, the minimum strength and stiffness requirements for the DMRSF should be based on the guidelines presented in Section 8.2. The building should then be re-analyzed to ensure that: (1) the initial design assumptions were adequate; and (2) the inter-story drifts were sufficiently small so as to preclude non-structural damage.

Design for the Collapse (Safety) Limit State:

The basic premise in the design for the collapse (safety), limit state is that structural collapse or damage hazardous to human life, is avoided during severe earthquake shaking. A deterministic approach to earthquake-resistant design of a building is shortsighted because both the building's dynamic characteristics and the characteristics of an earthquake that will drive the building to its maximum response, are rarely known with any degree of certainty. The design procedure discussed below attempts to ensure that the building's stiffness, strength and energy dissipation capacity (Steps 2, 3, 5 and 6) exceeds that required to survive severe earthquake shaking (Steps 1 and 4), that is, the "building's *supply*" exceeds the "earthquake's *demand*".

To implement such a rational design method, a broad database of earthquake records would be required for a wide variety of fault types, geological conditions and so on. These earthquake records would be used to develop

- Smoothed Inelastic Design Response Spectra, $IDRS(\eta,\xi,T)$

- Smoothed Input Energy Design Response Spectra, $EDRS(\eta,\xi,T)$.

A six-step procedure for designing a building against collapse during severe earthquake shaking is outlined below. The following procedure assumes that the building has already been designed to satisfy the serviceability requirements for minor earthquake shaking and that a range for each of the building's dynamic characteristics has been established.

Step 1: Construct an IDRS that is indicative of: (1) the characteristics of previously recorded severe ground motions at the site (or at sites of similar seismicity and local and global geology); (2) the building's damping properties; (3) the ductility that can be developed in the structural system without exceeding the maximum acceptable inter-story drift index; and (4) the expected hysteretic behavior (bilinear, trilinear, strength-degrading, and so on) of the structural system.

Step 2: Perform static load-to-collapse analyses of the building using nonlinear computer programs [34,35], for both rectangular and triangular load patterns, to determine the following:

- the strength of the building at the level of first significant yielding (R_y);

- the maximum strength of the building (R_{max}) at the maximum allowable inter-story drift index;

- the building's collapse mechanisms for both the rectangular and triangular lateral load distributions;

- the maximum plastic rotations in the hinging regions.

Step 3: Review the results of the analyses performed in **Step 2** to ensure that:

- the effective yielding strength of the building (determined for example using R_y and R_{max} and the equal energy method - Figures 7.10 and 7.11) is approximately equal to, or greater than, that strength demanded by the IDRS;

- the collapse mechanism is acceptable, that is, the distribution of inelastic deformation over the height of the building is relatively uniform;

- the maximum plastic rotations in the hinging regions can be developed in the structural sections;

- the distribution of strength and stiffness between the braced frames and the DMRSF (dual system only) is acceptable.

If either: (1) the effective yielding strength of the building, (2) the collapse mechanisms; (3) the maximum plastic rotations, or (4) the distribution of strength and stiffness between the braced frames and the DMRSF (dual system only) are unacceptable, redesign the building and return to **Step 2**.

Step 4: For the site under consideration, select an input energy design response spectrum (EDRS) that reflects: (1) the characteristics of the previously recorded severe ground motions at the site (or at sites having similar seismicity and local and global geology); (2) the damping properties of the building, and (3) the hysteretic characteristics of the structural system. This spectrum would be used to estimate the maximum amount of energy that could be imparted to the building during severe earthquake shaking.

Step 5: In the period range under consideration, select those earthquake ground motions that maximize the input energy for the building. In order to account for the stochastic nature of earthquake shaking, a number of earthquake ground motions should be selected. Perform non-linear dynamic analysis of the building using these earthquake ground motions, and determine:

- the performance of the building in terms of: (1) the maximum inter-story drift indices, and (2) the uniformity of the maximum inter-story drift indices, that is, the damage distribution;

- the plastic hinge rotation time histories in the critical regions and therefore the cumulative plastic rotations in these regions;

- the sensitivity of the strength of the building, the maximum inter-story drift indices and the uniformity of the damage distribution, to minor changes in the mechanical characteristics of those elements that control the response of the building; for example, a 20% decrease in the strength of the shear link in the bottom story of an EBDS.

Step 6: Using damage laws such as those summarized by Allahabadi [56] and the plastic hinge rotation time histories in the critical regions of the building, determine the likelihood of failure of these critical regions by low-cycle fatigue or incremental collapse. If either: (1) the performance of the building is unacceptable; or (2) its sensitivity to minor variations in mechanical characteristics is too great, or (3) there is a high probability of the failure of certain critical regions by low-cycle fatigue or incremental collapse, redesign the building and return to **Step 2**.

Discussion:

It must be recognized that internal force redistribution is the primary means of increasing the strength of a structure above its first significant yielding strength and that this redistribution is controlled by the degree of stable ductile behavior in the critical yielding regions. Accordingly, the structure must be designed and detailed to facilitate this redistribution. The detailing of the plastic hinge zones to maximize their ductility and to facilitate the strain-hardening of the material in the hinging regions cannot be over-emphasized.

Steps 2 to 5 of this design methodology is based on nonlinear planar frame analysis. The elastic and inelastic torsional response of buildings to seismic input has received insufficient attention in current seismic regulations. The elastic torsional response of structures, especially single story structures, to seismic input (resulting from the center of stiffness and the center of reactive weight not coinciding) is reasonably well understood. The inelastic torsional response of buildings to seismic input (resulting from the yielding and/or failure of sections of the primary lateral load resisting system) is not explicitly addressed in current seismic regulations. The ATC has wisely recommended that the primary lateral load resisting system be comprised of a minimum of four separate lines of framing in two orthogonal directions and that they be symmetrically located around the center of mass of the building. A minimum of four separate lines of framing of comparable stiffness in a given direction would: reduce the increased lateral load demand on a given line of framing resulting from the yielding of a parallel line of framing, and enhance the torsional stiffness, strength and redundancy of the entire building. In

design for the elastic and inelastic torsional response of braced and unbraced steel buildings, the following factors should be considered:

- The accidental eccentricity used to calculate the torsional moment on the building at a given level should reflect the in-plane stiffness of the floor system and the number and disposition of the lines of framing in the primary lateral load resisting system.

- A minimum of four separate vertical lines of framing of comparable stiffness and symmetrically located about the center of mass, in orthogonal directions should form the basis of the primary lateral load resisting system. These vertical framing lines should be symmetrically located about the center of mass of the building and positioned to maximize the torsional stiffness of the building. If the number of lines of framing in the primary lateral load resisting system is less than three in a given direction, those lines of framing should be designed assuming the loss of stiffness in a line of parallel framing.

As the profession's understanding of inelastic analysis and design procedures improve, the six-step, two-dimensional procedure noted above should be extended to three-dimensions and should explicitly account for accidental torsion and torsion due to unsymmetrical inelastic response. This would eliminate one of the major uncertainties associated with this design procedure.

It is of paramount importance to recognize that the procedure outlined above is by no means complete and rigorous. In order to implement this procedure, realistic LEDRS, IDRS, EDRS and response modification factors must be derived. As noted in Section 8.4, a great deal of research in these subject areas is required.

8.4 Recommendations for Future Research

It was noted in Section 8.3.1 that a rational design method for the earthquake-resistant design of steel structures is currently unavailable. Although a rational procedure is discussed in Section 8.3.3, it cannot be implemented into the current seismic regulations in the short-term. The interim method proposed by Bertero [30] makes use of realistic linear elastic design

response spectra and response modification factors.

In order to develop a more rational approach to the design of steel dual systems, many aspects require intensive investigation; in particular the following:

Response Modification Factors: The ATC and SEAOC response modification factors (R and R_w) overestimate the maximum possible reductions in the required elastic strengths of CBFs, CBDSs, EBFs and EBDSs. There is a need to evaluate, both analytically and experimentally, the strengths of steel dual systems that have been designed and constructed according to current seismic regulations. This information should result in response modification factors that are functions of the natural period, ductility supply and redundancy of the structural system.

Code Seismic Forces: The minimum seismic forces specified by the 1985 UBC, 1984 ATC and 1986 SEAOC are significantly smaller than those forces that were developed in the CBDS and EBDS during severe earthquake shaking. The minimum seismic forces must be upgraded to a level whereby a dual system, designed for these forces and the other code-based minimum requirements, will survive severe earthquake shaking.

Structural Layout: For the interim design method suggested by Bertero [30], the seismic regulations should provide guidelines regarding: (1) the minimum number of braced frames in the dual system; (2) the optimal plan distribution of braced frames in the dual system; and (3) the effects of diaphragm stiffness on the response of dual systems.

Dual System Compatibility: The interaction of braced frames and DMRSFs in a dual system requires further study. Emphasis should focus on determining the requirements for the DMRSF such that the strength and deformation envelope of the dual system remains stable after yielding of the braced frame, up to inter-story drift indices between 1.5% and 2.0%. The relationships between the relative lateral stiffness, deformability, ductility and yielding strengths of the braced frame and the DMRSF must be quantified if dual systems are to perform successfully in regions of high seismic risk.

Energy Methods: A rational design procedure incorporating energy methods must be based on reliable energy spectra; these spectra should reflect a number of parameters that include the local and global geological conditions, distance from the active fault, the characteristics of previously recorded earthquake ground motions and so on. Damage laws must be developed to estimate the fatigue life of structures at both the global and local levels in order to utilize the energy spectra noted above (Section 8.3.3).

SDOFS Spectra: SDOFS response spectra are currently being used to describe the response of MDOFS. Although the studies presented in Chapter 7 suggest that SDOFS spectra can be used to predict MDOFS response with a reasonable degree of accuracy, further studies are needed to establish bounds on the characteristics of the MDOFS that permit the assumption of SDOFS response. These studies should focus on the different types of structural systems, that is: flexural-type response exhibited by braced frames and shear walls, and shear-type response exhibited by moment-resisting space frames.

REFERENCES

[1] Whittaker A.S., Uang C.M. and Bertero V.V., "Earthquake Simulation Tests and Associated Studies of a 0.3-Scale Model of a Six-Story Eccentrically Braced Steel Structure," *Report No. UCB/EERC-87/02,* Earthquake Engineering Research Center, University of California, Berkeley, CA, July 1987.

[2] Uang C.M. and Bertero V.V., "Earthquake Simulation Tests and Associated Studies of a 0.3-Scale Model of a Six-Story Concentrically Braced Steel Structure", *Report No. UCB/EERC-86/10,* Earthquake Engineering Research Center, University of California, Berkeley, CA, December 1986.

[3] Kasai, K. and Popov, E.P., "A Study of Seismically Resistant Eccentrically Braced Steel Frame Systems," *Report No. UCB/EERC-86/01,* Earthquake Engineering Research Center, University of California, Berkeley, CA, January 1986.

[4] Hjelmstad, K.D. and Popov, E.P., "Seismic Behaviour of Active Beam Links in Eccentrically Braced Frames," *Report No. UCB/EERC-83/15,* Earthquake Engineering Research Center, University of California, Berkeley, CA, July 1983.

[5] Bertero, V.V., Uang, C.M. and Whittaker, A.S., "Test Structures : Experimental Response and Code Compliance," *ASCE Specialty Conference,* Orlando, Florida, August 1987.

[6] U.S.-Japan Planning Group, Cooperative Research Program Utilizing Large-Scale Testing Facilities, "Recommendations for a US-Japan Cooperative Research Program Utilizing Large Scale Facilities," *Report No. UCB/EERC-79/26,* Earthquake Engineering Research Center, University of California, Berkeley, CA, 1979.

[7] Foutch, D.A., Goel, S.C. and Roeder, C.W., "Preliminary Report on Seismic Testing of a Full-Scale Six-Story Steel Building," *Report No. UILU-ENG-86-2009,* University of Illinois at Urbana-Champaign, Urbana, Illinois, November 1986.

[8] Foutch, D.A., Goel, S.C. and Roeder, C.W., "Seismic Testing of Full-Scale Steel Building - Parts I and II," *Journal of Structural Engineering,* ASCE, Volume 113, No. 11, November 1987.

[9] Watabe, M., "Earthquake Resistant Regulations for Building Structures in Japan," *Earthquake Resistant Regulations - A World List*, July 1984.

[10] International Conference of Building Officials, *Uniform Building Code*, 1985 Edition, Whittier, California.

[11] Applied Technology Council, *"Tentative Provisions for the Development of Seismic Regulations for Buildings,"* ATC 3-06, National Bureau of Standards, U.S. Department of Commerce, Washington, D.C., 1984.

[12] Structural Engineers Association of California, *Recommended Lateral Force Requirements*, Final Draft, San Francisco, CA, December 1986.

[13] Khatib, I., Mahin, S.A. and Pister, K.S., "Seismic Behavior of Concentrically Braced Steel Frames," *Report No. UCB/EERC-88/01*, Earthquake Engineering Research Center, University of California, Berkeley, CA, January 1988.

[14] Tang, X. and Goel, S.C., "Seismic Analysis and Design Considerations of Braced Steel Structures," *Report No. UMCE 87-4*, The University of Michigan, Ann Arbor, Michigan, 1987.

[15] Ricles, J.M. and Popov, E.P., "Experiments on Eccentrically Braced Frames with Composite Floors," *Report No. UCB/EERC-87/06*, Earthquake Engineering Research Center, University of California, Berkeley, CA, June 1987.

[16] Ricles, J.M. and Popov, E.P., "Dynamic Analysis of Seismically Resistant Eccentrically Braced Frames," *Report No. UCB/EERC-87/07*, Earthquake Engineering Research Center, University of California, Berkeley, CA, June 1987.

[17] Engelhardt, M.D., "Long Links in Eccentrically Braced Frames - A Preliminary Assessment," *CE299 Report*, Department of Civil Engineering, University of California, Berkeley, CA, 1987.

[18] Khan, F.R. and Sbarounis, J.A., "Interaction of Shear Walls and Frames," *Journal of the Structural Division*, ASCE, Volume 90, No. ST3, June 1964, Part 1.

[19] Foutch, D.A. et. al., "Summary of the Design and Construction of the Full-Scale Specimen and Results of the Phase 1 Tests," *Structures Congress 3*, ASCE Annual Convention, San Francisco, CA, October 1984.

[20] Yamanouchi, H., and Midorikawa, M., "Design of the Full-Scale Six-Story Steel Building," *The Third Joint Technical Coordinating Committee*, U.S.-Japan Cooperative Research Program Utilizing Large Scale Test Facilities, Tsukuba, Japan, July 1982.

[21] Roeder, C.W. and Popov, E.P., "Inelastic Behaviour of Eccentric Braced Steel Frames Under Cyclic Loading," *Report No. UCB/EERC-77/18*, Earthquake Engineering Research Center, University of California, Berkeley, CA, August 1977.

[22] Malley, J.O. and Popov, E.P., "Design of Links and Beam-Column Connections for Eccentric Braced Steel Frames" *Report No. UCB/EERC-83/03*, Earthquake Engineering Research Center, University of California, Berkeley, CA, January 1983.

[23] Manheim, D., "On the Design of Eccentric Braced Frames," *Thesis presented to the University of California, Berkeley, in partial fulfillment of the degree of Doctor of Engineering*, Berkeley, CA, 1982.

[24] California Institute of Technology, "Strong Motion Accelerograms : Volumes 1-4"; *EERL Reports*, Earthquake Engineering Research Laboratory, California Institute of Technology, Pasadena, CA, July 1969 - present.

[25] Kawakami, Y., Midorikawa, M. and Nishiyama, I., "U.S.-Japan Cooperative Large Scale Earthquake Research Program : Earthquake Simulation Tests of a Full-Scale Model of a Six-Story Test Structure," *Building Research Institute*, Tsukuba, Japan, May 1985.

[26] Yamanouchi, H., Midorikawa, M. et al., "Inelastic Seismic Tests on a Full-Scale Six Story Eccentric K-Braced Steel Building," *Proceedings of the 17th Joint Panel Meeting of the U.S.-Japan Cooperative Program in Wind and Seismic Effects*, Tsukuba, Japan,

May 1985.

[27] B.R.I. Steel Group, "Phase II Test Results," *The Sixth Joint Technical Coordinating Committee*, U.S.-Japan Cooperative Research Program Utilizing Large Scale Testing Facilities, June 1985.

[28] B.R.I. Steel Group, "Phase III Test Results," *The Sixth Joint Technical Coordinating Committee*, U.S.-Japan Cooperative Research Program Utilizing Large Scale Testing Facilities, June 1985.

[29] Wilson, E.L., *The SAP-80 Series of Structural Analysis Programs for CP/M-80 Microcomputer Systems*, February 1984.

[30] Bertero, V.V., "Implications of Recent Earthquakes and Research on Earthquake-Resistant Design and Construction of Buildings," *Report No. UCB/EERC-86/03*, Earthquake Engineering Research Center, University of California, Berkeley, CA, March 1986.

[31] Rea, D. and Penzien, J., "Dynamic Response of a 20 ft x 20 ft Shaking Table, " *Proceedings of the Fifth World Conference on Earthquake Engineering*, Vol. 2, Rome, Italy, 1974.

[32] Becker, R.A. and Chambers, J.M., *S - An Interactive Environment for Data Analysis and Graphics*, The Wadsworth Statistics/Probability Series, 1984.

[33] Kannan, A.E. and Powell, G.H., "DRAIN-2D, A General Purpose Computer Program for Dynamic Analysis of Inelastic Plane Structures," *Report No. UCB/EERC-73/6*, Earthquake Engineering Research Center, University of California, Berkeley, CA, April, 1973.

[34] Allahabadi, R. and Powell, G.H., "DRAIN-2DX, Users Guide," *Report No. UCB/EERC-88/06* Earthquake Engineering Research Center, University of California, Berkeley, CA, May 1988.

[35] Mondkar, D.P. and Powell, G.H., "ANSR-1, General Purpose Computer Program for Analysis of Non-linear Structure Response," *Report No. UCB/EERC-75/17*, Earthquake Engineering Research Center, University of California, Berkeley, CA, 1975.

[36] Clough, R.W. and Penzien, J., *Dynamics of Structures*, McGraw-Hill, New York, 1975.

[37] Mahin, S.A. and Lin, J., "Construction of Inelastic Response Spectra for Single Degree of Freedom System," *Report No. UCB/EERC-83/17*, Earthquake Engineering Research Center, University of California, Berkeley, CA, March 1983.

[38] Ormsby, J.F., "Design of Numerical Filters with Applications to Missile Data Processing," *Journal of the Association for Computing Machinery*, Volume 8, No. 3, July 1961.

[39] Blondet, J.M., "Studies on Evaluation of Shaking Table Response Analysis Procedures," *Report No. UCB/EERC-81/18*, Earthquake Engineering Research Center, University of California, Berkeley, CA, November 1981.

[40] Kaba, S.A. and Mahin, S.A., "Interactive Computer Analysis Methods for Predicting the Inelastic Cyclic Behavior of Structural Sections,"
Report No. UCB/EERC-83/18, Earthquake Engineering Research Center, University of California, Berkeley, CA, July 1983.

[41] Zahrah, T.H. and Hall, W.J., "Seismic Energy Absorption in Simple Structures," *Report No. UILU-ENG-82-2011*, University of Illinois at Urbana-Champaign, Urbana, Illinois, 1982.

[42] American Institute of Steel Construction, *Specification for the Design, Fabrication and Erection of Structural Steel for Buildings*, New York, N.Y., 1980.

[43] Brokken, S. and Bertero, V.V., "Studies on the Effects of Infills in Seismic Resistant R/C Construction," *Report No. UCB/EERC-81/12*, Earthquake Engineering Research Center, University of California, Berkeley, CA, September 1981.

[44] Uang, C.M., Whittaker, A.S and Bertero, V.V., "Effects of Scaling and Testing Methods on the Seismic Response of a Braced Steel Frame," *Paper submitted for publication in the Journal of the Structural Division, ASCE*.

[45] Bertero, V.V. and Moustafa, S.E., "Steel Encased Expansive Cement Concrete Columns," *Journal of the Structural Division*, ASCE, Volume 96, No. ST11, November 1970.

[46] Liu, Z. and Goel, S.C., "Investigation of Concrete-Filled Steel Tubes Under Cyclic Bending and Buckling," *Report No. UMCE 87-3*, The University of Michigan, Ann Arbor, Michigan, 1987.

[47] Jain, A.K., Goel, S.C. and Hanson, R.D., "Static and Dynamic Hysteresis Behavior of Steel Tubular Members with Welded Gusset Plates," *Report No. UMEE 77R3*, The University of Michigan, Ann Arbor, Michigan, June 1977.

[48] Jain, A.K., Goel, S.C. and Hanson, R.D., "Hysteresis Behavior of Bracing Members and Seismic Response of Braced Frames with Different Proportions," *Report No. UMEE 78R3*, The University of Michigan, Ann Arbor, Michigan, July 1978.

[49] Gugerli, H. and Goel, S.C., "Inelastic Cyclic Behavior of Steel Bracing Members," *Report No. UMEE 82R1*, The University of Michigan, Ann Arbor, Michigan, January 1982.

[50] Astaneh-Asl, A., Goel, S.C. and Hanson, R.D., "Cyclic Behavior of Double Angle Bracing Members with End Gusset Plates," *Report No. UMEE 82R7*, The University of Michigan, Ann Arbor, Michigan, August 1982.

[51] Foutch, D.A., "Evaluation of Performance of the Phase Two Structure and Implications for Design," *Paper presented to the Seventh Joint Technical Coordinating Committee*, U.S.-Japan Cooperative Research Program Utilizing Large Scale Testing Facilities, July 1987.

[52] Uang, C.M. and Bertero V.V., "Implications of Recorded Earthquake Ground Motions on the Seismic Design of Building Structures," *Report No. UCB/EERC-88/13*, Earthquake Engineering Research Center, University of California, Berkeley, CA, September 1988.

[53] Newmark, N.M. and Hall, W.J., *Earthquake Spectra and Design*, Earthquake Engineering Research Institute, 1982

[54] Housner, G.W., "Limit Design of Structures to Resist Earthquakes," *Proceedings of the World Conference on Earthquake Engineering*, Berkeley, California, 1956.

[55] Akiyama, H., "Earthquake Resistant Limit-State Design for Buildings," University of Tokyo Press, 1985.

[56] Allahabadi, R., "Seismic Response and Damage Assessment for 2D Structures," *Thesis presented to the University of California, Berkeley, in partial fulfillment of the degree of Doctor of Engineering,* Berkeley, CA, 1987.

APPENDICES

APPENDIX A

ENERGY DISSIPATION IN ECCENTRICALLY BRACED FRAMES

The ability of an EBF to dissipate energy has been demonstrated both in this testing program (Chapter 7) and elsewhere [3,4,21]. For the six-story EBF tested on the earthquake simulator, the distribution of energy dissipation was highly nonuniform and was concentrated in the first story.

A comparison of the energy dissipation in a six-story EBF: (a) deforming uniformly over its height (Figure 7.9c), and (b) forming a soft first story (Figure 7.9d), clearly demonstrates the benefits of optimizing the distribution of the plastic shear strengths of the links in an EBF.

Consider a six-story, constant story height and story mass EBF similar to that shown in Figure 7.9. If the EBF forms a single degree-of-freedom (DOF) mechanism involving all six shear links, the state vector of nodal displacements ($\underline{U}$) can be expressed as

$$\underline{U} = \{ 1\ 2\ 3\ 4\ 5\ 6 \}\Theta h = \underline{\lambda}\Theta h \qquad (A.1)$$

where Θ = plastic inter–story drift index

      h = story height

      $\underline{\lambda}$ = vector of displacement ordinates,

where the ith DOF corresponds to the lateral displacement of the ith floor. For the purposes of this discussion, the six-story EBF is idealized as a six DOF lumped mass system with the building mass concentrated at the floor levels.

The state vector of nodal accelerations ($\underline{\ddot{U}}$) is directly proportional to the nodal displacements ($\underline{U}$), that is,

$$\underline{\ddot{U}} = \alpha\ \underline{U} = \alpha\underline{\lambda}\Theta h \qquad (A.2)$$

For a uniform mass distribution over the height of the EBF,

$$\underline{M} = \text{diag}\ [1\ 1\ 1\ 1\ 1\ 1]m \qquad (A.3)$$

where $\underline{M}$ = diagonal mass matrix (6×6)

m = story mass.

The state vector of nodal inertia forces (P) can be expressed as

$$\underline{P} = \underline{M}\underline{\ddot{U}} = m\alpha\lambda\Theta h = \beta\lambda\Theta \tag{A.4}$$

and the corresponding vector of story shear forces ($\underline{V}$) as

$$\underline{V} = \{\ 21\ 20\ 18\ 15\ 11\ 6\ \}\beta\Theta \tag{A.5}$$

where the story shear force at the *ith* level is the sum of the story inertia forces above the *ith* level, that is

$$V_i = \sum_{j=i}^{6} P_j$$

If the EBF forms a soft first story, the corresponding state vectors are

$$\underline{U} = \{\ 1\ 1\ 1\ 1\ 1\ 1\ \}\Theta h = \underline{\lambda}\Theta h \tag{A.6}$$

$$\underline{\ddot{U}} = \alpha\ \underline{U} = \alpha\underline{\lambda}\Theta h \tag{A.7}$$

$$\underline{P} = \beta\lambda\Theta \tag{A.8}$$

$$\underline{V} = \{\ 6\ 5\ 4\ 3\ 2\ 1\ \}\beta\Theta \tag{A.9}$$

Consider the shear yielding mechanism in the single story, single bay, pin-based, split-K EBF of story height h, span length L and link length e, shown in Figure A1. The story yielding strength (R_y) is related to the plastic yielding strength (V_p) of the link by

$$R_y = \frac{V_p L}{2h} \tag{A.10}$$

where a point of contraflexure is assumed at the center-line of the link. The kinematically admissible displacement field associated with the mechanism shown in Figure A1 is well established as

$$\Theta_p = \gamma_p\left(\frac{e}{L}\right) \tag{A.11}$$

where Θ_p = plastic inter–story drift index

$$= \Theta_{TOTAL} - \Theta_e \approx \Theta_{TOTAL}$$

Θ_e = elastic inter-story drift index

γ_p = plastic shear strain

$= \gamma_{TOTAL} - \gamma_e \simeq \gamma_{TOTAL}$

γ_e = elastic shear strain

Assuming an e/L ratio of between 1/7.5 and 1/12.5, that is,

$$0.08 \le \frac{e}{L} \le 0.13$$

and a maximum shear strain of approximately 10% [3], the maximum inter-story drift index (Θ) is limited to

$$0.80\% \le \Theta \le 1.33\%$$

An optimal design of an EBF would result in its forming a SDOF collapse mechanism and ideally, all shear links yielding simultaneously. For this six-story EBF, this would result in a link plastic shear force distribution ($\underline{V_p}$) over the height of the building as

$$\underline{V_p} = \{\ 21\ 20\ 18\ 15\ 11\ 6\ \}\ \Pi \qquad \text{(A.12)}$$

where Π is a constant, and V_{pi} is the plastic shear force in the link at the *ith* level.

The formation of a soft first story will generally preclude shear yielding in the remaining links unless the shear link in the first story undergoes a significant degree of strain-hardening. That is, energy dissipation will be confined primarily to the first story rather than being distributed over the height of the EBF.

The comparison below of the energy dissipation capacity of: (a) the six-story EBF forming a SDOF mechanism involving all six stories; and (b) the six-story EBF forming a soft first story, clearly shows the value of mobilizing all of the shear links to dissipate energy.

Case 1: SDOF Mechanism

Assuming that all six links yield simultaneously, the link shear strains, assuming an e/L ratio equal to 0.1, at a uniform inter-story drift index of 1%, are

$$\underline{\gamma} = \{\ 1\ 1\ 1\ 1\ 1\ 1\ \}\ 0.1\ \text{radian} \qquad \text{(A.13)}$$

where γ_i is the link shear strain at the ith level. The energy dissipated by all six links (E_L) is therefore approximately equal to

$$E_L \approx V^T_p \; \underline{\gamma} \; e \tag{A.14}$$

where the first term on the right hand side of A.14 is transpose of the vector V_p and the product of the following two terms is the shear displacement vector for the links. From equations A.12, A.13 and A.14

$$E_L = 91 \text{ units (kip–in).} \tag{A.15}$$

Case 2: Soft First Story Mechanism

The link shear strains, corresponding to the formation of a soft first story, an e/L ratio equal to 0.1 and a first inter-story drift index of 1%, are

$$\underline{\gamma} = \{ 1 \; 0 \; 0 \; 0 \; 0 \; 0 \} \; 0.1 \text{ radian.} \tag{A.16}$$

and the energy dissipated by all six links (E_L) is equal to

$$E_L \approx V^T_p \; \underline{\gamma} \; e = 21 \text{ units (kip–in).} \tag{A.17}$$

Summary

The difference between the energy dissipated by the complete mechanism and the soft first story mechanism is by a factor of

$$\frac{E_L^{\text{Case 1}}}{E_L^{\text{Case 2}}} = \frac{91}{21} = 4 \tag{A.18}$$

ignoring the effects of strain-hardening and assuming elastic response in the remaining elements in the EBF. The advantages of obtaining a complete SDOF mechanism are obvious, namely a four-fold increase in the capacity of the EBF to dissipate energy. That is, an EBF forming a complete SDOF mechanism would be capable of surviving a far more severe earthquake, in terms of increased acceleration and/or duration, than an EBF forming a soft first story.

Clearly a design objective with EBFs is to achieve a complete SDOF mechanism (Case 1) in the event of severe earthquake shaking. As a starting point, the procedure followed above can be used for the preliminary design of an EBF or a dual system incorporating EBFs. It must be noted however that the ground motion characteristics will affect the inertia force distribution in the structure. An impulsive-type earthquake will tend to concentrate demand in the lower stories of a building while an harmonic-type earthquake will place greater demand in the upper stories of a building. Inelastic dynamic analyses of an EBF (or dual system) should be undertaken for the types of earthquake ground motions expected at the site in order to refine the distribution of link plastic shear capacities over the height of the EBF.

Energy methods have been recently proposed by the authors as a design tool in earthquake-resistant design. The unique energy dissipation characteristics of an EBF, that is: (a) stable hysteretic behavior; and (b) controlled inelastic behavior in the links; as opposed to other systems in which: (a) the energy is dissipated in a more random manner throughout the structure; and (b) degrades with an increasing number of yielding reversals, suggest that the design of EBFs can be based in part on energy methods. The energy dissipation capacity (**SUPPLY**) of an EBF, in a given cycle of loading can be estimated with a reasonable degree of accuracy as being:

$$E_L = \sum_{i=1}^{n} 4 \, V_p \, \gamma_i \, e_i \qquad (A.19)$$

if all n links yield simultaneously. Assuming that the maximum rate of energy input (power) can be estimated for a given loading cycle (**DEMAND**), the **DEMAND** can be compared with the **SUPPLY** to ensure that the former is less than the latter. Once the "energy supply" exceeds the "critical earthquake demand", inelastic dynamic analysis should be undertaken as noted above.
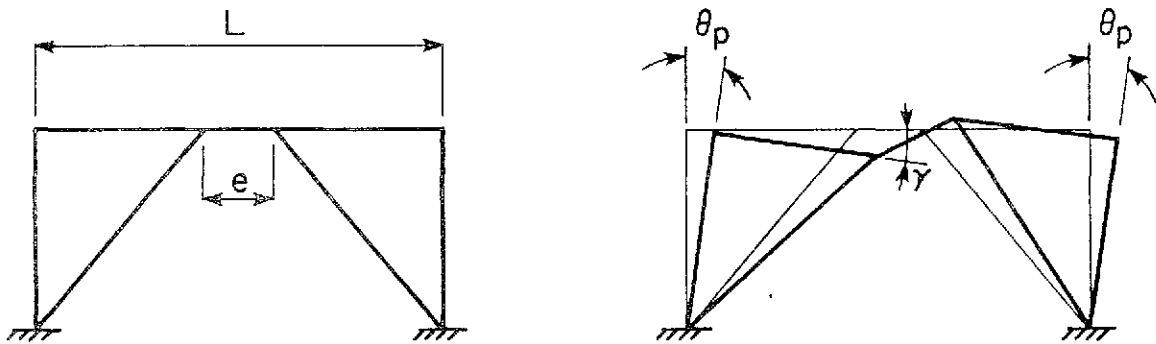
FIGURE A1 KINEMATICS OF A SPLIT-K EBF [1]

TABLES

Quantity	Multiply	by	to obtain
Length	inch	25.400	millimeter
	foot	0.3048	meter
Area	square inch	0.64516×10^{-3}	square millimeter
	square foot	0.92903×10^{-1}	square meter
Mass	pound	0.45359	kilogram
Stress	pound-force per square inch	6.894757	kilopascal
Force	pound-force	4.448222	newton
	kip	4.448222	kilonewton
Bending Moment	pound-force-inch	0.11298	newton-meter
	kip-in	0.11298	kilonewton-meter
	pound-force-foot	1.255818	newton-meter

TABLE 1.1 S.I. CONVERSION FACTORS

	Floor (psf)	Roof (psf)
Metal Deck	6	6
3.5" Lightweight Concrete	39	39
Ceiling & Floor Finishes	10	
Ceiling & Roofing		20
Partitions	20	
Structural Steel & Fireproofing	15	10
Total	90	75

Exterior Wall Weight = 30 psf

(a) DEAD LOAD

	Typical Floor (psf)	Roof (psf)
Live Load	60	20

(b) LIVE LOAD

TABLE 2.1 PROTOTYPE DESIGN LOADS

Story	Column Designation Mark No's				
	C1	C2	C3	C4	C5
5-6	10W49	10W33	10W33	12W49	12W49
3-4	12W65	12W53	10W89	10W60	12W72
2	12W79	12W65	12W50	12W79	12W106
1	12W87	12W87	12W65	12W106	12W136

(a) COLUMNS

Level	Girder Designation Mark No's			
	G1	G2	G3	G4
Roof,6	16W31	16W31	18W35	21W50
5	16W31	18W35		
4	18W35	18W35		
3	18W35	18W40		
2	18W40	18W40		

(b) GIRDERS

Story	Brace Designation Mark No's	
	B1	B2
5-6	4×4×0.180	8×6×0.313
5	5×5×0.180	8×6×0.313
2-4	6×6×0.250	8×6×0.375
1	6×6×0.500	8×6×0.375

(c) BRACES

TABLE 2.2 PROTOTYPE SECTION SIZES

Floor	Design Weight (kips) incl. External Wall	Design Weight (kips) excl. External Wall	As-Built Weight (kips)
Roof	227.7	193.7	166.9
6th	300.6	232.5	195.5
5th	300.6	232.5	195.5
4th	300.6	232.5	195.5
3rd	300.6	232.5	195.5
2nd	311.7	232.5	205.2
Total	1742	1356	1154

TABLE 2.3 PROTOTYPE FLOOR WEIGHTS

Level	W_x (kips)	H_x (ft)	F_x (kips)
Level Roof	193.7	70.5	36.9
Level 6	232.5	59.4	37.3
Level 5	232.5	48.2	30.3
Level 4	232.5	37.1	23.3
Level 3	232.5	25.9	16.3
Level 2	232.5	14.8	9.3
TOTAL	1356		153.4

TABLE 2.4 UBC LATERAL FORCE DISTRIBUTION

Dual System	CBDS		EBDS	
Level	Peak Displacement (in)	Inter-story Drift Index (%)	Peak Displacement (in)	Inter-story Drift Index (%)
Level Roof	0.86	0.11	0.76	0.08
Level 6	0.74	0.16	0.67	0.11
Level 5	0.58	0.15	0.55	0.12
Level 4	0.42	0.15	0.42	0.12
Level 3	0.27	0.13	0.29	0.12
Level 2	0.12	0.09	0.16	0.11

TABLE 2.5 UBC INTER-STORY DRIFT INDICES

Level	W_x (kips)	H_x (ft)	F_x (kips)
Level Roof	193.7	70.5	43.5
Level 6	232.5	59.4	44.0
Level 5	232.5	48.2	35.7
Level 4	232.5	37.1	27.4
Level 3	232.5	25.9	19.2
Level 2	232.5	14.8	10.9
Total			180.7

TABLE 2.6 ATC LATERAL FORCE DISTRIBUTION

Dual System	CBDS		EBDS	
Level	Peak Displacement (in)	Inter-story Drift Index (%)	Peak Displacement (in)	Inter-story Drift Index (%)
Level Roof	1.02	0.52	0.90	0.38
Level 6	0.88	0.73	0.80	0.56
Level 5	0.68	0.69	0.65	0.56
Level 4	0.50	0.69	0.50	0.56
Level 3	0.31	0.64	0.35	0.60
Level 2	0.15	0.41	0.19	0.54

TABLE 2.7   ATC INTER-STORY DRIFT INDICES

Dual System			CBDS	EBDS
Level	W_x (kips)	H_x (ft)	F_x (kips)	F_x (kips)
Level Roof	193.7	70.5	29.4	24.5
Level 6	232.5	59.4	29.8	24.8
Level 5	232.5	48.2	24.1	20.1
Level 4	232.5	37.1	18.5	15.4
Level 3	232.5	25.9	13.0	10.8
Level 2	232.5	14.8	7.4	6.2
Total	1356		122.0	101.8

TABLE 2.8 SEAOC LATERAL FORCE DISTRIBUTION

Dual System	CBDS		EBDS	
Level	Peak Displacement (in)	Inter-story Drift Index (%)	Peak Displacement (in)	Inter-story Drift Index (%)
Level Roof	0.69	0.07	0.51	0.05
Level 6	0.59	0.10	0.45	0.06
Level 5	0.46	0.09	0.37	0.07
Level 4	0.34	0.09	0.28	0.07
Level 3	0.21	0.08	0.19	0.06
Level 2	0.10	0.05	0.11	0.06

TABLE 2.9 SEAOC INTER-STORY DRIFT INDICES

	UBC	ATC	SEAOC	
			CBDS	EBDS
Nominal Base Shear Coefficient (C_s)	0.113	0.133	0.090	0.075
Braced Frame Base Shear Coefficient	1.25×0.113 $= 0.141$	0.8×0.133 $= 0.106$	$1.5 \times 0.8 \times 0.090$ $= 0.108$	0.8×0.075 $= 0.060$
Moment Frames Base Shear Coefficient	0.25×0.113 $= 0.028$	0.25×0.133 $= 0.033$	0.25×0.090 $= 0.023$	0.25×0.075 $= 0.019$
Total Base Shear Coefficient (C_t)	0.169	0.139	0.131	0.079
C_t at Working Stress Level (C_{tw})	0.169	0.111	0.131	0.079
C_t Extrapolated to Yield Level (C_{ty})	0.211	0.139	0.164	0.100

TABLE 2.10 CODE BASE SHEAR COEFFICIENTS

Floor	Prototype Weight As-Built (kips)	Similitude Scaled Weight (kips)	Model Weight As-Built (kips)
Roof	166.9	15.52	15.52
6th	195.5	18.18	18.16
5th	195.5	18.18	18.14
4th	195.5	18.18	18.08
3rd	195.5	18.18	18.10
2nd	205.2	19.09	19.08
Total	1154	107.3	107.1

TABLE 3.1 MODEL FLOOR WEIGHT DISTRIBUTION

	Roof	6 th	5 th	4 th	3 rd	2 nd
Roof	27.022	19.953	14.269	10.945	6.097	2.887
6th	20.080	18.622	13.266	9.750	5.974	2.609
5th	14.555	13.130	12.627	9.242	5.856	2.741
4th	9.884	9.539	9.153	8.684	5.586	2.619
3rd	6.150	6.074	5.944	5.634	5.142	2.632
2nd	3.041	2.924	2.774	2.911	2.763	2.327

(a) EXPERIMENTAL FLEXIBILITY MATRIX $(\times 10^{-3}$ inch/kip)

	Roof	6 th	5 th	4 th	3 rd	2 nd
Roof	189.1	-184.4	-24.6	-20.2	78.2	-51.9
6th	-184.4	395.0	-186.1	-1.0	-60.1	59.2
5th	-184.4	-186.1	557.0	-328.7	-62.8	58.6
4th	20.2	-1.0	-328.7	763.7	-440.9	17.0
3rd	78.2	-60.1	-62.8	-440.9	1081.7	-679.7
2nd	-51.9	59.2	58.6	17.0	-679.7	1117.9

(b) EXPERIMENTAL STIFFNESS MATRIX (kip/inch)

Mode	1st	2nd	3rd	4th	5th	6th
Period (sec)	0.328	0.116	0.067	0.055	0.042	0.032
Mode Shapes						
Roof	1.00	1.00	1.00	1.00	1.00	1.00
6th	0.85	0.28	-0.81	-2.19	-19.13	-0.88
5th	0.67	-0.49	-0.83	1.45	84.6	0.33
4th	0.52	-0.78	0.05	0.92	-104.4	-4.14
3rd	0.33	-0.82	0.65	-0.83	4.77	9.60
2nd	0.16	-0.50	0.87	-1.00	62.0	-8.01

(c) EXPERIMENTAL NATURAL PERIODS AND MODE SHAPES

TABLE 4.1 CBDS STATIC FLEXIBILITY TEST RESULTS

	Roof	6th	5th	4th	3rd	2nd
Roof	24.196	18.706	13.922	9.421	6.804	3.440
6th	19.852	17.165	13.059	9.223	6.516	3.419
5th	14.345	13.029	11.548	8.463	6.079	3.203
4th	9.882	8.946	8.264	7.224	5.375	3.020
3rd	6.782	6.200	5.597	5.382	5.052	2.916
2nd	3.838	3.648	3.140	3.147	2.975	2.690

(a) EXPERIMENTAL FLEXIBILITY MATRIX ($\times 10^{-3}$ inch/kip)

	Roof	6th	5th	4th	3rd	2nd
Roof	404.6	-542.7	92.1	41.5	-46.2	69.1
6th	-542.7	1144.5	-680.8	84.9	58.8	-143.3
5th	92.1	-680.8	1316.6	-939.3	117.5	172.0
4th	41.5	84.9	-939.3	1743.7	-881.6	-89.1
3rd	-46.2	-58.8	117.4	-881.6	1355.8	-636.3
2nd	69.1	-143.3	172.0	-89.1	-636.3	1064.1

(b) EXPERIMENTAL STIFFNESS MATRIX (kip/inch)

Mode	1st	2nd	3rd	4th	5th	6th
Period (sec)	0.322	0.103	0.057	0.039	0.030	0.025
Mode Shapes						
Roof	1.00	1.00	1.00	1.00	1.00	1.00
6th	0.94	0.37	-0.34	-1.50	-2.06	-4.43
5th	0.75	-0.37	-1.39	-0.16	1.48	10.4
4th	0.55	-0.88	-0.44	1.01	0.45	-14.17
3rd	0.40	-1.01	0.78	0.81	-2.06	8.55
2nd	0.23	-0.79	1.26	-1.52	1.74	-0.83

(c) EXPERIMENTAL NATURAL PERIODS AND MODE SHAPES

TABLE 4.2 EBDS STATIC FLEXIBILITY TEST RESULTS

		Free Vibration		Forced Vibration		Flexibility Test	
Mode		1st	2nd	1st	2nd	1st	2nd
CBDS	T_i (sec)	0.342	0.118	0.344	0.119	0.328	0.116
	ξ_i (%)	1.3	0.7	1.6	0.7	-	-
EBDS	T_i (sec)	0.316	0.105	0.320	0.106	0.322	0.103
	ξ_i (%)	0.7	0.5	0.7	0.9	-	-

TABLE 4.3 CBDS AND EBDS DYNAMIC CHARACTERISTICS

TEST NO.	FILENAME	TABLE MOTION	PA[*1] (%g)	V_b^{max} (kips)	IDI[*2] (%)	RDI[*3] (%)	REMARKS
1	850213.01	MO	0.4				Preliminary
2	850213.02	MO	0.7				Dynamic
3	850213.03	MO	1.0				Testing
4	850213.04	MO	2.1				
5	850214.01	MO	2.4				
6	850214.02	MO	4.5				Elastic Limit
7	850214.03	MO	6.3	14.8	0.15	0.11	State Testing
8	850215.01	FR.V[*4]					
9	850215.02	MO	6.2				
10	850215.03	FR.V					
11	850215.04	FR.V					
12	850215.05	MO	8.5				
13	850215.06	MO	9.9				
14	850215.07	FR.V					
15	850215.08	MO	16.1				
16	850215.09	FR.V					
17	850215.10	MO	14.7				
18	850215.11	FR.V					
19	850219.01	FR.V					
20	850219.02	MO	14.7				
21	850219.03	FR.V					
22	850219.04	MO	19.9				Damageability
23	850219.05	FR.V					Limit
24	850220.01	FR.V					State Testing
25	850220.02	MO	27.6				
26	850220.03	FR.V					
27	850220.04	MO	33.5	60.1	0.69	0.55	
28	850220.05	FR.V					Collapse Limit
29	850220.06	MO	64.9	78.6	1.89	0.94	State Testing
30	850220.07	FR.V					
31	850221.01	FR.V					After-Shock
32	850221.02	MO	30.1	57.9	1.47	0.70	Testing
33	850221.03	MO	27.6				
34	850221.04	FR.V					
35	850221.05	MO	26.5				
36	850221.06	FR.V					

*1 PA = Peak Table Acceleration   *3 RDI = Maximum Roof Drift Index

*2 IDI = Maximum Inter-Story Drift Index   *4 Free Vibration Test

TABLE 5.1 CBDS MODEL TEST SCHEDULE

TEST NO.	FILENAME	TABLE MOTION	PA[*1] (%g)	V_b^{max} (kips)	IDI[*2] (%)	RDI[*3] (%)	REMARKS
1	850415.01	MO	16.2	30.7	0.44	0.23	Preliminary
2	850419.01	FR.V[*4]					Dynamic
3	850419.02	FR.V					Testing
4	850424.02	FO.V[*5]					
5	850514.01	MO	9.51	17.2	0.13	0.10	Elastic Limit
6	850514.02	TAFT	3.0	7.9	0.07	0.11	State Testing
7	850514.03	TAFT	7.8	16.9	0.12	0.11	
8	850514.04	TAFT	9.9	31.2	0.22	0.19	
9	850514.05	FR.V					
10	850514.06	MO	7.8	15.1	0.11	0.09	
11	850514.07	MO	7.0	11.9	0.09	0.07	
12	850516.01	MO	14.3	25.1	0.20	0.17	
13	850517.01	MO	17.6	37.2	0.28	0.24	Damageability
14	850517.02	TAFT	21.4	50.7	0.42	0.36	Limit State
15	850517.03	FR.V					Testing
16	850518.01	TAFT	27.0	52.5	0.48	0.35	
17	850518.02	MO	27.5	57.0	0.58	0.40	
18	850518.03	FR.V					
19	850520.01	TAFT	33.8	64.1	0.67	0.45	
20	850520.02	FR.V					
21	850520.03	TAFT	40.3	82.7	1.04	0.62	Collapse Limit
22	850520.04	FR.V					State Testing
23	850520.05	TAFT	57.3	90.6	1.25	0.66	
24	850520.06	FR.V					
25	850522.01	TAFT	9.4	20.9	0.18	0.16	
26	850522.02	TAFT	66.3	91.6	1.28	0.72	
27	850522.03	PACO	7.7	10.8	0.11	0.08	After-Shock
28	850522.04	PACO	21.8	48.4	0.54	0.38	Testing
29	850522.06	PACO	12.8	17.1	0.17	0.10	
30	850522.07	PACO	96.0	70.9	0.98	0.63	
31	850522.08	FR.V					
32	850523.01	SINE	24.2	46.1	0.47	0.31	
33	850523.02	SINE	54.7	62.6	0.79	0.43	
34	850523.03	SINE	69.5	75.6	1.14	0.65	
35	850523.04	FR.V					
36	850524.02	FR.V					

*1 PA = Peak Table Acceleration *4 Free Vibration Test

*2 IDI = Maximum Inter-story Drift Index *5 Forced Vibration Test

*3 RDI = Maximum Roof Drift Index

TABLE 5.2 EBDS MODEL TEST SCHEDULE

	Natural Period (sec)			Damping Factor (%) [1]		
	1 st	2 nd	3 rd	1 st	2 nd	3 rd
Before MO 6.3%g [2]	0.342	0.119	0.069	1.3	0.7	0.5
Before MO 6.3%g	0.361	0.121	0.070	2.0	1.8	----
After MO 6.3%g	0.366	0.122	0.070	2.0	1.7	----
After MO 9.9%g	0.359	0.121	0.070	2.0	1.6	----
After MO 14.7%g	0.366	0.122	0.071	2.0	1.9	----
Before MO 27.6%g	0.367	0.123	0.071	2.1	2.0	----
Before MO 33.5%g	0.371	0.123	0.071	2.0	2.1	----
Before MO 64.9%g	0.367	0.124	0.071	2.0	2.6	----
After MO 64.9%g	0.392	0.150	0.073	----	----	----
After MO 26.5%g	0.434	0.162	0.075	2.0	2.1	----
DMRSF [2]	0.672	0.240	0.139	0.7	0.4	0.3

*1   Free Vibration Tests
*2   Earthquake Simulator Locked in Position

TABLE 6.1   DYNAMIC CHARACTERISTICS OF THE CBDS [2]

	Natural Period (sec)			Damping Factor (%) [1]		
	1 st	2 nd	3 rd	1 st	2 nd	3 rd
DMRSF [2]	0.672	0.240	0.139	0.7	0.4	0.3
Before MO 9.5%g [2]	0.316	0.105	0.057	0.7	0.5	----
After Taft 21.4%g	0.326	0.106	0.058	2.2	1.1	----
After MO 27.5%g	0.326	0.107	0.058	2.2	1.3	----
After Taft 33.8%g	0.326	0.107	0.058	2.3	1.3	----
After Taft 57.3%g	0.333	0.108	0.060	2.3	1.3	----
Before Sine 24.2%g	0.333	0.108	0.060	2.3	1.3	----
After Sine 69.5%g	0.333	0.111	0.060	2.3	1.3	----
After Sine 69.5%g [2]	0.333	0.111	0.060	2.3	1.3	----

*1   Free Vibration Tests
*2   Earthquake Simulator Locked in Position

TABLE 6.2   DYNAMIC CHARACTERISTICS OF THE EBDS [1]

Floor/Story	6	5	4	3	2	1
Lateral Displ (in.)	-0.28	-0.23	-0.22	-0.15	-0.11	-0.06
Time (sec)	4.32	4.33	4.33	4.33	4.33	4.34
Inter-story Drift (in.)	-0.06	0.05	-0.060	-0.05	-0.04	-0.06
Inter-story Drift Index (%)	0.14	0.11	0.15	-0.12	-0.11	-0.11
Time (sec)	4.31	4.50	4.32	4.32	4.33	4.34
Story Shear (k)	-3.4	-6.0	-8.7	-11.2	-13.1	-14.8
Story Shear/Total Wt.(%)	3.1	5.6	8.2	10.5	12.3	13.9
Time (sec)	4.30	4.31	4.31	4.32	4.33	4.33
Inertia Force (k)	3.3	3.3	2.8	2.6	2.1	1.6
Time (sec)	4.30	4.31	4.35	4.34	4.34	4.33
Overturn. Moment (k-in)	136	409	788	1245	1763	2539
Time (sec)	4.30	4.31	4.31	4.31	4.32	4.32

TABLE 6.3 CBDS MO-06 TEST RESPONSE ENVELOPES [2]

Floor/Story	6	5	4	3	2	1
Lateral Displ (in.)	0.18	0.15	0.13	-0.11	-0.07	0.05
Time (sec)	6.28	6.28	6.28	4.33	4.33	6.29
Inter-story Drift (in.)	0.03	-0.02	0.02	-0.04	-0.03	0.05
Inter-story Drift Index (%)	0.07	0.06	0.06	0.10	0.07	0.09
Time (sec)	6.27	6.47	6.26	4.33	4.33	6.2
Story Shear (k)	2.8	5.3	7.3	8.5	-9.8	-11.4
Story Shear/Total Wt.(%)	2.6	4.9	6.8	7.9	9.2	10.7
Time (sec)	6.28	6.26	6.26	6.26	4.33	4.33
Inertia Force (k)	-2.8	-2.7	-2.2	-2.0	-2.0	-1.8
Time (sec)	6.28	6.26	6.30	4.53	4.14	4.14
Overturn. Moment (k-in)	-113	-330	-626	-974	-1351	-1891
Time (sec)	6.28	6.27	6.27	6.27	6.27	6.27

TABLE 6.4 EBDS MO-07 TEST RESPONSE ENVELOPES [1]

Floor/Story	6	5	4	3	2	1
Lateral Displ (in.)	-1.41	-1.21	-0.95	-.70	-0.51	-0.29
Time (sec)	4.35	4.35	4.35	8.54	8.55	8.55
Inter-story Drift (in.)	-0.20	-0.28	0.25	-0.23	-0.21	-0.28
Inter-story Drift Index (%)	0.50	0.69	0.61	0.56	0.51	0.51
Time (sec)	4.34	8.99	4.56	8.54	4.36	8.55
Story Shear (k)	-16.8	-30.8	-41.0	-49.4	-55.6	-60.1
Story Shear/Total Wt. (%)	15.7	28.8	38.3	46.2	51.9	56.1
Time (sec)	4.34	4.35	4.34	4.35	4.35	8.54
Inertia Force (k)	16.8	16.7	12.9	10.0	8.5	7.9
Time (sec)	4.34	4.37	8.52	8.52	4.29	4.28
Overturn. Moment (k-in)	685	1927	3604	5621	7887	11058
Time (sec)	4.34	4.35	4.35	4.35	4.35	4.35

TABLE 6.5 CBDS MO-33 TEST RESPONSE ENVELOPES [2]

Floor/Story	6	5	4	3	2	1
Lateral Displ (in.)	-1.00	-0.88	-0.72	-0.51	-0.41	-0.33
Time (sec)	4.34	4.35	4.35	4.35	4.35	4.32
Inter-story Drift (in.)	0.12	-0.14	-0.14	-0.19	-0.15	-0.25
Inter-story Drift Index (%)	0.29	0.35	0.34	0.47	0.36	0.46
Time (sec)	6.27	4.34	4.34	4.34	4.34	4.36
Story Shear (k)	13.9	-26.5	-36.0	-43.1	-48.5	53.0
Story Shear/Total Wt.(%)	13.0	24.8	33.6	40.2	45.3	49.5
Time (sec)	6.27	4.33	4.34	4.34	4.34	4.36
Inertia Force (k)	-13.9	12.9	10.3	-8.8	-7.4	-6.9
Time (sec)	6.27	4.35	4.36	4.54	4.54	6.21
Overturn. Moment (k-in)	-568	1642	3112	4857	6811	9603
Time (sec)	6.27	4.33	4.34	4.34	4.34	4.35

TABLE 6.6 EBDS MO-28 TEST RESPONSE ENVELOPES

Floor/Story	6	5	4	3	2	1
Lateral Displ (in.)	-2.37	-2.12	-1.55	-1.13	-0.83	-0.47
Time (sec)	8.61	8.61	8.61	4.36	4.37	4.37
Inter-story Drift (in.)	-0.27	0.77	0.49	-0.33	-0.34	-0.47
Inter-story Drift Index (%)	0.66	1.89	1.20	0.81	0.83	0.87
Time (sec)	8.59	8.87	8.86	4.36	4.36	4.37
Story Shear (k)	-20.5	-42.4	-54.4	-65.8	73.8	-78.6
Story Shear/Total Wt. (%)	19.2	39.6	50.8	61.5	69.0	73.4
Time (sec)	8.59	4.38	8.61	4.35	4.34	4.34
Inertia Force (k)	20.5	22.4	18.3	-16.6	13.6	14.0
Time (sec)	8.59	4.38	4.33	8.79	4.30	4.29
Overturn. Moment (k-in)	836	2543	4713	7256	10227	14344
Time (sec)	8.59	4.38	8.60	4.36	4.36	4.35

TABLE 6.7 CBDS MO-65 TEST RESPONSE ENVELOPES [2]

Floor/Story	6	5	4	3	2	1
Lateral Displ (in.)	1.73	1.58	1.37	1.17	0.98	0.69
Time (sec)	8.54	8.54	8.54	8.55	8.55	8.55
Inter-story Drift (in.)	-0.20	0.25	0.22	0.21	0.29	0.69
Inter-story Drift Index (%)	0.50	0.61	0.54	0.52	0.71	1.28
Time (sec)	8.30	4.53	8.51	4.54	8.55	8.55
Story Shear (k)	-22.2	-36.4	54.2	-66.1	80.6	90.6
Story Shear/Total Wt.(%)	20.7	34.0	50.6	61.7	75.2	84.5
Time (sec)	8.68	8.29	4.53	8.31	8.54	8.54
Inertia Force (k)	19.9	-18.0	-15.7	-17.0	-17.6	-15.3
Time (sec)	8.68	4.53	8.54	8.55	6.16	6.16
Overturn. Moment (k-in)	812	2311	-4322	-6722	-9422	-13280
Time (sec)	8.68	8.68	4.52	4.53	4.53	4.53

TABLE 6.8 EBDS TAFT-57 TEST RESPONSE ENVELOPES

FIGURES

(a) Ductile Moment Resisting Space Frame

(b) Concentrically Braced Frame

(c) Eccentrically Braced Frame
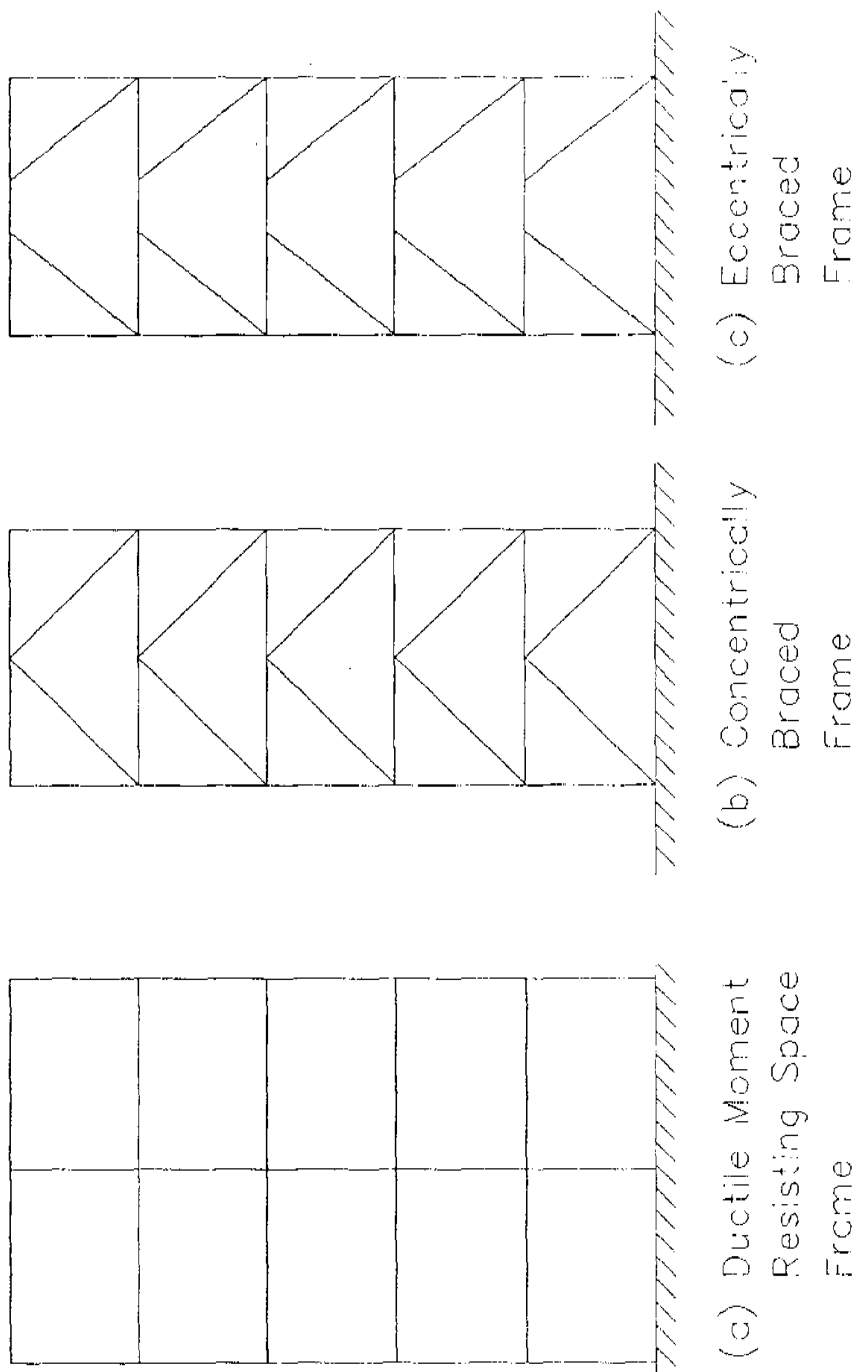
FIGURE 1.1 STRUCTURAL STEEL FRAMING SYSTEMS
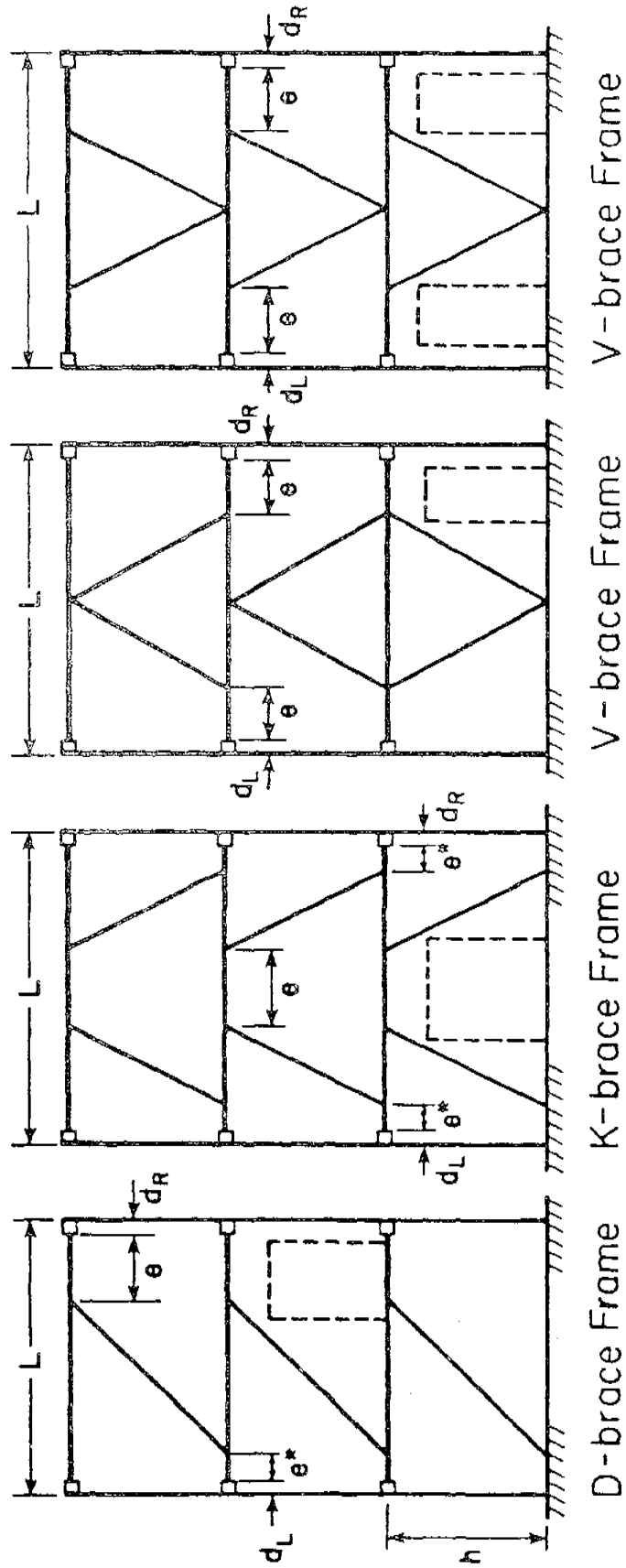
FIGURE 1.2 ECCENTRICALLY BRACED FRAMES [4]
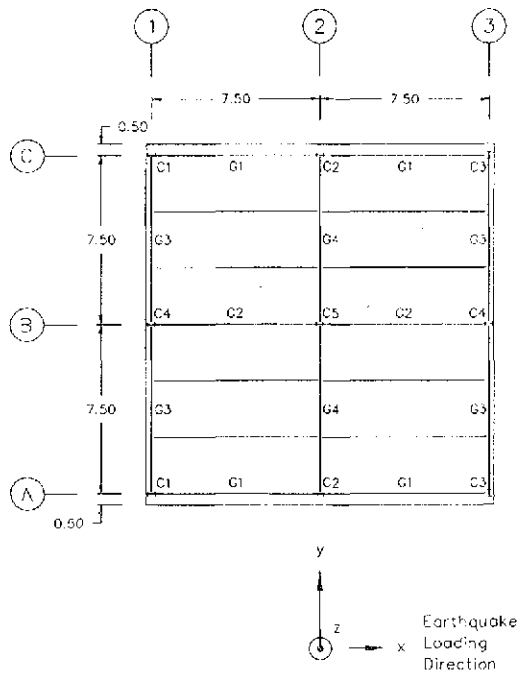
(a) Plan
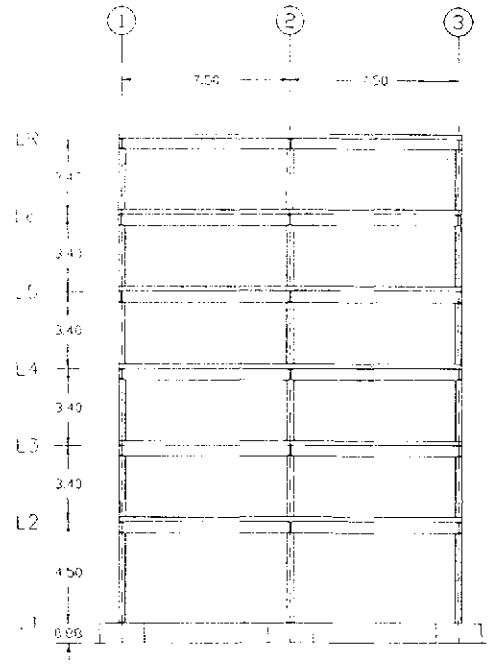
(b) Frames A & C

All dimensions in meters
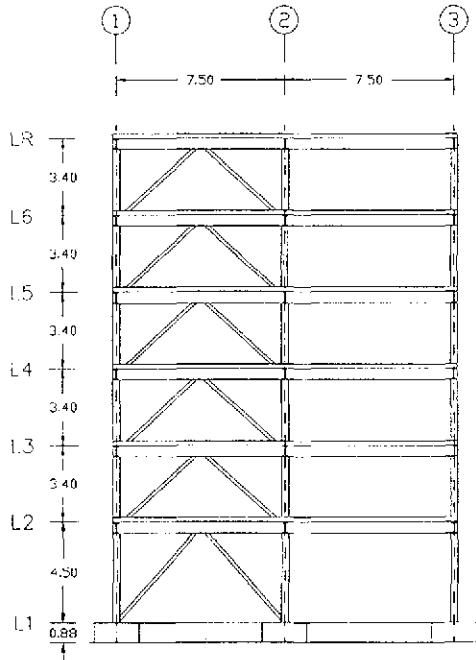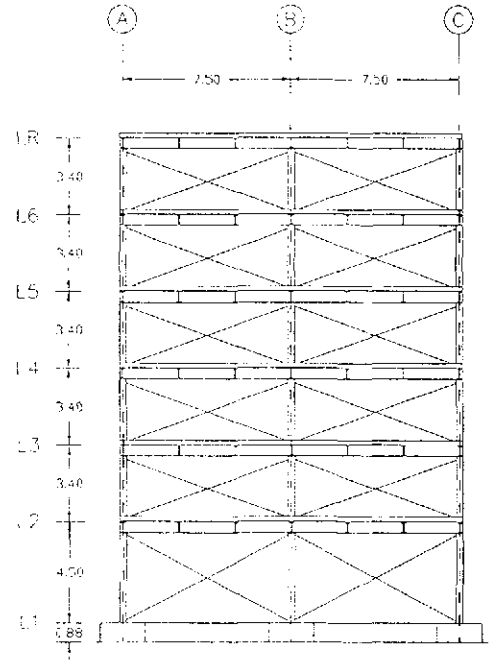
(c) Frame B

(d) Frames 1 & 3

FIGURE 2.1 PLAN AND ELEVATIONS OF THE CBDS PROTOTYPE
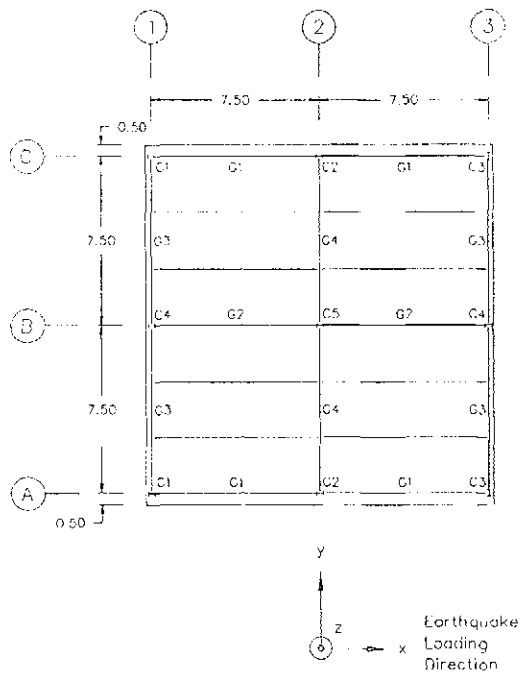
(a) Plan
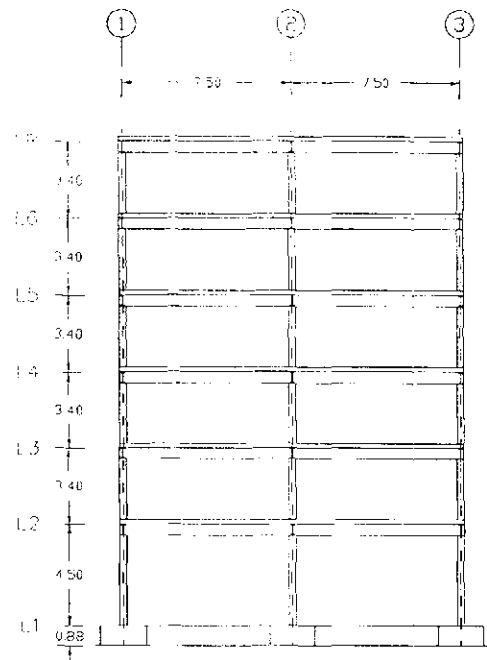
(b) Frames A & C

All dimensions in meters
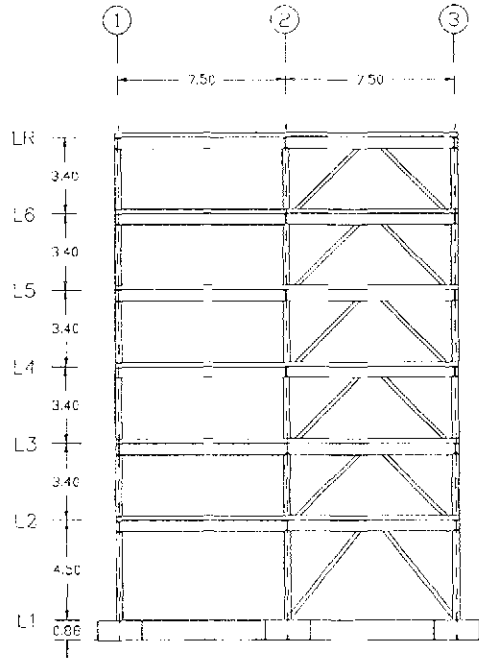
(c) Frame B
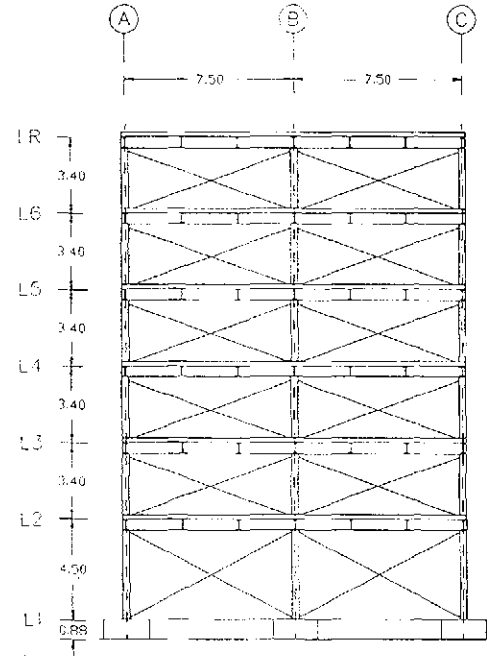
(d) Frames 1 & 3

FIGURE 2.2 PLAN AND ELEVATIONS OF THE EBDS PROTOTYPE

FIGURE 2.3 COMPOSITE GIRDER CROSS SECTION (FRAME B)

FIGURE 3.1 DYNAMIC PERFORMANCE OF THE EARTHQUAKE
SIMULATOR
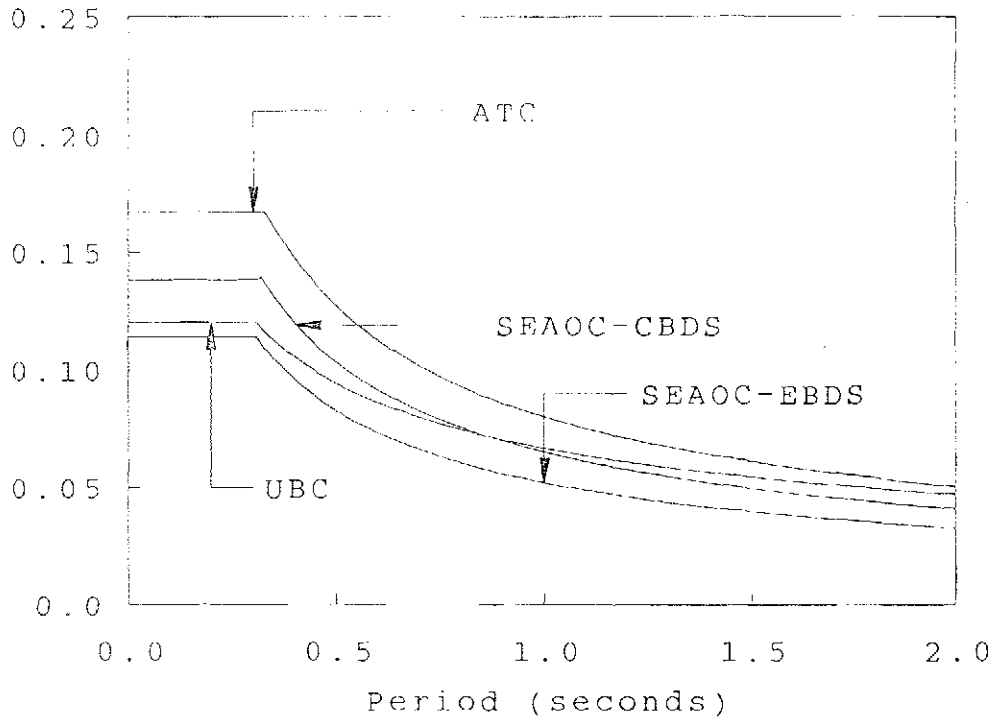
Design Base Shear (g)

(a) Firm Soil Spectra

Design Base Shear (g)
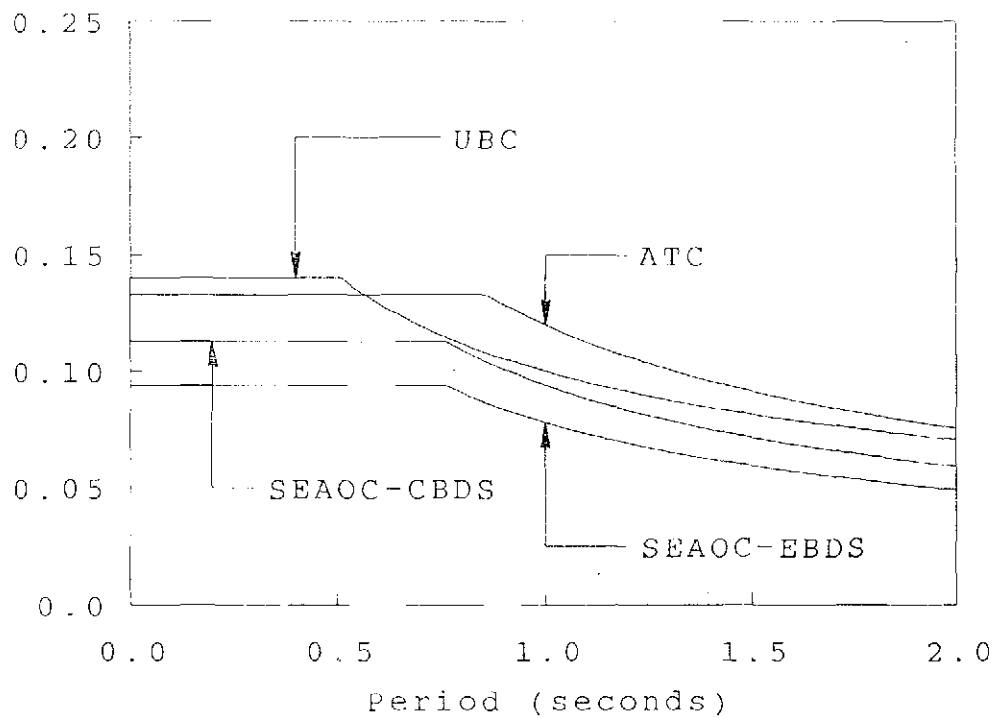
(b) Soft Soil Spectra

FIGURE 2.4 CODE-BASED DESIGN RESPONSE SPECTRA
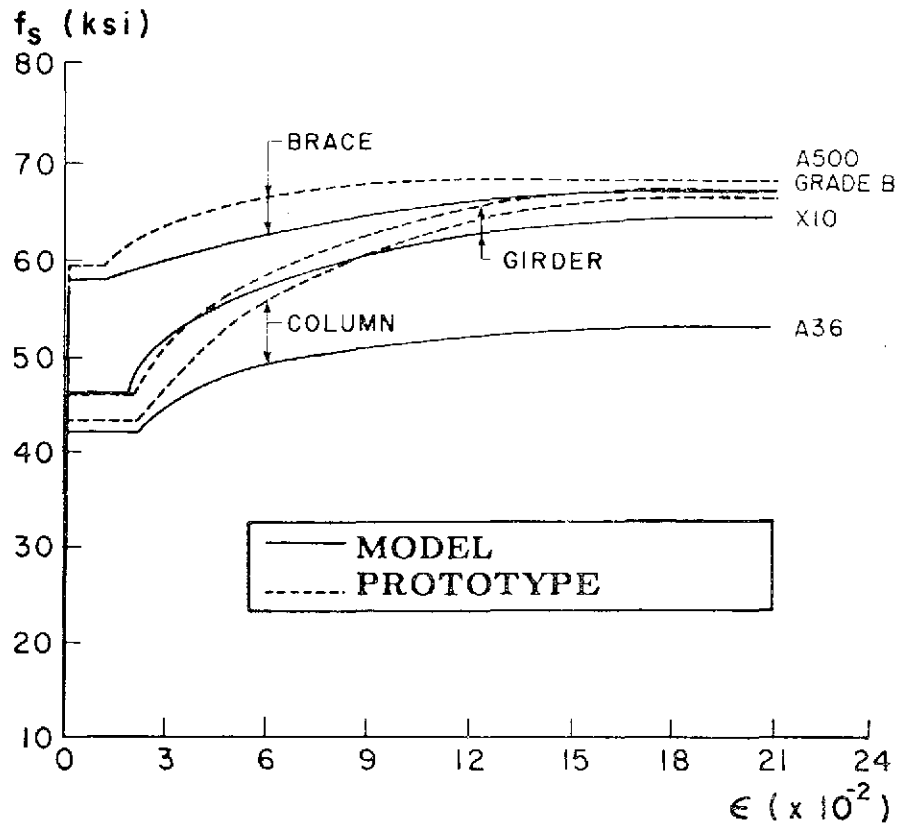
FIGURE 3.2 STEEL STRESS-STRAIN RELATIONSHIPS
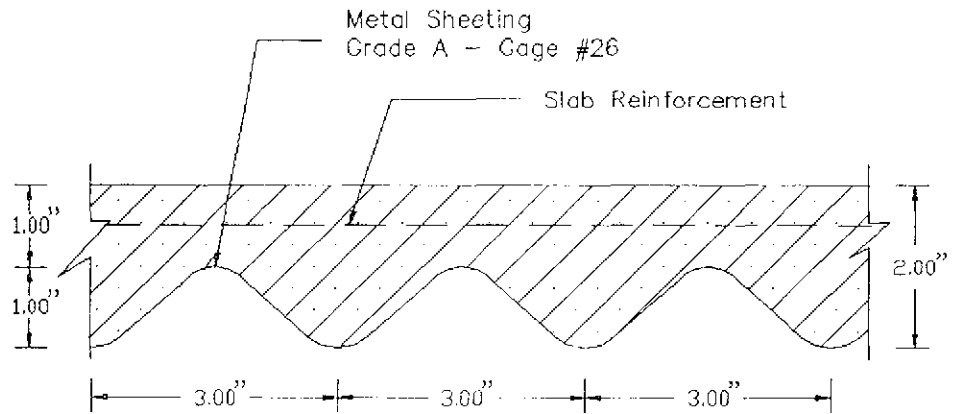
FIGURE 3.3 MODEL METAL DECK PROFILE

Strain Gage ⌐ DCDT – Shear Strain ⌐ ⌐ DCDT – Axial Strain
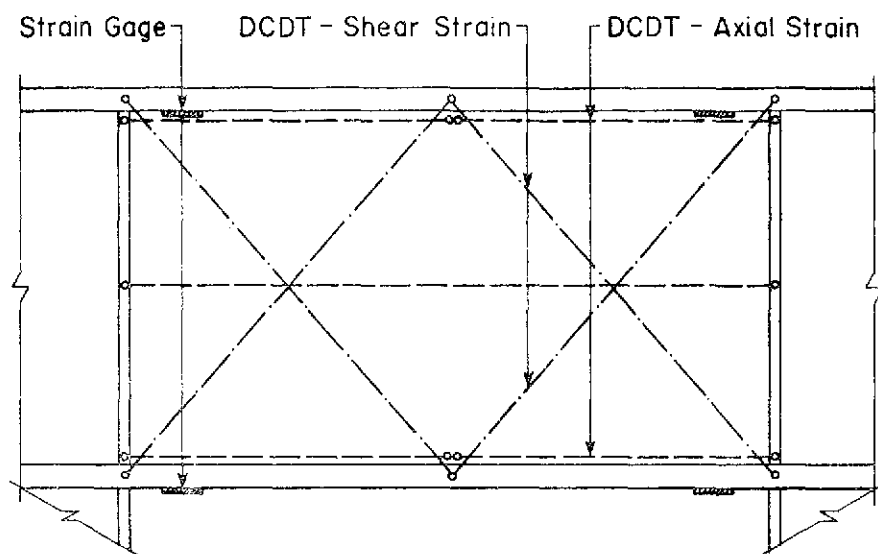
(a) Schematic Illustration
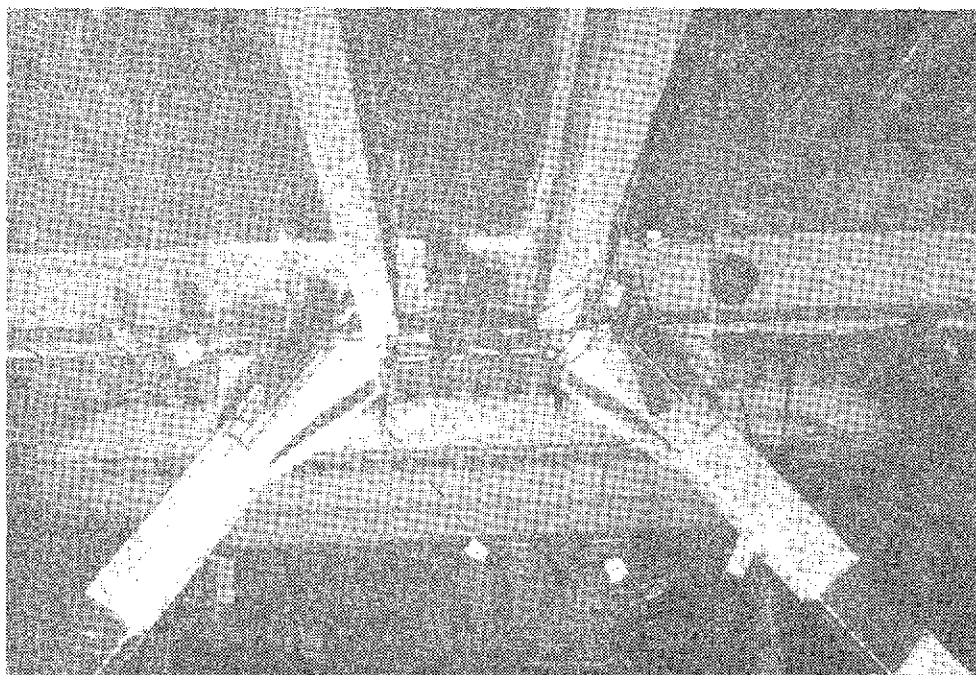
(b) Experimental Set-up

FIGURE 3.4 SHEAR LINK INSTRUMENTATION
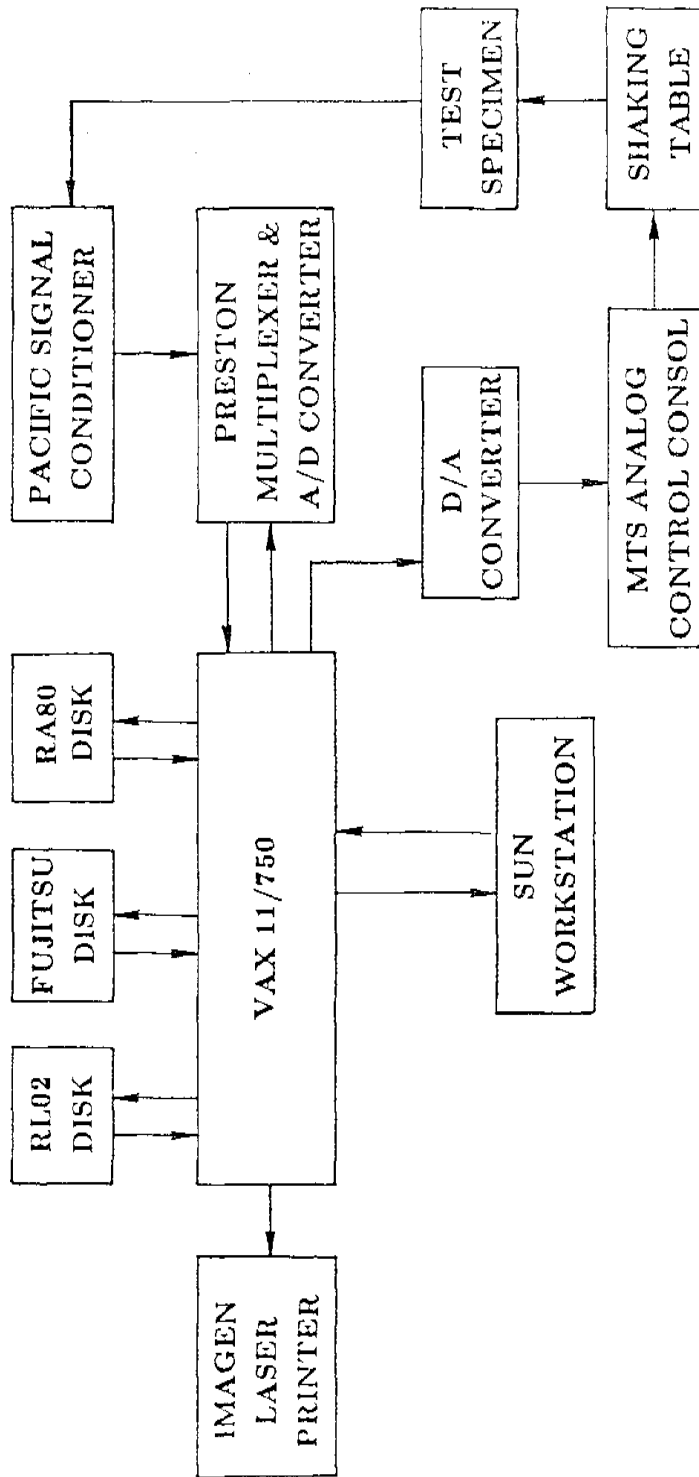
FIGURE 3.5 EARTHQUAKE SIMULATOR SYSTEM BLOCK DIAGRAM

(a) Plan View

(b) Elevation
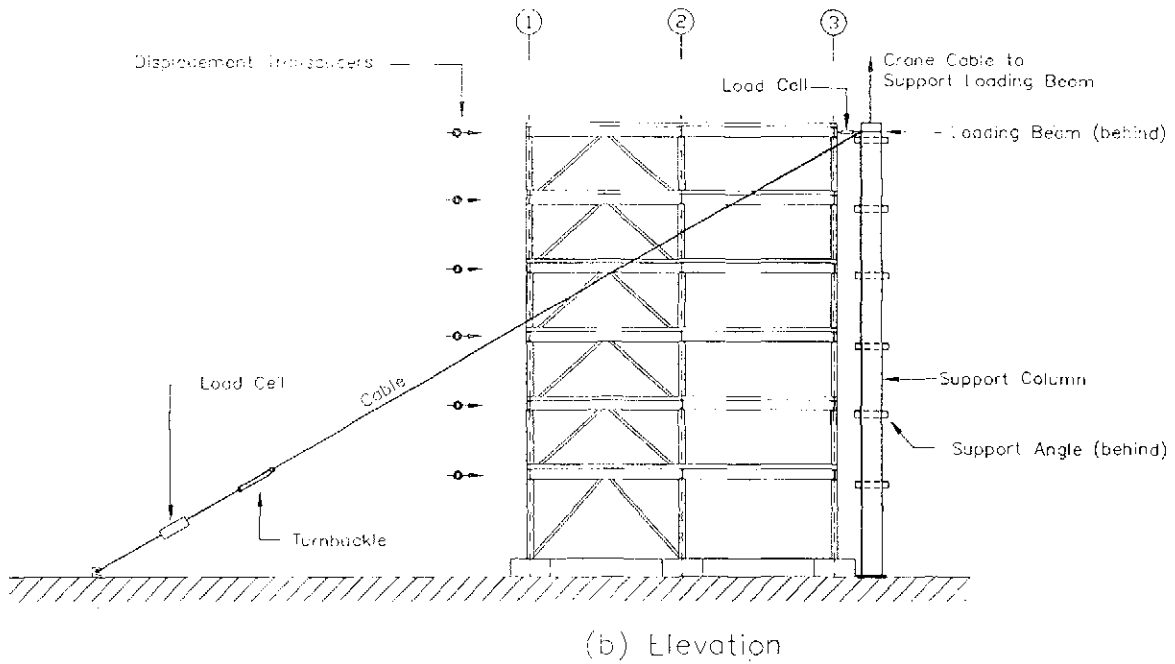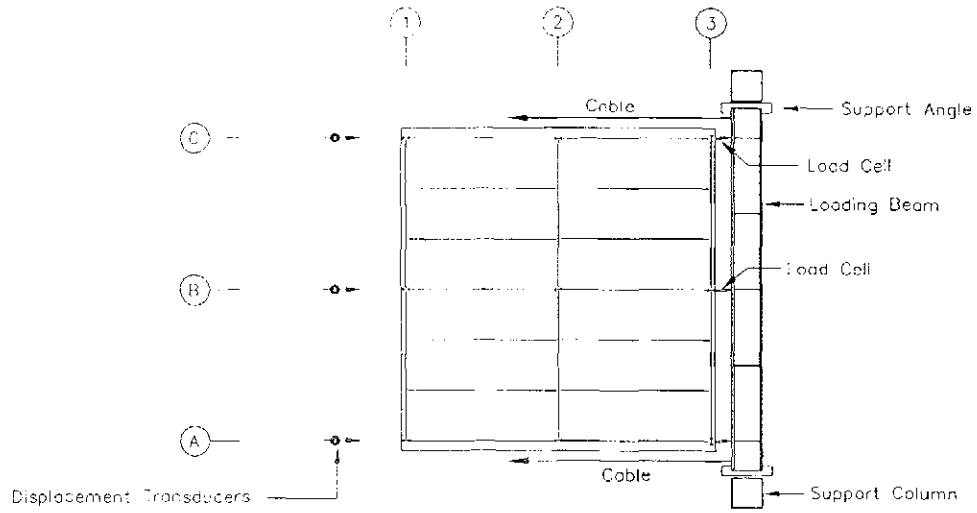
FIGURE 4.1 STATIC FLEXIBILITY TEST SET-UP
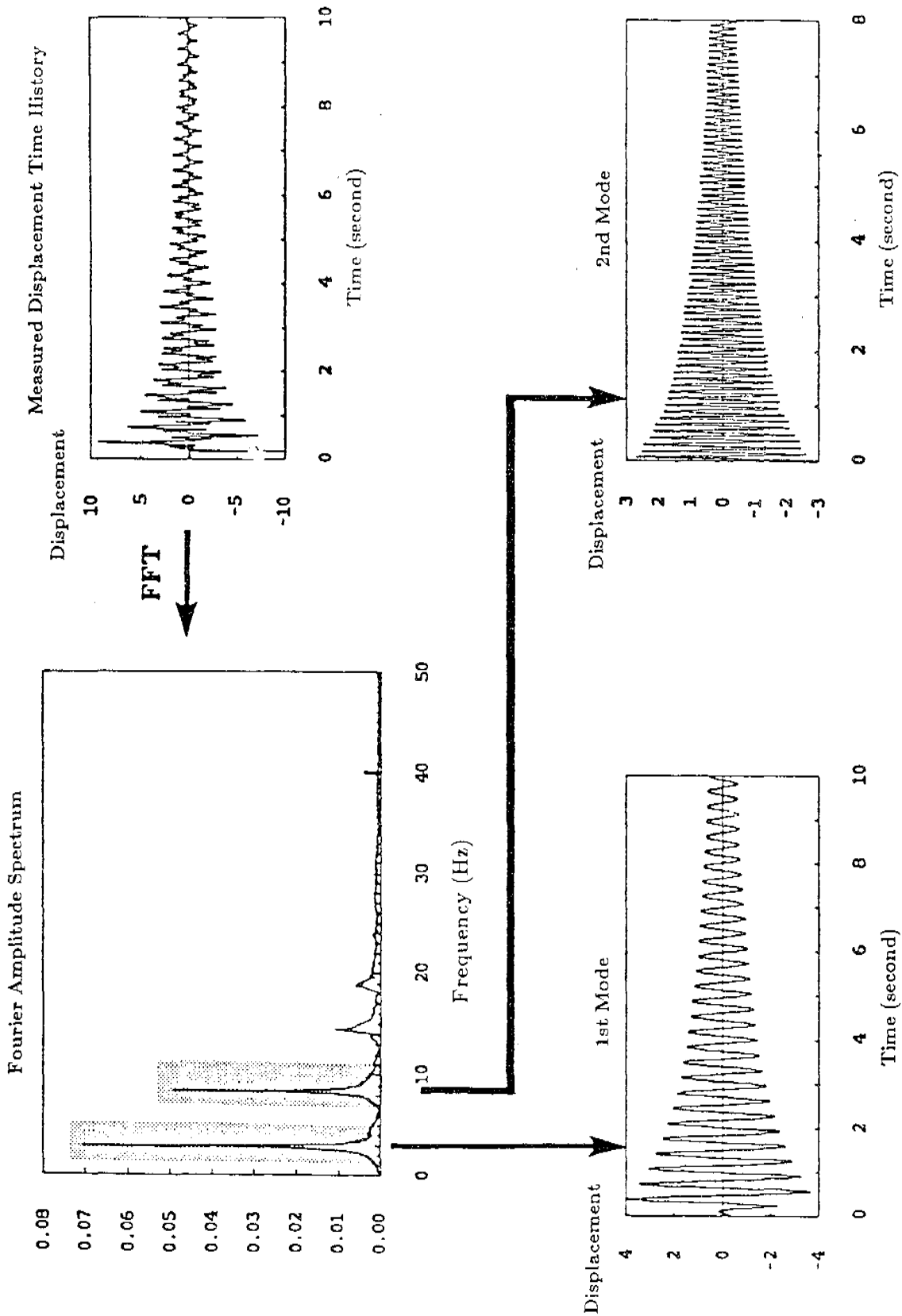
FIGURE 4.2 FREE VIBRATION TESTS AND FREQUENCY DOMAIN PROCEDURES

-1.0   0.0   1.0   -1.0   0.0   1.0   -1.0   0.0   1.0

Mode 1   Mode 2   Mode 3
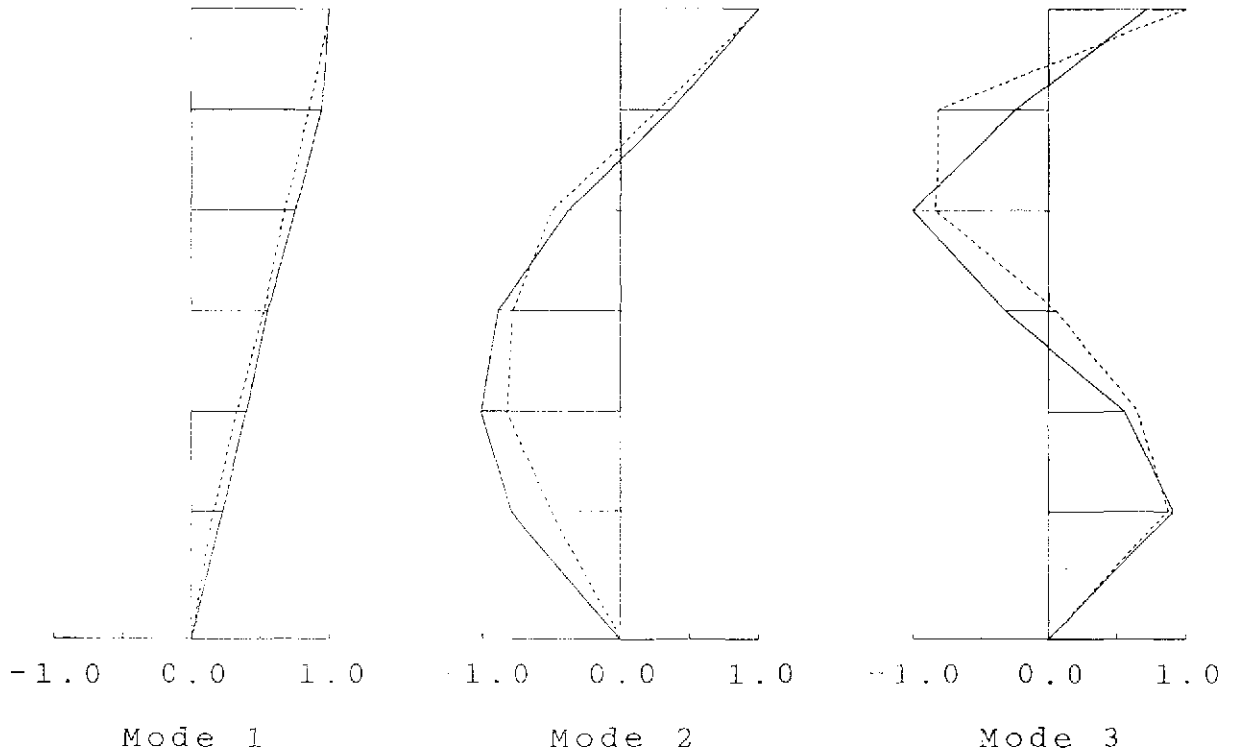
Dotted Line - CBDS, Solid Line - EBDS

FIGURE 4.3 CBDS AND EBDS MODEL MODE SHAPES
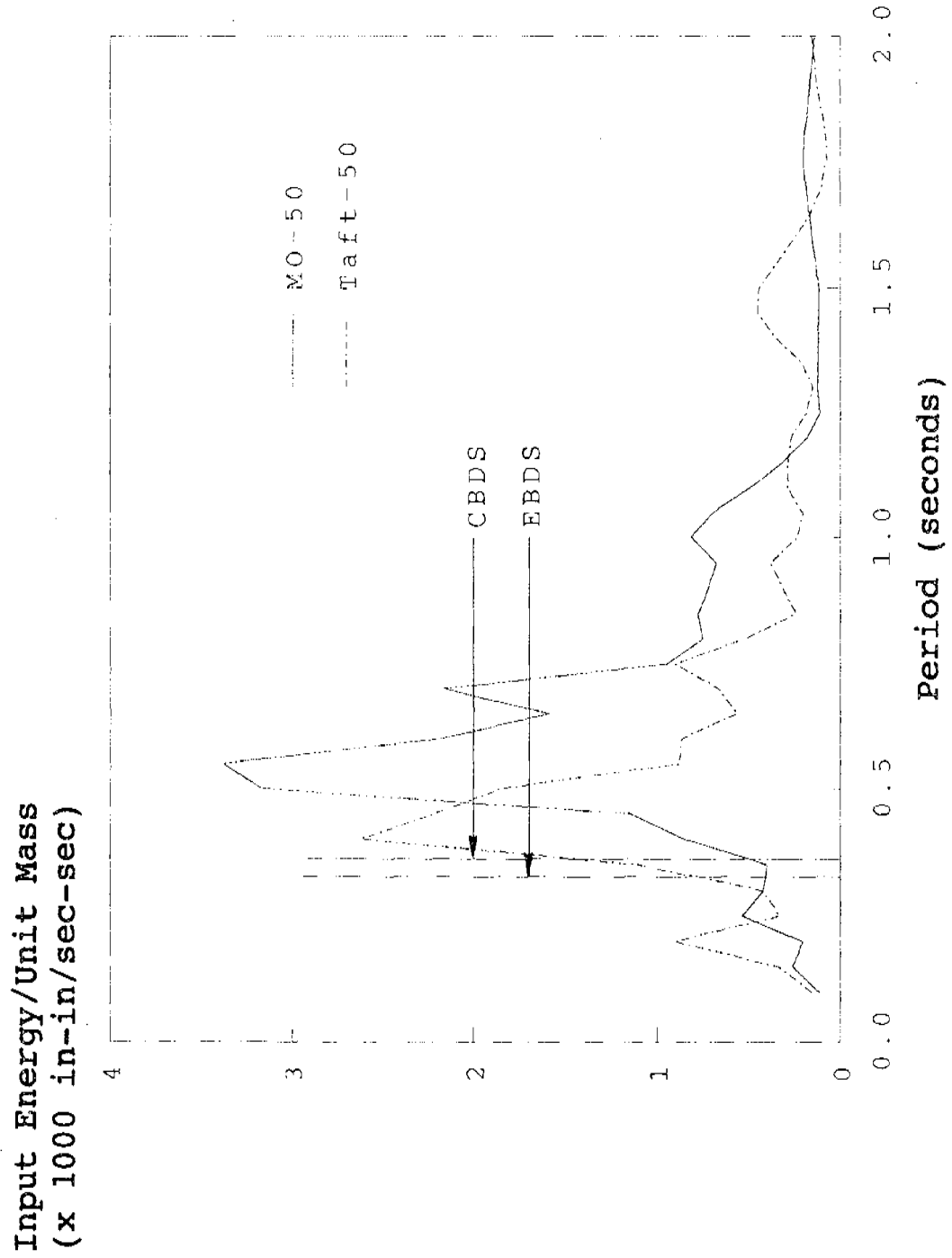
FIGURE 5.1 SDOF ELASTIC INPUT ENERGY SPECTRA ($\xi = 2\%$)
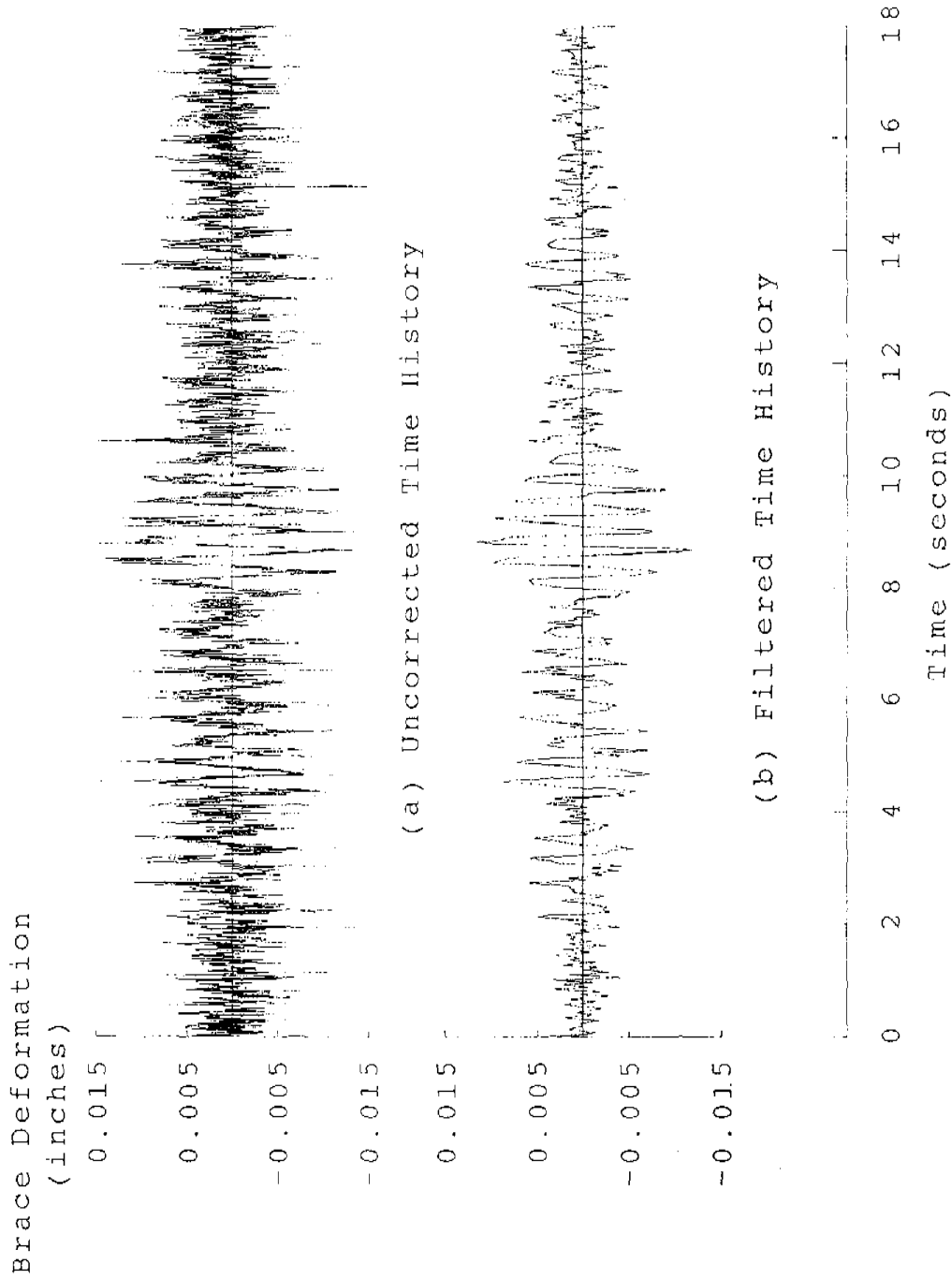
FIGURE 5.2 HIGH FREQUENCY NOISE FILTER
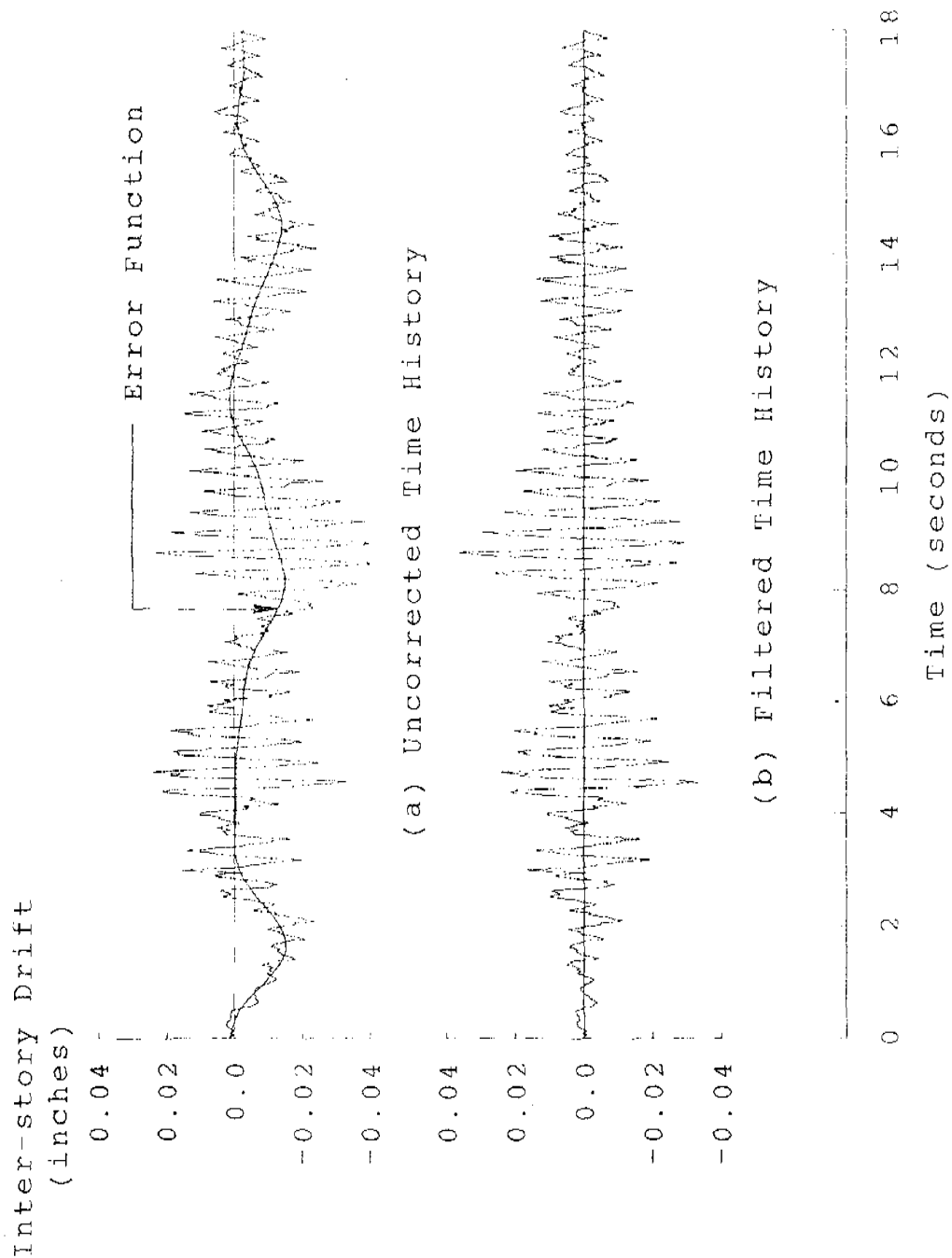
FIGURE 5.3 LOW FREQUENCY NOISE FILTER

+ve Inertia →

+ve Flexure

+ve Brace
Force

+ve Displacement
Acceleration

+ve Shear Force

+ve Overturning Moment

(a) CBDS Model

−ve Shear Force

+ve Inertia →

+ve Flexure

+ve Brace
Force

+ve Displacement
Acceleration

+ve Shear Force

+ve Overturning Moment
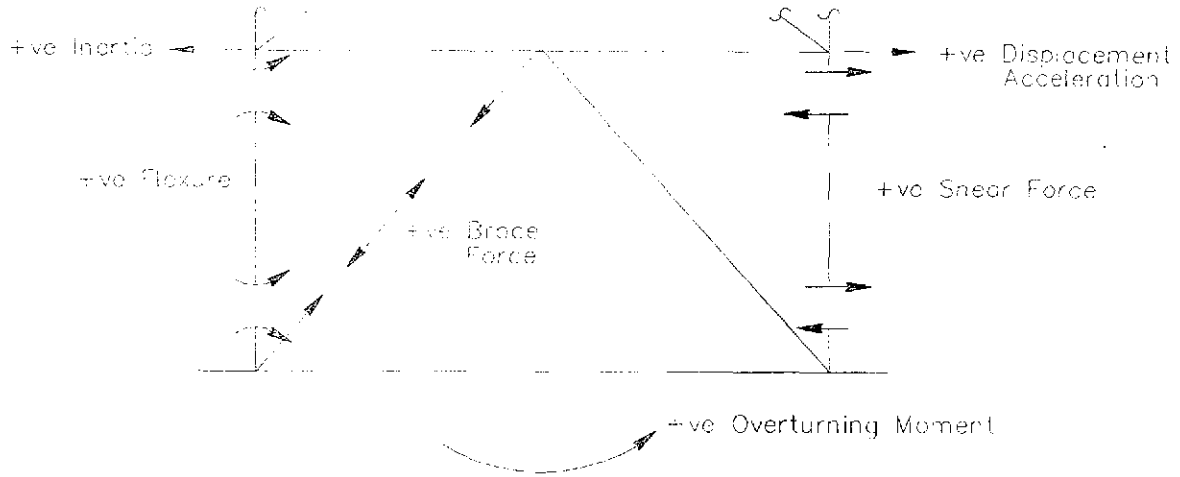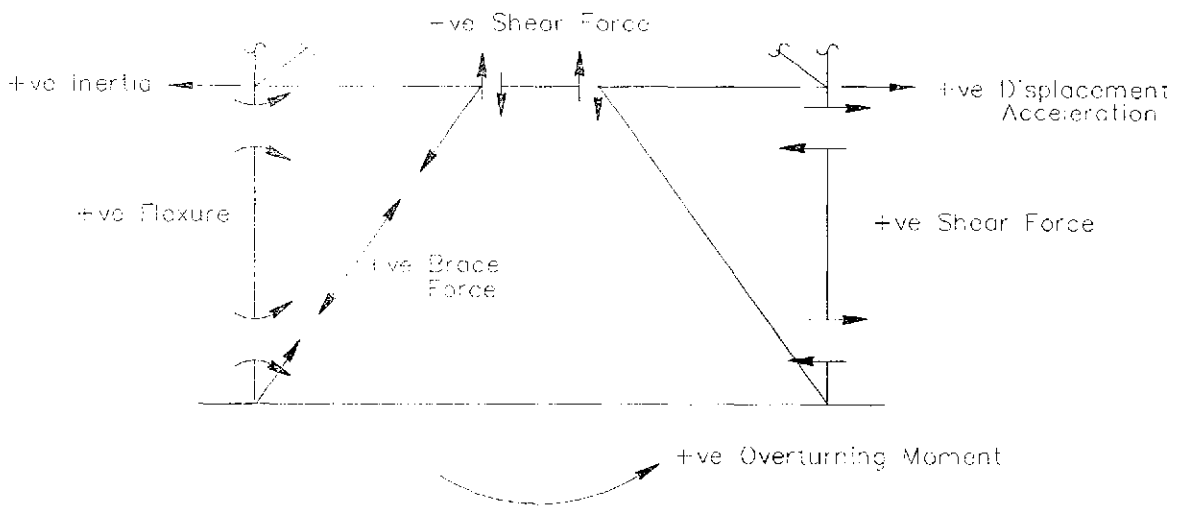
(b) EBDS Model

FIGURE 5.4   CBDS AND EBDS MODEL SIGN CONVENTION

Shear from Inertia Forces (kips)
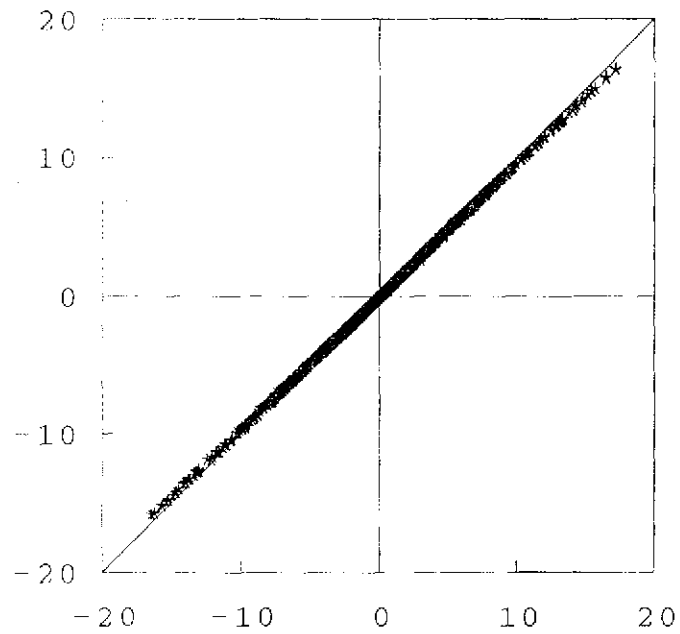
FIGURE 5.5 BASE SHEAR COMPARISON
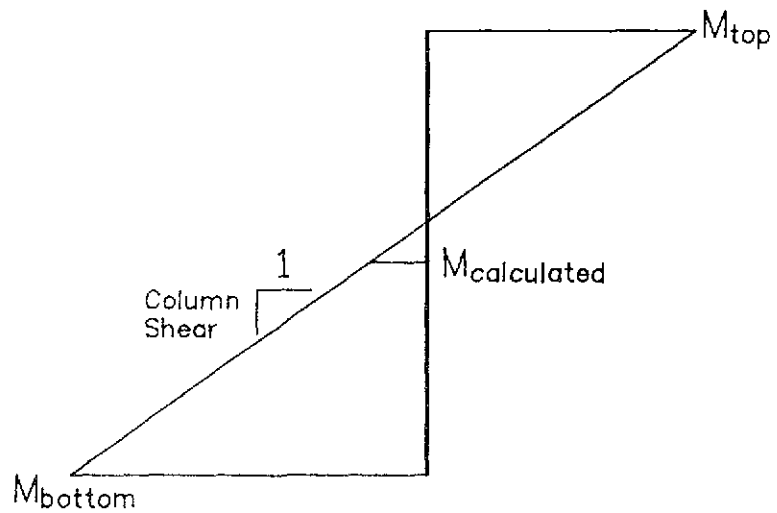
FIGURE 5.6 FIRST STORY COLUMN END MOMENT EVALUATION

FRAME A   FRAME B

(a) Columns and Braces

FRAME A   FRAME B
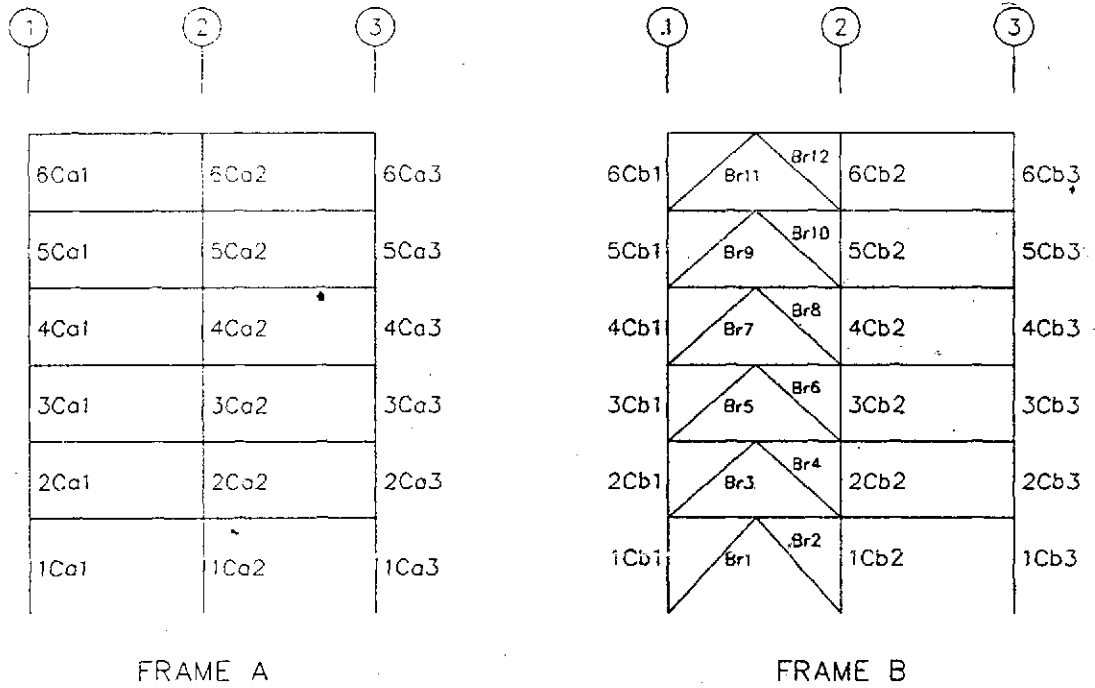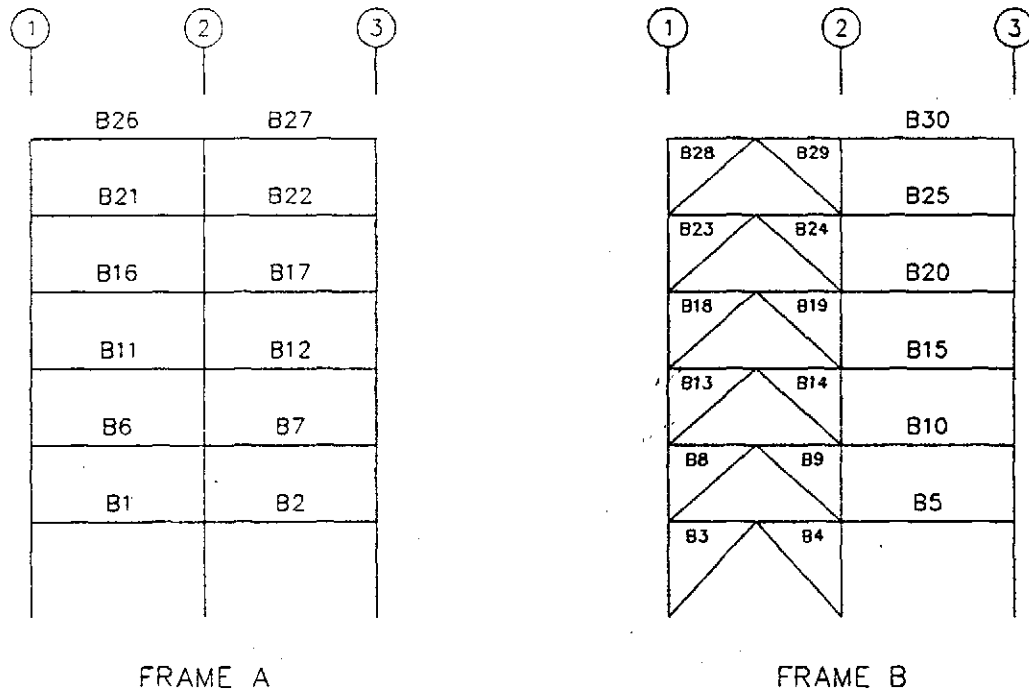
(b) Beams

FIGURE 5.7 CBDS MEMBER DESIGNATION

FRAME A

FRAME B

(a) Columns and Braces

FRAME A

FRAME B
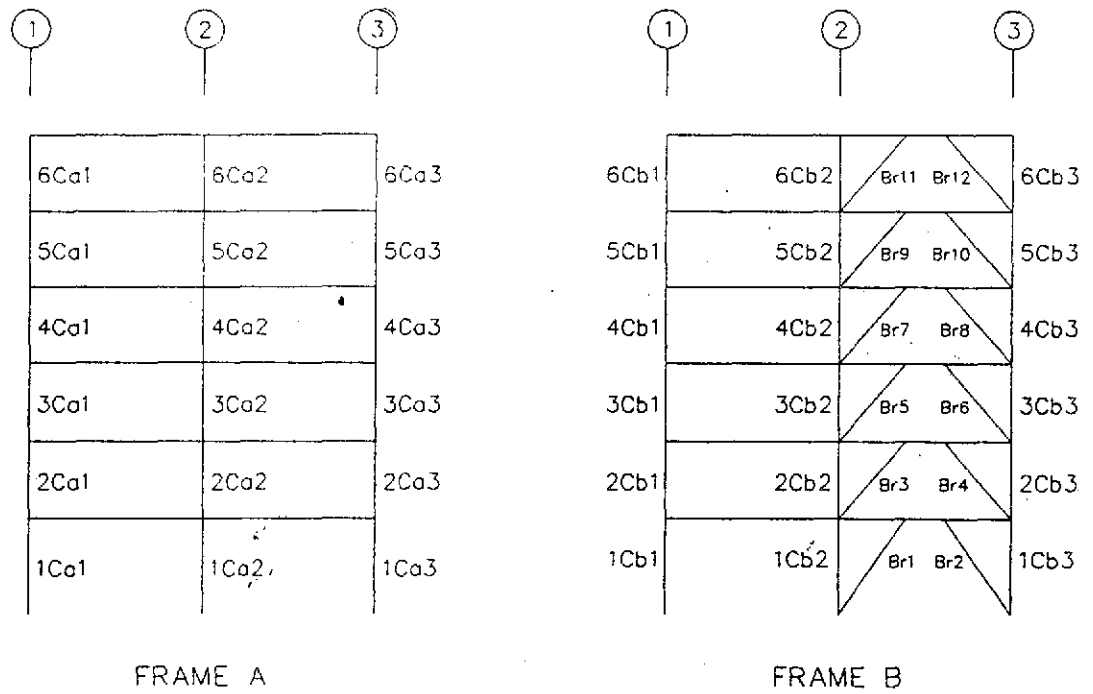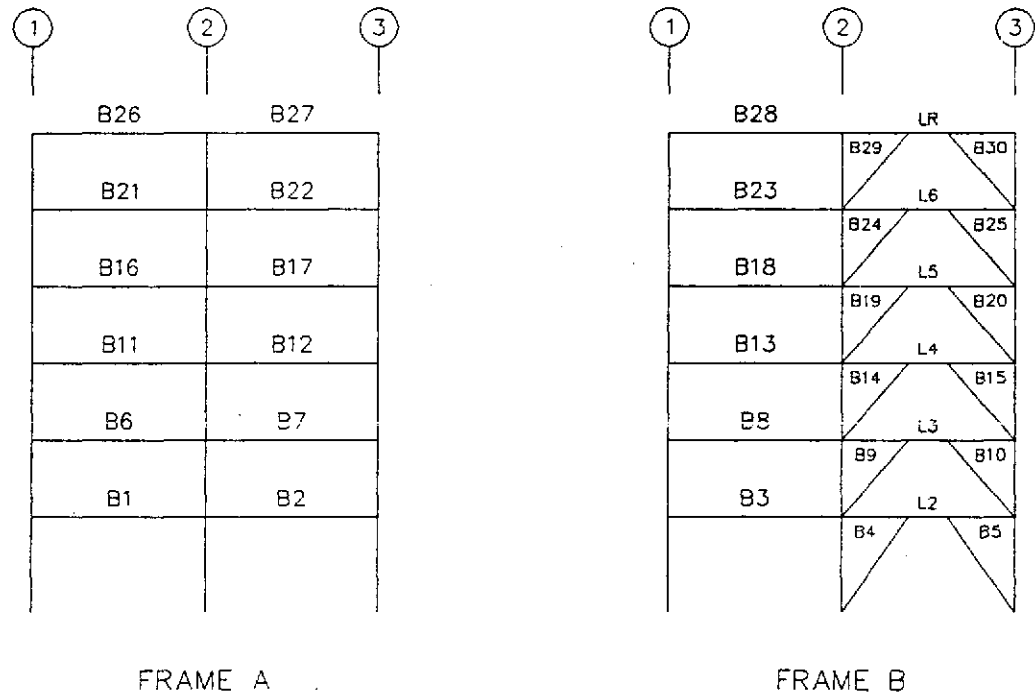
(b) Beams and Shear Links

FIGURE 5.8 EBDS MEMBER DESIGNATION
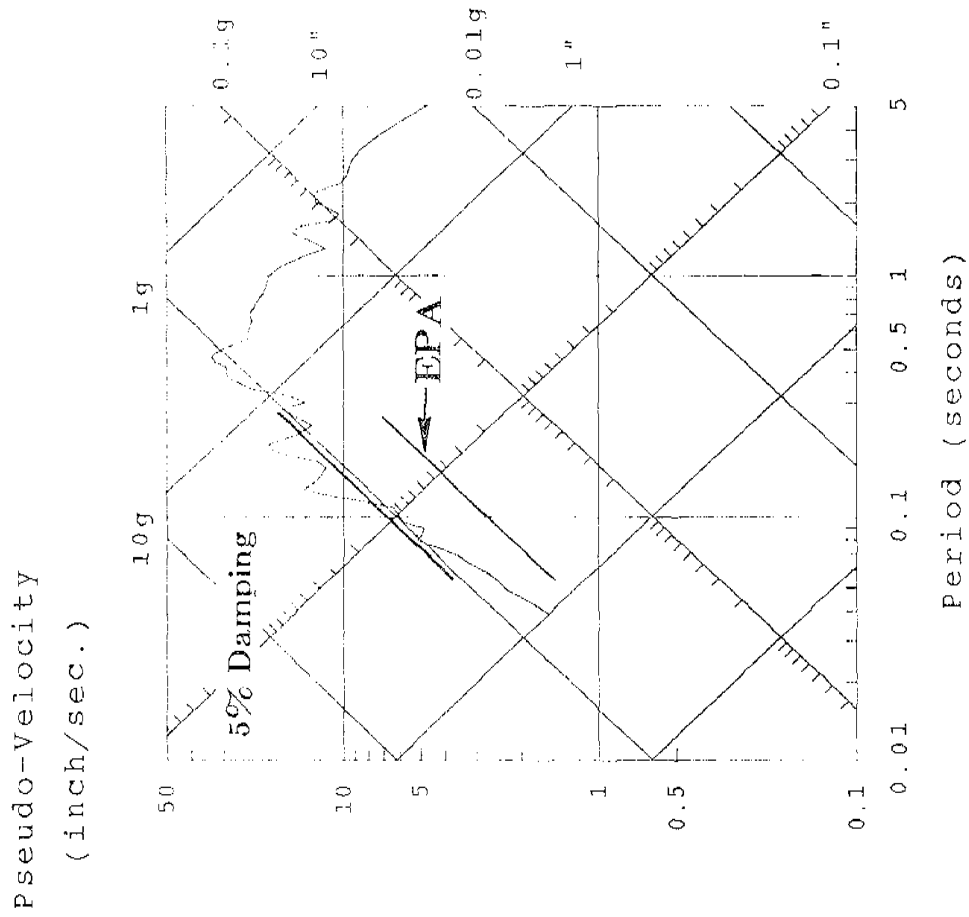
FIGURE 6.1 EVALUATION OF EPA FOR THE MODELS
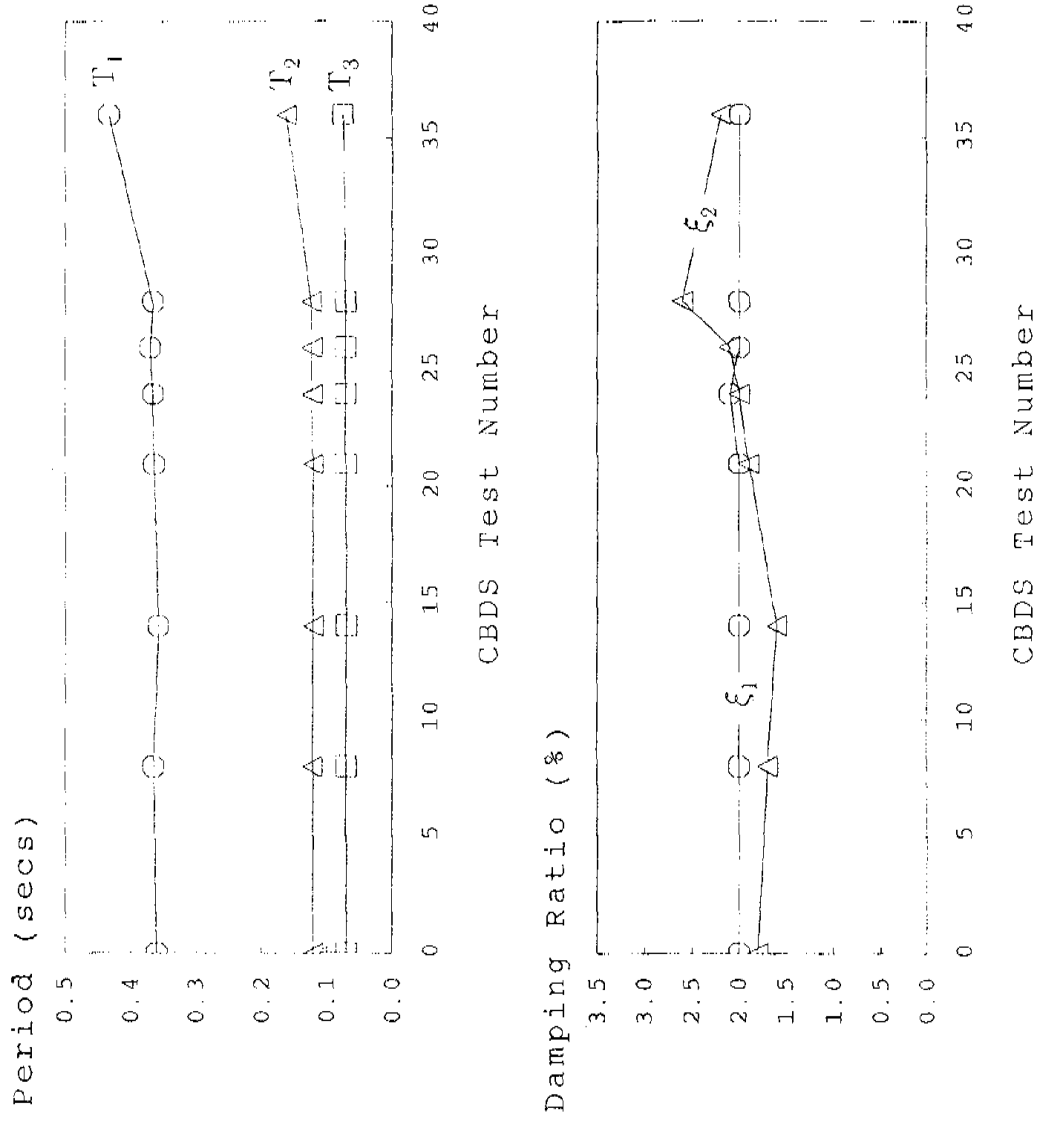
FIGURE 6.2 DYNAMIC CHARACTERISTICS OF THE CBDS
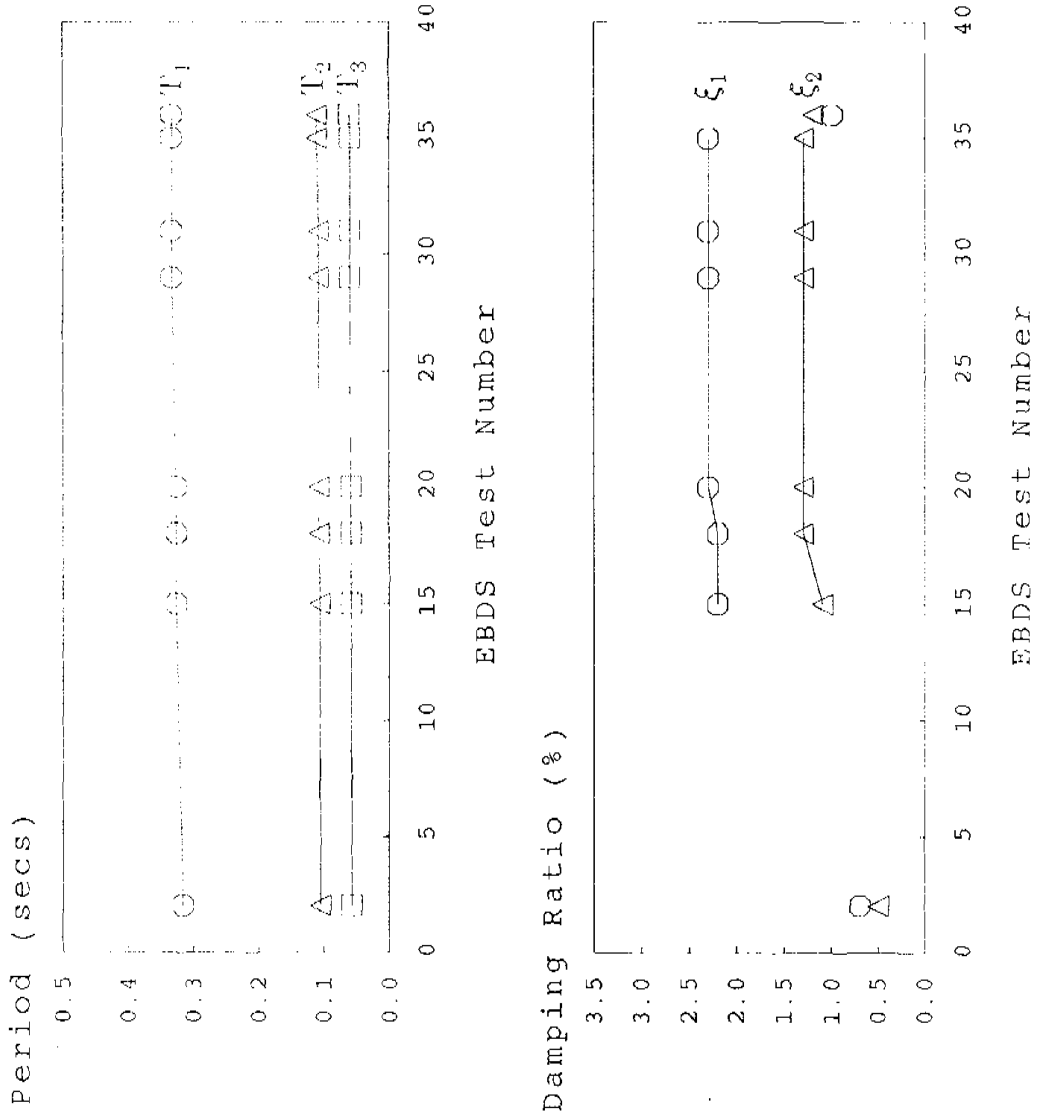
FIGURE 6.3 DYNAMIC CHARACTERISTICS OF THE EBDS
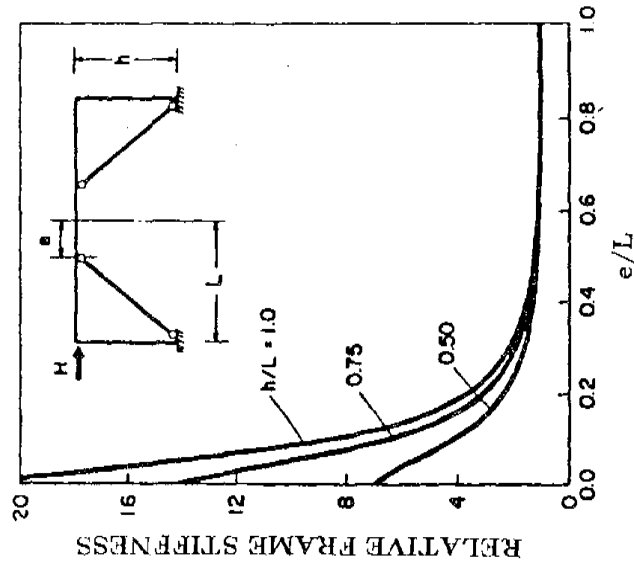
(a) D-Braced EBF
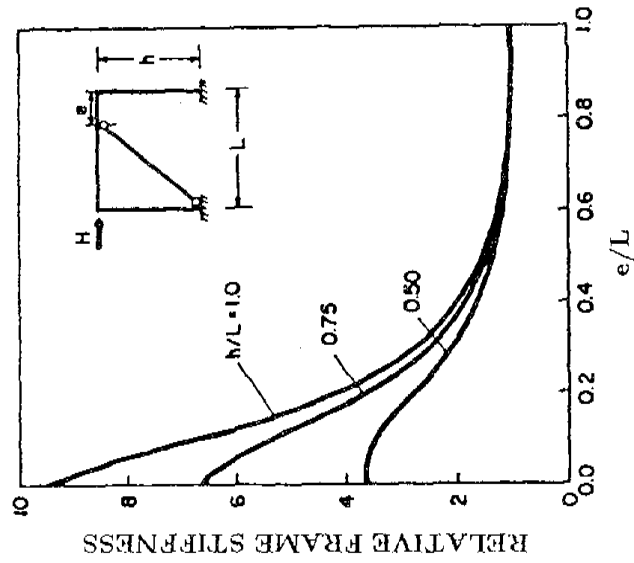
(b) Split K-Braced EBF

FIGURE 6.4 VARIATION IN THE ELASTIC STIFFNESS OF TWO EBFS [3]
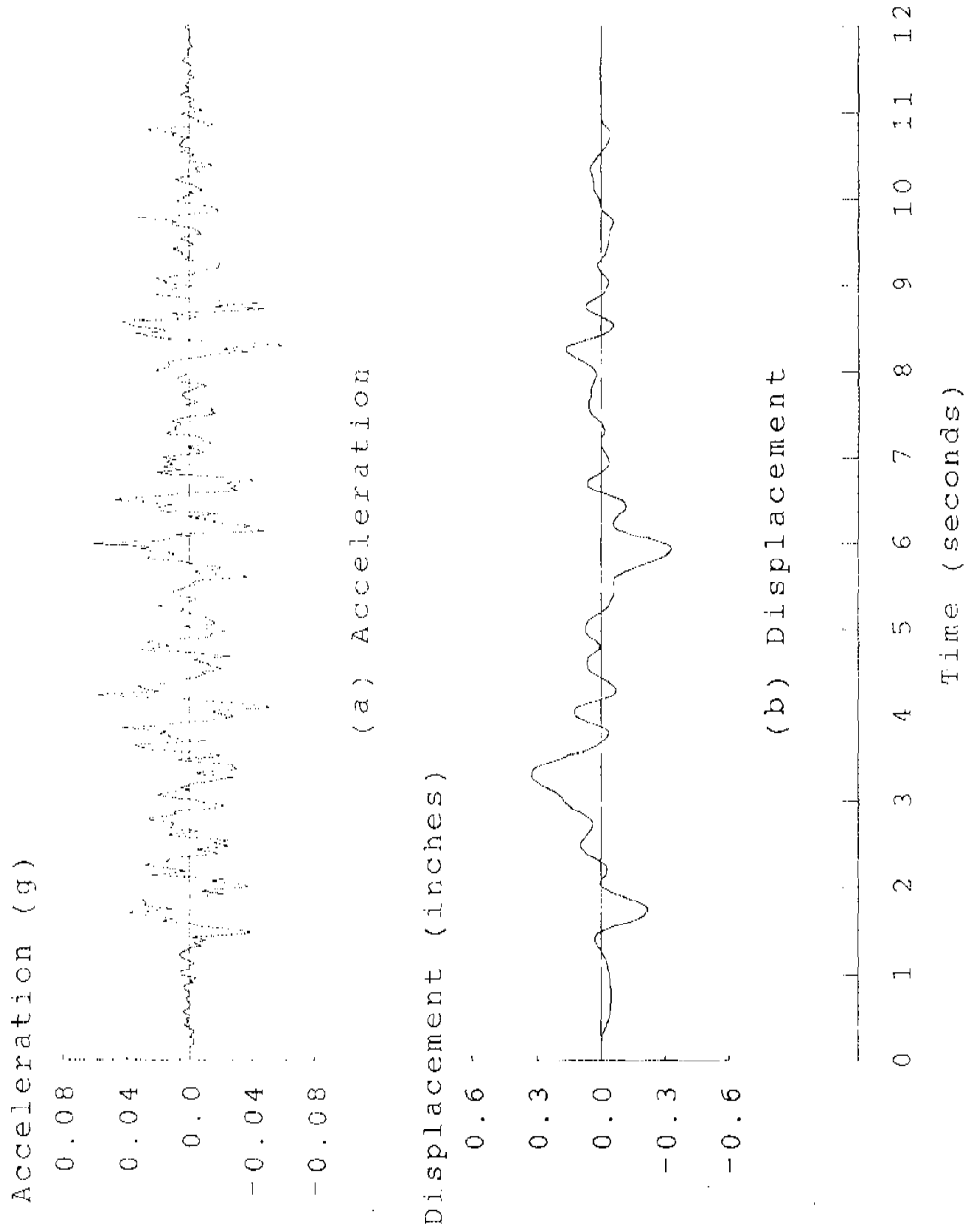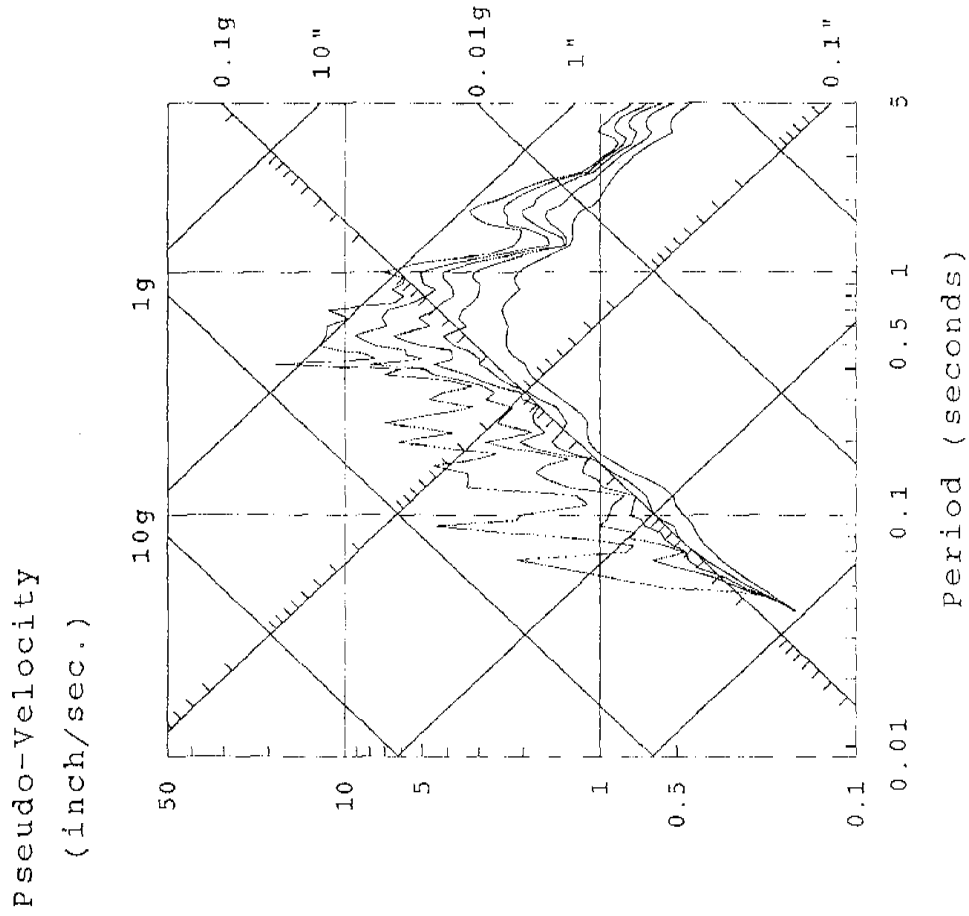
Acceleration (g)

(a) Acceleration

Displacement (inches)

(b) Displacement

Time (seconds)

FIGURE 6.5 CBDS MO-06 INPUT CHARACTERISTICS

FIGURE 6.5 CBDS MO-06 INPUT CHARACTERISTICS

(c) Response Spectra (0,2,5,10,20 % Damping)
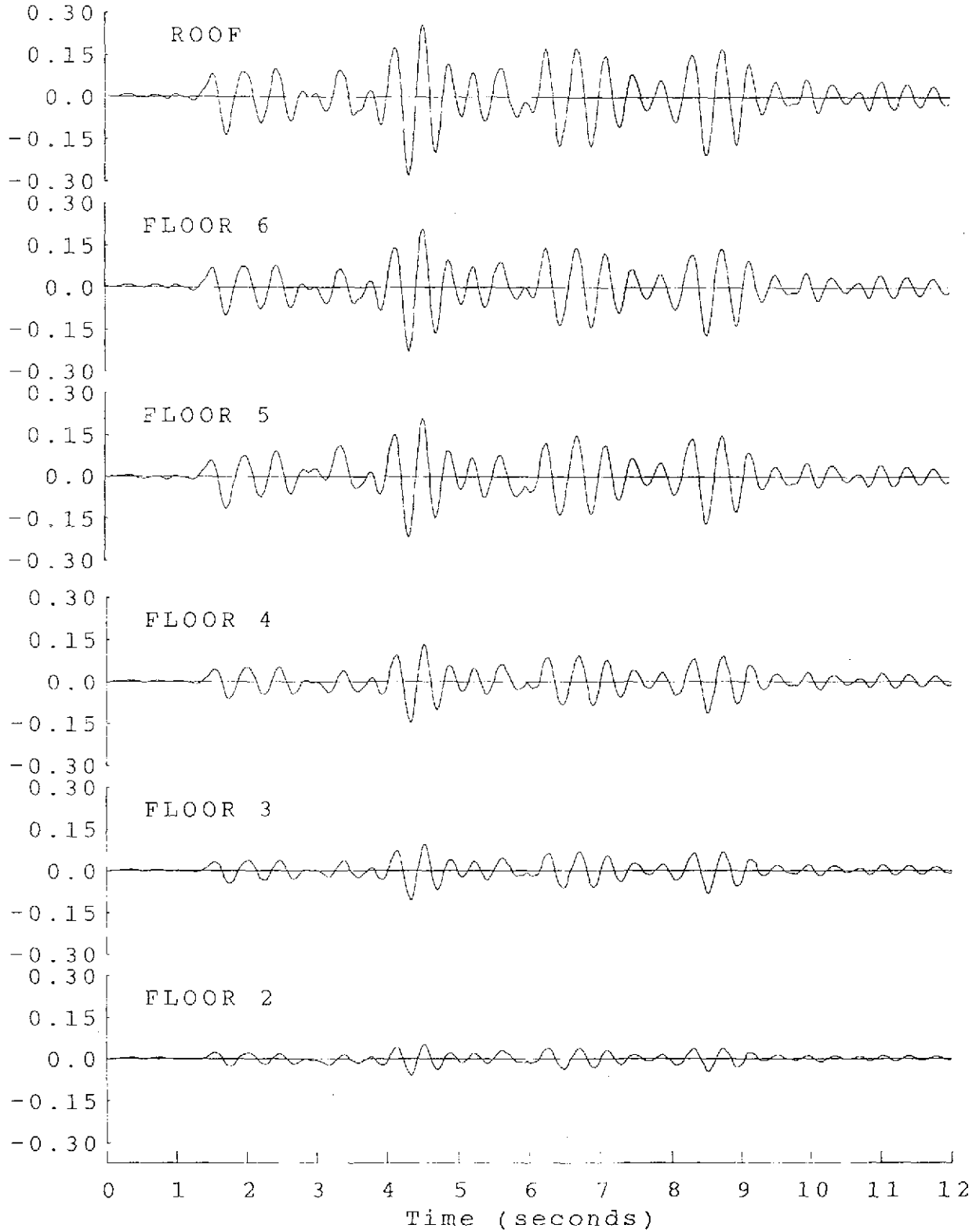
FIGURE 6.6 CBDS MO-06 LATERAL DISPLACEMENT TIME HISTORIES
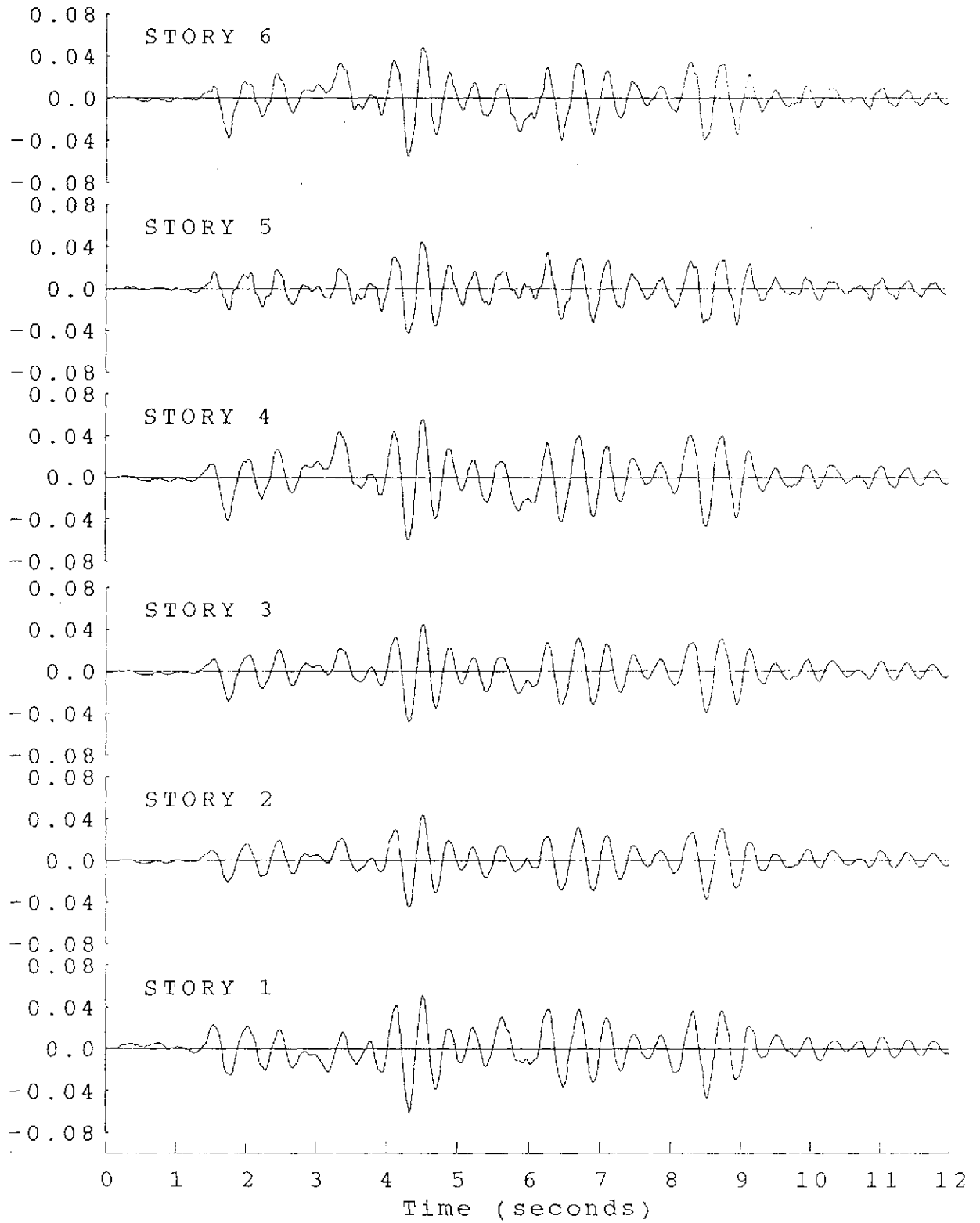
FIGURE 6.7 CBDS MO-06 INTER-STORY DRIFT TIME HISTORIES
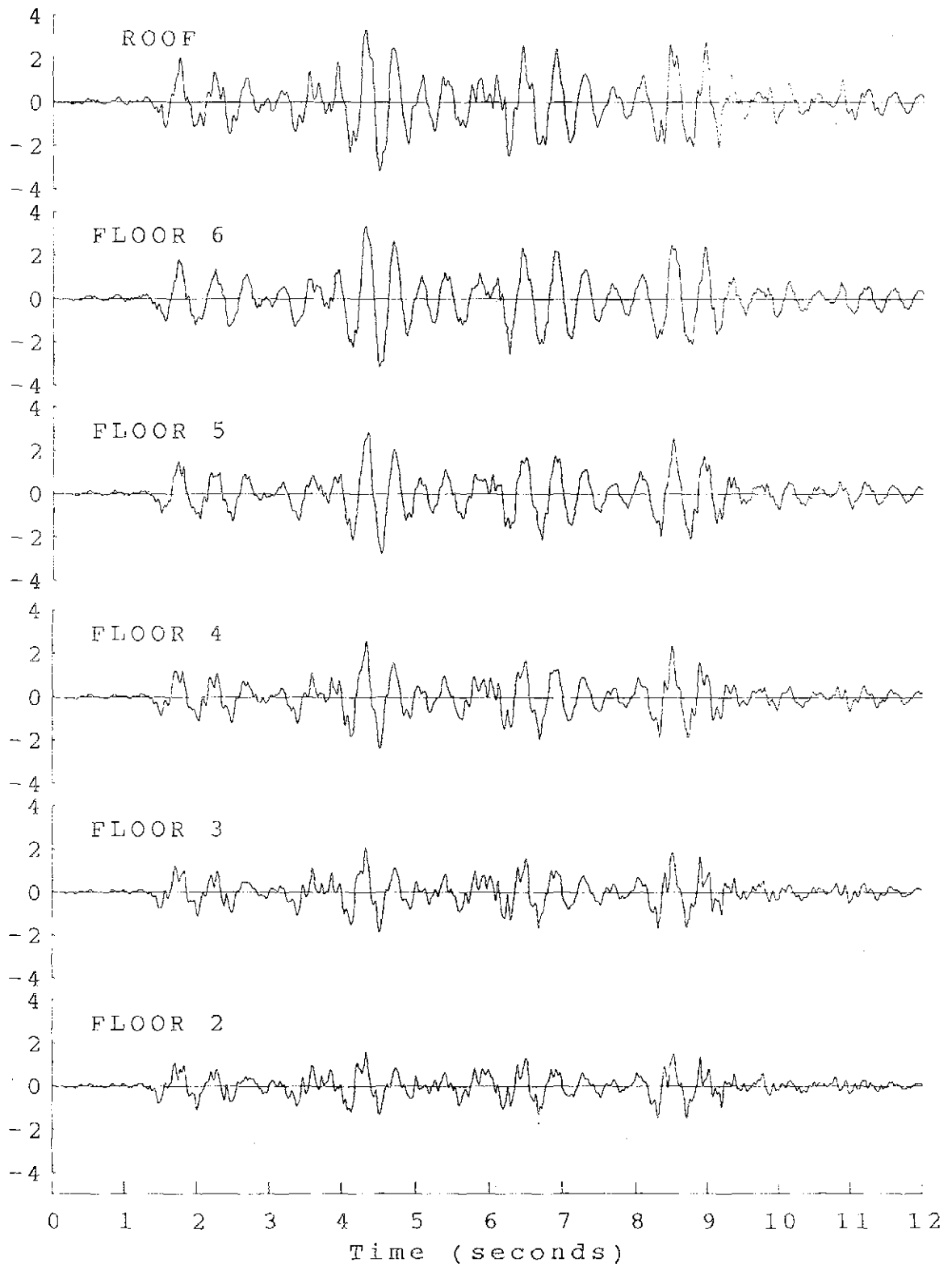
FIGURE 6.8 CBDS MO-06 INERTIA FORCE TIME HISTORIES
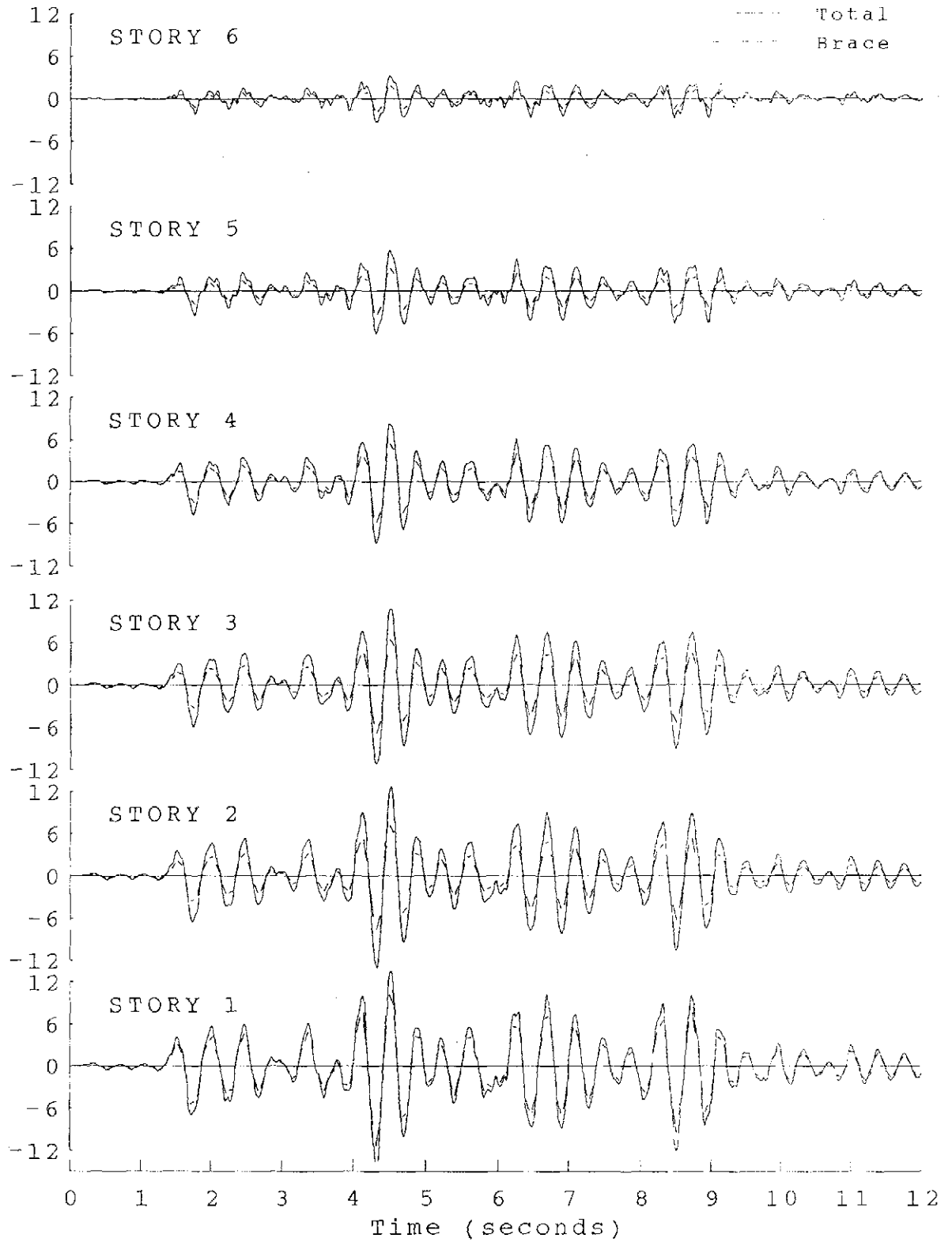
FIGURE 6.9 CBDS MO-06 STORY SHEAR TIME HISTORIES
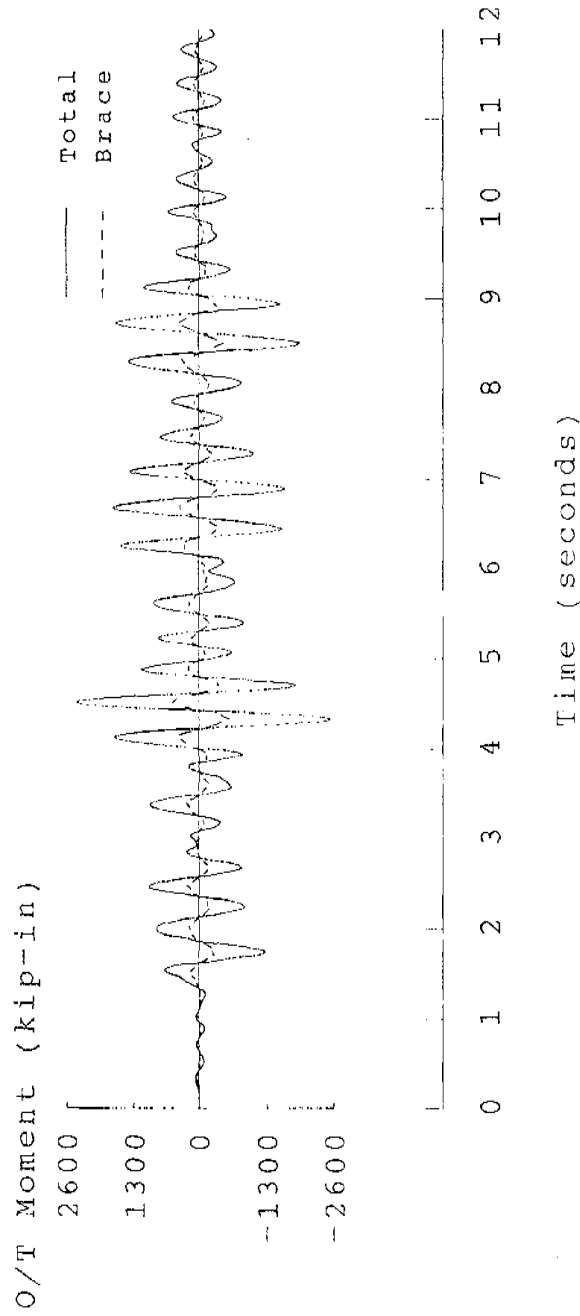
FIGURE 6.10 CBDS MO-06 OVERTURNING MOMENT TIME HISTORIES
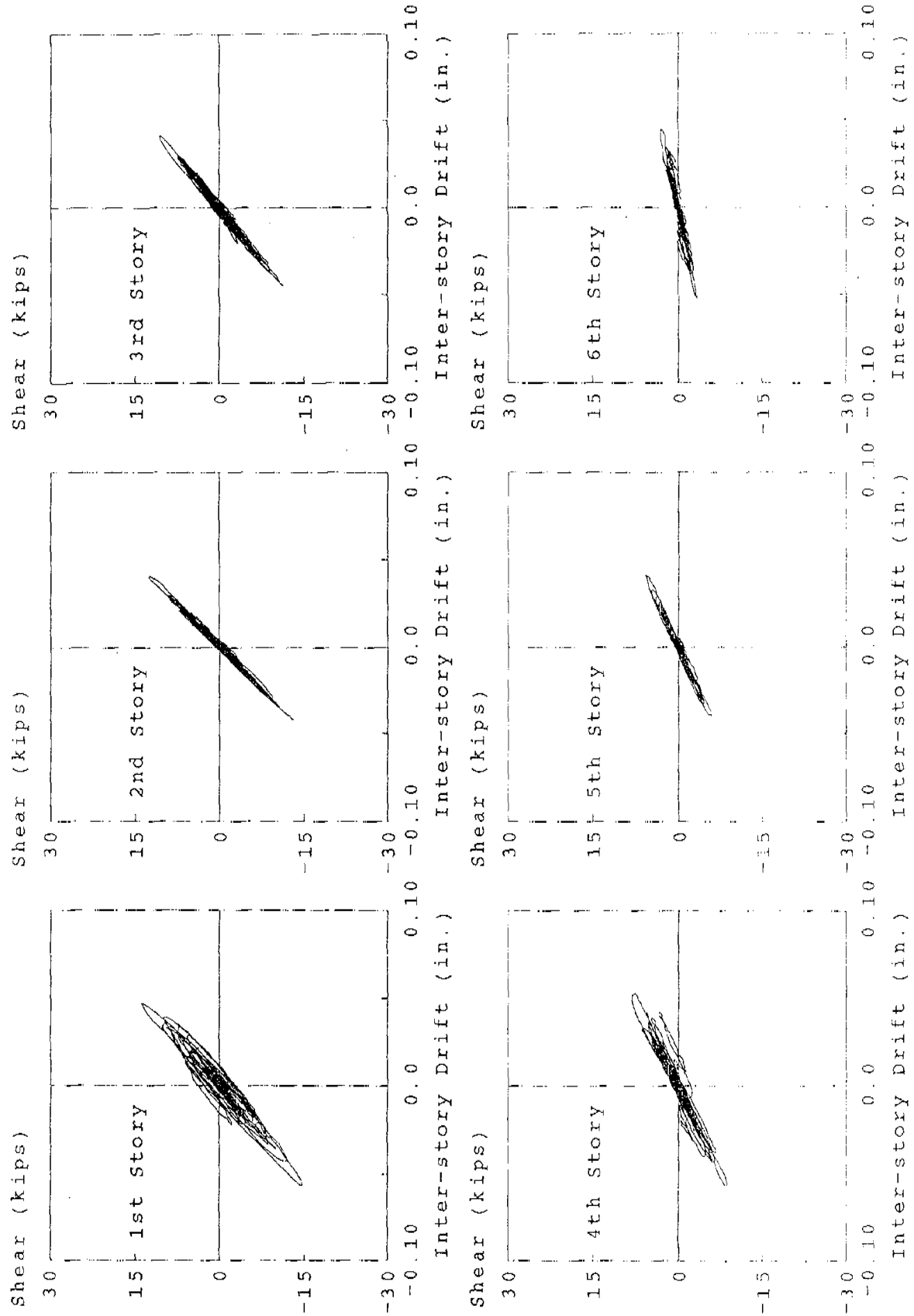
FIGURE 6.11 CBDS MO-06 STORY SHEAR AND INTER-STORY DRIFT RELATIONSHIPS

(a) Story Shear (kips)

(b) Inertia Force (kips)

(c) Lateral Displ. (inches)

(d) Inter-story Drift (inches)

(e) Overturning Moment (x1000 kip-inch)
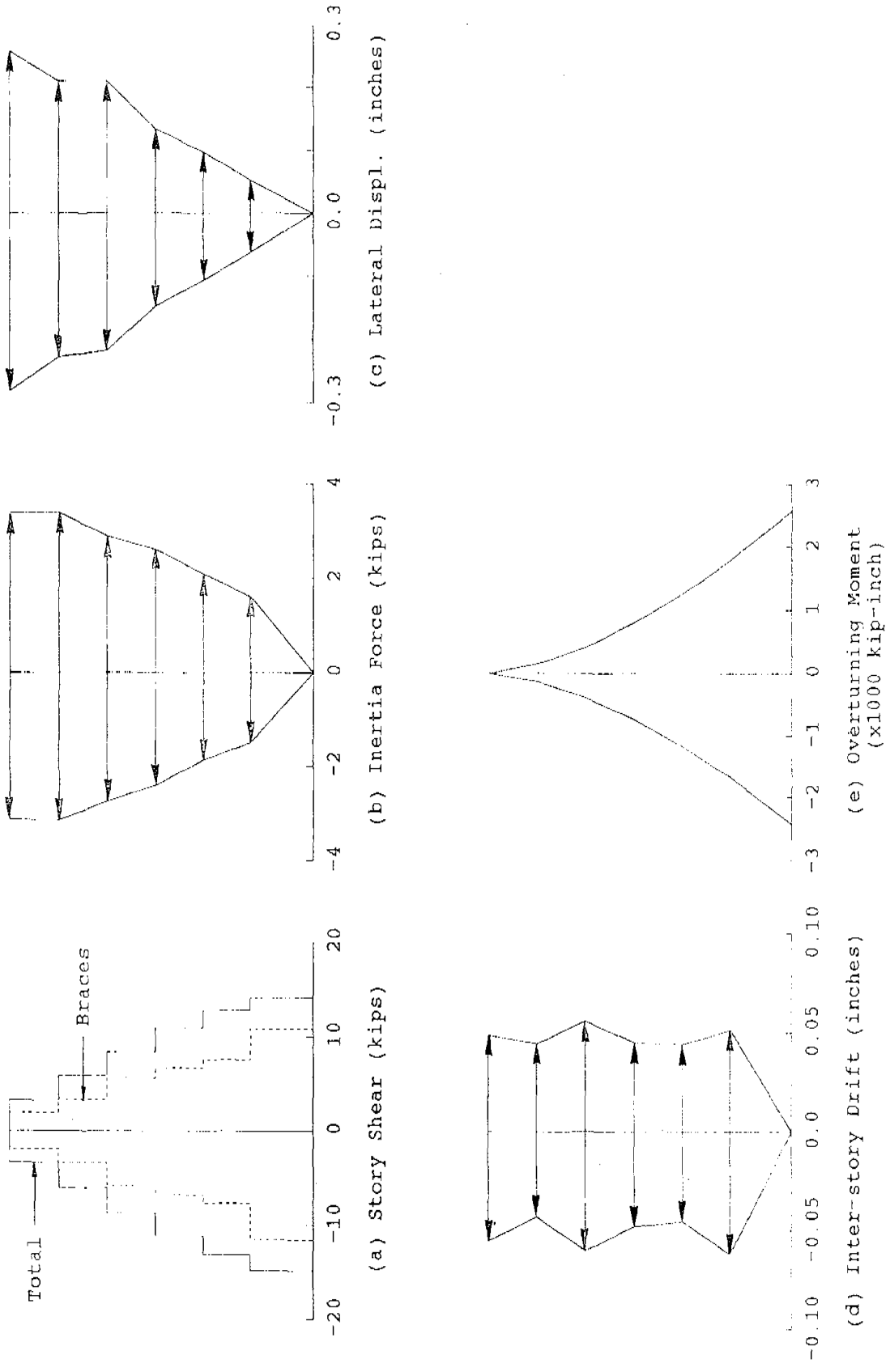
FIGURE 6.12 CBDS MO-06 RESPONSE ENVELOPES

(a) Lateral Displ. (inches)

(b) Inertia Force (kips)

(c) Story Shear (kips)

(d) Overturning Moment (x1000 kip-inch)

At Maximum Base Shear

(a) Lateral Displ. (inches)

(b) Inertia Force (kips)

(c) Story Shear (kips)

(d) Overturning Moment (x1000 kip-inch)

At Maximum Roof Displacement
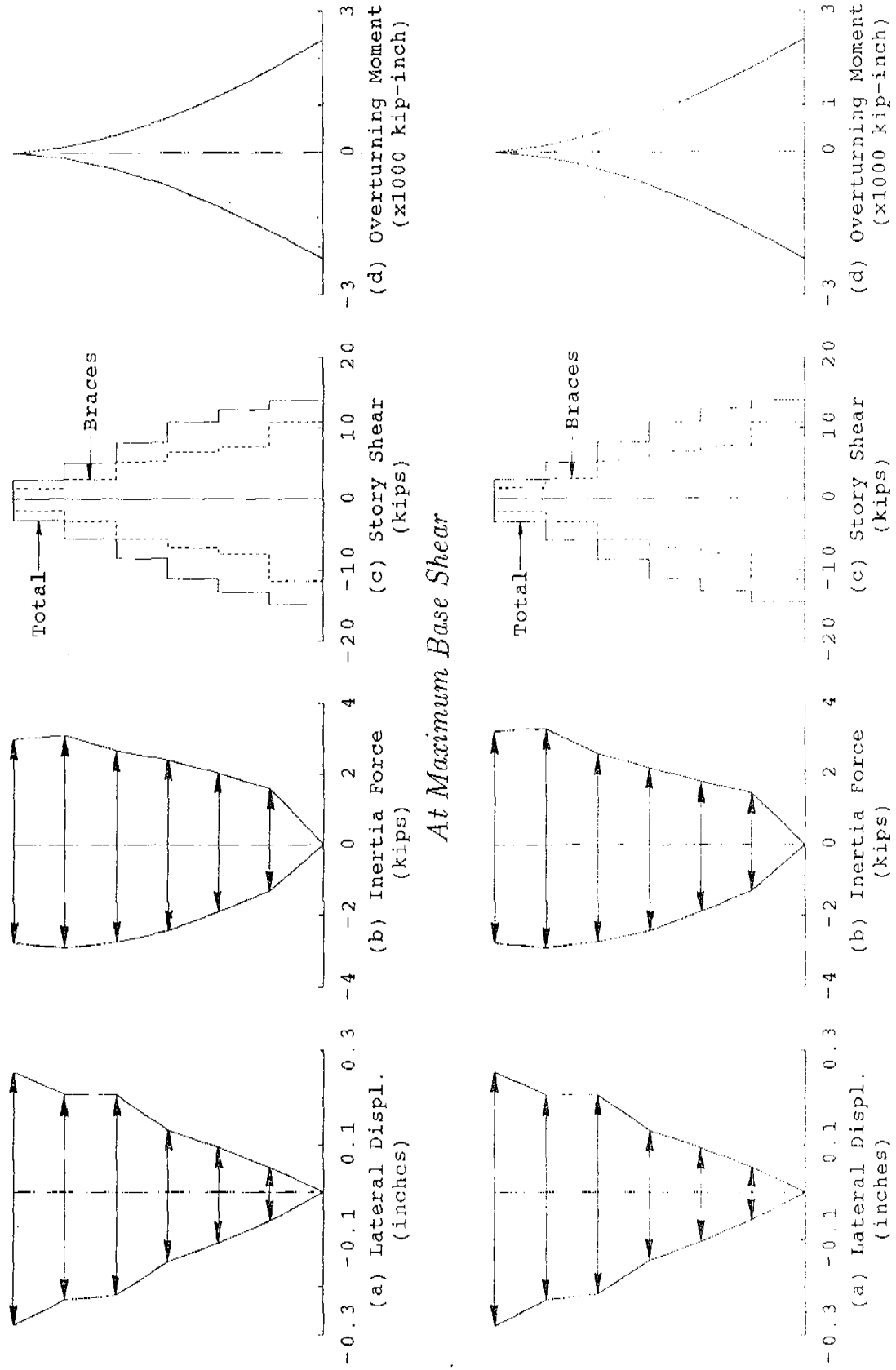
FIGURE 6.13 CBDS MO-06 RESPONSE PROFILES AT MAXIMUM RESPONSES

(a) Concentric Braces
(kips)

(b) DMRSF
(kips)

(c) Total
(kips)

At Maximum Base Shear

(a) Concentric Braces
(kips)

(b) DMRSF
(kips)

(c) Total
(kips)
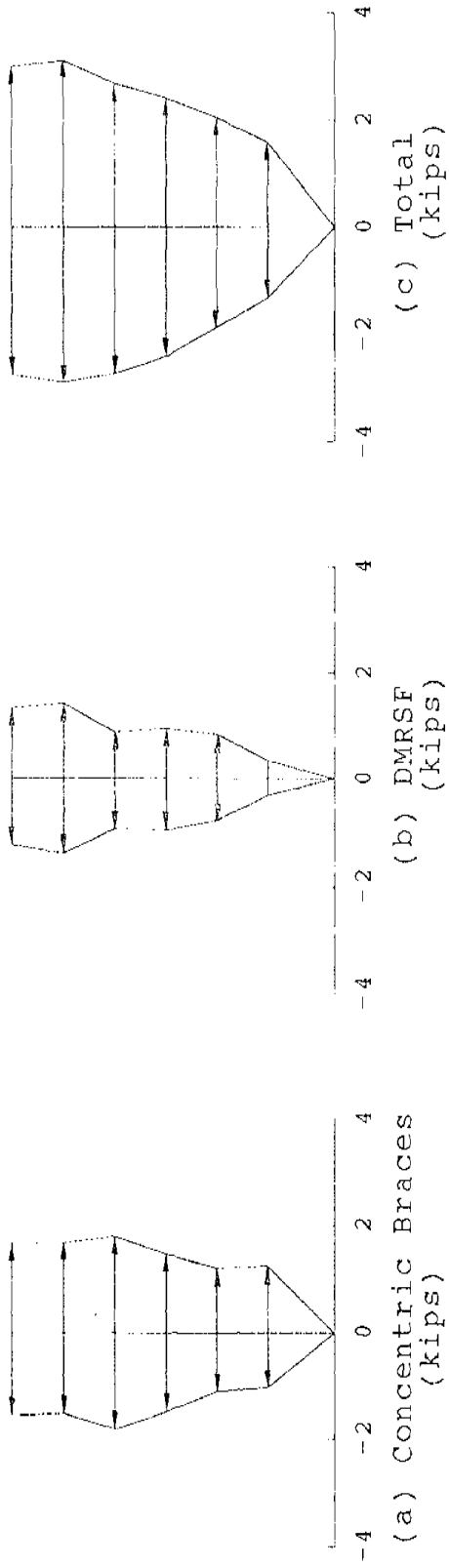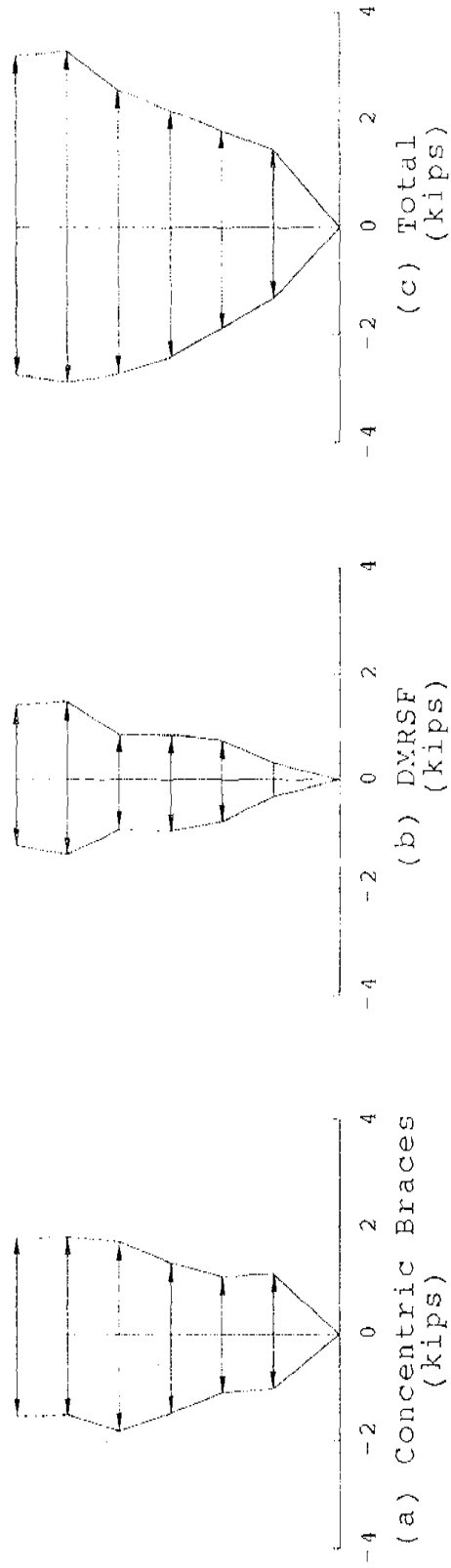
At Maximum Roof Displacement

FIGURE 6.14 CBDS MO-06 LATERAL FORCE DISTRIBUTIONS AT MAXIMUM RESPONSES
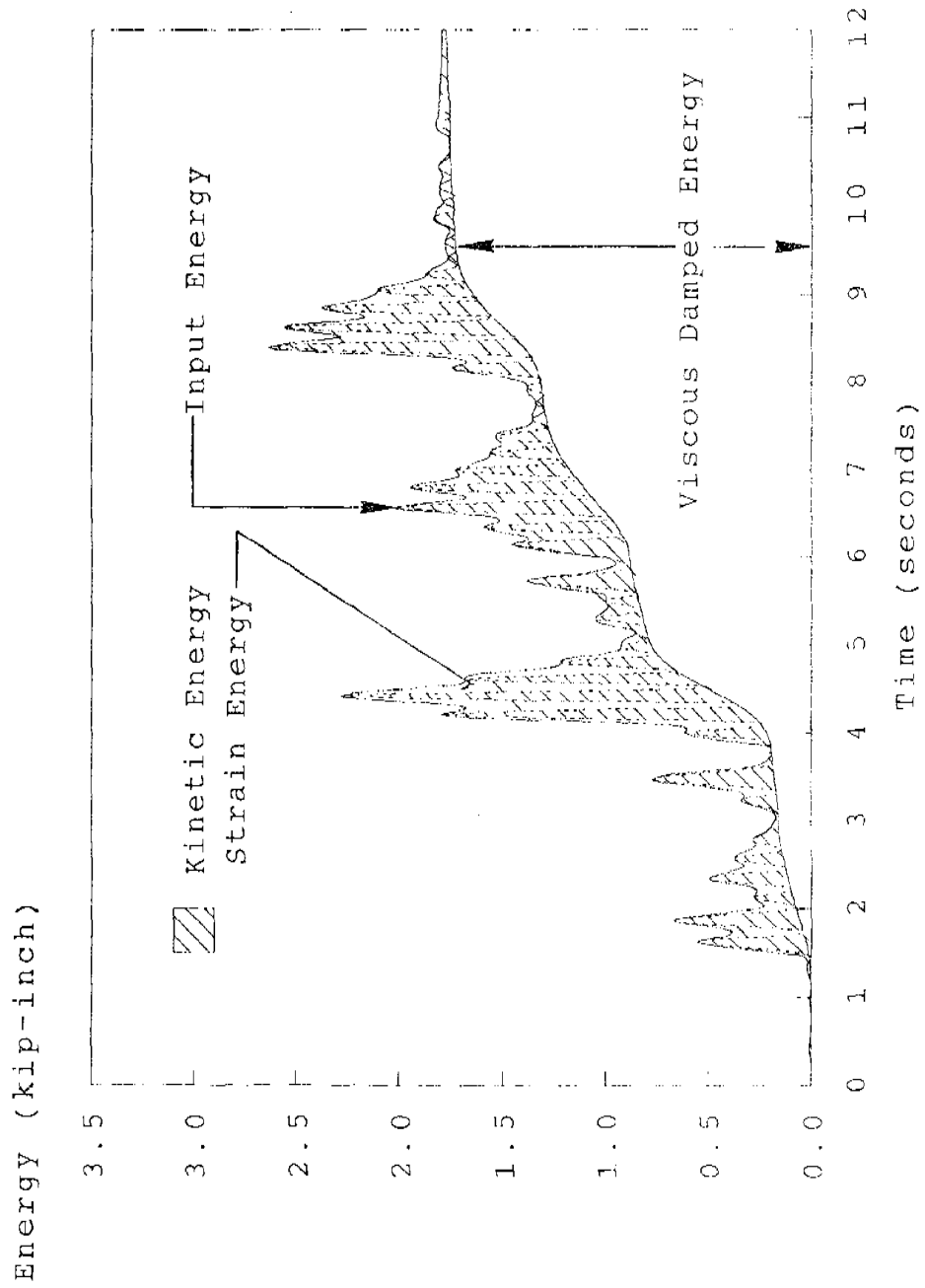
FIGURE 6.15 CBDS MO-06 ENERGY TIME HISTORIES
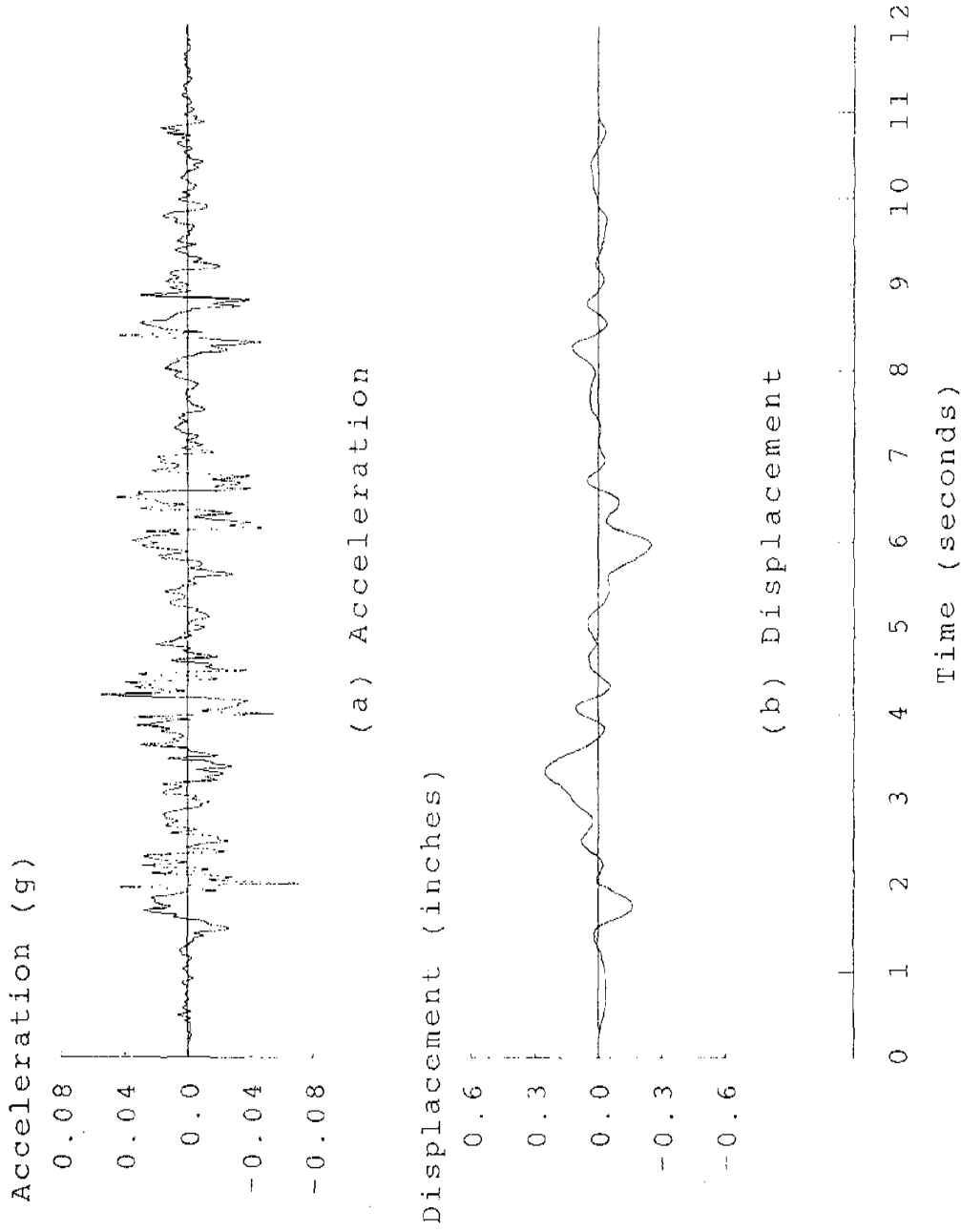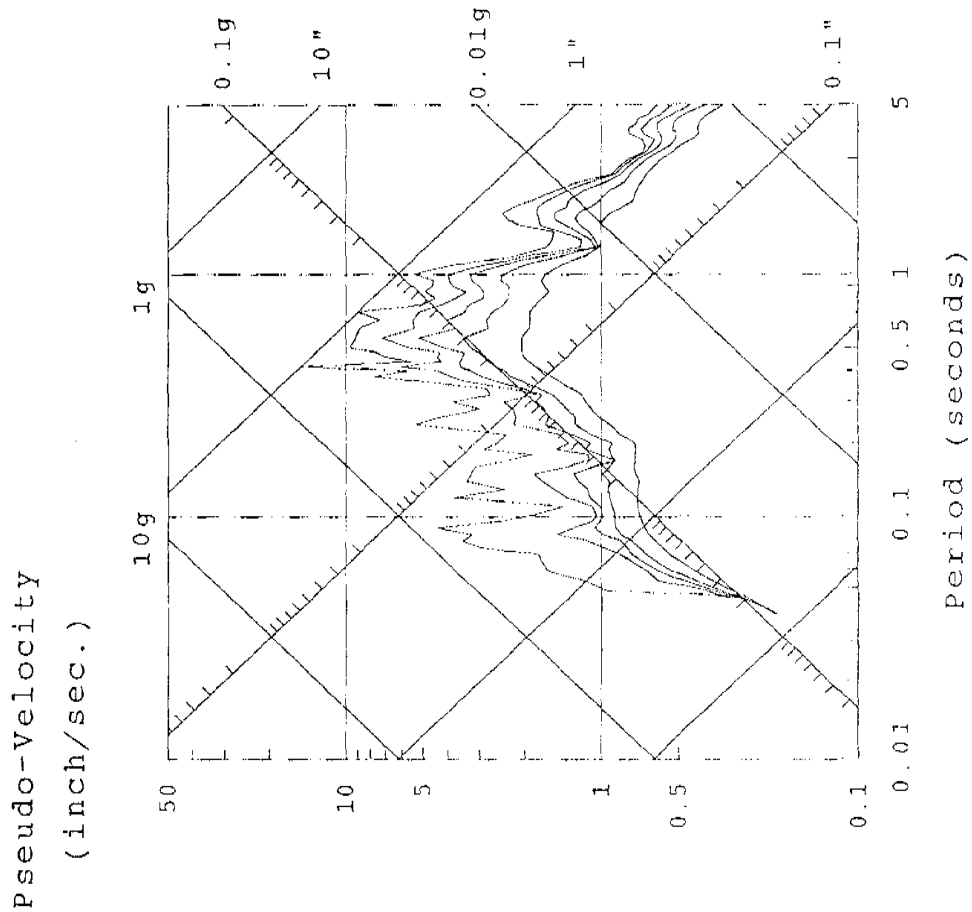
(a) Acceleration

(b) Displacement

FIGURE 6.16 EBDS MO-07 INPUT CHARACTERISTICS

FIGURE 6.16 EBDS MO-07 INPUT CHARACTERISTICS

(c) Response Spectra (0,2,5,10,20 % Damping)
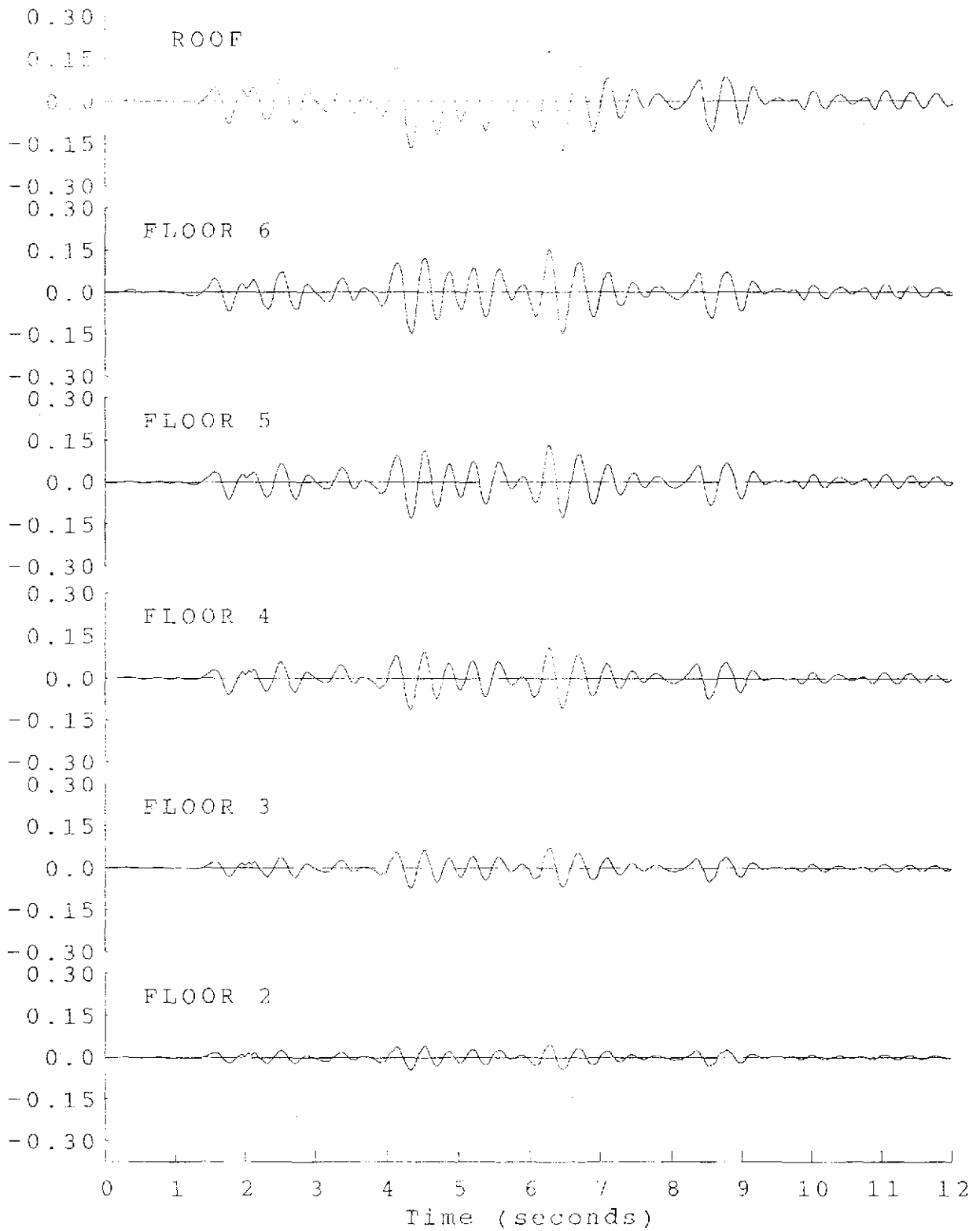
FIGURE 6.17 EBDS MO-07 LATERAL DISPLACEMENT TIME HISTORIES
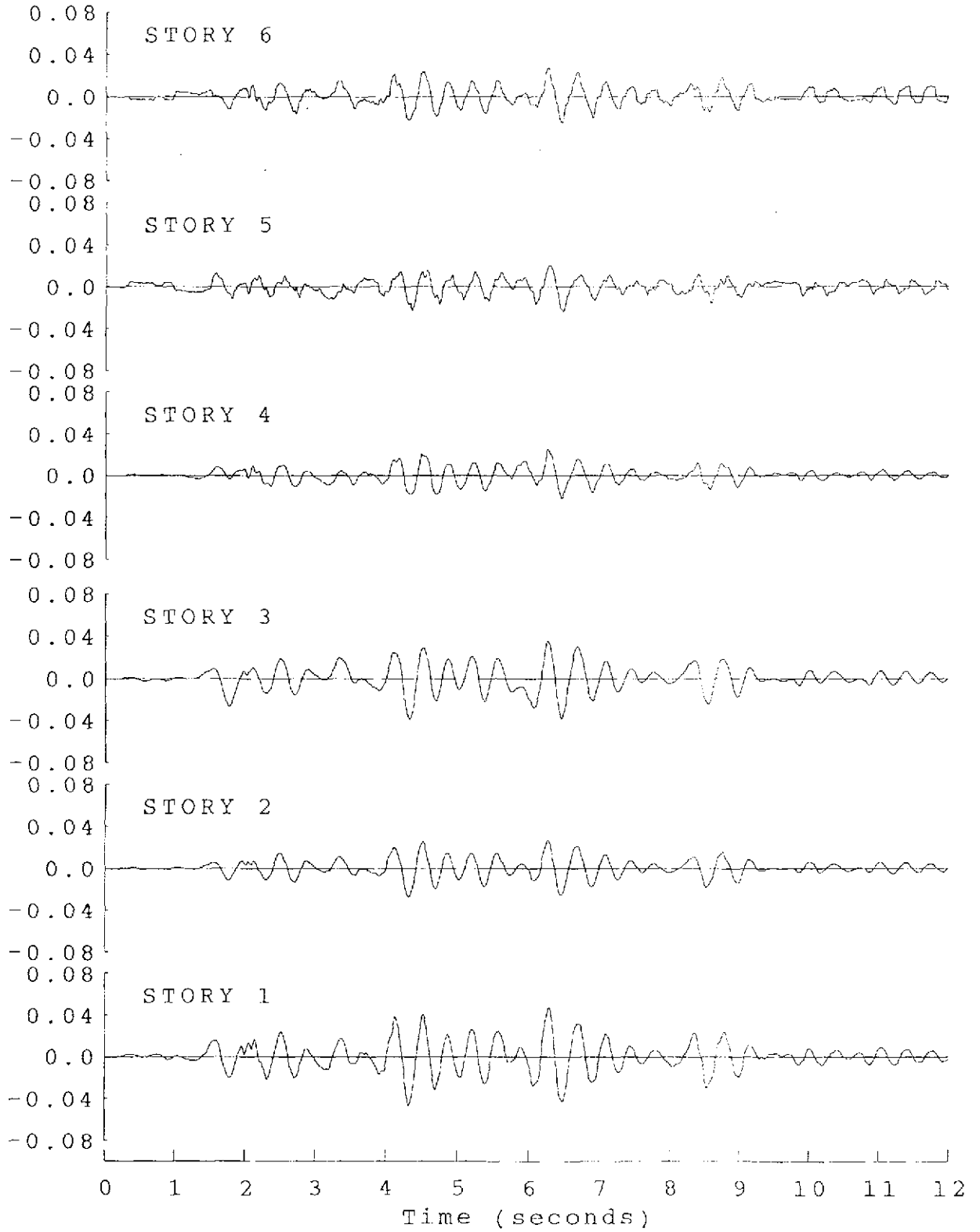
FIGURE 6.18 EBDS MO-07 INTER-STORY DRIFT TIME HISTORIES
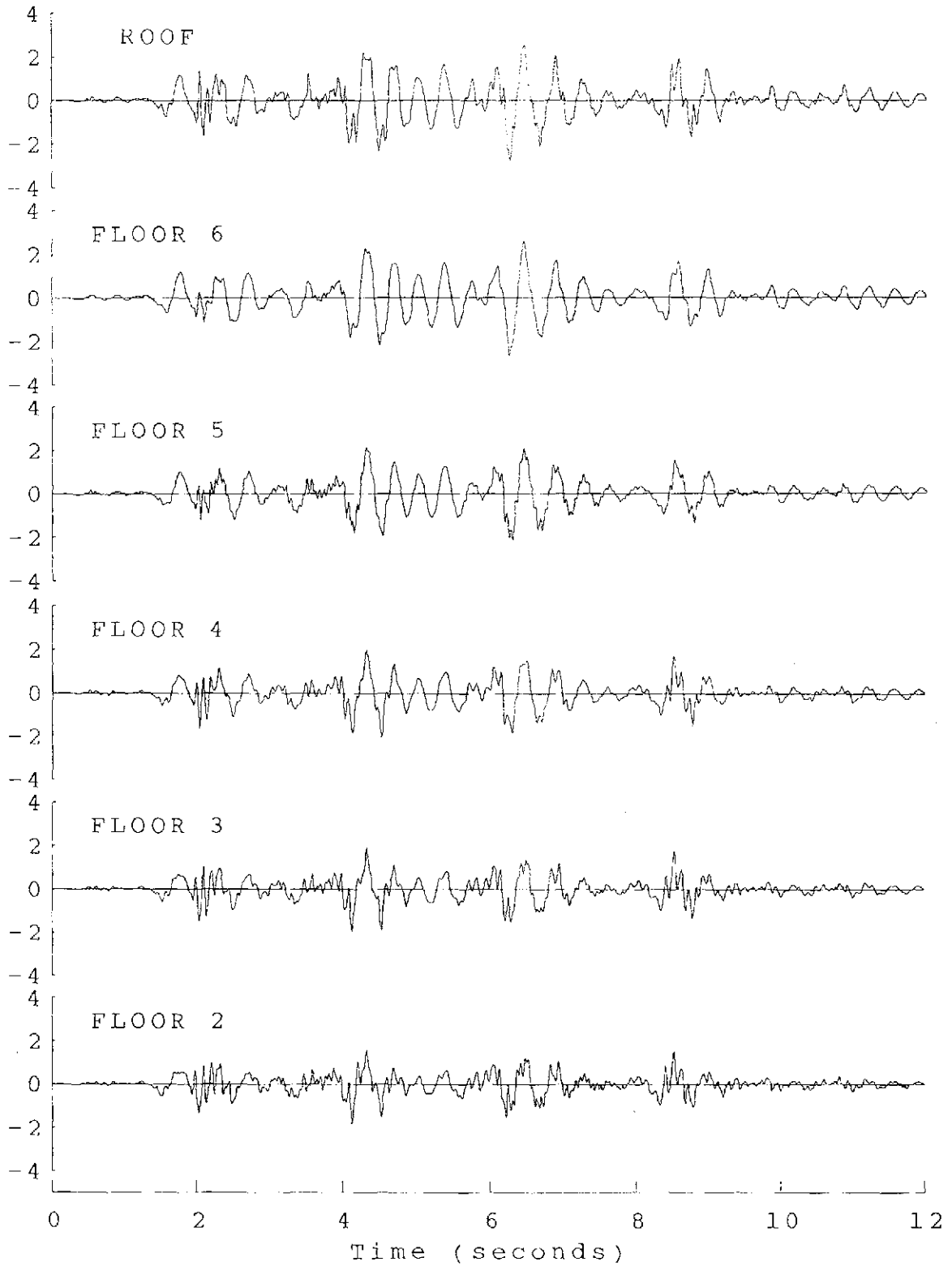
FIGURE 6.19 EBDS MO-07 INERTIA FORCE TIME HISTORIES
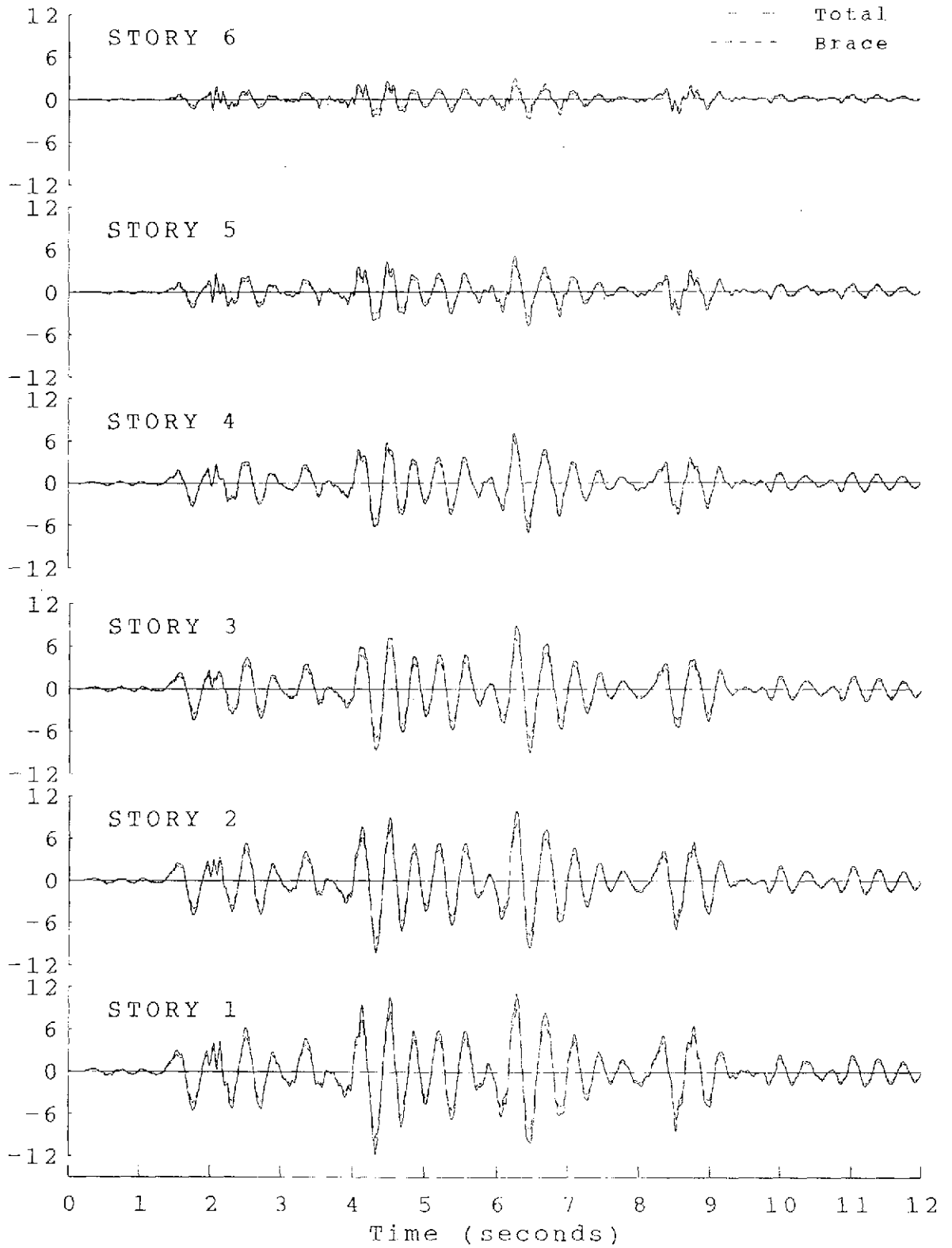
FIGURE 6.20 EBDS MO-07 STORY SHEAR TIME HISTORIES
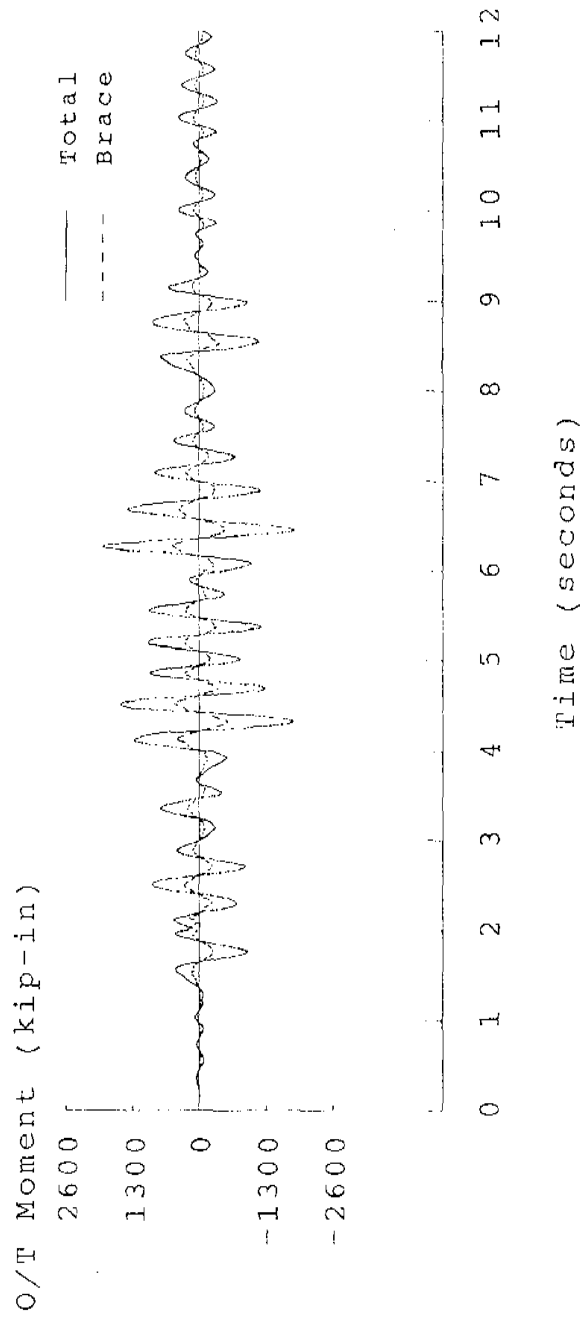
FIGURE 6.21 EBDS MO-07 OVERTURNING MOMENT TIME HISTORIES
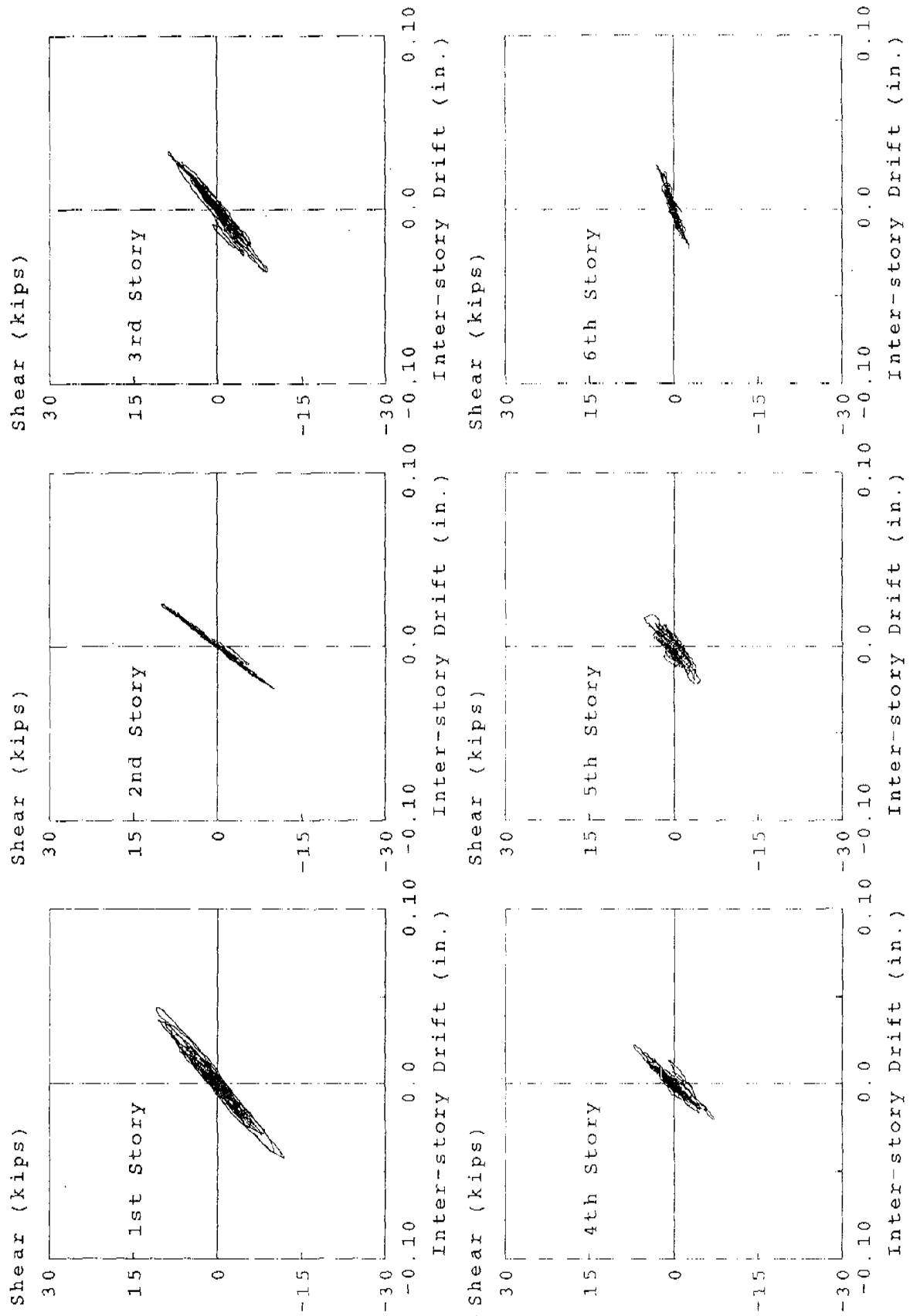
FIGURE 6.22 EBDS MO-07 STORY SHEAR AND INTER-STORY DRIFT RELATIONSHIPS
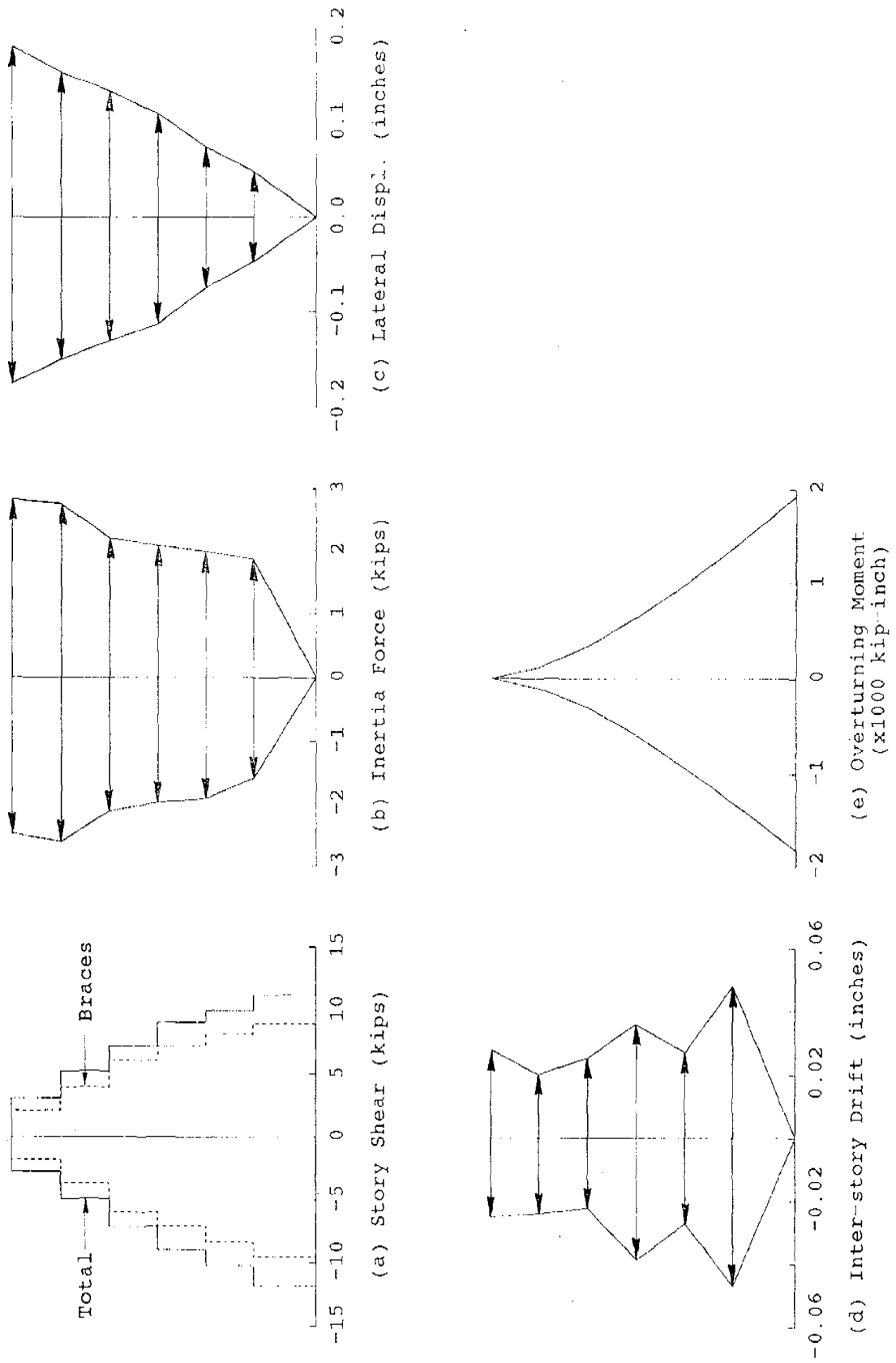
FIGURE 6.23 EBDS MO-07 RESPONSE ENVELOPES
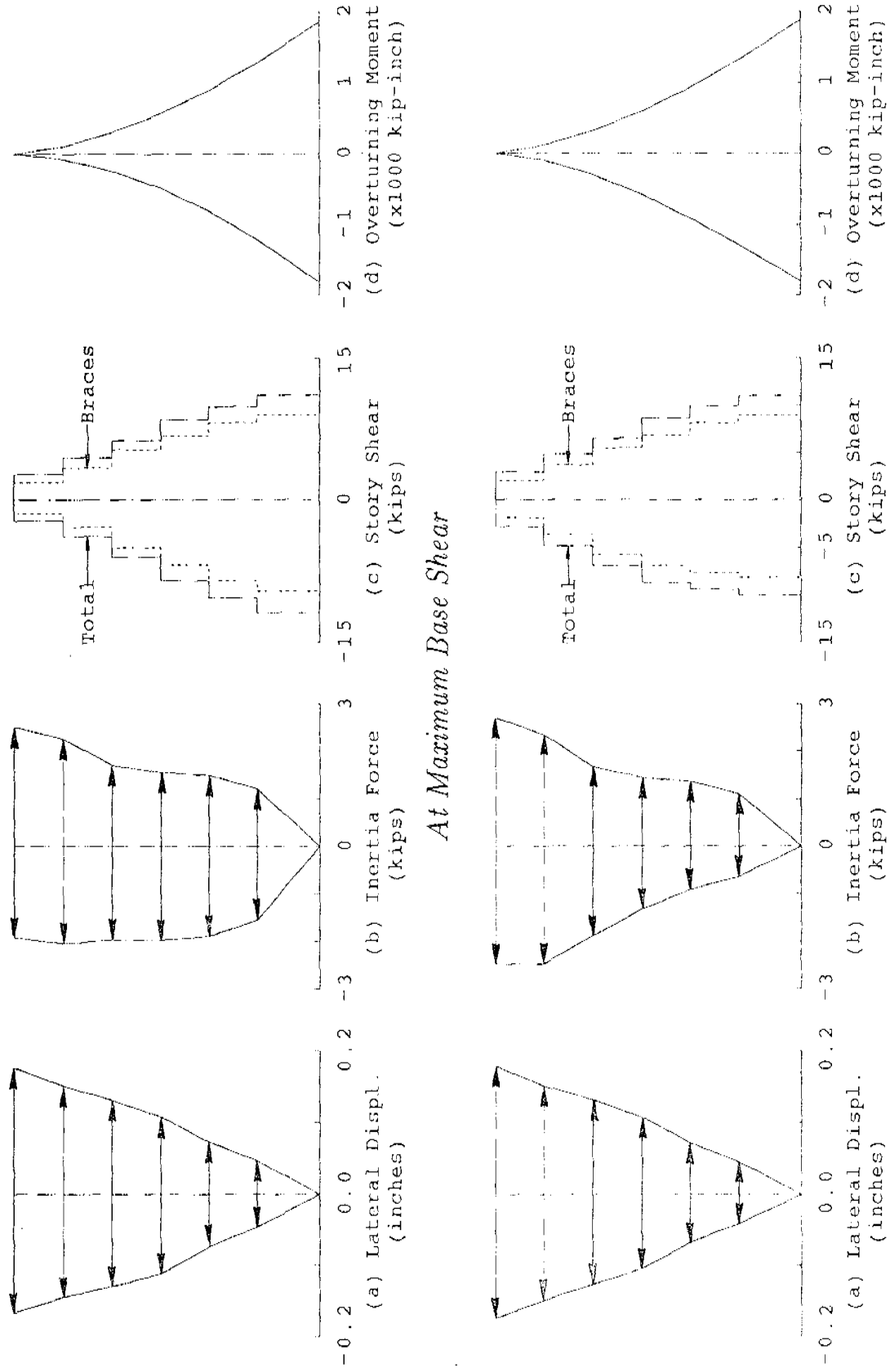
FIGURE 6.24 EBDS MO-07 RESPONSE PROFILES AT MAXIMUM RESPONSES

(a) Eccentric Braces
(kips)

(b) DMRSF
(kips)

(c) Total
(kips)

At Maximum Base Shear

(a) Eccentric Braces
(kips)

(b) DMRSF
(kips)

(c) Total
(kips)
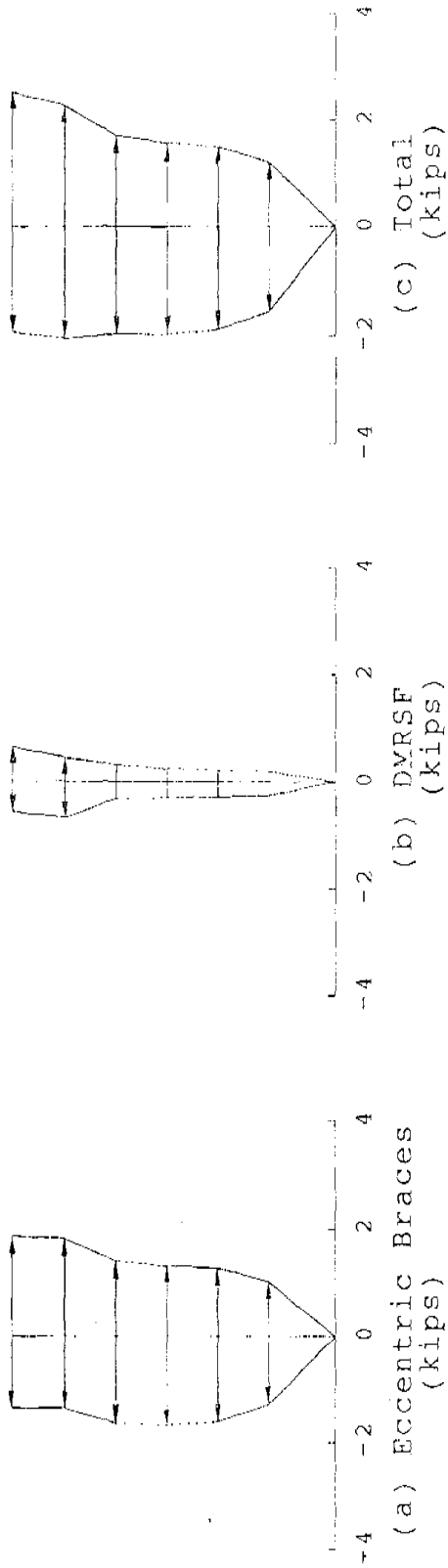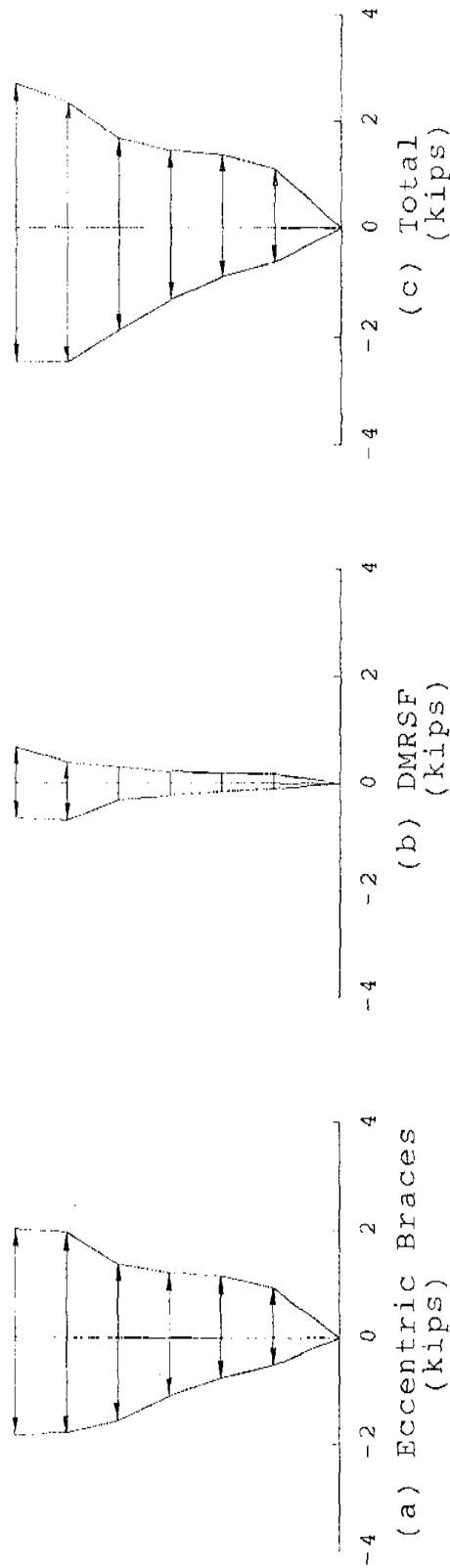
At Maximum Roof Displacement

FIGURE 6.25 EBDS MO-07 LATERAL FORCE DISTRIBUTIONS AT MAXIMUM RESPONSES
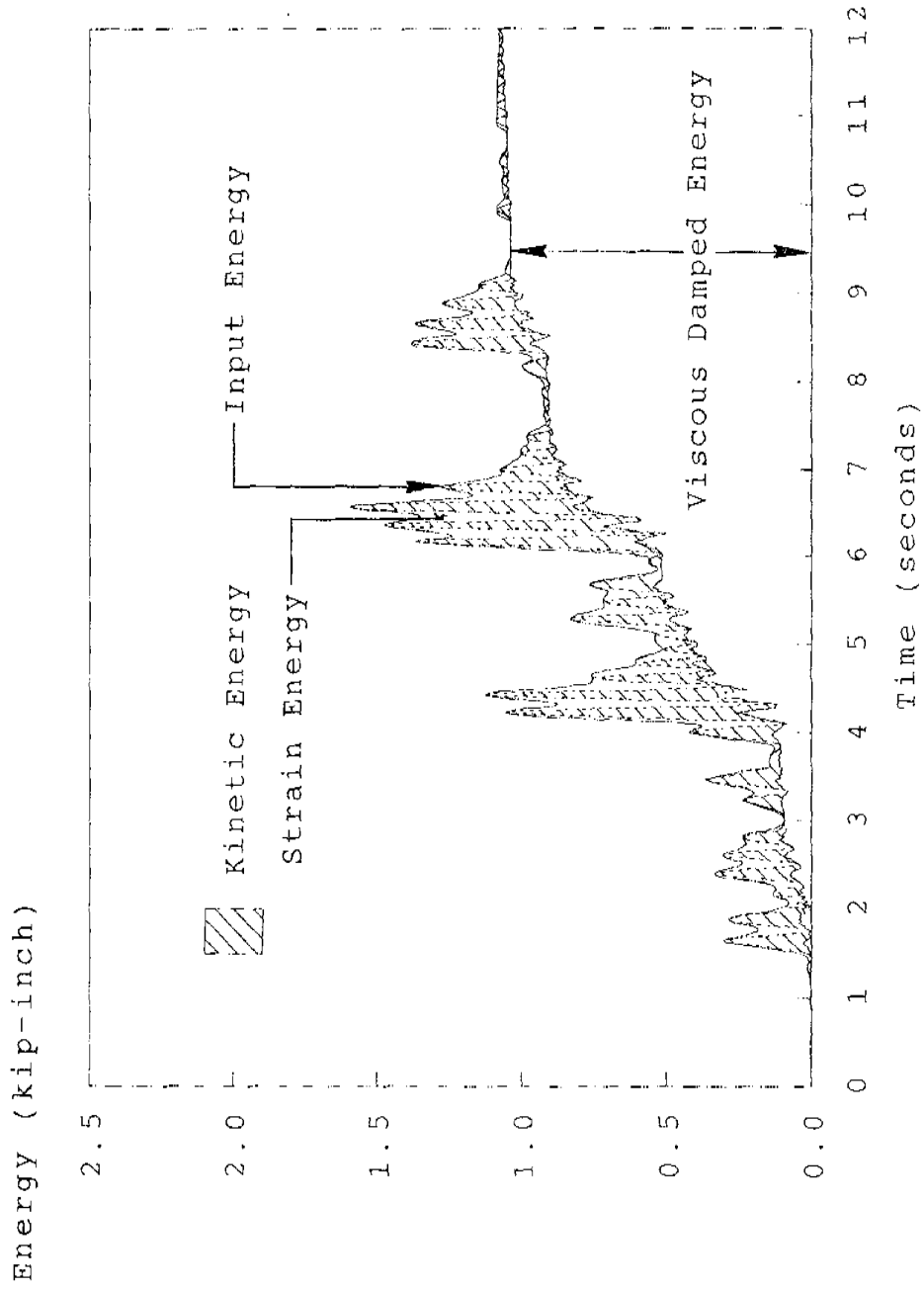
FIGURE 6.26 EBDS MO-07 ENERGY TIME HISTORIES

(a) Acceleration

(b) Displacement

FIGURE 6.27 CBDS MO-33 INPUT CHARACTERISTICS

Pseudo-Velocity (inch/sec.)

Period (seconds)
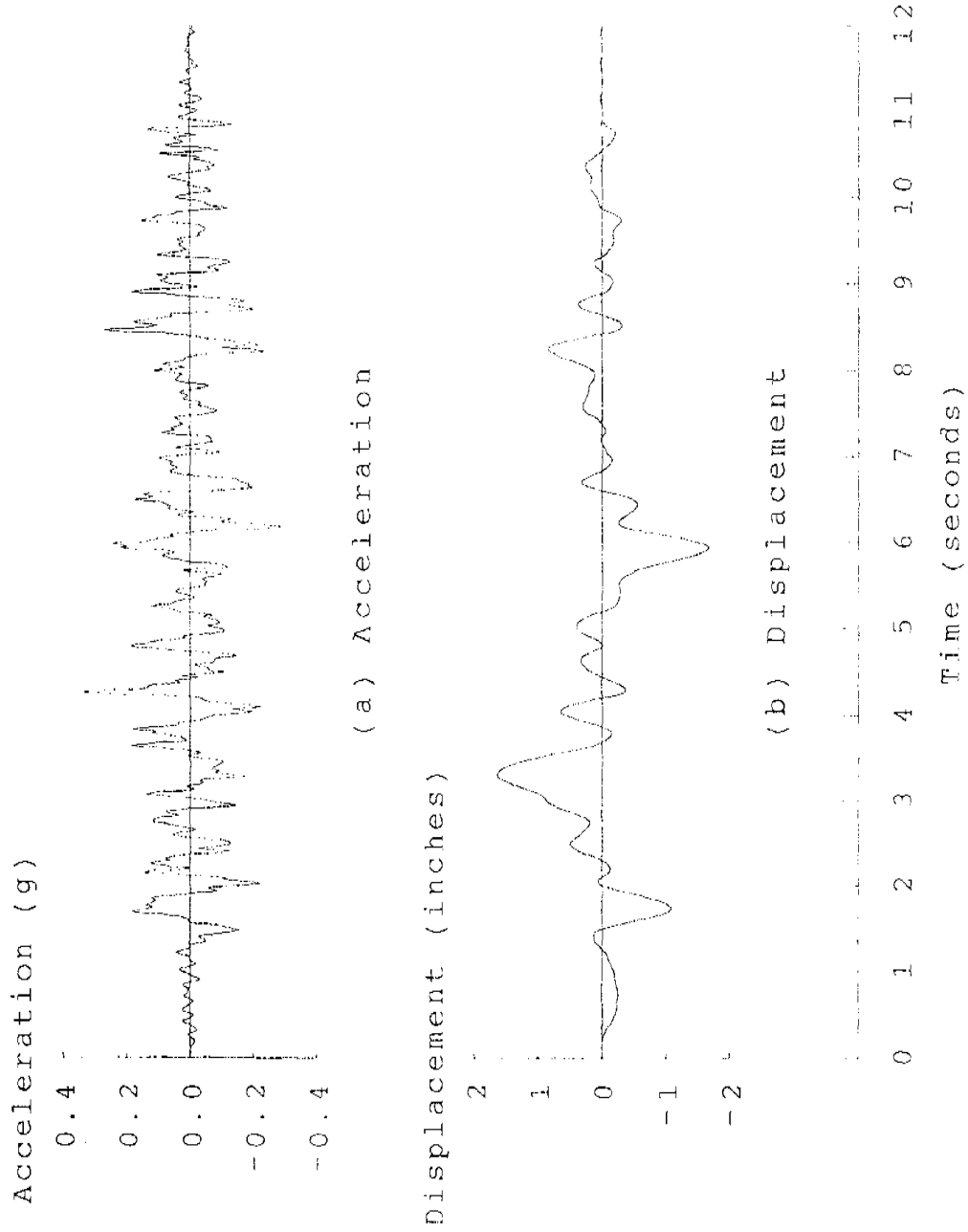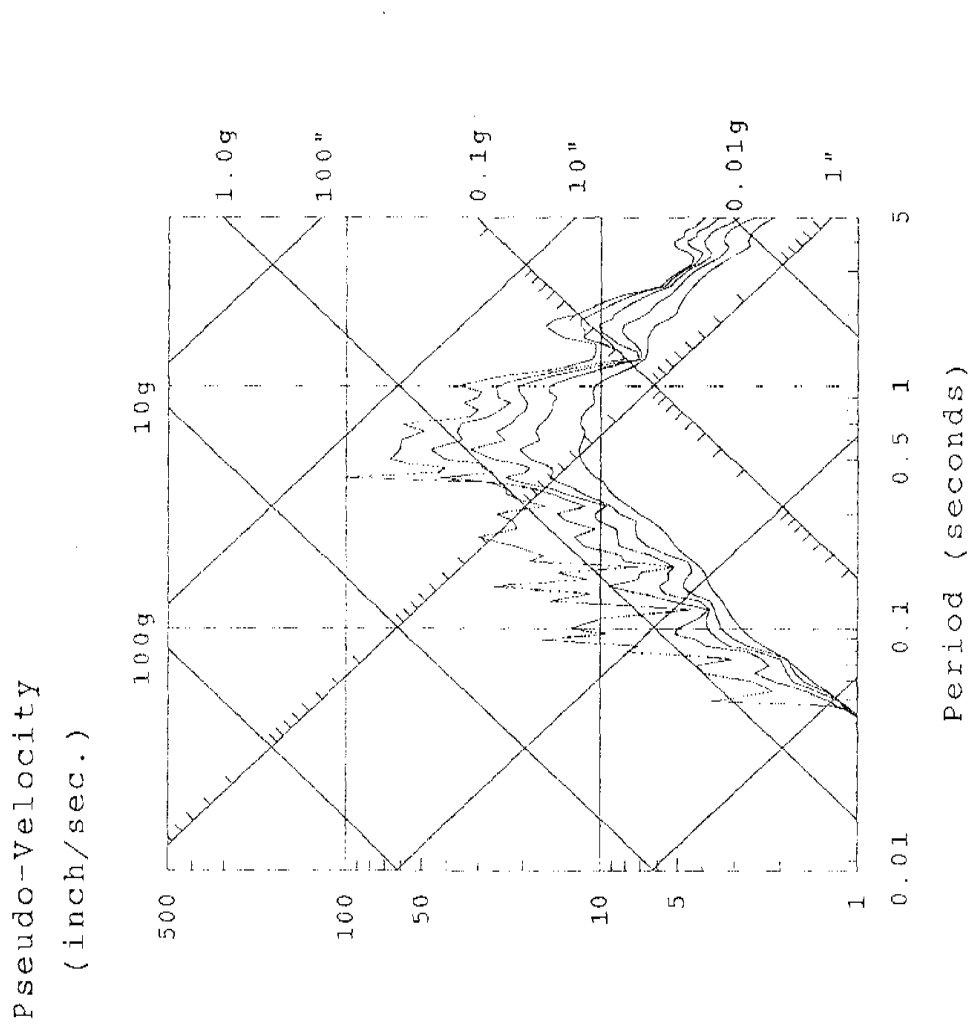
(c) Response Spectra (0,2,5,10,20 % Damping)

FIGURE 6.27 CBDS MO-33 INPUT CHARACTERISTICS
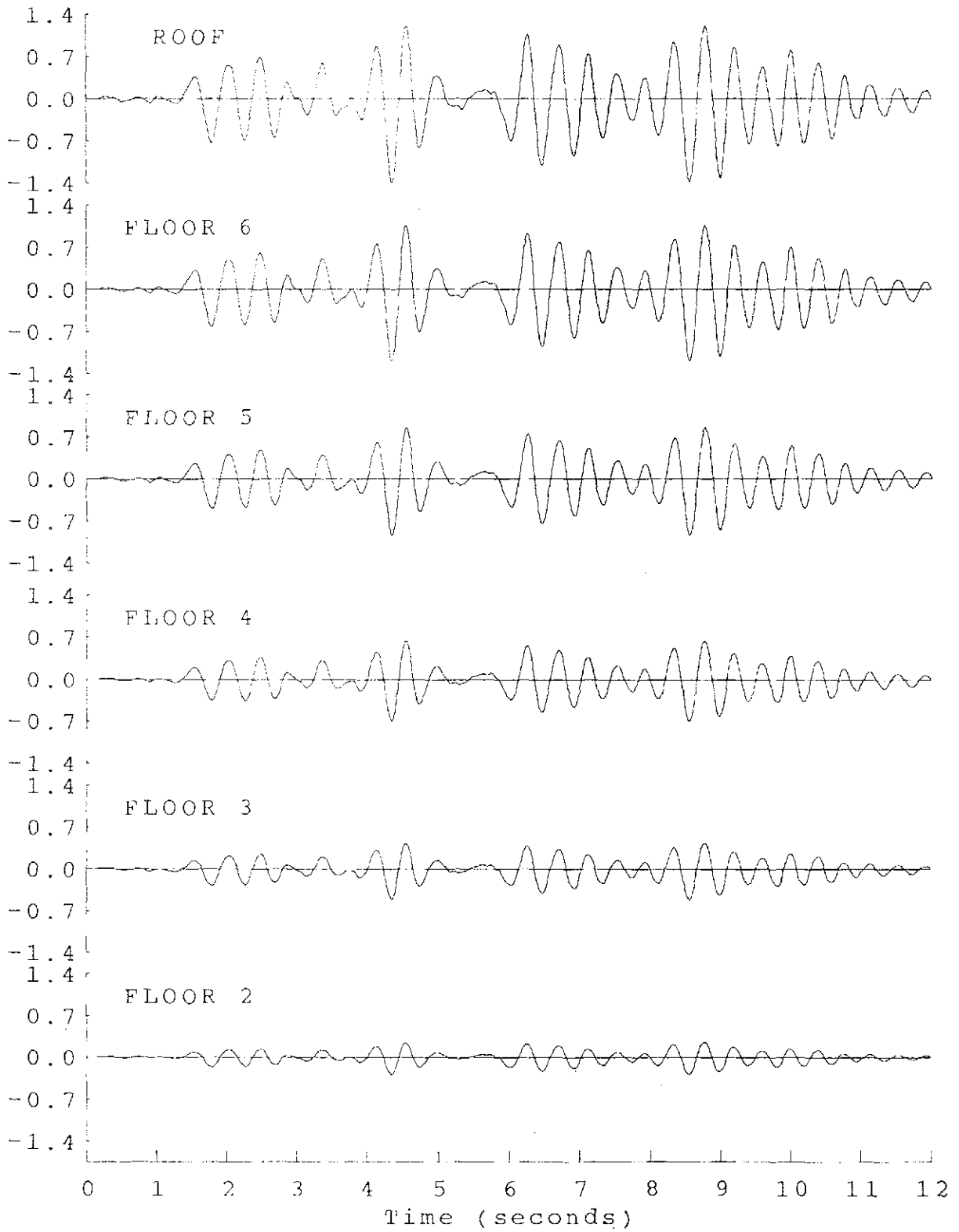
FIGURE 6.28 CBDS MO-33 LATERAL DISPLACEMENT TIME HISTORIES
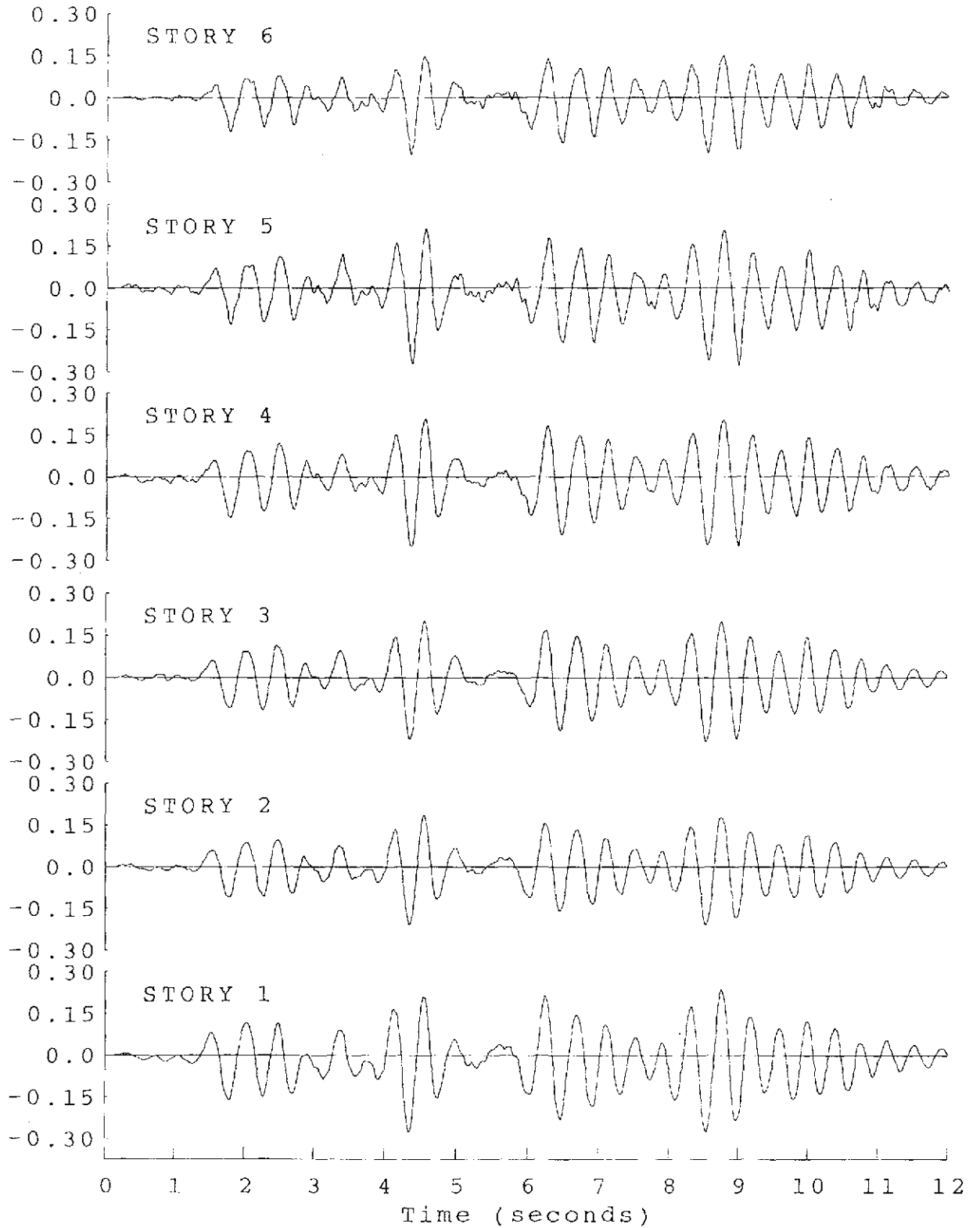
FIGURE 6.29 CBDS MO-33 INTER-STORY DRIFT TIME HISTORIES
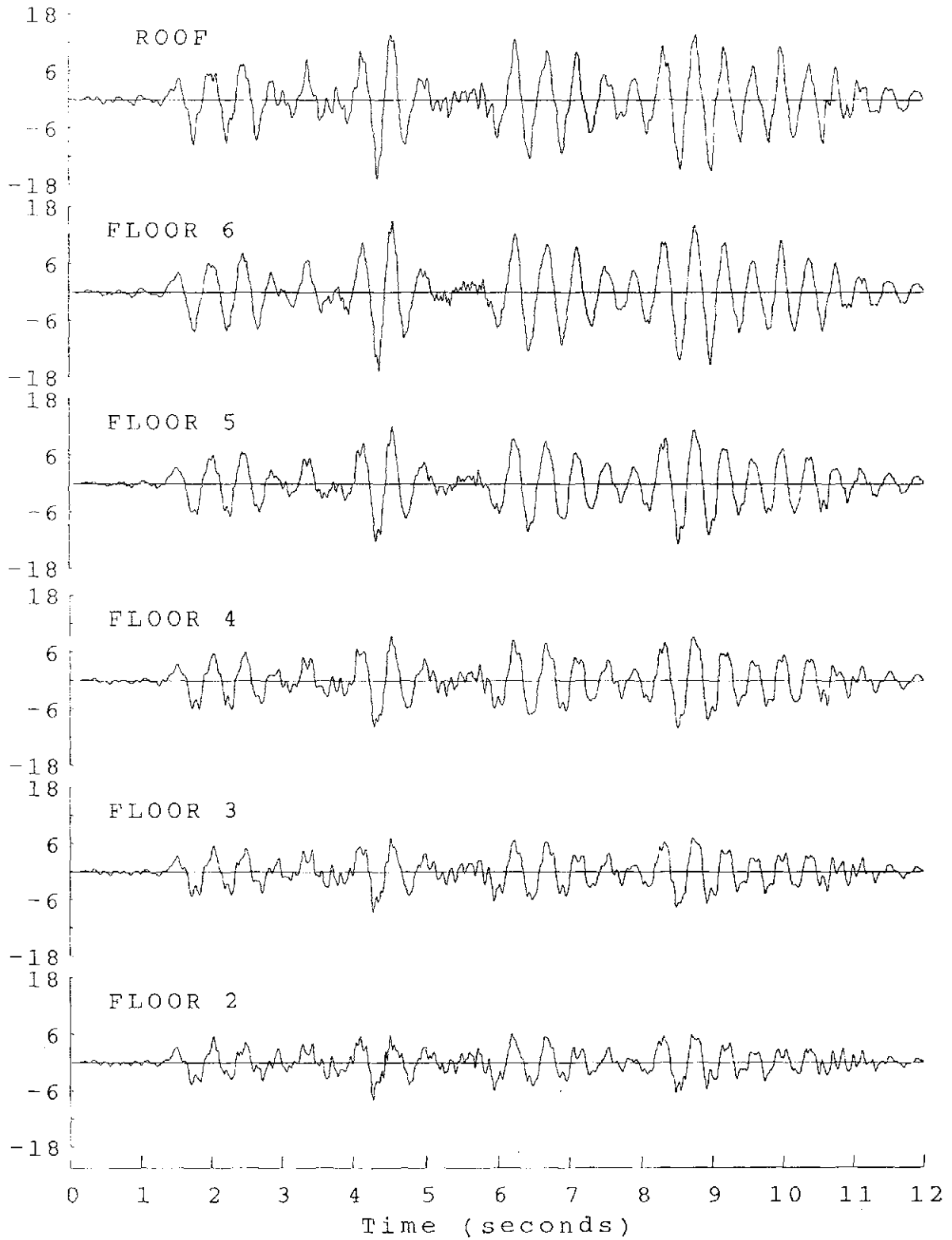
FIGURE 6.30 CBDS MO-33 INERTIA FORCE TIME HISTORIES
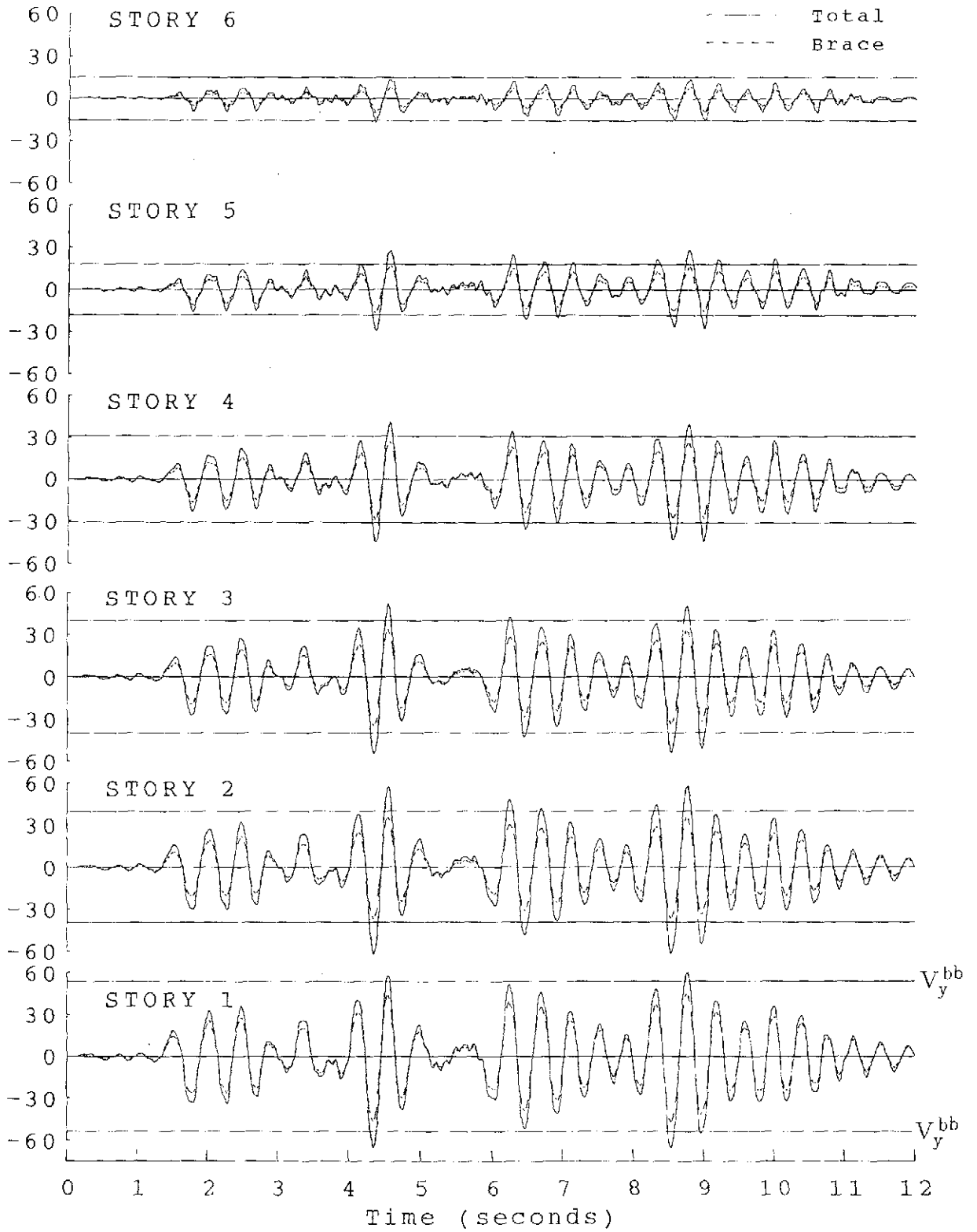
FIGURE 6.31 CBDS MO-33 STORY SHEAR TIME HISTORIES
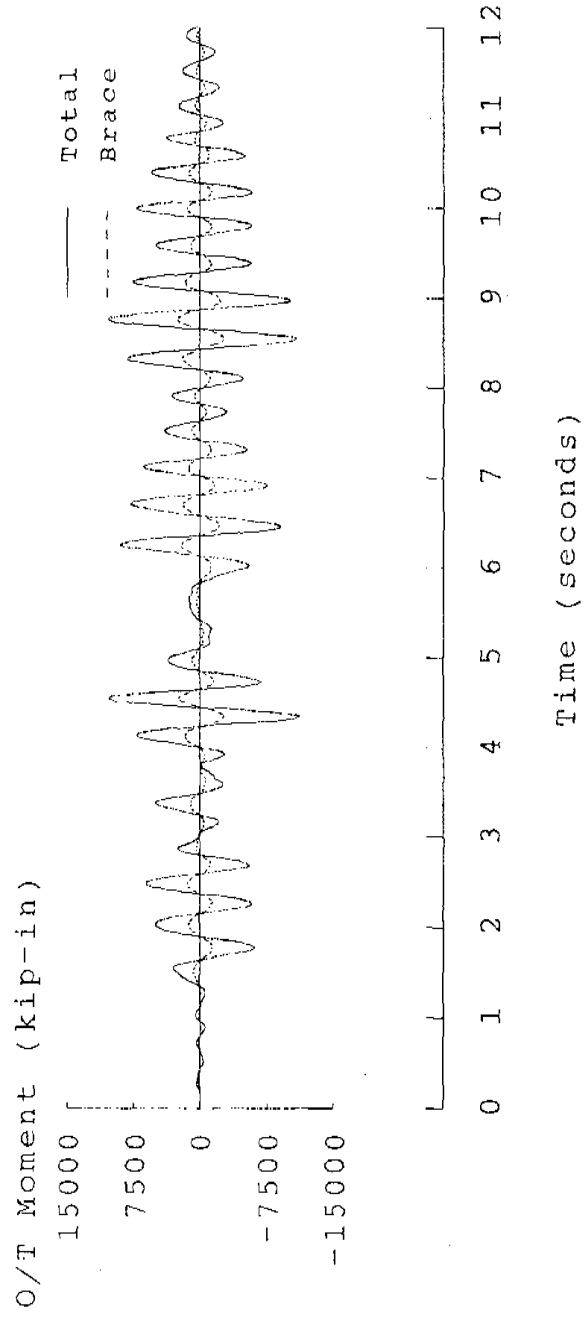
FIGURE 6.32 CBDS MO-33 OVERTURNING MOMENT TIME HISTORIES
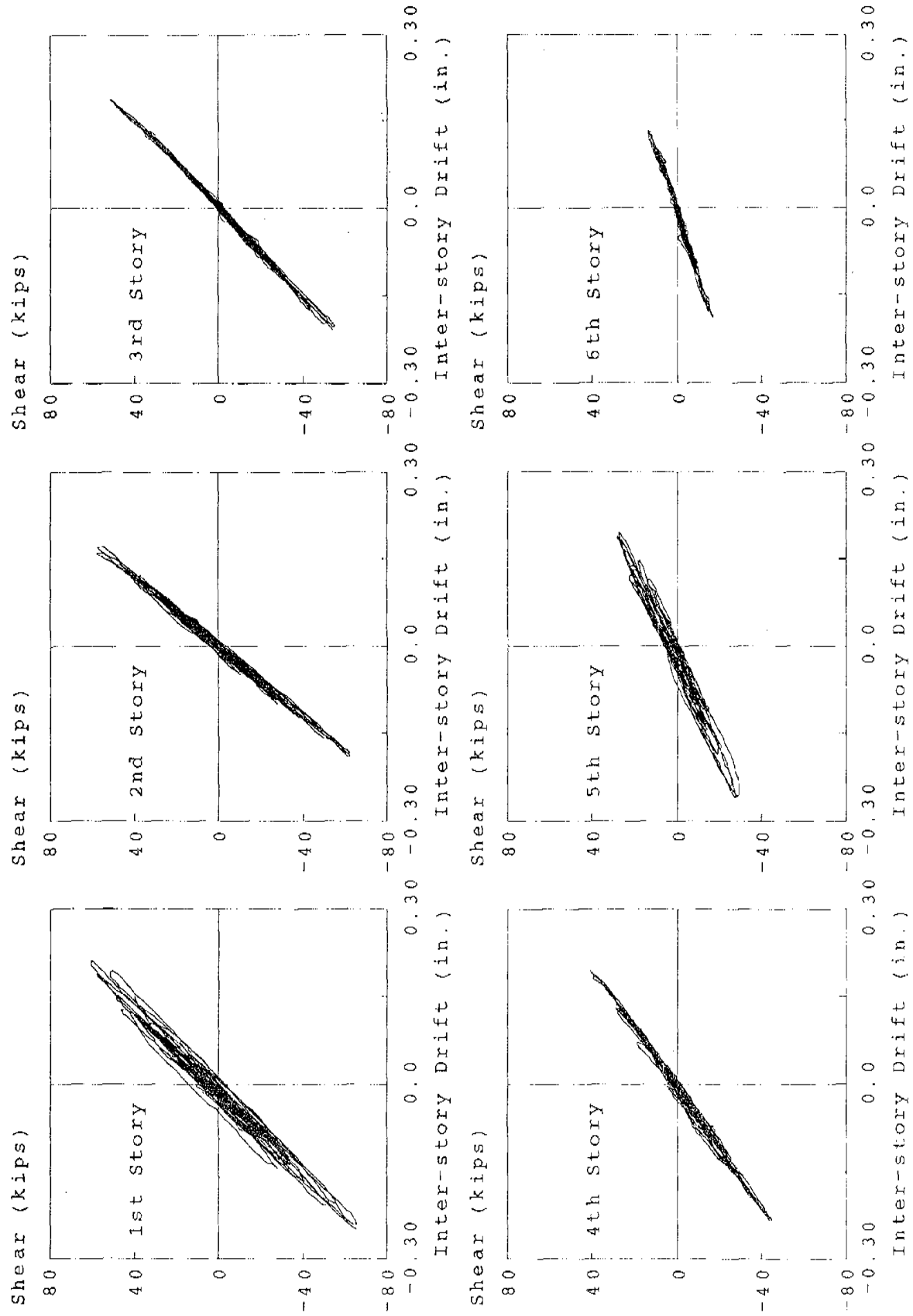
FIGURE 6.33 CBDS MO-33 TOTAL STORY SHEAR AND INTER-STORY DRIFT RELATIONSHIPS
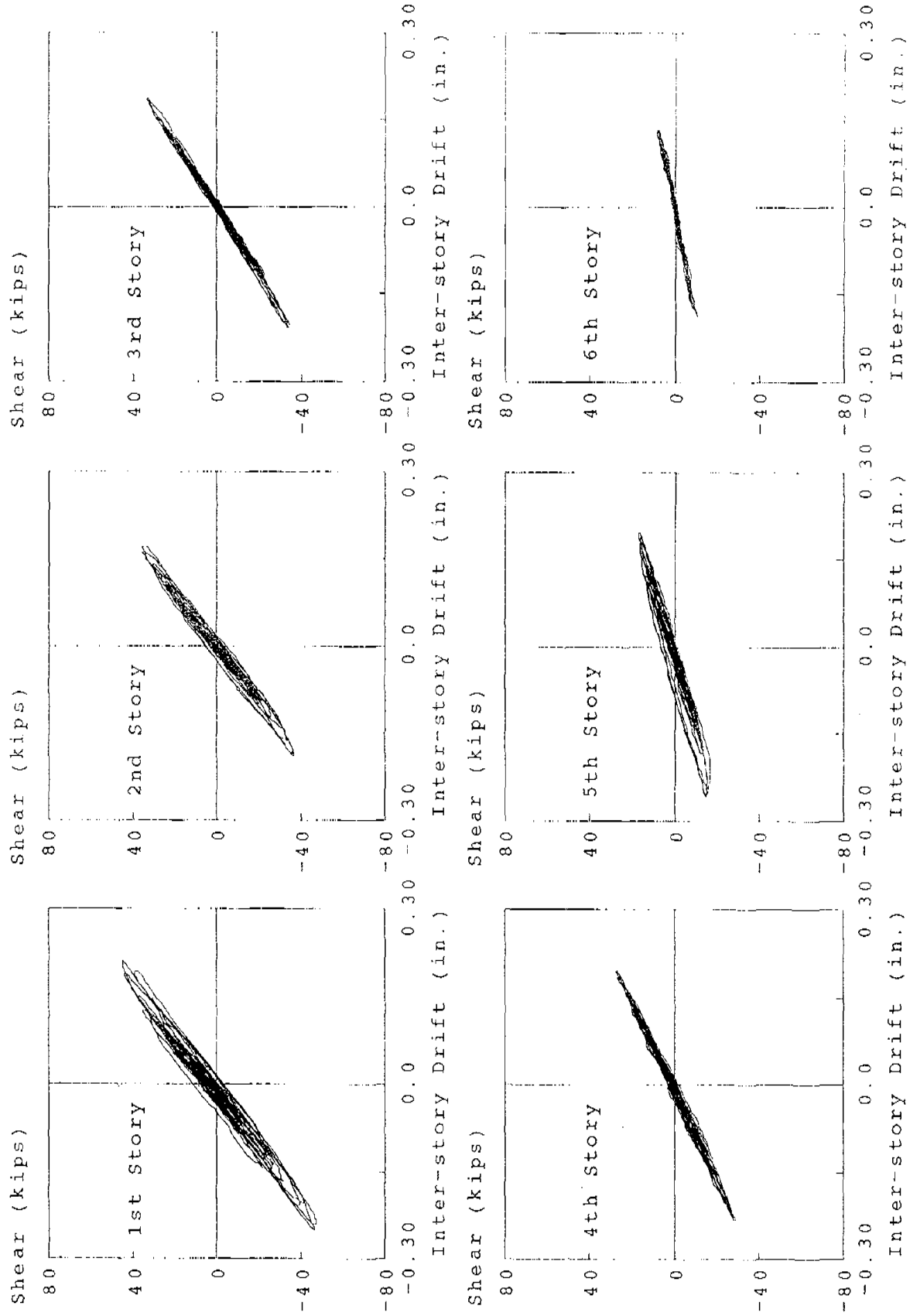
FIGURE 6.34 CBDS MO-33 BRACE STORY SHEAR AND INTER-STORY DRIFT RELATIONSHIPS
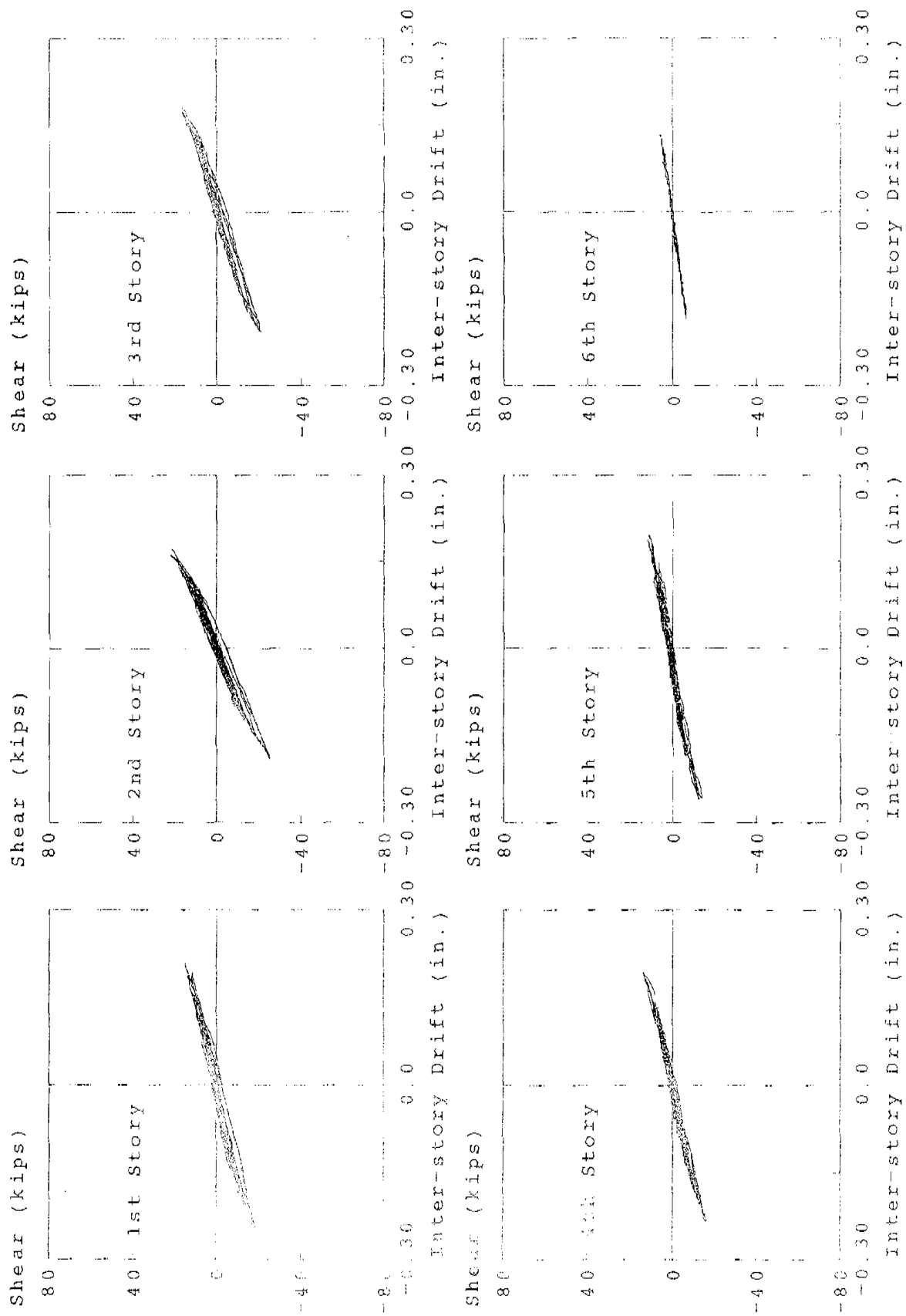
FIGURE 6.35 CBDS MO-33 DMRSF STORY SHEAR AND INTER-STORY DRIFT RELATIONSHIPS
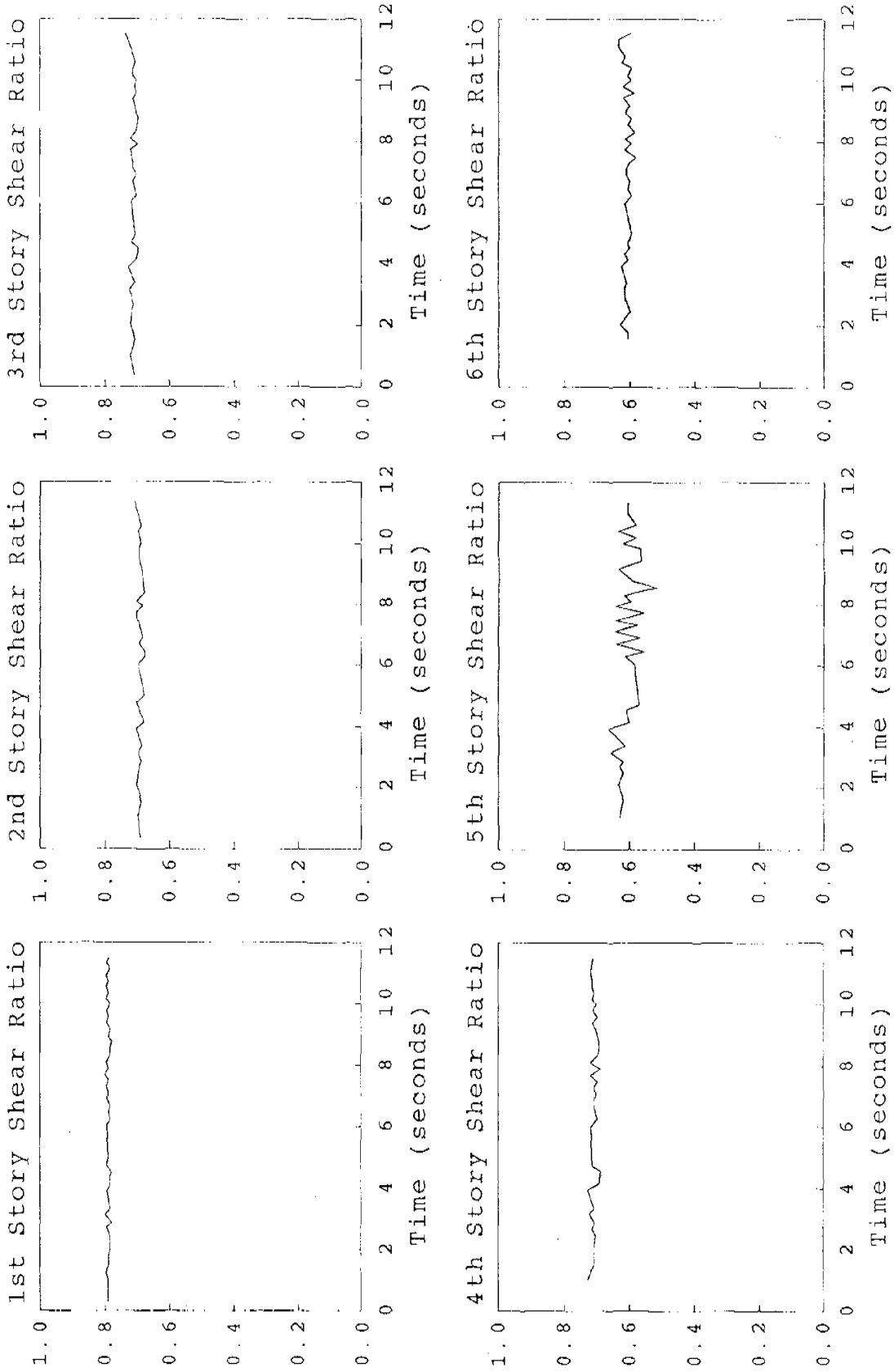
FIGURE 6.36 CBDS MO-33 STORY SHEAR RATIOS

(c) Lateral Displ. (inches)

(b) Inertia Force (kips)

(e) Overturning Moment (x1000 kip-inch)

(a) Story Shear (kips)

(d) Inter-story Drift (inches)
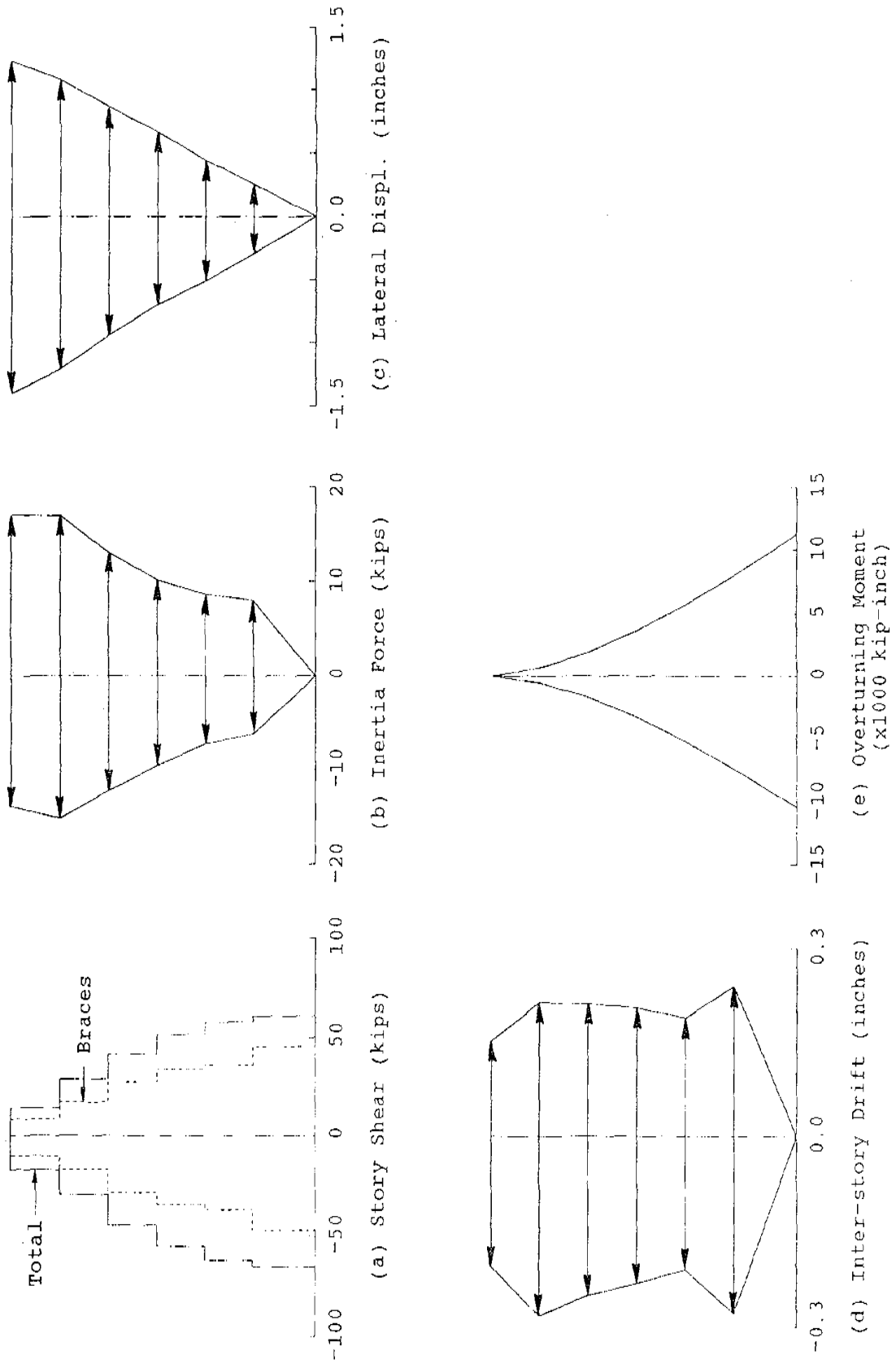
FIGURE 6.37 CBDS MO-33 RESPONSE ENVELOPES

At Maximum Base Shear

At Maximum Roof Displacement

(a) Lateral Displ. (inches) (b) Inertia Force (kips) (c) Story Shear (kips) (d) Overturning Moment (x1000 kip-inch)
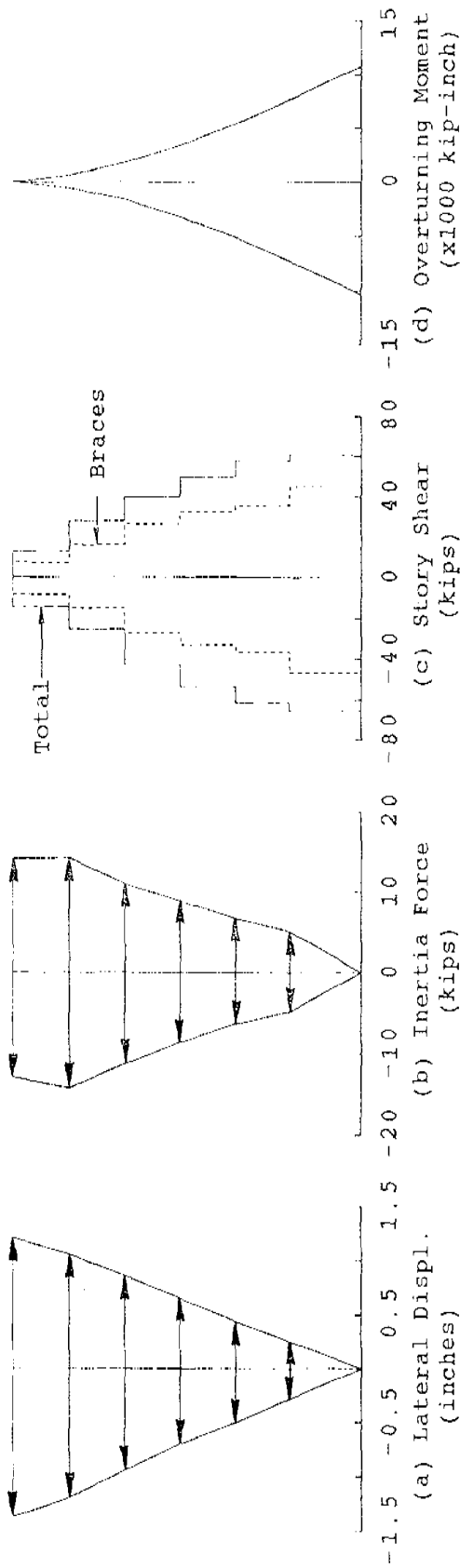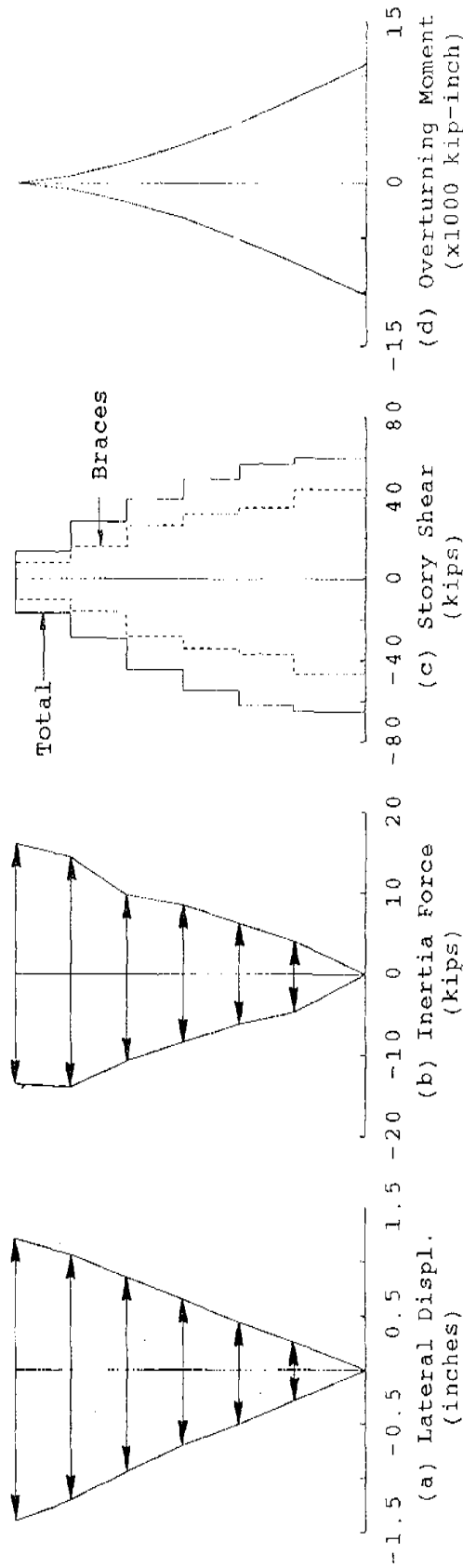
FIGURE 6.38 CBDS MO-33 RESPONSE PROFILES AT MAXIMUM RESPONSES
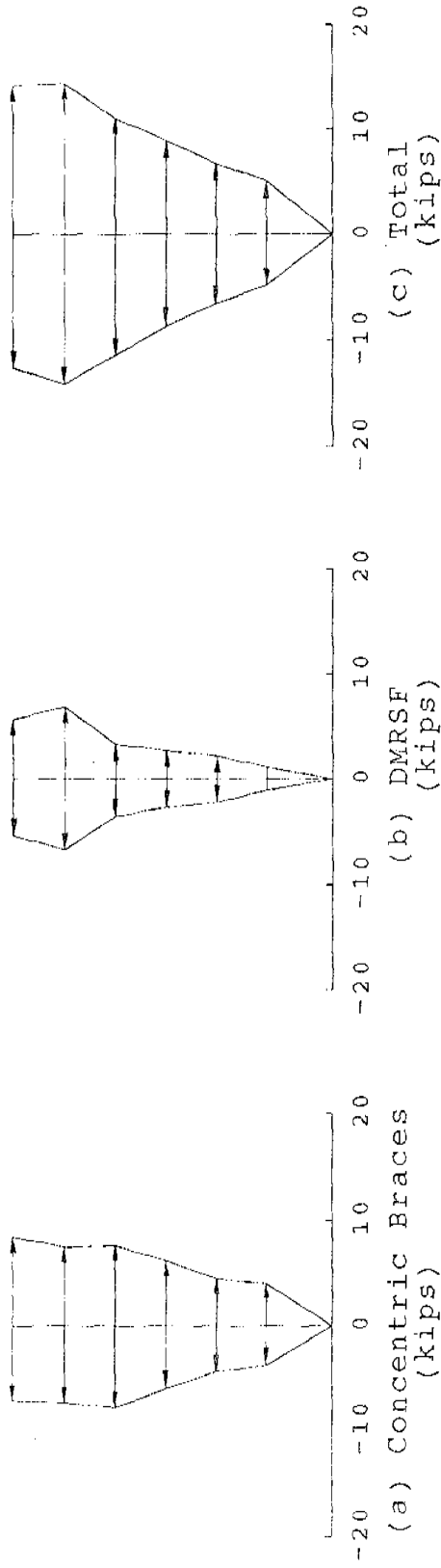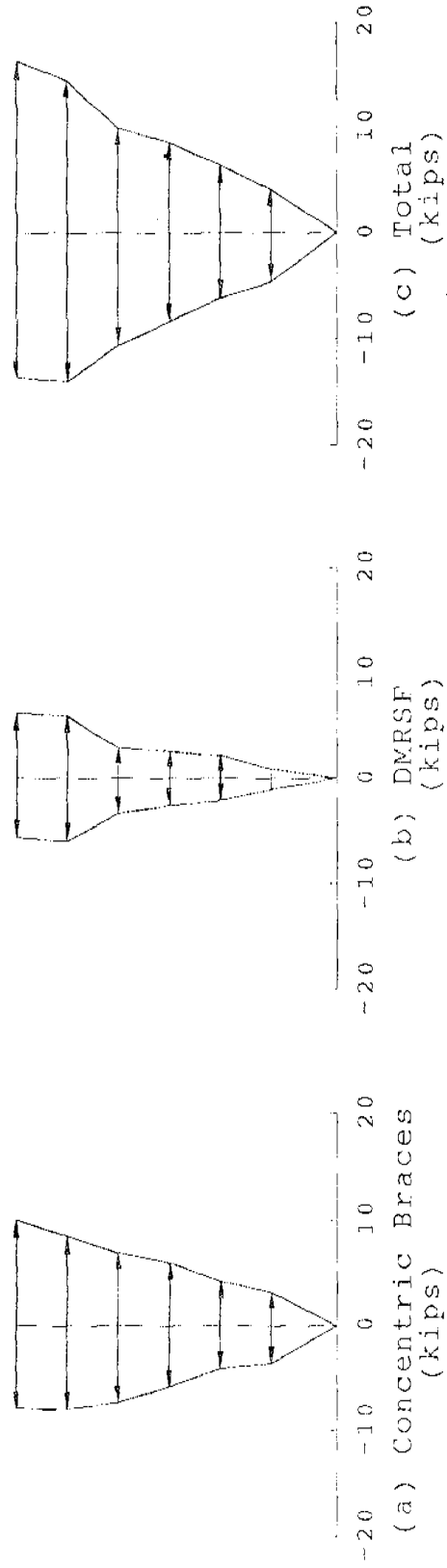
FIGURE 6.39 CBDS MO-33 LATERAL FORCE DISTRIBUTIONS AT MAXIMUM RESPONSES
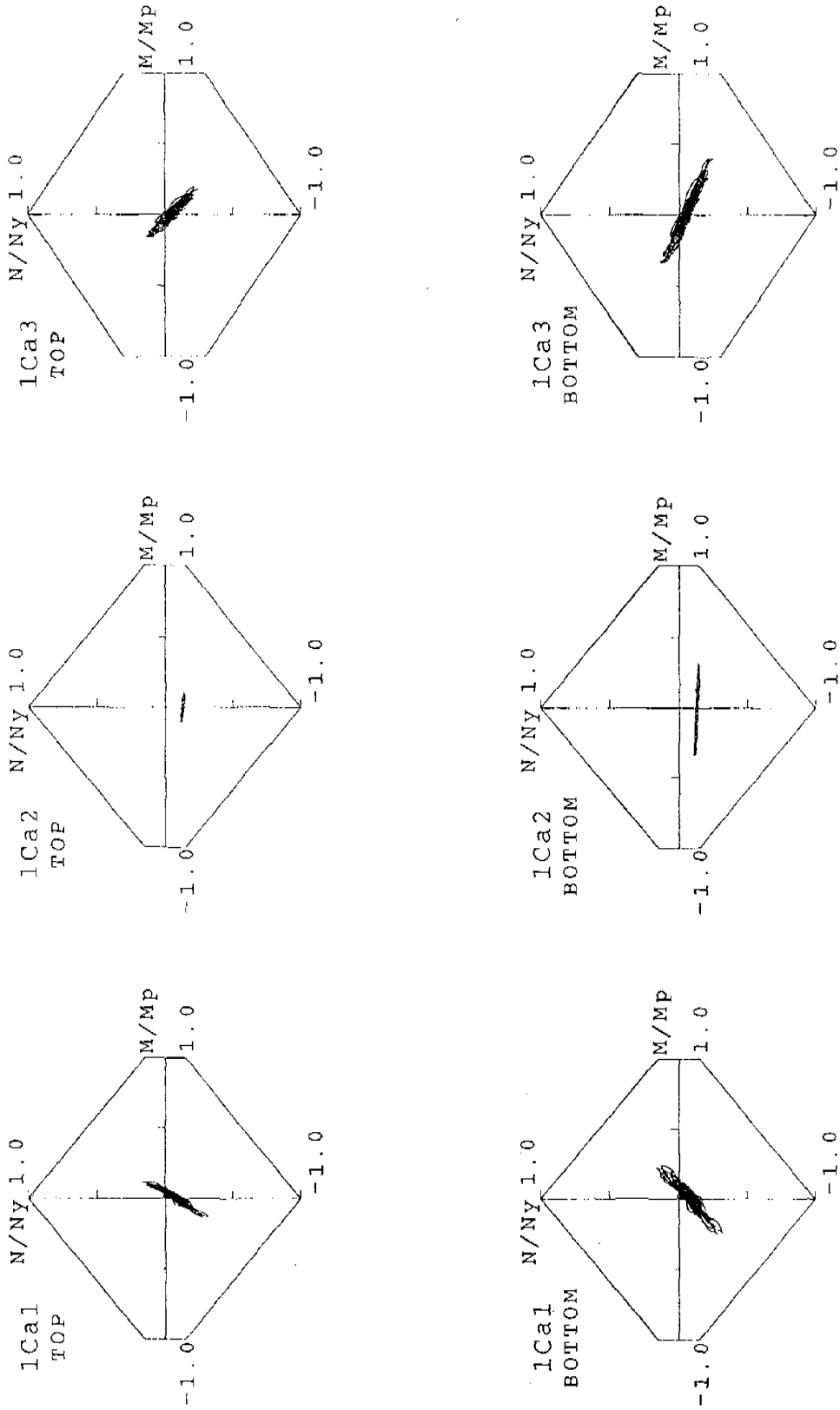
FIGURE 6.40 CBDS MO-33 FIRST STORY COLUMN AXIAL FORCE AND END MOMENT
INTERACTION CURVES (FRAME B)
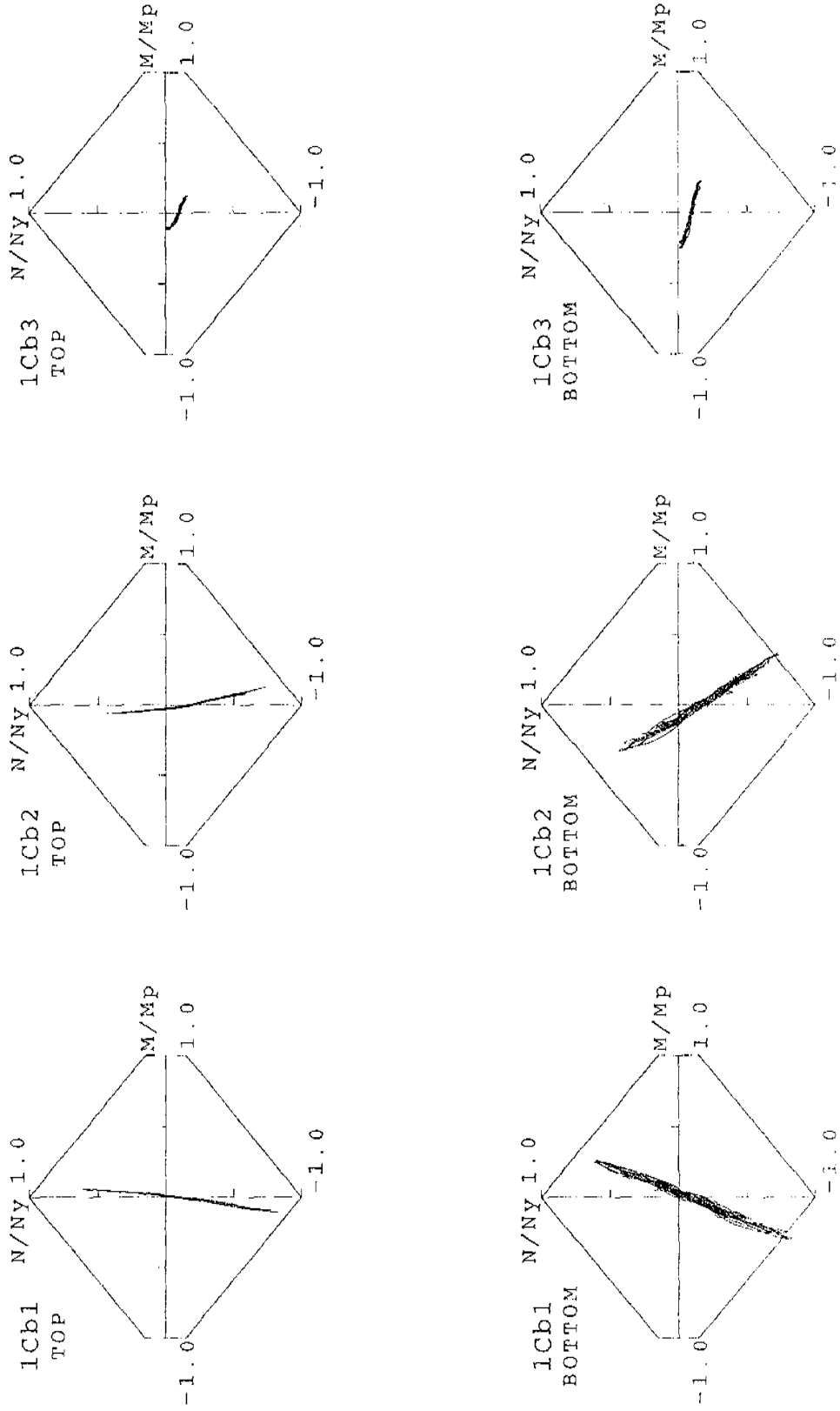
FIGURE 6.41 CBDS MO-33 FIRST STORY COLUMN AXIAL FORCE AND END MOMENT
INTERACTION CURVES (FRAME B)
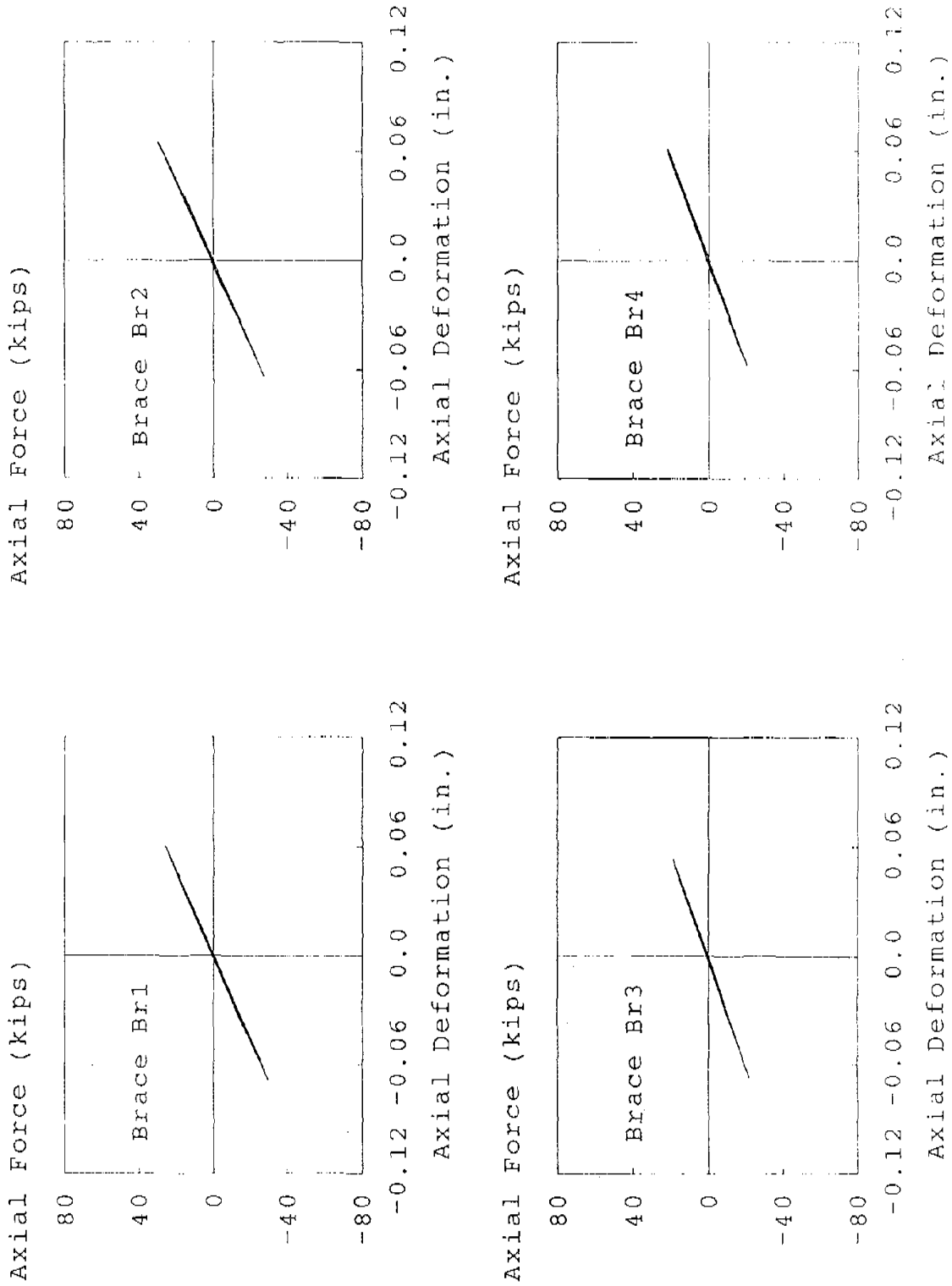
FIGURE 6.42 CBDS MO-33 BRACE FORCE AND DEFORMATION RELATIONSHIPS
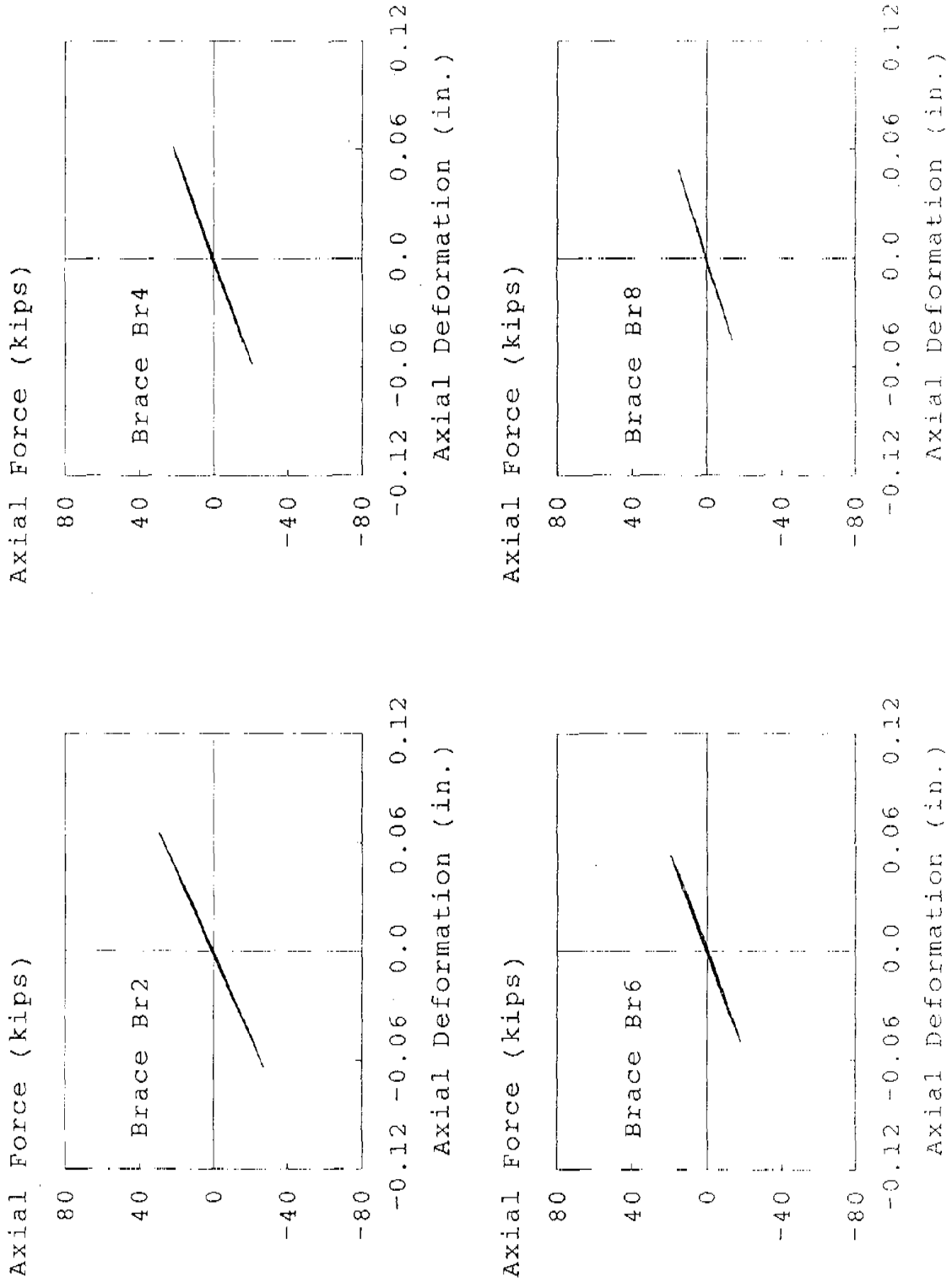
FIGURE 6.43 CBDS MO-33 BRACE FORCE AND DEFORMATION RELATIONSHIPS
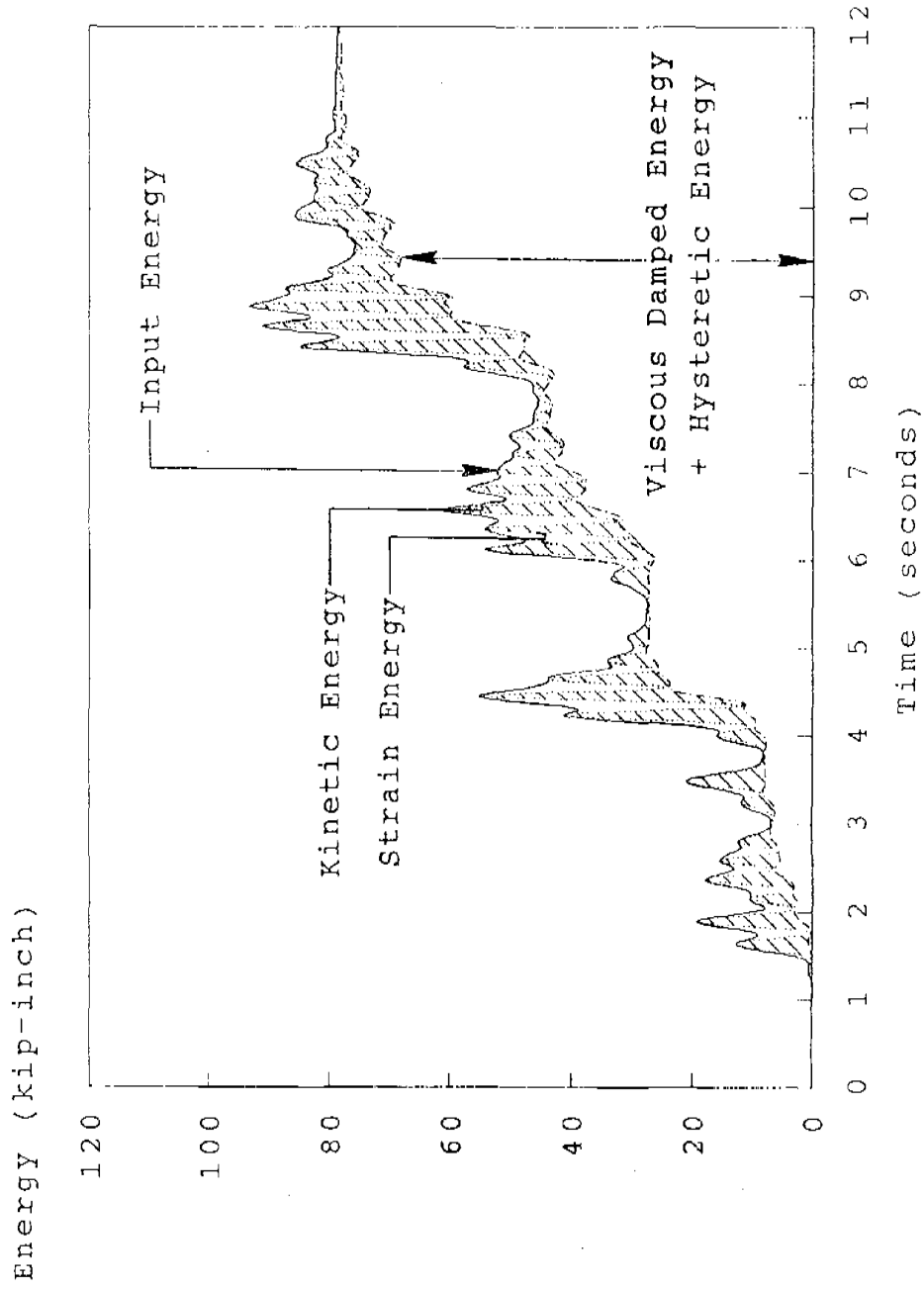
FIGURE 6.44 CBDS MO-33 ENERGY TIME HISTORIES

FIGURE 6.45 EBDS MO-28 INPUT CHARACTERISTICS

Pseudo-Velocity (inch/sec.)

Period (seconds)
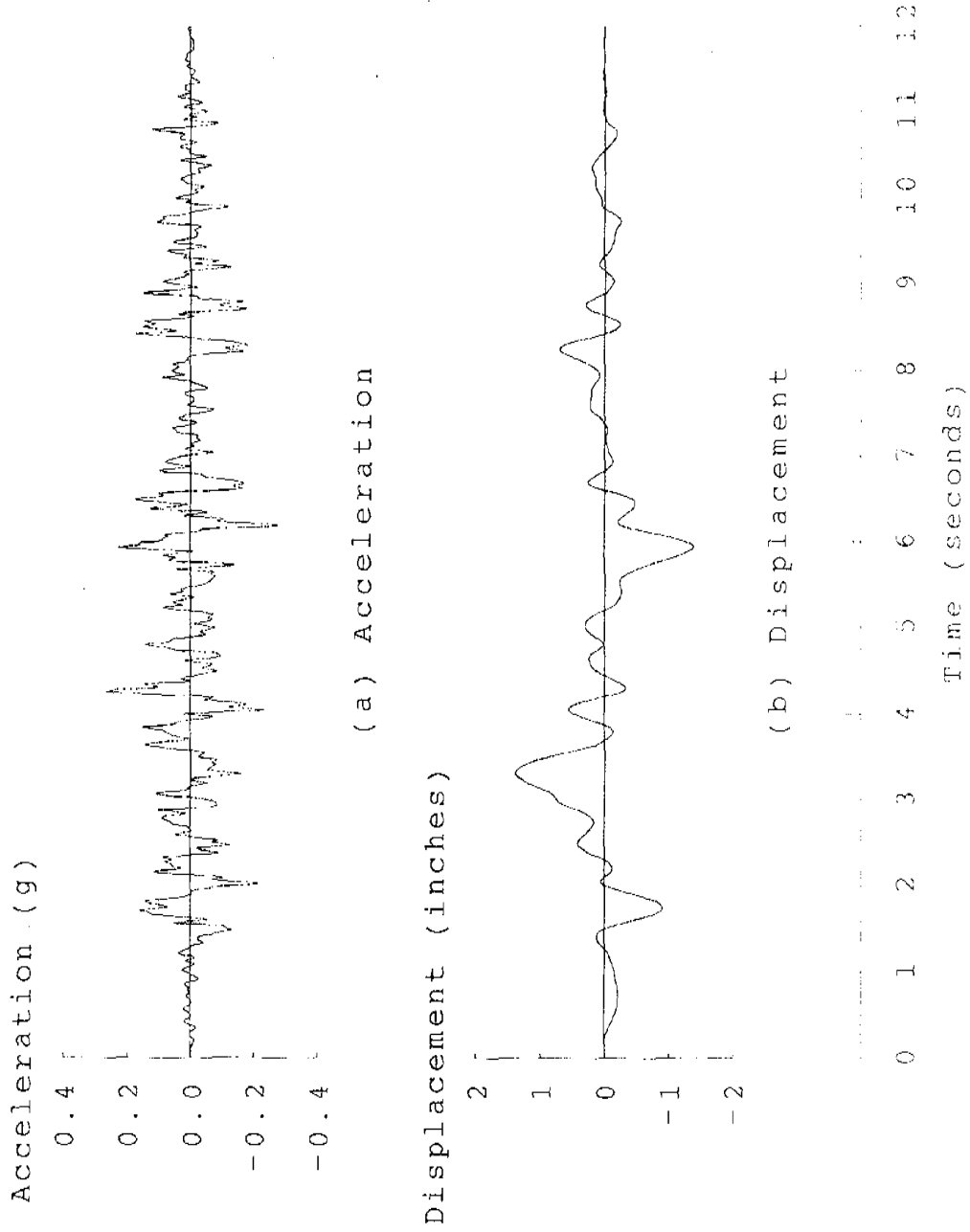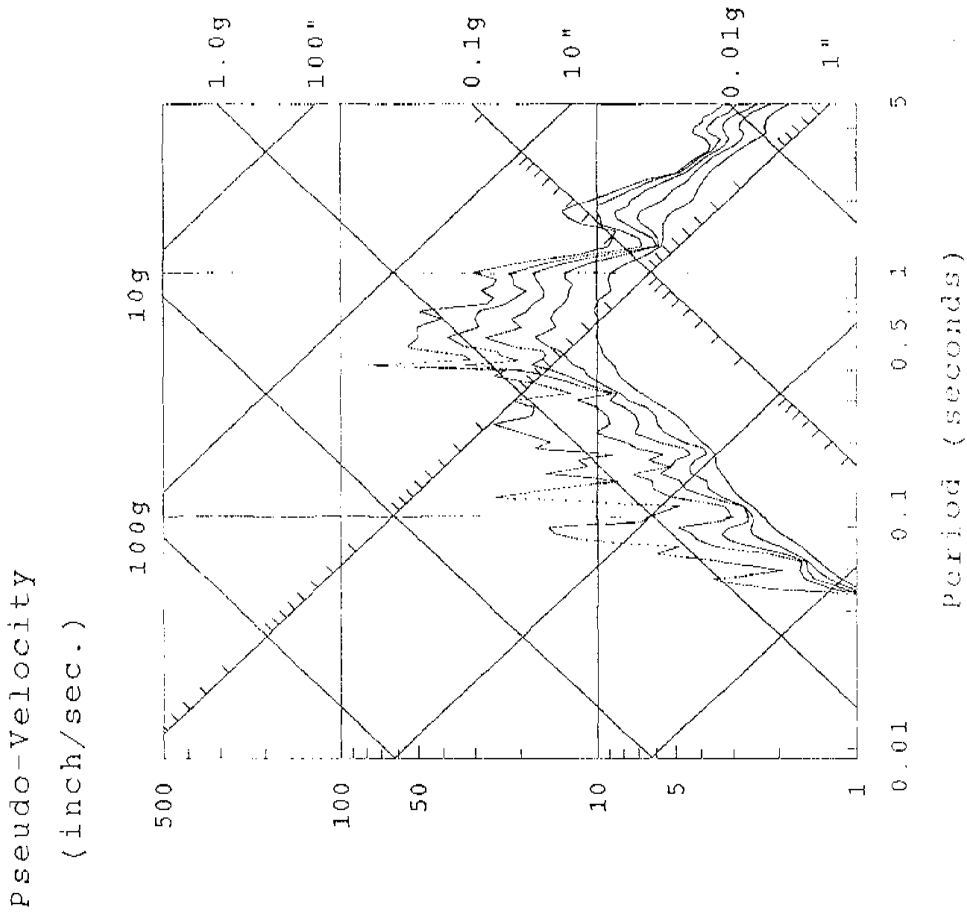
(c) Response Spectra (0,2,5,10,20 % Damping)

FIGURE 6.45 EBDS MO-28 INPUT CHARACTERISTICS
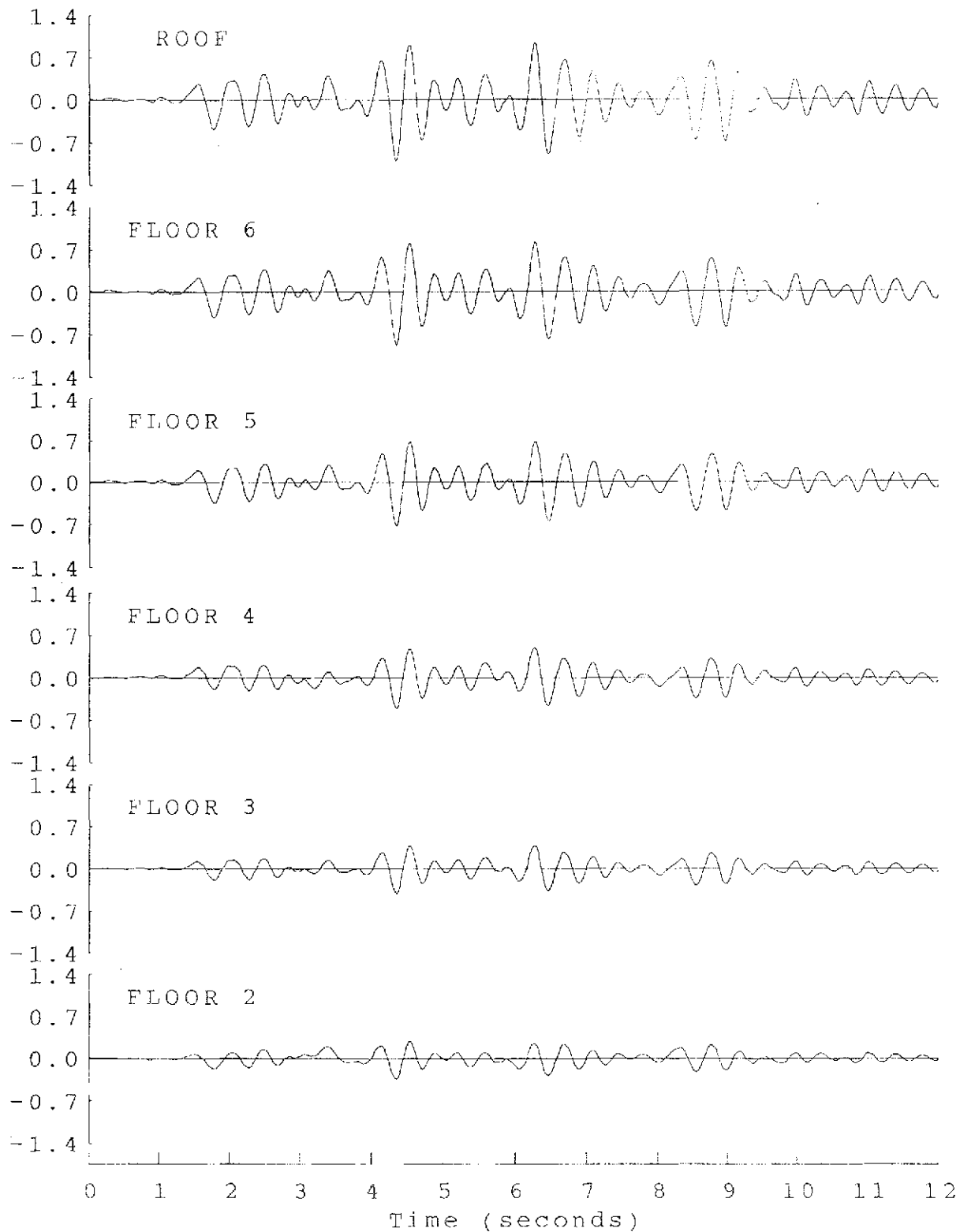
FIGURE 6.46 EBDS MO-28 LATERAL DISPLACEMENT TIME HISTORIES
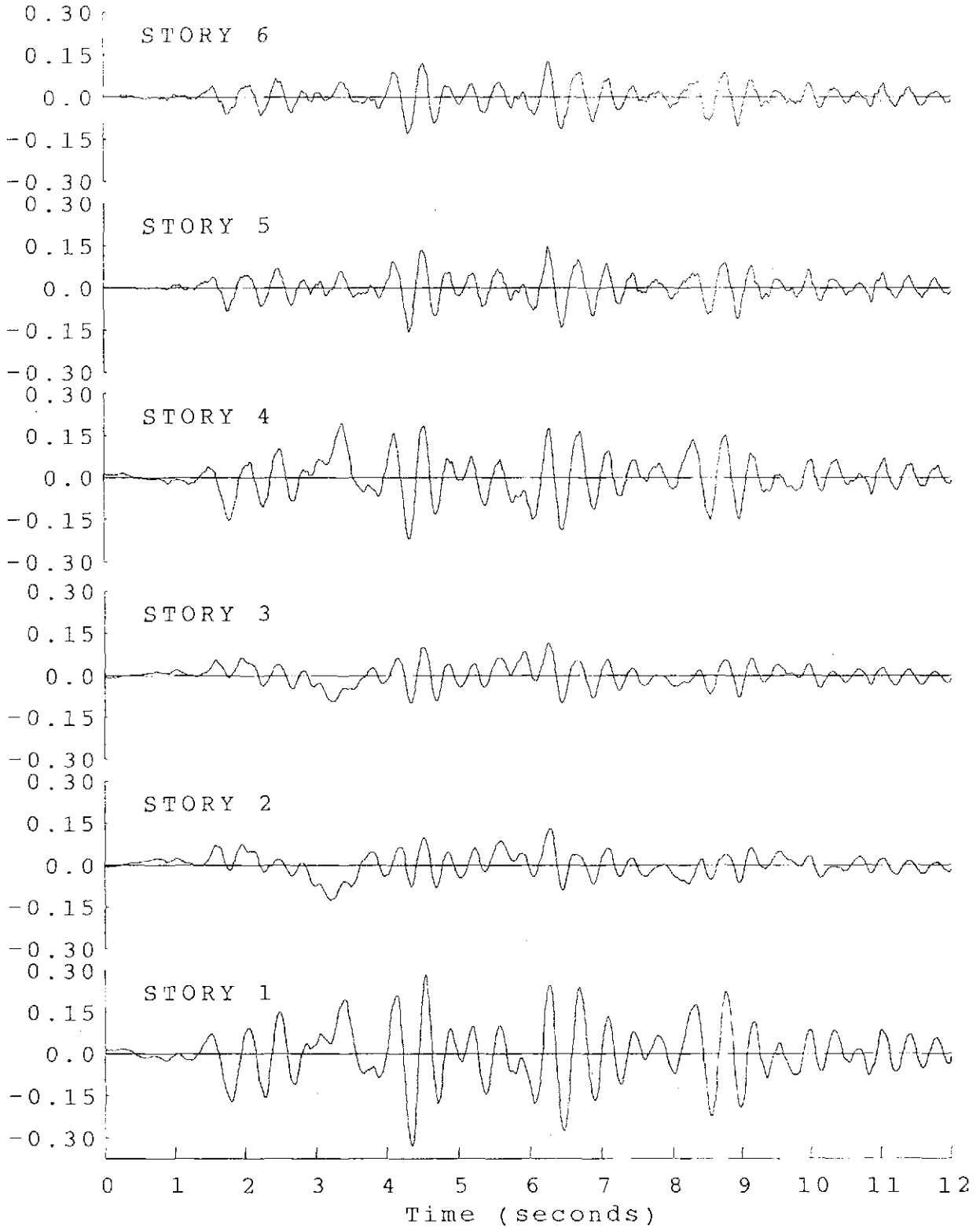
FIGURE 6.47 EBDS MO-28 INTER-STORY DRIFT TIME HISTORIES
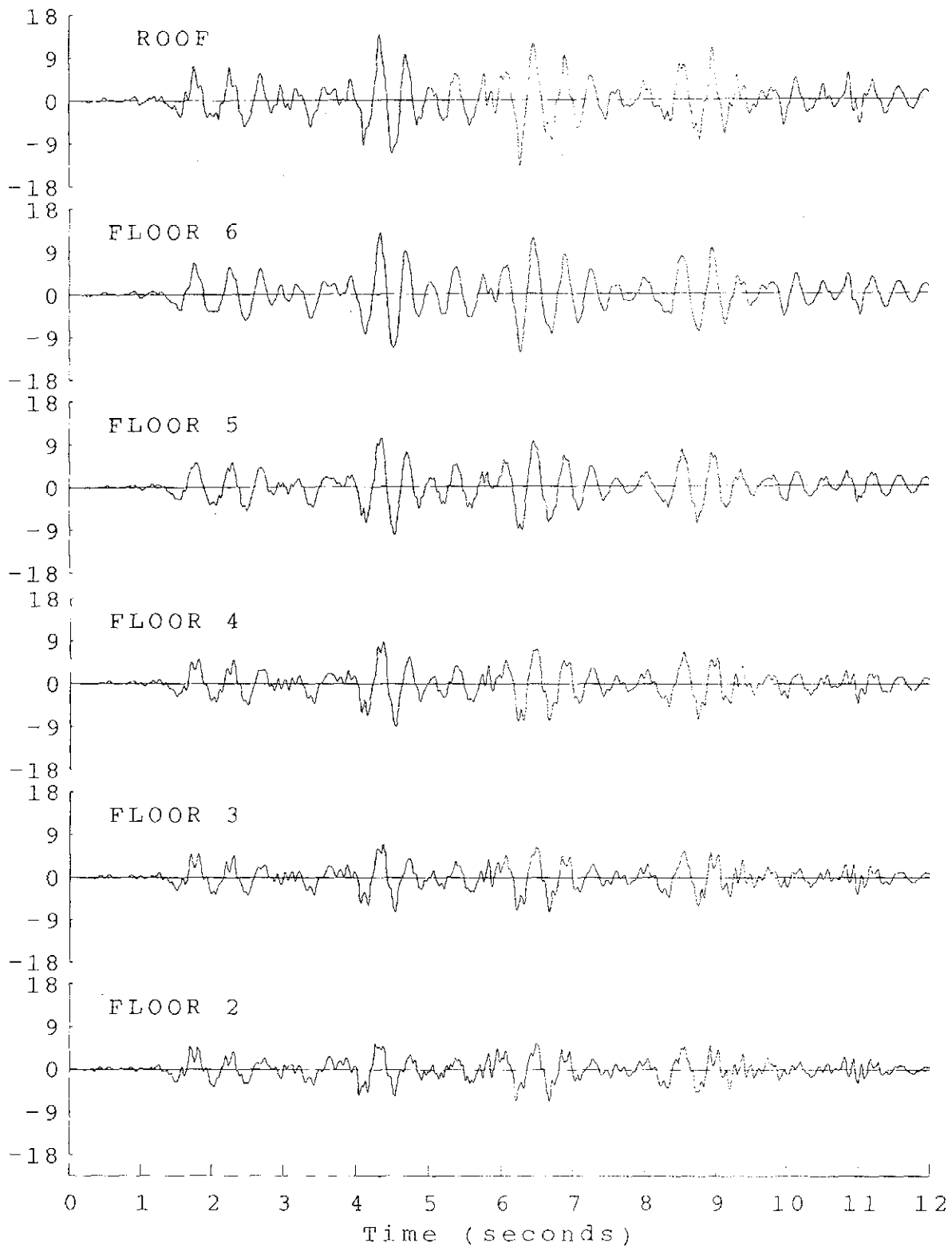
FIGURE 6.48 EBDS MO-28 INERTIA FORCE TIME HISTORIES
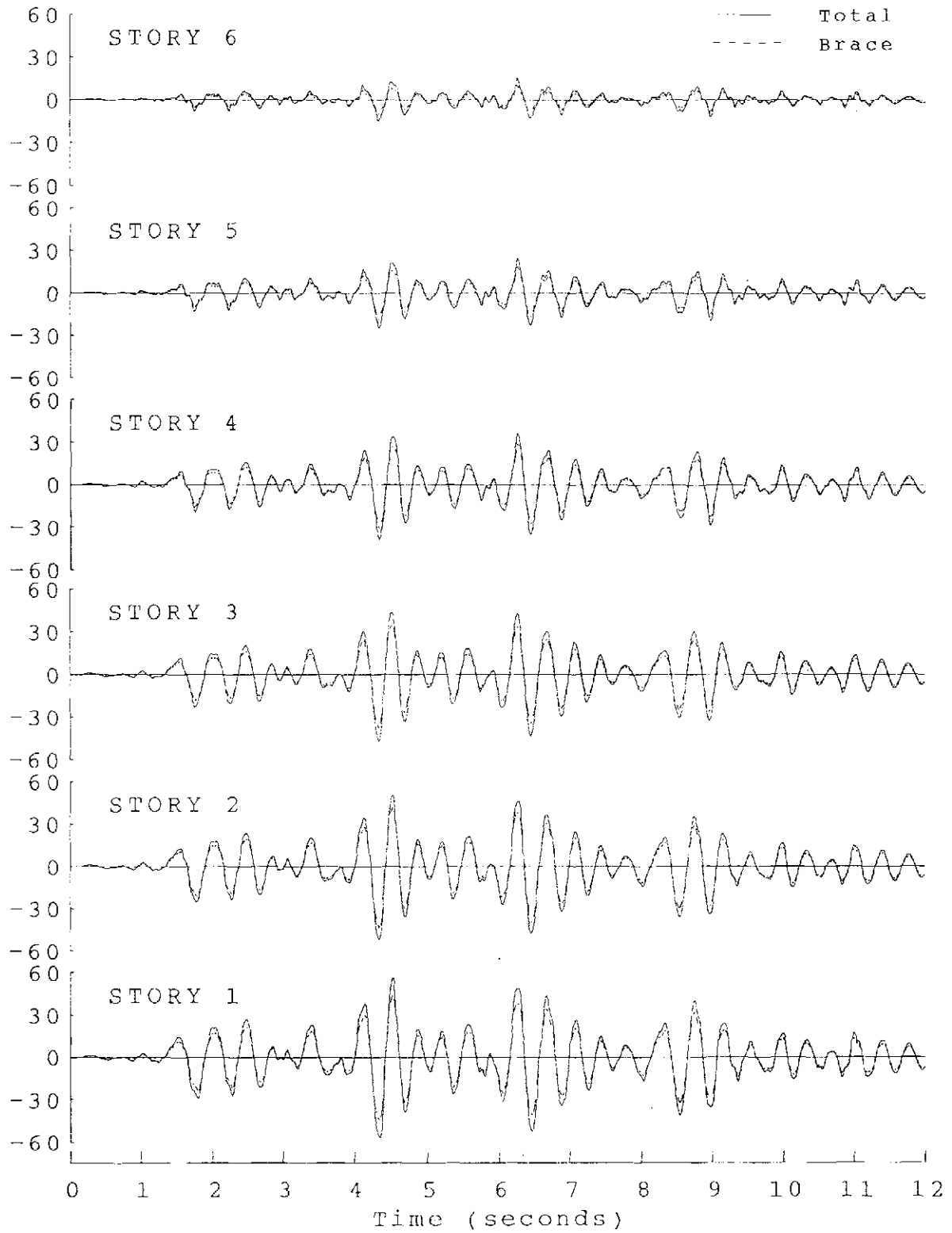
Story Shear
(kips)

FIGURE 6.49 EBDS MO-28 STORY SHEAR TIME HISTORIES
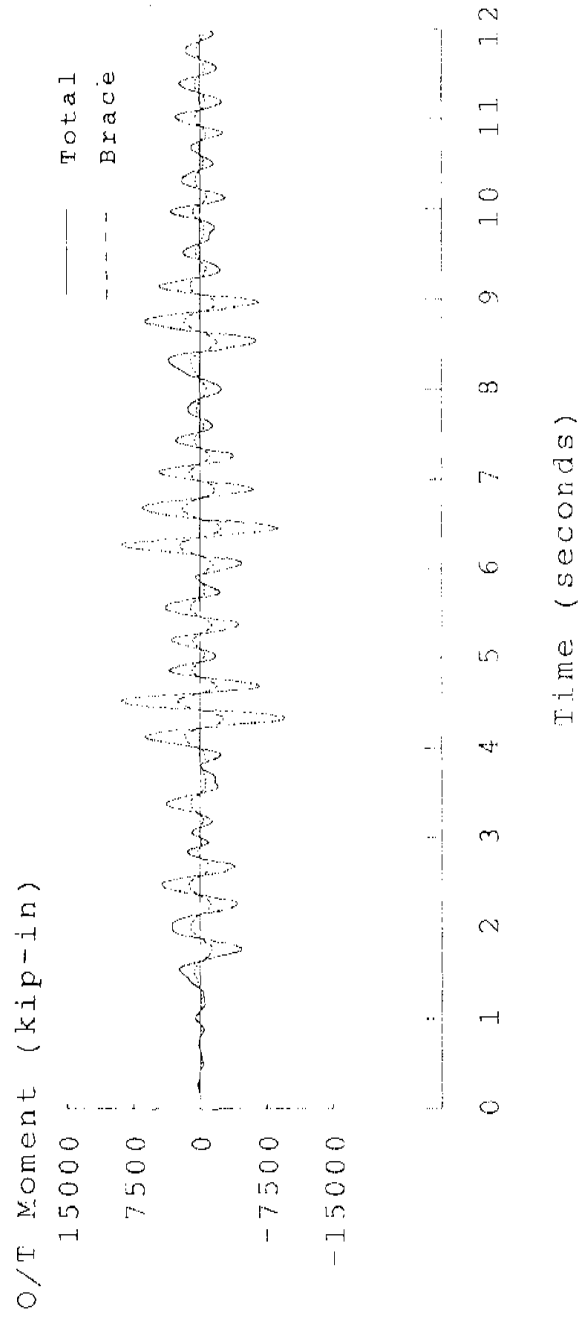
FIGURE 6.50 EBDS MO-28 OVERTURNING MOMENT TIME HISTORIES
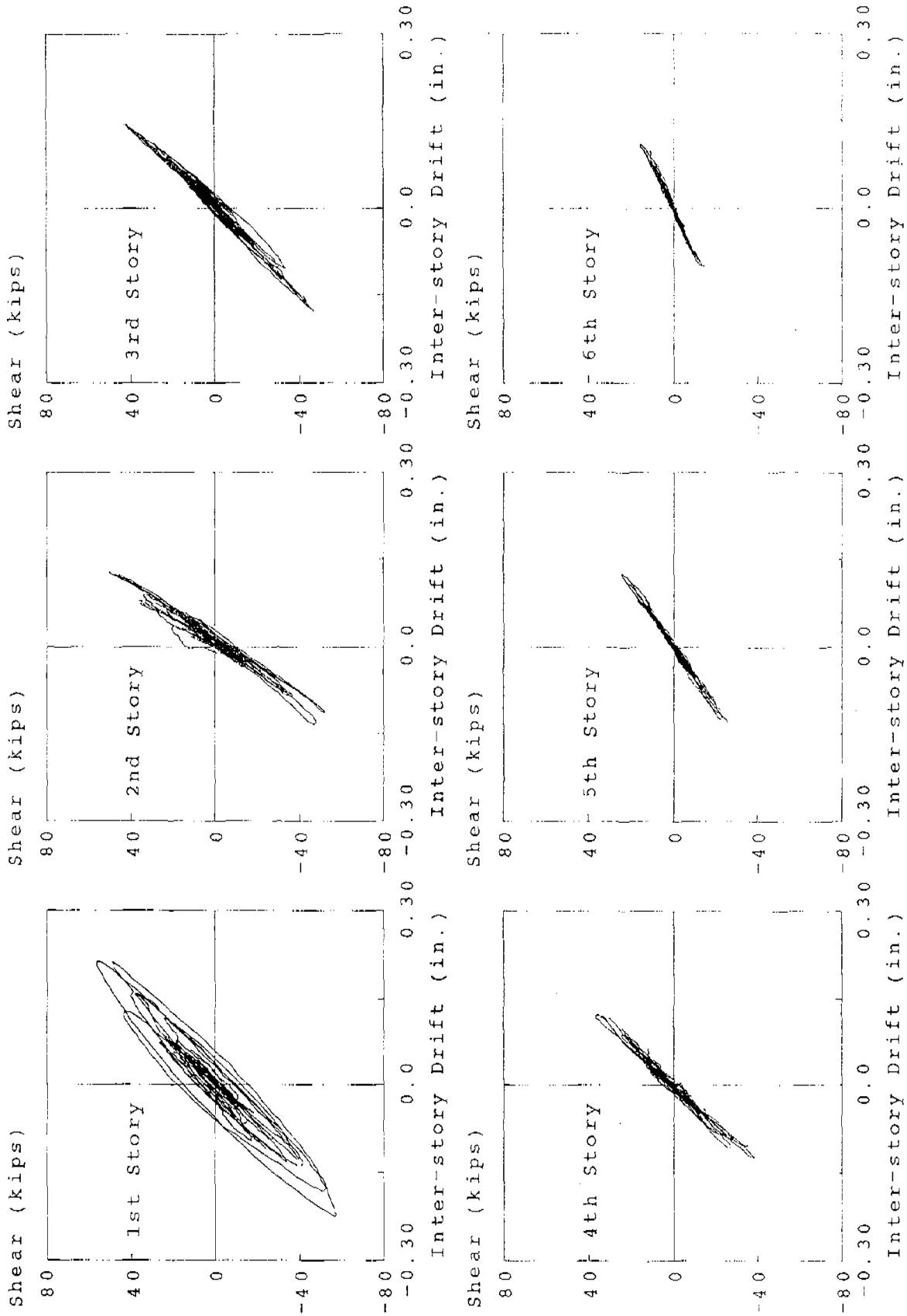
FIGURE 6.51 EBDS MO-28 TOTAL STORY SHEAR AND INTER-STORY DRIFT RELATIONSHIPS
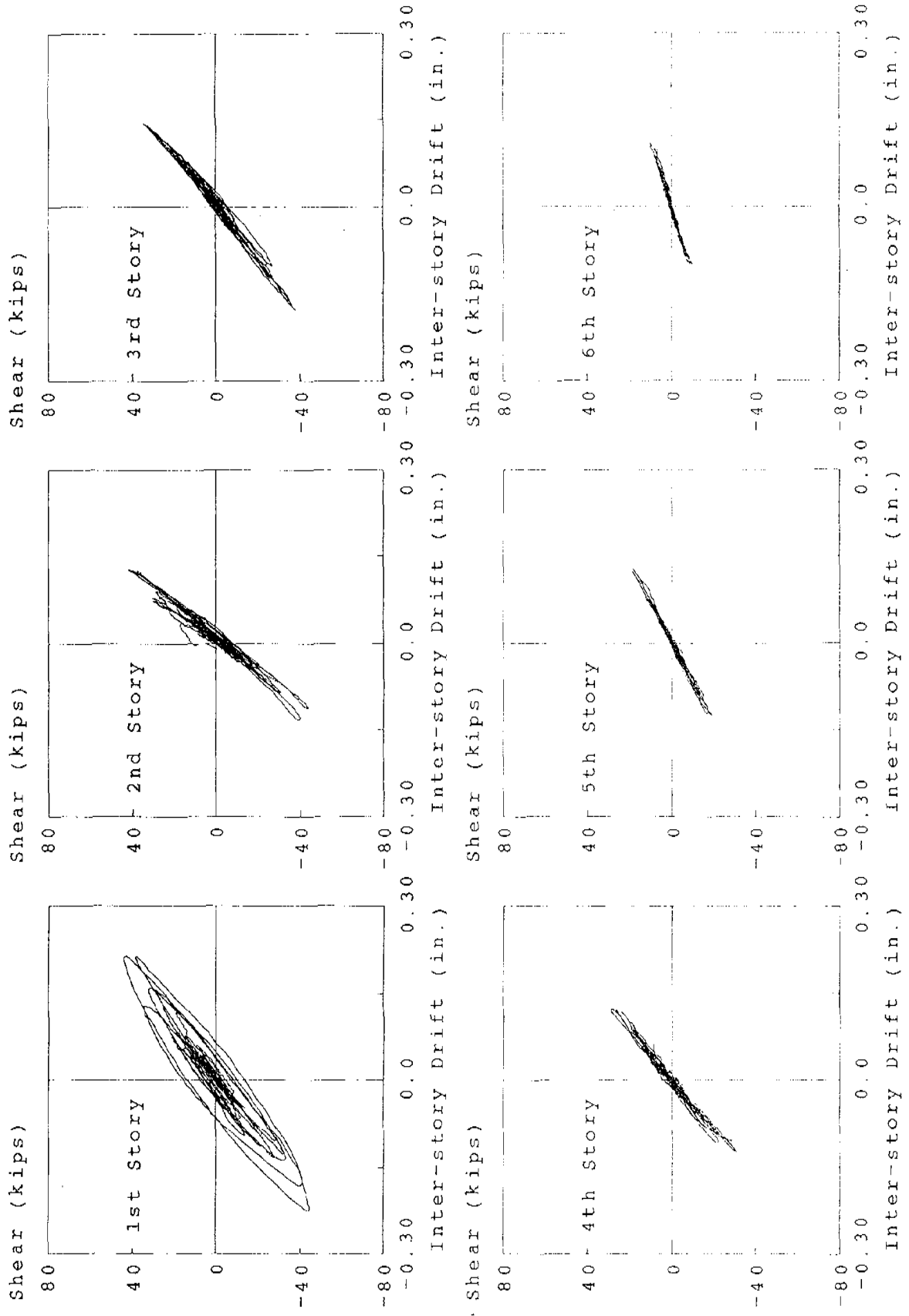
FIGURE 6.52 EBDS MO-28 BRACE STORY SHEAR AND INTER-STORY DRIFT RELATIONSHIPS
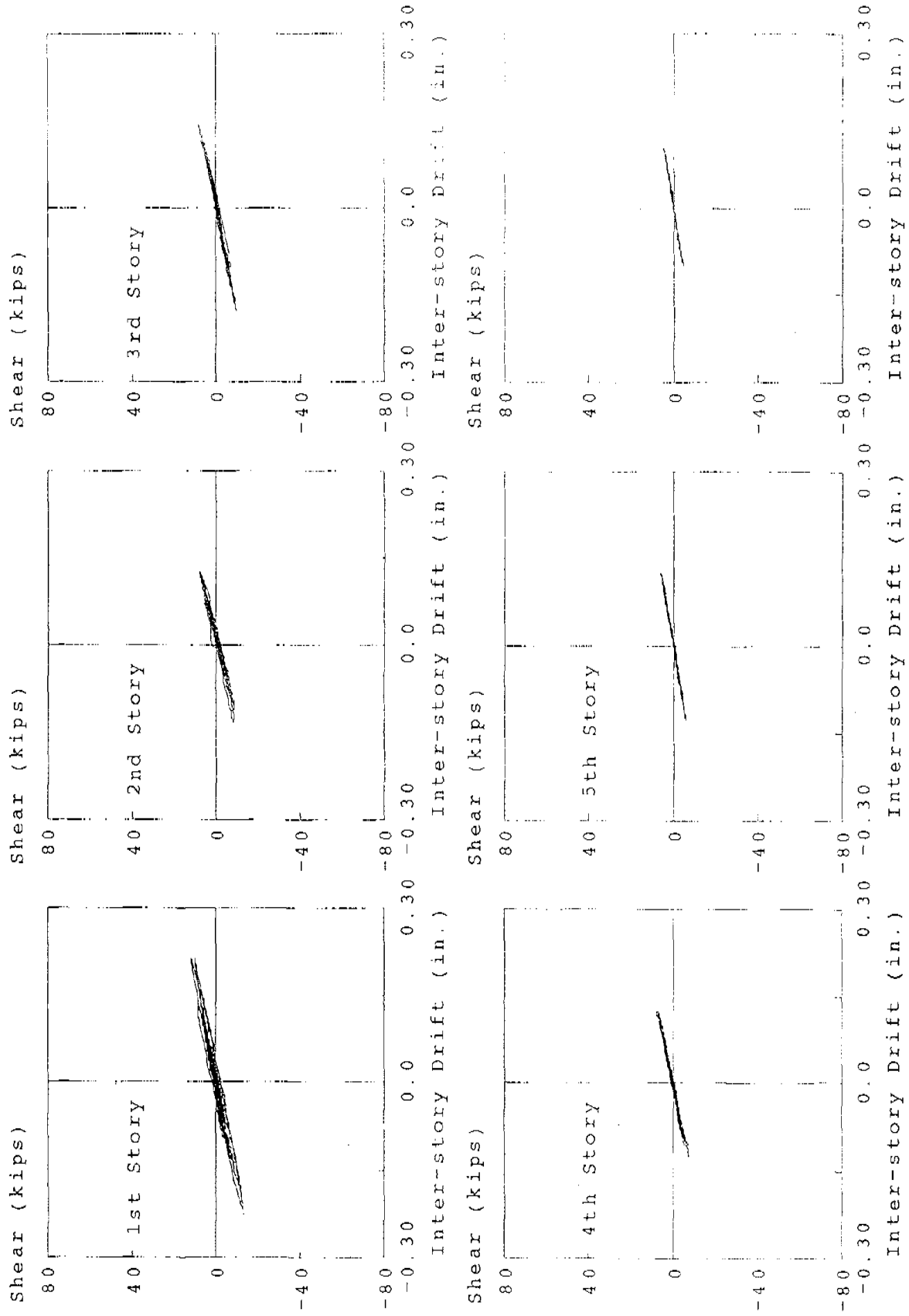
FIGURE 6.53 EBDS MO-28 DMRSF STORY SHEAR AND INTER-STORY DRIFT RELATIONSHIPS
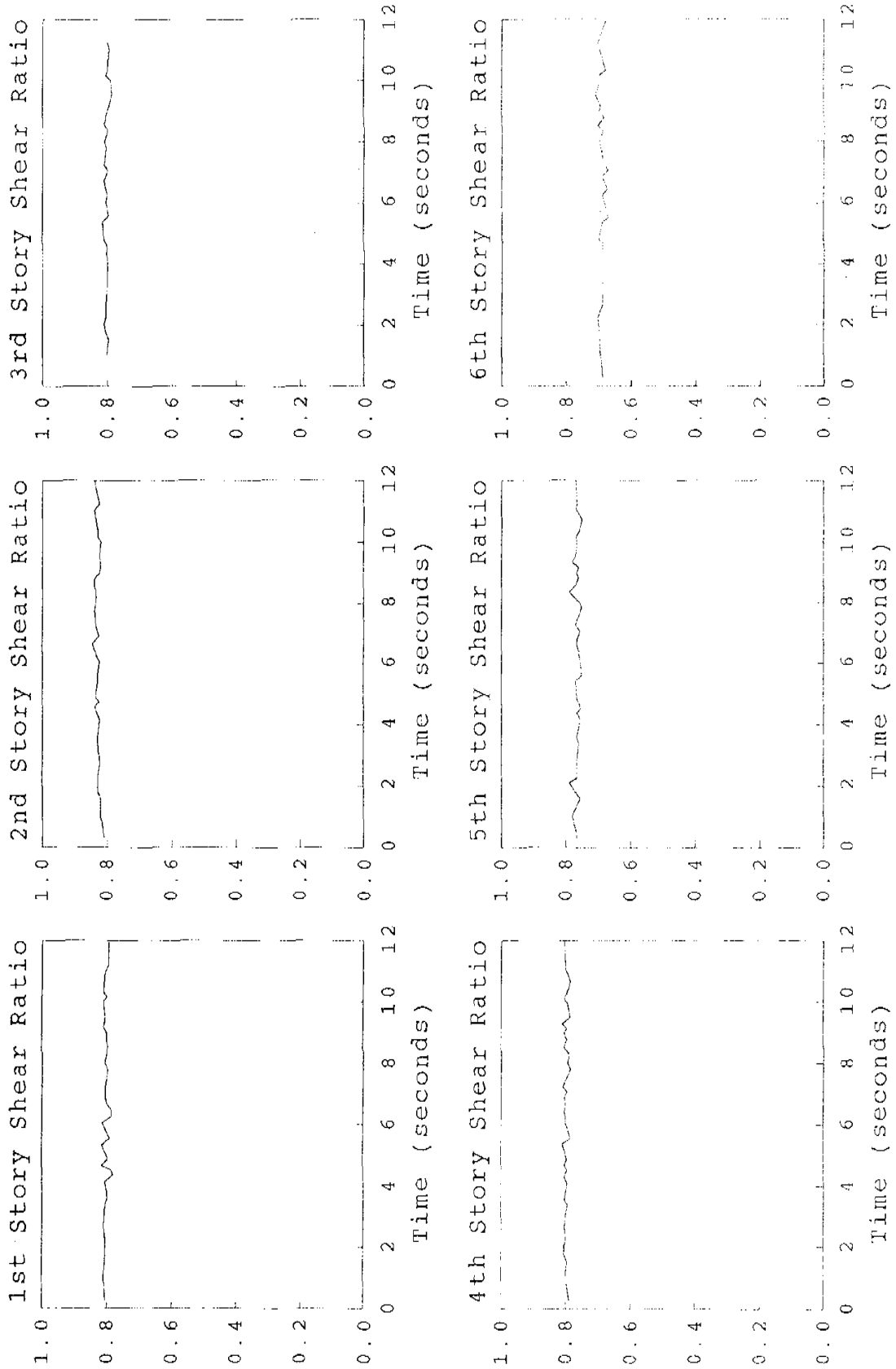
FIGURE 6.54 EBDS MO-28 STORY SHEAR RATIOS

(a) Story Shear (kips)

(b) Inertia Force (kips)

(c) Lateral Displ. (inches)

(d) Inter-story Drift (inches)

(e) Overturning Moment (x1000 kip-inch)
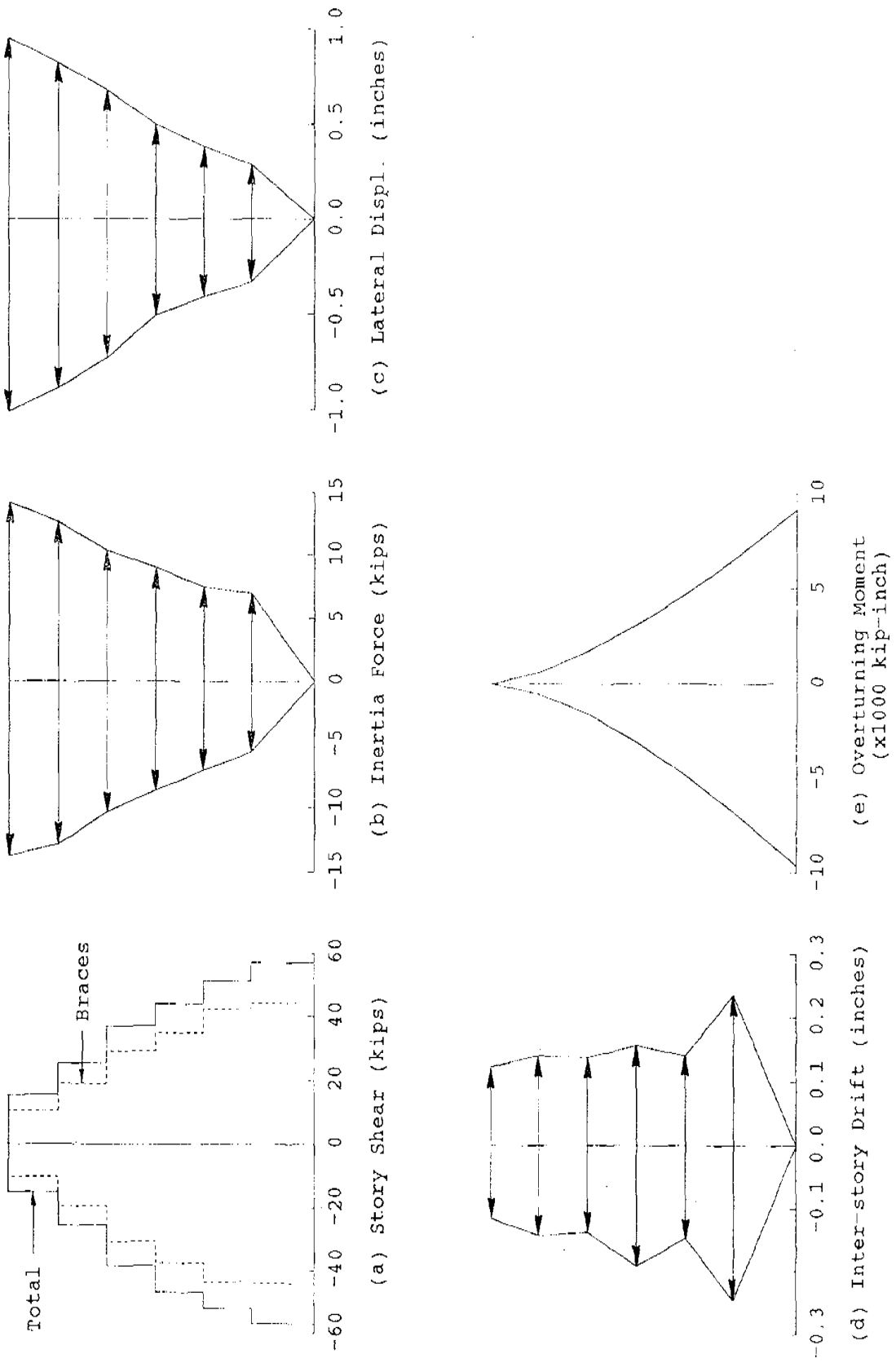
FIGURE 6.55 EBDS MO-28 RESPONSE ENVELOPES

At Maximum Base Shear

At Maximum Roof Displacement

(a) Lateral Displ. (inches)

(b) Inertia Force (kips)

(c) Story Shear (kips)

(d) Overturning Moment (x1000 kip-inch)
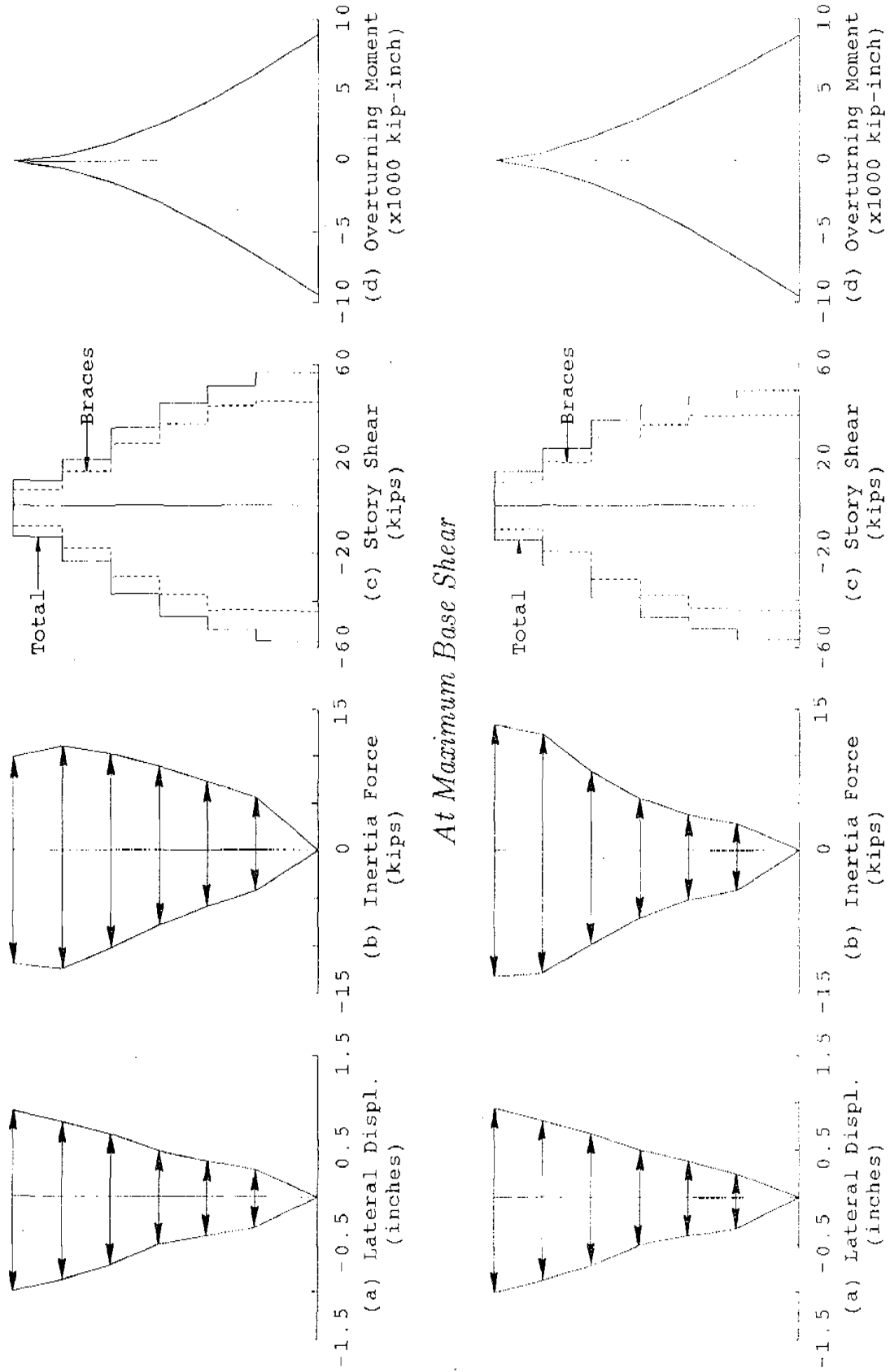
FIGURE 6.56 EBDS MO-28 RESPONSE PROFILES AT MAXIMUM RESPONSES
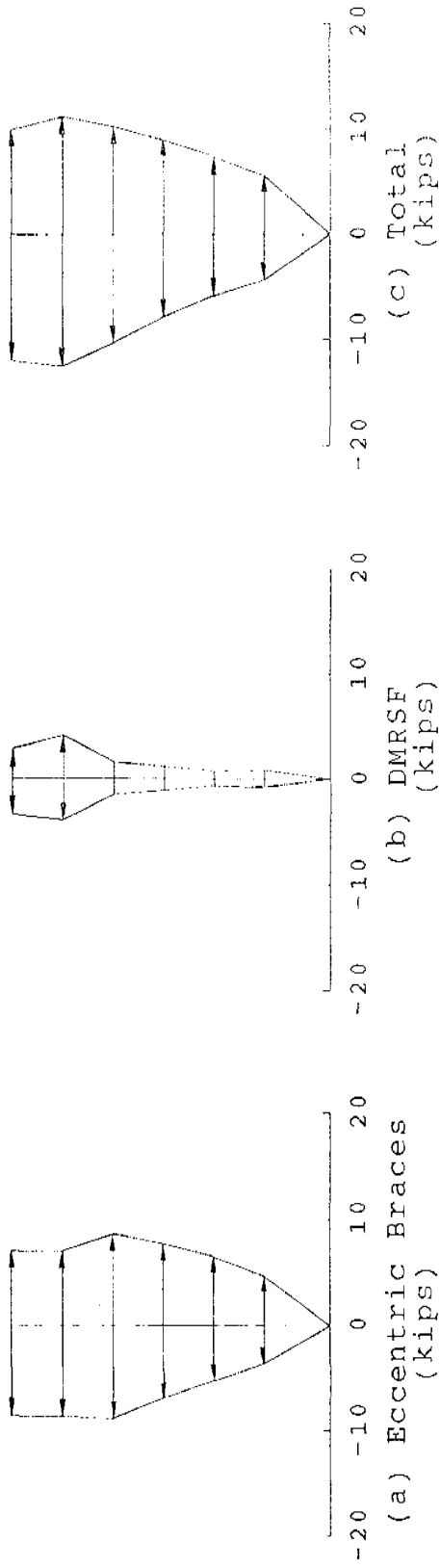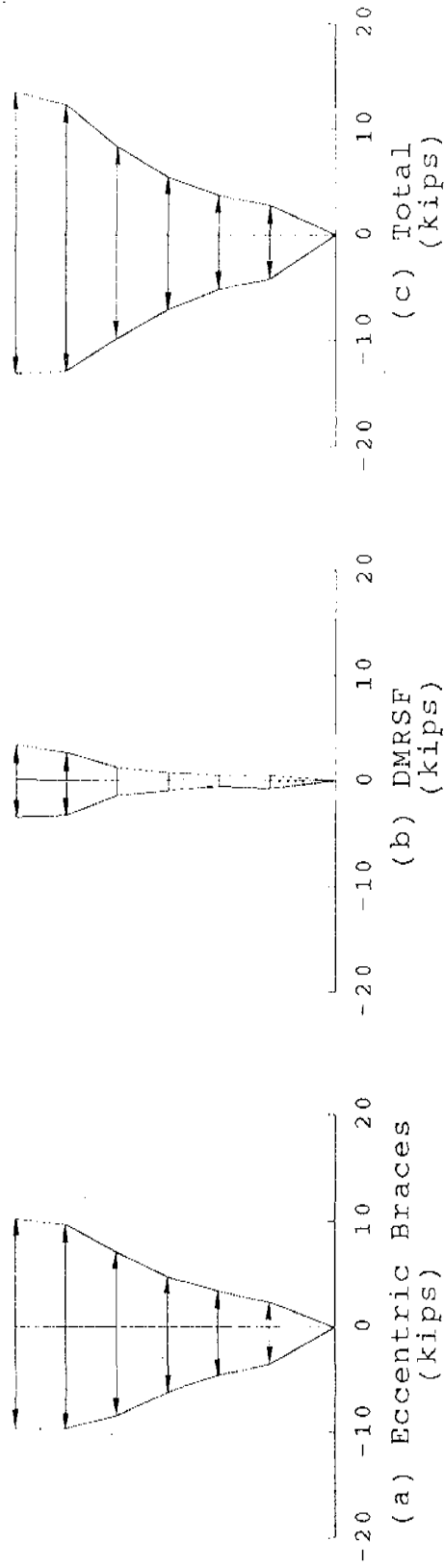
FIGURE 6.57 EBDS MO-28 LATERAL FORCE DISTRIBUTIONS AT MAXIMUM RESPONSES
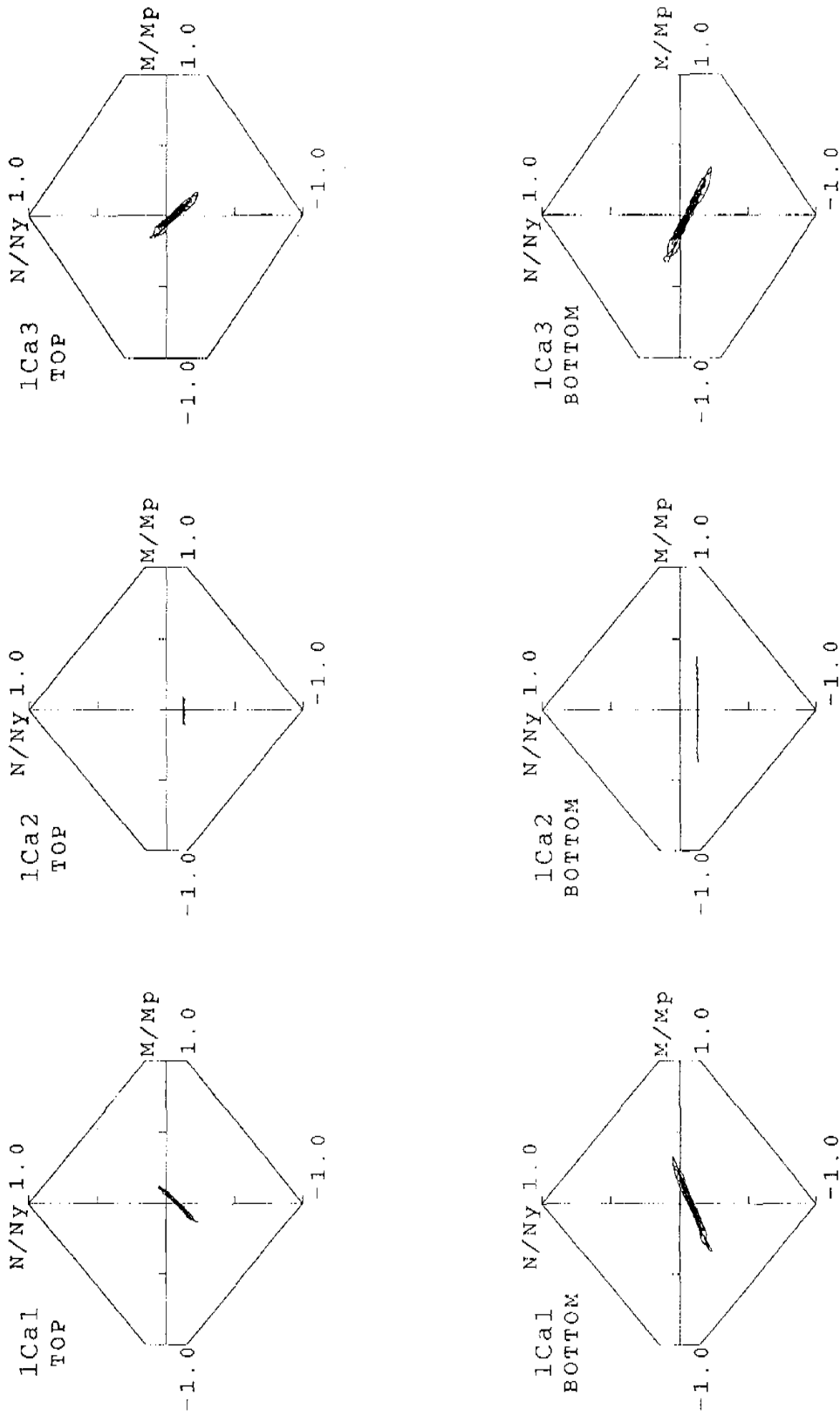
FIGURE 6.58 EBDS MO-28 FIRST STORY COLUMN AXIAL FORCE AND END MOMENT
INTERACTION CURVES (FRAME A)
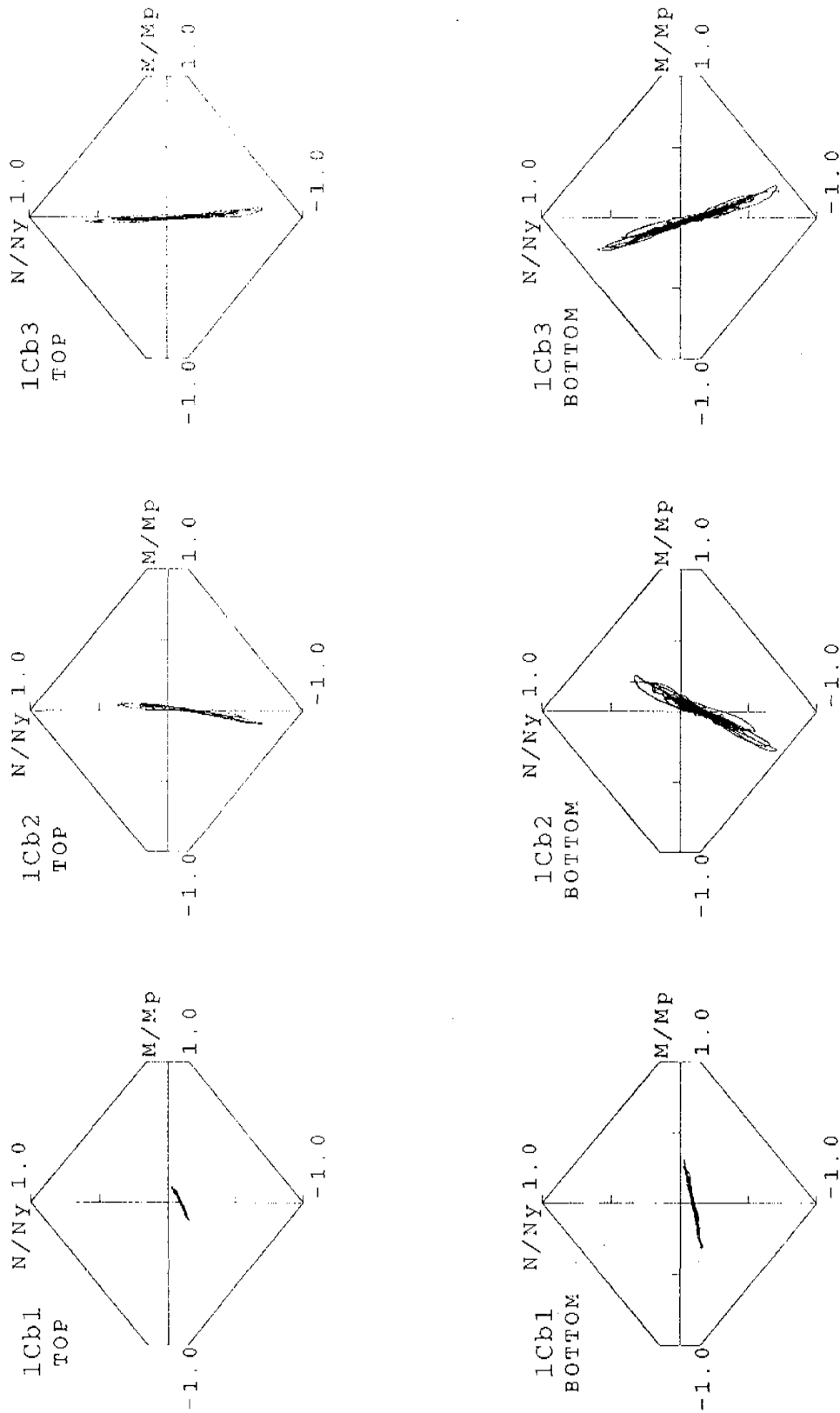
FIGURE 6.59 EBDS MO-28 FIRST STORY COLUMN AXIAL FORCE AND END MOMENT INTERACTION CURVES (FRAME B)
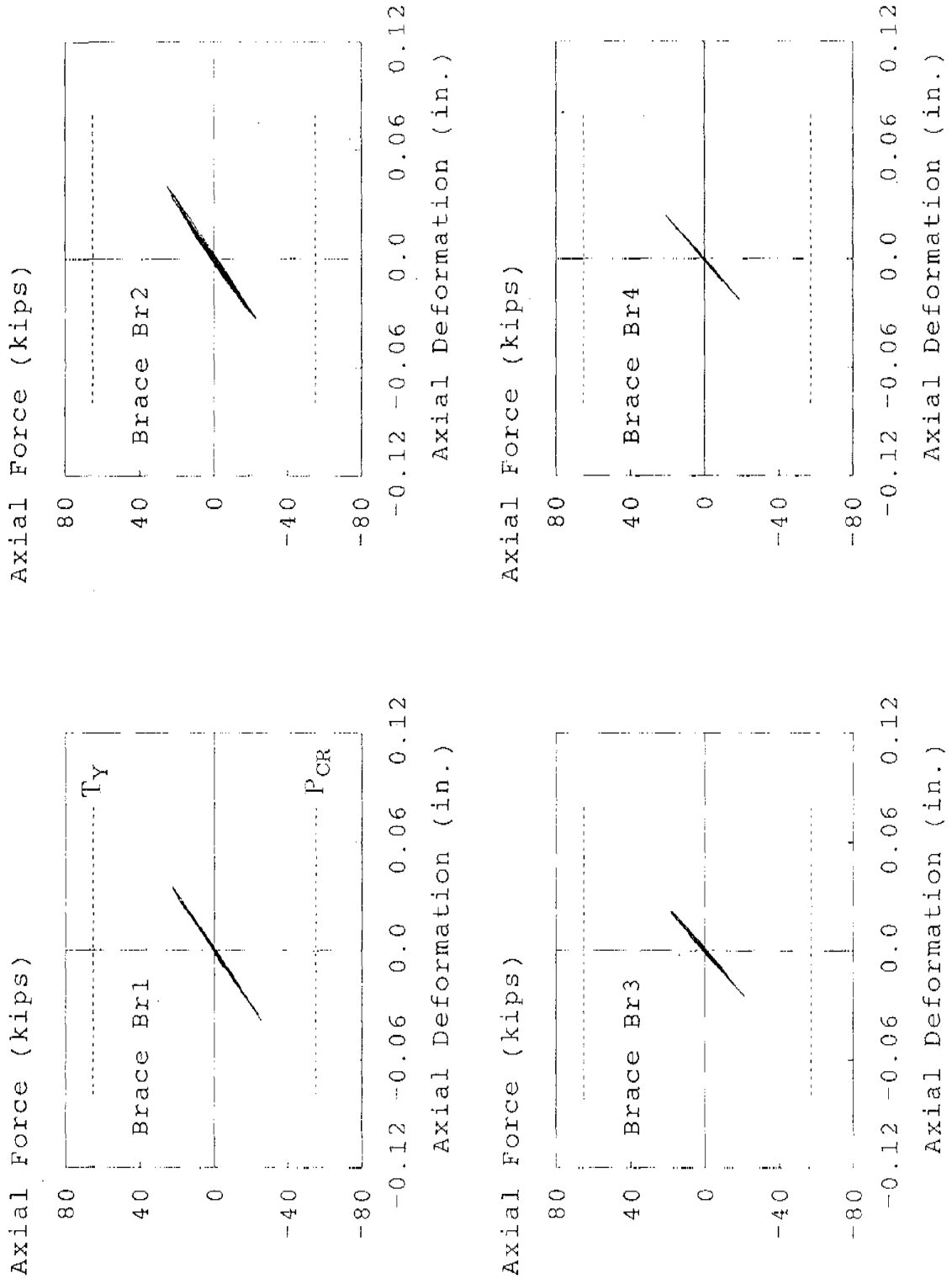
FIGURE 6.60 EBDS MO-28 BRACE FORCE AND DEFORMATION RELATIONSHIPS
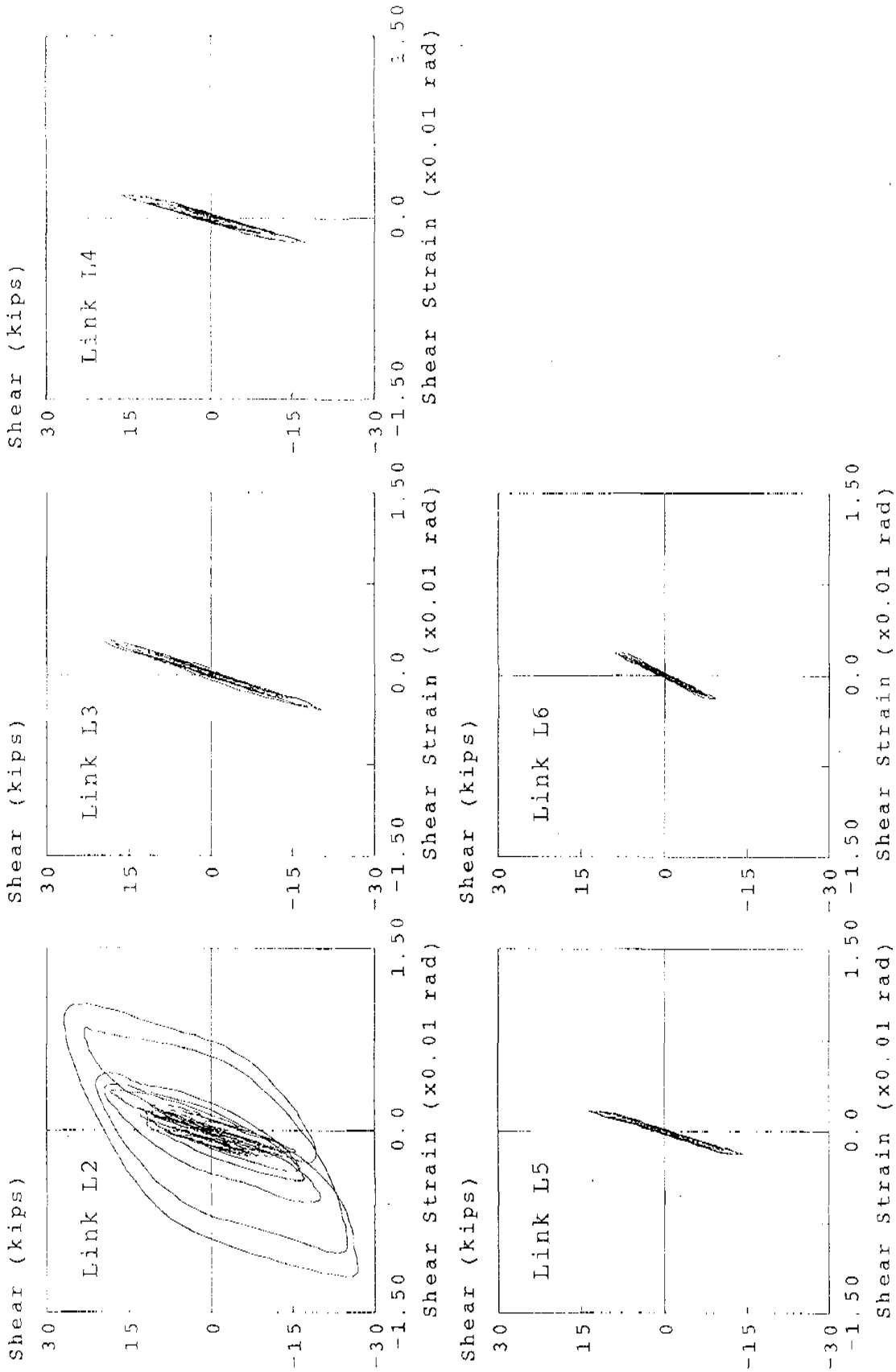
FIGURE 6.61 EBDS MO-28 LINK SHEAR FORCE AND SHEAR STRAIN RELATIONSHIPS
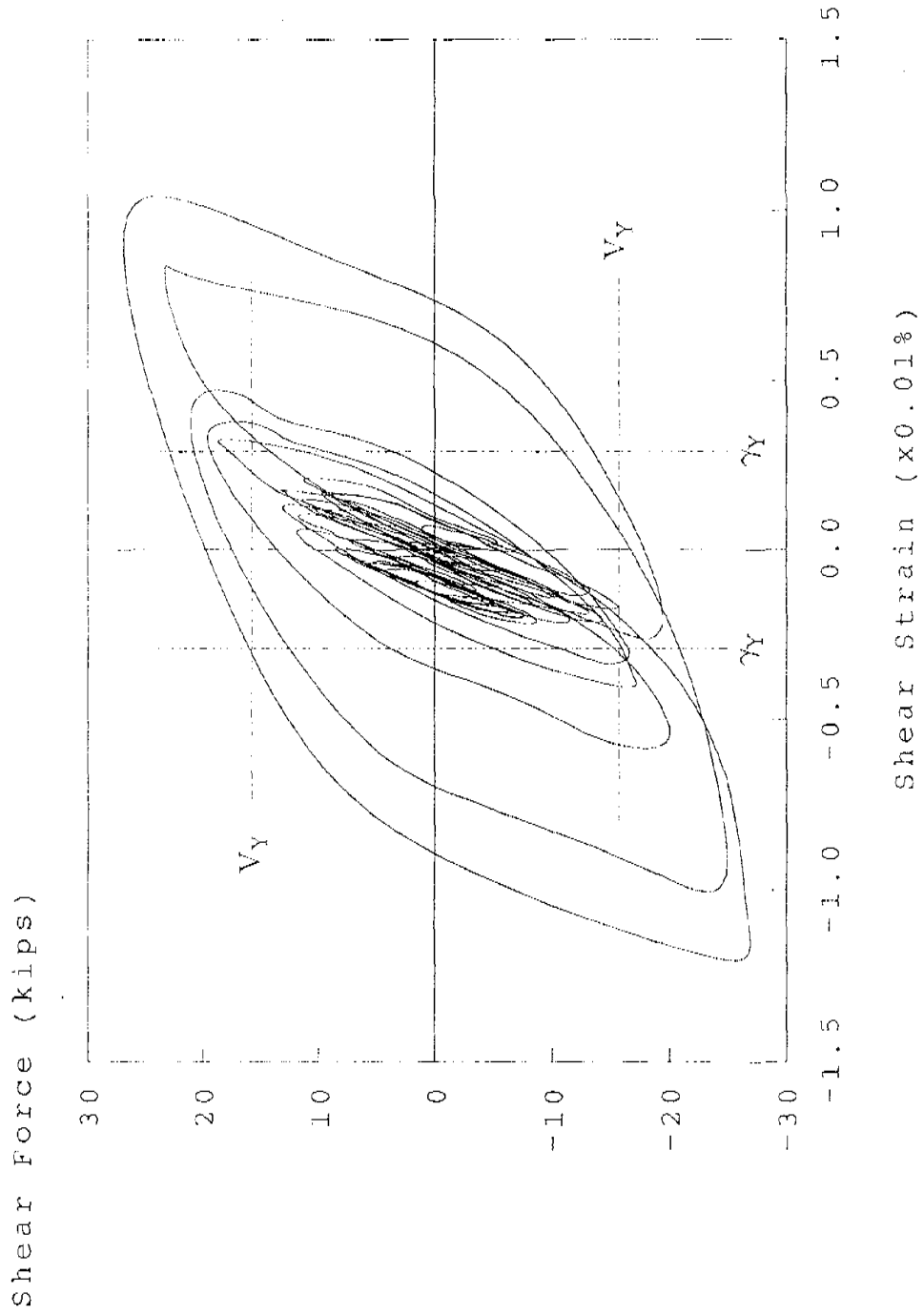
FIGURE 6.62 EBDS MO-28 LINK L2 SHEAR FORCE AND SHEAR STRAIN
RELATIONSHIP
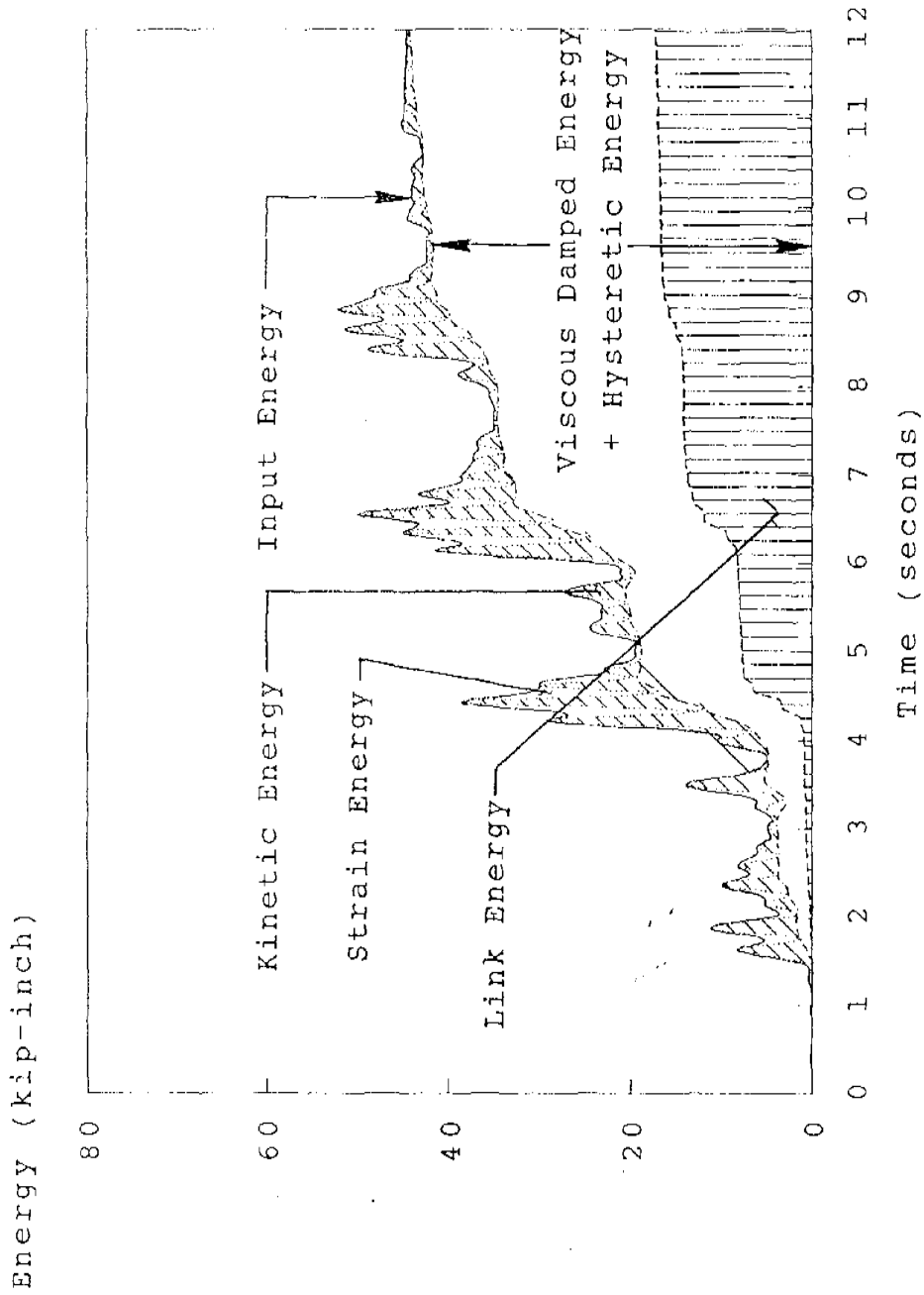
FIGURE 6.63 EBDS MO-28 ENERGY TIME HISTORIES

FIGURE 6.64 CBDS MO-65 INPUT CHARACTERISTICS

Pseudo-Velocity
(inch/sec.)

Period (seconds)
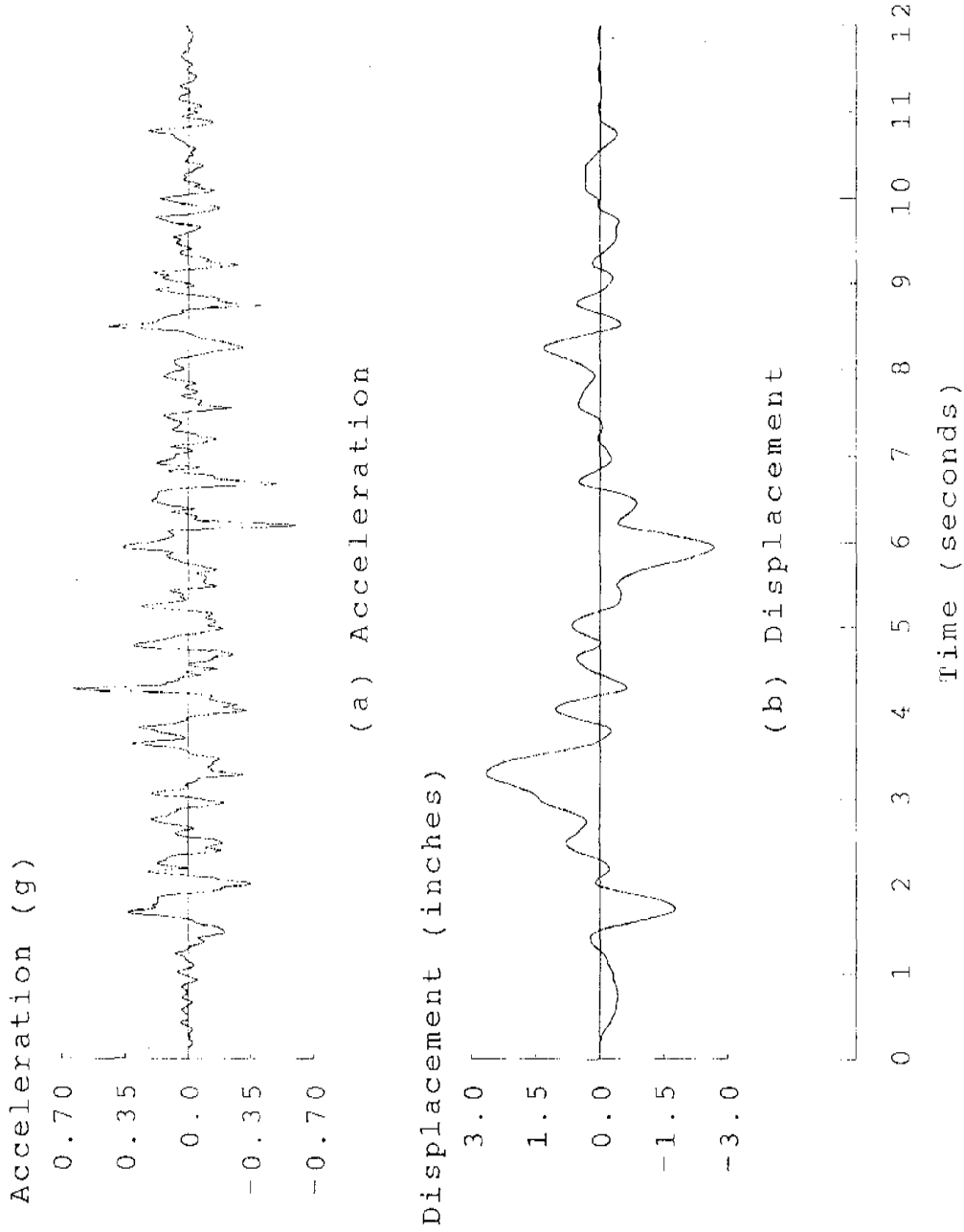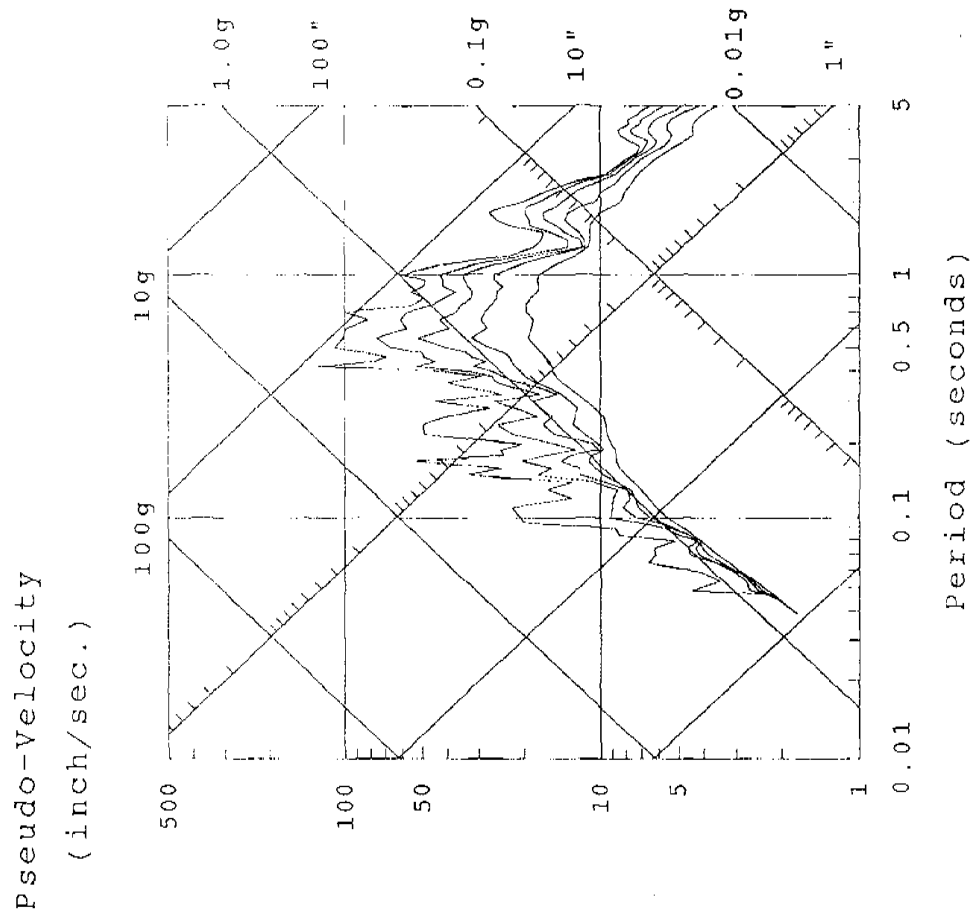
(c) Response Spectra (0,2,5,10,20 % Damping)

FIGURE 6.64 CBDS MO-65 INPUT CHARACTERISTICS

FIGURE 6.65 CBDS MO-65 LATERAL DISPLACEMENT TIME HISTORIES

FIGURE 6.66 CBDS MO-65 INTER-STORY DRIFT TIME HISTORIES
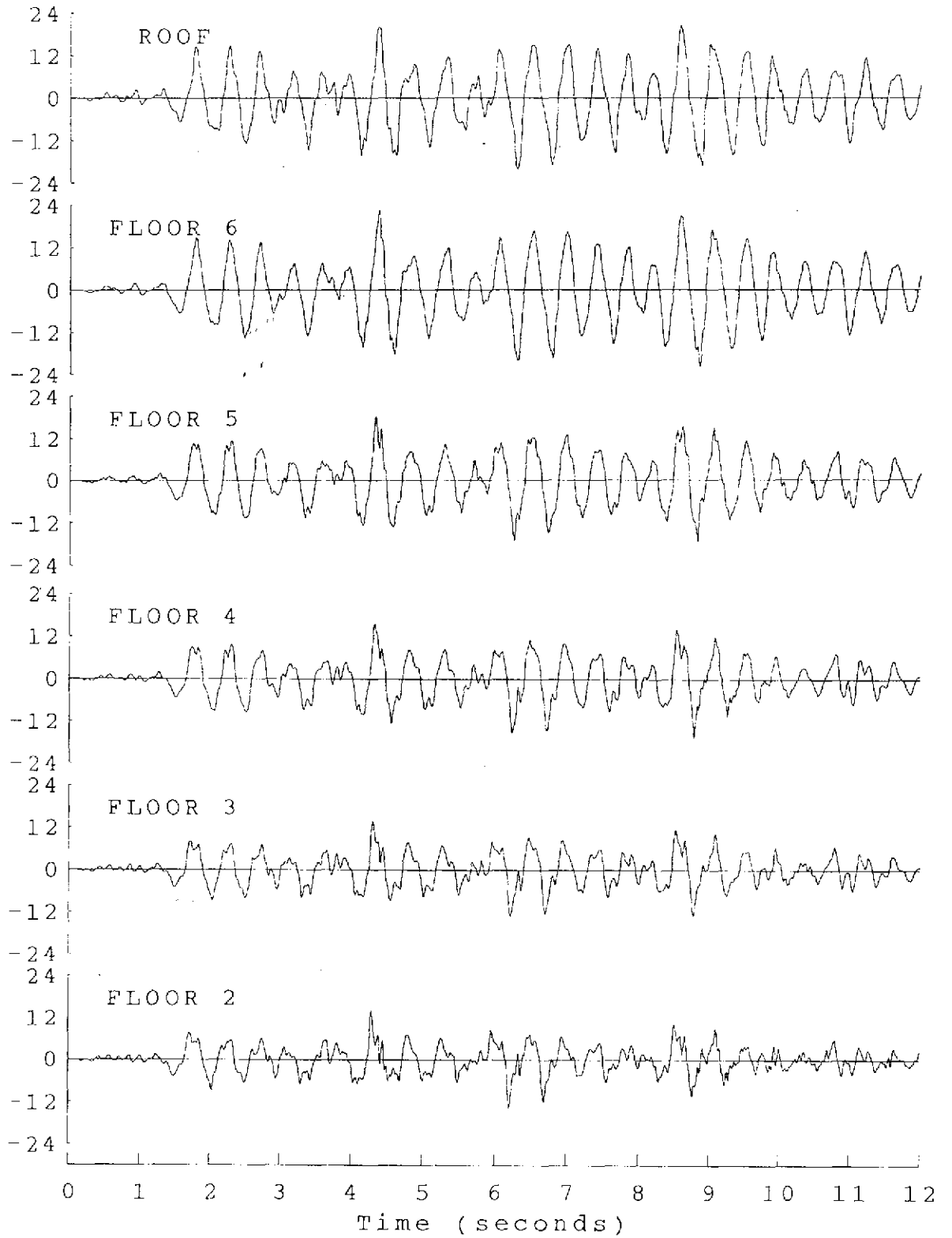
FIGURE 6.67 CBDS MO-65 INERTIA FORCE TIME HISTORIES
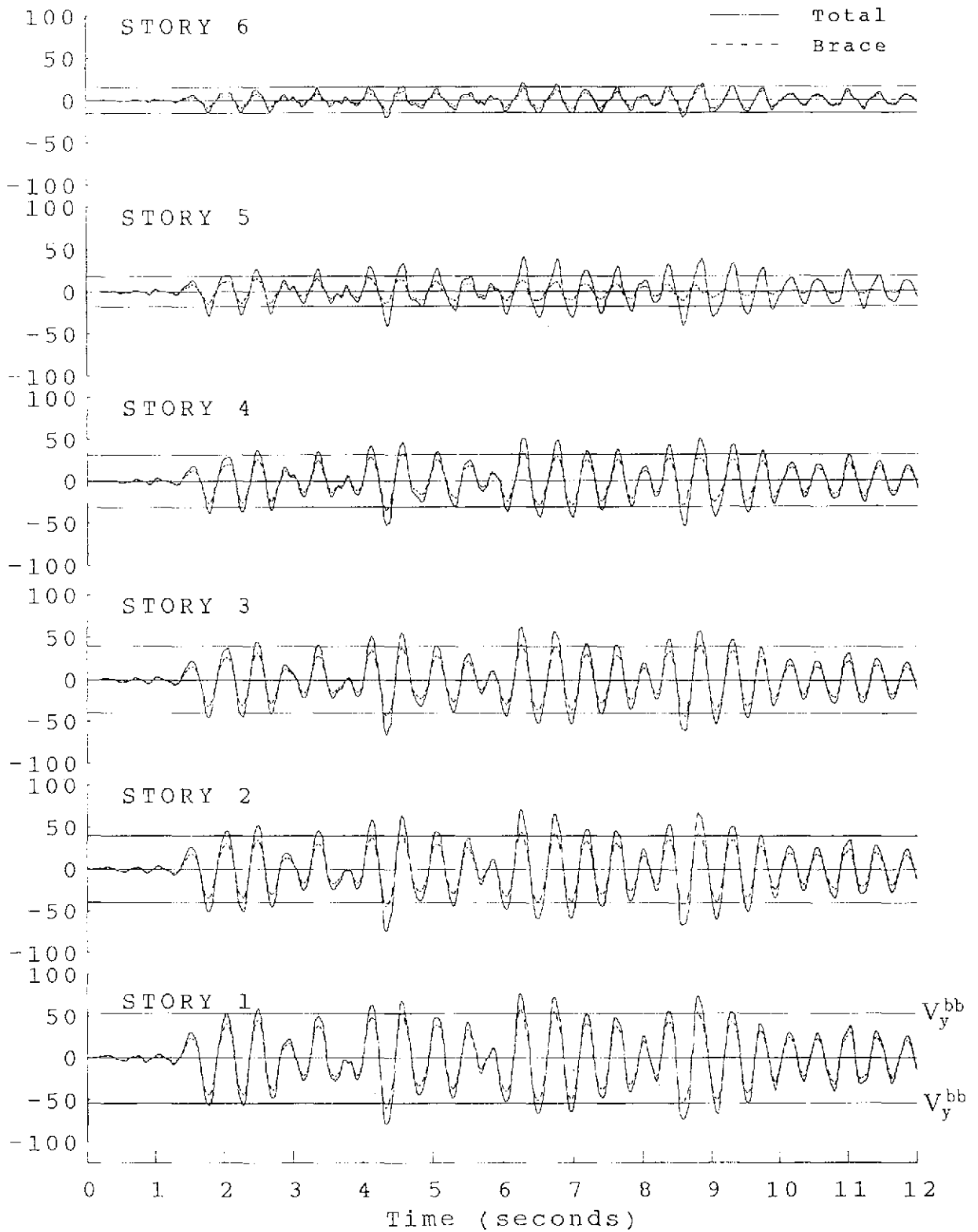
Story Shear
(kips)

FIGURE 6.68 CBDS MO-65 STORY SHEAR TIME HISTORIES
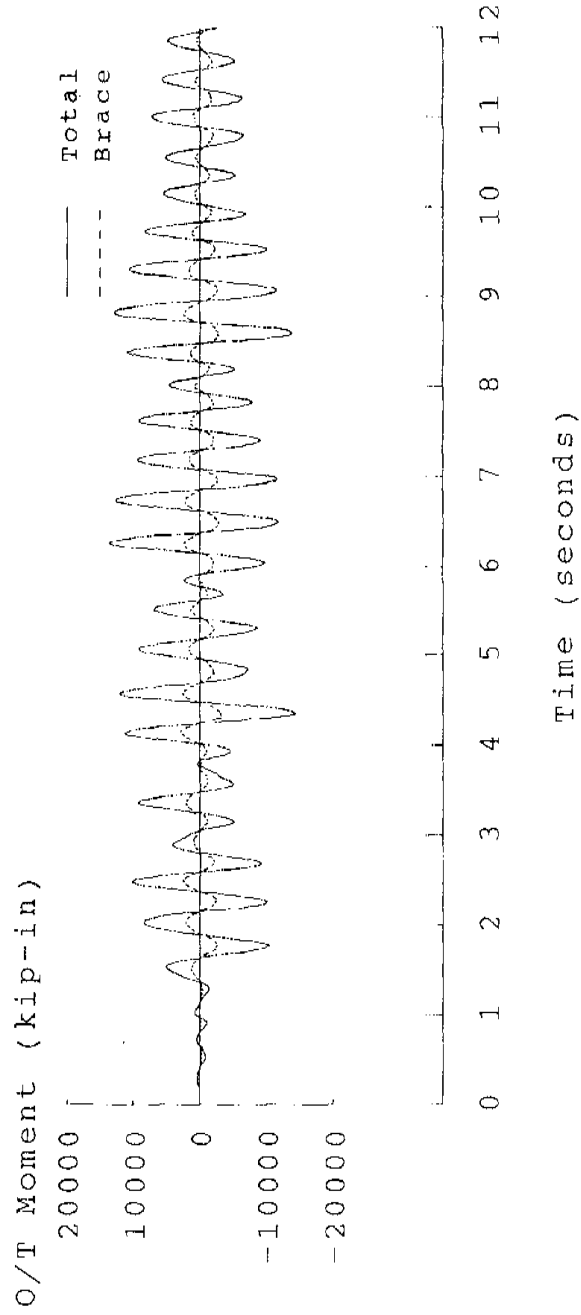
FIGURE 6.69 CBDS MO-65 OVERTURNING MOMENT TIME HISTORIES
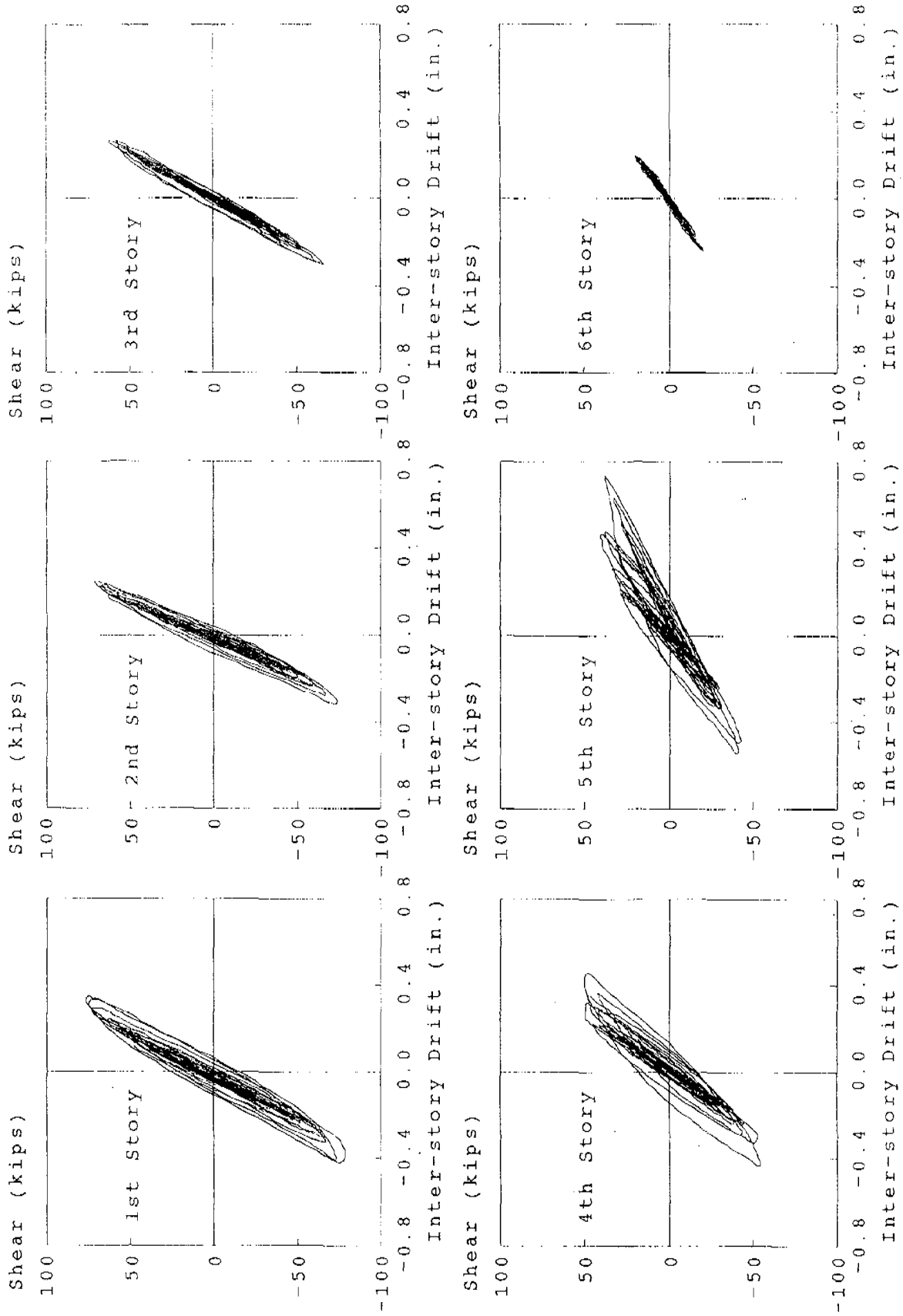
FIGURE 6.70 CBDS MO-65 TOTAL STORY SHEAR AND INTER-STORY DRIFT RELATIONSHIPS
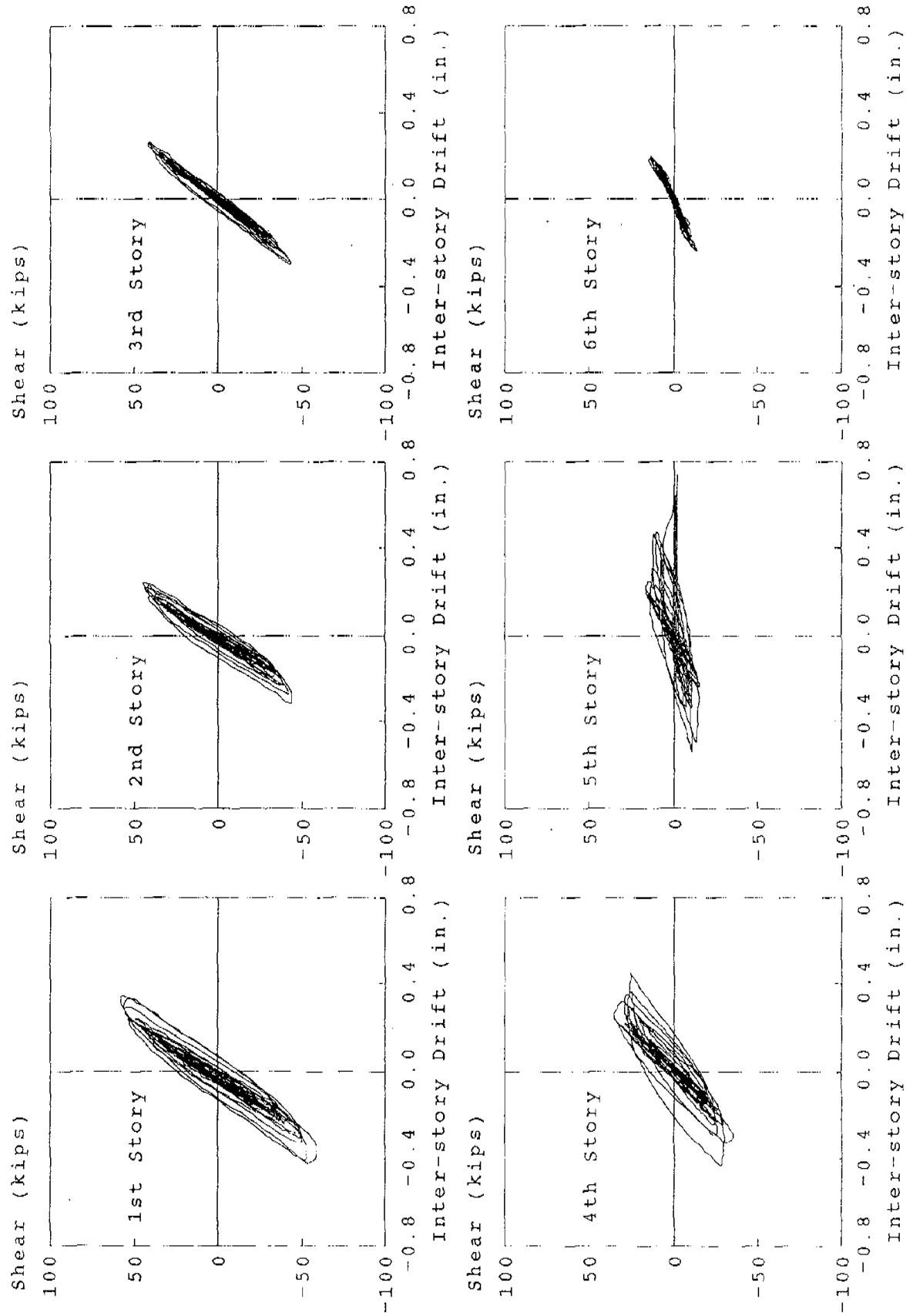
FIGURE 6.71 CBDS MO-65 BRACE STORY SHEAR AND INTER-STORY DRIFT RELATIONSHIPS
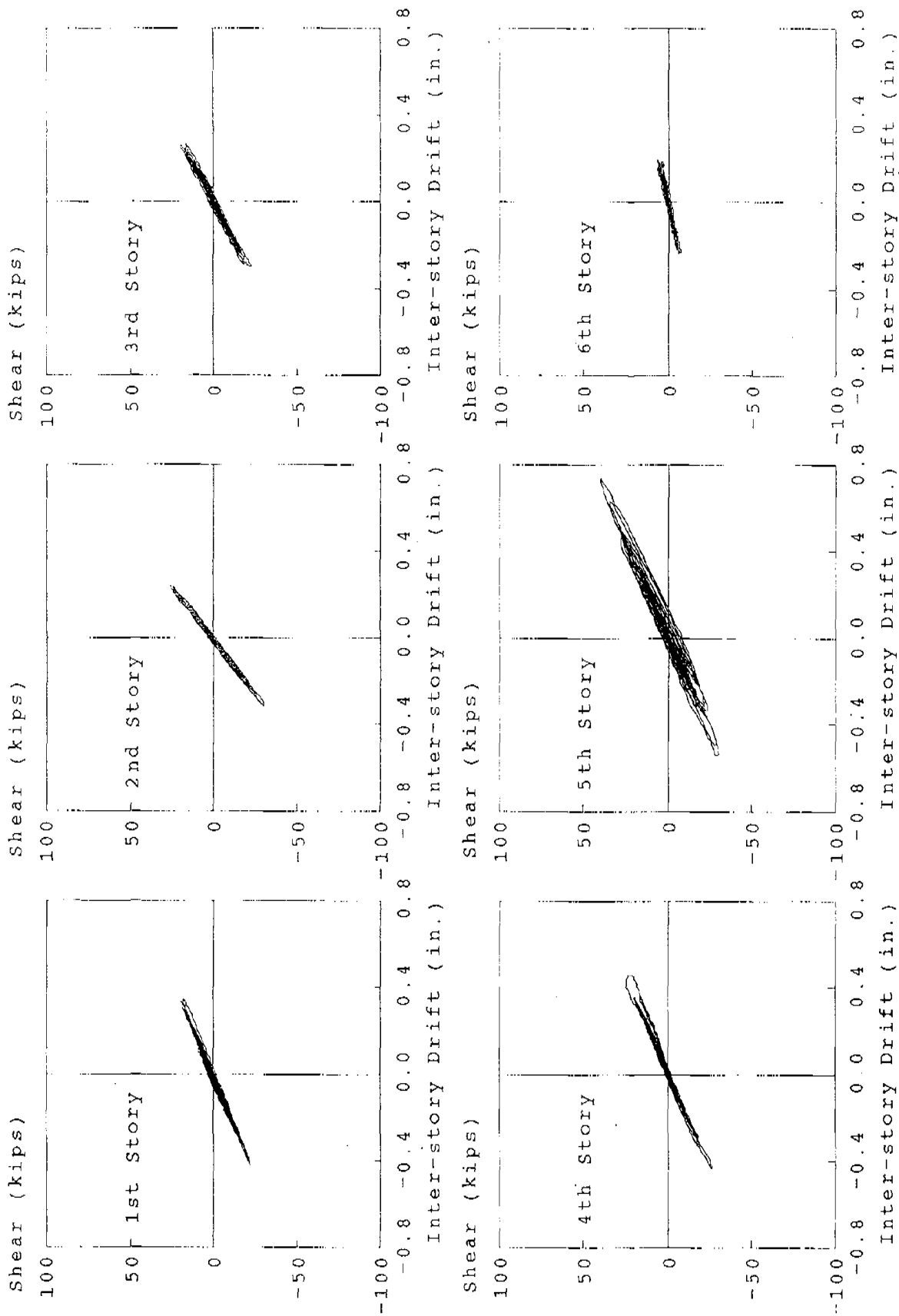
FIGURE 6.72 CBDS MO-65 DMRSF STORY SHEAR AND INTER-STORY DRIFT RELATIONSHIPS
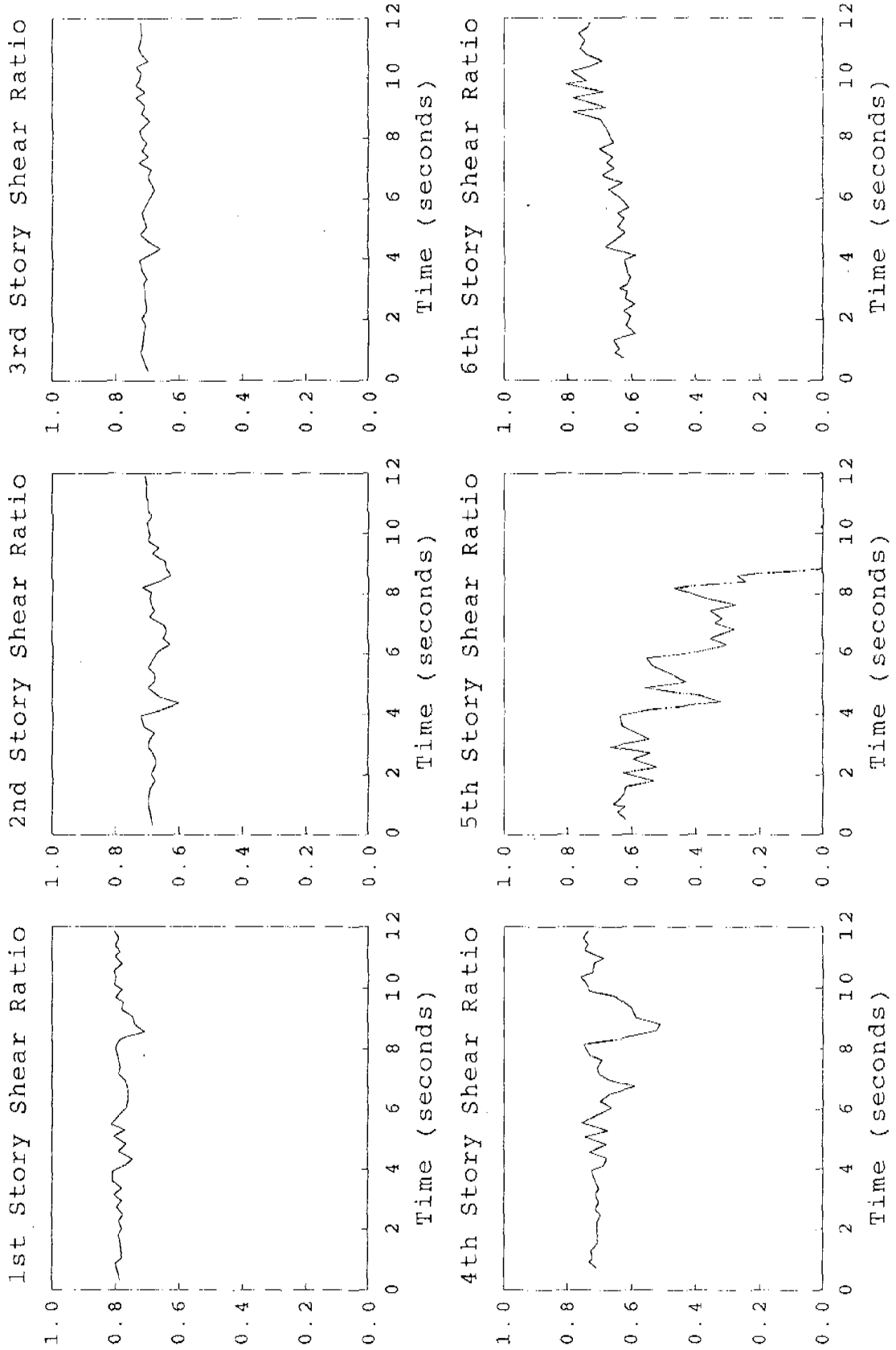
FIGURE 6.73 CBDS MO-65 STORY SHEAR RATIOS

(c) Lateral Displ. (inches)

(b) Inertia Force (kips)

(e) Overturning Moment (x1000 kip-inch)

(a) Story Shear (kips)

(d) Inter-story Drift (inches)
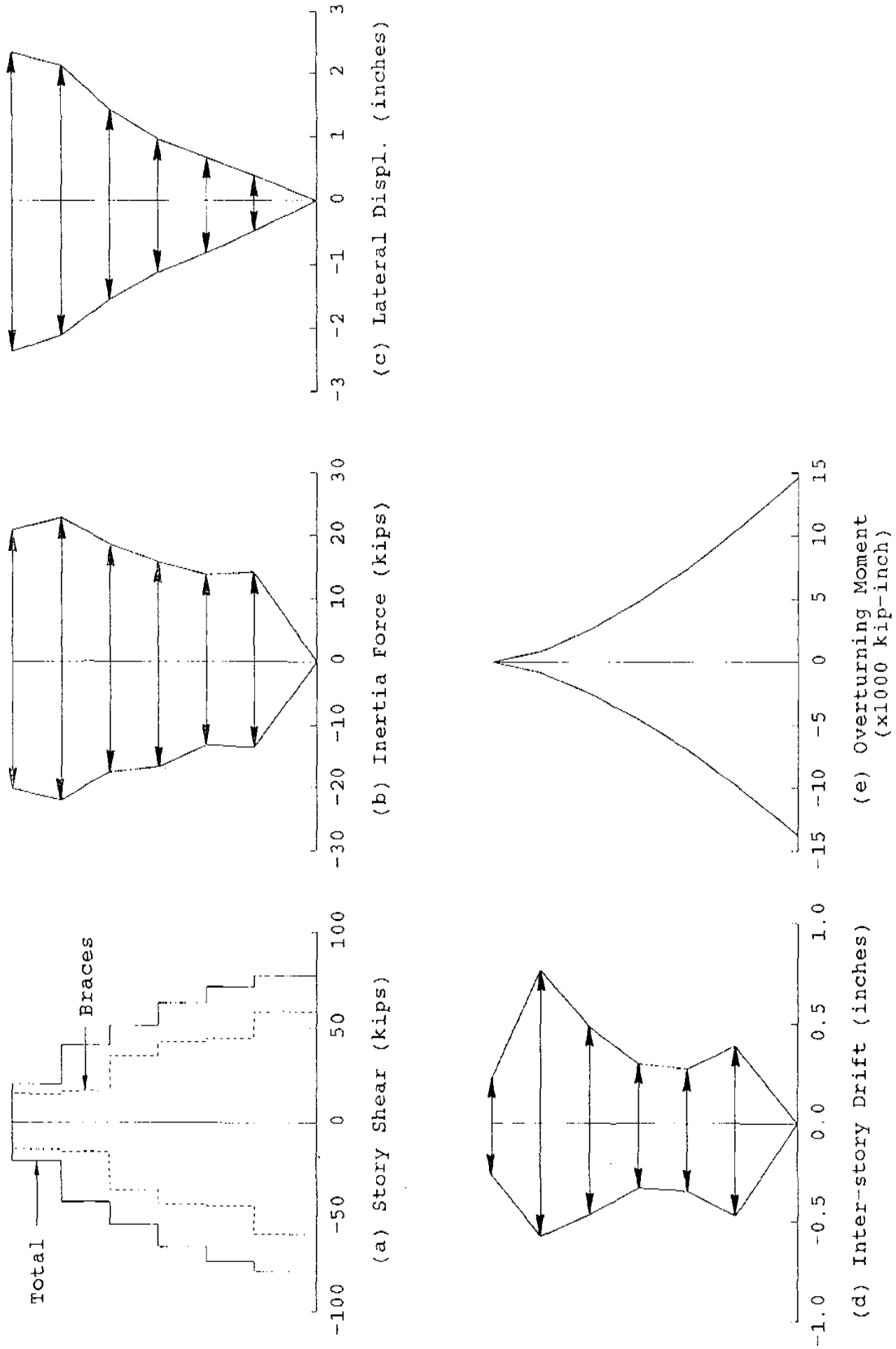
FIGURE 6.74 CBDS MO-65 RESPONSE ENVELOPES
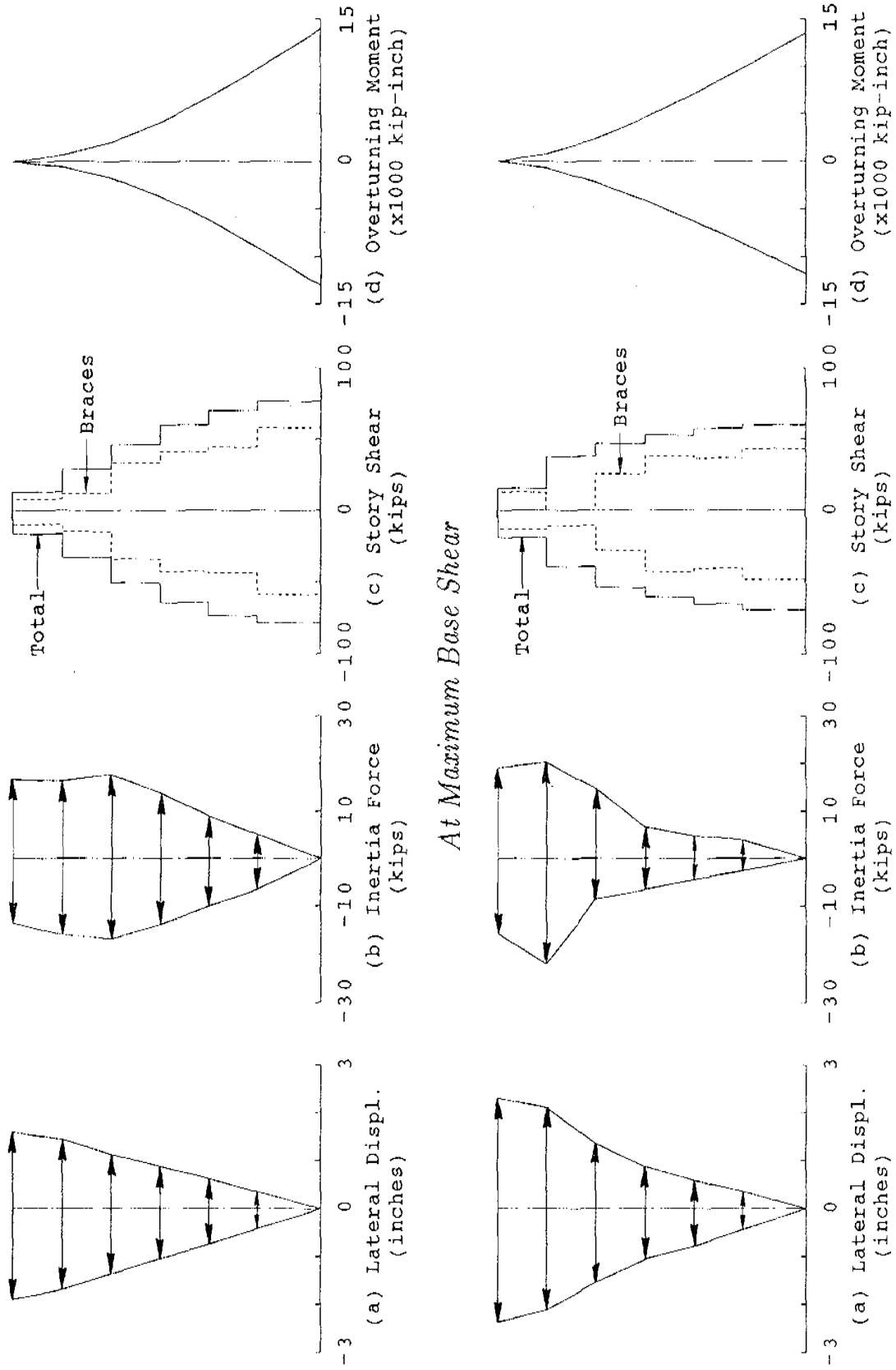
FIGURE 6.75 CBDS MO-65 RESPONSE PROFILES AT MAXIMUM RESPONSES
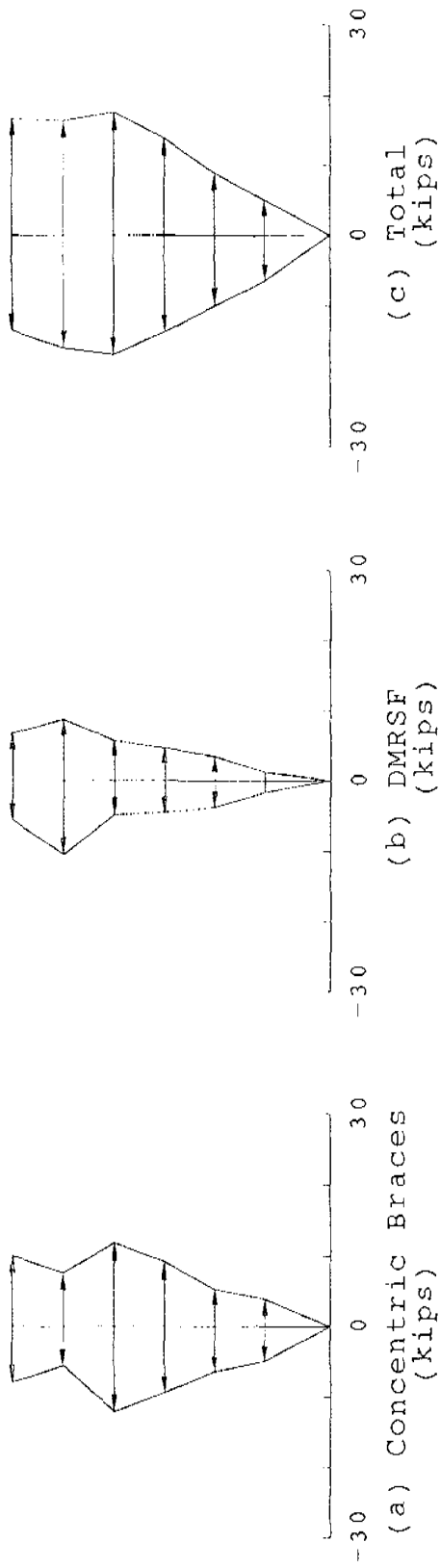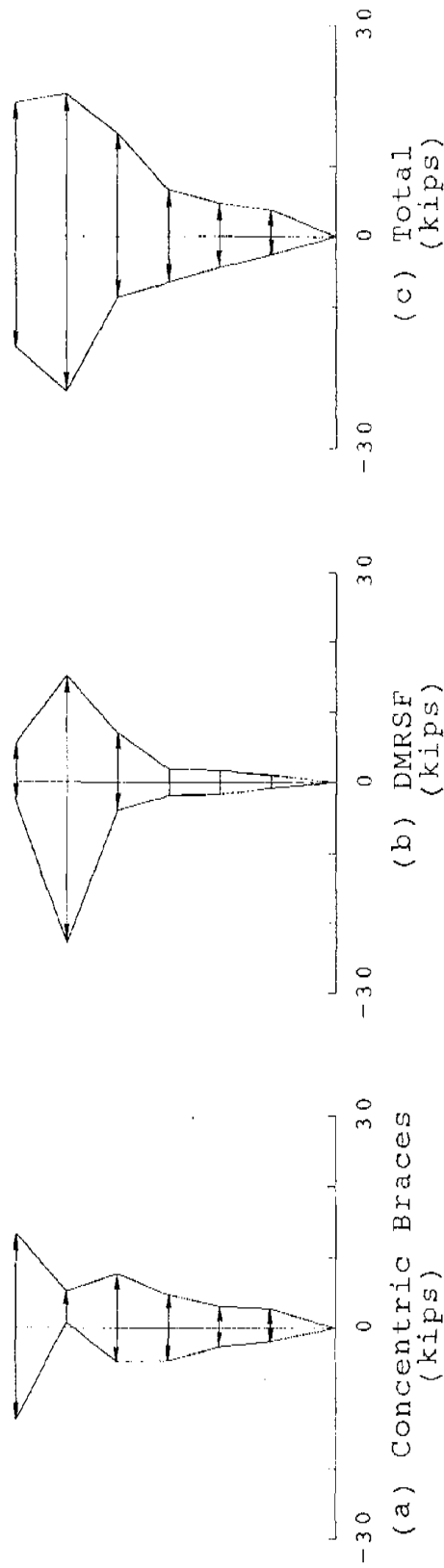
FIGURE 6.76 CBDS MO-65 LATERAL FORCE DISTRIBUTIONS AT MAXIMUM RESPONSES
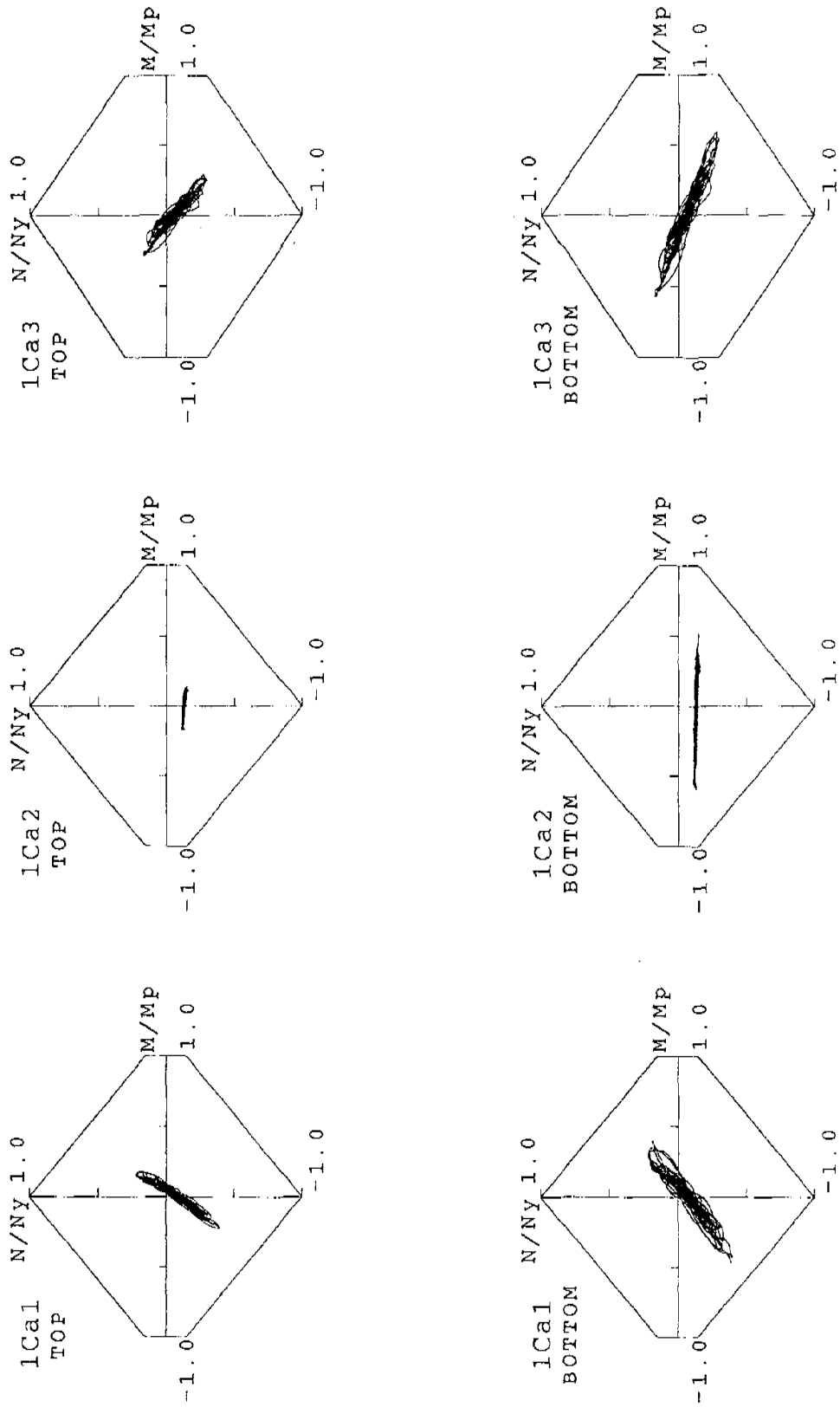
FIGURE 6.77 CBDS MO-65 FIRST STORY COLUMN AXIAL FORCE AND END MOMENT INTERACTION CURVES (FRAME A)
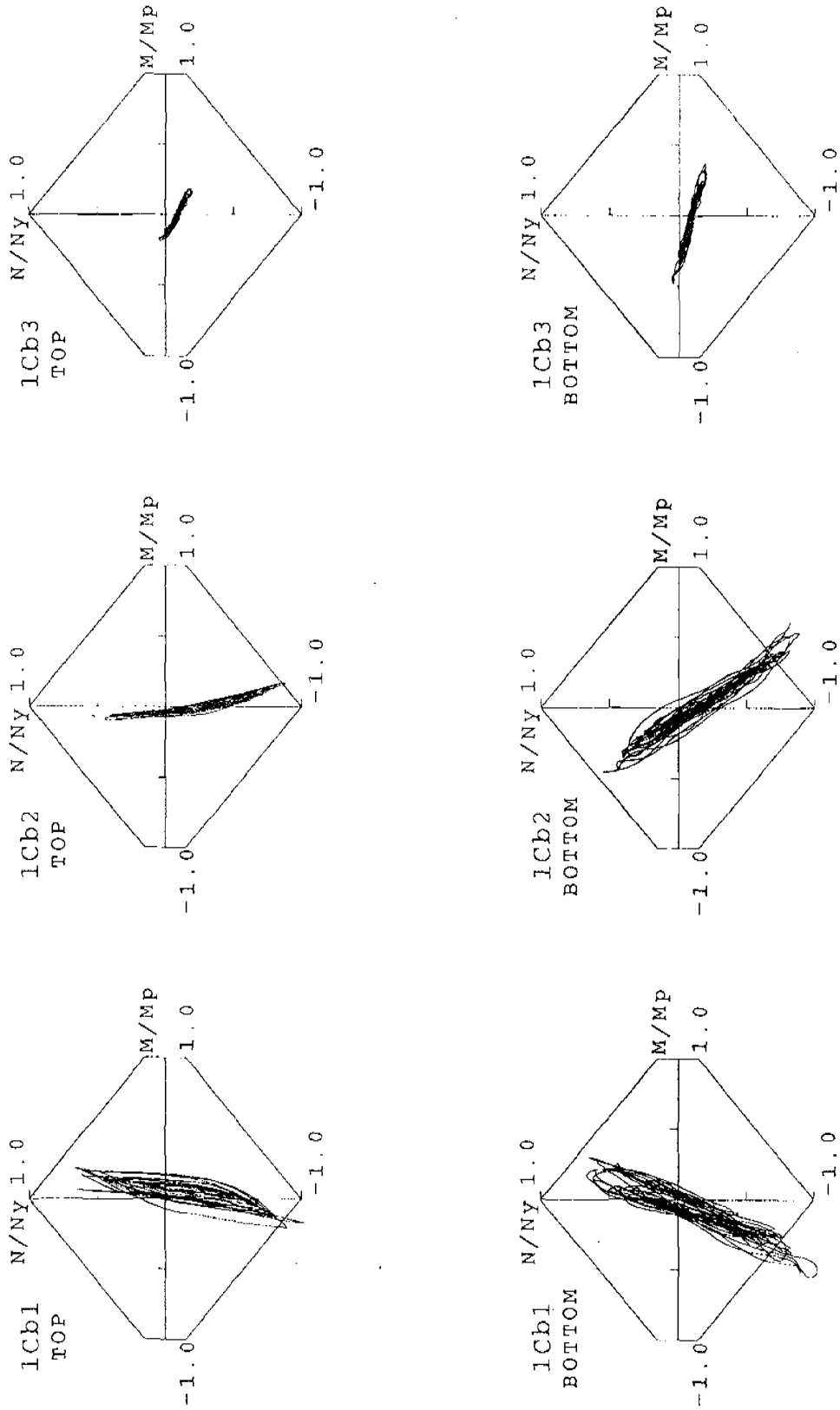
FIGURE 6.78 CBDS MO-65 FIRST STORY COLUMN AXIAL FORCE AND END MOMENT
INTERACTION CURVES (FRAME B)
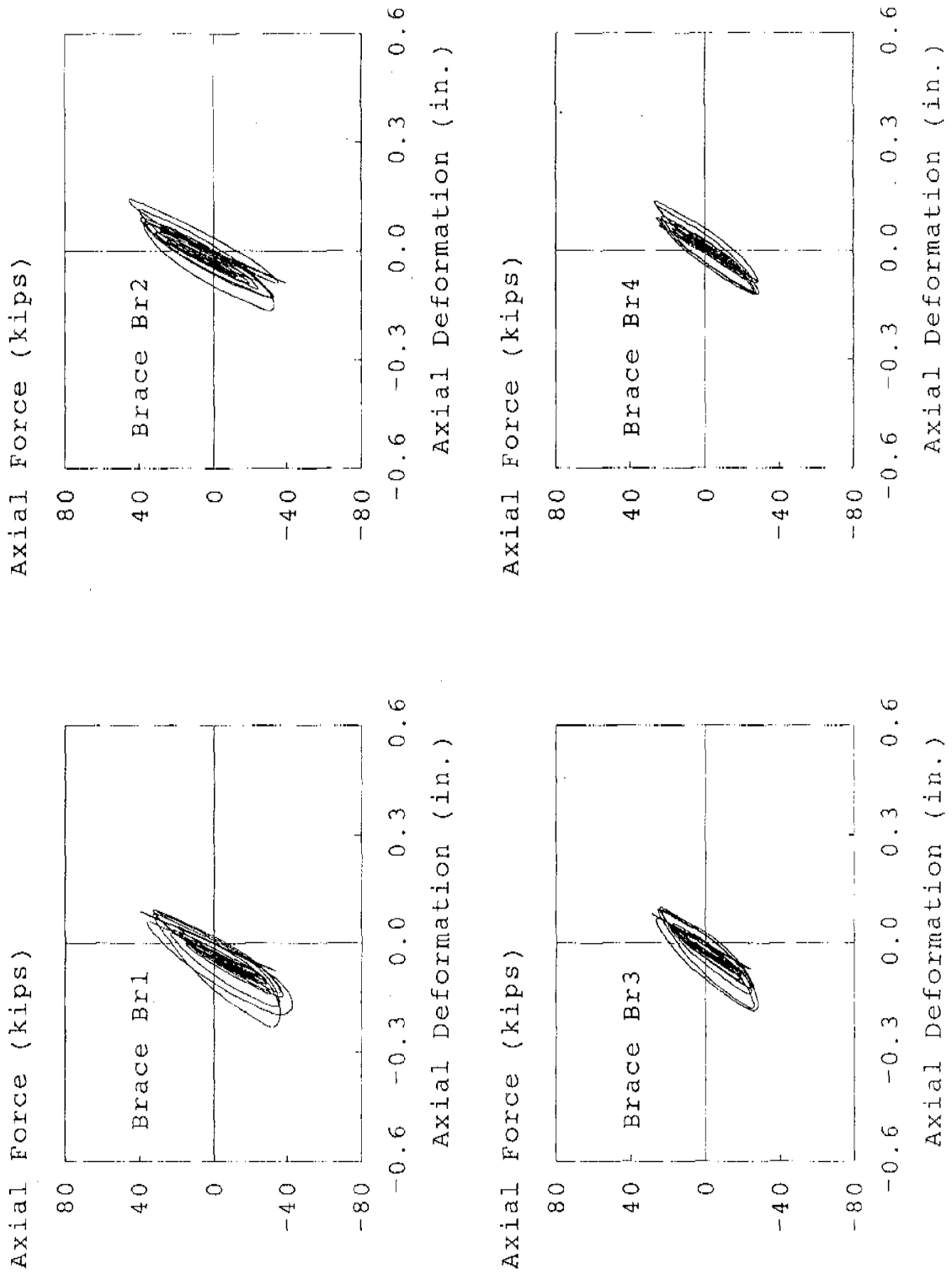
FIGURE 6.79 CBDS MO-65 BRACE FORCE AND DEFORMATION RELATIONSHIPS
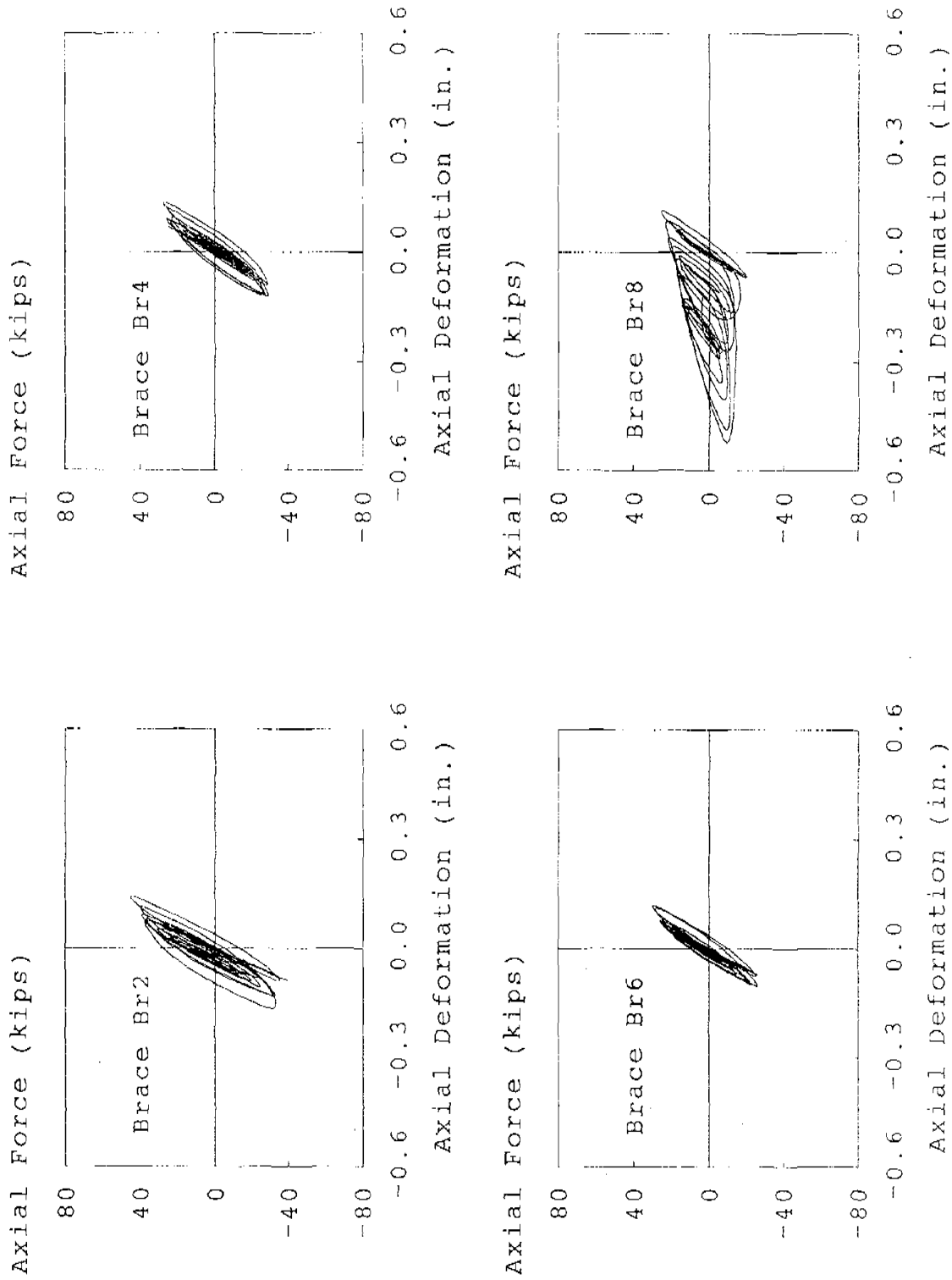
FIGURE 6.80 CBDS MO-65 BRACE FORCE AND DEFORMATION RELATIONSHIPS
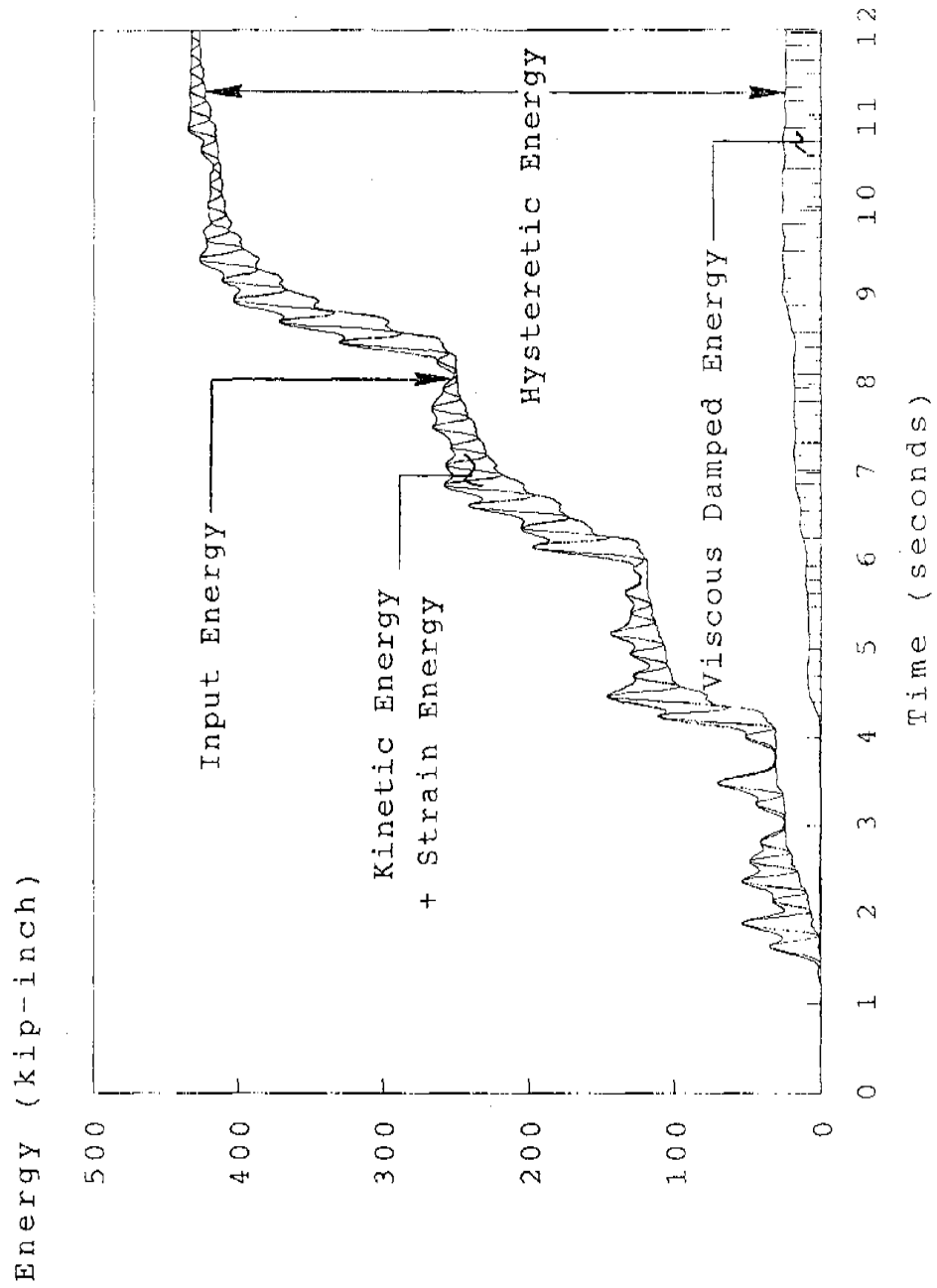
FIGURE 6.81 CBDS MO-65 ENERGY TIME HISTORIES
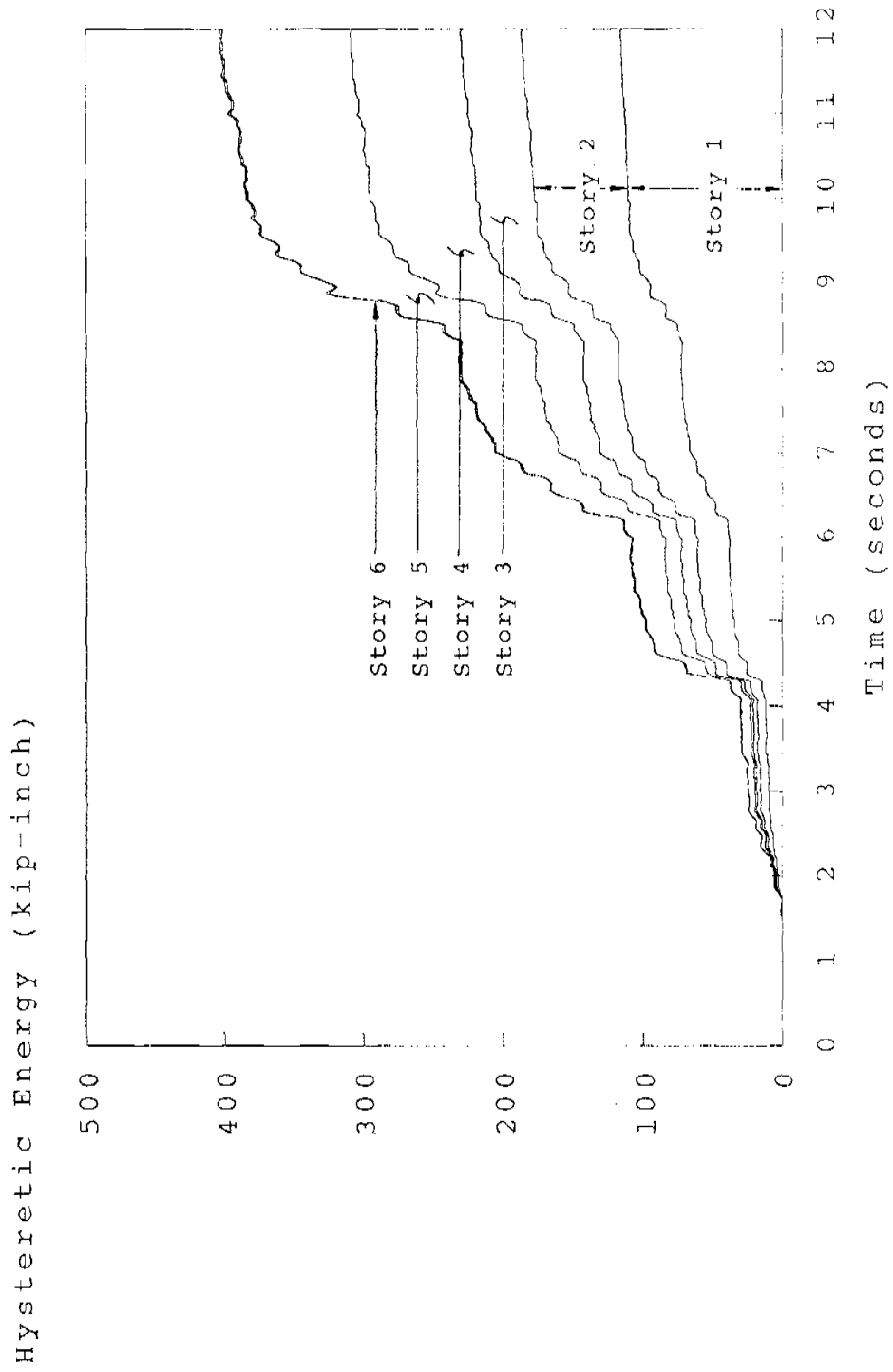
FIGURE 6.82 CBDS MO-65 HYSTERETIC ENERGY TIME HISTORIES
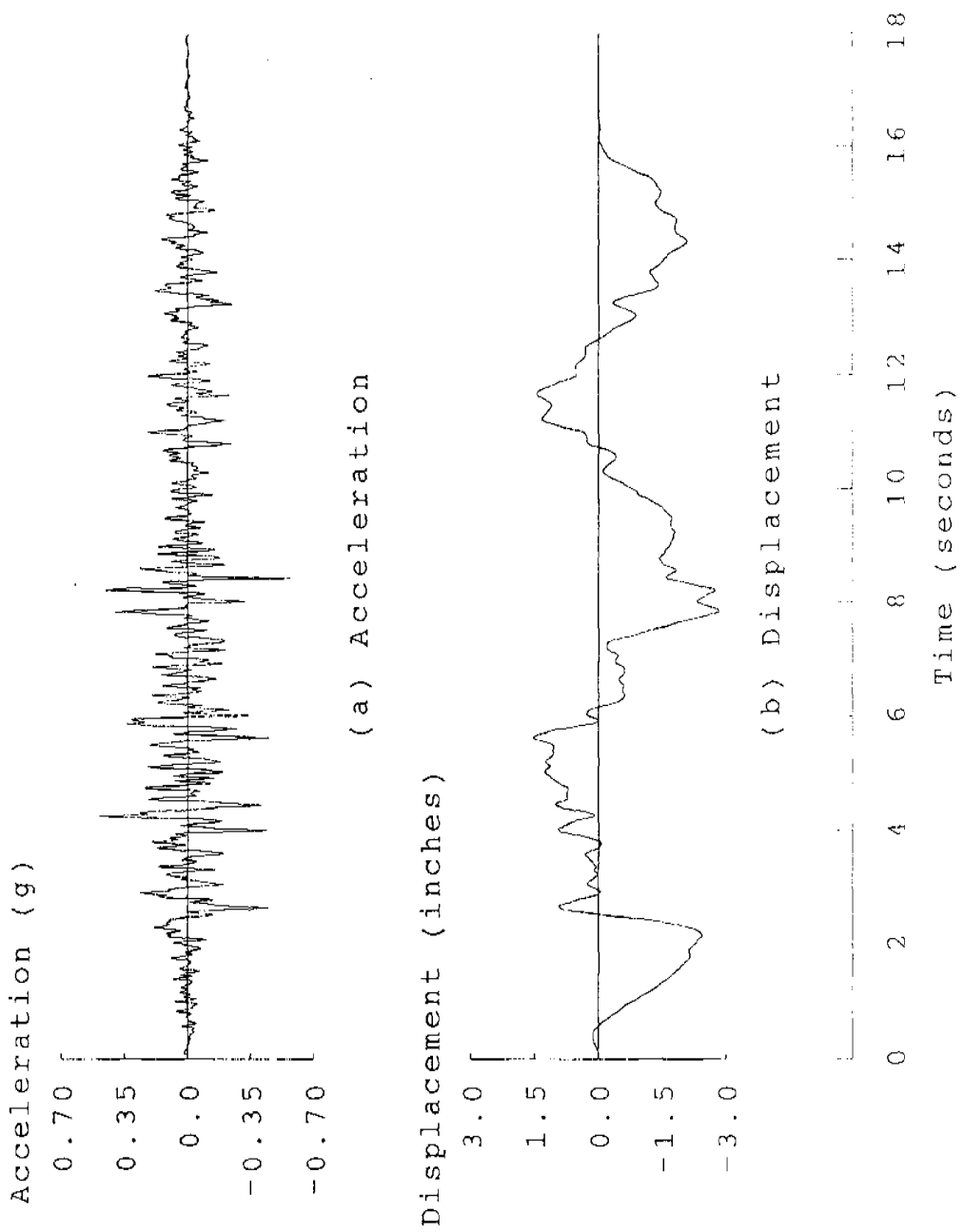
FIGURE 6.83 EBDS TAFT-57 INPUT CHARACTERISTICS

Pseudo-Velocity (inch/sec.)

Period (seconds)
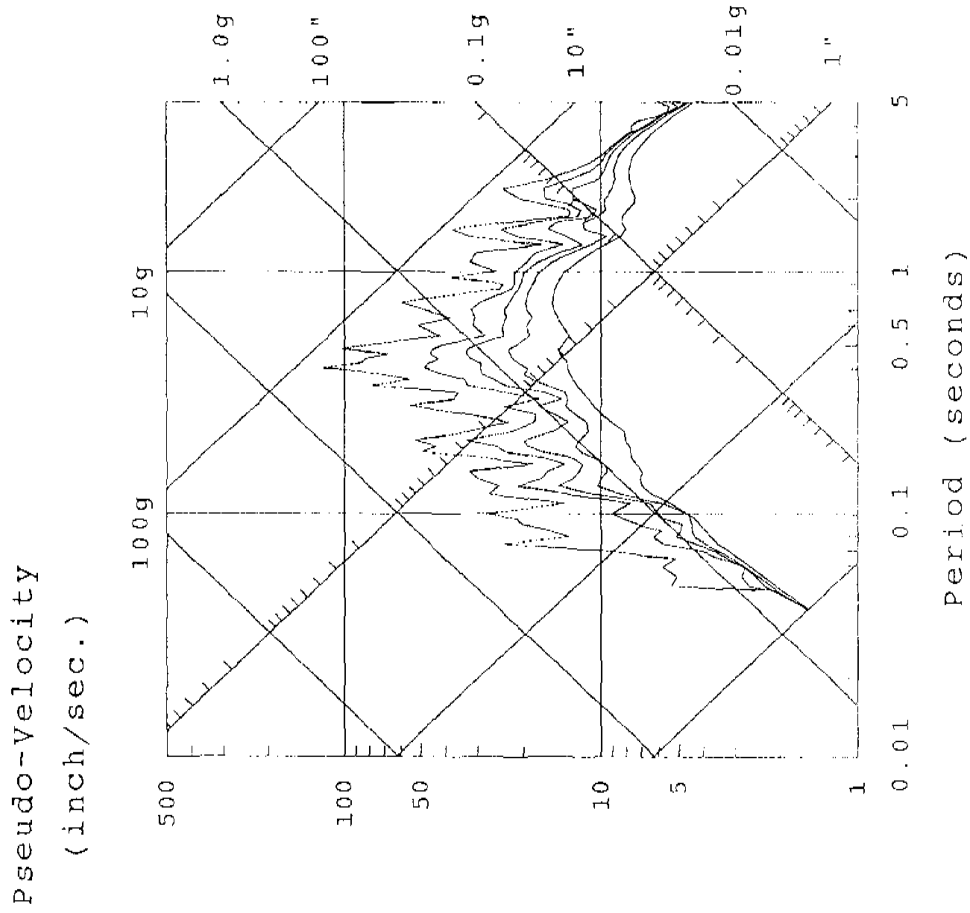
(c) Response Spectra (0,2,5,10,20 % Damping)

FIGURE 6.83 EBDS TAFT-57 INPUT CHARACTERISTICS

Displacement
(inches)
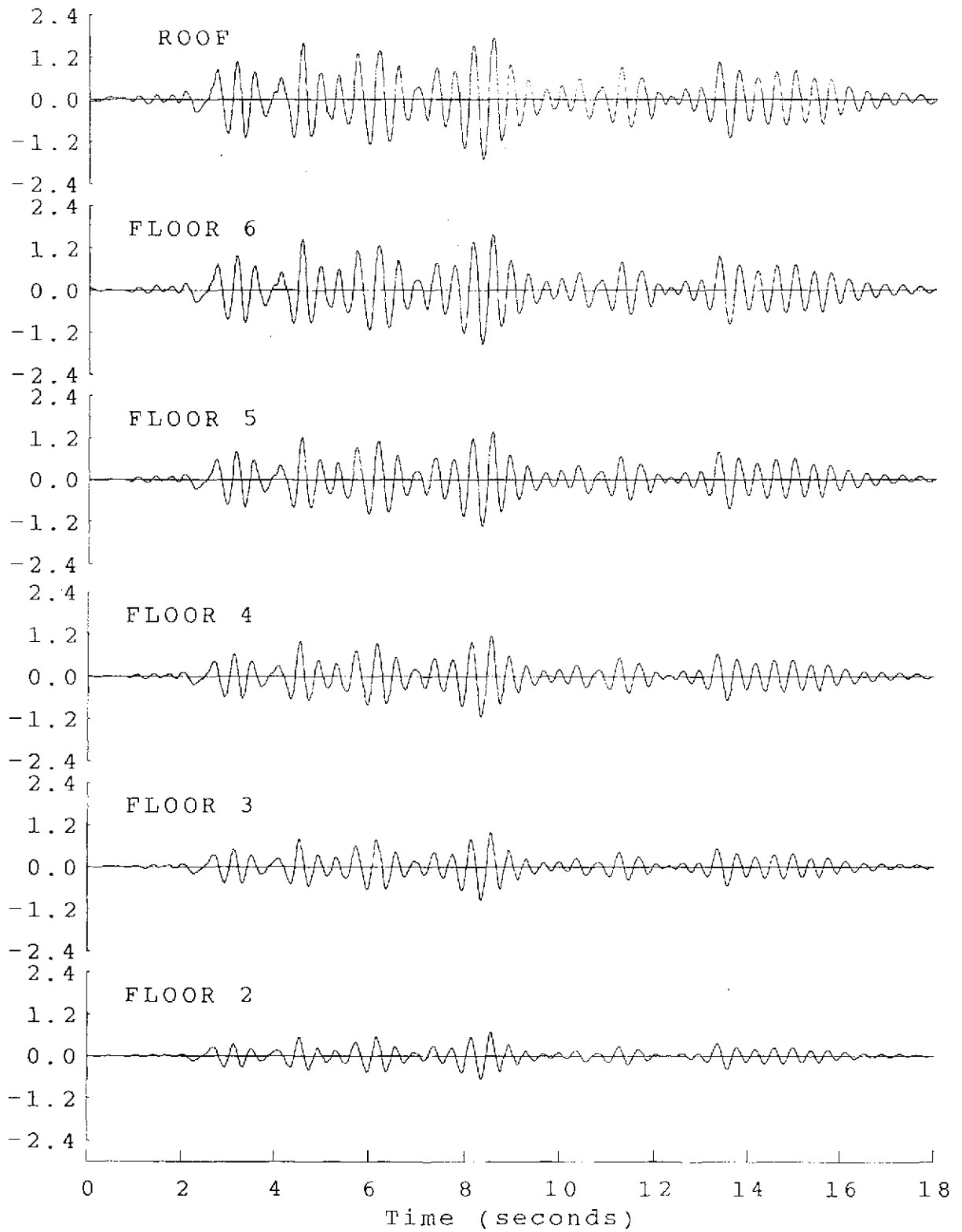
FIGURE 6.84 EBDS TAFT-57 LATERAL DISPLACEMENT TIME HISTORIES

Inter-story Drift
(inches)

Time (seconds)
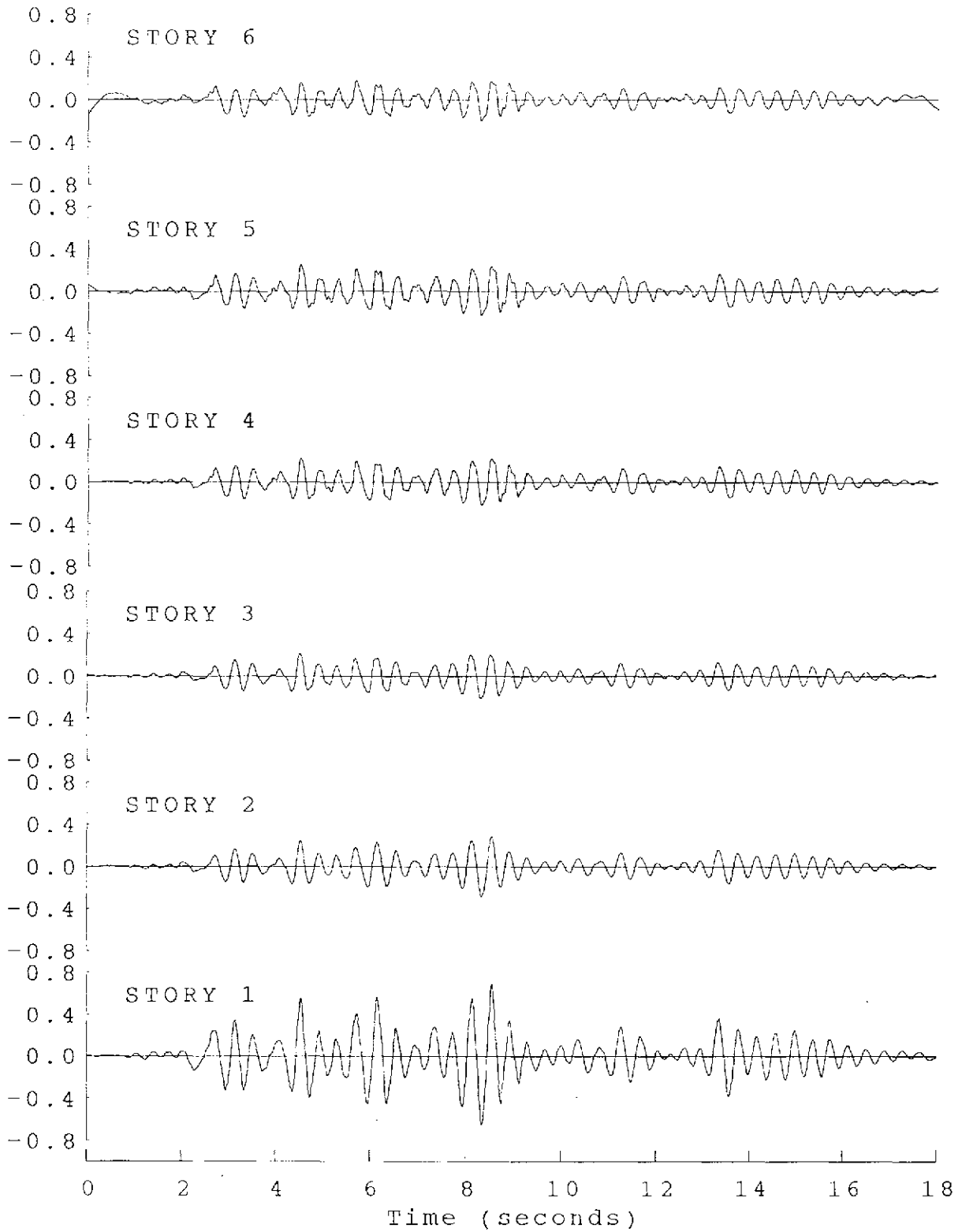
FIGURE 6.85 EBDS TAFT-57 INTER-STORY DRIFT TIME HISTORIES
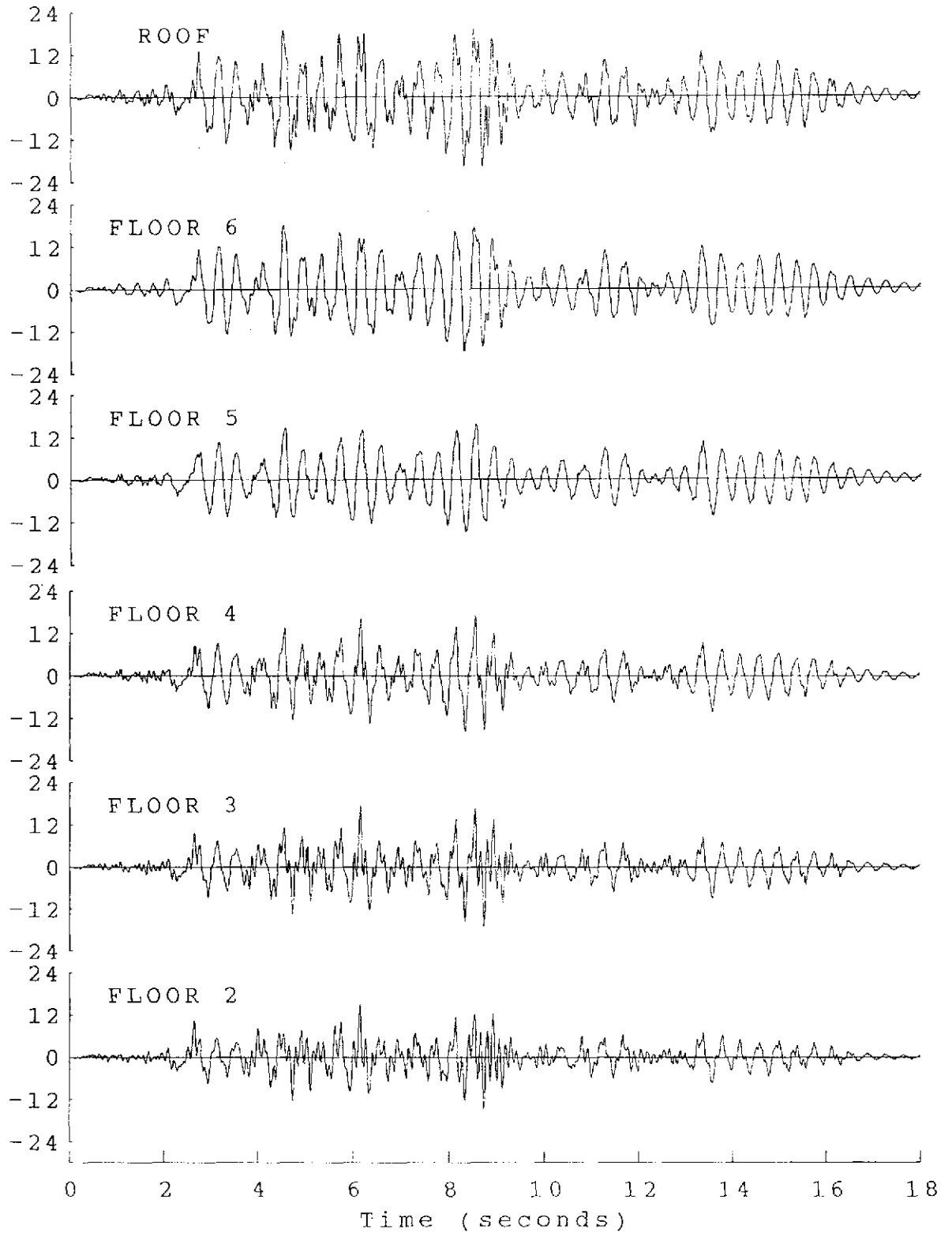
FIGURE 6.86 EBDS TAFT-57 INERTIA FORCE TIME HISTORIES
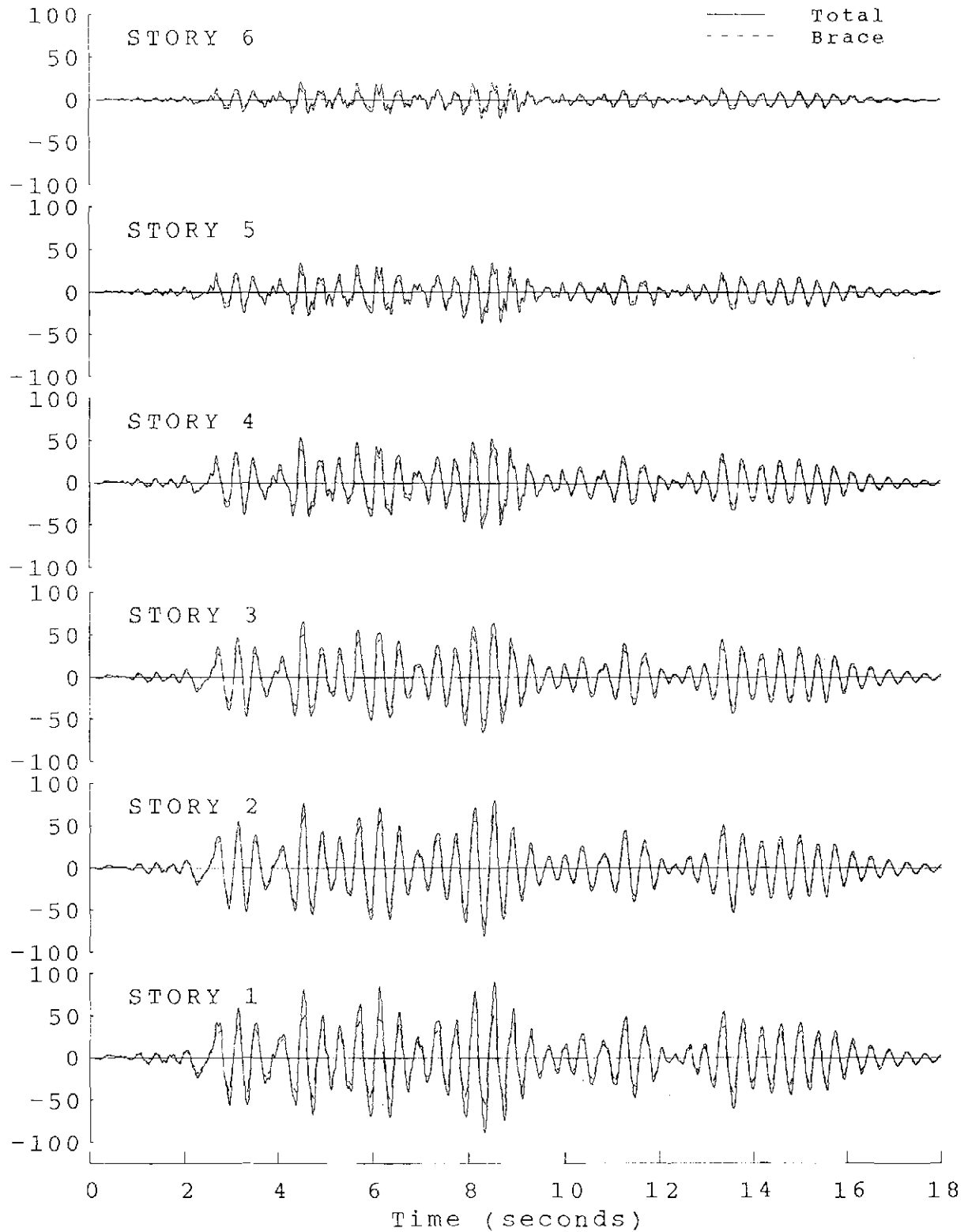
Story Shear
(kips)

FIGURE 6.87 EBDS TAFT-57 STORY SHEAR TIME HISTORIES

O/T Moment (kip-in)

Time (seconds)
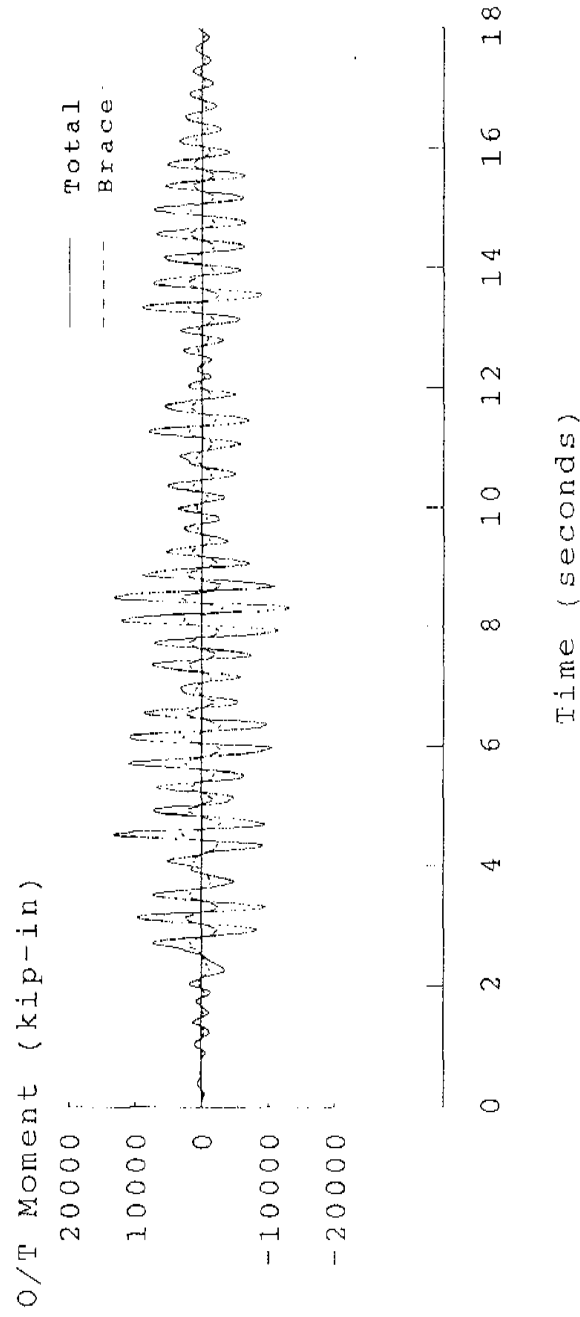
Total
Brace

FIGURE 6.88 EBDS TAFT-57 OVERTURNING MOMENT TIME HISTORIES
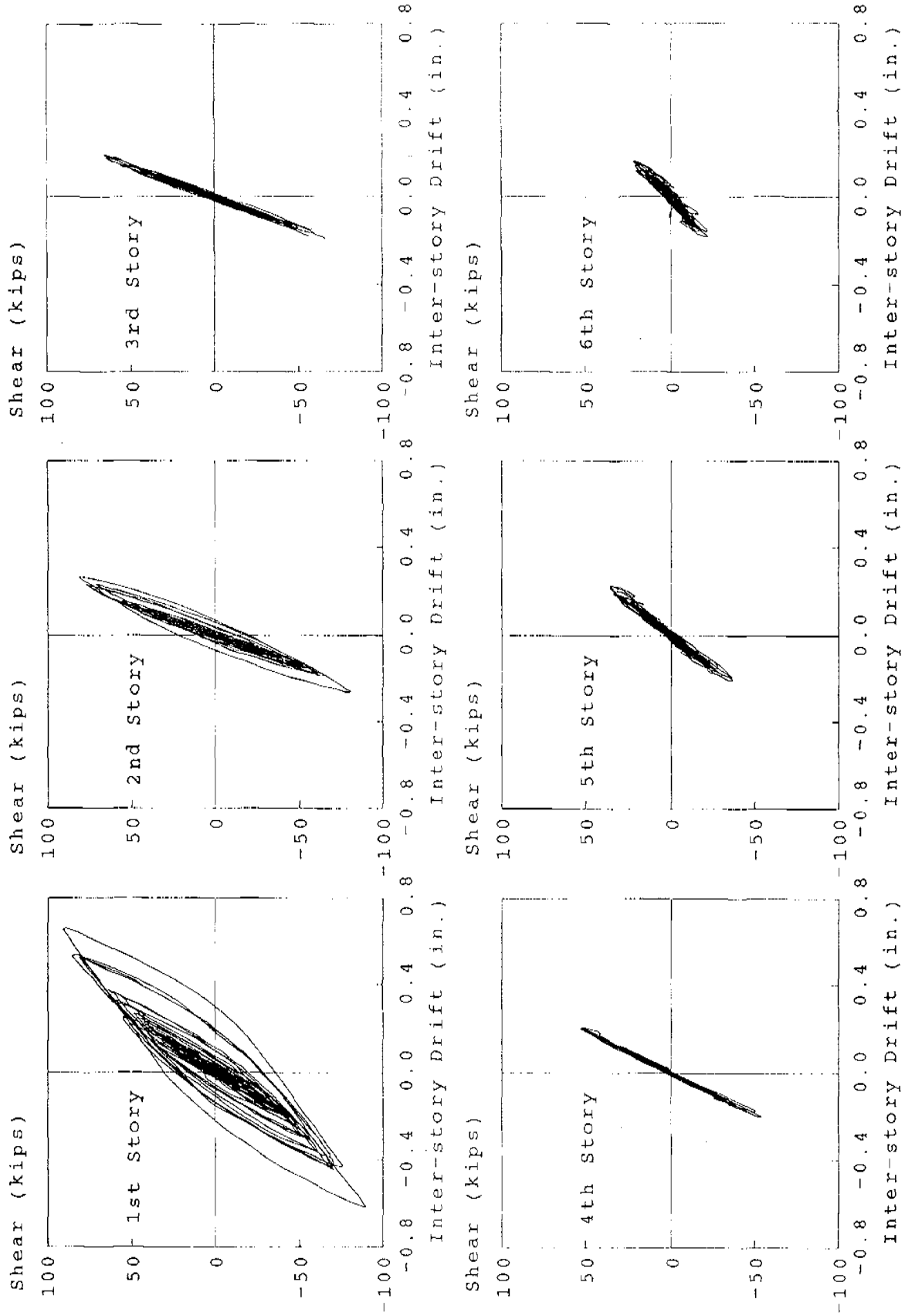
FIGURE 6.89 EBDS TAFT-57 TOTAL STORY SHEAR AND INTER-STORY DRIFT RELATIONSHIPS
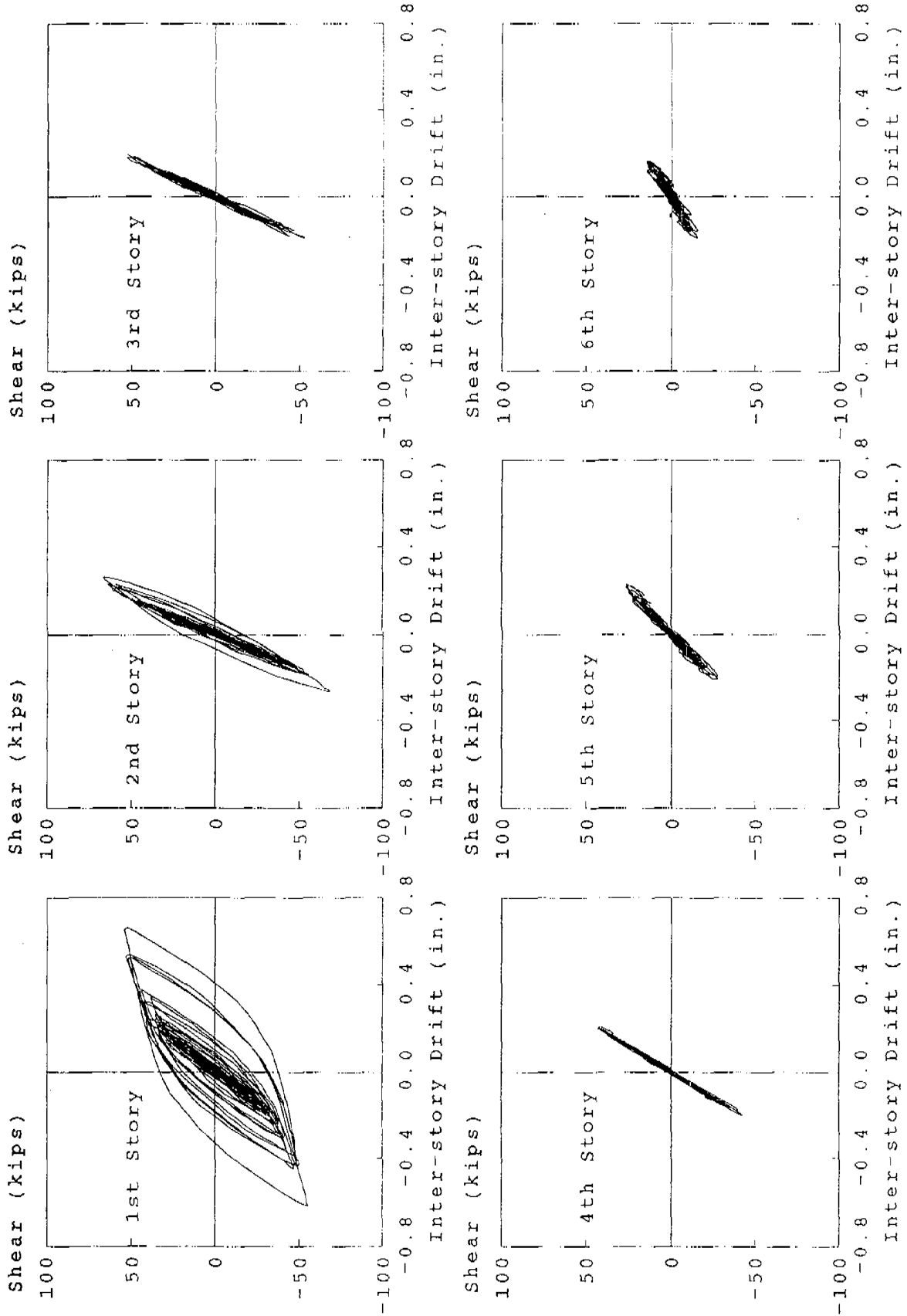
FIGURE 6.90 EBDS TAFT-57 BRACE STORY SHEAR AND INTER-STORY DRIFT RELATIONSHIPS
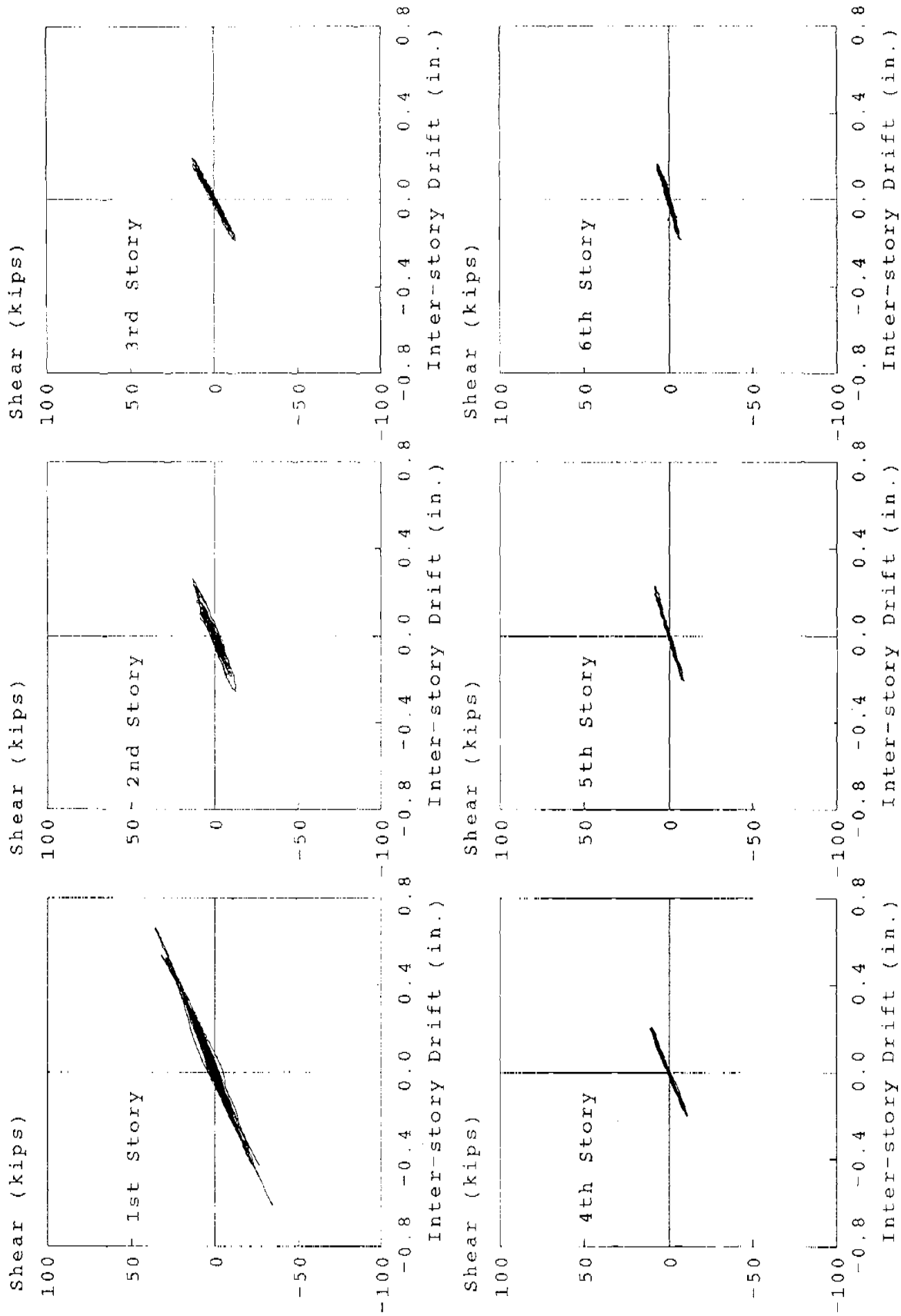
FIGURE 6.91 EBDS TAFT-57 DMRSF STORY SHEAR AND INTER-STORY DRIFT RELATIONSHIPS
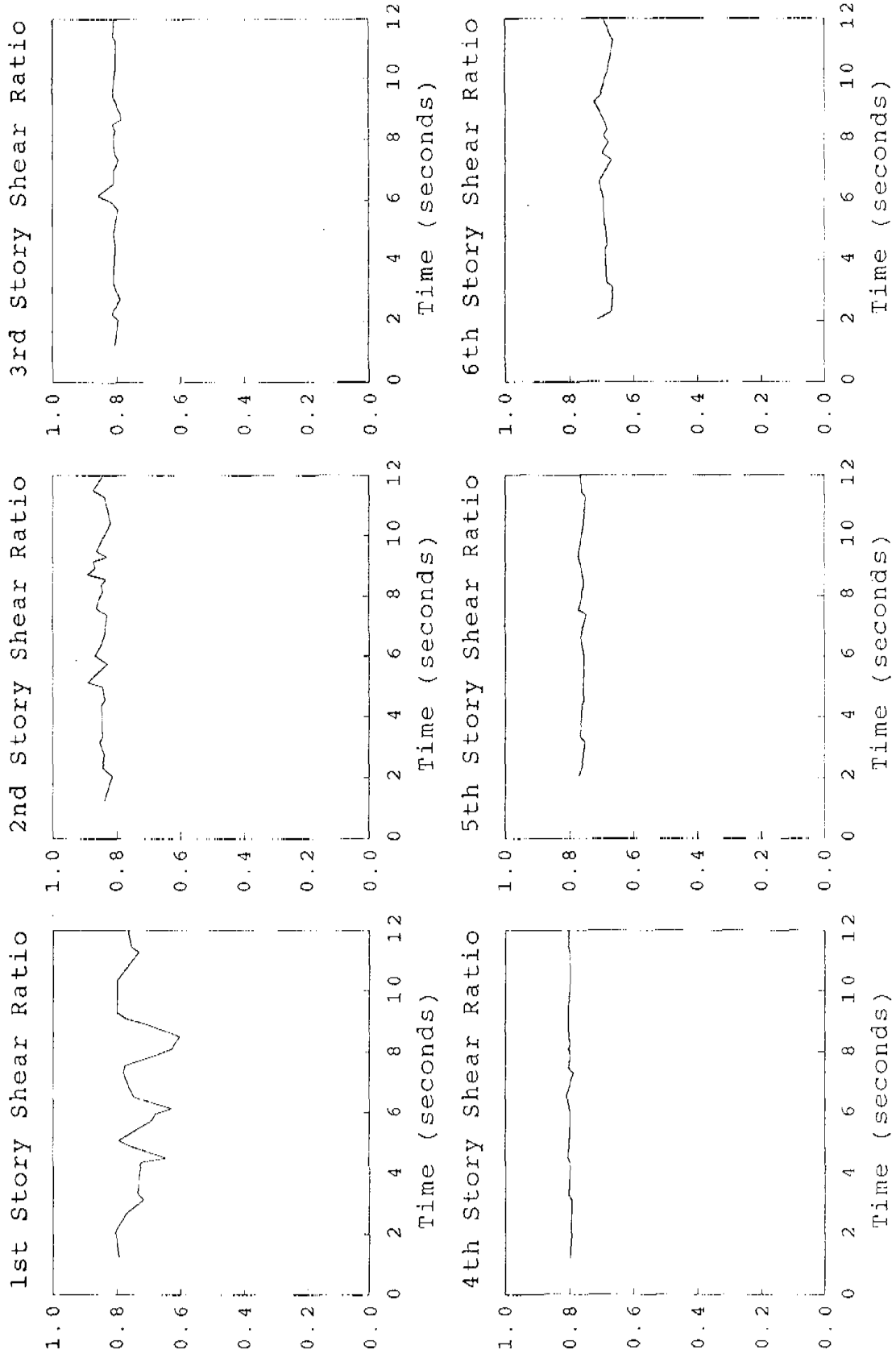
FIGURE 6.92 EBDS TAFT-57 STORY SHEAR RATIOS
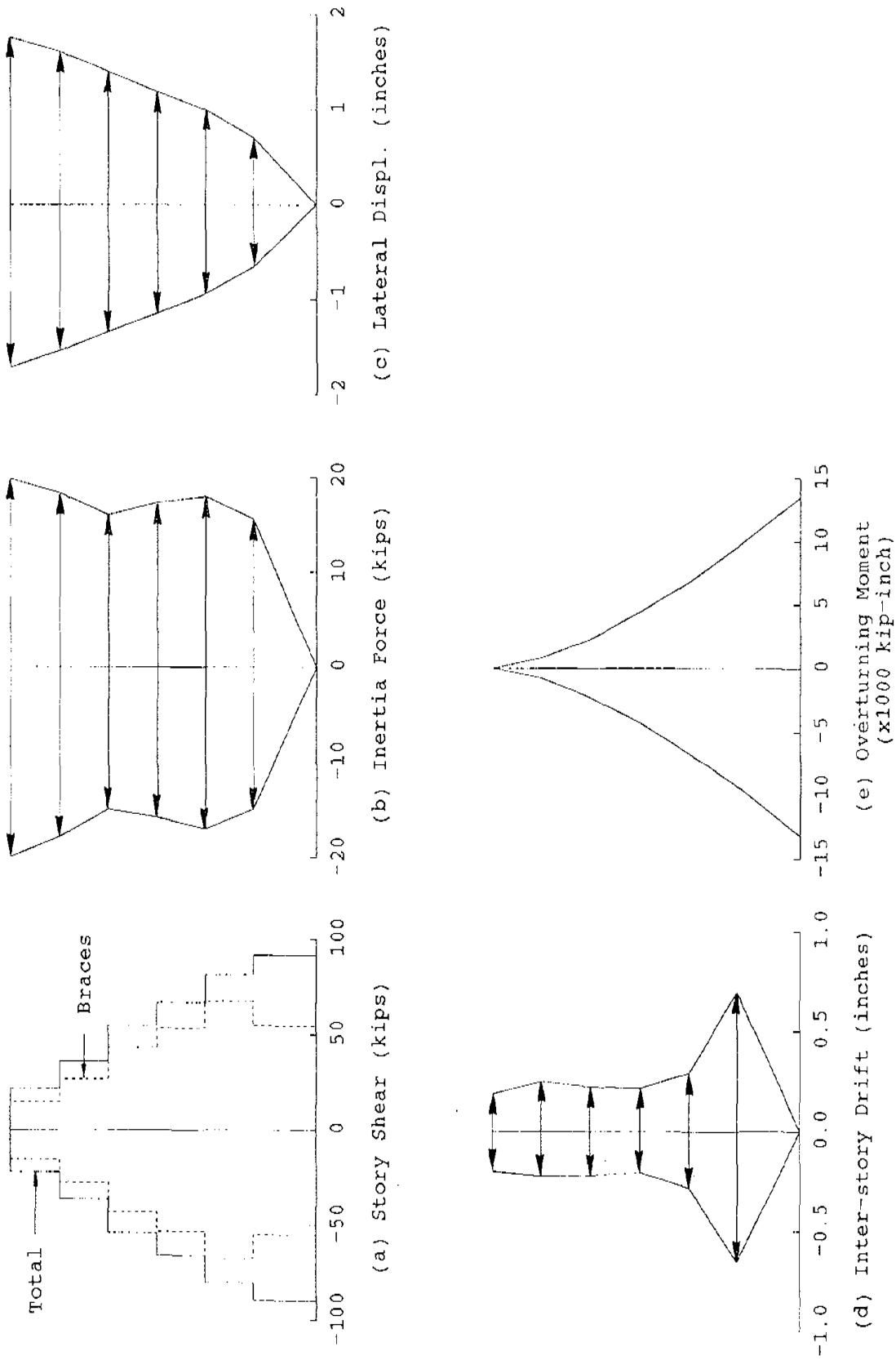
FIGURE 6.93 EBDS TAFT-57 RESPONSE ENVELOPES

(a) Story Shear (kips)

(b) Inertia Force (kips)

(c) Lateral Displ. (inches)

(d) Inter-story Drift (inches)

(e) Overturning Moment (x1000 kip-inch)

Braces

Total

At Maximum Base Shear

(a) Lateral Displ. (inches) (b) Inertia Force (kips) (c) Story Shear (kips) (d) Overturning Moment (x1000 kip-inch)

At Maximum Roof Displacement

(a) Lateral Displ. (inches) (b) Inertia Force (kips) (c) Story Shear (kips) (d) Overturning Moment (x1000 kip-inch)
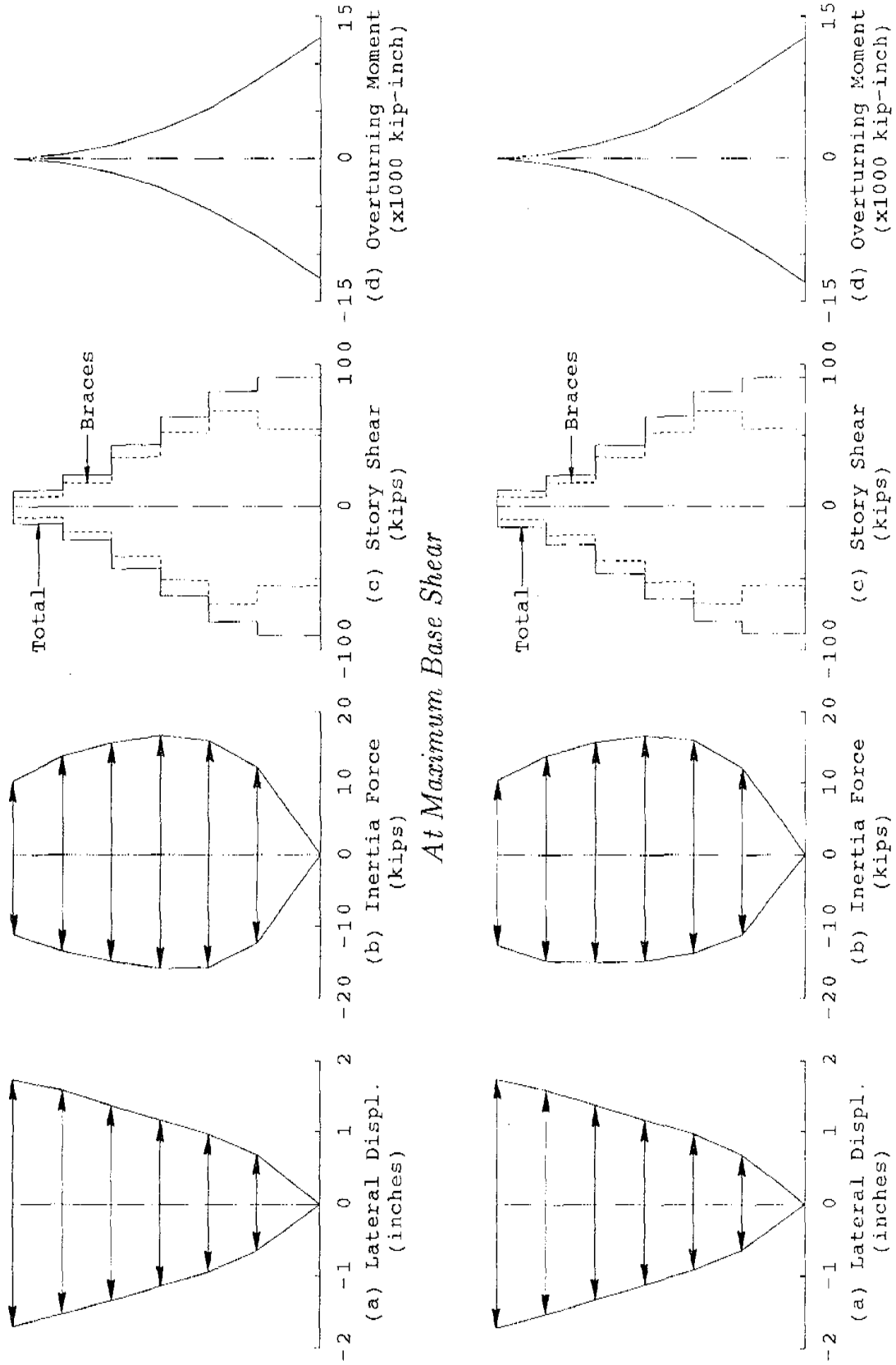
FIGURE 6.94 EBDS TAFT-57 RESPONSE PROFILES AT MAXIMUM RESPONSES

(a) Eccentric Braces (kips)   (b) DMRSF (kips)   (c) Total (kips)

At Maximum Base Shear

(a) Eccentric Braces (kips)   (b) DMRSF (kips)   (c) Total (kips)
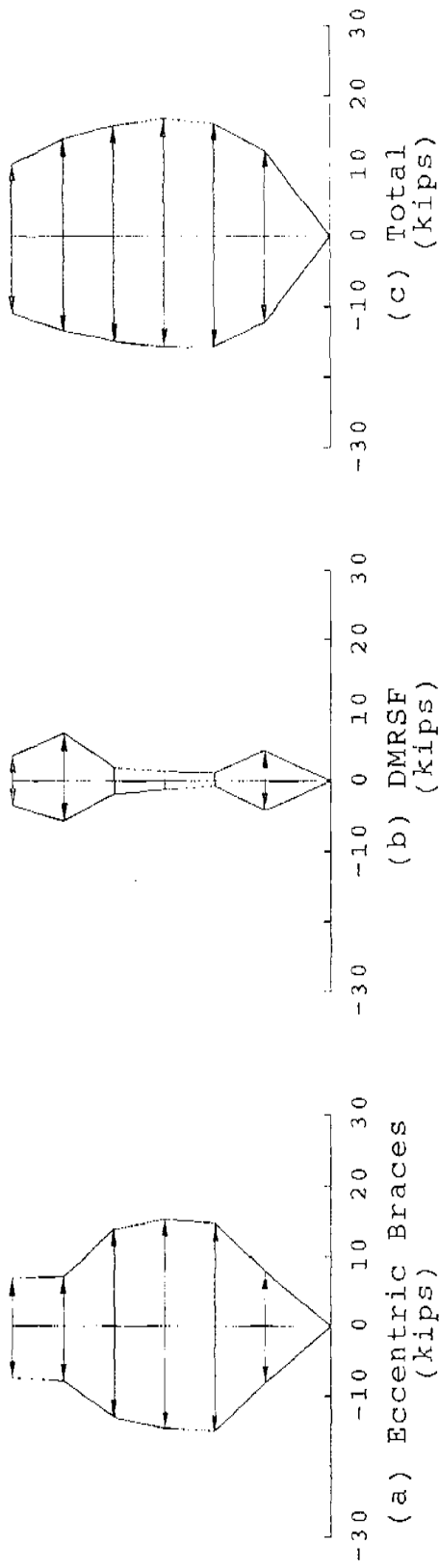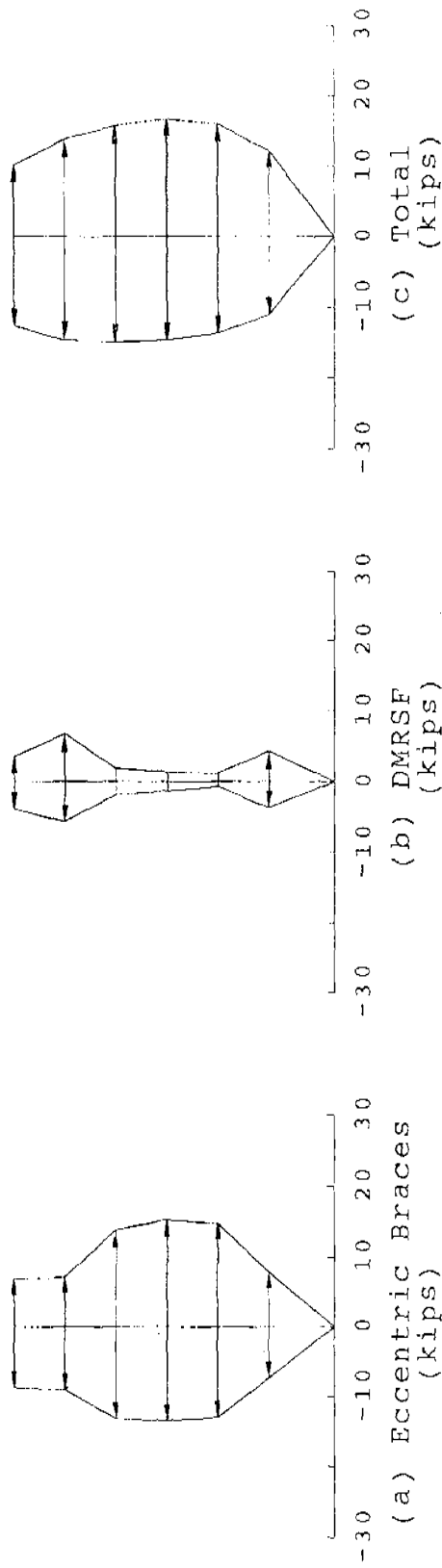
At Maximum Roof Displacement

FIGURE 6.95 EBDS TAFT-57 LATERAL FORCE DISTRIBUTIONS AT MAXIMUM RESPONSES
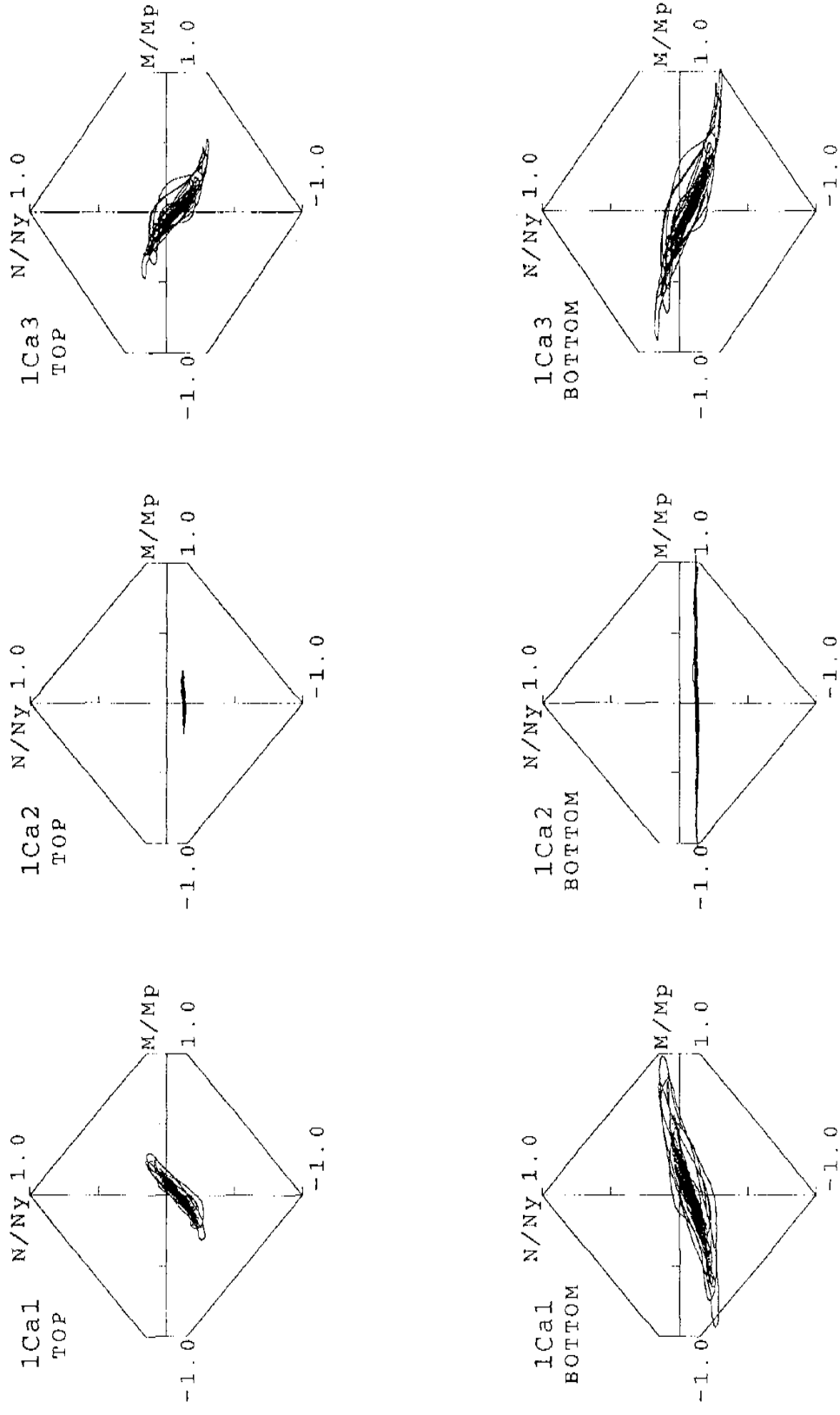
FIGURE 6.96 EBDS TAFT-57 FIRST STORY COLUMN AXIAL FORCE AND END MOMENT
INTERACTION CURVES (FRAME A)
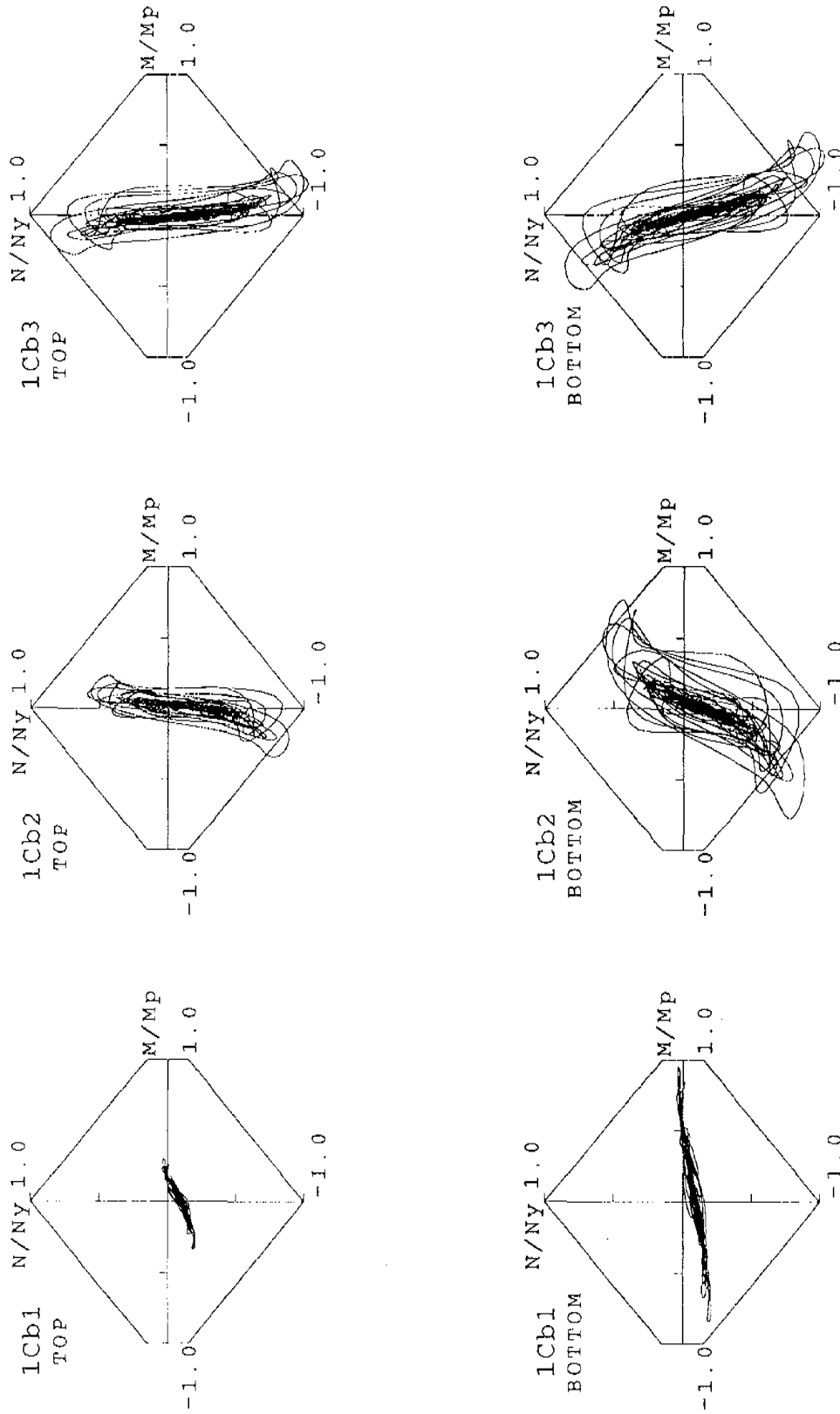
FIGURE 6.97 EBDS TAFT-57 FIRST STORY COLUMN AXIAL FORCE AND END MOMENT
INTERACTION CURVES (FRAME B)
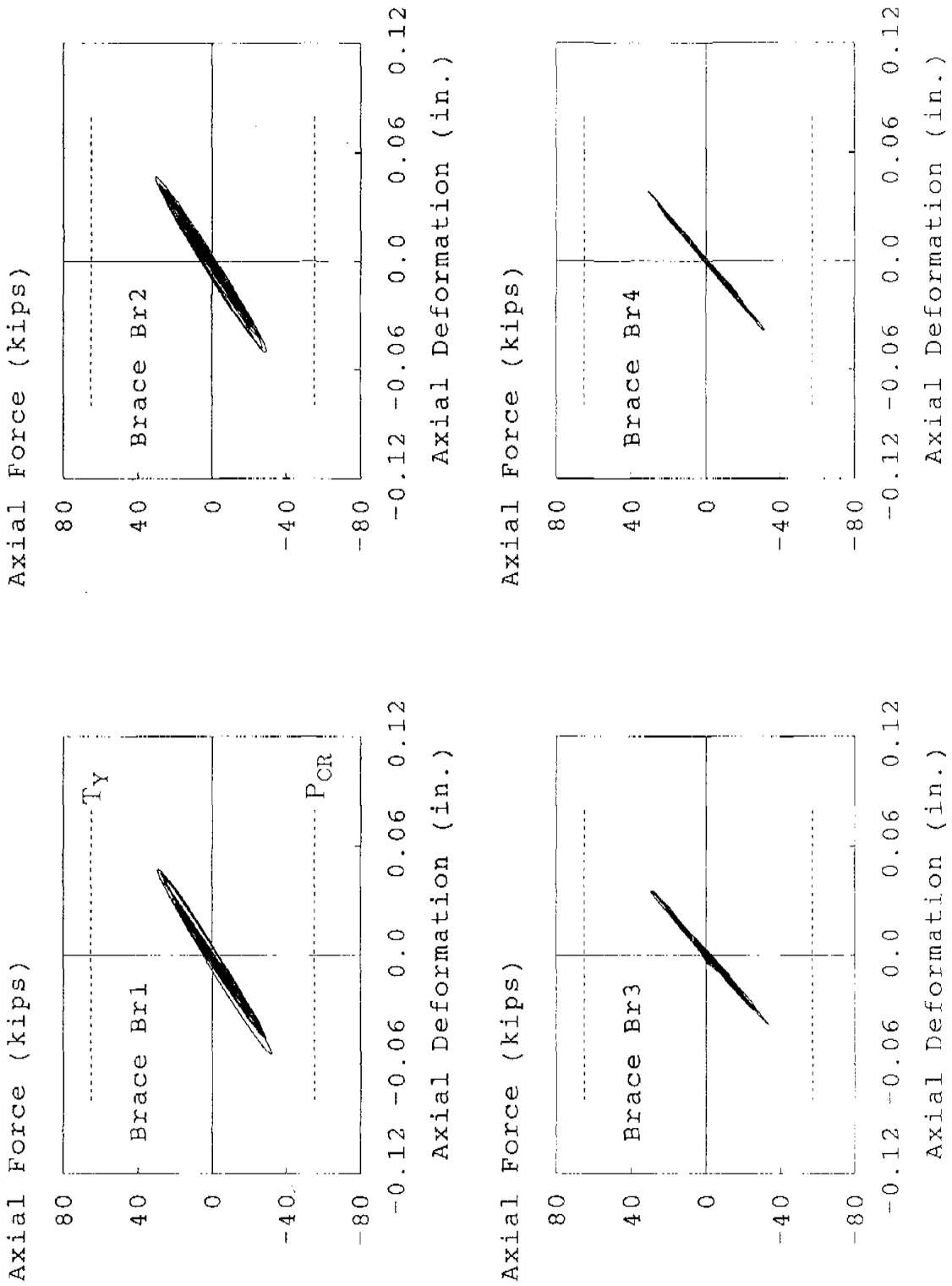
FIGURE 6.98 EBDS TAFT-57 BRACE FORCE AND DEFORMATION RELATIONSHIPS
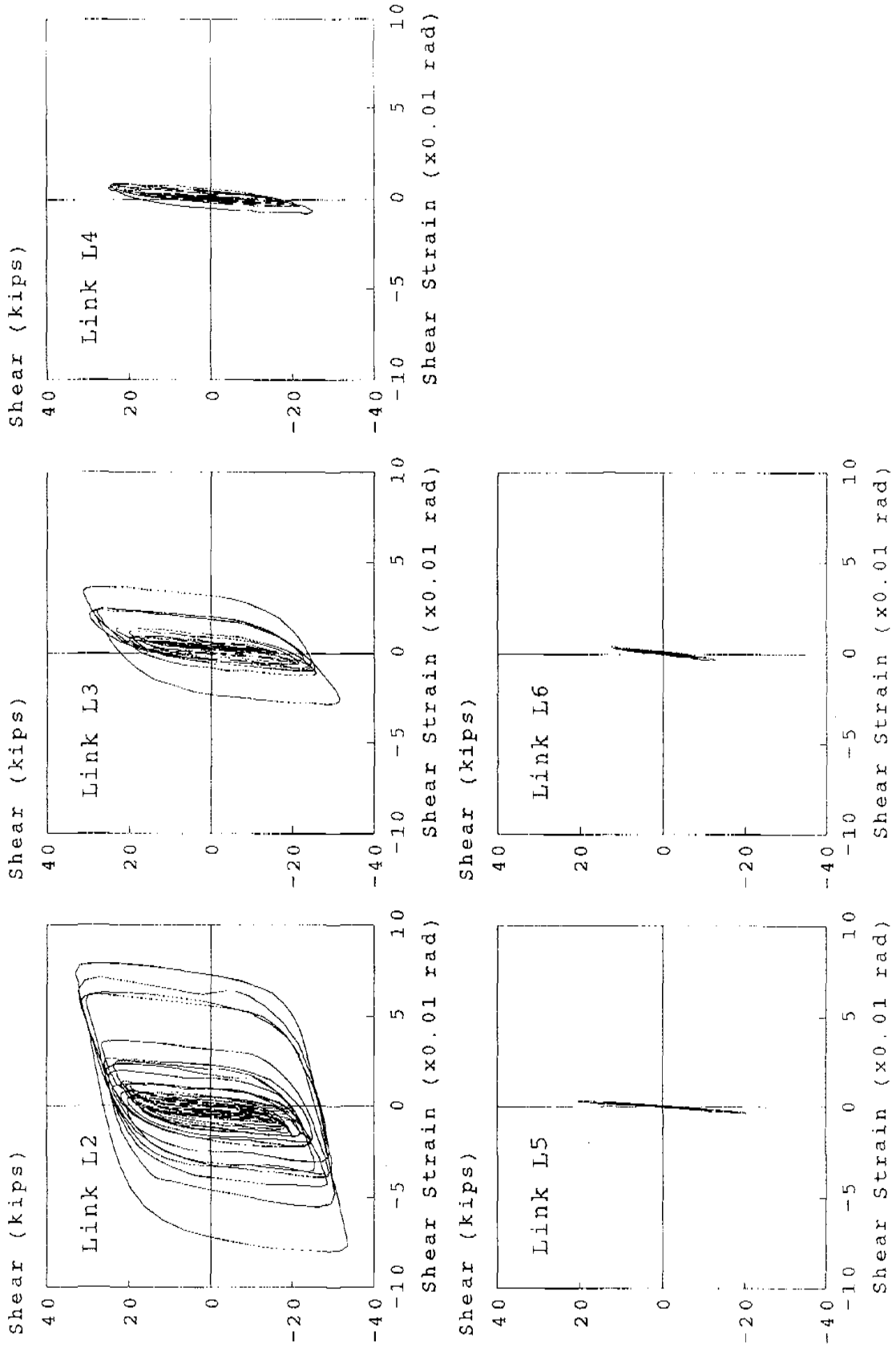
FIGURE 6.99 EBDS TAFT-57 LINK SHEAR FORCE AND SHEAR STRAIN RELATIONSHIPS
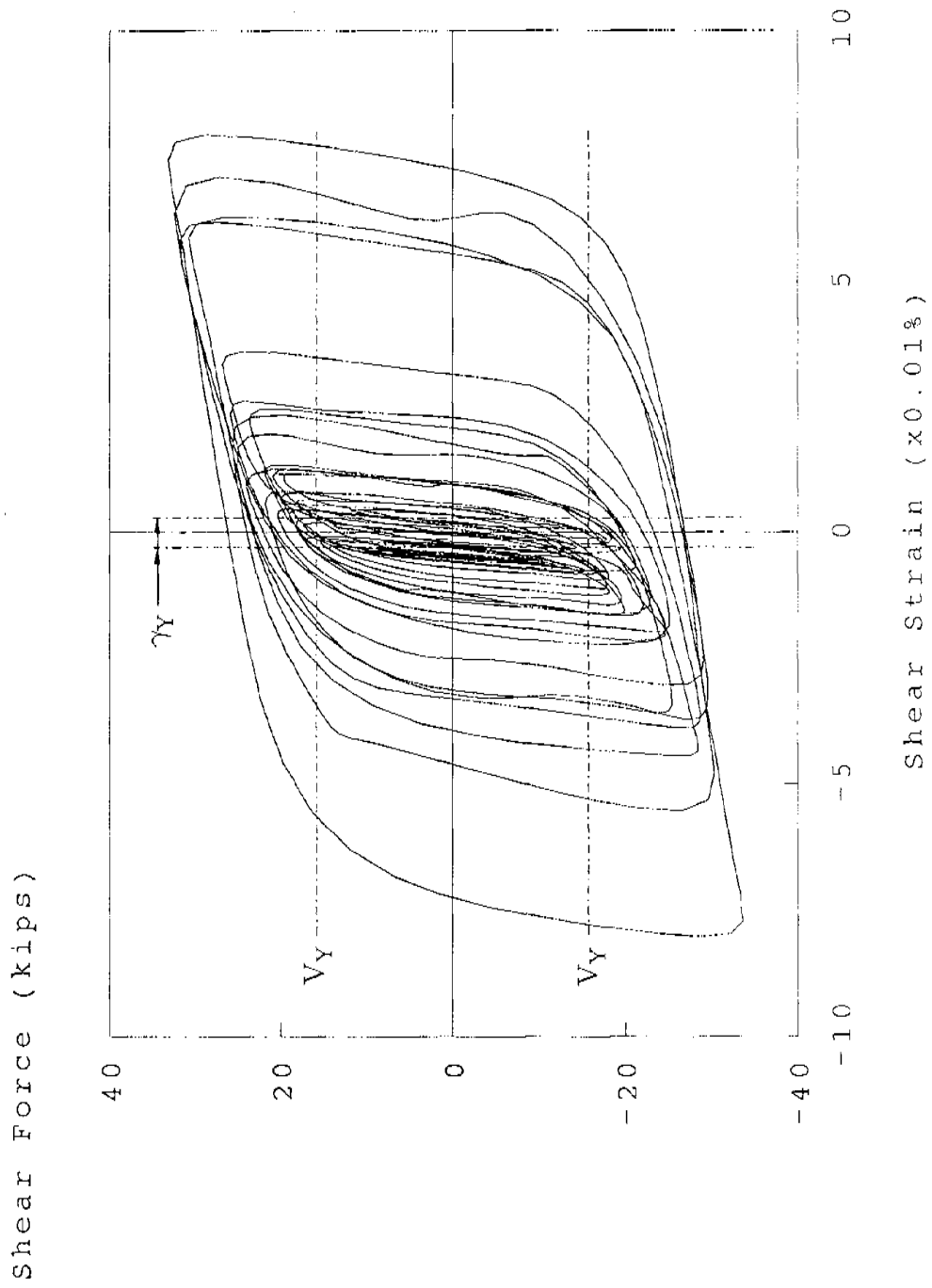
FIGURE 6.100 EBDS TAFT-57 LINK L2 SHEAR FORCE AND SHEAR STRAIN RELATIONSHIP
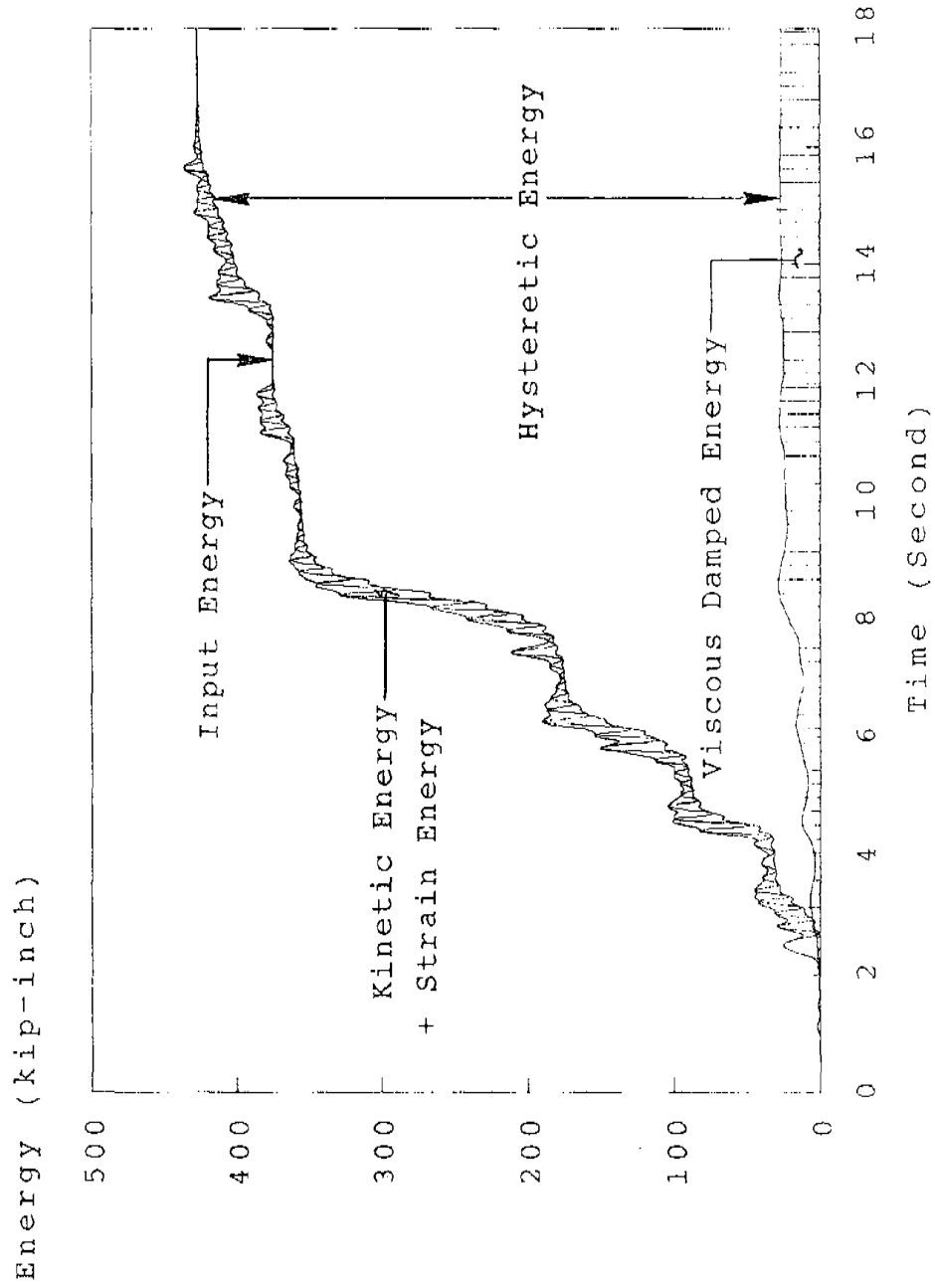
FIGURE 6.101 EBDS TAFT-57 ENERGY TIME HISTORIES
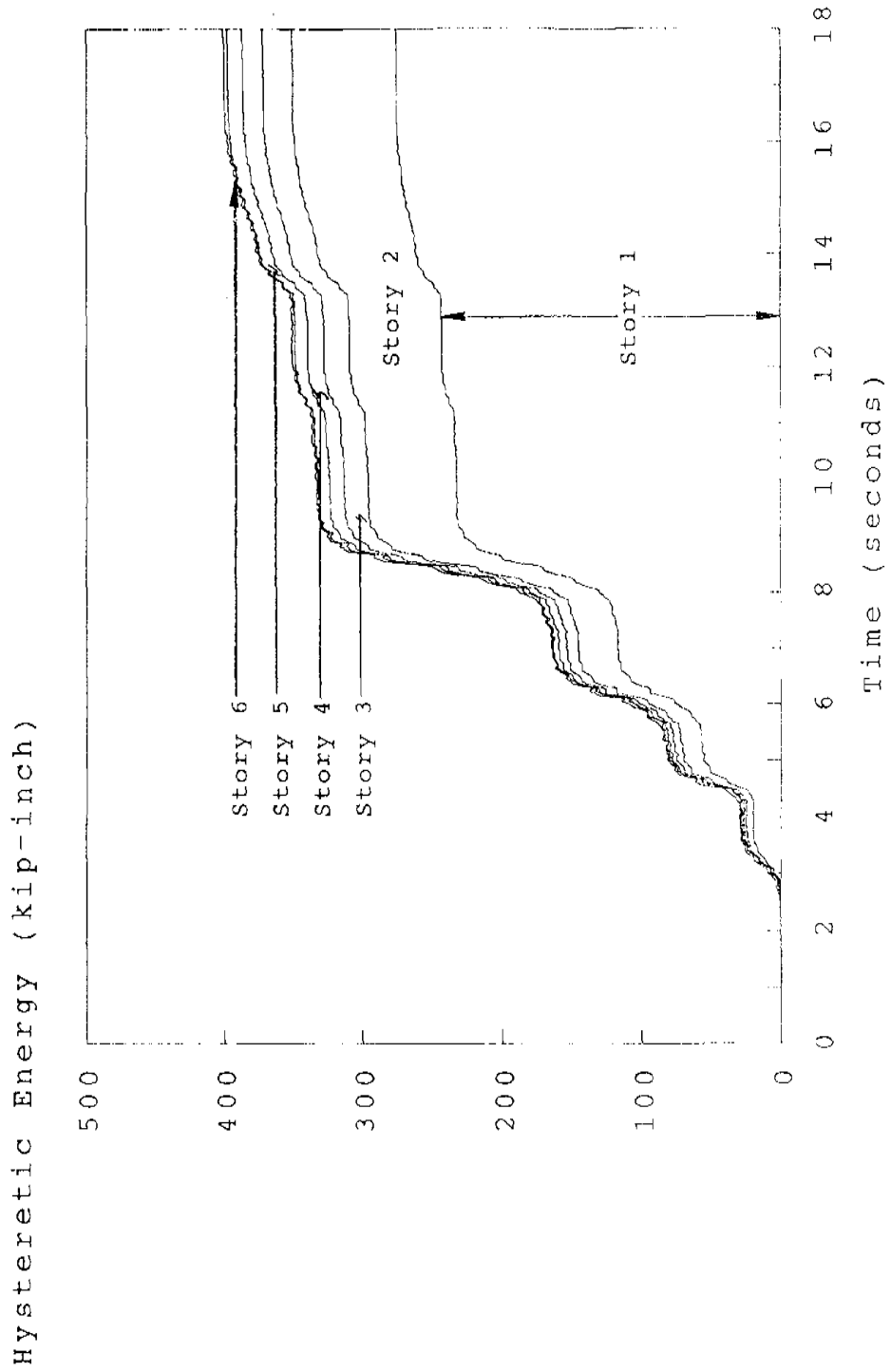
FIGURE 6.102 EBDS TAFT-57 HYSTERETIC ENERGY TIME HISTORIES

Link Energy (kip-inch)
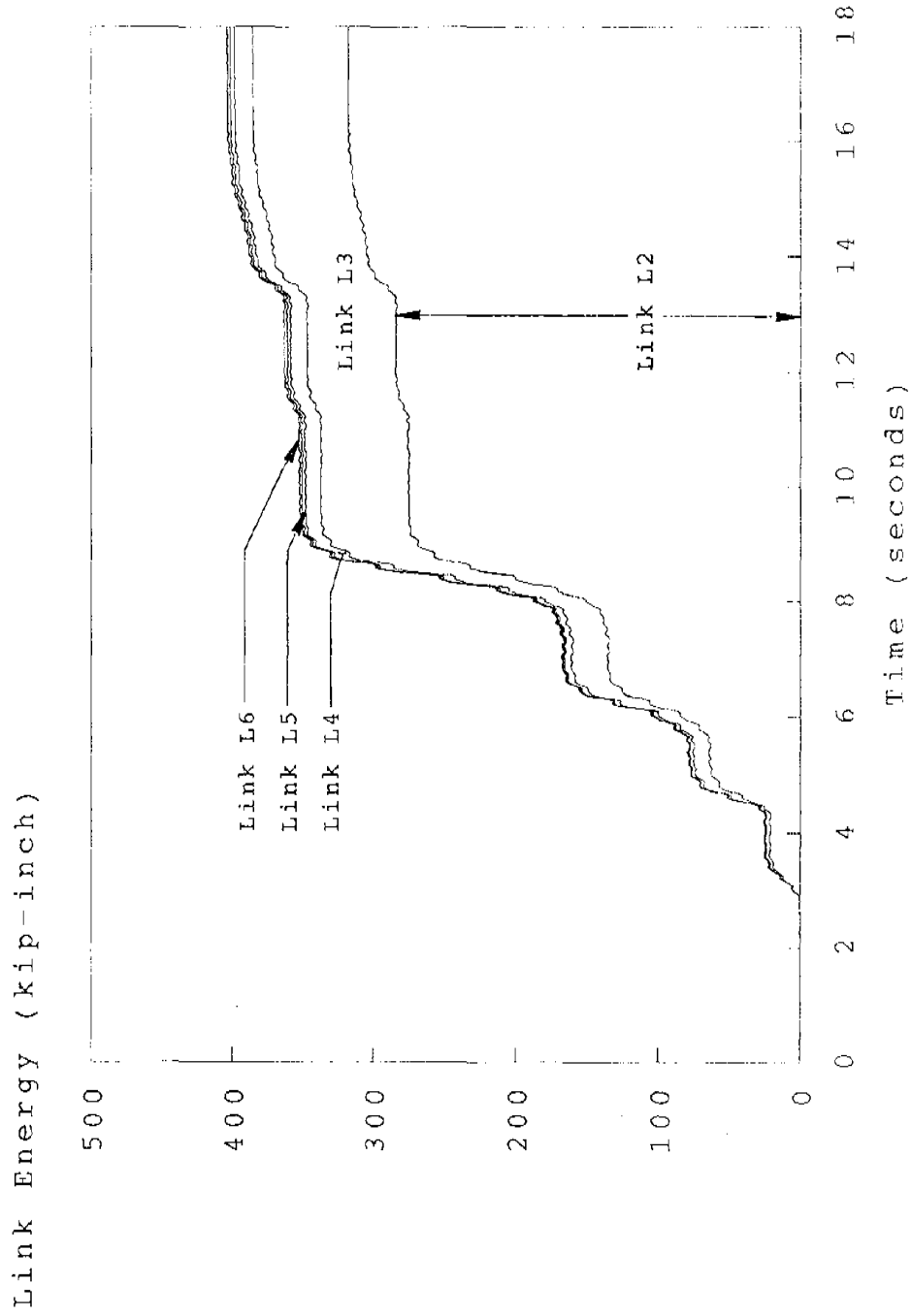
FIGURE 6.103 EBDS TAFT-57 LINK ENERGY TIME HISTORIES
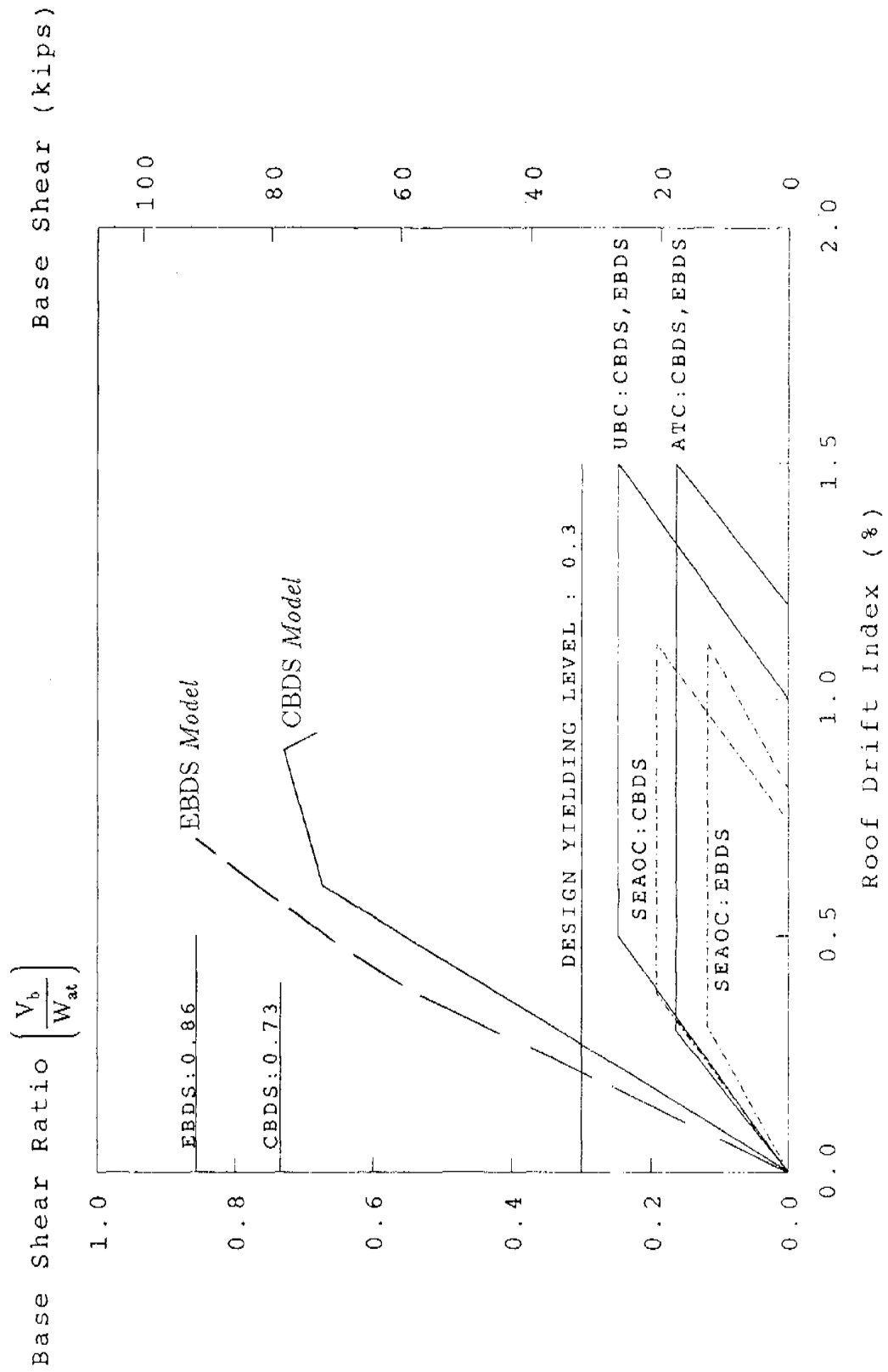
FIGURE 7.1 CBDS AND EBDS BASE SHEAR RATIO VERSUS ROOF DRIFT INDEX
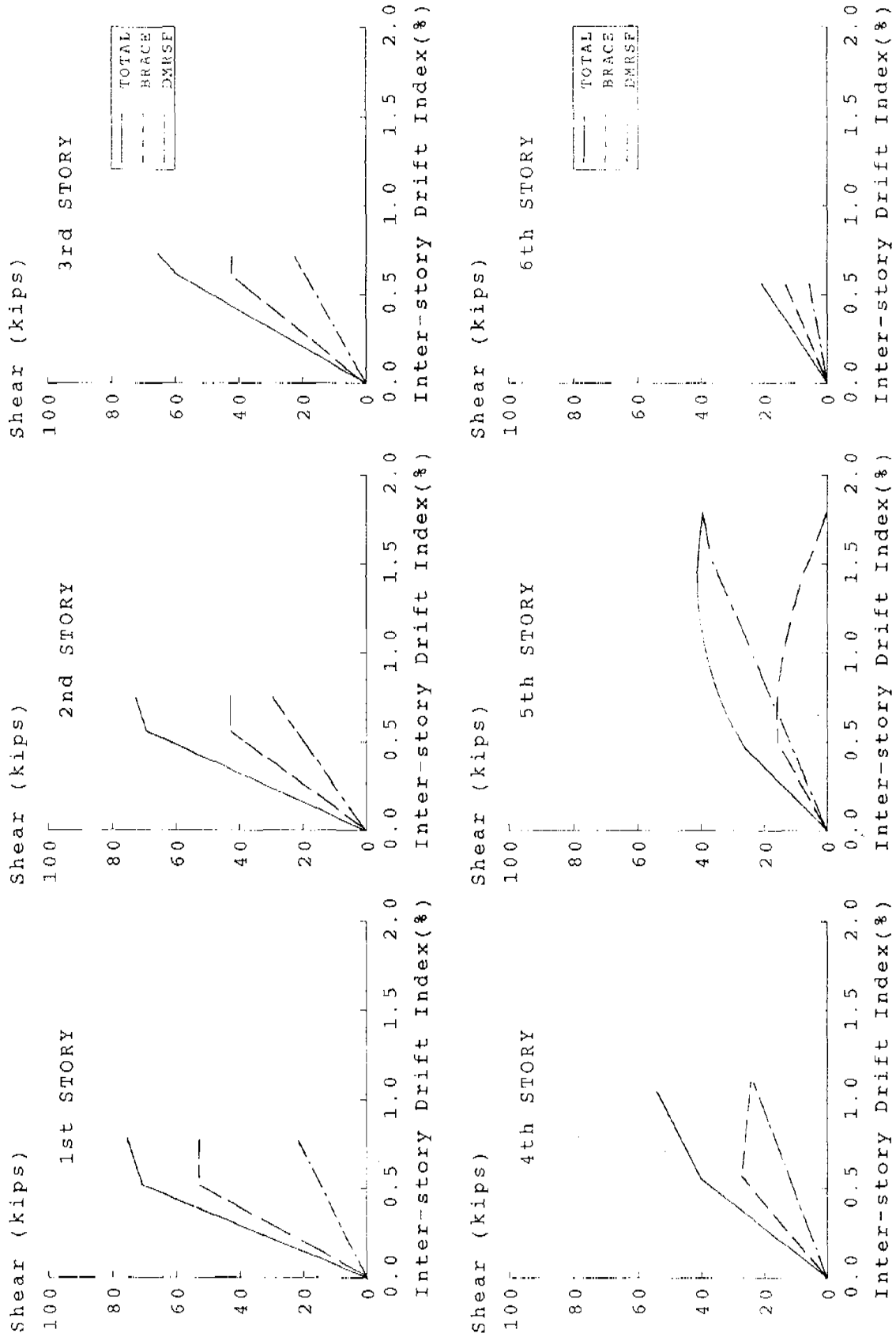
FIGURE 7.2 CBDS STORY SHEAR AND INTER-STORY DRIFT INDEX ENVELOPES
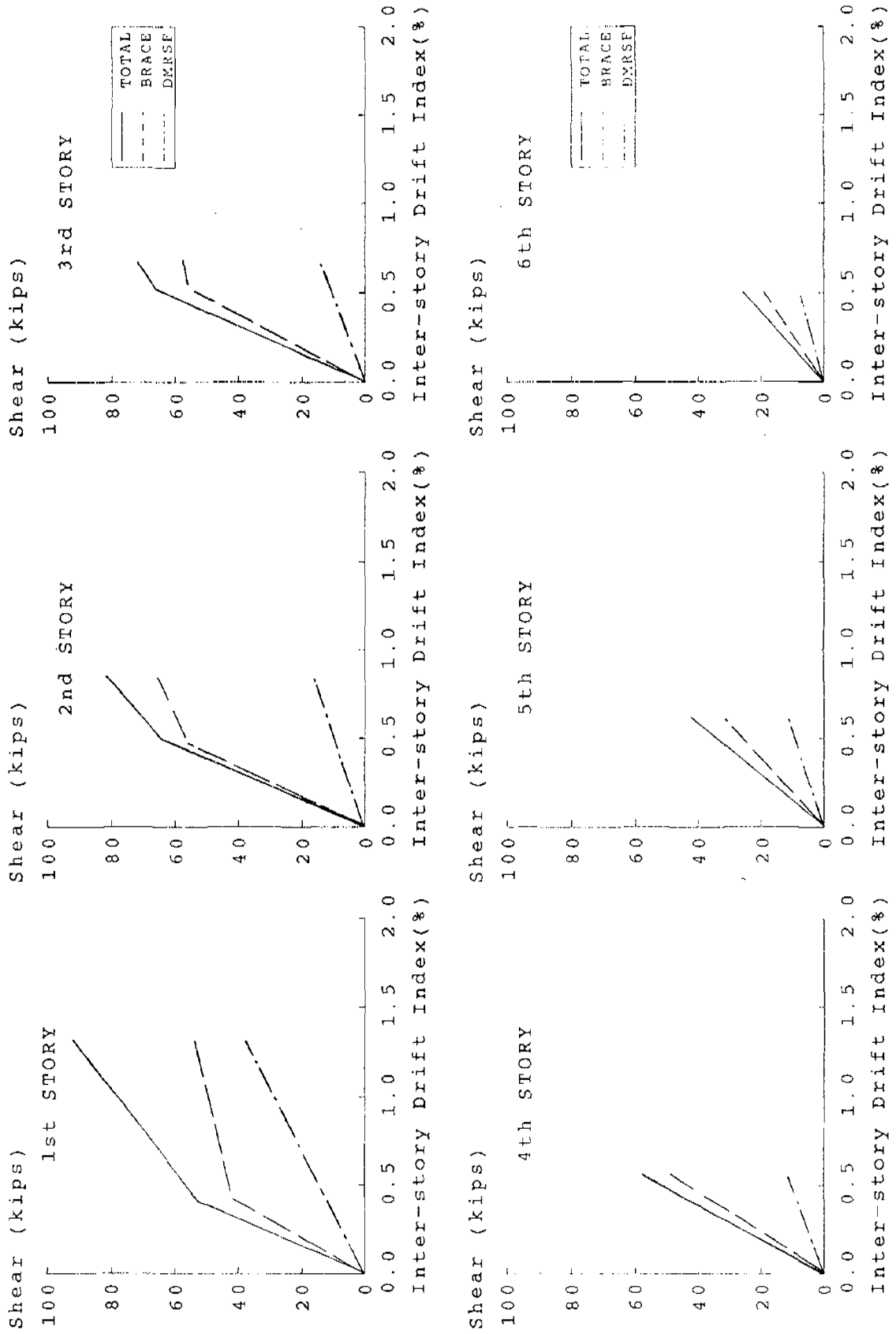
FIGURE 7.3 EBDS STORY SHEAR AND INTER-STORY DRIFT INDEX ENVELOPES
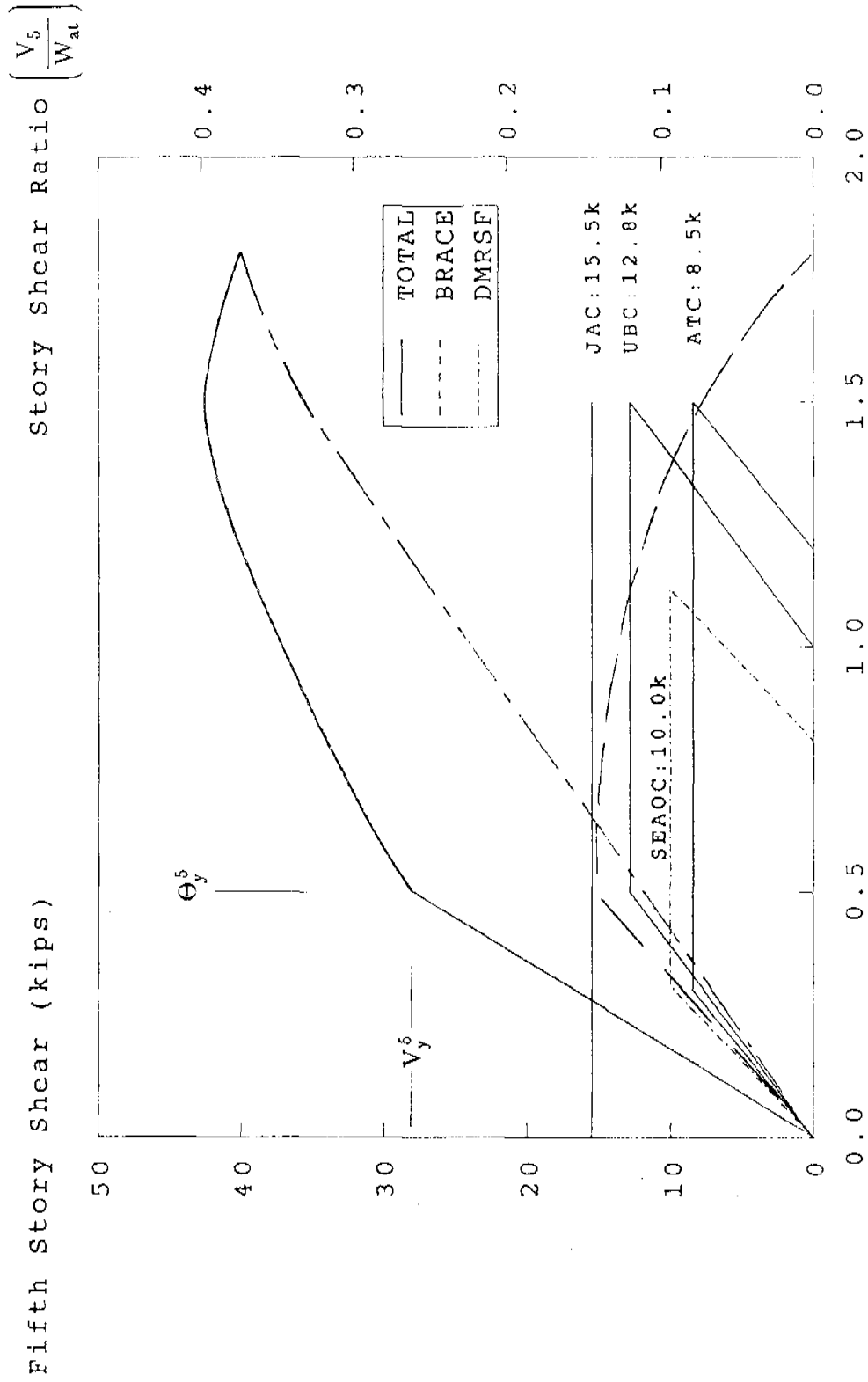
FIGURE 7.4 CBDS FIFTH STORY STRENGTH ENVELOPE
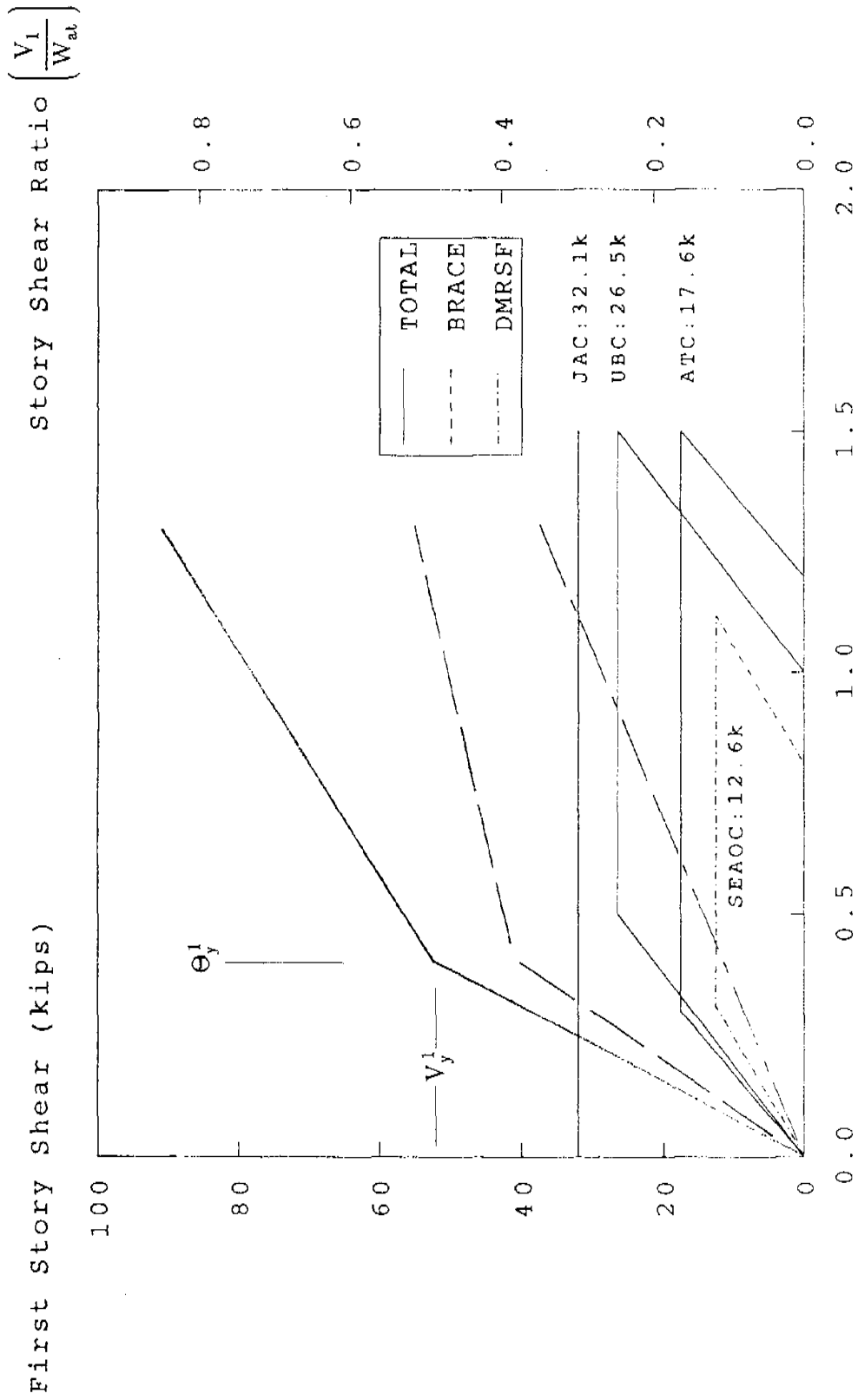
FIGURE 7.5 EBDS FIRST STORY STRENGTH ENVELOPE
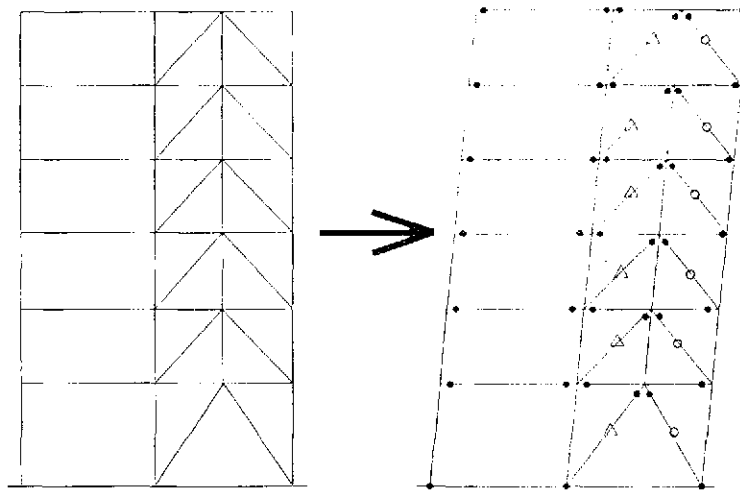
(a) Concentrically Braced Frame
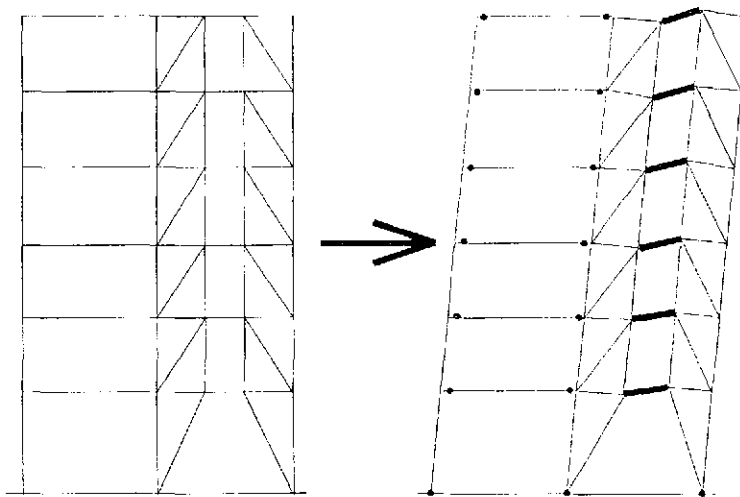
(b) Eccentrically Braced Frame

△ Tension Yielding   • Plastic Hinge

○ Buckling   — Shear Hinge

FIGURE 7.6 CBDS AND EBDS OPTIMIZATION SCHEMES
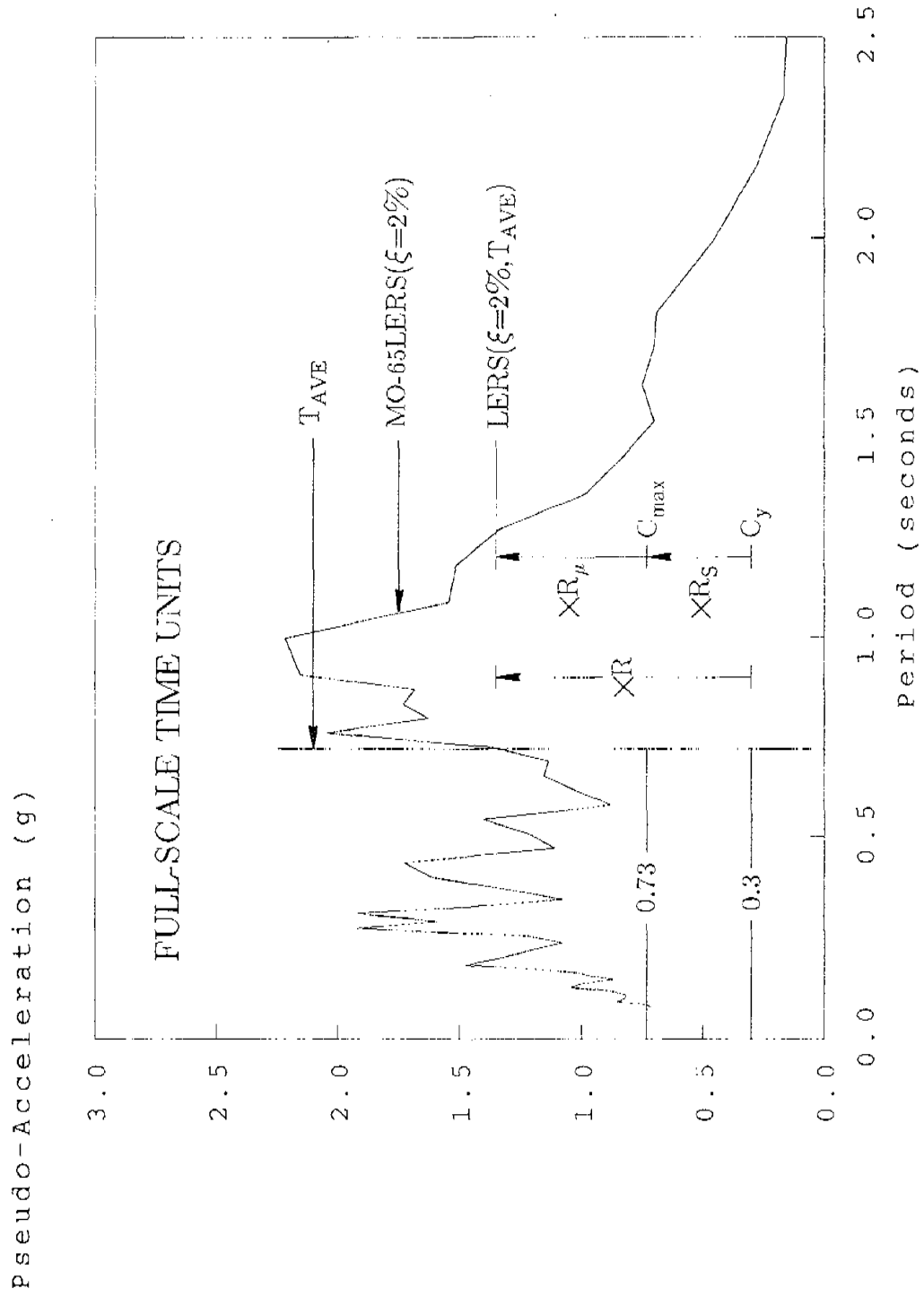
FIGURE 7.7 CBDS RESPONSE MODIFICATION FACTORS
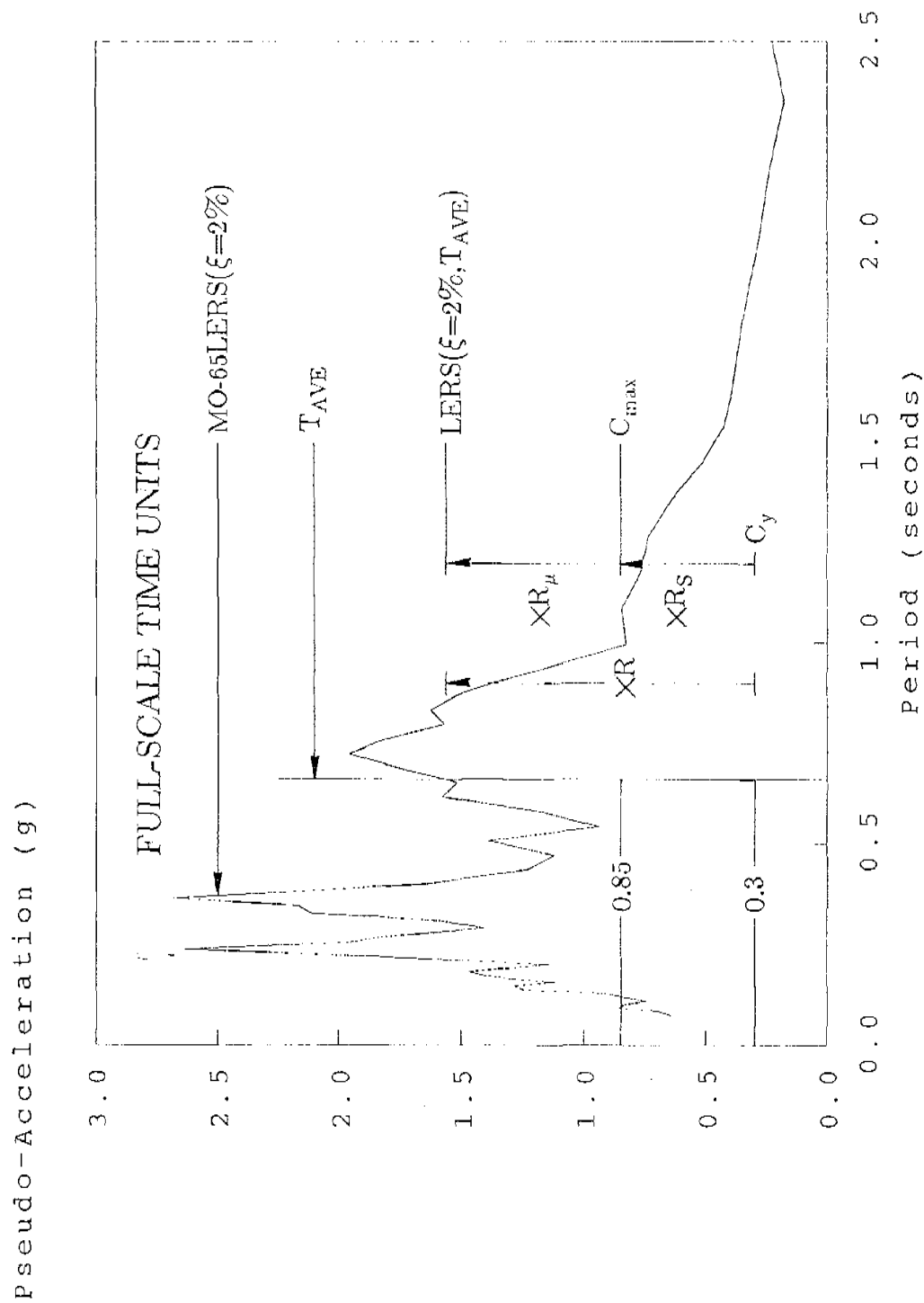
FIGURE 7.8 EBDS RESPONSE MODIFICATION FACTORS
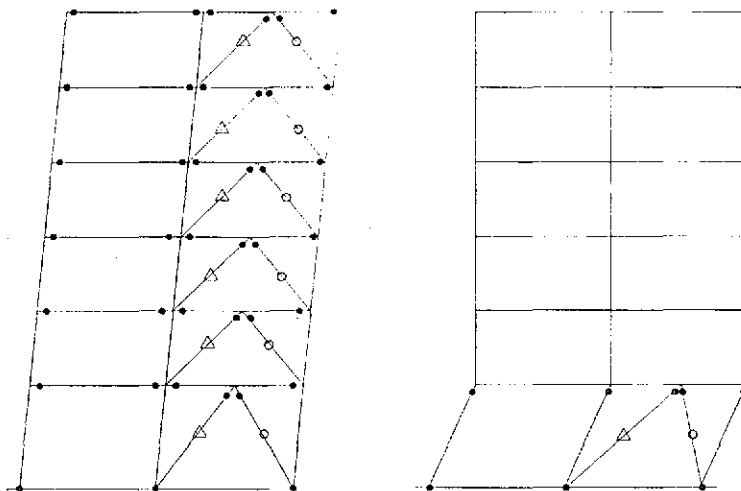
(a)   (b)

Concentrically Braced Frame
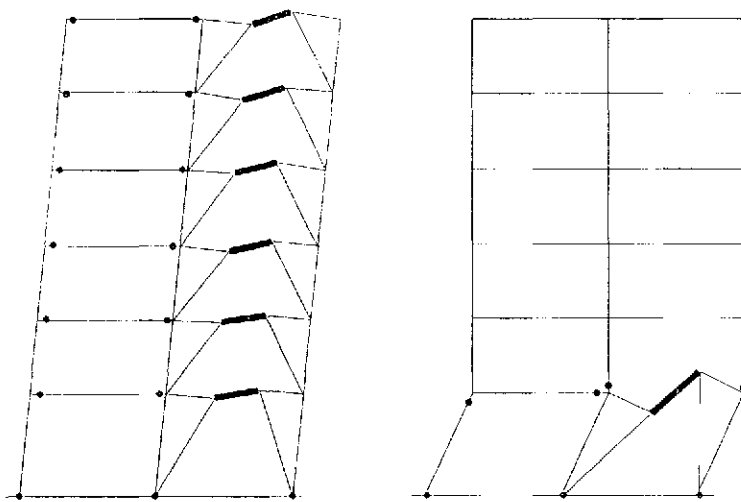
(c)   (d)

Eccentrically Braced Frame

△ Tension Yielding   • Plastic Hinge

○ Buckling   ▬ Shear Hinge

FIGURE 7.9   COLLAPSE MECHANSIMS

Base Shear Ratio

$C_y = 0.72$

$\mu_{ROOF} = 1.45$

$\Theta_y = 0.64$

$\Theta_{max} = 0.92$

0.0   0.5   1.0   1.5   2.0
Roof Drift Index (%)
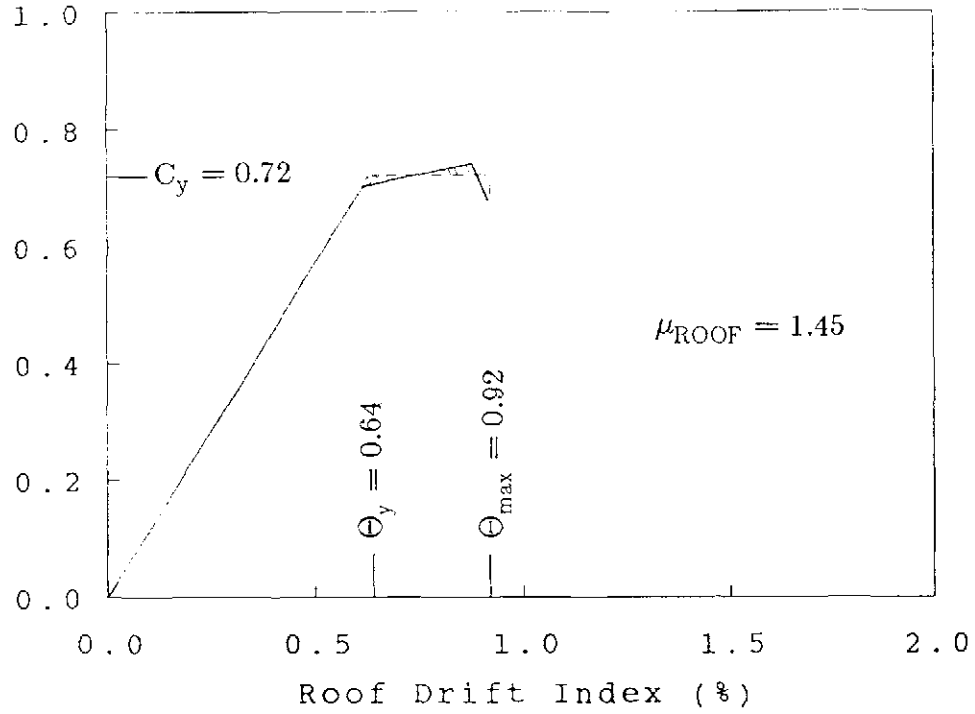
FIGURE 7.10 CBDS DISPLACEMENT DUCTILITY

Base Shear Ratio

$C_y = 0.72$

$\mu_{ROOF} = 1.40$

$\Theta_y = 0.50$

$\Theta_{max} = 0.70$

0.0   0.5   1.0   1.5   2.0
Roof Drift Index (%)
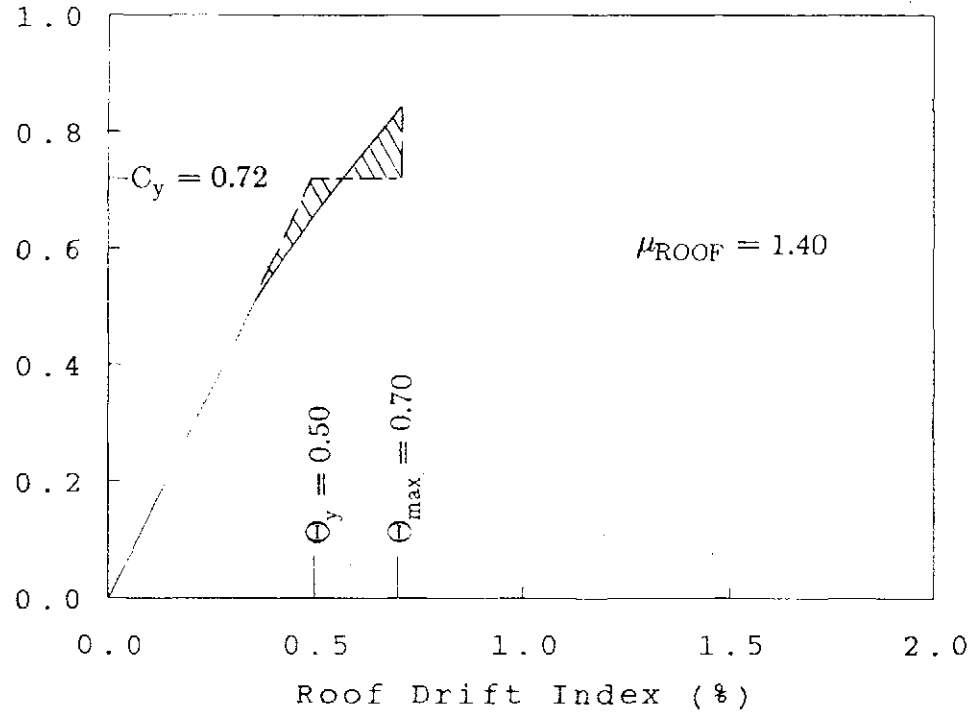
FIGURE 7.11 EBDS DISPLACEMENT DUCTILITY
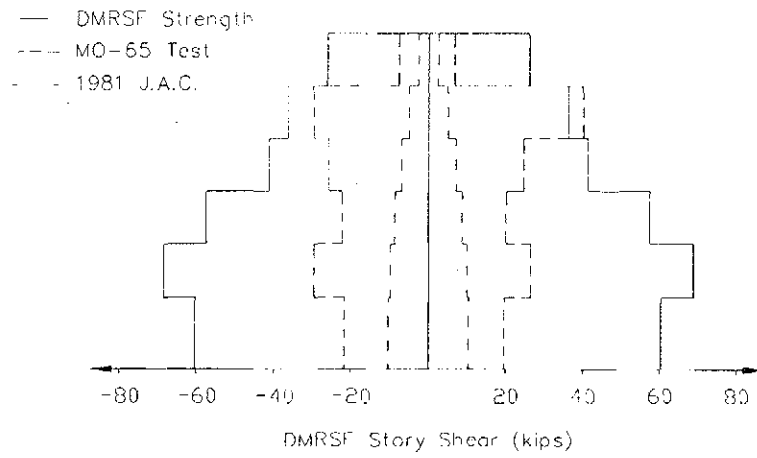
(a) CBDS MO-65 Test
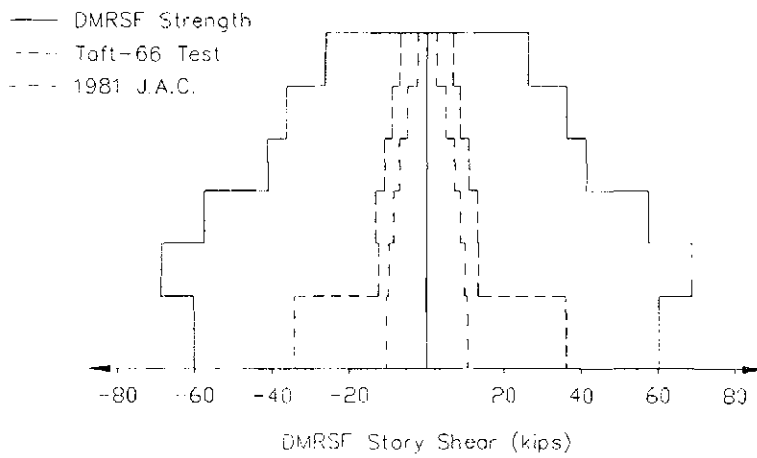
(b) EBDS Taft-66 Test

FIGURE 7.12 CBDS AND EBDS DMRSF STORY
SHEAR ENVELOPES
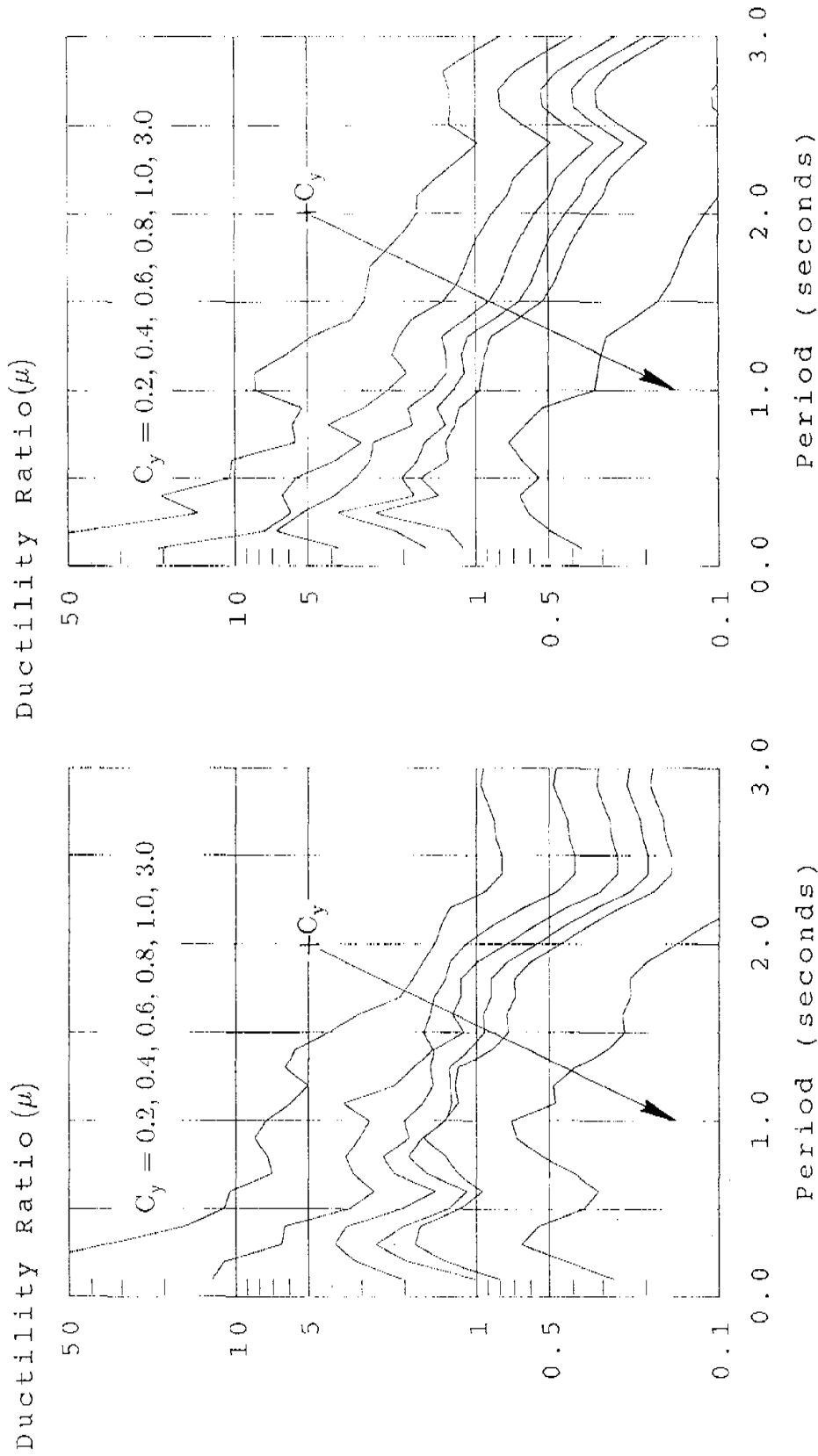
FIGURE 7.13 DISPLACEMENT DUCTILITY SPECTRA FOR 2% DAMPING
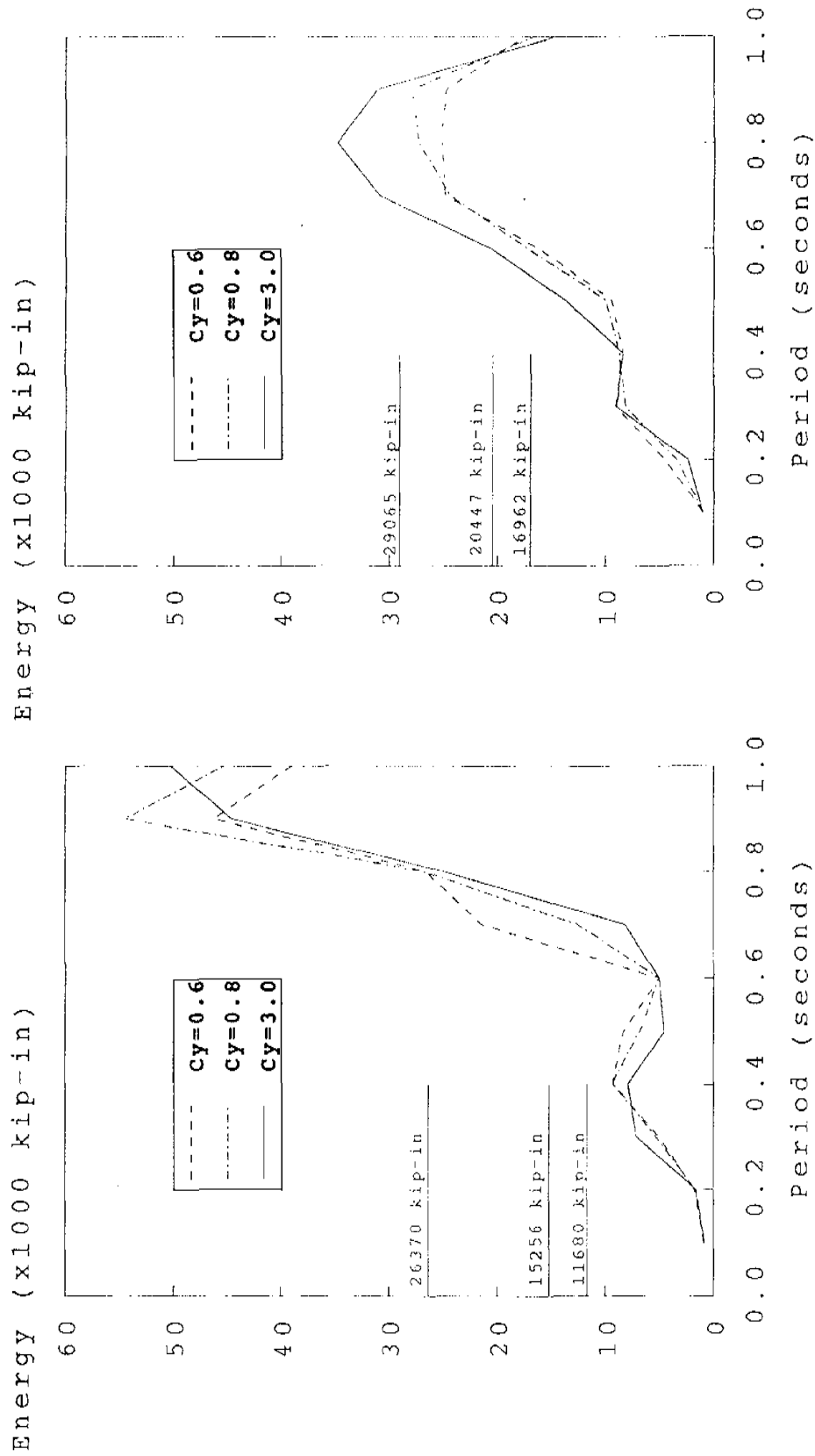
FIGURE 7.14 INPUT ENERGY SPECTRA FOR 2% DAMPING

EARTHQUAKE ENGINEERING RESEARCH CENTER REPORT SERIES

EERC reports are available from the National Information Service for Earthquake Engineering(NISEE) and from the National Technical Information Service(NTIS). Numbers in parentheses are Accession Numbers assigned by the National Technical Information Service; these are followed by a price code. Contact NTIS, 5285 Port Royal Road, Springfield Virginia, 22161 for more information. Reports without Accession Numbers were not available from NTIS at the time of printing. For a current complete list of EERC reports (from EERC 67-1) and availablity information, please contact University of California, EERC, NISEE, 1301 South 46th Street, Richmond, California 94804.

UCB/EERC-80/01 "Earthquake Response of Concrete Gravity Dams Including Hydrodynamic and Foundation Interaction Effects," by Chopra, A.K., Chakrabarti, P. and Gupta, S., January 1980, (AD-A087297)A10.

UCB/EERC-80/02 "Rocking Response of Rigid Blocks to Earthquakes," by Yim, C.S., Chopra, A.K. and Penzien, J., January 1980, (PB80 166 002)A04.

UCB/EERC-80/03 "Optimum Inelastic Design of Seismic-Resistant Reinforced Concrete Frame Structures," by Zagajeski, S.W. and Bertero, V.V., January 1980, (PB80 164 635)A06.

UCB/EERC-80/04 "Effects of Amount and Arrangement of Wall-Panel Reinforcement on Hysteretic Behavior of Reinforced Concrete Walls," by Iliya, R. and Bertero, V.V., February 1980, (PB81 122 525)A09.

UCB/EERC-80/05 "Shaking Table Research on Concrete Dam Models," by Niwa, A. and Clough, R.W., September 1980, (PB81 122 368)A06.

UCB/EERC-80/06 "The Design of Steel Energy-Absorbing Restrainers and their Incorporation into Nuclear Power Plants for Enhanced Safety (Vol 1a): Piping with Energy Absorbing Restrainers: Parameter Study on Small Systems," by Powell, G.H., Oughourlian, C. and Simons, J., June 1980.

UCB/EERC-80/07 "Inelastic Torsional Response of Structures Subjected to Earthquake Ground Motions," by Yamazaki, Y., April 1980, (PB81 122 327)A08.

UCB/EERC-80/08 "Study of X-Braced Steel Frame Structures under Earthquake Simulation," by Ghanaat, Y., April 1980, (PB81 122 335)A11.

UCB/EERC-80/09 "Hybrid Modelling of Soil-Structure Interaction," by Gupta, S., Lin, T.W. and Penzien, J., May 1980, (PB81 122 319)A07.

UCB/EERC-80/10 "General Applicability of a Nonlinear Model of a One Story Steel Frame," by Sveinsson, B.I. and McNiven, H.D., May 1980, (PB81 124 877)A06.

UCB/EERC-80/11 "A Green-Function Method for Wave Interaction with a Submerged Body," by Kioka, W., April 1980, (PB81 122 269)A07.

UCB/EERC-80/12 "Hydrodynamic Pressure and Added Mass for Axisymmetric Bodies.," by Nilrat, F., May 1980, (PB81 122 343)A08.

UCB/EERC-80/13 "Treatment of Non-Linear Drag Forces Acting on Offshore Platforms," by Dao, B.V. and Penzien, J., May 1980, (PB81 153 413)A07.

UCB/EERC-80/14 "2D Plane/Axisymmetric Solid Element (Type 3-Elastic or Elastic-Perfectly Plastic)for the ANSR-II Program," by Mondkar, D.P. and Powell, G.H., July 1980, (PB81 122 350)A03.

UCB/EERC-80/15 "A Response Spectrum Method for Random Vibrations," by Der Kiureghian, A., June 1981, (PB81 122 301)A03.

UCB/EERC-80/16 "Cyclic Inelastic Buckling of Tubular Steel Braces," by Zayas, V.A., Popov, E.P. and Mahin, S.A., June 1981, (PB81 124 885)A10.

UCB/EERC-80/17 "Dynamic Response of Simple Arch Dams Including Hydrodynamic Interaction," by Porter, C.S. and Chopra, A.K., July 1981, (PB81 124 000)A13.

UCB/EERC-80/18 "Experimental Testing of a Friction Damped Aseismic Base Isolation System with Fail-Safe Characteristics," by Kelly, J.M., Beucke, K.E. and Skinner, M.S., July 1980, (PB81 148 595)A04.

UCB/EERC-80/19 "The Design of Steel Energy-Absorbing Restrainers and their Incorporation into Nuclear Power Plants for Enhanced Safety (Vol.1B): Stochastic Seismic Analyses of Nuclear Power Plant Structures and Piping Systems Subjected to Multiple Supported Excitations," by Lee, M.C. and Penzien, J., June 1980, (PB82 201 872)A08.

UCB/EERC-80/20 "The Design of Steel Energy-Absorbing Restrainers and their Incorporation into Nuclear Power Plants for Enhanced Safety (Vol 1C): Numerical Method for Dynamic Substructure Analysis," by Dickens, J.M. and Wilson, E.L., June 1980.

UCB/EERC-80/21 "The Design of Steel Energy-Absorbing Restrainers and their Incorporation into Nuclear Power Plants for Enhanced Safety (Vol 2): Development and Testing of Restraints for Nuclear Piping Systems," by Kelly, J.M. and Skinner, M.S., June 1980.

UCB/EERC-80/22 "3D Solid Element (Type 4-Elastic or Elastic-Perfectly-Plastic) for the ANSR-II Program," by Mondkar, D.P. and Powell, G.H., July 1980, (PB81 123 242)A03.

UCB/EERC-80/23 "Gap-Friction Element (Type 5) for the Ansr-II Program," by Mondkar, D.P. and Powell, G.H., July 1980, (PB81 122 285)A03.

UCB/EERC-80/24 "U-Bar Restraint Element (Type 11) for the ANSR-II Program," by Oughourlian, C. and Powell, G.H., July 1980, (PB81 122 293)A03.

UCB/EERC-80/25 "Testing of a Natural Rubber Base Isolation System by an Explosively Simulated Earthquake," by Kelly, J.M., August 1980, (PB81 201 360)A04.

UCB/EERC-80/26 "Input Identification from Structural Vibrational Response," by Hu, Y., August 1980, (PB81 152 308)A05.

UCB/EERC-80/27 "Cyclic Inelastic Behavior of Steel Offshore Structures," by Zayas, V.A., Mahin, S.A. and Popov, E.P., August 1980, (PB81 196 180)A15.

UCB/EERC-80/28 "Shaking Table Testing of a Reinforced Concrete Frame with Biaxial Response," by Oliva, M.G., October 1980, (PB81 154 304)A10.

UCB/EERC-80/29 "Dynamic Properties of a Twelve-Story Prefabricated Panel Building," by Bouwkamp, J.G., Kollegger, J.P. and Stephen, R.M., October 1980, (PB82 138 777)A07.

UCB/EERC-80/30 "Dynamic Properties of an Eight-Story Prefabricated Panel Building," by Bouwkamp, J.G., Kollegger, J.P. and Stephen, R.M., October 1980, (PB81 200 313)A05.

UCB/EERC-80/31 "Predictive Dynamic Response of Panel Type Structures under Earthquakes," by Kollegger, J.P. and Bouwkamp, J.G., October 1980, (PB81 152 316)A04.

UCB/EERC-80/32 "The Design of Steel Energy-Absorbing Restrainers and their Incorporation into Nuclear Power Plants for Enhanced Safety (Vol 3): Testing of Commercial Steels in Low-Cycle Torsional Fatigue," by Spanner, P., Parker, E.R., Jongewaard, E. and Dory, M., 1980.

UCB/EERC-80/33 "The Design of Steel Energy-Absorbing Restrainers and their Incorporation into Nuclear Power Plants for Enhanced Safety (Vol 4): Shaking Table Tests of Piping Systems with Energy-Absorbing Restrainers," by Stiemer, S.F. and Godden, W.G., September 1980, (PB82 201 880)A05.

UCB/EERC-80/34 "The Design of Steel Energy-Absorbing Restrainers and their Incorporation into Nuclear Power Plants for Enhanced Safety (Vol 5): Summary Report," by Spencer, P., 1980.

UCB/EERC-80/35 "Experimental Testing of an Energy-Absorbing Base Isolation System," by Kelly, J.M., Skinner, M.S. and Beucke, K.E., October 1980, (PB81 154 072)A04.

UCB/EERC-80/36 "Simulating and Analyzing Artificial Non-Stationary Earth Ground Motions," by Nau, R.F., Oliver, R.M. and Pister, K.S., October 1980, (PB81 153 397)A04.

UCB/EERC-80/37 "Earthquake Engineering at Berkeley - 1980," by , September 1980, (PB81 205 674)A09.

UCB/EERC-80/38 "Inelastic Seismic Analysis of Large Panel Buildings," by Schricker, V. and Powell, G.H., September 1980, (PB81 154 338)A13.

UCB/EERC-80/39 "Dynamic Response of Embankment, Concrete-Gavity and Arch Dams Including Hydrodynamic Interation," by Hall, J.F. and Chopra, A.K., October 1980, (PB81 152 324)A11.

UCB/EERC-80/40 "Inelastic Buckling of Steel Struts under Cyclic Load Reversal.," by Black, R.G., Wenger, W.A. and Popov, E.P., October 1980, (PB81 154 312)A08.

UCB/EERC-80/41 "Influence of Site Characteristics on Buildings Damage during the October 3,1974 Lima Earthquake," by Repetto, P., Arango, I. and Seed, H.B., September 1980, (PB81 161 739)A05.

UCB/EERC-80/42 "Evaluation of a Shaking Table Test Program on Response Behavior of a Two Story Reinforced Concrete Frame," by Blondet, J.M., Clough, R.W. and Mahin, S.A., December 1980, (PB82 196 544)A11.

UCB/EERC-80/43 "Modelling of Soil-Structure Interaction by Finite and Infinite Elements," by Medina, F., December 1980, (PB81 229 270)A04.

UCB/EERC-81/01 "Control of Seismic Response of Piping Systems and Other Structures by Base Isolation," by Kelly, J.M., January 1981, (PB81 200 735)A05.

UCB/EERC-81/02 "OPTNSR- An Interactive Software System for Optimal Design of Statically and Dynamically Loaded Structures with Nonlinear Response," by Bhatti, M.A., Ciampi, V. and Pister, K.S., January 1981, (PB81 218 851)A09.

UCB/EERC-81/03 "Analysis of Local Variations in Free Field Seismic Ground Motions," by Chen, J.-C., Lysmer, J. and Seed, H.B., January 1981, (AD-A099508)A13.

UCB/EERC-81/04 "Inelastic Structural Modeling of Braced Offshore Platforms for Seismic Loading," by Zayas, V.A., Shing, P.-S.B., Mahin, S.A. and Popov, E.P., January 1981, (PB82 138 777)A07.

UCB/EERC-81/05 "Dynamic Response of Light Equipment in Structures," by Der Kiureghian, A., Sackman, J.L. and Nour-Omid, B., April 1981, (PB81 218 497)A04.

UCB/EERC-81/06 "Preliminary Experimental Investigation of a Broad Base Liquid Storage Tank," by Bouwkamp, J.G., Kollegger, J.P. and Stephen, R.M., May 1981, (PB82 140 385)A03.

UCB/EERC-81/07 "The Seismic Resistant Design of Reinforced Concrete Coupled Structural Walls," by Aktan, A.E. and Bertero, V.V., June 1981, (PB82 113 358)A11.

UCB/EERC-81/08 "Unassigned," by Unassigned, 1981.

UCB/EERC-81/09 "Experimental Behavior of a Spatial Piping System with Steel Energy Absorbers Subjected to a Simulated Differential Seismic Input," by Stiemer, S.F., Godden, W.G. and Kelly, J.M., July 1981, (PB82 201 898)A04.

UCB/EERC-81/10 "Evaluation of Seismic Design Provisions for Masonry in the United States," by Sveinsson, B.I., Mayes, R.L. and McNiven, H.D., August 1981, (PB82 166 075)A08.

UCB/EERC-81/11 "Two-Dimensional Hybrid Modelling of Soil-Structure Interaction," by Tzong, T.-J., Gupta, S. and Penzien, J., August 1981, (PB82 142 118)A04.

UCB/EERC-81/12 "Studies on Effects of Infills in Seismic Resistant R/C Construction," by Brokken, S. and Bertero, V.V., October 1981, (PB82 166 190)A09.

UCB/EERC-81/13 "Linear Models to Predict the Nonlinear Seismic Behavior of a One-Story Steel Frame," by Valdimarsson, H., Shah, A.H. and McNiven, H.D., September 1981, (PB82 138 793)A07.

UCB/EERC-81/14 "TLUSH: A Computer Program for the Three-Dimensional Dynamic Analysis of Earth Dams," by Kagawa, T., Mejia, L.H., Seed, H.B. and Lysmer, J., September 1981, (PB82 139 940)A06.

UCB/EERC-81/15 "Three Dimensional Dynamic Response Analysis of Earth Dams," by Mejia, L.H. and Seed, H.B., September 1981, (PB82 137 274)A12.

UCB/EERC-81/16 "Experimental Study of Lead and Elastomeric Dampers for Base Isolation Systems," by Kelly, J.M. and Hodder, S.B., October 1981, (PB82 166 182)A05.

UCB/EERC-81/17 "The Influence of Base Isolation on the Seismic Response of Light Secondary Equipment," by Kelly, J.M., April 1981, (PB82 255 266)A04.

UCB/EERC-81/18 "Studies on Evaluation of Shaking Table Response Analysis Procedures," by Blondet, J. M., November 1981, (PB82 197 278)A10.

UCB/EERC-81/19 "DELIGHT.STRUCT: A Computer-Aided Design Environment for Structural Engineering," by Balling, R.J., Pister, K.S. and Polak, E., December 1981, (PB82 218 496)A07.

UCB/EERC-81/20 "Optimal Design of Seismic-Resistant Planar Steel Frames," by Balling, R.J., Ciampi, V. and Pister, K.S., December 1981, (PB82 220 179)A07.

UCB/EERC-82/01 "Dynamic Behavior of Ground for Seismic Analysis of Lifeline Systems," by Sato, T. and Der Kiureghian, A., January 1982, (PB82 218 926)A05.

UCB/EERC-82/02 "Shaking Table Tests of a Tubular Steel Frame Model," by Ghanaat, Y. and Clough, R.W., January 1982, (PB82 220 161)A07.

UCB/EERC-82/03   "Behavior of a Piping System under Seismic Excitation: Experimental Investigations of a Spatial Piping System supported by Mechanical Shock Arrestors," by Schneider, S., Lee, H.-M. and Godden, W. G., May 1982, (PB83 172 544)A09.

UCB/EERC-82/04   "New Approaches for the Dynamic Analysis of Large Structural Systems," by Wilson, E.L., June 1982, (PB83 148 080)A05.

UCB/EERC-82/05   "Model Study of Effects of Damage on the Vibration Properties of Steel Offshore Platforms," by Shahrivar, F. and Bouwkamp, J.G., June 1982, (PB83 148 742)A10.

UCB/EERC-82/06   "States of the Art and Pratice in the Optimum Seismic Design and Analytical Response Prediction of R/C Frame Wall Structures," by Aktan, A.E. and Bertero, V.V., July 1982, (PB83 147 736)A05.

UCB/EERC-82/07   "Further Study of the Earthquake Response of a Broad Cylindrical Liquid-Storage Tank Model," by Manos, G.C. and Clough, R.W., July 1982, (PB83 147 744)A11.

UCB/EERC-82/08   "An Evaluation of the Design and Analytical Seismic Response of a Seven Story Reinforced Concrete Frame," by Charney, F.A. and Bertero, V.V., July 1982, (PB83 157 628)A09.

UCB/EERC-82/09   "Fluid-Structure Interactions: Added Mass Computations for Incompressible Fluid," by Kuo, J.S.-H., August 1982, (PB83 156 281)A07.

UCB/EERC-82/10   "Joint-Opening Nonlinear Mechanism: Interface Smeared Crack Model," by Kuo, J.S.-H., August 1982, (PB83 149 195)A05.

UCB/EERC-82/11   "Dynamic Response Analysis of Techi Dam," by Clough, R.W., Stephen, R.M. and Kuo, J.S.-H., August 1982, (PB83 147 496)A06.

UCB/EERC-82/12   "Prediction of the Seismic Response of R/C Frame-Coupled Wall Structures," by Aktan, A.E., Bertero, V.V. and Piazzo, M., August 1982, (PB83 149 203)A09.

UCB/EERC-82/13   "Preliminary Report on the Smart 1 Strong Motion Array in Taiwan," by Bolt, B.A., Loh, C.H., Penzien, J. and Tsai, Y.B., August 1982, (PB83 159 400)A10.

UCB/EERC-82/14   "Shaking-Table Studies of an Eccentrically X-Braced Steel Structure," by Yang, M.S., September 1982, (PB83 260 778)A12.

UCB/EERC-82/15   "The Performance of Stairways in Earthquakes," by Roha, C., Axley, J.W. and Bertero, V.V., September 1982, (PB83 157 693)A07.

UCB/EERC-82/16   "The Behavior of Submerged Multiple Bodies in Earthquakes," by Liao, W.-G., September 1982, (PB83 158 709)A07.

UCB/EERC-82/17   "Effects of Concrete Types and Loading Conditions on Local Bond-Slip Relationships," by Cowell, A.D., Popov, E.P. and Bertero, V.V., September 1982, (PB83 153 577)A04.

UCB/EERC-82/18   "Mechanical Behavior of Shear Wall Vertical Boundary Members: An Experimental Investigation," by Wagner, M.T. and Bertero, V.V., October 1982, (PB83 159 764)A05.

UCB/EERC-82/19   "Experimental Studies of Multi-support Seismic Loading on Piping Systems," by Kelly, J.M. and Cowell, A.D., November 1982.

UCB/EERC-82/20   "Generalized Plastic Hinge Concepts for 3D Beam-Column Elements," by Chen, P. F.-S. and Powell, G.H., November 1982, (PB83 247 981)A13.

UCB/EERC-82/21   "ANSR-II: General Computer Program for Nonlinear Structural Analysis," by Oughourlian, C.V. and Powell, G.H., November 1982, (PB83 251 330)A12.

UCB/EERC-82/22   "Solution Strategies for Statically Loaded Nonlinear Structures," by Simons, J.W. and Powell, G.H., November 1982, (PB83 197 970)A06.

UCB/EERC-82/23   "Analytical Model of Deformed Bar Anchorages under Generalized Excitations," by Ciampi, V., Eligehausen, R., Bertero, V.V. and Popov, E.P., November 1982, (PB83 169 532)A06.

UCB/EERC-82/24   "A Mathematical Model for the Response of Masonry Walls to Dynamic Excitations," by Sucuoglu, H., Mengi, Y. and McNiven, H.D., November 1982, (PB83 169 011)A07.

UCB/EERC-82/25   "Earthquake Response Considerations of Broad Liquid Storage Tanks," by Cambra, F.J., November 1982, (PB83 251 215)A09.

UCB/EERC-82/26   "Computational Models for Cyclic Plasticity, Rate Dependence and Creep," by Mosaddad, B. and Powell, G.H., November 1982, (PB83 245 829)A08.

UCB/EERC-82/27   "Inelastic Analysis of Piping and Tubular Structures," by Mahasuverachai, M. and Powell, G.H., November 1982, (PB83 249 987)A07.

UCB/EERC-83/01   "The Economic Feasibility of Seismic Rehabilitation of Buildings by Base Isolation," by Kelly, J.M., January 1983, (PB83 197 988)A05.

UCB/EERC-83/02   "Seismic Moment Connections for Moment-Resisting Steel Frames.," by Popov, E.P., January 1983, (PB83 195 412)A04.

UCB/EERC-83/03   "Design of Links and Beam-to-Column Connections for Eccentrically Braced Steel Frames," by Popov, E.P. and Malley, J.O., January 1983, (PB83 194 811)A04.

UCB/EERC-83/04   "Numerical Techniques for the Evaluation of Soil-Structure Interaction Effects in the Time Domain," by Bayo, E. and Wilson, E.L., February 1983, (PB83 245 605)A09.

UCB/EERC-83/05   "A Transducer for Measuring the Internal Forces in the Columns of a Frame-Wall Reinforced Concrete Structure," by Sause, R. and Bertero, V.V., May 1983, (PB84 119 494)A06.

UCB/EERC-83/06   "Dynamic Interactions Between Floating Ice and Offshore Structures," by Croteau, P., May 1983, (PB84 119 486)A16.

UCB/EERC-83/07   "Dynamic Analysis of Multiply Tuned and Arbitrarily Supported Secondary Systems," by Igusa, T. and Der Kiureghian, A., July 1983, (PB84 118 272)A11.

UCB/EERC-83/08   "A Laboratory Study of Submerged Multi-body Systems in Earthquakes," by Ansari, G.R., June 1983, (PB83 261 842)A17.

UCB/EERC-83/09   "Effects of Transient Foundation Uplift on Earthquake Response of Structures," by Yim, C.-S. and Chopra, A.K., June 1983, (PB83 261 396)A07.

UCB/EERC-83/10   "Optimal Design of Friction-Braced Frames under Seismic Loading," by Austin, M.A. and Pister, K.S., June 1983, (PB84 119 288)A06.

UCB/EERC-83/11   "Shaking Table Study of Single-Story Masonry Houses: Dynamic Performance under Three Component Seismic Input and Recommendations," by Manos, G.C., Clough, R.W. and Mayes, R.L., July 1983, (UCB/EERC-83/11)A08.

UCB/EERC-83/12   "Experimental Error Propagation in Pseudodynamic Testing," by Shiing, P.B. and Mahin, S.A., June 1983, (PB84 119 270)A09.

UCB/EERC-83/13   "Experimental and Analytical Predictions of the Mechanical Characteristics of a 1/5-scale Model of a 7-story R/C Frame-Wall Building Structure," by Aktan, A.E., Bertero, V.V., Chowdhury, A.A. and Nagashima, T., June 1983, (PB84 119 213)A07.

UCB/EERC-83/14   "Shaking Table Tests of Large-Panel Precast Concrete Building System Assemblages," by Oliva, M.G. and Clough, R.W., June 1983, (PB86 110 210/AS)A11.

UCB/EERC-83/15   "Seismic Behavior of Active Beam Links in Eccentrically Braced Frames," by Hjelmstad, K.D. and Popov, E.P., July 1983, (PB84 119 676)A09.

UCB/EERC-83/16   "System Identification of Structures with Joint Rotation," by Dimsdale, J.S., July 1983, (PB84 192 210)A06.

UCB/EERC-83/17   "Construction of Inelastic Response Spectra for Single-Degree-of-Freedom Systems," by Mahin, S. and Lin, J., June 1983, (PB84 208 834)A05.

UCB/EERC-83/18   "Interactive Computer Analysis Methods for Predicting the Inelastic Cyclic Behaviour of Structural Sections," by Kaba, S. and Mahin, S., July 1983, (PB84 192 012)A06.

UCB/EERC-83/19   "Effects of Bond Deterioration on Hysteretic Behavior of Reinforced Concrete Joints," by Filippou, F.C., Popov, E.P. and Bertero, V.V., August 1983, (PB84 192 020)A10.

UCB/EERC-83/20   "Correlation of Analytical and Experimental Responses of Large-Panel Precast Building Systems," by Oliva, M.G., Clough, R.W., Velkov, M. and Gavrilovic, P., May 1988.

UCB/EERC-83/21   "Mechanical Characteristics of Materials Used in a 1/5 Scale Model of a 7-Story Reinforced Concrete Test Structure," by Bertero, V.V., Aktan, A.E., Harris, H.G. and Chowdhury, A.A., October 1983, (PB84 193 697)A05.

UCB/EERC-83/22   "Hybrid Modelling of Soil-Structure Interaction in Layered Media," by Tzong, T.-J. and Penzien, J., October 1983, (PB84 192 178)A08.

UCB/EERC-83/23   "Local Bond Stress-Slip Relationships of Deformed Bars under Generalized Excitations," by Eligehausen, R., Popov, E.P. and Bertero, V.V., October 1983, (PB84 192 848)A09.

UCB/EERC-83/24   "Design Considerations for Shear Links in Eccentrically Braced Frames," by Malley, J.O. and Popov, E.P., November 1983, (PB84 192 186)A07.

UCB/EERC-84/01   "Pseudodynamic Test Method for Seismic Performance Evaluation: Theory and Implementation," by Shing, P.-S.B. and Mahin, S.A., January 1984, (PB84 190 644)A08.

UCB/EERC-84/02   "Dynamic Response Behavior of Kiang Hong Dian Dam," by Clough, R.W., Chang, K.-T., Chen, H.-Q. and Stephen, R.M., April 1984, (PB84 209 402)A08.

UCB/EERC-84/03   "Refined Modelling of Reinforced Concrete Columns for Seismic Analysis," by Kaba, S.A. and Mahin, S.A., April 1984, (PB84 234 384)A06.

UCB/EERC-84/04   "A New Floor Response Spectrum Method for Seismic Analysis of Multiply Supported Secondary Systems," by Asfura, A. and Der Kiureghian, A., June 1984, (PB84 239 417)A06.

UCB/EERC-84/05   "Earthquake Simulation Tests and Associated Studies of a 1/5th-scale Model of a 7-Story R/C Frame-Wall Test Structure," by Bertero, V.V., Aktan, A.E., Charney, F.A. and Sause, R., June 1984, (PB84 239 409)A09.

UCB/EERC-84/06   "R/C Structural Walls: Seismic Design for Shear," by Aktan, A.E. and Bertero, V.V., 1984.

UCB/EERC-84/07   "Behavior of Interior and Exterior Flat-Plate Connections subjected to Inelastic Load Reversals," by Zee, H.L. and Moehle, J.P., August 1984, (PB86 117 629/AS)A07.

UCB/EERC-84/08   "Experimental Study of the Seismic Behavior of a Two-Story Flat-Plate Structure," by Moehle, J.P. and Diebold, J.W., August 1984, (PB86 122 553/AS)A12.

UCB/EERC-84/09   "Phenomenological Modeling of Steel Braces under Cyclic Loading," by Ikeda, K., Mahin, S.A. and Dermitzakis, S.N., May 1984, (PB86 132 198/AS)A08.

UCB/EERC-84/10   "Earthquake Analysis and Response of Concrete Gravity Dams," by Fenves, G. and Chopra, A.K., August 1984, (PB85 193 902/AS)A11.

UCB/EERC-84/11   "EAGD-84: A Computer Program for Earthquake Analysis of Concrete Gravity Dams," by Fenves, G. and Chopra, A.K., August 1984, (PB85 193 613/AS)A05.

UCB/EERC-84/12   "A Refined Physical Theory Model for Predicting the Seismic Behavior of Braced Steel Frames," by Ikeda, K. and Mahin, S.A., July 1984, (PB85 191 450/AS)A09.

UCB/EERC-84/13   "Earthquake Engineering Research at Berkeley - 1984," by , August 1984, (PB85 197 341/AS)A10.

UCB/EERC-84/14   "Moduli and Damping Factors for Dynamic Analyses of Cohesionless Soils," by Seed, H.B., Wong, R.T., Idriss, I.M. and Tokimatsu, K., September 1984, (PB85 191 468/AS)A04.

UCB/EERC-84/15   "The Influence of SPT Procedures in Soil Liquefaction Resistance Evaluations," by Seed, H.B., Tokimatsu, K., Harder, L.F. and Chung, R.M., October 1984, (PB85 191 732/AS)A04.

UCB/EERC-84/16   "Simplified Procedures for the Evaluation of Settlements in Sands Due to Earthquake Shaking," by Tokimatsu, K. and Seed, H.B., October 1984, (PB85 197 887/AS)A03.

UCB/EERC-84/17   "Evaluation of Energy Absorption Characteristics of Highway Bridges Under Seismic Conditions - Volume I and Volume II (Appendices)," by Imbsen, R.A. and Penzien, J., September 1986.

UCB/EERC-84/18   "Structure-Foundation Interactions under Dynamic Loads," by Liu, W.D. and Penzien, J., November 1984, (PB87 124 889/AS)A11.

UCB/EERC-84/19   "Seismic Modelling of Deep Foundations," by Chen, C.-H. and Penzien, J., November 1984, (PB87 124 798/AS)A07.

UCB/EERC-84/20   "Dynamic Response Behavior of Quan Shui Dam," by Clough, R.W., Chang, K.-T., Chen, H.-Q., Stephen, R.M., Ghanaat, Y. and Qi, J.-H., November 1984, (PB86 115177/AS)A07.

UCB/EERC-85/01   "Simplified Methods of Analysis for Earthquake Resistant Design of Buildings," by Cruz, E.F. and Chopra, A.K., February 1985, (PB86 112299/AS)A12.

UCB/EERC-85/02   "Estimation of Seismic Wave Coherency and Rupture Velocity using the SMART 1 Strong-Motion Array Recordings," by Abrahamson, N.A., March 1985, (PB86 214 343)A07.

UCB/EERC-85/03 "Dynamic Properties of a Thirty Story Condominium Tower Building," by Stephen, R.M., Wilson, E.L. and Stander, N., April 1985, (PB86 118965/AS)A06.

UCB/EERC-85/04 "Development of Substructuring Techniques for On-Line Computer Controlled Seismic Performance Testing," by Dermitzakis, S. and Mahin, S., February 1985, (PB86 132941/AS)A08.

UCB/EERC-85/05 "A Simple Model for Reinforcing Bar Anchorages under Cyclic Excitations," by Filippou, F.C., March 1985, (PB86 112 919/AS)A05.

UCB/EERC-85/06 "Racking Behavior of Wood-framed Gypsum Panels under Dynamic Load," by Oliva, M.G., June 1985.

UCB/EERC-85/07 "Earthquake Analysis and Response of Concrete Arch Dams," by Fok, K.-L. and Chopra, A.K., June 1985, (PB86 139672/AS)A10.

UCB/EERC-85/08 "Effect of Inelastic Behavior on the Analysis and Design of Earthquake Resistant Structures," by Lin, J.P. and Mahin, S.A., June 1985, (PB86 135340/AS)A08.

UCB/EERC-85/09 "Earthquake Simulator Testing of a Base-Isolated Bridge Deck," by Kelly, J.M., Buckle, I.G. and Tsai, H.-C., January 1986, (PB87 124 152/AS)A06.

UCB/EERC-85/10 "Simplified Analysis for Earthquake Resistant Design of Concrete Gravity Dams," by Fenves, G. and Chopra, A.K., June 1986, (PB87 124 160/AS)A08.

UCB/EERC-85/11 "Dynamic Interaction Effects in Arch Dams," by Clough, R.W., Chang, K.-T., Chen, H.-Q. and Ghanaat, Y., October 1985, (PB86 135027/AS)A05.

UCB/EERC-85/12 "Dynamic Response of Long Valley Dam in the Mammoth Lake Earthquake Series of May 25-27, 1980," by Lai, S. and Seed, H.B., November 1985, (PB86 142304/AS)A05.

UCB/EERC-85/13 "A Methodology for Computer-Aided Design of Earthquake-Resistant Steel Structures," by Austin, M.A., Pister, K.S. and Mahin, S.A., December 1985, (PB86 159480/AS)A10 .

UCB/EERC-85/14 "Response of Tension-Leg Platforms to Vertical Seismic Excitations," by Liou, G.-S., Penzien, J. and Yeung, R.W., December 1985, (PB87 124 871/AS)A08.

UCB/EERC-85/15 "Cyclic Loading Tests of Masonry Single Piers: Volume 4 - Additional Tests with Height to Width Ratio of 1," by Sveinsson, B., McNiven, H.D. and Sucuoglu, H., December 1985.

UCB/EERC-85/16 "An Experimental Program for Studying the Dynamic Response of a Steel Frame with a Variety of Infill Partitions," by Yanev, B. and McNiven, H.D., December 1985.

UCB/EERC-86/01 "A Study of Seismically Resistant Eccentrically Braced Steel Frame Systems," by Kasai, K. and Popov, E.P., January 1986, (PB87 124 178/AS)A14.

UCB/EERC-86/02 "Design Problems in Soil Liquefaction," by Seed, H.B., February 1986, (PB87 124 186/AS)A03.

UCB/EERC-86/03 "Implications of Recent Earthquakes and Research on Earthquake-Resistant Design and Construction of Buildings," by Bertero, V.V., March 1986, (PB87 124 194/AS)A05.

UCB/EERC-86/04 "The Use of Load Dependent Vectors for Dynamic and Earthquake Analyses," by Leger, P., Wilson, E.L. and Clough, R.W., March 1986, (PB87 124 202/AS)A12.

UCB/EERC-86/05 "Two Beam-To-Column Web Connections," by Tsai, K.-C. and Popov, E.P., April 1986, (PB87 124 301/AS)A04.

UCB/EERC-86/06 "Determination of Penetration Resistance for Coarse-Grained Soils using the Becker Hammer Drill," by Harder, L.F. and Seed, H.B., May 1986, (PB87 124 210/AS)A07.

UCB/EERC-86/07 "A Mathematical Model for Predicting the Nonlinear Response of Unreinforced Masonry Walls to In-Plane Earthquake Excitations," by Mengi, Y. and McNiven, H.D., May 1986, (PB87 124 780/AS)A06.

UCB/EERC-86/08 "The 19 September 1985 Mexico Earthquake: Building Behavior," by Bertero, V.V., July 1986.

UCB/EERC-86/09 "EACD-3D: A Computer Program for Three-Dimensional Earthquake Analysis of Concrete Dams," by Fok, K.-L., Hall, J.F. and Chopra, A.K., July 1986, (PB87 124 228/AS)A08.

UCB/EERC-86/10 "Earthquake Simulation Tests and Associated Studies of a 0.3-Scale Model of a Six-Story Concentrically Braced Steel Structure," by Uang, C.-M. and Bertero, V.V., December 1986, (PB87 163 564/AS)A17.

UCB/EERC-86/11 "Mechanical Characteristics of Base Isolation Bearings for a Bridge Deck Model Test," by Kelly, J.M., Buckle, I.G. and Koh, C.-G., November 1987.

UCB/EERC-86/12 "Effects of Axial Load on Elastomeric Isolation Bearings," by Koh, C.-G. and Kelly, J.M., November 1987.

UCB/EERC-87/01 "The FPS Earthquake Resisting System: Experimental Report," by Zayas, V.A., Low, S.S. and Mahin, S.A., June 1987.

UCB/EERC-87/02 "Earthquake Simulator Tests and Associated Studies of a 0.3-Scale Model of a Six-Story Eccentrically Braced Steel Structure," by Whittaker, A., Uang, C.-M. and Bertero, V.V., July 1987.

UCB/EERC-87/03 "A Displacement Control and Uplift Restraint Device for Base-Isolated Structures," by Kelly, J.M., Griffith, M.C. and Aiken, I.D., April 1987.

UCB/EERC-87/04 "Earthquake Simulator Testing of a Combined Sliding Bearing and Rubber Bearing Isolation System," by Kelly, J.M. and Chalhoub, M.S., 1987.

UCB/EERC-87/05 "Three-Dimensional Inelastic Analysis of Reinforced Concrete Frame-Wall Structures," by Moazzami, S. and Bertero, V.V., May 1987.

UCB/EERC-87/06 "Experiments on Eccentrically Braced Frames with Composite Floors," by Ricles, J. and Popov, E., June 1987.

UCB/EERC-87/07 "Dynamic Analysis of Seismically Resistant Eccentrically Braced Frames," by Ricles, J. and Popov, E., June 1987.

UCB/EERC-87/08 "Undrained Cyclic Triaxial Testing of Gravels-The Effect of Membrane Compliance," by Evans, M.D. and Seed, H.B., July 1987.

UCB/EERC-87/09 "Hybrid Solution Techniques for Generalized Pseudo-Dynamic Testing," by Thewalt, C. and Mahin, S.A., July 1987.

UCB/EERC-87/10 "Ultimate Behavior of Butt Welded Splices in Heavy Rolled Steel Sections," by Bruneau, M., Mahin, S.A. and Popov, E.P., July 1987.

UCB/EERC-87/11 "Residual Strength of Sand from Dam Failures in the Chilean Earthquake of March 3, 1985," by De Alba, P., Seed, H.B., Retamal, E. and Seed, R.B., September 1987.

UCB/EERC-87/12   "Inelastic Seismic Response of Structures with Mass or Stiffness Eccentricities in Plan," by Bruneau, M. and Mahin, S.A., September 1987.

UCB/EERC-87/13   "CSTRUCT: An Interactive Computer Environment for the Design and Analysis of Earthquake Resistant Steel Structures," by Austin, M.A., Mahin, S.A. and Pister, K.S., September 1987.

UCB/EERC-87/14   "Experimental Study of Reinforced Concrete Columns Subjected to Multi-Axial Loading," by Low, S.S. and Moehle, J.P., September 1987.

UCB/EERC-87/15   "Relationships between Soil Conditions and Earthquake Ground Motions in Mexico City in the Earthquake of Sept. 19, 1985," by Seed, H.B., Romo, M.P., Sun, J., Jaime, A. and Lysmer, J., October 1987.

UCB/EERC-87/16   "Experimental Study of Seismic Response of R. C. Setback Buildings," by Shahrooz, B.M. and Moehle, J.P., October 1987.

UCB/EERC-87/17   "The Effect of Slabs on the Flexural Behavior of Beams," by Pantazopoulou, S.J. and Moehle, J.P., October 1987.

UCB/EERC-87/18   "Design Procedure for R-FBI Bearings," by Mostaghel, N. and Kelly, J.M., November 1987.

UCB/EERC-87/19   "Analytical Models for Predicting the Lateral Response of R C Shear Walls: Evaluation of their Reliability," by Vulcano, A. and Bertero, V.V., November 1987.

UCB/EERC-87/20   "Earthquake Response of Torsionally-Coupled Buildings," by Hejal, R. and Chopra, A.K., December 1987.

UCB/EERC-87/21   "Dynamic Reservoir Interaction with Monticello Dam," by Clough, R.W., Ghanaat, Y. and Qiu, X-F., December 1987.

UCB/EERC-87/22   "Strength Evaluation of Coarse-Grained Soils," by Siddiqi, F.H., Seed, R.B., Chan, C.K., Seed, H.B. and Pyke, R.M., December 1987.

UCB/EERC-88/01   "Seismic Behavior of Concentrically Braced Steel Frames," by Khatib, I., Mahin, S.A. and Pister, K.S., January 1988.

UCB/EERC-88/02   "Experimental Evaluation of Seismic Isolation of Medium-Rise Structures Subject to Uplift," by Griffith, M.C., Kelly, J.M., Coveney, V.A. and Koh, C.G., January 1988.

UCB/EERC-88/03   "Cyclic Behavior of Steel Double Angle Connections," by Astaneh-Asl, A. and Nader, M.N., January 1988.

UCB/EERC-88/04   "Re-evaluation of the Slide in the Lower San Fernando Dam in the Earthquake of Feb. 9, 1971," by Seed, H.B., Seed, R.B., Harder, L.F. and Jong, H.-L., April 1988.

UCB/EERC-88/05   "Experimental Evaluation of Seismic Isolation of a Nine-Story Braced Steel Frame Subject to Uplift," by Griffith, M.C., Kelly, J.M. and Aiken, I.D., May 1988.

UCB/EERC-88/06   "DRAIN-2DX User Guide.," by Allahabadi, R. and Powell, G.H., March 1988.

UCB/EERC-88/07   "Cylindrical Fluid Containers in Base-Isolated Structures," by Chalhoub, M.S. and Kelly, J.M., April 1988.

UCB/EERC-88/08   "Analysis of Near-Source Waves: Separation of Wave Types using Strong Motion Array Recordings," by Darragh, R.B., June 1988.

UCB/EERC-88/09   "Alternatives to Standard Mode Superposition for Analysis of Non-Classically Damped Systems," by Kusainov, A.A. and Clough, R.W., June 1988.

UCB/EERC-88/10   "The Landslide at the Port of Nice on October 16, 1979," by Seed, H.B., Seed, R.B., Schlosser, F., Blondeau, F. and Juran, I., June 1988.

UCB/EERC-88/11   "Liquefaction Potential of Sand Deposits Under Low Levels of Excitation," by Carter, D.P. and Seed, H.B., August 1988.

UCB/EERC-88/12   "Nonlinear Analysis of Reinforced Concrete Frames Under Cyclic Load Reversals," by Filippou, F.C. and Issa, A., September 1988.

UCB/EERC-88/13   "Implications of Recorded Earthquake Ground Motions on Seismic Design of Building Structures," by Uang, C.-M. and Bertero, V.V., November 1988.

UCB/EERC-88/14   "An Experimental Study of the Behavior of Dual Steel Systems," by Whittaker, A.S., Uang, C.-M. and Bertero, V.V., September 1988.